Observational Studies of

Pre-Main Sequence Stars.

Mark Gerard Hutchinson.

Submitted for the degree of Ph. D.

University of Keele.

1988.

BRITISH LIBRARY HSIRB

IMAGING SERVICES NORTH

Boston Spa, Wetherby
West Yorkshire, LS23 7BQ
www.bl.uk

The following have been excluded at the request of the university:

Figs 2.2.1a, 2.2.1b & 2.2.1c (between pgs 10 & 11)

Figs 2.2.3 & 2.2.4 (between pgs 14 & 15)

Figs 2.2.7a & 2.2.7b (between pgs 24 & 25)

MISSING PRINT

This work is dedicated to my dear parents, brother and grandmother, who have all been an inspiration to me. Also thanks to all my friends for their prayer and support throughout.

The Heavens declare the glory of God;
and the Firmament sheweth His handiwork.
Day unto day uttereth speech, and night unto
night sheweth knowledge.

Let the words of my mouth, and the meditation
of my heart, be acceptable in Thy sight,
O Lord, my Strength and my Redeemer

Psalm 19: 1, 2 and 14. R.S.V.

Acknowledgements.

The author would like to express his gratitude for the invaluable support and patient guidance given by Dr. A. Evans who supervised this work.

Thanks are due to the following persons: Drs. J. S. Albinson, P. Barrett, B. S. Carter, J. K. Davies, J. S. Jones, R. C. Maddison, K. Sekiguchi, H. Winckler, and all the staff at the South African Astronomical Observatory; M. Fisher, Dr. D. Pike and the staff at Los Muchachos who assisted in the work at La Palma; Drs. J. S. Albinson, B. Gregory, M. J. Goldsmith, and all the staff at Cerro Tololo; M. Shenton who obtained data from the Infra-Red Astronomical Satellite database and from the International Ultraviolet Explorer.

Thanks are also due to: Drs. M. Bailey and P. Bastien for useful discussions; Dr. J. S. Albinson for the loan of drawing equipment; J. White for supplying an algorithm for a least-squares cubic spline; M. Daniels and staff at Jodrell Bank and University College, London for assistance in producing finding charts; Drs. P. M. Allen and D. Pike for help in data reduction; collegues in the Physics Department, particularly the Head of Department, Prof. W. Fuller and the Physics departmental secretaries.

I gratefully acknowledge funding of this work by the Science and Engineering Research Council.

Finally, I give thanks to the Lord God for His Creation, and without Whom none of this would have been possible.

Abstract.

This work investigates selected young stars, paying particular attention to their photometric and polarimetric characteristics. The stars observed represent particular sub-classes of the Orion Population of young stars: stars of about one solar mass; stars of a few solar masses; a star which is thought to be still accreting matter; and a star which lies away from a star-forming dark cloud.

Data was acquired at ultraviolet, optical and infrared wavelengths, along with optical polarimetric data. The subsequent analysis of data for the well-studied stars can be summarised as follows: the spectroscopic characteristics of the star are defined; possible mechanisms for the photometric variability are discussed; and given the spectral type of the star, the intrinsic flux distribution is determined and the parameters of the optical and infrared emission are thus established. The implications of any polarimetric variability found are also discussed. A possible model of polarisation is discussed and the wavelength dependence of polarisation in eleven young stars is analysed.

It is found that the circumstellar environment plays a role in many of the observed characteristics of the stars studied. Several of the stellar spectra show lines which form in a stellar envelope. Each star is found to be affected by circumstellar extinction and to exhibit infrared emission from circumstellar dust. In most cases the circumstellar dust also gives rise to the optical polarisation. The photometric and/or polarimetric variability exhibited by some of the stars is ascribable to changes in the circumstellar dust shell opacity.

Contents.

Page.

Chapter 5. The T Tauri Stars RY Lup and RU Lup.

Page.

Chapter 6. Additional stars of the Orion Population.

Page.

Chapter 7. Polarisation from a Circumstellar Dust Shell.

Chapter 1. Introduction.

Up until the 1960's the problem of how a star such as the sun, and the sun's associated system of planets, was formed remained essentially a matter of conjecture. However, with the identification of groups of very young stars around the 1950's, work pioneered particularly by A. H. Joy and G. H. Herbig, the theoretical investigation of star formation and early stellar evolution began in earnest.

The familiar constituents of the solar system, the planets and other smaller bodies are believed to have condensed out of a pre-solar nebula when the sun was very young. Characteristics of the sun itself, such as its chromosphere, corona and its magnetic field for example, also must have had their origins at this early stage. It is believed that identification of stars of around one solar mass which are at different stages in their early evolution can mark out signposts in the process of formation of the sun and the solar system. Thus an understanding of the extreme characteristics of such young stars, such as strong line emission and the ultraviolet (UV) and infrared (IR) excess continuum emission will, it is suggested, inevitably contribute to the understanding of why the sun and our solar system are as they are today.

Thus whilst the results of research into the formation of solar mass stars will be rewarding in the sense that it will help further the understanding of the early history of the sun and the planets, the difficulties in understanding the complex nature of the young stars observed cannot be underestimated.

The phenomena which are observed in both low mass young stars, and their higher mass analogues, extend throughout the electromagnetic spectrum, from emission at X-ray wavelengths through to radio wavelengths, and each potentially revealing a different aspect of the formation of the different physical characteristics of a star and its circumstellar region: a stellar chromosphere, a stellar wind, a planetary system etc. Whilst the manifold and exotic characteristics of such young stars makes an understanding of this stage of stellar evolution no simple matter, they represent a richness and beauty in the history of our own sun (a star which is too often taken for granted) which would otherwise not have been realised.

The aim of this thesis is to make a useful contribution to the understanding of particular phenomena exhibited by a given number of young stars. The main phenomena which are studied here are the variability, the continuum emission from optical out to far-IR wavelengths and also the polarisation of light at optical wavelengths. Analysis of these characteristics will particularly determine the extent of the intrinsic variability of a given star, and also the role of the circumstellar environment in contributing to the observed reddening, IR emission, polarisation and variability.

It is hoped that this work will complement the understanding of the particular stars studied here, and also encourage others to further pursue the avenues of investigation explored here.

Chapter 2. Review of the Orion Population stars.

2.1. Introduction.

The purpose of this review is to collate the known properties of the Orion Population of young stars and thereby to summarise the current understanding of the nature of these stars. Although no two Orion Population stars are exactly alike, unless a general physical picture of the visible pre-main sequence (PMS) stage of stellar evolution, as represented by the Orion Population, can be drawn, no suitable framework will exist with which to analyse a given star. An Orion Population star cannot be studied and properly understood purely in isolation.

The two essential criteria which define an Orion Population star are: physical location, an association with a molecular cloud and/or bright or dark nebulosity; and line emission (Herbig and Rao 1972). Variables associated with nebulosity but which do not exhibit line emission are usually more numerous in nebulous regions than stars of the Orion Population (Herbig and Rao 1972). Variability is therefore only a secondary criterion for membership of the Orion Population.

Ambartsumian (1947) was first to recognise that stars of the Orion Population (as then represented essentially by T Tauri stars) are young stars evolving onto the main sequence (MS). That T Tauri stars are PMS stars is borne out by studying physical associations of T Tauri stars (a fact ascertained by radial velocity measurements), which are called T associations. T associations are not only associated with regions of active star formation (e.g. OB associa-

tions), but comparison of Hertzsprung-Russell (H-R) diagrams of T associations with theoretical PMS evolutionary tracks (Cohen and Kuhi 1979) confirms the youth of T associations. Thus the hypothesis that T Tauri stars are PMS stars is now widely accepted.

The Orion Population can be divided into three main groups: the T Tauri stars, the FU Ori stars and the Herbig Ae/Be stars. The classification system introduced by Kukarkin et al. (1969) which designates these stars as InT, FU and Ina respectively, was adopted by the International Astronomical Union (IAU) Commission 27, although is not commonly used. Throughout the rest of this work, the designations InT for T Tauri stars and Ina for Herbig Ae/Be stars, will be used as convenient shortened forms.

2.1.1. The T Tauri stars.

The original criteria employed by Joy (1945) to define the T Tauri (named after the prototype, T Tau) or InT class were: (i) irregular light variations (up to 3 mag.); (ii) spectral type F5 - G5 with emission lines resembling the solar chromosphere; (iii) low luminosity (i.e. dwarfs or sub-giants); (iv) association with bright or dark nebulosity. His study of eleven stars included R Mon and R CrA (now known to have spectral types earlier than F5, i.e. high mass analogues of InT stars), and therefore what Joy referred to as InT stars, are essentially now known as Orion Population stars.

Herbig (1962) stressed and refined the spectral criteria to include the following specific emission lines: the Balmer line series; CaII K and H, 3934 and 3968Å respectively; the FeI fluorescent lines 4063 and 4132Å; the forbidden lines of [SII] 4068, 4076, 6717, 6731Å

and [OI] 6300, 6363Å. Also he noted the presence of the strong LiI 6707Å photospheric absorption line. In more recent years, with the taking of spectrograms of fainter objects associated with nebulosity, these spectral criteria have been extended down to mid-M dwarfs.

Only a minority of InT stars satisfy **all** the spectral criteria of Herbig, and some InT stars (e.g. RY Lup, Herbig and Rao 1972) do not always exhibit line emission. The optical spectroscopic properties will be further discussed in Section 2.2.3. Briefly, other characteristic features of InT stars include variability (Section 2.2.4), UV (Section 2.2.2) and IR (Section 2.2.6) excesses, and optical polarisation (Section 2.2.5).

Several other groups of Orion Population stars exhibit similar spectral characteristics to InT stars:

A number of dMe flare stars, stars which can exhibit an InT-like spectrum during flaring activity, are associated with nebulosity and therefore these stars may represent the extreme low-mass tail of the Orion Population;

The YY Ori (or In(YY)) stars (so named after the prototype, YY Ori) are a sub-group of the InT class which were differentiated by Walker (1972) because they exhibited inverse P Cygni (often referred to as YY Ori) line profiles. The observation of inverse P Cygni line profiles aroused interest as they indicate mass infall, an occurrence expected in at least the early stages of star formation. However, the exact nature of the mass infall is uncertain, particularly in view of the fact that at least some YY Ori stars (e.g. DR Tau, S CrA) can also exhibit P Cygni profiles (i.e. mass outflow). See also Section 4.4.1;

The "isolated" InT stars are located far from a dark cloud, but exhibit a typical InT emission spectrum (Rucinski and Krautter 1983

See also Section 6.4.1;

The "naked" InT stars have been introduced by Walter (1987) in view of their comparatively weak Hα emission and also the observed lack of other InT features such as line emission and variability;

The Post-InT stars are stars in stellar clusters which are older than T associations, but which exhibit spectroscopic emission features similar to, but much weaker than, those observed in InT stars.

It is generally thought that the "isolated", "naked" and Post-InT stars are essentially "evolved" versions of InT stars, and that only the YY Ori stars can be properly classed as InT stars. Further discussion on InT stars in this work will concentrate on the "classical" InT stars, except where mention of the properties of the YY Ori and "isolated" InT stars is relevant, i.e. in the discussions of S CrA (a YY Ori star) in Section 4.4 and V4046 Sgr (an "isolated" InT star) in Section 6.4.

2.1.2. The FU Ori stars.

FU Ori underwent a remarkable eruptive event in 1936-37, brightening from about 16 mag. to 10 mag. in six months and then gradually faded back to a quiescent level. Other stars, V1057 Cyg, V1515 Cyg and V1375 Cyg have all since been observed to undergo similar outbursts. All FU Ori stars are associated with molecular clouds and nebulosity and exhibit line emission, and are therefore *bona fide* members of the Orion Population.

At maximum light the optical spectrum resembles that of a F or G supergiant, but the IR spectrum resembles that from a M-type star. Both IR and UV excesses are observed and ring-shaped nebulae are

associated with FU Ori stars (Goodrich 1987). Theoretical investigation to interpret the FU Ori phenomenon are centred on the following possibilities: M-type and F-G type binary systems (Elias 1978; Mould et al., 1978); F-G type giants which are rotating close to break up velocity (Larson 1980); an accretion disc model (Hartmann and Kenyon 1985). As the models currently stand, it would seem that the latter model best fits the observations with least difficulty.

It is believed that the spectra of all FU Ori stars resemble the spectra of ordinary InT stars before outburst (this is certainly known to be true of V1057 Cyg; Herbig 1958), and thus are taken to be closely related to the InT stars. Therefore, a consideration of the possible "event" statistics, i.e. comparison of the relative number of stars which have been observed to undergo outburst (FU Ori stars) with those that have not (InT stars), led Herbig (1977b) to suggest that FU Ori outbursts are recurrent. However, the exact nature of the FU Ori phenomenon, and therefore the actual nature of the relation to InT stars (if any), is still not clear.

2.1.3. The Herbig Ae/Be stars.

In the 1960's G. H. Herbig pioneered the work which sought to identify the early-type analogues of the InT stars, thereby making a complete spectral catalogue (from mid-B to mid-M) of the Orion Population possible. He carried out an initial survey (Herbig 1960) of 23 Ae and Be stars associated with nebulosity, applying the spectral criteria he determined for InT stars (Section 2.1.1). In recognition of his pioneering work in this field, these Orion Population stars have become known as Herbig Ae/Be stars. Since the 1960's the number

of known Herbig Ae/Be or Ina stars has grown, with a major contribution to this increase being made by Finkenzeller and Mundt (1984). Association of Ina stars with star forming regions and H-R plots have served to confirm these stars as PMS objects. The properties of these stars will be discussed in Section 2.3.

2.2. Properties of the T Tauri stars.

2.2.1. X-ray properties of T Tauri stars.

Observations of InT stars using the HEAO 2 (or *Einstein*) X-ray Satellite have been carried out by several groups, with the main surveys concentrating on the Taurus-Auriga region (Gahm 1980, Feigelson and DeCampli 1981; Walter and Kuhi 1981). The surveys of stars in Taurus-Auriga, did not detect X-ray emission for InT stars fainter than V $\simeq$ 13 mag., which indicates that the X-ray luminosity L_x probably scales with L_{Bol}. Also, for those stars detected, it was found that L_x in InT stars is about 10^{-3} - 10^{-4} L_{Bol}, which is a factor of $\simeq 10^3$ greater than the X-ray emission of normal dwarfs, a level of emission more comparable to active MS dwarfs, e.g. RS CVn.

Prior to these observations, theoretical work predicted that if the winds of InT stars are thermally driven, then the more active, extreme emission line InT stars would exhibit stronger X-ray emission (Bisnovatyi-Kogan and Lamzin 1977). However, the observations showed clearly that the reverse case is true. The InT stars with the strongest optical line emission spectra (known as "extreme" InT stars), such as RW Aur and XZ Tau, were not detected, whilst the weaker emission line stars (such as SU Aur) were bright at X-ray

wavelengths. Thus it seems clear that the X-rays are not formed in a stellar wind, but either in an enhanced hot stellar corona (e.g. Walter and Kuhi 1981) or by enhanced flares (or "superflares") (e.g. Montmerle et al., 1983). The level of X-ray emission between ≃ 0.5 and 4.5 keV detected in several InT stars indicates envelope or "coronal" temperatures ≃ a few x 10^7 K.

In order to look for flaring activity, there have been several searches for X-ray variability. Such observing campaigns have provided evidence for variability (on 10^2 - 10^5 s timescales) for several X-ray luminous stars, including DG Tau and SU Aur (Feigelson and DeCampli 1981). However, the observations of 23 PMS (mainly InT) stars in Taurus-Auriga (Walter and Kuhi 1981) failed to find any X-ray variability in the InT stars observed (including DG Tau, observed to exhibit variability by Feigelson and DeCampli 1981). This would suggest that the X-ray emission observed in their sample of stars is probably quiescent, i.e. emitted from a stellar corona, although previous studies clearly indicate that X-ray flares do occur. Montmerle et al. (1983) found that most of the X-ray sources in the ρ Oph cloud were variable (i.e. flaring), but of the ten InT stars in their sample of PMS stars, none gave a positive detection.

Although the exact origin of the X-ray emission has not yet been ascertained, several proposals to account for the lack of X-ray emission in the more (optically) active stars have been forwarded. The proposals are more applicable to coronal X-ray models, although as pointed out by Feigelson (1983), the distinction between an enhanced X-ray emitting corona and an enhanced flare model is probably not very great, and therefore the status of these hypotheses is not greatly affected whether the X-rays originate in coronae and/or flares. The

proposals for the lack of observable X-ray emission in "extreme" InT stars can be summarised as follows:

(i) X-rays *are* emitted from coronae/flaring activity in "extreme" InT stars, but are absorbed (or "smothered") by the dense, surrounding winds (Gahm 1980, Walter and Kuhi 1981);

(ii) energy which would have gone into heating the corona/flaring activity up to the temperatures required to emit X-rays ($T_e \geq 10^6$K) is instead carried off in accelerating a cool stellar wind (which produces the extreme line emission observed) (Imhoff and Giampapa 1980);

(iii) the "extreme" InT stars are considered to have just entered the InT stage of PMS evolution, at which stage they are yet to begin to emit X-rays (Gahm and Krautter 1982);

Further, the observations of Walter and Kuhi (1981) also indicate a possible inverse correlation between L_x and Hα equivalent width. The fact that X-rays are not detected in "extreme" InT stars, is by extrapolation, not inconsistent with this suggested anti-correlation.

2.2.2. Ultraviolet properties of T Tauri stars.

The UV spectra of InT stars as observed by the International Ultraviolet Explorer (IUE) generally exhibit (variable) emission lines of high ionisation such as CII-IV and SiII-IV, with the lines of slightly higher ionisation, NV (1239, 1243Å) and HeII (1640Å) (formed at $T_e \simeq 2 \times 10^5$K) being observed in only a few stars. Thus the transition region temperature in InT stars is generally $\simeq$ 1-2 x 10^5K. The strongest UV lines typically observed are the MgII h and k (2796 and 2803Å) resonance lines.

That the transition region lines of highest ionisation (e.g. CIV,

Fig 2.2.1a.

Fig. 2.2.1b.

Fig 2.2.2. Schematic temperature profile of a deep chromosphere.

SiIV) are often strong in InT stars with moderate optical line emission (e.g. GW Ori, Fig. 2.2.1a) but usually either weak or absent in the "extreme" InT stars (e.g. RW Aur, Fig. 2.2.1b) (Imhoff and Appenzeller 1987), indicates that for InT stars with strong optical emission, temperatures of only $\simeq 10^5$ K are attained in the transition line region. This suggests that non-thermal (e.g. Alfvenically driven) mass loss is the dominant cooling mechanism in the atmospheres of the more "extreme" optical emission InT stars (cf. Section 2.2.1).

Although the UV continua are usually brighter than expected for the spectral class (i.e. an UV excess), only a few high resolution spectra (usually centred on the strong lines) have been obtained. In only some stars (e.g. SU Aur) is the photospheric spectrum apparent in the UV.

To produce the observed degree of enhanced UV line and continuous emission requires a high degree of non-radiative heating in a dense (usually referred to as a *deep*) chromosphere. The idea of a deep chromosphere was first suggested by Herbig (1970), and was initially introduced to explain the optical emission characteristics; see Section 2.2.3. A deep chromosphere places the temperature minimum deeper than $\tau_{continuum} \simeq 1$, so that many emission lines (see Fig. 2.2.2), an UV and an IR excess (beyond 1.68μm) are produced (see Cram 1979 and Calvet et al., 1984).

The UV observations would therefore indicate a two-component atmosphere in InT stars, which can be viewed as a scaled-up version of the solar chromosphere: a compact high density region (the deep chromosphere) analagous to closed magnetic field structures observed in the sun, and open regions of relatively strong mass loss (preventing formation of strong transition region lines), analagous to solar coronal holes (Giampapa 1983).

2.2.3. Optical Spectroscopic properties of T Tauri stars.

The basic spectroscopic characteristics of InT stars are summarised in Section 2.1, although the majority of InT stars exhibit only moderate Hα and CaII K and H line emission. InT stars can exhibit "veiling" (infilling by emission) of the photospheric lines, but in only about 10% of InT stars does the emission spectrum so dominate that no photospheric spectrum is observable. The optical spectra of the InT stars which exhibit particularly strong line emission, the "extreme" InT stars (e.g. RW Aur and RU Lup) and the YY Ori stars (e.g. DG Tau and S CrA), have been the most intensively studied.

The catalogue (obtained at 7Å resolution) of Cohen and Kuhi (1979) indicates that NaI emission occurs in 7% of InT stars, FeII in 18% and HeI in 40% (indicating the presence of hot gas, $T_e \simeq 1 - 5 \times 10^4$ K, in the atmospheres of a large number InT stars). Also Cohen and Kuhi (1979) point out a correlation between Hα, FeII and [OI] emission with HeI, indicating a common (probably chromospheric) origin for the emission spectra. Their conclusion that the level of emission activity tends to decrease with age was *not* however verified (although in a somewhat smaller sample of stars) by Herbig et al. (1986) who indicate that emission-line intensity and age are not simply related.

The "degree" of emission in an InT optical spectrum is usually described by emission class (see Herbig 1962):

class 1 - emission only at Hα;

class 2 - weak emission at red wavelengths;

class 3 - moderate Balmer and CaII K and H emission;

class 4 - strong Balmer, CaII K and H emission with other, weak lines;

class 5 - strong Balmer, CaII K and H and metallic line emission.

Thus a star which exhibits a very weak emission spectrum, such as SU Aur is typically only class 1-2, whereas an "extreme" InT star such as RW Aur is always class 5. The stronger lines in particular, usually exhibit a degree of variability.

Balmer emission lines typically dominate the optical spectrum and the lower members can often exhibit variable absorption features, e.g. P Cygni profiles. The intense Hα line in InT stars can be Gaussian, or can exhibit one or two absorption features, although unlike the other Balmer lines, **true** P Cygni or inverse P Cygni profiles (i.e. the absorption extends below the continuum) are **never** seen in Hα.

The CaII K and H lines and NaI D lines also usually exhibit variable profiles and absorption features. The lines can exhibit very different extremes: rapid variability on a timescale of hours, e.g. the NaI D lines of RW Aur; or exhibit a stable blue-shifted absorption feature, e.g. the NaI D lines of DG Tau, indicative of an extended, expanding shell (Mundt 1984). Rapid variability of the NaI D line profiles is presumably due to flaring activity (cf. solar flares).

The presence of the strong FeI 4063, 4076Å fluorescent lines in the spectrum of an InT star is also strongly suggestive of flaring activity, as these lines are only otherwise observed in solar flares or in dMe dwarfs during flaring.

Detailed, semi-empirical modelling (Cram 1979; Calvet et al., 1984) has been carried out to interpret the optical (and UV; see Section 2.2.2) emission properties of InT spectra in terms of a homogeneous deep chromosphere (an over-simplification where InT stars are concerned, e.g. see Section 2.2.2; a schematic temperature profile such as that expected in InT stars is represented in Fig. 2.2.2). The models successfully account for the observed veiling, the FeI

(excepting the fluorescent FeI lines) and FeII emission spectra, the profiles of the CaII K and H, NaI D and the Hγ and Hβ lines, and also the observed continuous energy distribution (from UV to near-IR wavelengths) in a number of InT stars (e.g. AA Tau and BP Tau, see Fig. 2.2.3). However, the deep chromosphere model cannot account for the observed strength of the Hα line nor the size of the observed Balmer jump. Emission from an extended envelope is required to interpret these, e.g. Calvet et al. (1984).

The likely extension and geometry of such extended envelopes have been investigated by studies of the forbidden and Hα line emission in ten InT stars (including RY Tau and HL Tau) by Edwards et al. (1987). Their work provides evidence that the winds of these stars are essentially conical or bipolar, and that the blueshifted nature of the forbidden lines is due to obscuration of the receding lobe by circumstellar dust discs (of typical radius ≃ 40 A.U.).

A significant fraction of InT stars exhibit forbidden line emission, e.g. 29% of the stars studied by Cohen and Kuhi (1979) show [OI] emission, and about one-third of these stars are associated with tiny nebulosities (which also exhibit forbidden emission).

Although many prominent Herbig-Haro (HH) objects in star forming regions have been shown to be associated (by proper motion measurements) with massive, embedded sources (e.g. HH28 and 29 with L1551 IRS5; Cudworth and Herbig 1979), smaller scale HH nebulosities and optical jets have been shown to associated with several InT stars, e.g. DG Tau, HL Tau/XZ Tau (Mundt and Fried 1983). However, the observed luminosities and winds of InT stars are not capable of powering the HH phenomenon (for a review of possible mechanisms of production, see Canto 1983). This fact, coupled with the estimated

Fig. 2.2.3.

Fig. 2.2.4. Optical lightcurves of DN Tau.
(From Vrba *et al.*, 1986)

time since ejection (inferred from the proper motion) of such objects has led to the suggestion that HH objects associated with InT stars are probably ejected during an earlier, more energetic phase in their evolution, possibly whilst the stars were still embedded, e.g. the "turn-on" of the stellar wind, or an FU Ori-type outburst (Lada 1985).

Recent studies of the rotation velocties of InT stars (Vogel and Kuhi 1981; Bouvier et al., 1986b; Hartmann et al., 1986) showed that InT stars are slow rotators, with typical observed $v\sin i \simeq 10 - 15$ kms^{-1}. This result shows that: (1) the angular momentum problem (the angular momentum of stars is $\simeq 10^{-4} - 10^{-5}$ that for the protostellar clouds from which the stars form) in low mass stars is solved *prior* to the InT stage of PMS evolution, i.e. the "missing" angular momentum is probably lost during star formation via magnetic braking (Mestel and Spitzer 1956); (2) the observed rotation velocities are consistent with a modified version of the Skumanich (1972) relation (modified by replacing rotation velocity by angular momentum), i.e. $(J/M) \simeq t^{-1/2}$ (Vogel and Kuhi 1981). Also Hartmann et al. (1986) find no correlation between $v\sin i$ and Hα emission, leading them to conclude that InT activity is probably not driven by an enhanced solar-type magnetic dynamo as was suggested by Bouvier and Bertout (1986).

The LiI 6707Å absorption line is typically $\simeq 10^{2}$ times stronger than is observed in MS dwarfs. In MS dwarfs the photospheric lithium is destroyed by proton collisions when it is convectively transported to deeper atmospheric layers. Therefore the relative strength of the observed LiI line suggests that the convective envelopes of InT stars (inferred from the strong chromospheric activity) are young. It is noted that the strength of the LiI line is enhanced by a factor of two in solar penumbrae relative to the solar photosphere. Although this is

hardly the order of magnitude observed in InT stars relative to MS dwarfs, it does suggest that "starspot" activity in InT stars (see Section 2.2.4) may also give rise to variations in the strength of the LiI line, and thus a relationship between the LiI line strength and photometric variations may be worth looking for in certain InT stars.

2.2.4. Optical Photometric properties of T Tauri stars.

InT stars are generally found to appear redder than would be expected for their spectral type and interstellar (IS) reddening. This general result is obviously dependent on adequate representation of the intrinsic optical colours of InT stars by the colours of normal dwarf stars. The colour excess is usually attributable to InT stars being affected by circumstellar reddening (e.g. Rydgren et al., 1982). The most notable star in this respect is HL Tau which suffers $A_V \simeq 7$ mag. of extinction by an edge-on circumstellar disc (Cohen 1983).

The light variability of InT stars is generally irregular. Two schemes of categorising the irregular lightcurves have been formulated. The first involves assigning the stars which exhibit rapid variability to one class, the RW Aur variables, whilst the stars which exhibit smoother, more regular variability being referred to as T Tau variables (Wenzel 1969). However this classification has found little favour (e.g. Herbig 1962) and is rarely used. A more widely used classification for InT lightcurves was introduced by Parenago (1954):

type I - stars which are most often bright;

type II - stars which prefer the middle of their range;

type III - stars which are most often faint;

type IV - stars with no preferred brightness level.

This scheme was slightly extended by Herbig (1962) to include the typical timescale of variation.

Periodic/quasi-periodic light variations were first observed in InT stars by Hoffmeister (1965) (e.g. S CrA, RY Lup), variations which he attributed to the presence of "starspots"; but only recently have observations provided convincing evidence of sinusoidally varying, periodic light variations due to "spotted" photospheres, the first of these being in SY Cha (Schaefer 1983). Subsequent studies (e.g. Vrba et al., 1986; Bouvier et al., 1986a) have increased the number of stars with sinusoidally varying lightcurves to a handful (e.g. DN Tau, see Fig. 2.2.4; Vrba et al., 1986). The term "starspot" is used in analogy with solar sunspots, i.e. essentially a tube of magnetic flux escaping from deep within a convective envelope. The presence of starspots in InT stars is an idea not inconsistent with the two component atmosphere suggested by Giampapa (1983) - see Section 2.2.2.

Appenzeller and Dearborn (1984) showed the feasibility of large cool starspot regions covering about half the observed disc, causing large (up to 3.5 mag.) amplitude light variations in InT stars; however, the large fractional "spot" coverage of the stellar disc which is inferred to interpret some observed variations (e.g. 0.8 for CO Ori, Herbst et al., 1983; 0.73 for GI Tau, Vrba et al., 1986) stretches considerably current physical concepts of a spotted photosphere. There is almost certainly a definite physical constraint on the diameter of an individual starspot, D, which is expected to scale with the depth of the convection zone H (e.g. $D \simeq 3H$, Mullan 1975). The most comparable starspot model is the $\simeq$ 20% surface coverage required to successfully interpret the lightcurves of RS CVn binaries (Eaton and Hall 1979).

In most instances (e.g. DN Tau), both hot *and* cool spot temperatures (relative to the photospheric effective temperature) are required to interpret the observations, with the "hot spot" or plage region usually occupying a much smaller fraction of the stellar disc than the cool spot. It should be stressed that the observed light-curves of stars with "spotted" photospheres suffer many phase changes, indicative that the spot areas are **not** constant, which in itself provides another constraint on physically realisitic starspot sizes.

Given the current understanding of starspots, it is to be expected that starspots and flaring activity should be related (e.g. Mullan 1975), and therefore flaring activity (seen as a large scatter in U points and/or X-ray variability) should be looked for in InT stars which exhibit sinusoidally varying lightcurves and *vice versa*.

A search for "flare" activity in the optical, by monitoring the U (3600Å) lightcurve in five InT stars, was carried out by Worden and Schneeberger (1981). They interpret the observed variations at U in terms of the superposition of many solar-like flare light curves. They found timescales for individual flare events of 10^2 - 10^4 s, similar to that observed for solar flares, but they computed that InT flare events are about 10^3 times more energetic than solar flares.

The optical colour slopes of variation show that InT stars generally become redder when fainter. This behaviour can be successfully interpreted either in terms of a starspot model (i.e. due to surface activity) or variable extinction by circumstellar dust (e.g. Schmelz 1984). However, particularly in some of the earlier InT spectral types (e.g. RY Tau), the U-B and B-V colours can become bluer when faint (a colour reversal), and such behaviour cannot be accounted for purely by changes in circumstellar extinction.

The underlying longer term (possibly quasi-periodic; Herbst 1986) changes, over timescales ≃ weeks - years, in the level of light emission which is generally exhibited by InT stars cannot be attributed to a rotational modulation; thus such behaviour is presumably due to either variable circumstellar extinction and/or due to changes in the (convective) transport of surface energy (Herbst 1986).

The overall impression from the literature would thus appear to be that both surface activity (e.g. Worden and Schneeberger 1981; Vrba et al., 1986) and circumstellar dust shell opacity (e.g. Evans et al., 1982; Schmelz 1984) can play a part in the light variability of InT stars. Surface activity, such as flares and starspots almost certainly dominate the short-term (≃ hours - days) variability seen in many InT stars, with changes in either the line-of-sight circumstellar opacity and/or the global effective temperature affecting the underlying, longer term (≃ weeks - years) variations.

An example of a well-studied star which exhibits both long-term and short-term variability is RY Tau. It exhibits short-term (≃ days) fluctuations indicative of starspot/flaring activity (Vrba et al., 1986), and also long-term (≃ months-years) changes in the level of quiescent brightness and also in the degree of polarisation (Schulte-Ladbeck 1983). The lightcurve has a quasi-period of ≃ 32 days (Herbig and Rao 1972) and the lightcurve over the past 20 years is shown in Fig. 2.2.5. The long-term light (Fig. 2.2.5) and polarimetric (Fig. 2.2.6) changes in RY Tau have been ascribed to a single mechanism, "orbiting" clumps of circumstellar dust (Efimov 1980; Schulte-Ladbeck 1983), although the long-term light variability has also been ascribed to global changes in effective temperature (Vrba et al., 1986).

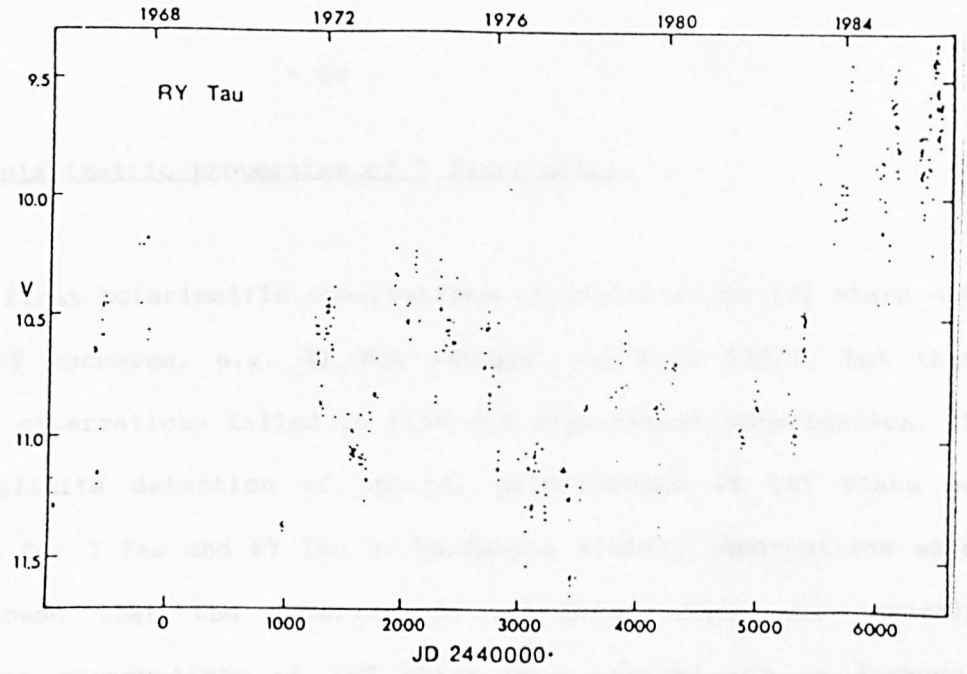

Fig. 2.2.5. The visual lightcurve of RY Tau spanning the last 20 years. Data prior to 1981 are from Zajtseva (1982). More recent points were obtained at Van Vleck Observatory. The dramatic increase in mean brightness level, which occurred in 1984 (Herbst and Stine 1984), is clearly seen.
(From Herbst 1986)

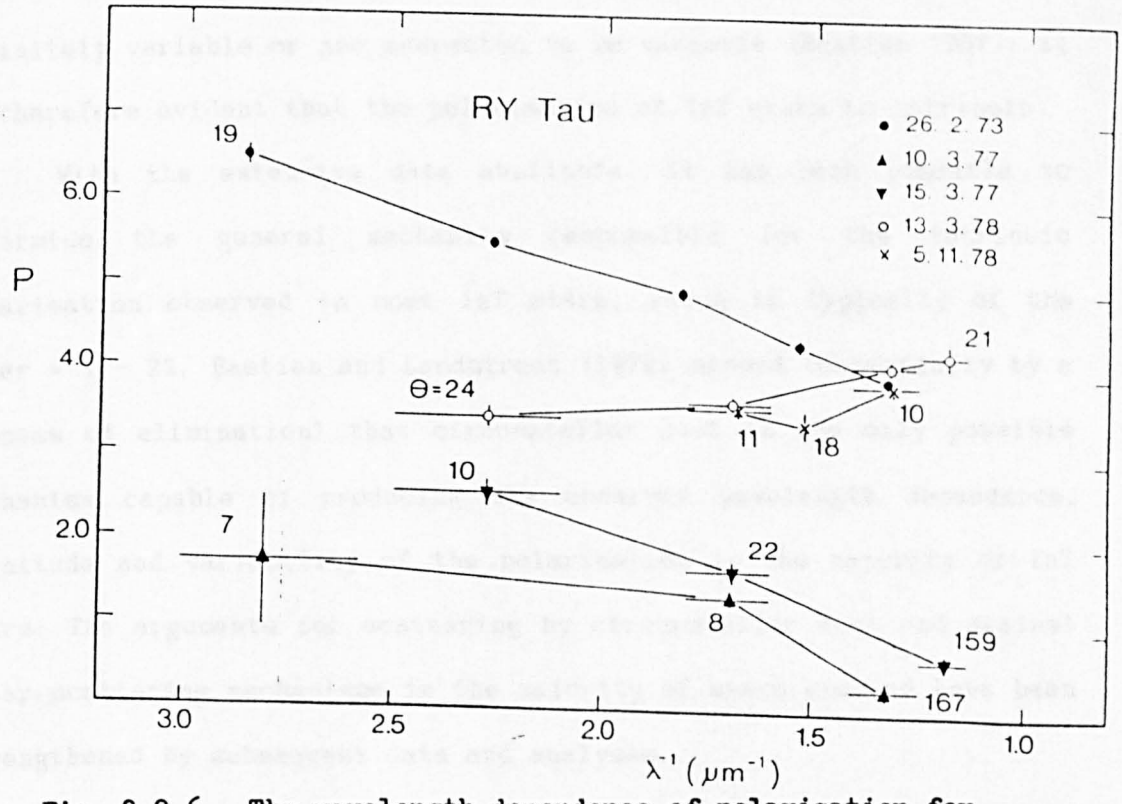

Fig. 2.2.6. The wavelength dependence of polarisation for RY Tau on the dates indicated. The corresponding position angles are indicated. The 1973 data are from Breger (1974).
(From Bastien and Landstreet 1979)

2.2.5. Polarimetric properties of T Tauri stars.

The first polarimetric observations concentrated on InT stars with strong UV excesses, e.g. NX Mon (Hunger and Kron 1957), but these earliest observations failed to find any significant polarisation. The first definite detection of optical polarisation in InT stars was obtained for T Tau and RY Tau by Vardanian (1964), observations which also showed that the polarisation of these stars was variable. Subsequent observations of InT stars were carried out by Serkowski (1969a), Breger (1974) and Abuladze et al. (1975) which confirmed the varibility of T Tau and RY Tau and increased the number of known InT polarimetric variables. Polarimetric variability is now known to be widespread amongst InT stars (e.g. Bastien 1982; Schulte-Ladbeck 1983; Bastien 1985): almost 85% of the InT stars observed are either definitely variable or are suspected to be variable (Bastien 1987); it is therefore evident that the polarisation of InT stars is intrinsic.

With the extensive data available, it has been possible to determine the general mechanism responsible for the intrinsic polarisation observed in most InT stars, which is typically of the order $\simeq$ 1 - 2%. Bastien and Landstreet (1979) showed (essentially by a process of elimination) that circumstellar dust is the only possible mechanism capable of producing the observed wavelength dependence, magnitude and variability of the polarisation in the majority of InT stars. The arguments for scattering by circumstellar dust and against other scattering mechanisms in the majority of stars studied have been strengthened by subsequent data and analyses.

For example, studies by Bastien (1982, 1985) show that the optical polarisation and the optical emission characteristics of InT stars (in

the majority of cases) are found not to be correlated, and therefore do not have a common mechanism, i.e. produced within a stellar envelope. However, there is a correlation between the magnitude of the polarisation and the optical-IR colours, particularly <V> - <L>, i.e. stars which are strongly polarised also have large near-IR excesses (attributable to thermal emission from dust; see Section 2.2.6).

It is stressed however that the form of the wavelength dependence of polarisation can differ greatly from star to star (see Section 7.3). Therefore it cannot be simply assumed that the polarisation of an InT star is necessarily due to scattering by circumstellar dust.

The largest optical polarisation observed in an InT star is 12% for HL Tau. The high polarisation of this star is clearly attributable to multiple scattering within an optically thick, edge-on circumstellar disc (Cohen 1983); this value is close to the theoretical limit of ≈ 11-12% (Daniel 1980), which can be produced by multiple scattering by unaligned grains in an uniform ellipsoidal shell.

The polarisation is generally a function of both wavelength and time, i.e. $p(\lambda,t)$. The range of variability can be as much as 6% (as in UY Aur), but more typically lies between 0.5 and 1.0% (Bastien 1985). In most cases the variability would appear to be irregular (as would be expected in random changes in the dust shell opacity), although the data obtained are often too inadequate to be conclusive. At present, only for one star, RY Lup (which can vary by as much as 0.5% in a few days; see Section 5.1.5), is there any evidence for periodic changes in the polarisation (as indicated in Bastien 1987). Periodic variations could be due to the non-uniform illumination of a dust shell by a rotating, "spotted" star (see Section 7.4).

The marked variability observed in the wavelength dependence

observed in several stars (e.g. RY Tau, Fig. 2.2.6), is more difficult to interpret however. The usual suggestion is that the grain size (or grain size distribution) changes with time. This led Burke and Silk (1976) to propose a model of grain growth in the environments of InT stars. But the effects of multiple scattering within a complex, varying dust distribution is also likely to be able to reproduce the observed variations in the wavelength dependence (Bastien 1987).

Also the position angle of the polarisation of many InT stars is known to be variable. A variable position angle indicates that the circumstellar dust distribution giving rise to the polarisation has no fixed axis, i.e. it is non-symmetric. Variations can be as large as 45°, but changes of this magnitude are only ever associated with limited changes in the magnitude of the polarisation (as with SU Aur), and the variation in the Stokes (Q,U) plane is therefore well confined (Bastien 1987). This fact indicates that, for such stars, the scattering dust is confined to a narrow solid angle (e.g. a disc).

Hough et al. (1981) observed substantial IR polarisation in five of six InT stars they observed and found a reversal of almost exactly 90° in the position angle between the optical and the IR polarisation for both T Tau and SU Aur. Monte Carlo computations by Daniel (1980) show that such reversals are in fact a natural property of scattering by dielectric grains (grains with a purely real refractive index).

Positive detection of circular polarisation in T Tau, RY Tau and SU Aur has also been made (Nadeau and Bastien 1986). The search for, and analysis of, circular polarisation in young stars is still in its early stages, but it is suggested by Nadeau and Bastien (1986) that circularly polarised light in InT stars is an indication of either partially aligned dust grains and/or multiple scattering within an

asymmetric dust shell (Nadeau and Bastien 1986).

2.2.6. Infrared properties of T Tauri stars.

The near-IR colours from 1 - 5μm of several InT stars observed by Mendoza (1968) were larger than expected for the given spectral types (i.e. an IR excess), even after correcting for IS extinction. He ruled out anomalous reddening (i.e. the value of $R = A_V/E(B-V) > 3.1$, the value for a "normal" IS reddening law) as the cause, and suggested that the strong near-IR excesses were due to thermal re-radiation of absorbed (UV and optical) stellar radiation and the weaker IR excesses were caused by heating of a stellar wind by cosmic rays.

Rydgren et al. (1976) however interpreted the near-IR excess of a number of InT stars in the Taurus and the ρ Oph clouds in terms of free-free and free-bound emission in the IR from a circumstellar envelope, which is affected by an anomalous cloud extinction law ($R \simeq 7$). Therefore they predicted that the more "extreme" InT stars should exhibit the larger near-IR excesses. However, Cohen and Kuhi's (1979) analysis of a much larger number of InT stars failed to substantiate this prediction, and showed quite clearly that the near-IR excesses in the majority of InT stars require some thermal dust emission, and that about half the InT stars in Taurus-Auriga can be explained *only* by thermal dust emission. It should however be noted that anomalous extinction *is* found towards the centres of some dark cloud regions, e.g. Cha T1 and R CrA; Vrba and Rydgren (1984).

For a reddened star with an IR excess attributable to dust emission, once the colours have been corrected for IS extinction, the dust shell parameters can, in principle, be estimated. An analysis of

InT stars in Taurus and NGC 2264 by Rydgren et al. (1982) show very well-defined near-IR colour-colour loci (Fig. 2.2.7) once the colours have been dereddened. This strongly indicates that the maximum dust temperature surrounding InT stars is remarkably uniform (T_{max} ≃ 1300K). They also find a correlation between E(V-I) (a reddening indicator) and H-K (an IR excess indicator), a result which strongly suggests that the reddening affecting their sample of stars is essentially circumstellar in origin.

The near-IR colours of InT stars typically vary by no more than a magnitude, and the variations can be attributed to variation in either the intrinsic emission (e.g. XZ Tau) or the dust shell opacity (e.g. CW Tau) (Schmelz 1984). Schmelz also indicates that near-IR colour changes due to shell opacity tend to be biased towards stars which have the stronger IR excesses, i.e. the more substantial dust shells.

The different spectral forms of the near- and mid-IR (1 - 10μm) excesses in InT stars have been successfully modelled by either blackbody emission or in a few cases by free-free emission (e.g. Cohen and Kuhi 1979), and for those InT stars with fairly flat IR excesses in λF_λ, by models which consider emission from discs with realistic grain and density parameters (e.g. Adams et al., 1987). In many cases, IR excesses have been shown to extend out to the 12 - 100μm wavelength region covered by the Infra-Red Astronomical Satellite (IRAS), e.g. Rucinski (1985), Walker and Marsden (1986). Such results indicate the ubiquity of both hot and cool dust emission in most InT stars.

Adams and Shu (1986) showed that a circumstellar disc can intercept and re-radiate only ≃ 25% of the stellar luminosity, a result which they suggest requires self-luminous discs (i.e. discs heated both by stellar radiation and internally, by viscous and/or accretion

K-L

FIG. 2.2.7a. FIG. 2.2.7b.

FIG. a —Plot of $H-K$ against $K-L$ for T Tauri stars we have observed in the Taurus region. Filled circles, filled squares, and filled triangles indicate stars of spectral type K0 to K4, K5 to K7–M0, and M0 to M1, respectively. Stars of unknown spectral type are represented by an X. The line extending from each point of known spectral type indicates the correction for IS reddening if the entire $E(V-I)$ is due to IS reddening. The dashed curve is the locus of dust shell models with a maximum grain temperature of 1300 K and a K7 V central star.

FIG. b —Plot of $J-H$ against $H-K$ for T Tauri stars we have observed in the Taurus region. Otherwise, similar to Fig. a

(From Rydgren et al., 1982)

processes) for stars with large, flat (in λF_λ) IR excesses. However, Kenyon and Hartmann (1988) in a similar treatment showed that, provided a disc is not spatially thin, flat IR continua can be explained without invoking the need for self-luminous discs. Thus only in cases where the $\simeq$ 1 - 10μm IR luminosity exceeds the stellar bolometric luminosity do self-luminous discs seem essential.

Further, the inferred mass infall rate of $\simeq 10^{-6}$ $M_\odot$ yr^{-1}, which Adams and Shu (1985) suggest to power a self-luminous disc should produce observable inverse P Cygni profiles if the nebular gas is coupled with the nebular dust. Thus, if their idea is correct, it suggests that YY Ori stars (which are much more likely than "classical" InT stars to be still accreting nebular matter) should exhibit larger IR excesses than "classical" InT stars, which does not seem to be observationally substantiated.

Two IR spectral features which have been observed in a significant number of InT stars are of particular note. First, the wavelength region 7500 - 8700Å is typically dominated by CaII IR triplet 8498, 8542 and 8662Å emission (Herbig and Soderblom 1980), and for the twelve stars Herbig and Soderblom observed, these lines were generally seen to be saturated, irrespective of the intensity of the lines. This strongly indicates that the relative area of the emission region varies from star to star, an interpretation further strengthened by the observed proportionality of OI 8446Å to CaII 8498Å emission (Herbig and Soderblom 1980). These IR observations further support the idea forwarded by Petrov and Shcherbackov (1976) that the surfaces of InT stars are inhomogeneous, covered by both active (hot) and quiet (cool) surface regions, i.e. further evidence in favour of two component starspot/flare models of InT activity (e.g. Giampapa 1983).

Spectrophotometry of a larger number of InT stars by Cohen and Whitteborn (1985) confirmed the presence of 10μm silicate features (either in absorption or emission) in the spectra of the InT stars they observed, indicating that silicate grain material is probably a typical constituent of the dust shells associated with InT stars.

2.2.7. Radio properties of T Tauri Stars.

Particular InT stars have been well studied at radio wavelengths (e.g. T Tau) and statistically, the most important radio survey (as regards InT stars) of a region of star formation was of the Taurus-Auriga region (Bieging et al., 1984). This survey was luminosity limited ($\log L \geq 0.2\ L_\odot$) for 4.885 GHz continuum radio emission, and about a quarter of those InT stars observed gave a positive detection.

A summary of the general properties of the InT stars at radio wavelengths can be given thus: most of the InT stars which exhibit radio emission are the "extreme" InT stars such as RW Aur, DG Tau and NX Mon (a notable exception is RU Lup, Brown 1987a); the observed radio continua indicate the presence of highly ionised winds which probably originate in hot ($T_* \simeq 10^6$ K) envelopes (Felli and Panagia 1981) and show no evidence for mass-loss rates higher than $\simeq$ few x $10^{-8}\ M_\odot yr^{-1}$.

Also a survey of InT stars mainly in Taurus-Auriga and Monoceros at the 110 GHz ^{12}CO J = 1-0 transition was carried out by Edwards and Snell (1982) in search of high velocity gas associated with InT stars. Several stars (e.g. RY Tau, SU Aur) gave a positive detection. Also radio mapping by Grasdalen et al. (1984) of another detected source, HL Tau, indicates the presence of a molecular disc (cf. resolution of a disc by Beckwith et al., 1984 using speckle interferometry).

For two of the sources detected (T Tau and AS 353A), if continuous spherical outflow is assumed, then the mass loss rates implied exceed 7×10^{-8} $M_\odot$ yr^{-1}, which is greater than the theoretical limit of 3×10^{-8} $M_\odot$ yr^{-1} imposed by DeCampli (1981) for sustained mass loss. That this limit is exceeded for two, and possibly other InT stars would suggest that, in several cases, (large-scale) mass loss from InT stars is either bipolar (Cohen 1982) or episodic (Edwards and Snell 1982). It is perhaps worth recognising that the possibly recurrent (Herbig 1977b) mass-loss suffered by FU Ori stars may possibly be collimated by a circumstellar disc (Hartmann and Kenyon 1985).

2.3. Properties of the Herbig Ae/Be Stars.

2.3.1. X-ray properties of Herbig Ae/Be stars.

In comparison to the InT stars, the Ina stars have not been well studied at X-ray wavelengths. Of the few stars that have been observed (e.g. AB Aur, R CrA), most lie in the Taurus-Auriga (Feigelson and DeCampli 1981) and R CrA (Walter and Kuhi 1981) clouds, and only a few definite identifications (e.g. TY CrA) were made. This would suggest that X-ray emission in Ina stars is not as enhanced as is generally observed in InT stars (Section 2.2.1).

2.3.2. Ultraviolet properties of Herbig Ae/Be stars.

Typically, the strongest UV emission lines observed in Ina stars are the MgII h and k resonance lines. Also, absorption lines of high excitation such as CIV can be observed (as in AB Aur; Catala et al.,

1986). Such lines are more typically characterisic of early B spectral types, and are therefore probably indicative of strong stellar winds in the Ina stars for which they are observed. The comparative lack of study of Ina stars with IUE (cf. InT stars) probably reflects a relative faintness of Ina stars at UV wavelengths, a fact in itself noteworthy (cf. the UV excess of InT stars, Section 2.2.2).

Only two stars, AB Aur (Catala et al., 1986 and references therein) and V856 Sco (Tjin A Djie et al., 1982) have been studied by IUE in any great detail. The UV spectra of AB Aur (A0V) and V856 Sco (A7III-IV) are quite different, with V856 Sco exhibiting a similiar UV spectrum to that observed in InT stars. Modelling of the (variable) MgII h and k UV resonance lines in AB Aur by Catala et al. (1984) indicates that these lines originate in both a dense chromosphere which extends out to a few stellar radii, and a wind which extends out to several tens of stellar radii. Most interestingly, the work of Catala et al. (1984, 1986) has shown evidence for periodic variations in the line profiles of the MgII h and k ($t \simeq 45$ hours) and CIV ($t \simeq$ 32 hours) UV lines. They view this activity in the stellar wind as magnetic in origin, and they hope to interpret these findings in terms of streaming within a differentially rotating envelope.

2.3.3. Optical Spectroscopic properties of Herbig Ae/Be stars.

The optical spectra of Ina stars tend to be dominated by strong Balmer absorption lines, although the lower members of the series, particularly Hα and Hβ, are often observable in emission (as is the case for classical Be stars). Both the lower Balmer lines and the CaII K and H lines are usually variable (typically on timescales of

months - years) and often exhibit P Cygni profiles (e.g. MWC 1080, Z CMa), indicating that significant, variable mass loss is probably common in Ina stars (a conclusion substantiated by available UV spectral observations). Absorption lines of singly ionised metals, such as FeII and TiII are also commonly observed.

Herbst et al. (1983) indicate a trend between emission class and spectral type within Herbig and Rao's (1972) catalogue of Orion Population stars, i.e. the Ina stars are less likely to exhibit strong emission line spectra than the InT stars. However, Herbig and Rao did caution against the use of their catalogue in a purely statistical analysis, and supporting data are needed. Such a correlation (if substantiated) may well be related to a comparative "lack" of formation of a convective envelope and an increasing domination of photospheric lines (e.g. HI) in the earlier spectral types, i.e. Ina stars.

The shape of the Hα profile is typically either Gaussian (as in V380 Ori), double peaked (as in R Mon) or P Cygni (as in Z CMa), as shown in Fig. 2.3.1. The Hα profile is commonly used to sub-classify Ina stars. The large width (≃ 10 - 20Å) of the Hα line usually observed in Ina stars, indicates that the stellar envelopes are probably expanding with velocities typically of several hundred kms^{-1} (Pogodin 1985). Although the stellar continua are often strongly affected by IS/circumstellar extinction, the observed Balmer jump and decrement in many Ina stars indicates a typical envelope electron temperature of only ≃ 8000K (Pogodin 1985).

A study by Edwards et al. (1987) of the line profiles of Hα and the forbidden lines in Z CMa and R Mon indicate that the outflow from both these stars is bipolar in nature, with the receding lobes of forbidden emission obscured by a circumstellar dust disc (of radius ≃ 10^3 A.U.).

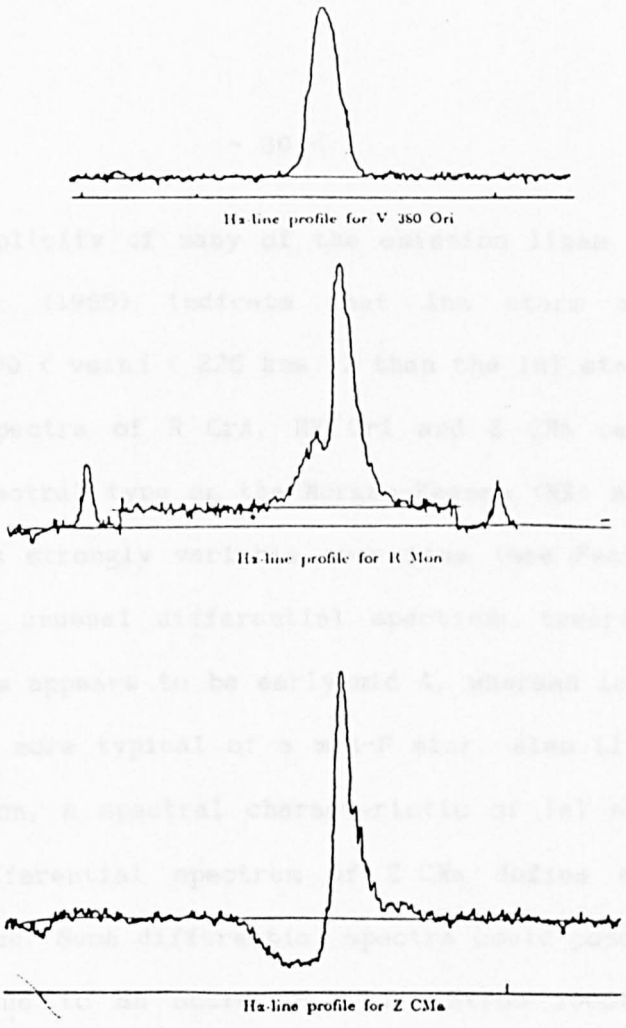

Fig. 2.3.1. Characteristic Hα line profiles observed in Herbig Ae/Be stars: gaussian (V380 Ori); double peaked (R Mon); P Cygni (Z CMa).

(From Dijab and Esipov 1968)

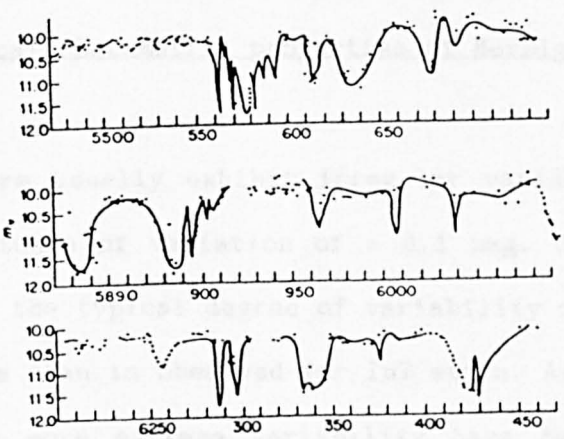

Light curve of T Orionis (Inas) from 1927 to 1931 (according to G. B. Lacchini, *Asiago Oss. Contributi* No. 70, 1956)

Fig. 2.3.2.

The duplicity of many of the emission lines and measurements of Finkenzeller (1985) indicate that Ina stars are notably faster rotators ($100 < v\sin i < 225$ kms^{-1}) than the InT stars (Section 2.2.3).

The spectra of R CrA, HK Ori and Z CMa cannot be assigned a definite spectral type on the Morgan-Keenan (MK) system. The spectrum of R CrA is strongly variable over time (see Section 4.2.1). HK Ori exhibits an unusual differential spectrum: towards blue wavelengths the spectrum appears to be early-mid A, whereas longward of 5500Å the spectrum is more typical of a mid-F star. Also LiI 6707Å is strongly in absorption, a spectral characteristic of InT stars. The even more unusual differential spectrum of Z CMa defies even such a simple decomposition. Such differential spectra could possibly be caused by a "hotspot" due to an accretion flow (Strom 1983), an inhomogeneous photosphere or a contribution from two stars of different spectral type in a binary system (although there is no supportive evidence for this). The former interpretation would suggest HK Ori and Z CMa as possible candidates to exhibit a future FU Ori-type outburst according to the FU Ori accretion model of Hartmann and Kenyon (1985).

2.3.4. Optical Photometric properties of Herbig Ae/Be stars.

Ina stars usually exhibit irregular variability, with characteristic amplitudes of variation of $\simeq$ 0.1 mag. over a timescale of $\simeq$ a month, i.e. the typical degree of variability observed in Ina stars is less extreme than is observed for InT stars. Also some Ina stars which can exhibit more extreme variability have been quiescent in recent years (AB Aur, Z CMa; Herbst *et al.*, 1982). The extent of the variability tends to increase towards shorter wavelengths (Pogodin

1985), indicating that the variations can be interpreted in terms of variable circumstellar extinction (note that many Ina stars are probably affected by significant circumstellar extinction, Pogodin 1985) and/or due to intrinsic variations in the photospheric emission.

A significant number of Ina stars exhibit lightcurves which are occasionally punctuated by deep (typically $\simeq$ 0.5 - 3 mag.) minima occurring over only a few days, i.e. Parenago type I lightcurves. Such stars, e.g. BF Ori, WW Vul, are often referred to as T Ori variables (after the prototype, T Ori; see also Fig. 2.3.2). Such type I lightcurves would seem to be more common in Ina stars than in InT stars (Herbig and Rao 1972; Herbst et al., 1983).

Whilst it is possible that such type I behaviour of the lightcurve can be attributed to variable circumstellar extinction (e.g. Evans et al., 1989 for BF Ori), some of the T Ori variables (e.g. UX Ori, BF Ori) can exhibit a colour reversal and an increase in Hα equivalent width at minimum light. Thus some of the T Ori minima are better explained in terms of a cool starspot model (cf. Herbst et al., 1983).

Although the starspot phenomenon is not unusual in active late type dwarf stars such as InT and RS CVn (Eaton and Hall 1979) stars, a starspot model is not as readily applicable to the earlier Ina stars as the energy transport in B-A type stars is essentially radiative throughout the stellar atmosphere. Therefore, for a starspot model to be applicable to early type Ina stars, either a reasonable theory to explain the formation of a convective envelope in B-A type PMS stars, or a theory of producing a "starspot"-like inhomogeneous photosphere without a convective zone, must be developed.

Additionally, starspot models are difficult to substantiate in T Ori stars due to: (i) the sizes of "spot" required (fractional area

of "spotted" photospheric disc ≃ 85% for UX Ori and BF Ori; Herbst et al., 1983); (ii) a lack of any sinusoidal behaviour (clearly observed in the lightcurves of a few InT stars) in T Ori lightcurves (see Fig. 2.3.2); (iii) the lack of any flare-like behaviour (presumably associated with starspot activity) in Ina stars; (iv) the large amplitudes (≃ 3 - 4 mag.) of some of the observed minima. Models of the energy transport in early spectral type T Ori envelopes must address these stringent parameters if the starspot hypothesis is to be upheld, parameters which pose no interpretative difficulty for variable extinction models.

2.3.5. Polarimetric properties of Herbig Ae/Be stars.

The earliest polarimetric observations of Ina stars concentrated on R CrA (Serkowski 1969b) and Z CMa (Serkowski 1970; Vrba 1975), which were both found to be polarimetrically variable. The magnitude of the polarisation exhibited by Ina stars (e.g. R Mon, p_v > 10%) is typically significantly greater than is usually observed in InT stars. Vrba et al. (1979) showed that about half of the known Ina stars are polarimetric variables, i.e. the polarisation is intrinsic. It is interesting to note that those Ina stars which exhibit no significant polarisation are not photometrically variable (Herbst et al., 1982), and that those stars which exhibit large polarimetric variations also exhibit large photometric variations. Thus it would seem likely that the polarimetric and photometric variations in Ina stars are in some way related. For example: R CrA - 1 ≤ p_v ≤ 18% and 9.7 ≤ V ≤ 14.4 mag. (Sections 4.2.5 and 4.2.1); BF Ori - 2.5 ≤ p_v ≤ 21% (P. Barrett 1987, private communication) and 9.8 ≤ V ≤ 13.4 mag. (Herbig and Rao 1972).

For Ina stars, attempts to determine the polarising mechanism have not been conclusive. Garrison and Anderson (1978) found that, for their observed sample of stars, the wavelength dependence of polarisation is not significantly different from that observed in classical Be stars. This was evidence in favour of the polarisation orignating within a stellar envelope, as is the case for classical Be stars (Poeckert and Marlborough 1978). A very different conclusion was drawn by Vrba et al. (1979), who studied the wavelength dependence of a larger number of Ina stars, and suggested that the likely mechanism was scattering by circumstellar and/or nebular dust. In view of the statistically more significant result of this latter analysis, and that many Ina stars exhibit a significant level of polarisation (typically $p \simeq 1 - 6\%$), it would seem appropriate to consider that multiple scattering in a circumstellar dust shell is an important contributor to the polarisation seen in many Ina stars. But as for InT stars, it is stressed that there is no standard form of the wavelength dependence of polarisation observed in Ina stars and that the origin of the polarisation in each star must be determined individually.

Although multiple scattering in a homogeneous dust shell can produce the magnitude of polarisation typically observed, the maximum polarisation exhibited by stars such as R CrA (18% - Serkowski 1969b) and BF Ori (21% - P. Barrett 1987, private communication) demands multiple scattering by partially aligned grains in dense, inhomogeneous and/or non-symmetrical dust distributions (Daniel 1980). Also Ward-Thompson et al. (1985) have obtained polarisation maps centred on R CrA and T CrA (Fig. 2.3.3) which, in their interpretation, provides direct evidence for aligned grains in a circumstellar disc associated with each star.

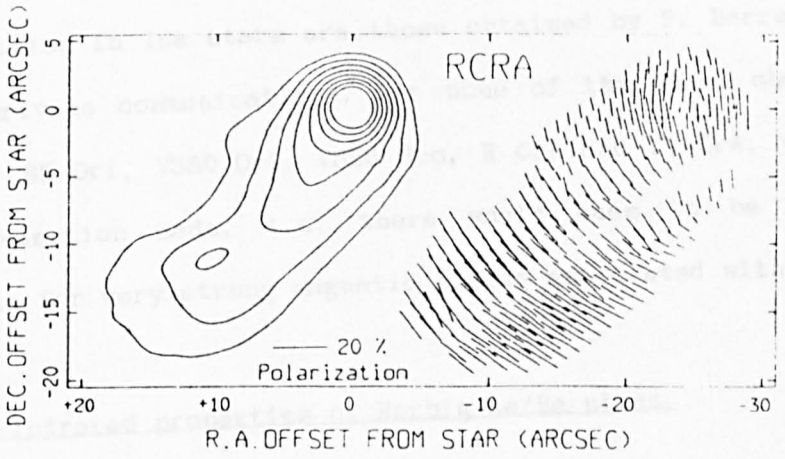

(a)

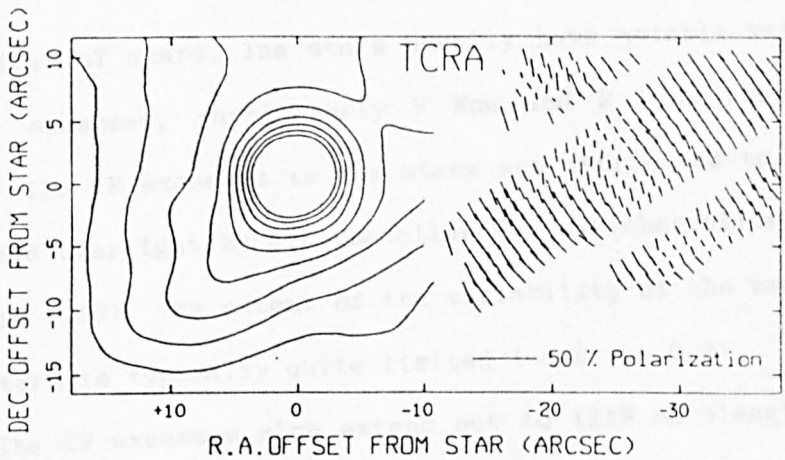

(b)

. Polarization map and intensity contour map of (a) R Cr A and (b) T Cr A. The integration bins are 1×1 arcsec. The offset coordinates refer to the contour map. For the polarization map the star is centred at offset coordinates RA = −25, Dec = 0.

Fig. 2.3.3.
(From Ward-Thompson et al., 1985)

As far as the author is aware, the only observations of circular polarisation in Ina stars are those obtained by P. Barrett at SAAO in 1987 (private communication). For none of the stars observed: T Ori, UX Ori, BF Ori, V380 Ori, V856 Sco, R CrA and TY CrA, was a positive (3σ) detection made, i.e. there would seem to be no compelling evidence for very strong magnetic fields associated with Ina stars.

2.3.6. Infrared properties of Herbig Ae/Be stars.

Like InT stars, Ina stars usually have notable near-IR (1 - 5μm) colour excesses, particularly R Mon and R CrA (Imhoff and Mendoza 1974). The IR excesses in Ina stars are attributed to re-radiation of absorbed starlight by circumstellar dust (Finkenzeller and Mundt 1984; Pogodin 1985). The extent of the variability of the near-IR colours of Ina stars is typically quite limited ($\simeq$ 0.1 - 0.2).

The IR excesses also extend out to IRAS wavelengths for many Ina stars (e.g. MWC 1080, Walker and Marsden 1986; HD 97300, Thé and Dawanas 1987), indicating that the circumstellar shells are usually quite extensive. The form of the IR excess out to 100μm can often be well fitted by several superposed blackbodies (Thé and Dawanas 1987). That the strength of the near-IR excess is seemingly correlated to the presence of H_2O absorption (Pogodin 1985), would suggest that the more massive dust shells are also the more extensive. Other circumstellar IR spectral features observed in Ina stars are the 3.3μm emission feature (e.g. TY CrA, Whittet et al. 1983) and the 10μm silicate feature, either in absorption (HK Ori, Z CMa, MWC 1080) or emission (AB Aur, V380 Ori, R Mon) (Cohen and Whitteborn 1985), although no extensive searches for either feature in Ina stars have been made.

2.3.7. Radio Properties of Herbig Ae/Be stars.

Of the handful of Ina stars that have been observed at radio wavelengths (e.g. Z CMa, Bieging et al., 1984; R CrA and V856 Sco, Brown 1987a), only TY CrA has given a positive detection (Brown 1987b). The non-detections give an upper-limit on the rate of spherically symmetric ionised mass-loss of $\simeq 10^{-8}$ $M_\odot$ yr^{-1}.

CO molecular emission has been observed for R Mon (Edwards and Snell 1982) and also CO maps have resolved sources for not only R Mon (Sargent and Beckwith 1987), but also for R CrA (Levreault 1984, unpublished). The radio maps indicate that both sources are slightly elongated (i.e. an outflow) in the direction of the cometary nebulae associated with each star; also the presence of a molecular circumstellar disc around R Mon has been indicated (Kaifu 1987).

2.4. Summary.

There is strong evidence for an active, deep chromosphere in a significant number of InT stars which gives rise to the observed UV excess and the enhanced UV and optical line emission. It would seem that such "active" regions can cover the stellar surface inhomogeneously, as is indicated by the optical and UV spectra and the saturation of the CaII IR triplet lines in several InT stars. Also there is strong, more direct observational evidence for inhomogeneous coverage in a limited number of InT stars, with the inferred presence of starspots (sinusoidal light variations) and flares (variable X-ray emission, fluorescent FeI emission lines). Additionally, there is evidence for a wind, or an extended envelope in a number of InT stars:

blueshifted forbidden emission and narrow, stable NaI D absorption features. Strong winds are particularly evident in the more active, "extreme" InT stars: the notable absence of both X-ray and strong UV transition line emission; significant radio continuum emission; the observed size of the Balmer jump and the intensity of the Hα line.

It would seem likely that such winds are driven from the stellar surface by Alfvén waves, and in a number of cases, may well be bipolar, i.e. possibly collimated by a magnetic field. The strength of magnetic fields associated with InT stars would however seem to be limited by the observational upper limits placed by Johnstone and Penston (1986, 1987) in three InT stars (RU Lup, CoD -34 7151 and GW Ori) and the low rotation velocity of the majority of InT stars, i.e. seemingly limiting the possible role of the dynamo effect.

The IR excess emission from InT stars is almost certainly dominated by re-radiation from circumstellar dust, dust which may surround a number of InT stars in the form of a circumstellar disc (e.g. HL Tau). Also the observed polarimetric variations and the long-term light variations in InT stars are potentially explicable in terms of changes in the circumstellar dust shell opacity.

There are two extreme views on the essential origin of the active and variable nature of InT stars. Firstly Herbst et al. (1982) suggest that although the InT stars are essentially defined by spectroscopic criteria, the fact that they are all also found to be variable, would strongly indicate that there is a single underlying mechanism for both the variability and the spectral characteristics, a mechanism which is almost certainly intrinsic to the star (Herbst 1986).

On the other hand, Walter (1987) compares the properties of "naked" InT PMS stars with those of InT stars, and he concludes that

the emission properties of InT stars are essentially dominated by the interaction of the star with its circumstellar environment (see also Chevalier 1983).

However, both views cannot fully accommodate the range of observed characteristics, and it is suggested that a combination of both intrinsic and extrinsic phenomena are required to fully explain the "T Tauri" phenomenon. With evidence for starspots, flares and/or non-thermal stellar winds clearly associated with some of the more well-studied InT stars, it would seem clear that intrinsic magnetic activity plays a major, if not dominant, role in giving rise to the characteristic "T Tauri" properties of line emission, UV excesses and (at least) the short-term variability. Also, InT stars clearly do interact with their environment to some extent: the infall of nebular material has occurred or is possibly still occurring (as is suggested for YY Ori stars) around InT stars, and circumstellar discs are thereby formed (e.g. Shu and Adams 1987); winds, in a number of cases bipolar (i.e. collimated), whether episodic or continuous, can give rise to observable molecular outflows and optical emission nebulae (jets and HH objects), particularly in some of the more active stars.

For the less well studied group of Ina stars, the underlying physics which gives rise to the observed activity and variability is less clear. Undoubtedly the level of "chromospheric" line and continuum emission seen in InT stars does not generally extend to the Ina stars: there is no enhanced X-ray or UV continuum emission as is typically observed in InT stars; rather it would seem that the UV and optical lines arise predominantly in an extended, ionised stellar envelope. The IR excesses, silicate features and significant polarisation observed in many Ina stars infer the presence of

substantial dust shells, although a contribution to the observed polarisation from the stellar envelope in several Ina stars cannot be ruled out. It would also seem likely that such circumstellar dust causes the significant reddening observed in a number of Ina stars, and that changes in the line-of-sight opacity may well be the predominant underlying cause of the T Ori lightcurve variability. Also there is increasing evidence for extensive circumstellar discs associated with a number of Ina stars such as Z CMa and R Mon from studies of the Hα and forbidden lines, and for R CrA and T CrA from polarimetric mapping.

Observations of the target stars have been particularly directed towards an understanding of a few key properties of the Orion Population stars discussed here: the photometric and polarimetric variability; the circumstellar reddening; the IR excess emission. As these properties are essentially ubiquitous to both the early (Ina) and late (InT) type Orion Population stars, successful interpretation of these properties is integral to an understanding of the nature of the Orion Population stage in PMS evolution. In addition, observations of the wavelength dependence of polarisation in a further number of stars will help delineate circumstellar grain parameters in a sample of Orion Population stars.

Chapter 3. Observations and Data Reduction.

3.1. Introduction.

The observations taken for this work were obtained at several observing sites from May 1987 to January 1988. Also some of the data published by Kilkenny *et al.* (1985) and Bastien (1985) are used to supplement the data obtained, but only the Hβ photometry of Kilkenny *et al.* (1985) needs introduction here (Section 3.4.1). Where the author took part in the acquisition and reduction of data, some details of the methods used are given, plus a brief description of the instruments used. A few observations using the IUE satellite were made (by M. Shenton) on 29th and 30th May, 1987 just prior to the observing run in the first week of June, 1987 at the Cerro Tololo Inter-American Observatory (CTIO), and these will be commented on first.

3.2. IUE Observations.

IUE time was allocated for stars in the R CrA dark cloud on HJD 2446945 and 2446946, just before the run at CTIO. Unfortunately only TY CrA and HD 176386 were bright enough for good IUE spectra to be obtained, although no IR spectra of either star were obtained at CTIO. Both were observed however in subsequent observations at the South African Astronomical Observatory (SAAO). As neither star was strongly variable between May and July, 1987, the IUE spectra and SAAO data can be compared.

The IUE satellite is used to obtain UV spectra of stars between

the wavelength ranges of 1150-2000Å (using the Short Wavelength Prime (SWP) camera) and 1825-3300Å (using the Long Wavelength Prime (LWP) camera). IUE can take spectra at both high ($\lambda/\Delta\lambda \simeq 10^4$) and low ($\lambda/\Delta\lambda \simeq 300$) dispersion. None of the target stars are bright enough in the UV to obtain high resolution IUE spectra.

A value for the V mag. of a star at the time of the IUE observation is also useful, so that it is known whether the star was visually bright or faint at the time. It is preferable if the V mag. is measured with a co-ordinated ground-based observation, but as this was not possible, an estimate of the V mag. can actually be made from the IUE Fine-Error Sensor (FES) count.

The FES 'prime' mode is used to image the observed field on a TV monitor, so that the target star (if brighter than V ≃ 13 mag.) can be accurately centred in the aperture for observing. Although it was not designed as a photometer, a relation between the observed FES count (essentially a measure of a star's brightness), the (B-V) colour, and the V magnitude has been determined for normal stars, and allows it to be used as such (see Stickland 1980). Thus using the relation

$$V = M(FES) - 0.28\ (B-V) \qquad (3.1)$$

where $M(FES) = -2.5 \log CT_{corr} + 16.58$,

and $CT_{corr} = CT\ (\ 1 - 1.8 \times 10^{-5}\ CT\ )$,

an estimate for V can be evaluated from the observed FES count CT. The value of V determined in this way should not be necessarily interpreted as a "true" V mag.; this is particularly true for PMS stars, many of which are known to exhibit UV excesses. The values of V estimated from the FES count are given in Table 3.2.1, where the log

Table 3.2.1.

Log of IUE Observations.

Star/Date	Camera/ obs. no.	FES	V mag.	Start (HH:MM:SS)	Duration (MM:SS)	Cont.
HJD 2446945:						
R CrA	LWP 10872	84	11.55	04:00:10	157:00	3
HJD 2446926:						
HD176386	SWP 30166	3450	7.63	00:47:18	2:00	5
HD176386	LWP 10877	3335	7.67	00:53:00	2:00	7
TY CrA	SWP 30167	413	9.89	01:40:47	40:00	4
TY CrA	LWP 10878	367	10.16	02:33:47	25:00	7
HD176386	LWP 10879	3228	7.70	03:37:11	00:40	5

FES = Fine Error Sensor count, from which the V mag. was calculated. The exposure began at the UT given in the column **Start** and the exposure time is given in the column **Duration**. The number under the column **Cont.** gives an indication of how well exposed the spectrum was in the continuum. A number less than 5 is under-exposed, 5 is an optimally-exposed spectrum and a number greater than 5 is over-exposed.

of the IUE observations are tabulated.

As the IUE satellite has lost the use of three of its four gyro's since launch, the close proximity of HD 176386 to TY CrA was very useful, as it allowed HD 176386 to be used as a guide star for the observations of TY CrA. This also meant that the time taken in slewing was negligible, but this did not allow spectra to be taken directly after one another. This is because, once a spectrum has been taken, the detector array of vidicon cameras has to be "cleared" before the next spectrum can be started, a process which takes some 15 minutes.

In order to produce a good quality IUE spectrum, the integration time for an observation has to be carefully decided upon: a spectrum can easily be either under- or over-exposed. A spectrum which is under-exposed can only be useful to estimate an upper limit for the UV flux of a very faint star, but an over-exposed spectrum can be useful to define the continuum or to obtain better spectral coverage at wavelengths where the detector sensitivity falls off (e.g. $\lambda \leq 2400$Å in LWP). For normal stars, it is possible to estimate an exposure time by evaluating the expected UV flux from the known V mag. and reddening. However, as the PMS target stars may have slight UV excesses and are variable, a more practical method is to note from the IUE log the exposure time of previous IUE spectra and the quality of the exposure obtained for the observed FES count. A useful guide is that the premium exposure time for a LWP spectrum is usually about two-thirds of that needed for a SWP spectrum.

For both TY CrA and HD 176386, the FES count was similar to that for previous IUE exposures, and so the exposure times decided upon were similar to those which had been previously used, although, the SWP spectrum (a 40 minute exposure) for TY CrA was slightly under-

exposed, and the LWP spectra for both stars (2 minutes for HD 176386 and 25 minutes for TY CrA) were slightly over-exposed. Thus a second, optimum 40 second exposure was taken for HD 176386. The quality of the SWP spectrum of TY CrA is perfectly adequate for identifying lines. The UV spectra obtained are displayed and discussed in Section 4.1.2.

Although R CrA was slightly fainter (from the FES count) than when a 220 minute exposure had been previously taken (when the spectrum was under-exposed), only a 157 minute exposure was possible for this star, due to limitation of time. Thus only a limit on the UV flux can be obtained from these data. This flux is proportional to the response function of the camera used and inversely proportional to the integration time (see the IUE "Notes for Applicants" manual, 1988).

3.3. Observations taken at CTIO.

3.3.1. Observations.

IR spectroscopy and photometry were obtained at CTIO in Chile, from HJD 2446952 to 2446959. The observatory is situated near La Serena, at an approximate elevation of 2200m in the Andean mountain range.

The observations were taken at the f/15 Cassegrain focus on the 1.5m telescope using two interchangable detector systems - a helium-cooled bolometer (with a nitrogen-cooled outer casing) and a nitrogen-cooled photometer/spectrometer. The operating temperature of the nitrogen-cooled detectors was 53K and about 1-2K for the helium-cooled system. Both instruments used photovoltaic InSb detector systems, with a BaF_2 field lens entrance window. The aperture was fully opened to 40" for calibration and set at 20" for the near-IR photometry and

spectroscopy. The chopper throw on each instrument was 30". Both instruments were made at CTIO, and each was used for four nights.

The spectrometer (see Fig. 3.3.1) was fitted with two back-to-back gratings placed on a rotatable mounting. One grating was used for the IJK and M wavelength ranges, and the other for the H and L wavelength ranges. The wavelength ranges of the filters used are: I (0.92-1.13μm), J (1.14-1.41μm), H (1.42-1.85μm), K (1.98-2.46μm), L (3.30-4.15μm) and M (4.5-5.2μm). The line spacing on the grating used was 210 lines per mm, achieving a spectral resolution of $\lambda/\Delta\lambda \simeq 1000$. Filter change was remotely operated by a pneumatic system and rotation of the gratings by a worm gear and stepping motor with 6 motor steps per resolution element. On two nights, some problems were experienced with the stepping motor, which resulted in unreliable data for some of the stars, particularly affecting one of the standard stars (α PsA) on HJD 2446954 and XX Oph on HJD 2446955 (see Fig. A.2.2).

An incandescent lamp was used to initially position the grating and to check the correct response of the detectors at the start and end of each night. Wavelength calibration was carried out using various inert-gas discharge lamps to calibrate the grating at the start of each night by peaking the signal at a particular emission line, e.g. the 2.320μm Xenon line.

The feedback resistance was set as high as was permitted by the background flux, in order to minimise system noise. The resistor settings were set "high" for the IJHK filters, "medium" for the L filter and "low" for the M filter. For the fainter stars, the integration time per grating spacing was 2 s at I, through to 10 s at M.

Photometry was carried out on the IJHKL and M CTIO set of filters on three nights and it had been hoped to take some 10-20μm measure-

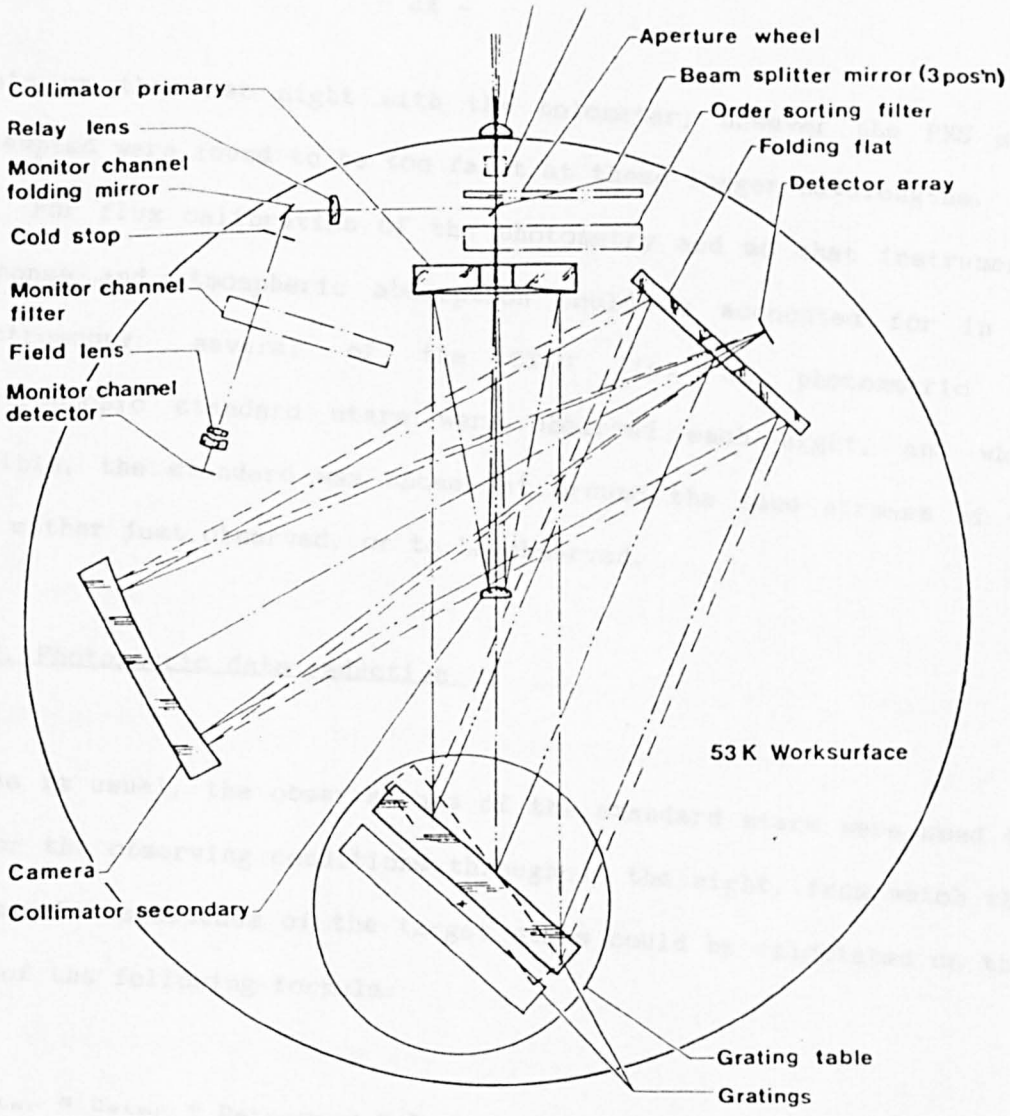

IR SPECTROMETER
Optical Layout

Fig. 3.3.1

Fig. 3.3.1. Optical layout of the CTIO IR Spectrometer.
(From the CTIO IR Spectrometer Users Manual 1986)

ments on the last night with the bolometer; however the PMS stars attempted were found to be too faint at these longer wavelengths.

For flux calibration of the photometry and so that instrumental response and atmospheric absorption could be accounted for in the spectroscopy, several of the CTIO list of photometric and spectroscopic standard stars were observed each night, and where possible, the standard was chosen at around the same airmass of the star either just observed, or to be observed.

3.3.2. Photometric data reduction.

As is usual, the observations of the standard stars were used to monitor the observing conditions throughout the night, from which the photometric magnitudes of the target stars could be calculated on the basis of the following formula:

$$m_{star} = n_{star} + n_{standard} - m_{standard} \qquad (3.2)$$

where n represents an observed magnitude, and m represents the actual magnitude of the star. Any difference in the atmospheric optical depth between the calibrating standard used and the observed target star, was also accounted for when necessary, but generally any such difference was within the observational error ($\simeq$ 0.05 mag.). The actual magnitudes of the standard stars used were either supplied in the observatory list of photometric standards, or taken from the published NASA list of IR observations (Gezari et al., 1984). The JHKL and M photometry was readily reduced, but no data taken using the CTIO I filter were found for the standard stars. The reduced photometry is

tabulated in Table 3.3.1. The observational errors are typically ≃ 0.05 mag. at JHK and ≃ 0.1 mag. at L and M.

3.3.3. Spectroscopic data reduction.

For the spectroscopy, it was particularly important that the adjacent standard star observed was free of any spectral features in the wavelength ranges observed, as well as being at a similar airmass. With these constraints, it would be possible to eliminate any contamination from strong lines from the standard, and to reduce to a minimum any differences in the atmospheric absorption between the spectra of the target star and standard star. If the atmospheric absorption was not divided out successfully, the calibrated spectra would still contain atmospheric bands, especially at the edges of each spectrum, where atmospheric absorption is more pronounced.

The standards used for the reduction process had to be selected on the basis that they were free of intrinsic spectral features over the wavelength range of interest. For the IJKL and M bands either an O or A type star was required (Ridgway 1984) because over these wavelength ranges the continuum is well-defined, and reasonably free of the stronger IR hydrogen lines. Contamination over the observed wavelength ranges comes from lines at: Paϵ 0.955μm, Paδ 1.005μm and Paγ 1.094μm at I; Paβ 1.282μm at J; Bγ 2.167μm and the Pfund series limit at 2.279μm at K; Pfγ 3.742μm at L; Pfβ 4.652μm at M. In the wavelength range of the H spectra however there is strong contamination from the higher Brackett series lines down to Bϵ at 1.818μm, particularly for A stars; therefore a G star (preferably, although not essentially, of luminosity class III) should be chosen to avoid this contamination. In

Table 3.3.1.

CTIO IR Photometry.

Star	HJD (2440000+)	J	H	K	L	M
RU Lup	6953.607	8.83	7.96	7.21	6.08	5.07
RY Lup	6953.631	8.79	7.85	6.99	5.94	5.47
	6958.691	9.20	8.28	7.33	6.03	5.35
AK Sco	6953.696	7.63	7.13	6.55	5.63	5.22
	6958.709	7.51	7.19	6.68	5.66	
XX Oph	6953.772	4.39	3.35	2.84	2.47	2.25
	6958.728	4.29	3.19	2.72	2.42	2.60
R CrA	6958.808	7.50	7.05	6.60		
S CrA	6958.786	7.61	6.91	6.05	4.95	4.29
TY CrA	5953.813	7.50	6.98	6.68		
	6958.819	7.31	6.84	6.55		
	6958.899	7.47		6.68		

Typical photometric errors are ≃ 0.05 mag. at JHK and ≃ 0.10 mag. (≃ 0.30 mag. if fainter than ≃ 5 mag.) at L and M.

G-type spectra the IR hydrogen lines are weak, but the spectrum is still reasonably free of the strong molecular absorption features that are found in later spectral types (e.g. FeH, CO). Thus on the basis of this, the follwing standards chosen from the CTIO list of standards were α PsA (A3V), ϵ Sgr (B9IV-A0V) and α^1 Cen (G2V).

As a rule therefore, apart from the H spectra, the most appropriate (in time and quality) of either ϵ Sgr or α PsA were used to reduce the spectra, although α^1 Cen should be used to reduce any hydrogen lines observed in the original spectra. As α^1 Cen set before the end of each night, the fluxes of any observed hydrogen lines in spectra taken towards the end of each night cannot therefore be reliably calibrated.

Once the atmospheric absorption in the observed spectra have been divided out by the appropriate standard spectra, the spectra are then normalised to the photometric flux of the target star, as observed on either HJD 2446953 or 2446958, which ever was nearest to the spectroscopic observation (although no photometry of V856 Sco was obtained, and so the fluxes used were taken a month later at SAAO and adjusted slightly in order to match the continuum slope; see Fig. 6.1.2).

The reduction procedure was carried out by converting the data files into a DIPSO readable format (DIPSO is the standard Starlink spectral analysis package). It was necessary to remove noise (often present due to poor signal-to-noise and/or atmospheric contamination) at the edges of many of the spectra of the fainter stars, and for most of the L spectra taken it was necessary to remove spurious data around $\simeq 3.7\mu m$ (i.e. losing information on Pfγ 3.74μm), due to an instrumental light leak at this wavelength. The quality of the spectra were typically good enough to pick out strong hydrogen and helium lines, although usually not all the Brackett lines (where present) in the H

spectra were detectable, indicating that detection of the weaker, metallic lines in the spectra is uncertain.

Unfortunately, the target stars (other than R CrA, which is bright at M) were too faint (i.e. fainter than the limiting magnitude of the grating/detector system) to obtain good signal-to-noise at the M band, and even the M spectrum of R CrA was too noisy to be useful. The observing log for the spectroscopy is given in Table 3.3.2.

3.4. Observations taken at SAAO.

The SAAO is based in Sutherland, Cape Province, and situated at an altitude of 1758m. Three observing runs were carried out, using the three largest telescopes at the site, the 0.75m, the 1m and the 1.9m. Two of the runs were dedicated to obtaining simultaneous optical BVRI Johnson (1966) photometry and polarimetry, and IR (JHKL and MNQ) photometry, by co-ordinating the observations on all three telescopes.

3.4.1. Optical and Far-IR Observations.

Some of the observations used (Kilkenny et al., 1985) also include U and Hβ photometry. In the Hβ photometry, the Hβ line is observed through both a narrow and a wide filter, and the Hβ index is given by,

$$\beta = 1.086 \left[a_n/F_n - a_w/F_w \right] \qquad (3.3)$$

(Golay 1974) where the a values represent the profile of the Hβ line through the wide (w) and narrow (n) filters, and the F values represent the observed fluxes through the respective filters. The index β monitors whether the Hβ line profile is in net emission (β <

Table 3.3.2.

Log of CTIO Spectroscopic Observations.

HJD (2440000+)	Star	Bands
6954	V856 Sco	I,J,H,K,L and M
6955	RY Lup	L and H
	XX Oph	I,J,H and K
	R CrA	H and M
6956	RU Lup	J and K
	AK Sco	I,J,H and K
	S CrA	K and L

Table 3.4.1.

Characteristics of the SAAO Mark II IR photometer.

Filters: J, H, K, L (1.25, 1.65, 2.2, 3.4 μm)

Apertures: 1, 1.5, 2, 3, 4 mm diameter

F-ratio: f/15

Chopper speed: 12.5 Hz

Fabry Lens: CaF_2, 7.5 mm focal length

Acquisition field: 4 cm diameter

2.5) or net absorption ($\beta > 2.5$).

Optical polarimetry was obtained with the optical photometry by P. Barrett using the St. Andrews photometer at the f/15.8 Cassegrain focus of the 1.0m telescope. The photometer was switched from photometric to polarimetric mode throughout the night, where a rotating half-waveplate retarder was used to obtain the linear polarimetric data and a quarter-waveplate retarder was used to obtain the circular polarimetric data. Because of time limitations, it was only possible to carry out a few polarimetric observations using filters, and most of the observations were thus made using a clear optical filter. For details of the instrumentation of a polarimeter, see Section 3.5.1.

Optical photometric (on the 1.0m) and spectroscopic data (at the f/15 Cassegrain focus of the 1.9m) were obtained on HJD 2446998 and 2446999. The instruments used on the 1.9m were the grating spectrograph and the Reticon Photon Counting System as the detector. Throughout the night, standard Cu/Ar and Cu/Ne lamps were used to ensure correct angle setting of the grating, and for wavelength calibration. Also an illuminated NaI D filter was used for start- and end-of-the-night flat-field exposures, in order to monitor the count rate of the detector for an uniform illumination. Using a neutral density filter, two exposures per star were taken, and subsequently averaged to give reliable, good quality spectra. The averaged spectra were flux and wavelength calibrated and atmospheric features were removed by using a standard star spectrum taken on the same night. Cross-checking the original spectra showed that a few spurious features were present in the averaged spectra of only two stars (RY Lup and T CrA), stars which were fainter than $V \simeq 12$ mag. Such features were thus removed.

The wavelength range of the spectra is typically from 3350Å to

7965Å, with a spectral resolution of $\Delta\lambda \simeq 2.8$ Å. The stars that were faint (V > 10 mag.) on the night of observation (as determined by the brightness of the image on the TV monitor) were observed for about 900 seconds for each spectrum taken, and the brighter stars were observed for around 500-600 seconds. The signal-to-noise of the spectra was typically poor bluewards of ≃ 3600Å and redwards of ≃ 7000Å because of a fall in the response of the detector.

On other nights, the IR bolometer was used at the f/50 chopping secondary focus of the 1.9m telescope. The helium-cooled IR bolometer houses the InSb detector system used to obtain HMNQ data. Although using a non-standard H filter, the 1.9m H observation still provides a useful check when adding the 1.9m MNQ data to the 0.75m JHKL data.

3.4.2. Near-IR Observations.

The Mark II IR photometer was used at the main Cassegrain focus of the SAAO 0.75m telescope. The Mark II photometer was made at SAAO in 1974-75 and is set up for use with a focal ratio of f/15, and thus is interchangable between the 0.75m and 1.9m telescopes. The photometer consists of a liquid nitrogen dewar, fitted with an InSb detector. A CaF_2 Fabry lens acts as the entrance window, and the filter system, operated manually, consists of JHK and L bands. Table 3.4.1 gives a summary of the characteristics of the photometer, and it is shown in section in Fig. 3.4.1. The optimum sensitivity of the detector at the K band is 10.5 ± 0.1 mag. for a 140 second integration.

At the start of the night, and also at intervals during the night, the correct centring of the aperture (set to 2mm) was ascertained by centring a sufficiently bright (at both optical and IR wavelengths)

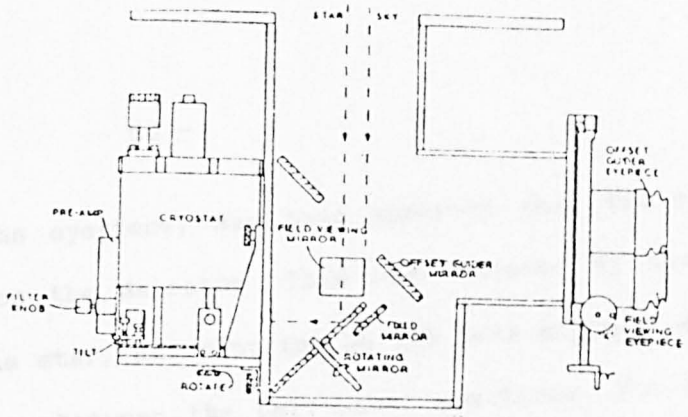

PEOPLE'S PHOTOMETER SCHEMATIC

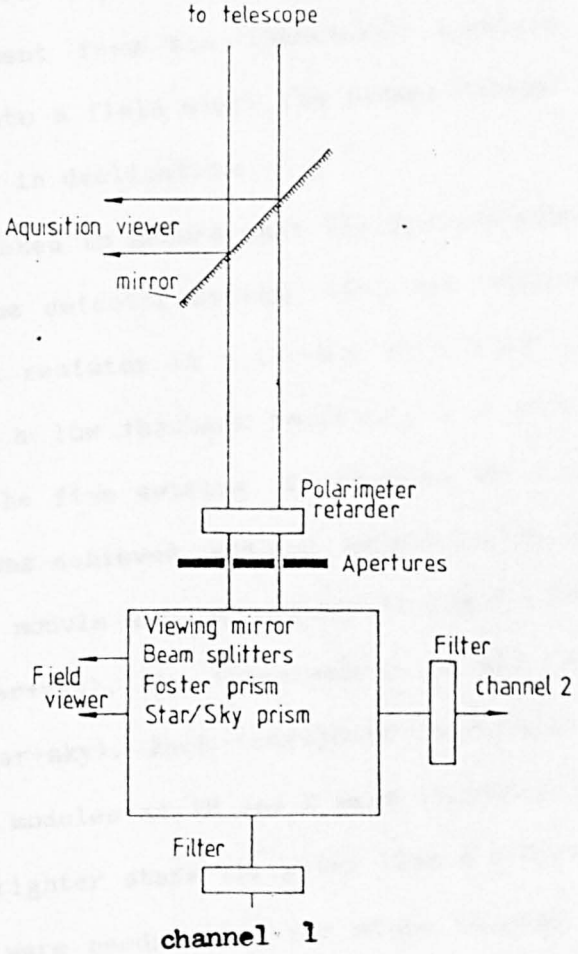

Fig. 3.4.1. Optical layout of the SAAO Mark II IR photometer.
(From the SAAO IR Tech. Ed. 1980)

Fig. 3.5.1. Schematic layout of the JKT People's photometer in polarimetry mode.
(From the UK Optical Telescopes Obs. Guide 1983)

star, firstly in the eyepiece, and then ensuring that the star was correctly centred on the detector. This was achieved by moving the telescope across the star, and centring on the peak signal, which was taken to lie halfway between the half-power positions. The star was then accurately re-centred in the eyepiece. Two eyepieces were used. The offset guider field eyepiece, with a 40 mm diameter, was used to ensure correct movement from the (star+sky) aperture to the sky aperture by fixing onto a field star. The offset "throw" corresponded to about an arcminute in declination.

Care had to be taken to ensure that the optimum electrical signal was obtained from the detector system. This was achieved by setting onto a high feedback resistor ($3 \times 10^{10}\Omega$), with a 30° phase lock for JH and K, and onto a low feedback resistor ($3 \times 10^{9}\Omega$), with a 80° phase lock for L. The fine setting of the gain was then adjusted so that a peak signal was achieved, without saturation occurring.

Each integration module was carried out in the following order; one integration of (star+sky), two integrations of sky, and one further integration of (star+sky). Each individual integration lasted 10 s. About two or three modules at JH and K were required for good signal-to-noise for the brighter stars (brighter than K ≃ 6-7th mag.), and at least six modules were needed at L for stars fainter than L ≃ 6 mag. For calibration of the instrumental magnitude, a standard star was observed at least every two hours.

Also, the Supernova in the Large Magellenic Cloud, SN1987A, was observed on every clear night on each telescope, the results of which are included in the third of a series of papers (Catchpole et al., 1988). The JHKL photometry of SN1987A obtained in September, 1987 by J. K. Davies and the author, along with the other photometry obtained

of the target stars and PMS stars in Orion are tabulated in Table 3.4.2. Typical photometric errors are 0.03 mag. at JH and K and ≃ 0.05 mag. at L, except where L > 6.0 mag. where the errors are ≃ 0.15 mag.

3.4.3. Data reduction.

All the data were reduced at SAAO by the collaborating staff astronomers, apart from the far-IR MN and Q data, which were reduced by hand back at Keele by Dr. A. Evans and the author. No air mass correction was necessary as it had been incorporated in the instrumental magnitude. Typical photometric errors are ≃ 0.1 mag.

3.5. Observations taken at Roque de Los Muchachos.

The Roque de Los Muchachos Observatory is at an altitide of 2369m on La Palma, in the Canary Islands. The optical telescopes based there are the 4.2m William Herschel telescope, the 2.5m Isaac Newton telescope and the 1.0m Jacobyn Kepteyn telescope (JKT).

3.5.1. Observations.

The polarimetric observations were carried out between the nights of HJD 2447160 and HJD 2447166, using the Peoples' photometer mounted at the f/15 Cassegrain focus of the JKT. The photometer was designed at RGO by R. Bingham. It has two photoelectric detector channels, one along and one orthogonal to the optical axis of the telescope.

The photometer has interchangable optics (e.g. a beamsplitter, a Foster prism) and filter slides. The slides can be operated either

Table 3.4.2.

SAAO IR Photometry.

Star	HJD (2440000+)	J	H	K	L
RU Lup	7047.284	8.70	7.66	6.93	
	7049.250	8.71	7.73	6.95	
RY Lup	7041.236	8.74	7.78	7.05	5.94
	7042.262	9.03	7.94	7.13	6.22
	7042.314	9.03	7.99	7.10	
	7043.287	8.69	7.68	6.97	6.00
	7043.314	8.67	7.68	6.98	
	7044.238	8.83	7.79	7.01	5.90
	7047.261	8.73	7.73	7.00	6.09
	7049.227	8.46	7.53	6.87	6.01
CoD -33°10685	7041.254	7.72	6.86	6.45	
	7042.238	7.66	6.84	6.43	
AK Sco	7042.321	7.91	7.31	6.70	
	7044.316	7.90	7.32	6.66	
V856 Sco	7044.268	6.04	5.17	4.30	3.14
R CrA	7040.380	7.03	4.97	3.35	1.71
	7041.413	7.12	4.95	3.34	1.68
	7042.447	7.18	4.96	3.32	1.66
	7045.442	7.25	5.01	3.37	1.71
	7048.428	7.28	5.04	3.35	1.72
	7050.271	7.32	5.02	3.35	1.67
S CrA	7041.355	8.07	6.90	6.00	4.85
	7042.372	7.86	6.68	5.78	4.80
	7042.438	7.92	6.78	5.88	4.72
	7044.355	7.83	6.65	5.76	
	7048.440	7.89	6.72	5.80	

Table 3.4.2. (Cont'd.)

Star	HJD (2440000+)	J	H	K	L
HD 176386	7044.402	6.80	6.67	6.61	
TY CrA	7040.274	7.39	6.85	6.59	5.72
	7041.389	7.43	6.89	6.60	5.41
	7042.434	7.43	6.88	6.61	
	7044.385	7.40	6.85	6.59	5.49
T Ori	7041.667	8.33	7.17	6.18	
	7044.631	8.42	7.19	6.20	5.06
	7052.596	8.34	7.25	6.25	
UX Ori	7040.542	9.02	8.26	7.43	
	7041.604	9.06	8.32	7.50	
	7044.601	9.05	8.31	7.48	
	7047.615	9.14	8.35	7.50	
	7048.575	9.20	8.38	7.49	
	7052.577	9.12	8.30	7.42	
BF Ori	7041.658	9.50	8.76	8.01	
	7044.651	9.83	8.93	8.10	
	7048.622	9.67	8.89	8.10	
	7052.626	9.92	9.01	8.17	
V380 Ori	7047.647	8.09	6.97	5.94	
	7050.669	8.12	7.00	5.99	
	7052.648	8.07	6.97	5.96	4.56

Table 3.4.2. (Cont'd.)

Star	HJD (2440000+)	J	H	K	L
SN 1987A	7040.587	2.99	2.85	2.29	1.82
	7041.545	2.94	2.81	2.32	1.88
	7043.542	2.99	2.84	2.34	1.90
	7044.556	3.00	2.88	2.37	1.98
	7047.566	2.98	2.90	2.40	1.97
	7048.562	3.02	2.93	2.43	2.01
	7049.628	3.04	2.95	2.45	2.04
	7052.532	3.07	3.00	2.50	2.07

Typical photometric errors are $\simeq$ 0.03 mag. at JHK, and $\simeq$ 0.05 mag. at L = 4 mag. and $\simeq$ 0.15 mag. at L = 6 mag.

manually or automatically by pneumatic pistons. The filter slide used contained the UBVRI Johnson (1966) set of filters. In polarimetric mode, only a single entrance aperture is used. The aperture was selected according to observing conditions, 14" when the conditions were good, and 28" when conditions were poor.

For linear polarimetry a rotating half waveplate retarder was inserted into the beam above the aperture selector and a Foster beam analyser (replacing the usual beam splitter used for photometry) is used to split the beam into two orthogonally polarised beams which then enter the photomultipliers. The waveplate rotates once every 960 milliseconds, and 96 x 10 microsecond bins of data are taken during each rotation. A reference pulse, defining a zero point for the optic axis of the waveplate, is produced by a magnet and a Hall field effect transistor. A schematic diagram showing the optical layout of the photometer is shown in Figure 3.5.1.

At the start of each night, a bright star was centred and focused in both the acquisition eyepiece and the TV monitor. A flood field light was used to provide illumination (so that the edge of the aperture could be clearly discerned) for centring in the eyepiece, and the position of the aperture was marked on the TV monitor at the observing console. This was necessary because each time the telescope was moved to a new position, the viewing mirror, which diverted light to the TV monitor, was inserted so that the star could be accurately positioned into the centre of the aperture before observing.

It was also important to keep a check at times throughout the night that the area marked on the TV monitor matched the actual aperture position, as, from time to time, the marked position could move slightly out of line from the actual aperture position - indeed

several times, when this was checked, positioning the stellar image at the "apparent" centre of the aperture, as seen from the TV monitor, actually placed the stellar image near the edge of the aperture. For the measurement of the sky for each observation, the telescope was moved approximately 30" in RA, and then re-centred back onto the star for a further (star+sky) measurement. This was especially important for the fainter objects observed, as the run was carried out during a week of bright moonlight (scattered moonlight being polarised). Also sky measurements are essential in subtracting the sky noise when reducing the photometric data.

At least two standard polarimetric stars were observed on each night, in order to determine the instrumental polarisation and position angle. The standard stars were sufficiently bright that the observed degree of polarisation (p) was unaffected by sky noise. Also they were used (along with other photometric standard stars) to calibrate the photometric observations.

3.5.2. Polarimetric data reduction.

The polarimetric standard stars observed are given in Table 3.5.1.

Table 3.5.1.

Star	Sp. type	p(%)	θ(°)	
χ^1 Ori	G0V	0.013	175	(Serkowski et al., 1975)
107 Psc	K1V	0.016	20	(Serkowski et al., 1975)
HD 23512	A0V	2.3	30	(Hsu and Breger 1982)
9 Gem	B3Ia	3.01	169.8	(Hsu and Breger 1982)

Further, the wavelength dependence of p and θ as observed at each filter is given for 9 Gem in 1981 by Hsu and Breger (1982) as:

	U	B	V	R	I
p (%)	2.58	2.83	2.94	2.86	2.71
θ (°)	169.8	169.3	169.8	170.7	170.3

During dark time, χ' Ori and 107 Psc are very good polarimetric standards, but as the polarisation of both χ' Ori and 107 Psc is virtually zero (as is the case for most polarimetric standard stars), there are (unfortunately) often large statistical errors in the observed position angle (θ), because of the high sky noise from polarised moonlight. The brighter standards (e.g. α CMi, V ≃ 0.3 mag.) were found to cause saturation of the detectors, as they were too bright for the instrument sensitivity. In the same paper by Hsu and Breger (1982), it is also pointed out that 9 Gem is not a reliable standard to use, as its polarisation has been known to be variable by as much as 0.25% and by as much as 2° in position angle over two years. Thus it was decided to determine the instrumental polarisation using HD 23512 on the first night, and from χ' Ori and 107 Psc for the remaining six nights. As the polarisation is essentially zero for the latter two stars and both are very bright, they thus give a reliable zero-point for the instrumental polarisation at each filter. From the observed polarisation of the standard star, the instrumental polarisation at that filter is given by

$$p_{observed} = p_{intrinsic} + p_{instrumental} \qquad (3.4).$$

Where more than one observation of a useful standard is taken on a night, the average value for the zero-point polarisation is taken.

The only two standards with well-determined observational values (i.e. with low observational errors) of the position angle, are 9 Gem and HD 23512. As the intrinsic position angle of 9 Gem has probably changed by as much as 6-12° since 1981, it was decided to rely on HD 23512 alone for calibration of $\theta_{instrumental}$ (using the equivalent of Eq. (3.4) for values of θ) for the first night. For the other nights, the weighted mean of the observed position angle for each star was used to determine the instrumental polarisation angle. For χ^1 Ori and 107 Psc the square of the observed uncertainty in θ was used as the weight. The standard deviation for 9 Gem was assigned as the sum of the estimated uncertainty in the intrinsic position angle and the statistical variation in the observed position angle.

The instrumental polarisation and position angle (and errors) determined for each night are tabulated in Table 3.5.2. As the observations of p and θ are slightly affected by the atmospheric conditions and strongly affected by the sky polarisation (which will change during each night as the moon moves across the sky, and from night to night as the moon changes its phase), the instrumental values of p and θ are expected to vary from night to night.

From comparing the observed values of p and θ for 9 Gem with the zero-point values thus determined, the intrinsic values of p and θ estimated for 9 Gem at the time of the observations (January 1988) are 2.5 ± 0.4 % and 21 ± 13° respectively. Unfortunately the combination of bright sky conditions and faintness of some of the target stars resulted in some of the data being below the 3σ detection level. For V380 Ori and UY Aur the polarisation was determined to be close to

Table 3.5.2.

Zero point values of p and θ observed on the JKT.

HJD (2440000+)	p(%)	σ(p)	θ(°)	σ(θ)
7160	0.36	0.12	95	10
7161	0.38	0.03	75	12
7162	0.77	0.05	81	9
7163	0.24	0.04	52	12
7164	0.21	0.04	68	10
7165	0.14	0.02	86	8
7166	0.26	0.05	67	23

The statistical uncertainty in the determination of p and θ on each night are given by σ(p) and σ(θ) respectively.

zero, within the observational uncertainty of ≃ 0.3%.

3.5.3. Photometric data reduction.

Although the beamsplitter in the photometer was not in use for sky chopping, it was still possible to estimate photometric magnitudes for the brighter stars, as star and (star+sky) measurements had been made for both target and standard stars. To estimate the instrumental response, and hence convert the observed ((star+sky)-sky) count rate into a magnitude, a number of photometric standard (including some of the polarimetric standards) stars were observed. These are given in Table 3.5.3, and are taken from the Astronomical Almanac 1987.

The observed count rates were converted into magnitudes using

$$m(\lambda) - m_{\odot}(\lambda) = - 2.5 \log (I_{*}(\lambda) / I_{\odot}(\lambda)) \qquad (3.5)$$

where $I_{\odot}(\lambda)$ was evaluated from a photometric standard observed in the same part of the night as the target star. This was done by inserting the known magnitude and the observed count rate into Eq. (3.5), and thus giving an estimate for $I_{\odot}(\lambda)$. The values of $I_{\odot}(\lambda)$ for the 14" and 28" aperture were used separately.

Because of the low signal-to-noise in the count rate for many of the target stars, the uncertainty in subtracting this noise (as the signal was not chopped), and the variation in $I_{\odot}(\lambda)$ every night, the photometric error is large, usually about 0.2 - 0.3 mag. Thus to attempt any colour and airmass corrections with such inherent uncertainty in the magnitude was felt inappropriate.

The reduced data (p, θ and m) are tabulated in Table 3.5.4.

Table 3.5.3.

List of Photometric Standards for the JKT.

Star	Sp. type	U	B	V	R	I
χ' Ori	G0 V	5.08	5.00	4.41	3.90	3.59
107 Psc	K1 V	6.57	6.08	5.24	4.55	4.12
9 Gem	B3 Ia	-	6.71	6.27	-	-
HD 23512	A0 V	-	8.47	8.11	-	-
HD 4550	G8 Vp	7.37	7.20	6.45	5.79	5.34
γ Peg	B2 IV	1.73	2.60	2.83	2.92	3.11

The spectral type and magnitudes of the photometric standards used for the JKT observations are given.

Table 3.5.4.

Polarimetric Observations on the JKT.

Star	HJD (2440000+)	p/θ/m	U	B	V	R	I	σ
RY Tau	7160.451	p(%)	2.8	2.0	2.6	2.7	3.5	0.4
	7161.576		1.1	0.9	1.1	1.1	1.6	0.3
	7162.388		0.3	0.6	1.2	-	1.5	0.6
	7162.676		3.4	-	-	2.0	-	0.4*
	7163.403		4.9	5.2	5.4	5.3	5.2	0.8*
	7163.615		5.8	6.9	6.5	7.8	8.4	1.3*
	7164.331		5.0	4.1	2.9	2.4	2.4	0.2*
	7165.355		7.3	4.5	2.4	2.3	2.3	0.3*
	7166.517		13.3	6.1	2.8	2.5	2.5	0.3

Table 3.5.4. (Cont'd.)

Star	HJD (2440000+)	p/θ/m	U	B	V	R	I	σ
RY Tau	7160.451	θ(°)	21	30	33	37	34	13
	7161.576		15	29	39	41	51	29
	7162.388		11	4	178	164	177	35
	7163.403		38	38	45	49	50	17
	7163.615		45	41	46	47	48	17*
	7164.331		14	19	36	46	55	12*
	7165.355		1	1	17	28	29	10*
	7166.517		21	26	44	58	64	26
	7160.451	m	11.1	11.1	10.1	9.4	9.0	0.2
	7161.576		-	11.4	10.4	9.3	8.5	0.3
	7166.517		11.8	11.2	9.4	9.1	8.1	0.2
FM Tau	7160.465	p(%)	-	2.6	1.4	1.0	1.5	0.5
	7162.480		1.7	1.7	1.1	1.0	0.9	0.3*
	7160.465	θ(°)	171	167	169	166	12	17
	7162.480		15	13	26	37	50	15*
RW Aur	7161.623	p(%)	1.2	0.7	1.0	1.1	1.3	0.4
	7162.684		-	-	-	1.3	-	0.3*
	7163.642		1.2	1.4	2.0	1.5	1.0	0.2*
	7161.623	θ(°)	173	175	177	171	173	24
	7161.623	m	-	11.0	10.4	9.7	9.2	0.3
SU Aur	7161.706	p(%)	1.2	0.4	1.2	0.8	1.1	0.3
	7162.723		-	-	1.7	1.4	-	0.2*
	7162.723	θ(°)	73	-	66	66	-	12*
	7162.723	m	-	10.3	9.4	8.6	8.4	0.3*

Table 3.5.4. (Cont'd.)

Star	HJD (2440000+)	p/θ/m	U	B	V	R	I	σ
AB Aur	7163.707	p(%)	0.9	0.6	1.4	1.7	2.1	0.3*
	7163.707	θ(°)	87	51	44	55	51	20*
	7163.707	m	8.3	7.5	7.3	6.9	6.2	0.2*
GW Ori	7164.619	p(%)	-	-	1.2	0.6	0.5	0.2
	7164.619	m	11.8	10.8	9.8	9.1	8.6	0.3
BF Ori	7161.687	p(%)	14.8	3.8	2.5	1.9	1.5	0.5
	7162.518		6.8	3.2	2.8	2.3	2.3	0.4*
	7163.528		7.1	4.0	3.3	2.7	3.4	0.3*
	7164.539		7.9	4.3	3.4	2.3	1.6	0.2*
	7166.636		8.7	2.8	2.1	2.3	2.1	0.3*
	7161.687	θ(°)	80	77	84	84	66	18
	7161.687	m	-	11.2	10.8	10.4	10.6	0.3
	7162.518		11.2	10.4	10.0	9.7	9.4	0.3*
Z CMa	7166.585	p(%)	-	-	1.8	1.1	0.9	0.3
	7166.585	θ(°)	156	156	101	173	173	28
	7166.585	m	11.8	11.0	9.4	8.5	7.8	0.3

Column p/θ/m indicates if the observation was polarisation/position angle/magnitude. The error value σ is typical for each filter, but on occasion the error at U and I is slightly higher. An asterisk at the end of a row indicates that the aperture setting was 28" - otherwise it was 14".

Chapter 4. Observations of PMS Stars in the R CrA Cloud.

4.1. The Herbig Ae/Be star TY CrA.

4.1.1. Introduction.

TY CrA (CoD -37°13024) is a B9V Ina star located in the R association within Corona Australis, which is centred on the variable Ina star R CrA. The R CrA R association lies in a dark cloud which forms the tip of a much larger dark cloud region in Corona Australis. TY CrA is associated with the bright, variable reflection nebulae NGC 6726 and 6727, along with the non-variable A0V star HD 176386 (CoD -37°13023). Because of the close association and the very similar spectral class of the two stars, HD 176386 serves as a useful comparison star for TY CrA.

The spectrum of TY CrA has very well-defined, strong Balmer absorption lines, and is classified as a B9Vea variable in Kholopov et al. (1987). The Hα line can, on occasion, be observed in emission but typically the Balmer lines are affected by shell absorption (Herbig and Rao 1972). Other than this, the spectral type of TY CrA is hardly variable; the only spectral classification other than B9 which has been given is B8 (Marraco and Rydgren 1981).

TY CrA varies in the range $8.9 < V < 12.1$ mag. and is generally close to maximum light, with $\langle V \rangle = 9.43$ mag. (Herbig and Rao 1972). TY CrA has been described as a triple system (Kholopov et al., 1987). Both of the companion stars are typically much fainter than TY CrA, e.g. the brighter companion is at $V \simeq 13.3$ mag. Therefore neither

companion is likely to affect either the photometric or spectroscopic observations of TY CrA itself.

When TY CrA is towards the bright end of its range, the lightcurve typically varies within a very restricted range, $9.39 \leq V \leq 9.81$ mag. (Kholopov et al, 1987) and is generally erratic in behaviour, although possible periods of 1.92, 2.9 and 4.0 days in the lightcurve have been suggested (see Kholopov et al., 1987). The lightcurve is known to exhibit occasional deep minima, down to as faint as $V \simeq 12$ mag., similar to the variations exhibited by T Ori (see Fig. 2.3.2). No doubt it was this behaviour which led to the early suggestion that TY CrA was an eclipsing variable, but the fact that the photospheric lines show no marked velocity shifts rules out this interpretation (Herbig and Rao 1972). Although the companion stars are unlikely to affect the lightcurve of TY CrA, Herbig (1960) pointed out that variability in the bright nebulae NGC 6726/7 may contribute to the erratic variations in the lightcurve of TY CrA, although this is probably only likely when TY CrA is faint ($V \geq 11$ mag.).

Polarimetric observations of TY CrA, HD 176386 and NGC 6726/7 have been obtained by Serkowski (1969b) at blue wavelengths. TY CrA is known not to be polarimetrically variable. TY CrA exhibits an IR excess beyond 5μm which is ascribable to thermal emission from circumstellar dust (Whittet et al., 1983; Thé and Dawanas 1987) and also exhibits an anomalous extinction law (Whittet et al., 1983).

Of the visible stars within the R CrA association, TY CrA is the only source which has been detected at both X-ray and millimetre/radio wavelengths. The X-ray luminosity of TY CrA is a factor $\simeq 10^{3}$ brighter than expected for a normal B9V star (Walter and Kuhi 1981). X-ray emission from a Be star may be expected to arise either within a hot

corona, or from shocks formed within a strongly accelerated wind.

Loren (1979) observed strong CO emission centred on TY CrA and HD 176386. This observation indicates that the dust surrounding TY CrA is heated by a star that is much hotter than TY CrA (B9), namely a B2 spectral type star. This therefore led Loren to suggest that another, more luminous source is embedded within the nebula, but obscured by the nebular dust. Similarly, the 6cm radio flux of 1.26 mJy associated with TY CrA is greater than that expected from the recombination radiation within the stellar atmosphere of a normal B9 star (Brown 1987b). But as pointed out by Brown (1987b) it can be assumed that the radio flux from TY CrA originates from optically thick free-free emission in a stellar wind, a not implausible assumption in view of the presence of the observed shell emission/absorption.

4.1.2. The Ultraviolet and Optical Spectra.

This section will be divided into four parts. Firstly, the optical spectrum of TY CrA obtained at SAAO in July, 1987 will be discussed. Then the SWP IUE spectrum obtained two months previously will be discussed, a discussion which will include a comparison with the "normal" A0V UV spectrum exhibited by HD 176386 and the SWP IUE spectrum of TY CrA obtained in 1980. An interpretation of some of the spectral features observed will be followed by a brief summary of the spectroscopic characteristics of TY CrA.

The line identifications (unless otherwise specified) for the spectra of TY CrA and in all the spectra throughout the rest of this work are based on the following line lists: The Massachusetts Institute of Technology Wavelength Tables (1969); Moore (1972); Kurucz and

Peytremann (1975). In addition, the partial Grotrian diagrams in this work are based on the diagrams presented in Moore and Merril (1968).

4.1.2.1. The Optical spectrum.

The optical spectrum of TY CrA was obtained on HJD 2446999. Simultaneous optical photometry showed that V = 9.32 mag., and B-V = 0.52, values which are fairly typical for TY CrA, as <V> ≃ 9.43 mag. and <B-V> = 0.56 (Herbig and Rao 1972). The spectrum, with identified lines, is given in Fig. 4.1.1.

The strengths of the Balmer lines and of the Balmer jump are characteristic of a reddened B9V star. This is clearly seen in Fig. 4.1.2 where the spectrum has been appropriately dereddened and fitted to an appropriate Kurucz (1979) model atmosphere with T_{eff} = 10000K and log g = 3.5. This procedure is further outlined in Section 4.1.4.2. The spectrum of TY CrA has been smoothed with a 10Å Gaussian filter. The fall in the spectral continuum below the model atmosphere redward of 6000Å is due to a fall in the detector response.

TY CrA is affected by shell emission and/or absorption, and at sufficient resolution an absorption core can be observed in the Balmer lines at a mean velocity of -30 ± 4 kms^{-1} (Herbig and Rao 1972). Unfortunately, at the resolution obtained here (Δλ ≃ 2.8Å) the Balmer lines cannot be adequately resolved, although clearly they are not strongly affected by either shell emission or absorption.

The CaII K and H shell lines are very weak, but the NaI D shell lines are clearly present. Several singly ionised metallic lines, lines typical of late B/early A spectra are present, e.g. the MgII 4388Å and the FeII 4923, 5018, 5644, and 6158Å lines.

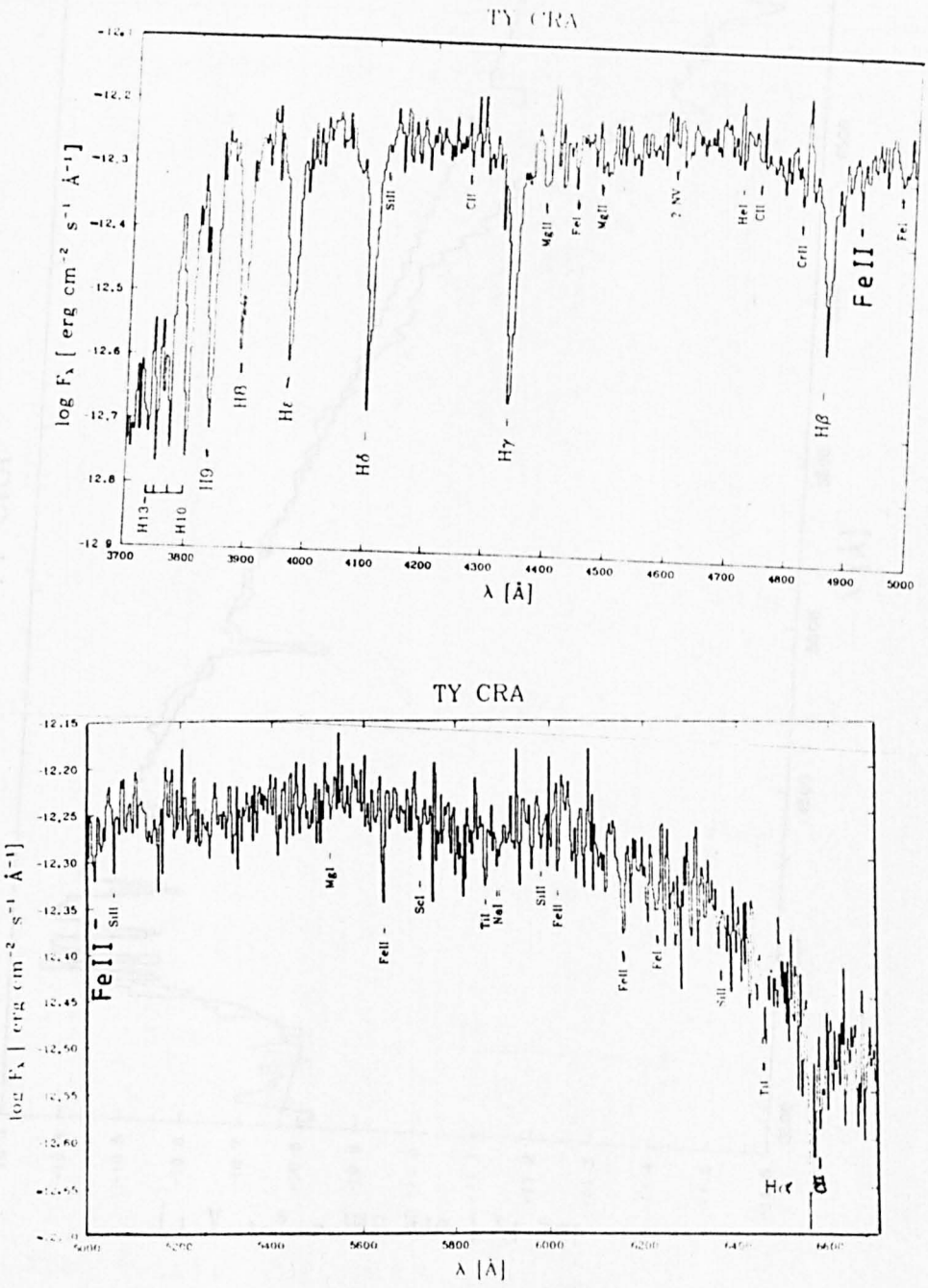

Fig. 4.1.1. Optical spectrum of TY CrA.
See also Section 4.1.2.1.

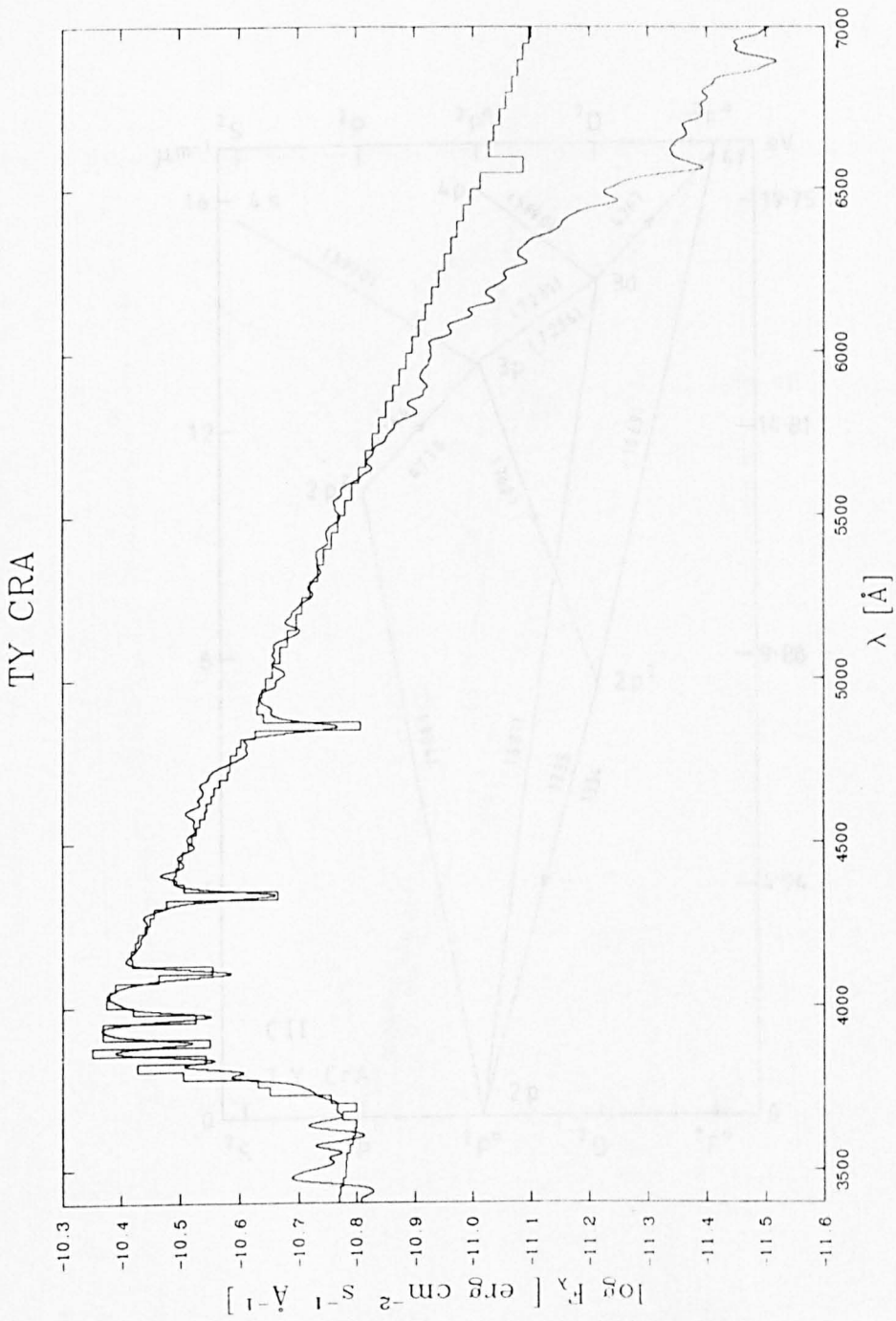

Fig. 4.1.2. Model atmosphere fit of optical spectrum of TY CrA.
See also Sections 4.1.2.1 and 4.1.4.2.

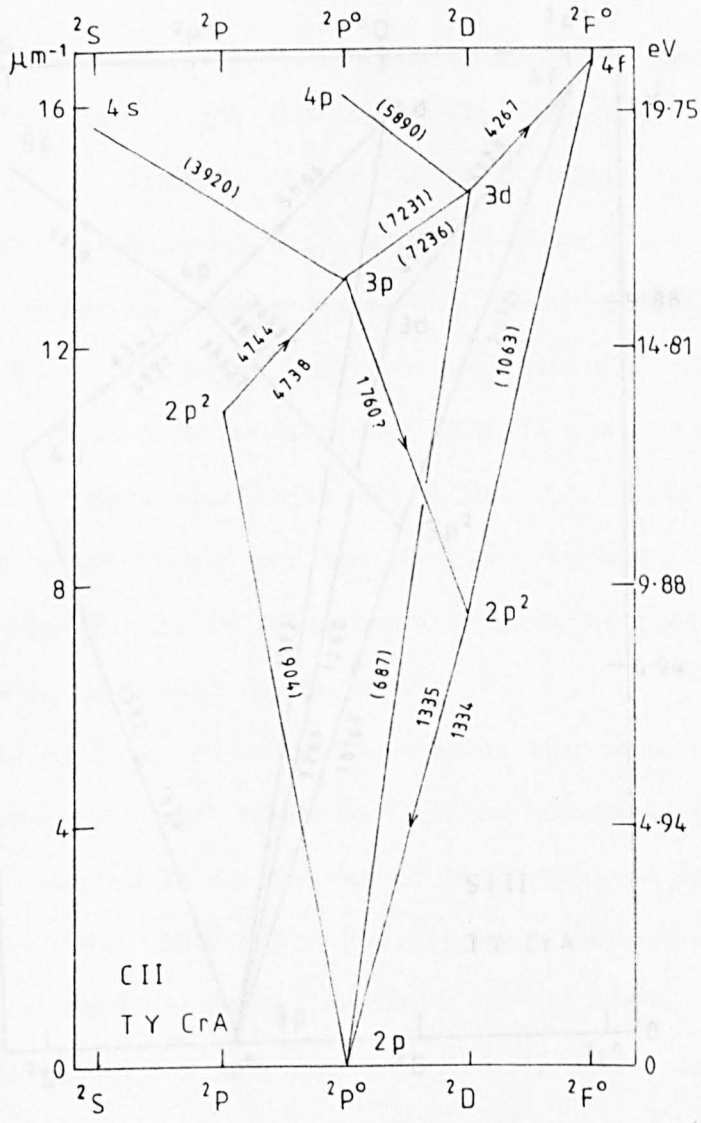

Fig. 4.1.3. CII Grotrian diagram for observed UV and optical transitions in TY CrA. See also Section 4.1.2.

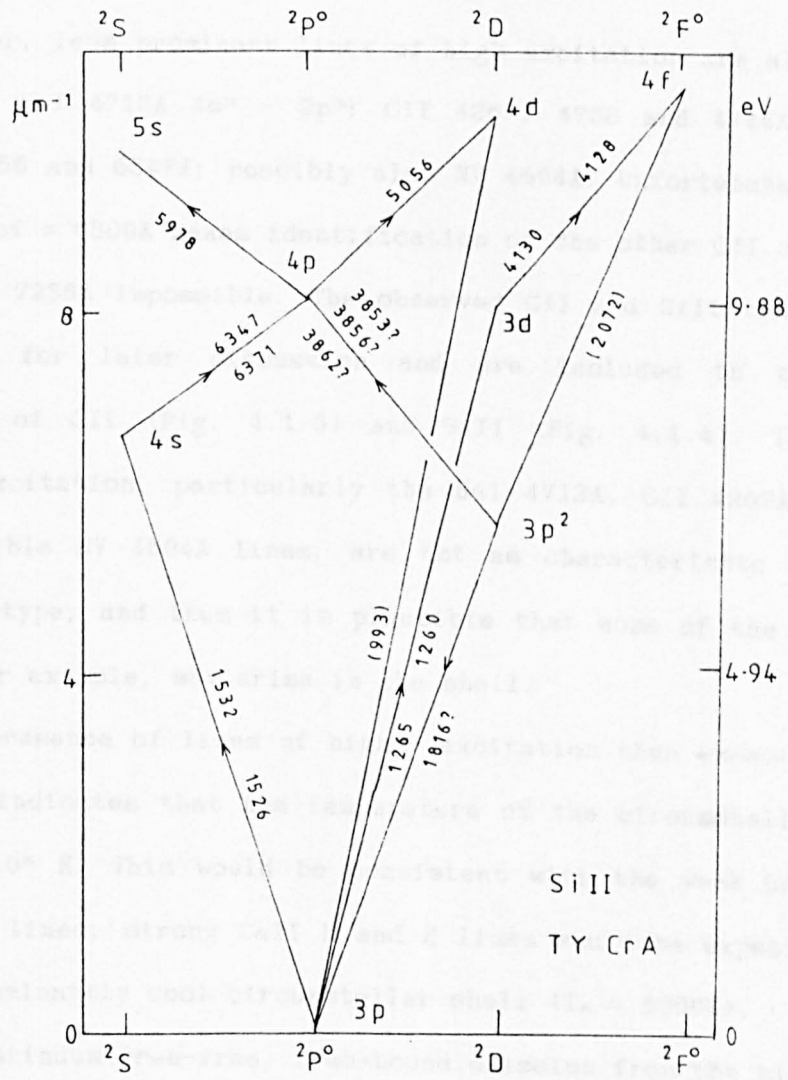

Fig. 4.1.4. SiII Grotrian diagram for observed UV and optical transitions in TY CrA. See also Section 4.1.2.

Other, less prominent lines of high excitation are also seen. For example: HeI 4713Å $4s^3 - 2p^3$; CII 4267, 4738 and 4744Å; SiII 4128, 4130, 5056 and 6347Å; possibly also NV 4604Å. Unfortunately the noise redward of ≃ 6800Å makes identification of the other CII optical lines at 7231, 7236Å impossible. The observed CII and SiII transitions are relevant for later discussion and are included in the Grotrian diagrams of CII (Fig. 4.1.3) and SiII (Fig. 4.1.4). The lines of higher excitation, particularly the HeI 4713Å, CII 4267Å (3d - 4f), and possible NV 4604Å lines, are not as characteristic of a late-B spectral type, and thus it is plausible that some of the HeI and CII lines, for example, may arise in the shell.

The presence of lines of higher excitation than expected in a B9V spectrum indicates that the temperature of the circumstellar envelope is $T_e \gtrsim 10^4$ K. This would be consistent with the weak CaII K and H resonance lines; strong CaII K and H lines would be expected to form in a predominantly cool circumstellar shell ($T_e \simeq 6000$K).

No continuum free-free, free-bound emission from the circumstellar shell affecting the size of the Balmer jump is indicated in the SAAO spectrum (see Fig. 4.1.2); although in view of the fact that several Ina stars exhibit continuum emission affecting the Balmer jump (Pogodin 1985), and that there is possible free-free continuum emission in TY CrA at longer wavelengths (Section 4.1.4.2 and Brown 1987b), the occurrence of optical continuum emission from the shell when the Hα line is in emission, cannot be precluded.

4.1.2.2. The Ultraviolet spectrum.

The IUE spectra of TY CrA and HD 176386 were obtained on HJD

2446946 (see Section 3.2). An estimate of the visual brightness of TY CrA from the FES count gives V ≈ 9.9 mag., which would indicate that TY CrA was fainter than when at normal light of V = 9.43 mag. (Herbig and Rao 1972). The corresponding FES V magnitude of 7.70 mag. of the non-variable HD 176386 is in good agreement with the observed V magnitude of 7.63 mag. obtained two months later at SAAO.

Unfortunately the LWP spectrum of TY CrA was over-exposed, and therefore it is not possible to clearly identify lines in the LWP spectral range, although the continuum is well-defined. However, in the SWP spectrum, although it was slightly under-exposed, two strong emission features (other than the strong geocoronal Lyα line) are well resolved and are also clearly evident on the IUE photowrite. Also a well-defined absorption spectrum with several strong lines, was evident. The observed spectrum, SWP 30167 along with likely line identifications is given in Fig. 4.1.5, and the identified lines, laboratory *gf* values and transistions (where known) are tabulated in Table 4.1.1. In the figure a gap in the spectrum denoted R refers to a camera reseau mark.

From comparison with the UV lines expected in normal B stars from Heck (1987), and from direct comparison with the standards in the IUE low resolution spectral atlas (Heck et al., 1984), the UV spectrum of TY CrA is identifiable as late B as, e.g. the SiII 1265Å and SiI 1300Å features are observed, although the characteristically strong CII 1336Å absorption feature seen in late B stars is evidently in emission, although the feature is partly covered by a reseau mark.

Also the features present in both TY CrA (B9V) and HD 176386 (A0V) can be compared, where the UV spectrum of HD 176386 is taken to represent that of a normal A0V star. The SWP 30166 and LWP 10879

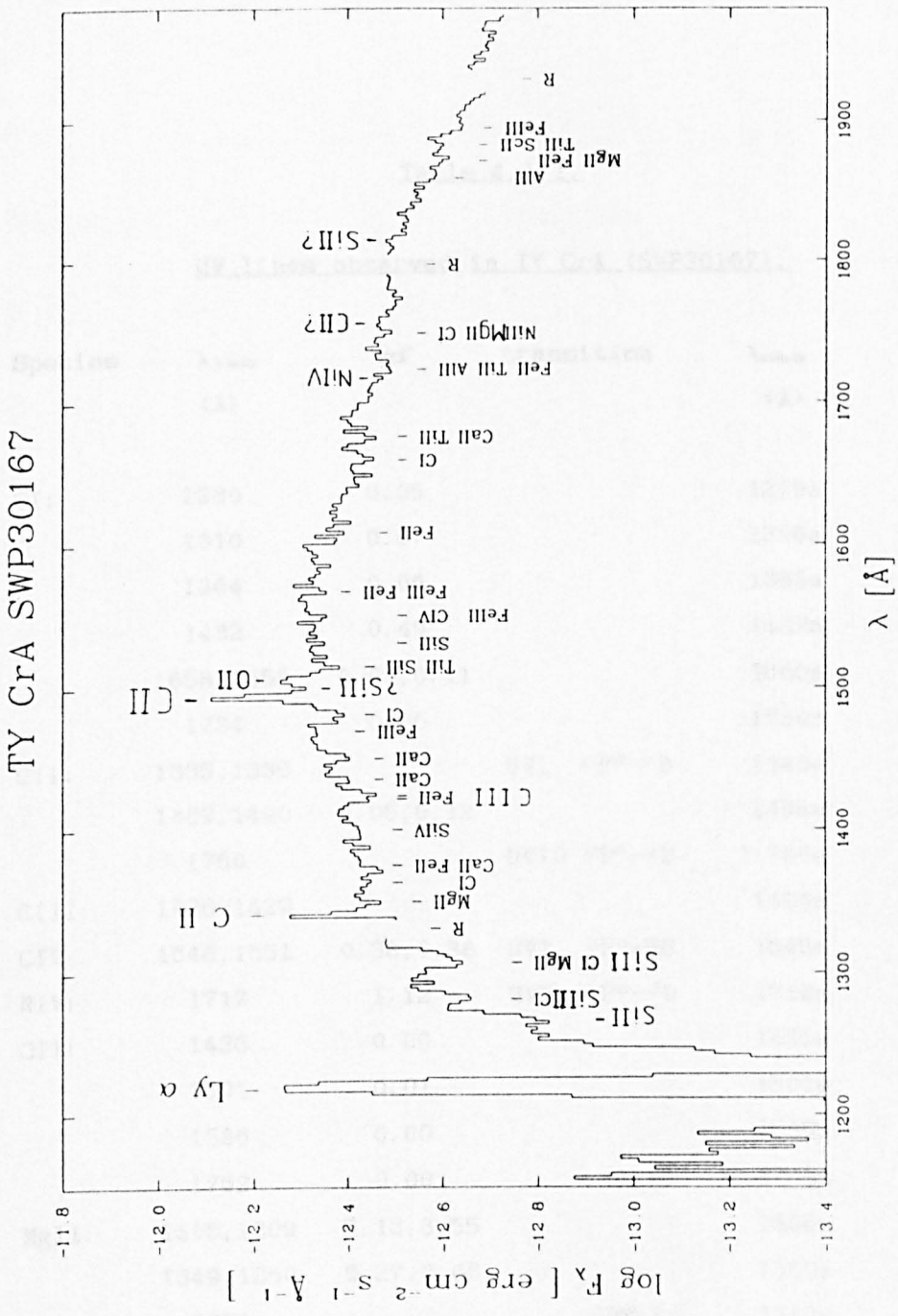

Fig. 4.1.5. IUE spectrum SWP30167 of TY CrA with identified lines. R denotes reseau mark. See also Section 4.1.2.2.

Table 4.1.1.

UV lines observed in TY CrA (SWP30167).

Species	λ_{lab} (Å)	gf	transition	λ_{obs} (Å)
CI:	1280	0.05		1279a
	1310	0.07		1306a
	1364	0.06		1363a
	1482	0.40		1482a
	1658,1658	0.09,0.11		1660a
	1734	0.00		1730a
CII:	1335,1336		UV1 $^2P^o-^2D$	1340e
	1489,1490	0.05,0.12		1494e
	1760		UV10 $^2P^o-^2D$	?1760e
CIII:	1426-1429			1425a
CIV:	1548,1551	0.38,0.38	UV1 $^2P^o-^2S$	1549a
NIV:	1717	1.12	UV7 $^1P^o-^2D$	1718a
OII:	1436	0.00		1436a
	1501	0.01		1501e
	1586	0.00		1585a
	1752	0.00		1750a
MgII:	1305,1309	5.13,3.55		1306a
	1349,1350	0.27,0.68		1350a
	1750		$^2P^o-^2D$	1750a
	1870,1870	0.43,0.68		1871a
SiII:	1265		UV4 $^2P^o-^2D$	1264a
	1305,1309	5.13,3.55		1307a
	1512,1517	0.37,0.40		1517a
	1533	0.36	UV2 $^2P^o-^2S$	1530a
	1817	1.35	UV1 $^2P^o-^2D$	?1816e

Table 4.1.1. (cont'd)

Species	λ_{lab}	*gf*	transition	λ_{obs}
SiIII:	1280	0.32		1281a
SiIV:	1394,1403	1.07,0.53		1400a
CaII:	1370	0.12		1372a
	1434	0.20		1436a
	1674	0.04		1675a
FeII:	1364	0.09		1363a
	1371	0.62		1371a
	1421	0.16		1421a
	1425	0.05		1425a
	1567	0.27		1567a
	1585,1585	0.20,0.17		1585a
	1609	0.35		1609a
	1642,1643	0.19,0.20		1642a
	1726	0.14		1724a
	1781	0.05		1781a
FeIII:	1469,1470	0.07,1.86		1469a
	1479	0.07		1478a
	1542,1544	1.39,5.74		1542a
	1548,1550	6.89,7.13		1549a
	1567,1569	1.59,2.04		1567a
	1895	3.00		1895a

The lines identified in the IUE spectrum SWP 30167 of TY CrA are listed. The rest wavelengths (λ_{lab}) of the multiplet transition are given, and where known the laboratory *gf* values and the transitions are also given. The feature the line contributes to is listed under λ_{obs}, and the letters a or e indicate whether the feature was in absorption or emission respectively. A ? denotes an uncertain identification.

spectra of HD 176386 are shown, with the strong lines identified, in Fig. 4.1.6. The two strong emission features centred at 1340 and 1494Å in TY CrA are both identifiable with CII blended lines at 1334, 1335 and 1489, 1490Å respectively. These two CII blended features are present in absorption in the spectrum of HD 176386, as expected in a normal A0V spectrum. There are lines that are strong in both spectra, namely SiII 1265, 1515Å, CI 1279, 1364 and 1482Å and the CIV, FeIII blend at 1550Å. The feature at 1550Å is typical of earlier B type stars and therefore the presence of this feature is unexpected in both stars. The remaining SiI, CI, MgII 1307Å and CaII 1436Å features are somewhat stronger in the spectrum of HD 176386.

There are several features which are observed in the SWP spectrum of TY CrA which are not present in the SWP spectrum of HD 176386, for example, the emission feature at 1501Å, attributed to OII. Also in the TY CrA spectrum, features at 1760 and 1817Å may represent weak emission from CII and SiII respectively. All the CII and SiII UV transitions are included in Figs. 4.1.3 and 4.1.4 respectively. As in the optical spectrum of TY CrA, there are also several lines of MgII and FeII observed in the UV (see Fig. 4.1.5 and Table 4.1.1).

Most notable are the lines of high ionisation present in the spectrum of TY CrA, lines which are more typical of hotter, early B spectral types, e.g. FeIII, AlIII. Of particular interest are the resonance lines of high ionisation, the SiIV 1394, 1403Å (3s - 3p) and CIV 1548, 1550Å (2s - 2p) doublets. The CIV doublet probably forms a blend with the FeIII 1548, 1550Å doublet. The presence of such lines indicates that temperatures of $\approx 10^5$ K are reached within the shell.

The NV 1239, 1243Å (2s - 2p) resonance doublet which is often seen when the CIV and SiIV resonance lines are observed, may be present but

HD 176386

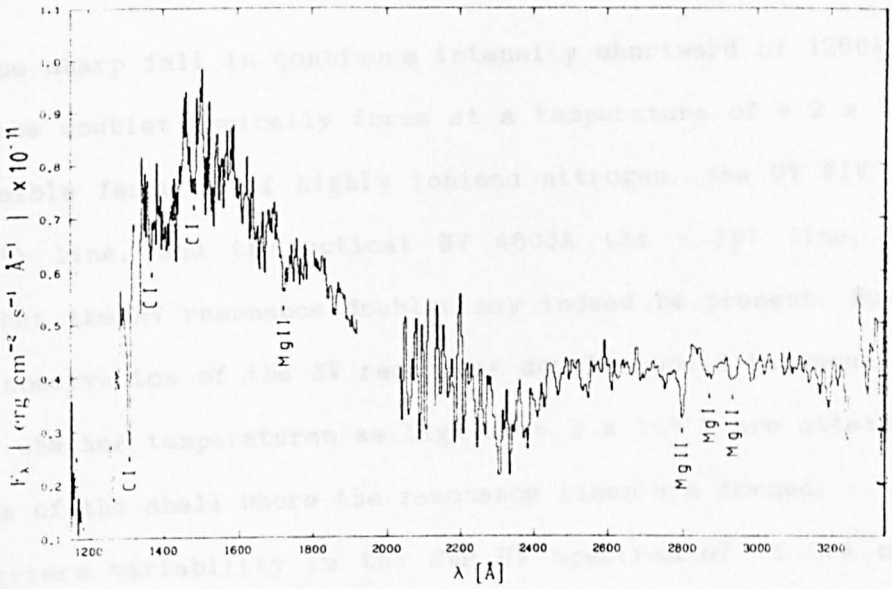

TY CRA 1980

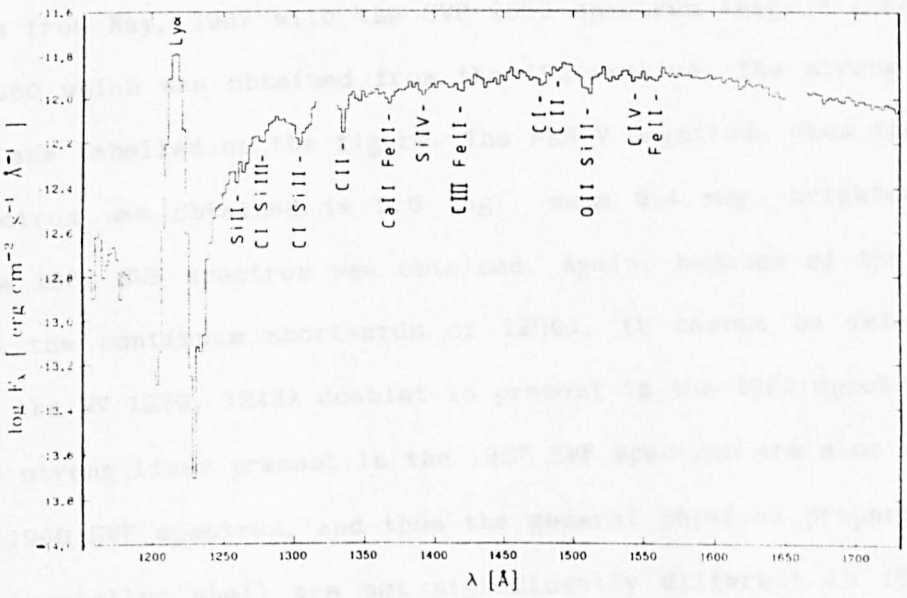

Fig. 4.1.6. IUE spectra SWP30166 and LWP10879 of HD176386 with identified lines.
See also Section 4.1.2.2.

Fig. 4.1.7. IUE spectrum SWP9850 of TY CrA with identified lines.
See also Section 4.1.2.2.

lost in the sharp fall in continuum intensity shortward of 1250Å. The NV resonance doublet typically forms at a temperature of $\simeq 2 \times 10^5$ K. Other possible features of highly ionised nitrogen, the UV NIV 1719Å ($2p - 2p^2$) line, and the optical NV 4603Å ($3s - 3p$) line, would suggest that the NV resonance doublet may indeed be present. However, a direct observation of the NV resonance doublet would be required to ascertain whether temperatures as high as $\simeq 2 \times 10^5$ K are attained in the region of the shell where the resonance lines are formed.

Long-term variability in the SWP UV spectrum of TY CrA over a timescale of $\simeq$ years, can be looked for by comparing the SWP 31067 spectrum from May, 1987 with the SWP 9850 spectrum (Fig. 4.1.7) from July, 1980 which was obtained from the IUE archive. The strong lines present are labelled on the figure. The PES V magnitude when the 1980 SWP spectrum was obtained is 9.5 mag., some 0.4 mag. brighter than when the 1987 SWP spectrum was obtained. Again, because of the sharp fall in the continuum shortwards of 1250Å, it cannot be determined whether the NV 1239, 1243Å doublet is present in the 1980 spectrum.

The strong lines present in the 1987 SWP spectrum are also evident in the 1980 SWP spectrum, and thus the general physical properties of the circumstellar shell are not significantly different in 1980 and 1987. There are however differences in some of the spectral lines. Notably the CIV and SiIV resonance lines appear weaker in the 1980 spectrum, and the SiII 1265 and 1305, 1309Å and SiIII 1280Å lines are also weaker in the 1980 spectrum. The most significant difference between the spectra is that the CII 1335 and 1490Å blends and the OII 1501Å line in emission in the 1987 spectrum, were in absorption in the 1980 spectrum, as would be expected in a B9 spectral type. Thus these features are clearly worthy of future study.

4.1.2.3. Discussion of the observed transitions.

It should be stressed that the optical and UV spectra were non-simultaneous and thus discussion of the optical and UV transitions should take this into account. The discussion will concentrate on the formation of the lines in the envelope, particularly the UV resonance lines and the unexpected CII UV emission blends.

The presence of UV and optical lines of high ionisation and excitation are an indication of either the presence of very hot "chromospheric" regions superposed on a normal B9V envelope (i.e. an extended envelope), and/or excitation within a dense, hot wind. An extended envelope and a stellar wind are not mutually exclusive; indeed a stellar wind would typically be expected to originate from an (expanding) extended envelope, as in AB Aur (Catala et al., 1984).

The observed UV doublet resonance transitions of CIV 1548 and 1550Å (2s - 2p) and SiIV 1395 and 1403Å (3s - 3p) are known to be excellent indicators of the presence of ionised, line-driven winds, particularly in Of and Be stars (Cassinelli and Lamers 1987). Clearly, high resolution spectroscopy of the lines of high ionisation, in particular the CIV and SiIV lines, is highly desirable in determining whether these lines in TY CrA are formed in an extended envelope and/or in a stellar wind. It is perhaps worth noting that none of the observations of TY CrA would be incompatible with the presence of an ionised wind: CIV and SiIV resonance lines; strong X-ray emission (Walter and Kuhi 1981); and 6cm radio emission (Brown 1987b).

Two methods of producing the highly ionised species such as SiIV and CIV in the envelopes of Ina stars have been proposed. The usual mode of production suggested is electron collisions within a very hot

($T_{max} \simeq 10^{5.5} - 10^{7}K$) "coronal" region, where the density is low enough to balance the radiative recombinations with the collisional ionisations. However, with the limited energy budget of a late B star, it is difficult to see how a "corona" of such a high temperature and excitation could be sustained around a star such as TY CrA (B9), unless there is continued input of energy from, for example, trapped magnetic flux or the final phase of the accretion process of star formation.

As an alternative, less energetic mechanism, Catala (1988) has produced a detailed scheme which solves the radiative transfer equations for the CIII - CIV - CV transitions in a $T_{max} \simeq 15000 - 18000K$ expanding envelope/chromosphere around an Ina star. This scheme has been successfully applied to the strong CIV lines in the most well studied (in the UV) Ina star, AB Aur, which has a spectral class A0Vep, i.e. very similar to TY CrA. In principle therefore this raises the possibility that the CIV lines can be formed in the envelope of TY CrA without temperatures as high as $T_{max} \simeq 10^{5}K$ being required.

However, as TY CrA is bright at X-ray wavelengths (Walter and Kuhi 1981), there is supportive observational evidence for high "coronal" temperatures in the stellar envelope. The detection of X-ray emission in TY CrA contrasts with the non-detection of X-ray emission from AB Aur as well as with other Ina stars observed (e.g. Feigelson and DeCampli 1981; see also Section 2.3.1). Therefore, unlike AB Aur, "coronal" temperatures are almost certainly attained in the envelope of TY CrA and thus the scheme of low temperature formation of the CIV lines (Catala 1988) is probably inappropriate in the case of TY CrA.

As a strong X-ray flux is observed in TY CrA (i.e. the optical depth to X-rays within the envelope region is probably low), it would seem reasonable to assume that the soft X-rays essentially pervade the

stellar envelope. In the case of TY CrA therefore, it is suggested that the observed X-ray flux could potentially cause ionisation of CI, NI and OI within the envelope by facilitating the removal of the two outer electrons (often referred to as Auger electrons) by the K shell absorption of X-rays. This is a spectral feature which should be observable with X-ray spectroscopy.

Such a process however could only be important in a cool region of the envelope, where C, N and O would be expected to be predominantly in a state of low ionisation, e.g. CI, CII. The cool region would be expected to be exterior to the inner, excited region of the envelope provided that the envelope density does not fall off too rapidly with distance. If the Auger absorption of X-rays were occurring in the envelope, it is suggested that this process may contribute to the formation of the C, N and O lines of high ionisation, e.g. CIV.

Now the problem of interpretation of the prominent CII 1335, 1490Å and the OII 1501Å emission features in the 1987 SWP spectrum, a spectrum otherwise dominated by absorption lines, will be addressed. In a B9/A0 star, it would be expected, as was the case in both the 1987 spectrum of HD 176386 and in the 1980 spectrum of TY CrA, that these lines should be observed in absorption.

As the CII blends are the more prominent features, discussion will concentrate on these, although the essential arguments are similar for the OII emission line. Unfortunately, despite a search of available catalogues, the CII transition which gives rise to the observed 1489 and 1490Å CII doublet is not known. Therefore discussion will necessarily concentrate on the formation of the 1334, 1335Å CII blend. This transition and the other observed CII transitions are indicated in Fig. 4.1.3, although it should be remembered that the UV and optical

spectra are non-simultaneous. Fortunately the pertinent transitions in the following discussion are all in the UV.

Now, all the excited transitions which occur within the envelope would be expected to lead to significant self-absorption effects (e.g. photo-excitation, scattering of line photons), and unless a line becomes optically thick (as can occur for Hα in TY CrA) or is unaffected by self-absorption (e.g. a line which forms in a geometrically thin region), a line would normally be expected in absorption.

Typically the CII transitions (see Fig. 4.1.3) will be affected by ionisation of CI, collisional excitation and photo-excitation of CII, and recombination from CIII (which will tend to populate the lower levels). However, as the CII $2p^2$ level is not metastable, it is difficult to see how (i.e. under what conditions) the CII 1334, 1335Å emission blend can be formed. It would normally be expected that the CII 1334, 1335Å $2p^2$ - 2p transition would form a strong absorption feature, as is seen in normal A0/B9 spectra and in the 1980 SWP spectrum of TY CrA (cf. the similarly energetic SiII 1265Å 3d - 3p line strongly in absorption in the 1987 spectrum of TY CrA).

However, if Auger absorption of X-rays by CI to form CIII does become important within the envelope (see above), then formation of additional CIII may possibly contribute to the expected CII transitions by recombination. Whether this becomes a dominant process however depends on the density of CI atoms, the X-ray flux and the X-ray absorption cross-section of CI. It is clear that Auger absorption of X-rays could only be important within a region of low excitation (presumed to be the outer envelope), as only in such a region could a substantial fraction of CI be expected. However, unless the envelope was inhomogeneous, it is difficult to see how, in the outer envelope,

the optical depth of CI to X-rays would be sufficient to give rise to a significant number of ionisations to CIII. Even given a high enough density of CI, the recombination rate to the CII 2p level would still need to exceed the rate of radiative de-excitation down to the 2p level. As pointed out above, the region in which excitation of the CII $2p^2$ - 2p transition would probably also need to be geometrically thin.

4.1.2.4. Summary.

In summary, optical (e.g. HI, FeII) and UV (e.g. CI, SiII) lines which are characteristic of a B9V star are observable in TY CrA, although lines of higher excitation and ionisation than would be expected are also present (e.g. CIV, FeIII, HeI). Thus the circumstellar envelope of TY CrA is likely to be hotter and probably more extended than would be suggested by a B9V spectral classification.

Both the lines of high ionisation and the observed strong X-ray flux (Walter and Kuhi 1981) are likely to originate within a hot ($T_e \approx 10^5$ - 10^7 K) "coronal" region. The possibility of an ionised, line-driven stellar wind would be not be inconsistent with the 6cm radio observation of TY CrA (Brown 1987b). However, the problem of the origin of such an energetic envelope surrounding a B9V star is one which is not well understood.

It would seem possible that Auger absorption of X-rays by CI and OI could, in principle at least, play a not insignificant role in the formation of the observed CII and OII emission blends, as well as other lines, e.g. CIV. However, given that the characteristic physical parameters of the envelope of TY CrA, the velocity, electron density and temperature, are not well known (thus high resolution spectroscopy

of the shell lines is highly desirable) and the uncertainties inherent in the proposed method of excitation, it would be unwise to advocate the mechanism of Auger absorption of X-rays in the envelope of TY CrA any further than this. When appropriate observations become available, the qualitative arguments presented here for the possible Auger absorption of X-rays can be examined quantitatively.

4.1.3. The Colour-colour variations.

The observed colour-colour variations of TY CrA from UBVRI and Hβ optical and JHKL near-IR photometry obtained at SAAO from 1981-1984 (published in Kilkenny et al., 1985), and from BVRI and JHKL photometry obtained at SAAO in 1987, will now be discussed. Although the dataset is fairly comprehensive, it is unfortunately too sparse to look for regularities in the lightcurve. Over the entire optical dataset (some 24 observations) TY CrA only varied from $8.95 < V < 9.38$ mag., (cf. $\langle V \rangle = 9.43$ mag.; Herbig and Rao 1972) with no night-to-night variations exceeding $\Delta V \simeq 0.05$ mag., except for a fall of $\Delta V = 0.25$ mag. between HJD 2447040 and HJD 2447041. Thus, over the epochs observed, TY CrA was not strongly variable, and the optical lightcurve exhibits only slowly varying, long-term changes around maximum light.

The variation of B-V with V is shown in Fig. 4.1.8 and clearly TY CrA is redder when fainter. Now, Whittet et al. (1983) interpreted the IR excess of TY CrA beyond 5μm as due to thermal re-radiation by circumstellar dust. Thus in view of the fact that TY CrA is significantly reddened: $(B-V)_{obs} \simeq 0.50$, cf. $(B-V)_{intrinsic} = 0.00$ for an A0V star (Johnson 1966); TY CrA may well be affected by extinction by circumstellar dust. Interestingly, the V, B-V slope of variation

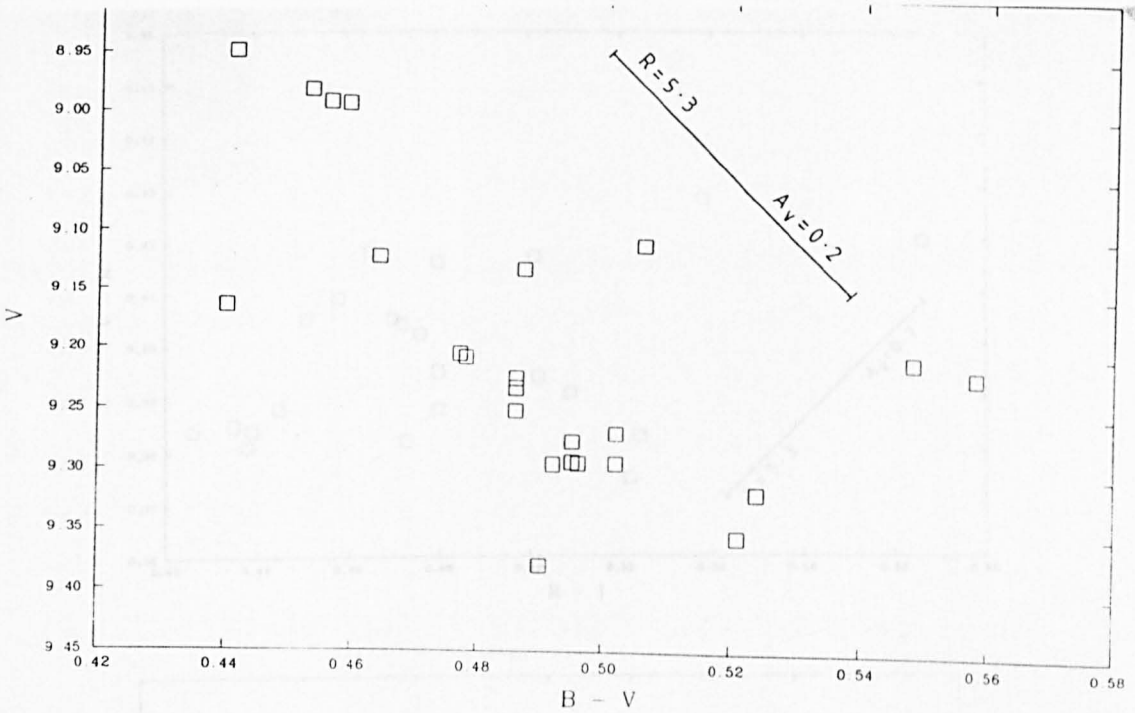

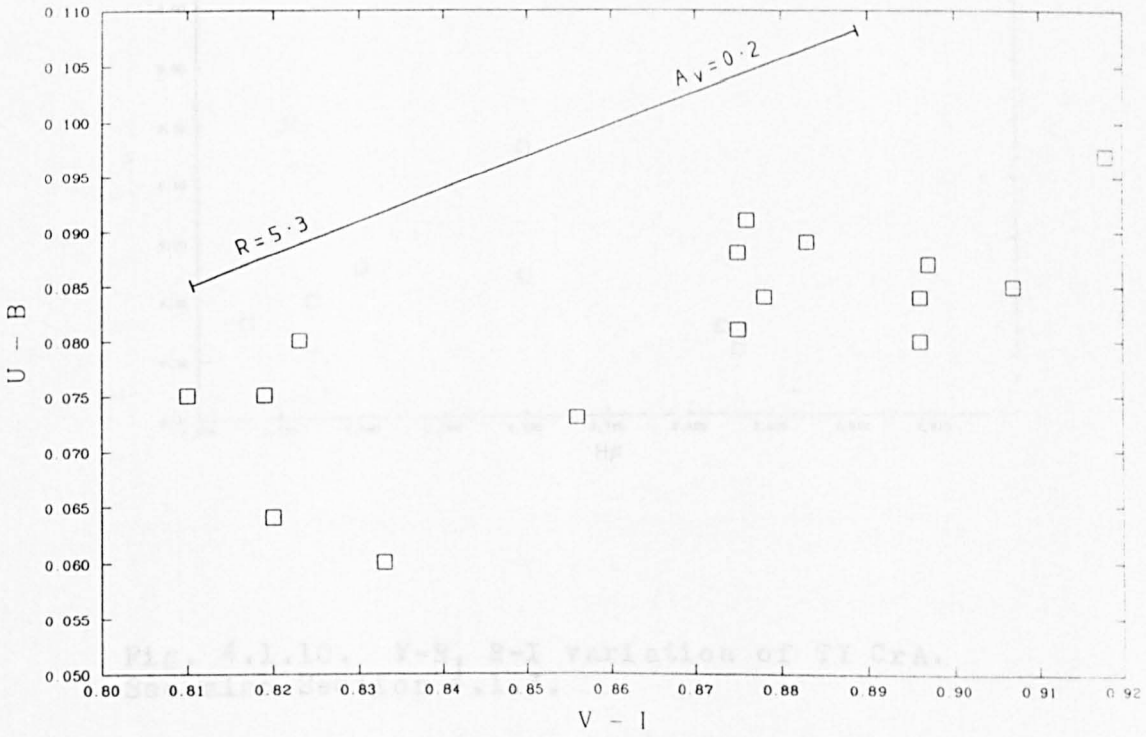

Fig. 4.1.8. V, B–V variation of TY CrA.
See also Section 4.1.3.

Fig. 4.1.9. U–B, V–I variation of TY CrA.
See also Section 4.1.3.

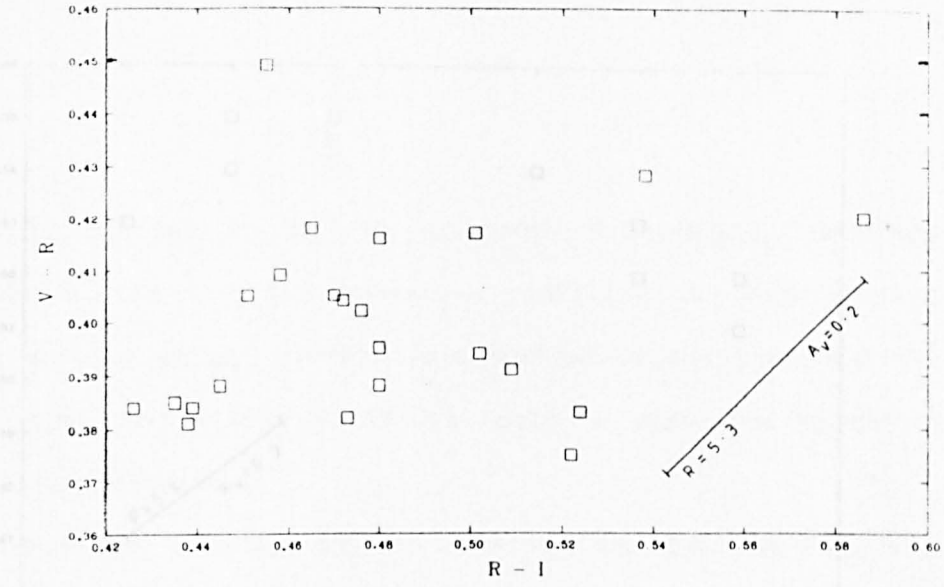

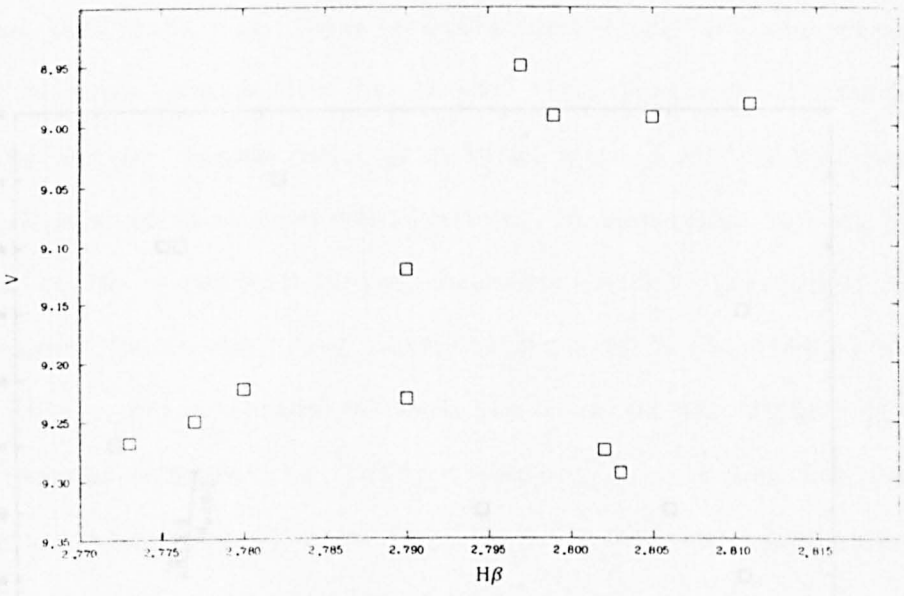

Fig. 4.1.10. V-R, R-I variation of TY CrA.
See also Section 4.1.3.

Fig. 4.1.11. V, Hß variation of TY CrA.
See also Section 4.1.4.

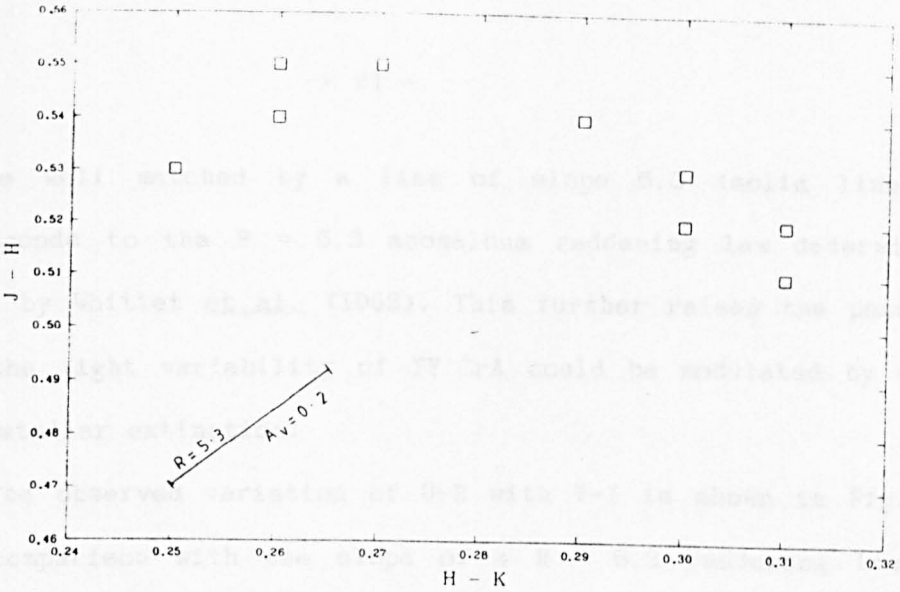

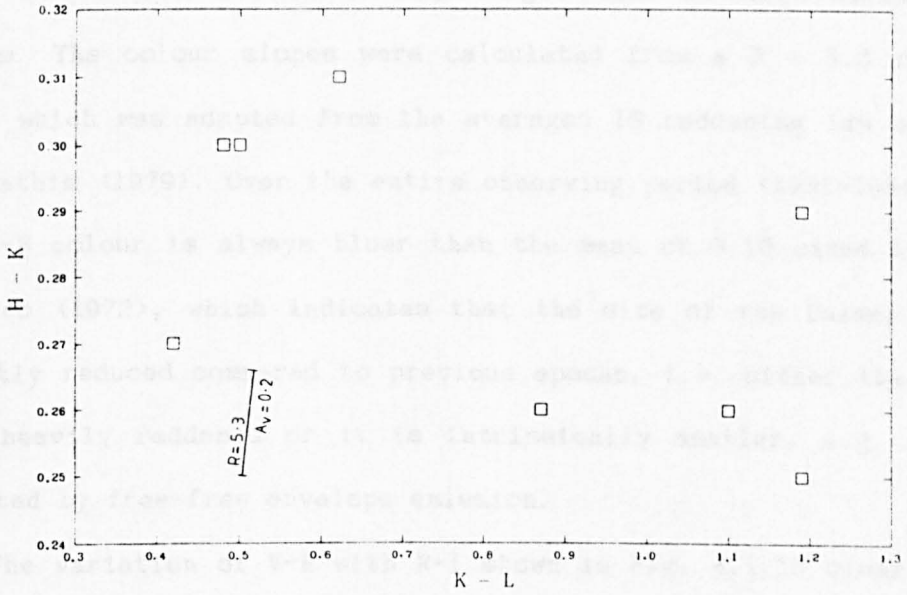

Fig. 4.1.12. J-H, H-K variation of TY CrA. See also Section 4.1.3.

Fig. 4.1.13. H-K, K-L variation of TY CrA. See also Section 4.1.3.

can be well matched by a line of slope 5.3 (solid line) which corresponds to the R = 5.3 anomalous reddening law determined for TY CrA by Whittet et al. (1983). This further raises the possibility that the light variability of TY CrA could be modulated by variable circumstellar extinction.

The observed variation of U-B with V-I is shown in Fig. 4.1.9. From comparison with the slope of a R = 5.3 reddening law (solid line), the variations in these colours can also be interpreted in terms of variable extinction by larger than IS-sized circumstellar grains. The colour slopes were calculated from a R = 5.3 reddening curve which was adapted from the averaged IS reddening law of Savage and Mathis (1979). Over the entire observing period (1981-1984; 1987), the U-B colour is always bluer than the mean of 0.10 cited by Herbig and Rao (1972), which indicates that the size of the Balmer jump is slightly reduced compared to previous epochs, i.e. either the jump is less heavily reddened or it is intrinsically smaller, e.g. possibly affected by free-free envelope emission.

The variation of V-R with R-I shown in Fig. 4.1.10 clearly shows more scatter than for the other optical colours. Despite the scatter, many of the points when TY CrA is blue lie roughly on the line appropriate for a R = 5.3 reddening law (solid line), although the trend here is certainly less convincing than for the other optical colours. However, given that the variable Hα line (Herbig and Rao 1972) will affect the R photometry point, it is therefore not improbable that the underlying variation could be due to variable circumstellar extinction, with R = 5.3.

Now, the Balmer lines of TY CrA are affected by shell emission and absorption (Kholopov et al., 1987). The variation of the Hβ index with

V is displayed in Fig. 4.1.11. In view of the lack of any significant short-term variations in V (i.e. in the continuum emission of TY CrA), it is perhaps not altogether surprising that there were no significant changes in the Hβ index, which will be affected by the degree of shell absorption/emission. This is because it would be expected that changes in the excitation of the shell are, to a significant degree, dependent on intrinsic changes in the star itself (where the shell originates).

Further, it is notable that there is no evidence in the literature for any significant changes in the spectral type (B8/9; see Section 4.1.1), and therefore in the effective temperature of TY CrA. The fact that the intrinsic variability of TY CrA, other than variability in the shell lines, is probably quite limited, would not be inconsistent with an extrinsic mechanism (such as variable circumstellar extinction) for the light variations. Therefore it would seem that the long-term (≃ weeks - months) optical light variability of TY CrA can indeed be attributed to changes in the degree of circumstellar extinction. It is also suggested that the occasional deep minima in the lightcurve of TY CrA (Herbig and Rao 1972), although none were observed here, could potentially be explicable in terms of variable circumstellar extinction, e.g. as for BF Ori (Evans et al., 1988).

As noted by Whittet et al. (1983), TY CrA exhibits no near-IR excess, although there is a 3.3μm emission feature in the spectrum. Thus the near-IR colours are unlikely to be affected by dust emission. The near-IR colour-colour variations are shown in Figs. 4.1.12 and 4.1.13. The observed variations are quite limited (except at K-L), but it is seen that they are not well described by the locus of variation of a R = 5.3 reddening law, particularly towards longer wavelengths.

As there is no (dust) near-IR excess affecting the near-IR

colours, any variation in the effective temperature of TY CrA would be expected to lead to strong changes in J-H essentially at constant H-K (Schmelz 1984). Such colour variability is not observed however, which is consistent with the constancy of the spectral type of TY CrA (see above). Indeed, if anything, the reverse colour-colour trend is indicated.

The variation in the H-K, K-L plane departs most notably from that expected from a R = 5.3 reddening law. The significant amplitude of variation in K-L is essentially attributable to the large variation in the L magnitude. The variation in L can be partly ascribed to the faintness of TY CrA at L ($\gtrsim$ 6 mag.), and therefore the typical observational error in L is $\simeq$ 0.15 mag. on the 0.75m telescope at SAAO (Kilkenny et al., 1985). However, even allowing for this, the actual variability of K-L ($\simeq$ 0.8) is still significantly greater than expected from the continuum variations arising from variable circumstellar extinction.

Thus it would seem clear that variable extinction cannot be the dominant cause of the near-IR variability. As there is unlikely to be significant near-IR excess emission from circumstellar dust (Whittet et al., 1983), nor any significant variability in the photospheric continuum emission of TY CrA, then it can only be suggested that an additional source(s) of variability is required. Possible sources of variability may include the 3.3μm feature affecting L (the band at which the variability is most notable) and free-free emission (which would also be expected to affect the visual flux; but see also Section 4.1.2.1). Clearly, simultaneous spectroscopic/photometric monitoring of TY CrA in the near-IR is highly desirable.

In conclusion, the observed long-term colour variability of TY CrA

would be consistent with TY CrA being affected by changes in the circumstellar dust shell opacity, with an anomalous circumstellar reddening law of R ≃ 5.3. A R = 5.3 reddening law (as determined for TY CrA by Whittet et al., 1983) would suggest a characteristic grain size of ≃ 0.3μm. However, the fact that behaviour of some of the colours towards longer wavelengths, most notably K-L, show departures from the variation expected from the R = 5.3 reddening law, indicates an additional component(s) affecting the near-IR colours.

4.1.4. The Reddening Law and the Flux Distribution.

This section comprises of three parts: firstly an investigation of the reddening law of TY CrA using the spectra and photometry obtained of both TY CrA and HD 176386; the subsequent determination of the stellar and circumstellar properties of TY CrA (and HD 176386) as obtained from the dereddened data; and finally there is a brief discussion of the R CrA cloud region in view of the derived reddening law and the IRAS flux maps obtained of the R CrA region.

4.1.4.1. The Reddening Law.

As TY CrA is likely embedded in the R CrA cloud and has a circumstellar dust shell (Whittet et al., 1983), it is therefore affected by IS extinction, cloud extinction and circumstellar extinction. Thus, once the IS reddening has been removed, the cloud and circumstellar reddening law affecting TY CrA can be determined.

Now, of the stars in the R CrA association, it is suggested that TY CrA is the star for which the reddening law can best be determined.

This is because TY CrA is bright in both the optical and the UV and, in comparison with the other stars observed here, its light variations are generally quite limited (see Section 4.1.3 and cf. Section 4.2.3). In addition, TY CrA is unaffected by dust emission out to 5μm and so the reddening law out to 5μm can be determined unambiguously. Note however the (variable) near-IR excess (Sections 4.1.3 and 4.1.4.2).

Another pertinent factor is that TY CrA (B9V) is closely associated with a non-variable star, HD 176386 (A0V). HD 176386 is also bright in the optical and UV, and thus a useful comparison of the extinction law of these two stars can be made. As HD 176386 is not heavily reddened (Marraco and Rydgren 1981), it is certainly not a background star, and as it may well be contributing to the illumination of the NGC 6726/7 nebulae associated with the two stars (Marraco and Rydgren 1981), it probably lies very close to TY CrA (and thus the R CrA cloud) in space. Therefore HD 176386 can be regarded as an ideal star with which to reliably estimate the foreground, IS extinction towards TY CrA, and thereby making an accurate removal of the IS reddening possible.

The IUE spectrum of HD 176386 was dereddened until the IS 2200Å absorption feature was removed. Removal of the 2200Å feature is known to be a very good method of unambiguously determining the IS reddening (assuming a normal R = 3.1 reddening law) of a star not affected by any anomalous reddening. In this way the IS reddening (with R = 3.1) of HD 176386 is estimated to be $E(B-V) = 0.17 \pm 0.02$, in excellent agreement with the value of 0.17 determined by Marraco and Rydgren (1981) from photometric observations. As a further check it is found that with this reddening correction, a 10000K, log g = 3.5 Kurucz (1979) model atmosphere (appropriate for an A0V spectral type, Allen 1973) can be fitted to the UV continuum.

Now, as TY CrA has no dust IR excess shortward of 5μm (Whittet et al., 1983), once the IS reddening has been removed, the reddening law of TY CrA out to ≈ 5μm can be determined. The reddening curve of TY CrA has been explicitly deduced by Whittet et al. (1983), where it was shown that the reddening law is anomalous, with a value of the total-to-selective extinction (from extrapolation to $1/\lambda = 0$) of R = 5.3. Other estimates of the reddening law of TY CrA have been given as R = 5.1 (Marraco and Rydgren 1981) and R = 5.9 (The and Dawanas 1987).

With a view to extending the wavelength range covered by Whittet et al. (1983), from the IUE spectra obtained (although the LWP spectrum was over-exposed, it can still be used here as the continuum is well-defined), the extinction properties of TY CrA in the UV can be determined. Also, an optical spectrum of TY CrA was taken at SAAO two months after obtaining the IUE spectrum; although the optical and UV spectra should ideally have been obtained simultaneously. With a suitable normalisation of the UV spectra (required in view of the difference in 0.4 mag. at V indicated between the optical and UV observations), the merged IUE SWP and LWP spectra are seen to match the optical spectrum well (See Fig. 4.1.14, in which the spectra have been smoothed with a Gaussian filter of 10Å).

Removal of the 2200Å feature in the IUE spectrum of TY CrA would indicate that the reddening affecting TY CrA in the UV is only E(B-V) = 0.22 ± 0.02 (assuming a normal reddening law), cf. the IS $E(B-V)_{IS}$ = 0.17 determined for HD 176386. Contrast this total E(B-V) = 0.22 from UV observations with the range in total E(B-V) of TY CrA determined from optical observations: 0.48 - 0.67 (Knacke et al., 1973 and Marraco and Rydgren 1981, respectively). Thus it would seem evident that the reddening law affecting TY CrA is anomalous. The discrepency

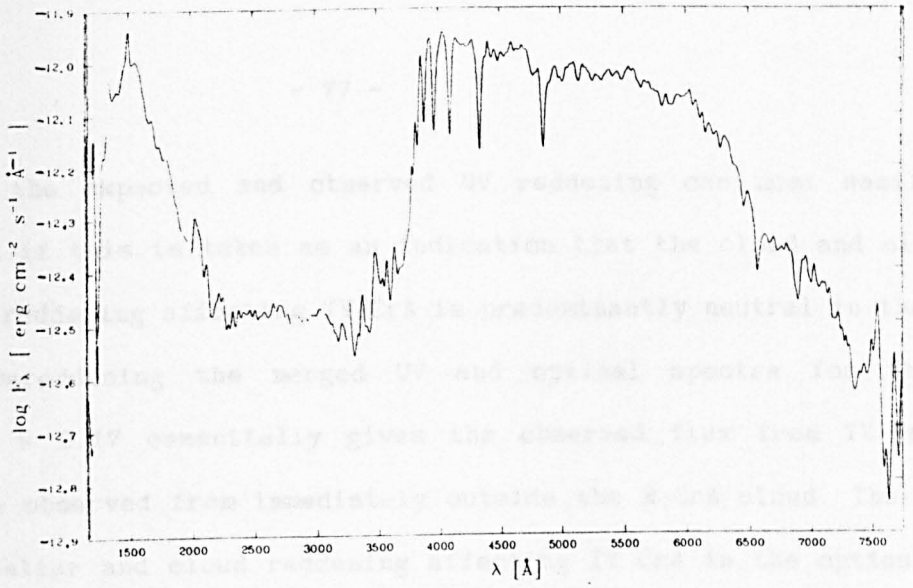

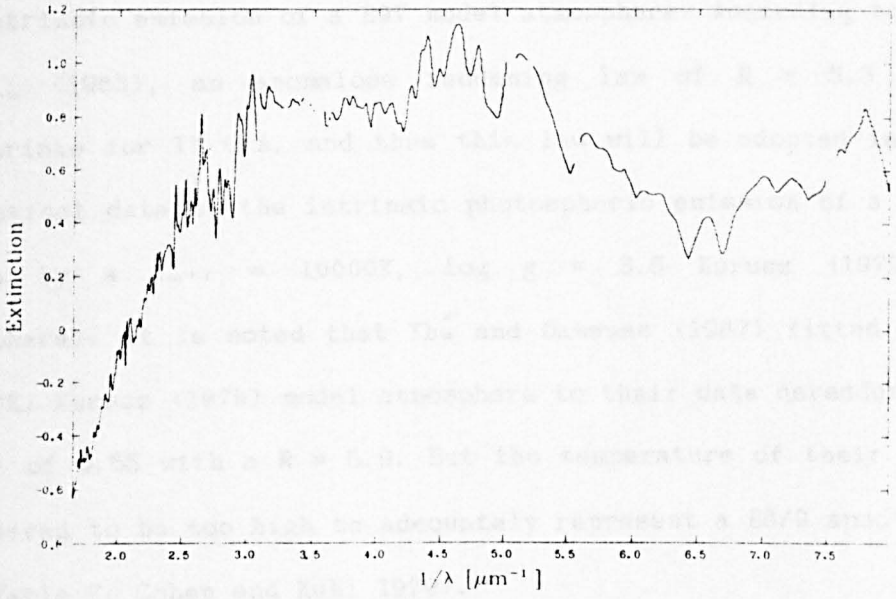

Fig. 4.1.14. Merged IUE and optical spectra of TY CrA. See also Section 4.1.4.1.

Fig. 4.1.15. The extinction law of TY CrA as determined from the merged IUE and optical spectra shown in Fig. 4.1.14.
See also Section 4.1.4.1.

between the expected and observed UV reddening can most easily be resolved if this is taken as an indication that the cloud and circumstellar reddening affecting TY CrA is predominantly neutral in the UV.

Dereddening the merged UV and optical spectra for the IS $E(B-V)_{IS}$ = 0.17 essentially gives the observed flux from TY CrA as would be observed from immediately outside the R CrA cloud. The total circumstellar and cloud reddening affecting TY CrA in the optical can then be estimated by dereddening the optical spectrum until it fits the intrinsic emission of a B9V model atmosphere. According to Whittet et al. (1983), an anomalous reddening law of R = 5.3 is most appropriate for TY CrA, and thus this law will be adopted in fitting the optical data to the intrinsic photospheric emission of a B9V star (given by a T_{eff} = 10000K, log g = 3.5 Kurucz (1979) model atmosphere). It is noted that Thé and Dawanas (1987) fitted a hotter (12000K) Kurucz (1979) model atmosphere to their data dereddened by an E(B-V) of 0.55 with a R = 5.9. But the temperature of their model is considered to be too high to adequately represent a B8/9 spectral type (see Table 7; Cohen and Kuhi 1979).

It was found that the adopted 10000K, log g = 3.5 model atmosphere was found to adequately reproduce the optical continuum, Balmer jump and the Balmer line strengths of the SAAO spectrum when the optical spectrum was dereddened by an IS $E(B-V)_{IS}$ = 0.17 and an additional (i.e. cloud and circumstellar) reddening of $E(B-V)_{CS}$ = 0.43 (with R = 5.3). The fit obtained is shown in Fig. 4.1.2, a fit initially presented in Section 4.1.2.2.

However, it is found that a cloud plus circumstellar reddening of only $E(B-V)_{CS} \simeq 0.01$ is required in order to fit a 10000K model atmosphere to the merged IUE spectra of TY CrA, i.e. the reddening in

the UV is essentially wholly IS. Now, unless the continuum slope (in either the optical or UV) changed markedly in the two months between the UV and optical spectroscopic observations, a possibility which is considered unlikely in view of the difference of ≈ 0.4 mag. in V between observations and the known limited variability in the spectral type of TY CrA (note also the similar UV continua of TY CrA observed in 1980, Fig. 4.1.7, and 1987, Fig. 4.1.5), the difference in $E(B-V)_{cs}$ required to fit the spectra with the same model atmosphere is almost certainly due to a difference in the circumstellar/cloud reddening from the UV into the optical. Of course, to unambiguously ascertain this, simultaneous optical and UV spectra would ideally be required.

When the intrinsic flux distribution (represented by the 10000K model atmosphere fitted to the dereddened optical spectrum) is divided by the smoothed, merged spectra, dereddened for the IS $E(B-V)_{IS}$ = 0.17, and then converted to magnitudes, the resultant plot of extinction with $1/\lambda$ (Fig. 4.1.15) gives an indication of the extinction law from 1200Å to 6000Å. Note however that in this figure the extinction has not been appropriately normalised, and that the ordinate is arbitrary. Given the spectral features which affect the smoothed "continuum", particularly in the UV (the Balmer lines in the optical have been effectively divided out), an error of ≈ 0.1 - 0.2 mag. is likely. The two absorption features around 1500Å are essentially due to the strong CII and OII emission features in the original SWP spectrum. It can be seen that the extinction is reasonably flat in the UV, i.e. no 2200Å feature is evident.

The reddening law out to 20μm was determined using the simultaneous optical and IR photometry obtained at SAAO on HJD 2447041 (note that no L photometry point was obtained on this date). Having removed

the IS reddening, and the dust IR excess beyond 5μm (by subtracting a 300K blackbody from the data; cf. Whittet et al., 1983) following the procedure outlined above, the cloud and circumstellar extinction law normalised to E(B-V) = 1 was determined. Note again however the possibility of a weak near-IR excess.

The resultant anomalous extinction law is plotted in Fig. 4.1.16 (represented by squares) and compared against the normalised IS curve (solid line) of Savage and Mathis (1979). The expected photometric errors are represented by vertical bars. A high value of R (from the extrapolated intercept at $1/\lambda = 0$) is clearly indicated, with $R \simeq 5 - 6$ depending on how the curve is extrapolated. However, with both the IR observational errors (for TY CrA at Q the typical error is $\simeq 0.1 - 0.2$ mag.) and variability (TY CrA was observed to vary by $\simeq 1$ mag. at N and Q; see also Section 4.1.4.2), the value of R can probably only be reliably determined to an accuracy of ± 0.5. Although a value of $R \simeq 6$ would be similar to the R = 5.9 adopted by Thé and Dawanas (1987), it would not be inconsistent to adopt R = 5.3 as was also explicitly derived by Whittet et al. (1983). Also, a R = 5.3 reddening law would not be incompatible with the observed optical colour variability of TY CrA (Section 4.1.3).

Therefore the reddening of TY CrA is shown to be anomalous from UV out to IR wavelengths. This fact will therefore be taken into account in the following section when the observed flux distribution of TY CrA is dereddened. The implications of the anomalous reddening law will be discussed in Section 4.1.4.3.

From the photometry of HD 176386, the distance modulus is estimated to be 6.12, given the IS extinction of $A_V = 0.53$ mag. and the absolute magnitude of an A0V star to be $M_V = 0.60$ mag. Marraco and Rydgren

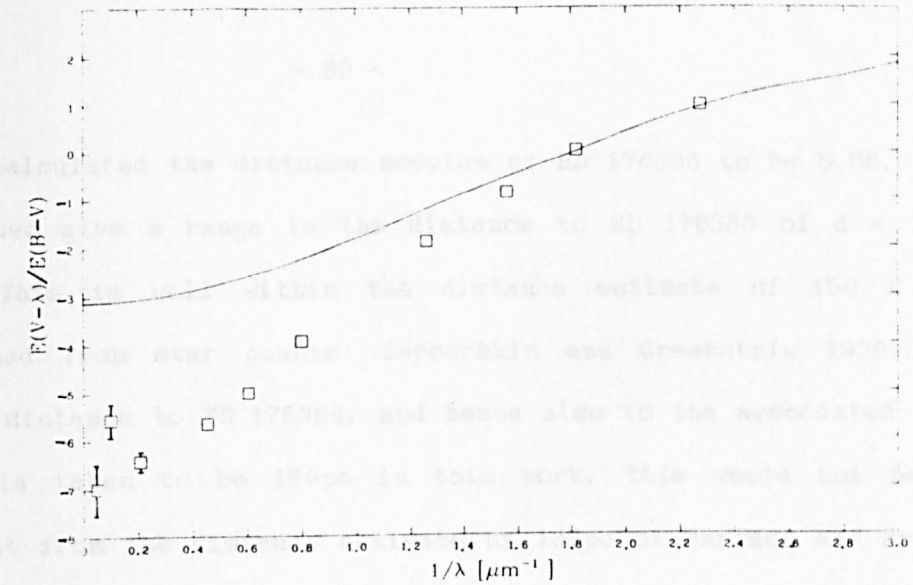

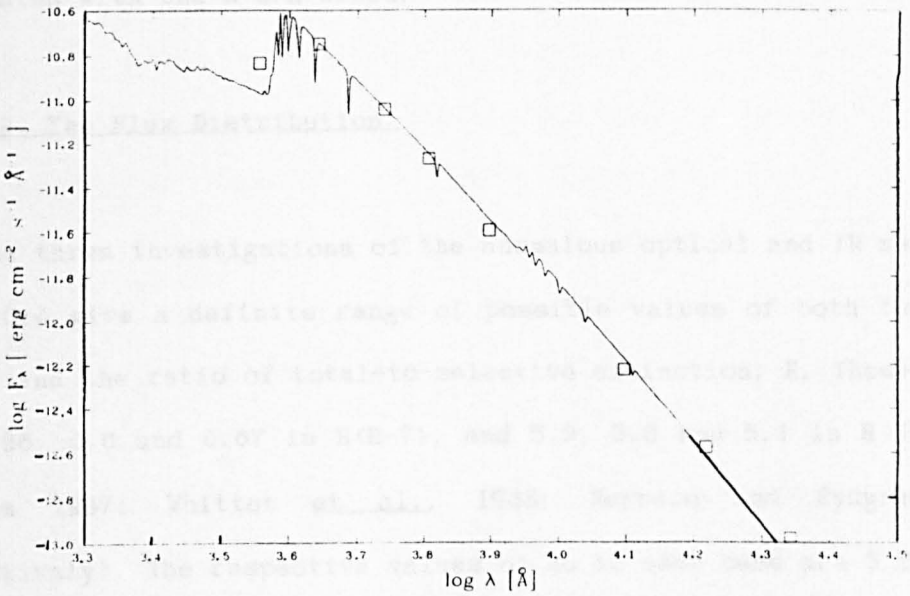

Fig. 4.1.16. The **reddening** law of TY CrA as determined from simultaneous optical and IR photometry normalised to E(B-V) = 1. See also Section 4.1.4.1.

Fig. 4.1.17. The flux distribution of TY CrA on HJD 2444742. See also Section 4.1.4.2.

(1981) calculated the distance modulus of HD 176386 to be 5.58. These two values give a range in the distance to HD 176386 of d ∝ 131 - 168pc. This is well within the distance estimate of 150 ± 50pc determined from star counts (Gaposchkin and Greenstein 1936). The adopted distance to HD 176386, and hence also to the associated R CrA cloud, is taken to be 150pc in this work. This would not be too different from the distance estimate of 138pc of Marraco and Rydgren (1981) determined for three lightly reddened stars assumed to be associated with the R CrA cloud.

4.1.4.2. The Flux Distribution.

The three investigations of the anomalous optical and IR reddening of TY CrA give a definite range of possible values of both the total E(B-V) and the ratio of total-to-selective extinction, R. These values are 0.55, 0.6 and 0.67 in E(B-V), and 5.9, 5.3 and 5.1 in R (Thé and Dawanas 1987; Whittet et al., 1983; Marraco and Rydgren 1981 respectively). The respective values of A_V in each case are 3.25, 3.18 and 3.42 mag., i.e. the total extinction of TY CrA is well-defined.

Given that the circumstellar reddening of TY CrA is probably variable (Section 4.1.3), once the IS reddening has been removed, the circumstellar and cloud reddening, denoted by $E(B-V)_{cs}$ is determined for each individual dataset by fitting the data to an appropriate model atmosphere. Given a B9V spectral class, the calibrations given in Allen (1973) and Cohen and Kuhi (1979) and the available Kurucz (1979) model atmospheres, model atmospheres of T_{eff} = 10000 and 11000K and log g = 3.5 and 4 are considered to be appropriate for TY CrA. Although a 10000K, log g = 3.5 model atmosphere was found to

give a best fit to the dereddened optical spectrum (Section 4.1.4.1), it was consistently found that an 11000K, log g = 3.5 model atmosphere gave the better fits to the optical UBVRI photometry, and thus this model was adopted in fitting the photometry. In view of this, it would seem that a 10500K model atmosphere (no Kurucz (1979) model of this temperature was available) would be more appropriate in fitting the continuum emission of TY CrA.

For each dataset, the optical and near-IR photometry could be fitted with the adopted Kurucz model atmosphere for reddening values of $E(B-V)_{IS}$ = 0.17, and a range in $E(B-V)_{CS}$ = 0.43 - 0.45 (with an assumed R = 5.3). Two fits are shown, from 0.36 - 2.2μm on HJD 2444742 (Fig. 4.1.17) and from 0.44 - 10μm on HJD 2447040 (Fig. 4.1.18). As was found by Whittet et al. (1983), no significant IR excess out to 3.5μm is prevalent. The persistent excess above the stellar continuum at 3.5μm is attributed to the emission feature observed at 3.3μm (Whittet et al., 1983). Beyond ≃ 5μm the excess clearly requires an additional emission component, presumably emission from the circumstellar dust (cf. Whittet et al., 1983).

With the inclusion of the IRAS Point Source Catalogue (PSC) (Beichman et al., 1985) data for TY CrA (TY CrA was not flagged as a variable source in the IRAS PSC) with the 0.44 - 20μm SAAO photometry obtained on HJD 2447041 (Fig. 4.1.19), it is seen that the notable IR excess beyond ≃ 5μm can indeed be explained by thermal emission from warm dust (note the flux units in this figure, F_ν and not F_λ). The N and Q data points on this night (when TY CrA was bright) correspond to the rise in the IRAS data points, except for the Band I flux at 12μm. As no discrepant 12μm flux was noted by Thé and Dawanas (1987) this probably indicates variability in the ≃ 10 - 20μm emission (note that

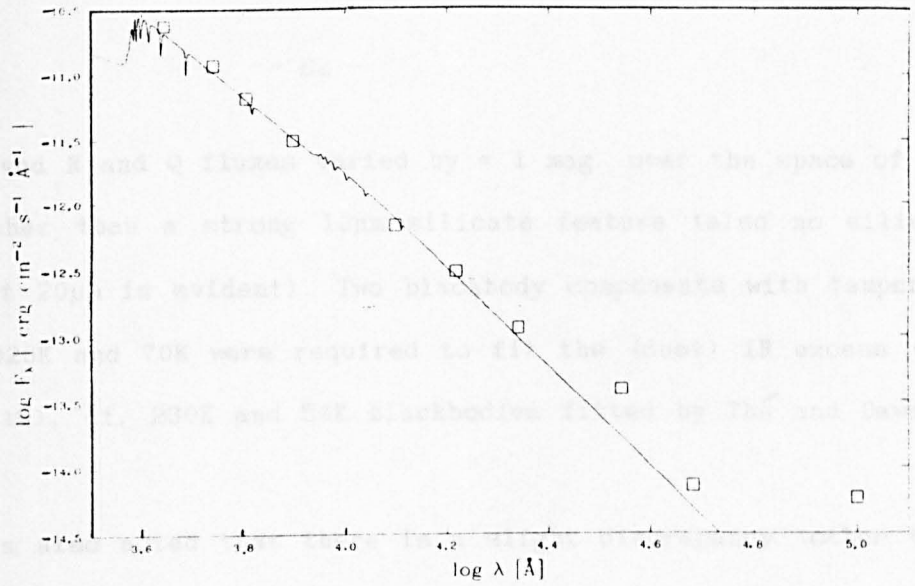

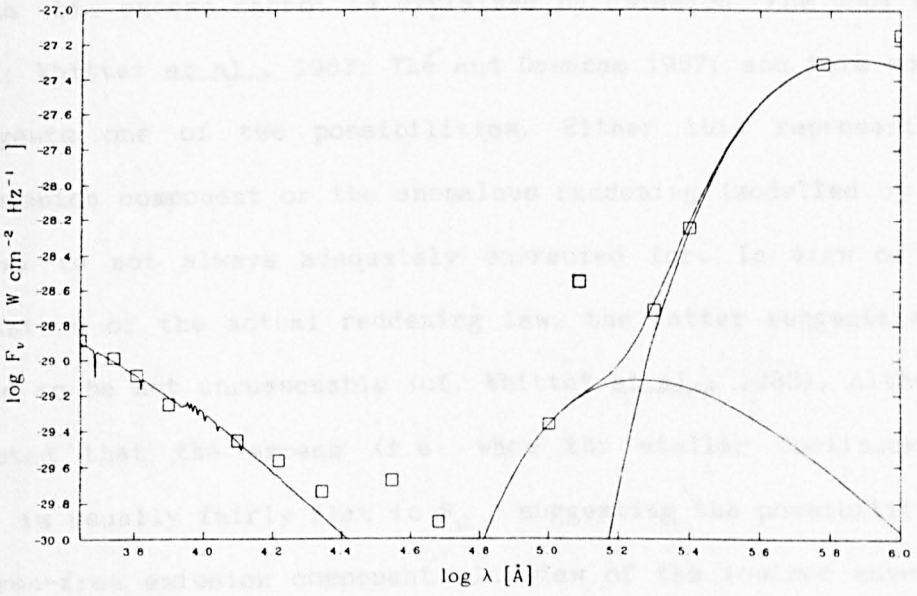

Fig. 4.1.18. Flux distribution of TY CrA on HJD 2447040. See also Section 4.1.4.2.

Fig. 4.1.19. Flux distribution of TY CrA on HJD 2447041 with IRAS data included. See also Section 4.1.4.2.

the observed N and Q fluxes varied by ≃ 1 mag. over the space of ten days) rather than a strong 10μm silicate feature (also no silicate feature at 20μm is evident). Two blackbody components with temperatures of 320K and 70K were required to fit the (dust) IR excess (see Fig. 4.1.19), cf. 230K and 54K blackbodies fitted by Thé and Dawanas (1987).

It is also noted that there is a slight discrepancy (other than the excess at 3.5μm) in the fits of the stellar continuum to the dereddened near-IR (≃ 2.5 - 5μm) photometry, e.g. see Figs. 4.1.18 and 4.1.19. As this excess cannot be explained by emission from cool dust (T ≃ 300K; Whittet et al., 1983; Thé and Dawanas 1987; and this work), this suggests one of two possibilities. Either this represents a "real" emission component or the anomalous reddening (modelled by a R = 5.3 law) is not always adequately corrected for. In view of the unusual nature of the actual reddening law, the latter suggestion is considered to be not unreasonable (cf. Whittet et al., 1983), although it is noted that the excess (i.e. when the stellar continuum is removed), is usually fairly flat in F_ν , suggesting the possibility of a weak free-free emission component. In view of the ionised envelope of TY CrA (Section 4.1.2), free-free emission is not implausible.

The average value for the normalisation required to fit the model atmosphere to the dereddened data gives an estimate of the stellar radius of 2.4 $R_\odot$ for an assumed distance of 150 pc. This radius estimate compares well with the radius of an A0V star of 2.5 $R_\odot$ (Allen 1973). Assuming that the luminosity equation, $L_{Bol} = 4\pi\sigma R_*^2 T_{eff}^4$, can be applied to Orion Population stars, for TY CrA with T_{eff} = 11000K and a R_* = 2.4 $R_\odot$, this gives a L_{Bol} = 75.5 $L_\odot$, which is in excellent agreement with the bolometric luminosity of 80 $L_\odot$ for a B9V star.

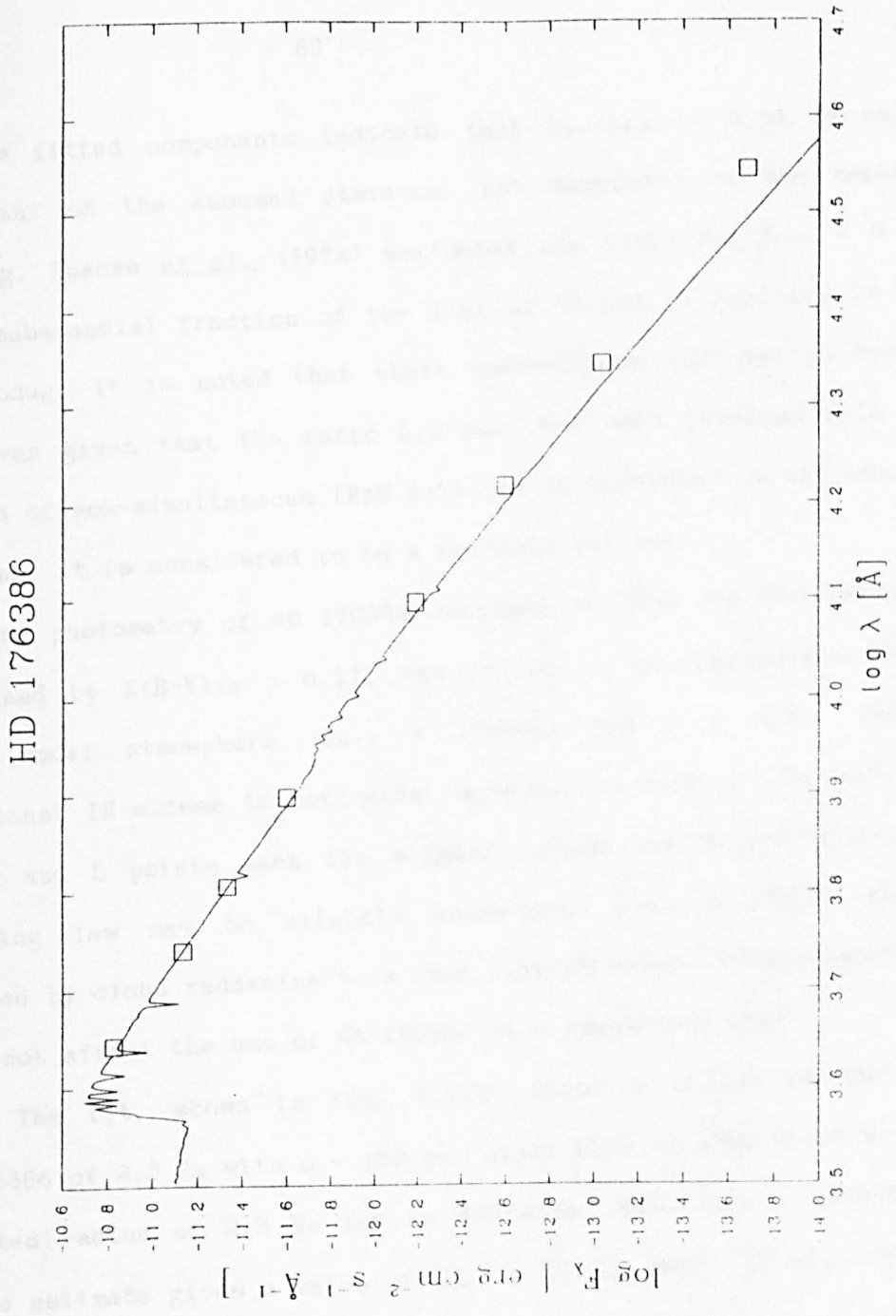

Fig. 4.1.20. Flux distribution of HD176386 on HJD 2447044. See also Section 4.1.4.2.

The fitted components indicate that $L_{IR}/L_{Bol} \simeq 0.38$, a value independent of the assumed distance, but dependent on the assumed reddening. Knacke et al. (1973) estimated the ratio $F_{IR}/F_{vis} \simeq 0.15$, i.e. a substantial fraction of the flux of TY CrA is radiated in the IR, although it is noted that their observations did not go beyond 20μm. Even given that the ratio L_{IR}/L_{Bol} has been obtained with the addition of non-simultaneous IRAS data and is dependent on the assumed reddening, it is considered to be a reliable estimate.

Also photometry of HD 176386 obtained at SAAO (on HJD 2447044), dereddened by $E(B-V)_{IS} = 0.17$, was fitted to an appropriate Kurucz (1979) model atmosphere ($T_{eff} = 10000K$, log g = 3.5), and no significant IR excess is noticable. However, in view of the fact that the HK and L points each lie slightly above the fitted model, the reddening law may be slightly anomalous, i.e. HD 176386 may be affected by cloud reddening to a very limited extent (this possibility would not affect the use of HD 176386 as a comparison star).

The fit, shown in Fig. 4.1.20 gives a radius estimate for HD 176386 of 2.3 $R_\odot$ with d = 150 pc. Again this is consistent with the expected radius of 2.5 $R_\odot$ for an A0V star. With $T_{eff} = 10000K$ this radius estimate gives a value of $L_{Bol} = 58\ L_\odot$, which is significantly larger than the value of 16 $L_\odot$, estimated by Wilking et al. (1986), and is in much better agreement with an expected luminosity of some 70 - 80 $L_\odot$ for an A0V star (Allen 1973).

4.1.4.3. Cloud Properties.

The R CrA cloud is known to be a region of fairly high extinction ($1.5 \lesssim A_V \lesssim 3.5$ mag.; Rossano 1978a). However, as the individual

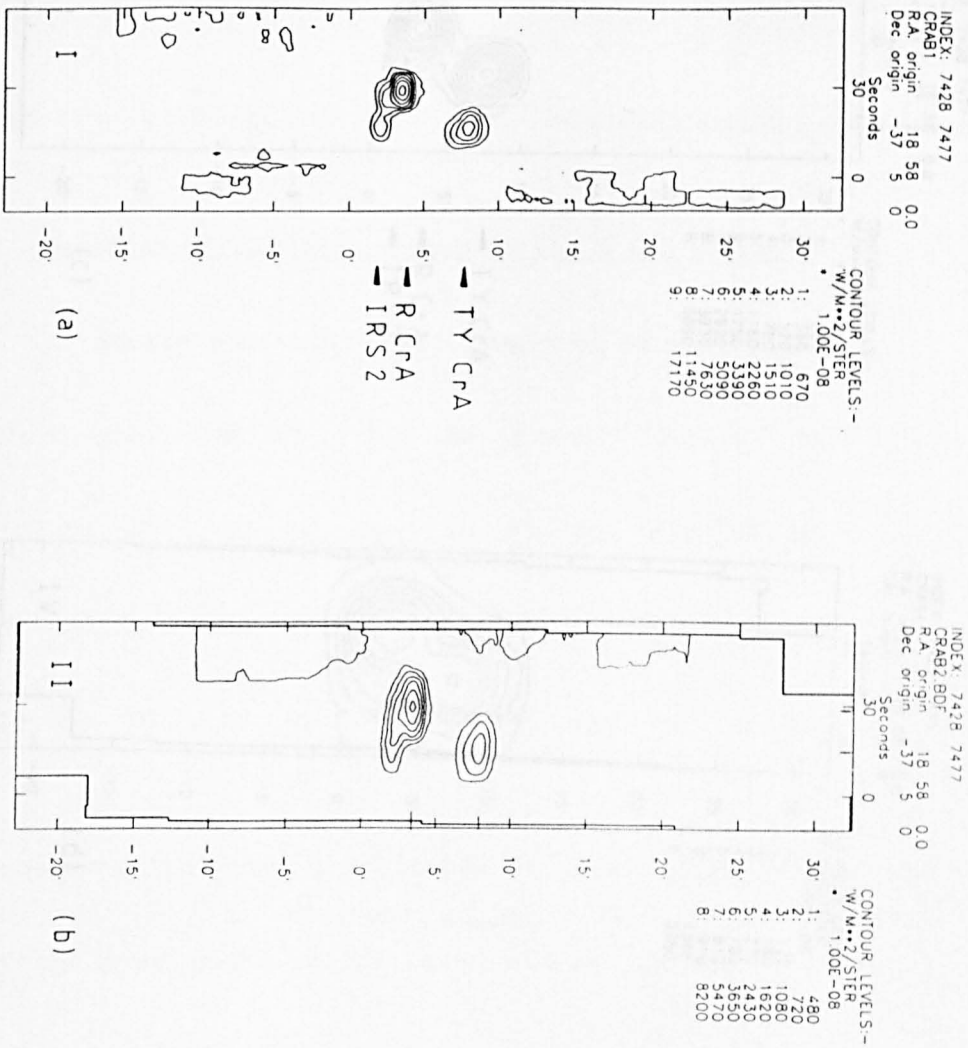

Fig. 4.1.21. IRAS flux maps of the R CrA cloud. The identified sources are TY CrA, R CrA and IRS2. See also Section 4.1.4.3.

(a) Band I flux map.

(b) Band II flux map.

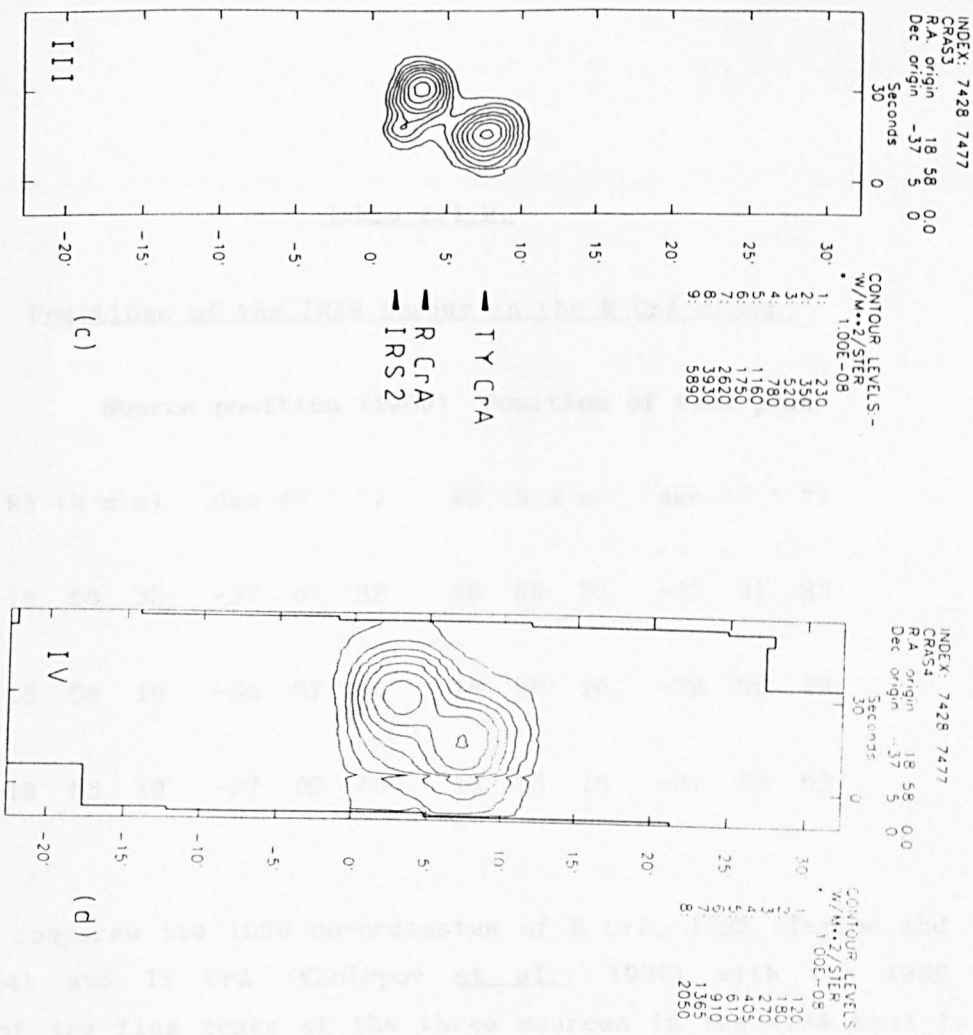

Fig. 4.1.21. (cont'd)

(c) Band III flux map.

(d) Band IV flux map.

Table 4.1.2.

Positions of the IRAS images in the R CrA cloud.

Source	Source position (1950)						Position of flux peak					
	RA (h m s)			dec (° ' ")			RA (h m s)			dec (° ' ")		
R CrA	18	58	32	-37	01	32	18	58	28	-37	01	20
TY CrA	18	58	18	-36	57	00	18	58	16	-36	56	45
IRS 2	18	58	19	-37	02	48	18	58	16	-37	02	52

This table compares the 1950 co-ordinates of R CrA, IRS2 (Taylor and Storey 1984) and TY CrA (Kholopov et al., 1987) with the 1950 positions of the flux peaks of the three sources in the IRAS band I flux map.

components of the cloud and circumstellar reddening affecting TY CrA cannot be extricated, the cloud reddening law cannot be unambiguously determined. The best that can be said therefore is that the reddening law determined for TY CrA may well indicate both the circumstellar and cloud grain properties. As TY CrA and HD 176386 probably lie towards the front edge of the R CrA cloud (Marraco and Rydgren 1981), and if it is assumed that the reddening law of TY CrA derived in Section 4.1.4.1 is representative of the cloud reddening law, then the likely grain properties towards the perimiter of the cloud can be commented upon.

From the derived anomalous ($R \simeq 5.3$) extinction law, it would seem that the grain population within the cloud is unlike that of the normal grain distribution within the IS medium. The absence of the 2200Å feature suggests that small ($\simeq 0.03\mu m$) grains (responsible for the 2200Å feature in the IS medium) may be depleted in the cloud/ circumstellar environment. Alternatively, the presence of grains of this size may be masked due to growth of grain mantles. The form of the UV/optical extinction in Fig. 4.1.15, with the curve reaching a plateau beyond $1/\lambda \simeq 2.5 - 3\mu m^{-1}$, indicates the presence of grains of a typical size, $a_{gr} \simeq 0.05 - 0.06\mu m$. Also there is a significant population of grains which are larger than IS grains, as inferred from the anomalous value of $R \simeq 5.3$, indicating a grain size, $a_{gr} \simeq 0.3\mu m$. These findings would therefore be consistent with grain growth occurring in the R CrA cloud (cf. Whittet et al., 1983), although destruction of the smaller grains is also tenable.

As part of the IRAS programme of Additional Observations, far-IR imaging of the R CrA region at each IRAS bandpass was carried out. These maps of the region (Fig. 4.1.21) indicate the presence of only

three far-IR sources, sources which are identifiable with R CrA, TY CrA and IRS2 (HH 100IR) (see also Table 4.1.2). These IRAS maps clearly fail to show evidence for any of the inferred embedded IR sources, other than IRS2, corresponding to the 2μm sources of Taylor and Storey (1984). Thus, in agreement with the conclusion of Vrba et al. (1981), it seems clear that the majority of the 2μm sources in this region must be heavily reddened background stars.

As radio mapping suggests that the R CrA cloud core may still be in free-fall collapse (Loren 1979), but yet there are very few embedded IR sources, it would indeed seem likely that the process of star formation is being held up within the cloud core (Loren 1975), even though the core itself is massive enough for star formation to occur (Vrba et al., 1981).

Now, Loren (1979) also showed that the CO emission associated with TY CrA required excitation by a spectral type of ≃ B2, which would be incompatible with the spectral type of TY CrA (B9) (see also Section 4.1.1). However, as there are no embedded IR sources associated with TY CrA, Loren's (1979) proposal of an additional luminous source cannot be considered tenable. In view of the fact that TY CrA is over-luminous at X-ray wavelengths and emits strongly at 6cm (Brown 1987b), emission Brown attributed to a stellar wind, it is therefore not inconceivable that TY CrA is sufficiently over-luminous at millimetre wavelengths to explain the observed CO emission peak.

4.1.5. Polarimetric observations.

In comparing the polarimetric observations of TY CrA obtained by Serkowski (1969b), it must be remembered that Serkowski made his

polarimetric observations using a blue filter, whereas the observations presented here were taken with a clear filter.

On HJD 2446991 the linear polarisation of HD 176386 observed through a clear filter was 0.72 ± 0.08%, cf. 0.57% observed by Serkowski (1969b) using a blue filter.

In 1969, when TY CrA was observed at B = 9.7 mag., Serkowski (1969b) measured the polarisation in the blue to be 1.1 ± 0.5%. The average value of B in the 1987 photometry was also 9.7 mag., and the average polarisation (with a clear filter) was 1.21 ± 0.13% (the error corresponds to the typical observational error). Overall, with five observations obtained over a ten day period in September, 1987, the polarisation of TY CrA varied by no more than 0.25% (± 0.1%). In addition, no significant change (within the observational errors of ± 7°) in the position angle was observed over the same ten day period. The average $\theta \simeq 90^{\circ}$ compares well with the $\theta \simeq 104^{\circ}$ observed (in the blue) by Serkowski (1969b).

Thus it is concluded that the linear polarisation and position angle of TY CrA are not strongly variable. However, the fact the polarisation of TY CrA is greater than expected if it were caused by the intervening IS (and cloud) dust, indicates that the observed polarisation is essentially intrinsic to the star (Serkowski 1969b).

Now, as the polarisation of TY CrA, like "classical" Be stars, is not strongly variable, it is possible that, as with Be stars, the polarisation may be due to electron scattering within a circumstellar envelope (Poeckert and Marlborough 1978). Alternatively, the polarisation may be caused by scattering by circumstellar dust grains. Observations of the wavelength dependence of polarisation are therefore desirable in determining the origin of the polarisation.

4.1.6. Summary and Conclusions.

Evidence for a highly ionised stellar envelope is indicated by the presence of lines of high ionisation (e.g. CIV, SiIV) in the SWP IUE spectrum of TY CrA. High resolution observations of such UV lines and also the Balmer lines would be useful in determining the envelope parameters, and further observations with a view to tying down the timescale of variability of these lines would also be desirable.

As there are no embedded sources associated with TY CrA, it is clear that TY CrA radiates strongly at both X-ray and radio/millimetre wavelengths, observations which would not be incompatible with the presence of a highly ionised stellar envelope. Further, TY CrA is suggested as a candidate for X-ray spectroscopic observations in order to look for the carbon and oxygen K shell absorption edges.

Optical and IR photometry, along with optical and UV spectroscopy have been used to determine the extinction law of TY CrA. The extinction law was found to be anomalous, and essentially neutral in the UV, of a form indicating typical grain sizes of $\simeq 0.06$ and $0.3\mu m$. Also, variable circumstellar extinction by large ($\simeq 0.3\mu m$) grains is proposed as the underlying cause of the long-term light variations in TY CrA, although this mechanism cannot fully account for the observed degree of near-IR variability.

TY CrA is found to have a strong far-IR excess attributable to thermal emission from circumstellar dust. Also there is a possible weak near-IR excess which may be attributable to either anomalous extinction or free-free emission. The intrinsic polarisation of TY CrA is not strongly variable, and further observations are required to determine the origin of the polarisation.

4.2. The Herbig Ae/Be star R CrA.

4.2.1. Introduction.

R CrA (CoD -37°13027) lies towards the centre of the R CrA dark cloud, and together with the fainter Ina star T CrA, is associated with a variable, cometary reflection nebula, NGC 6279. R CrA lies at the apex of the cometary nebula and is the dominant illuminating source, cf. the association of R Mon (also an Ina star) with a cometary nebula NGC 2261. The variability of NGC 6279 has been interpreted in terms of dense (but gravitationally unstable) cloudlets passing close by R CrA and thereby causing a "shadowing" effect in the illumination of the nebula from R CrA (Graham and Phillips 1987).

R CrA exhibits a large variation in visual magnitude, $9.7 < V < 14.4$ mag. (Joy 1945; Kholopov et al., 1987). The mean brightness is $\langle V \rangle = 10.74$ mag., but the lightcurve shows no preference for any particular brightness level and exhibits a quasi-period of $\simeq$ 32 days (Herbig and Rao 1972). Also the lightcurve suffers occasional, deep ($\simeq$ 2 mag.) T Ori-like minima (see Fig. 2.3.2) lasting only a few days.

The optical spectrum of R CrA exhibits strong Balmer absorption lines and variable emission of Hα and Hβ. The Balmer lines are occasionally affected by the occurrence of very deep shell absorption, giving the appearance of an A5 I/II spectral type. A similar phenomenon is also exhibited by R Mon. This transient phenomenon has been ascribed in both stars to the close passage of nebulous shells which strongly scatter Balmer radiation into the associated cometary nebulae (Herbig and Rao 1972). Note therefore that the variability of

NGC 6279 (Graham and Phillips 1987) and the transient shell absorption of R CrA (Herbig and Rao 1972) may well have a common origin.

Joy (1945) estimated the spectral type of R CrA as F5 and he noted that in 1920 Hubble initially estimated the spectral type as G. These initial studies mark the start of a prolonged quest to assign R CrA a definite spectral type. All subsequent designations have tended to favour a spectral type in the range A-F. Herbig (1962) and Herbig and Rao (1972) indicate a spectral type of ≃ F0, Mendoza et al. (1969) observed the spectrum as A5, and Marraco and Rydgren (1981) as late A. Kholopov et al. (1987) list the spectral type as A5IIpe.

With the Balmer lines being affected by variable shell absorption, it is unsurprising that changes in the spectral type have been observed. However, in view of the marked range in the spectral type of R CrA from A to G, it would seem evident that the intrinsic spectral type of R CrA is actually variable, and cannot therefore be uniquely assigned a spectral class on the MK system. A similar conclusion was reached by Mendoza et al. (1969) who suggest that that a spectral type of A5pe is probably most appropriate.

The spectrum also exhibits strongly variable CaII K and H, HeI and FeII emission lines (Joy 1945, Hartigan and Graham 1987). The HeI line profiles are particularly intruiging, with the 5875 triplet and 6678Å singlet lines exhibiting inverse P Cygni profiles (Hartigan and Graham 1987). Both the prominent HeI line profiles and the variable, central reversal of Hα observed by Graham and Phillips (1987) lead these authors to suggest that R CrA posseses a very strong, active extended chromosphere, from which the strong line emission predominantly arises. In view of the rapid time variability (≃ 24 hours, Graham and Phillips 1987) of the Hα line profile in R CrA, this region cannot be

much more extensive than $\simeq R_*$, and is possibly also highly turbulent.

However, as R CrA was not detected as a X-ray source by the *Einstein* satellite (Walter and Kuhi 1981), it would seem that "coronal" temperatures ($T_e \simeq 10^6 - 10^7$ K) are not attained within the extended "chromospheric" region.

R CrA is significantly reddened and the reddening law is probably anomalous, e.g. E(B-V) = 1.12 and R = 3.3 (Thé and Dawanas 1987). R CrA exhibits a remarkably steep rise in flux from the visual out into the IR. Typical colours are: (V-L) = 8.93 (Imhoff and Mendoza 1974) and (L-Q) = 5.26 (Taylor and Storey 1984), and R CrA is one of the brightest Orion Population stars longwards of $\simeq 8\mu m$ (Imhoff and Mendoza 1974). Again, the Ina star R Mon exhibits a similarly large rise in the IR.

Graham and Phillips (1987) note that the heating of the warm dust extending into the molecular cloud surrounding R CrA is probably attributable to R CrA itself. R CrA was not detected at 6cm by Brown (1987b), but does lie at the source of both strong far-IR and molecular emission, e.g. CO (Loren 1975), CH_2CO (Vrba et al., 1981). This would indicate that R CrA is the dominant energy source of the nearby HH objects and CO outflow. However, proper motion measurements of the HH objects indicate that they were probably ejected from the far-IR source IRS2 (Hartigan and Lada 1985), itself co-incident with the HH object HH100. Like R CrA, IRS2 is sufficiently luminous to excite the associated HH objects.

Polarimetric observations of R CrA have been obtained by Serkowski (1969b), Vrba et al. (1979) and Ward-Thompson et al. (1985). Serkowski (1969b) observed a steep rise in the polarisation (in the blue) from 7% to 18%, over a 38 day period in 1969, over which time the star

faded from V = 11.5 down to 13.5 mag. The corresponding variation in position angle was 170 - 185°. Serkowski (1969b) comments that in view of the rapid rise in the polarisation, the polarisation of R CrA probably originates close in to the star rather than in the associated nebula, NGC 6729, which was also observed to emit significantly polarised light, $p_v \simeq 14\%$.

The polarisation was observed to be ≃ 6-7% by Vrba et al. (1979) and Ward-Thompson et al. (1985). Vrba et al. (1979) interpreted this high polarisation in terms of transmission of light through a dense cloud of aligned particles. The polarimetric mapping of R CrA by Ward-Thompson et al. (1985) lends support to this interpretation and Ward-Thompson et al. (1985) suggest a disc-like geometry for the aligned, circumstellar grains (see also Fig. 2.3.3). Further, they interpret optical plates and CO maps obtained of the region in terms of collimation of an optical jet by a circumstellar disc and collimation of a CO outflow by a more extensive, intra-cloud disc.

4.2.2. The Optical Spectrum.

The optical spectrum of R CrA was obtained on HJD 2446998, when the star was observed to be down at V = 12.47 mag. and was also very red, B-V = 0.86 (cf. <V> = 10.74 mag., <B-V> = 0.56; Herbig and Rao 1972). The SAAO spectrum with the strong lines identified is shown in Fig. 4.2.1.

4.2.2.1. Spectral Classification.

As has been mentioned, the spectrum of R CrA is very variable,

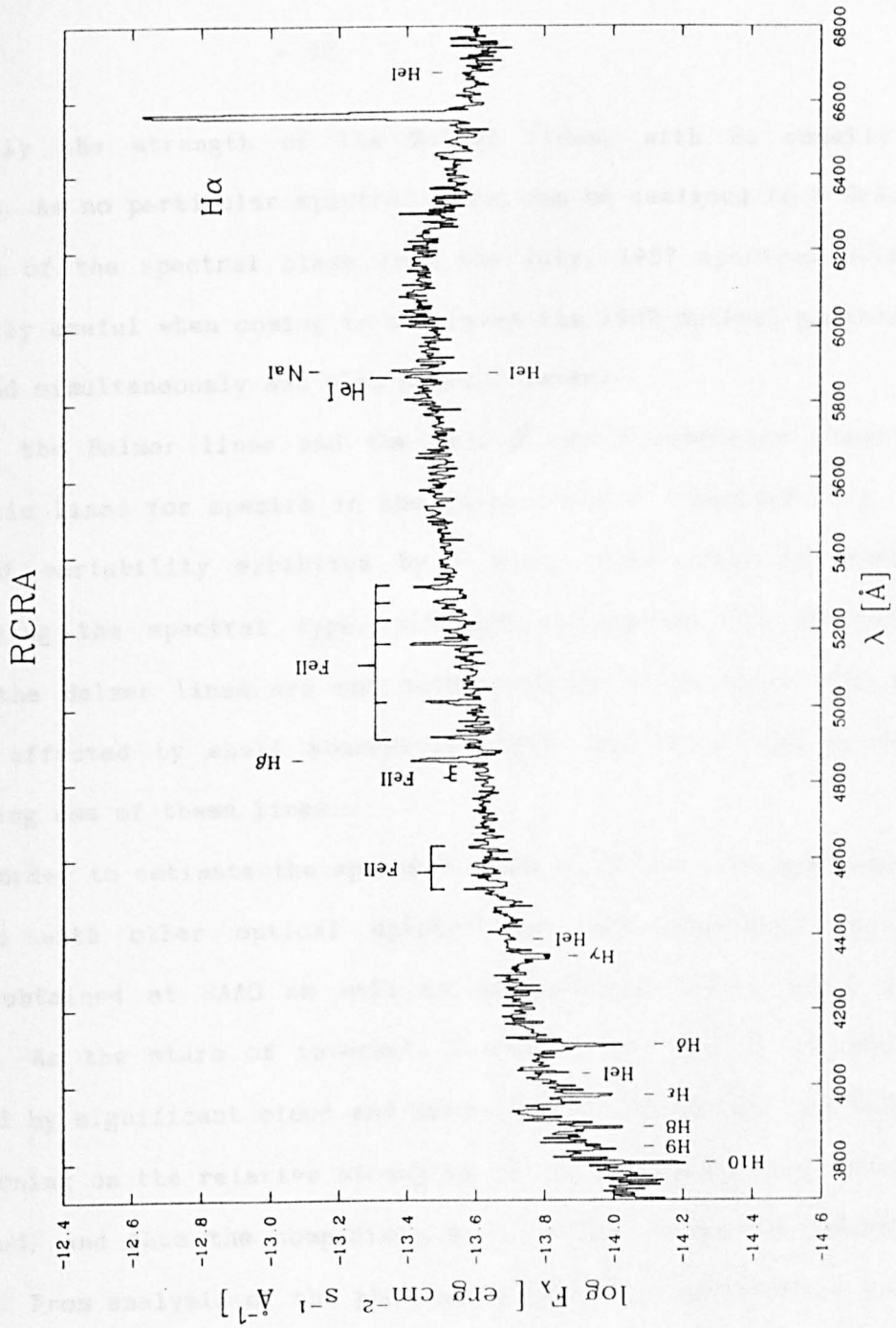

Fig. 4.2.1. Optical spectrum of R CrA. See also Section 4.2.2.

especially the strength of the Balmer lines, with Hα usually in emission. As no particular spectral class can be assigned to R CrA, an estimate of the spectral class from the July, 1987 spectrum will be especially useful when coming to interpret the 1987 optical photometry (obtained simultaneously and also a month later).

As the Balmer lines and the CaII K and H resonance lines are diagnostic lines for spectra in the range early A - early F (i.e. the range of variability exhibited by R CrA), they shall be used in determining the spectral type, although as pointed out in Section 4.2.1, the Balmer lines are not only affected by emission, but also can be affected by shell absorption. Note the Hα and Hβ emission, precluding use of these lines.

In order to estimate the spectral class of R CrA, the spectrum was compared with other optical spectra (of well-determined spectral class) obtained at SAAO as well as with Kurucz (1979) model atmospheres. As the stars of interest, R CrA, T CrA and TY CrA are all affected by significant cloud and circumstellar reddening, the effects of reddening on the relative strengths of the hydrogen lines cannot be neglected, and thus the comparison must be made using the dereddened spectra. From analysis of the photometry of R CrA (see Section 4.2.4), the cloud plus circumstellar reddening of R CrA is estimated to be $E(B-V)_{cs} \simeq 0.61 - 0.77$, with $R = 5.3$ (the IS reddening is $E(B-V)_{IS} = 0.17$; Section 4.1.4.1).

In the observed spectra, the Balmer lines of R CrA are not as strong as the corresponding lines in either TY CrA (B9) or T CrA (F0). However, after dereddening the spectra, the Balmer lines are still found to be weaker than the lines in TY CrA, but slightly stronger than in T CrA. That the lines are not notably strong indicates that

they are unaffected by shell absorption. It is clear that the spectrum of R CrA lies in the range B9 - F0 delineated by the two stars used for comparison, and probably closer to F0. That the CaII resonance lines are fairly strong (the CaII lines become important around late A), stronger than in TY CrA but weaker than in T CrA, also indicates that the spectral type of R CrA probably lies nearer F0 than B9.

From a comparison with a grid of Kurucz (1979) model atmospheres, the strengths of the Hδ and Hϵ lines (Balmer lines not affected by emission) suggest an effective temperature for R CrA in the range 8000 - 8500K, which corresponds to a range of A3 - A6 (Cohen and Kuhi 1979). That the estimate of spectral type from the strengths of both Balmer and CaII resonance lines are in general agreement, it would seem clear that the higher Balmer lines are not strongly affected by shell absorption. Therefore the spectrum of R CrA as observed in July, 1987 is determined to lie in the range mid to late A.

4.2.2.2. The Hydrogen lines.

The Hα and Hβ emission lines are as strong as have been observed when R CrA is brighter, indicating that the Balmer emission is not significantly diminished when R CrA is faint. The strength of the Hα line would be incompatible with it arising purely in a dense stellar chromosphere (Calvet et al., 1984), and as reviewed in Section 4.2.1, the strong Hα and Hβ line emission must arise in an extended, highly excited circumstellar envelope.

An IR spectrum of R CrA was also obtained at CTIO in June, 1987, at the H band wavelength range, which covers lines of the Brackett IR series. Although the star is very bright at this wavelength (H $\simeq$ 4

mag.), because of poor movement of the grating, the quality of the spectrum is affected by regularly-spaced "drop outs". Thus it is not possible to identify the whole of the series over this wavelength range, but the B12, B14, B15 and B18 lines can be seen in emission on both the original, and the reduced spectrum (see Fig. 4.2.2). Therefore both the Paschen and Brackett IR hydrogen series probably exhibit strong emission. In view of the variability of the Balmer lines, the IR hydrogen lines are probably also variable.

4.2.2.3. The Helium lines.

Several HeI lines are observed. The singlet 3d - 2p 6678Å line is predominantly in absorption, whilst the triplet 3d - 2p 5875Å line exhibits a very wide, ≈ 12Å prominent inverse P Cygni profile (cf. Hartigan and Graham 1987). The 5d - 2p 4387Å and $4d^3$ - $2p^3$ 4471Å and $5d^3$ - $2p^3$ 4026Å lines are all observed in absorption. The expected singlet 4d - 2p 4921Å line is in a blend dominated by the strong FeII 4923Å emission line.

That the higher HeI transitions are in absorption indicates that high temperatures (≈ a few x 10^4 K) are attained in the extended chromospheric region, whilst the wide, inverse P Cygni profiles typically exhibited by the triplet and singlet 3d - 2p lines indicate that the turbulent mass motion of the hot, dense plasma within the highly excited envelope is dominated by infall.

4.2.2.4. The FeII lines.

With many strong FeII lines in the spectrum, it was possible to

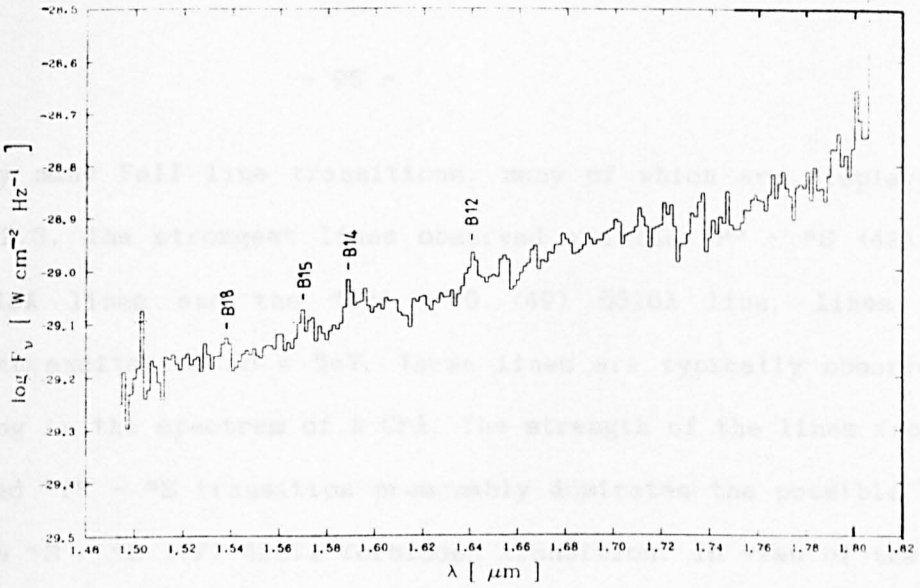

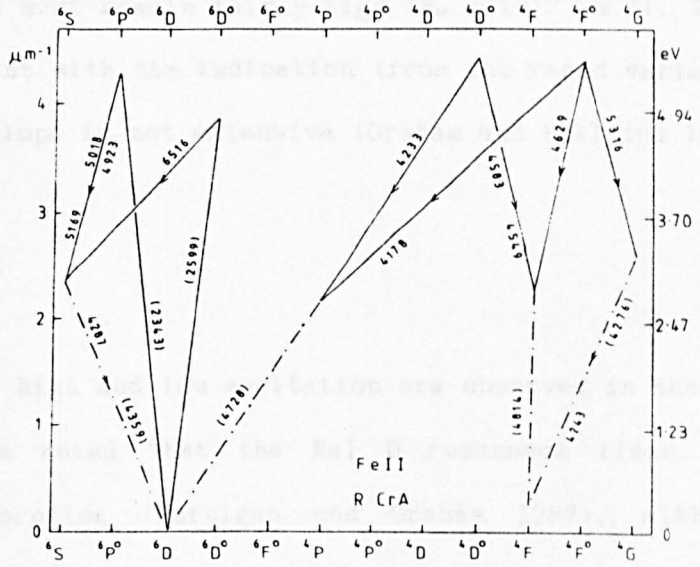

Fig. 4.2.2. H band IR spectrum of R CrA showing Brackett lines.
See also Section 4.2.2.2.

Fig. 4.2.3. FeII Grotrian diagram for optical transitions in R CrA.
See also Section 4.2.2.3.

identify many FeII line transitions, many of which are displayed in Fig. 4.2.3. The strongest lines observed are the $^6P^o$ - ^6S (42) 5169 and 5018Å lines and the $^4F^o$ - ^4G (49) 5316Å line, lines which represent excitation to ≃ 5eV. These lines are typically observed to be strong in the spectrum of R CrA. The strength of the lines from the permitted $^6P^o$ - ^6S transition presumably dominates the possible blend with the ^6S - ^6D (7F) 4287Å forbidden transition. In view of the lack of any prominent FeII forbidden emission (the transitions of which are shown in Fig. 4.2.3 as broken lines), the electron density within the emission envelope must remain fairly high (N_e ≥ 10^{10} cm^{-3}). This would not be inconsistent with the indication (from the rapid variability in Hα) that the envelope is not extensive (Graham and Phillips 1987).

4.2.2.5. Summary.

Both lines of high and low excitation are observed in the spectrum of R CrA. It is noted that the NaI D resonance lines, normally strongly in absorption (Hartigan and Graham 1987), although not resolved in the SAAO spectrum, are clearly dominated by emission at this epoch.

The formation of HeI absorption lines indicates the presence of a hot (≃ a few x 10^4 K), dense chromospheric region which is affected by substantial infall. The spectrum is dominated by strong emission lines such as HI and FeII of lower excitation (≃ 10^4 K), and a region of even lower excitation (≃ several x 10^3 K) is also indicated at this epoch, by the strong NaI D emission. Therefore it would seem that the extended envelope of R CrA is characterised by distinct regions of both high and low temperature. High resolution spectroscopy of the

different lines would be useful in delineating the physical parameters within the various regions.

4.2.3. The Colour-colour variations.

The UBVRI and JHKL photometry of Kilkenny et al. (1985) obtained from 1981 to 1984 and the BVRI and JHKL photometry obtained at SAAO in 1987 forms the database for investigation of the colour and light variations of R CrA. R CrA was observed to vary between 11.2 < V < 12.7 mag., fainter than the <V> = 10.74 mag. indicated by Herbig and Rao (1972). Therefore R CrA was observed throughout a long-term phase where the star was fainter than at "normal" light. Unfortunately the observations were not continuous enough (except for the photometry obtained in September 1987 - see Section 4.2.5) for an investigation of the short-term variations (≃ hours - days) in the lightcurve.

The variation of B-V with V is shown in Fig. 4.2.4. The B-V colour exhibits a tendency to redden as the star fades, particularly when fainter than V ≃ 11.8 mag. However, R CrA can also appear heavily reddened when comparatively bright, e.g. for five observations obtained on HJD 2444866, V ≃ 11.5 mag. and B-V ≃ 0.88, cf. <B-V> ≃ 0.56 (Herbig and Rao 1972). Typically R CrA is less heavily reddened even when much fainter than this, see Fig. 4.2.4. In view of the notable variation in spectral class (see Section 4.2.1), such epochs where R CrA is redder than expected for a certain light level are best attributed to a later spectral type of R CrA than is typically observed.

R CrA is clearly significantly reddened: $(B-V)_{obs} \simeq 0.8$, cf. $(B-V)_{intrinsic} \simeq 0.05$ for an A5I star (Johnson 1966), although it is noted that the spectral type of R CrA can typically range from early A

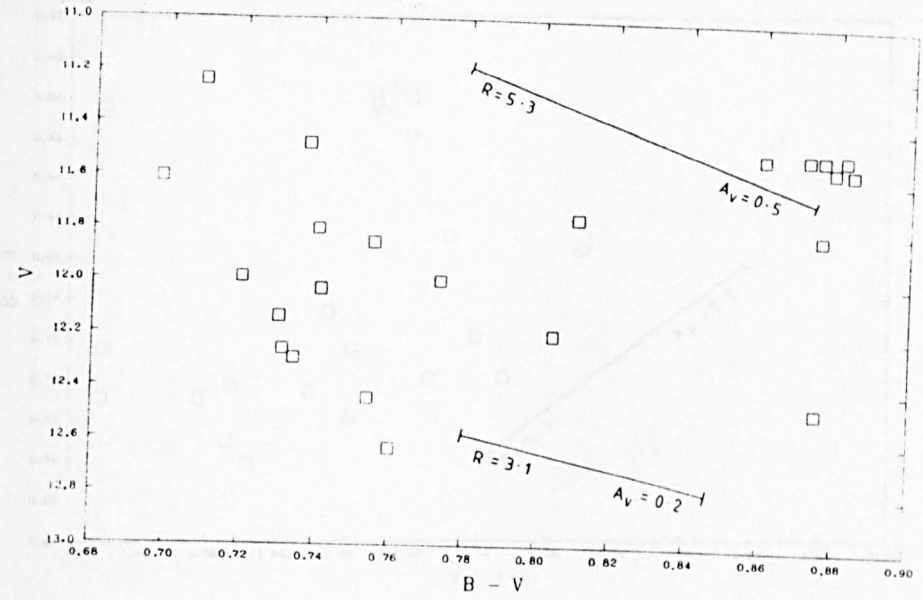

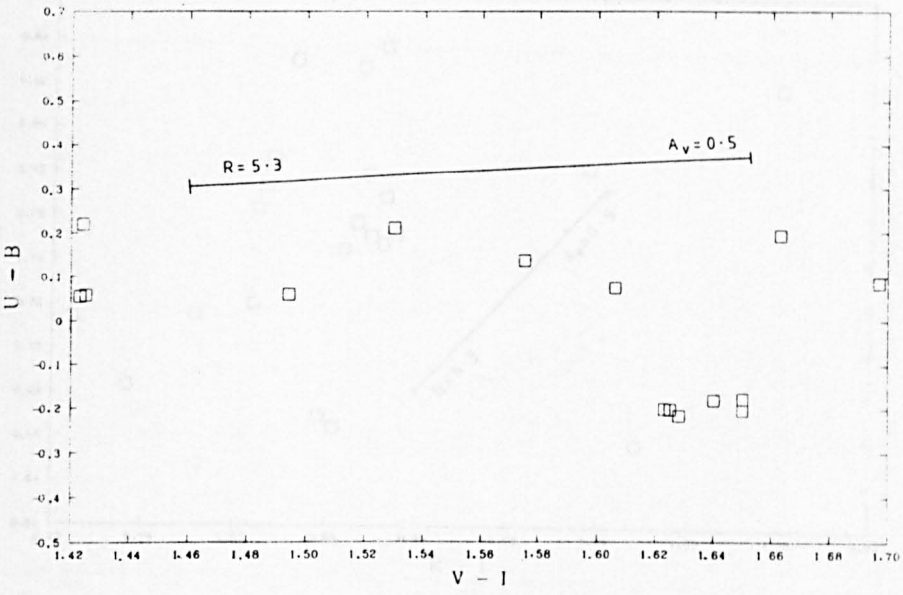

Fig. 4.2.4. V, B-V variation of R CrA.
See also Section 4.2.3.

Fig. 4.2.5. U-B, V-I variation of R CrA.
See also Section 4.2.3.

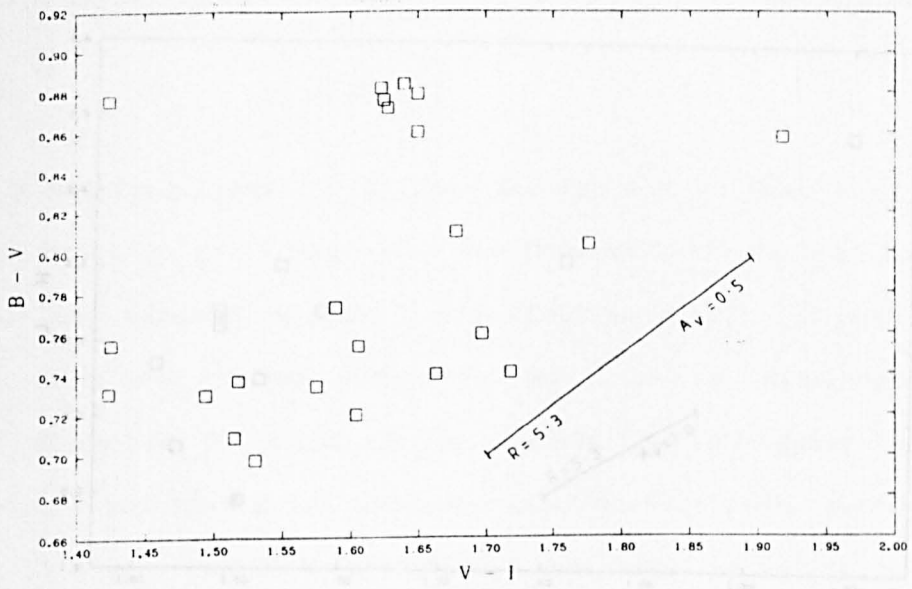

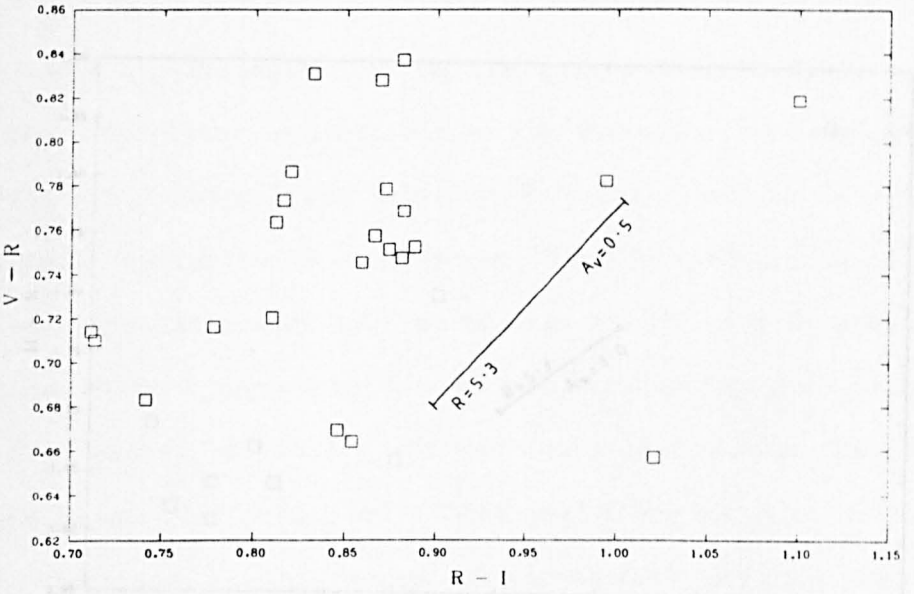

Fig. 4.2.6. B-V, V-I variation of R CrA. See also Section 4.2.3.

Fig. 4.2.7. V-R, R-I variation of R CrA. See also Section 4.2.3.

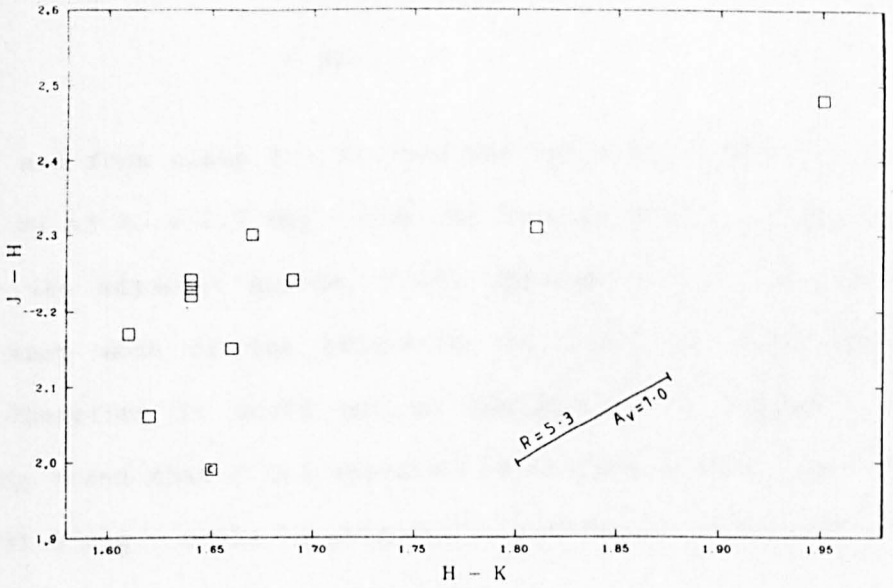

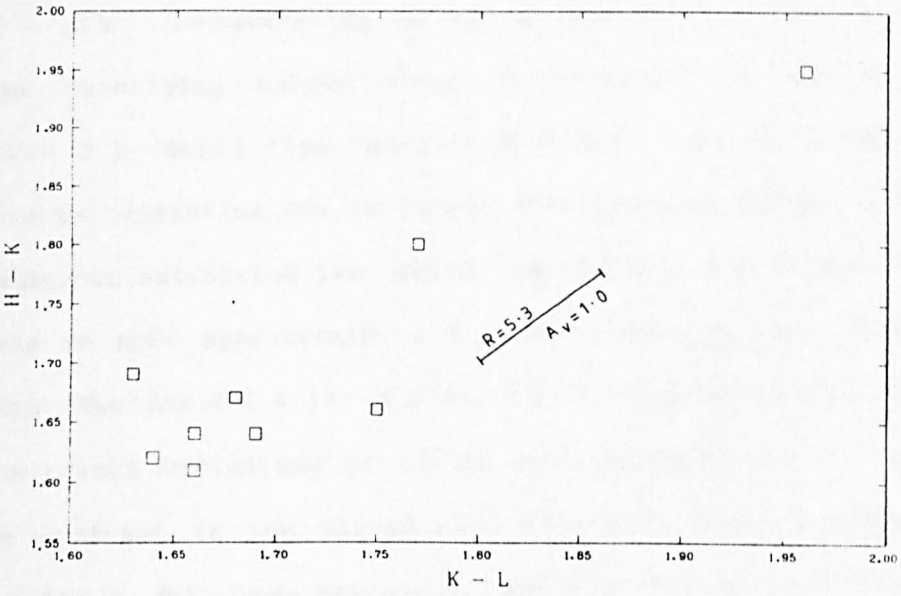

Fig. 4.2.8. J-H, H-K variation of R CrA. See also Section 4.2.3.

Fig. 4.2.9. H-K, K-L variation of R CrA. See also Section 4.2.3.

- late F and from class I - II (see Section 4.2.1). Now, as R CrA is reddened by an $A_V \simeq 3.7$ mag. (Thé and Dawanas 1987), cf. an $A_V \simeq 1.9$ mag. for the adjacent source, T CrA (Section 4.1.3), it would seem evident that much of the extinction of R CrA is circumstellar in origin. Therefore it would not be implausible to suggest that the underlying trend that R CrA appears redder when fainter, particularly for $V \gtrsim 11.8$ mag., could be potentially ascribable to variation in the degree of the circumstellar extinction.

Thé and Dawanas (1987) indicate an anomalous extinction law for R CrA (R = 3.3). Concentrating on the points fainter than $V \simeq 11.8$ mag., the underlying colour slope of variation is steeper than $\Delta V/\Delta(B-V) = 3.1$ (solid line labelled **R = 3.1**), and it is suggested that variable extinction due to larger than IS-sized grains, i.e. a R = 5.3 anomalous extinction law (solid line in Fig. 4.2.4 labelled **R = 5.3**) would be more appropriate. A R = 5.3 reddening law was derived for TY CrA (Section 4.1.4.1), and was found to describe the observed long-term colour variations of TY CrA well (Section 4.1.3). However, note the contrast in the degree of variability and the scatter in points in the V, B-V plane between TY CrA (Fig. 4.1.8), which exhibits little variation in spectral type and R CrA (Fig. 4.2.4), which exhibits significant variation in spectral type.

The other optical colours are all observed to generally redden as R CrA fades, as can be seen for U-B, V-I (Fig. 4.2.5), B-V, V-I (Fig. 4.2.6) and V-R, R-I (Fig. 4.2.7). If the degree of scatter of points about a $R \simeq 5.3$ locus (solid line) in each colour-colour diagram is attributed to changes in effective temperature (from the known variation in spectral type), and in addition, the more pronounced scatter at V-R and R-I is attributed to contamination from the

variable Hα line, it is suggested that the underlying, long-term (i.e. ≈ days - months) colour behaviour could plausibly be accounted for by variable circumstellar extinction by large grains.

The set of five observations obtained on HJD 2444866 mentioned above are notable as they represent a significant departure from the behaviour expected by variable extinction. Contrast the observed values from that night of V ≈ 11.5 mag., U-B ≈ - 0.20 and B-V ≈ 0.88 with the mean values of <V> = 10.74 mag., <U-B> = 0.10 and <B-V> = 0.56 (Herbig and Rao 1972). Now, all the optical colours were significantly redder than is typical for R CrA at V ≈ 11.5 mag., *except* the U-B colour which was bluer than is typical of R CrA at any light level. The red optical colours can best be attributed to R CrA exhibiting a much later spectral type at this time than is usual (i.e. ≈ A5), although no other observations were obtained either side of HJD 2444866 to estimate the length of time R CrA remained in this state. The anomalously blue U-B colour at this epoch could potentially be attributable to free-free, free-bound continuum emission affecting the size of the Balmer jump at this time, although such continuum emission (as may possibly arise from the highly excited extended chromosphere) is not known to be usually evident in R CrA.

The near-IR colour-colour plots (Figs. 4.2.8 and 4.2.9) show that the variations between the colours are fairly well correlated, and lie fairly well along the slope delineated by a R = 5.3 reddening law (solid line). The point with an inscribed letter C in Fig. 4.2.8 was from an observation obtained at CTIO.

The strong IR excess of R CrA is likely due to emission from dust (e.g. Thé and Dawanas 1987). However, the typical extent of the near-IR colour variability (except for the two reddest points in each plot)

and the near-IR colour slopes are not incompatible with the variability in the near-IR being essentially attributable to changes in the circumstellar extinction. The two reddest points in both plots would require several magnitudes of visual extinction, and thus are almost certainly due to the strength of the dust emission being intrinsically much weaker than is usual.

Thus it is clear that the notable optical variability observed almost certainly reflects the significant variation in spectral type exhibited by R CrA, and further, it is suggested that R CrA is also affected by variable circumstellar extinction by larger than IS-sized grains. Simultaneous photometric and spectroscopic monitoring of R CrA would be extremely useful in delineating the extent of the contribution of both mechanisms to the optical light variability of R CrA. The near-IR variations can, in part, be ascribed to changes in the line-of-sight opacity, cf. the interpretation of the polarimetric variability of R CrA in Section 4.2.5, although variability in the strength of the dust emission is also evident.

4.2.4. The Flux Distribution.

As R CrA radiates much of its energy in the IR, an understanding of the nature and origin of the IR continuum excess will be important if R CrA is to be fully understood.

The photometry of R CrA from 4.4 - 20μm obtained at SAAO in July and September, 1987 will be used here to determine the physical parameters of R CrA. As the spectral type of R CrA was estimated to be mid - late A in July, 1987 (see Section 4.2.2.1), despite the known variation in spectral type, it is unlikely that from July to September

the effective temperature of R CrA would be very different from $T_{eff} \simeq$ 8500K. The strength of the Balmer lines and the size of the Balmer jump would not be inconsistent with the usual luminosity classification of a bright giant (e.g. Kholopov et al., 1987), and thus a log g = 3 was assumed throughout, although as no photometry at U was obtained, the value of the gravity used is not an important parameter in fitting the photometry. Therefore Kurucz (1979) models with $T_{eff} \simeq$ 8500K and log g = 3 were initially adopted in fitting the photometry.

In this work (see Section 4.1.2.1) the IS reddening (denoted $E(B-V)_{IS}$) for stars within the R CrA cloud has been determined to be 0.17. After this correction for the IS reddening, the photometry is then dereddened for the significant cloud and circumstellar reddening, which will be denoted by $E(B-V)_{CS}$ (as in TY CrA), until a good fit to the BV and I photometry points (the R point is not reliable due to Hα emission) is obtained to the adopted 8500K model atmosphere.

Now, the circumstellar reddening law of R CrA (Thé and Dawanas 1987) is known to be anomalous, R ≃ 3.3. Although the optical colour slopes exhibit a significant degree of scatter, the underlying colour variability may well indicate that an anomalous reddening law for the circumstellar grains with R = 5.3 would not be inappropriate (Section 4.2.3). Therefore the circumstellar reddening was removed using a R = 5.3 reddening law.

Overall, it was found that the optical photometry dereddened by an $E(B-V)_{CS}$ = 0.61 could be well fitted with a T_{eff} = 8500K model atmosphere, *except* for the photometry obtained on HJD 2446998 and HJD 2447040, when the fits were clearly not as good. The dust shell parameters of the fits obtained to the dereddened photometry are tabulated in Table 4.2.1. Note that the difference between the value

Table 4.2.1.

Parameters of the fits to the photometry of R CrA.

Date (HJD)	T_1 (K)	$(R/D)_1$ ($R_\odot kpc^{-1}$)	T_2 (K)	$(R/D)_2$ ($R_\odot kpc^{-1}$)
2446998	1300	1680	-	-
2447040	1300	1770	-	-
2447041	1300	1770	300	18300
2447042	1300	1790	300	20800
2447044	1300	1740	300	23200
2447048	1300	1750	-	-
2447050	1300	1760	-	-

The parameters of the blackbody fits to the 1987 photometry of R CrA are given, where T_1 and T_2 represent the fitted dust temperatures and $(R/D)_1$ and $(R/D)_2$ represent the respective fitted ratio of (radius of fitted blackbody/distance to R CrA) in approriate units.

of the total E(B-V) obtained here of 0.78 and the value of 1.12 obtained by Thé and Dawanas (1987) is attributable to the different spectral type (B - A) and reddening law (R = 3.3) adopted by Thé and Dawanas (1987).

The fit of an 8500K model atmosphere to the HJD 2446998 photometry dereddened by $E(B-V)_{cs}$ = 0.61, photometry which was obtained simultaneously with the optical spectrum discussed in Section 4.2.2, is shown in Fig. 4.2.10. This observation is of particular interest because R CrA was observed to be very red at this time, and also the spectral type at the time was known to be mid to late A (Section 4.2.2.1). The fact that the dereddened photometry could not be well fitted by neither an 8000K nor an 8500K model atmosphere (appropriate for the known spectral type) with an $E(B-V)_{cs}$ = 0.61, indicates that R CrA was particularly red because it was more heavily reddened by circumstellar dust than is usual. An additional reddening correction of E(B-V) ≃ 0.16 (i.e. giving $E(B-V)_{cs}$ = 0.77) with R = 5.3 is required to give a good fit to the model atmosphere.

The typical variability of R CrA observed in the near-IR extends out to far-IR wavelengths as R CrA is observed to be variable in the MNQ data obtained over four consecutive nights. To supplement the MNQ photometry obtained when R CrA was brightest at this time (V = 11.76 mag. on HJD 2447042), and thus least likely to be heavily reddened, the appropriately dereddened IRAS PSC (Beichman et al., 1985) data of R CrA was also plotted. The fit to the dereddened dataset is shown in Fig. 4.2.11. The fit was obtained with an 8500K stellar component, and three blackbody components with temperatures of 1300K, 300K and 80K, cf. Thé and Dawanas (1987) fitted four blackbody components, with temperatures of 1285K, 367K, 116K and 33K to their data (plus IRAS

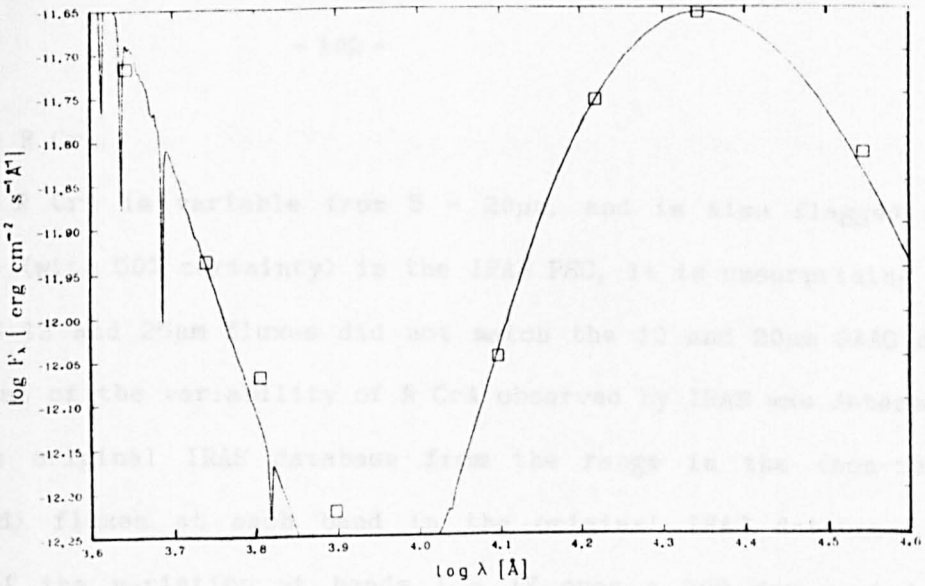

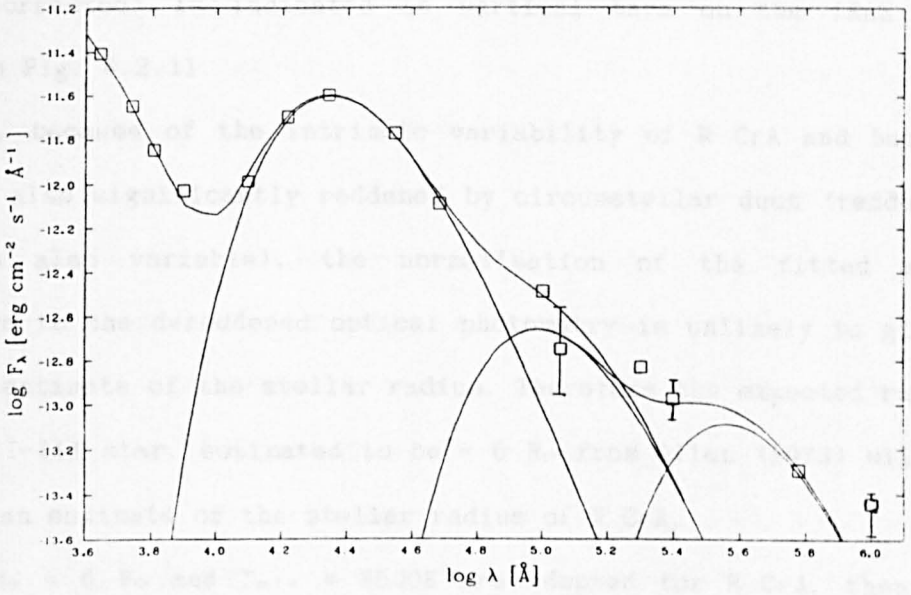

Fig. 4.2.10. Flux distribution of R CrA on HJD 2446998. See also Section 4.2.4.

Fig. 4.2.11. Flux distribution of R CrA on HJD 2447042 with IRAS data included. Vertical bars on the IRAS points indicate the range of variability observed by IRAS.
See also Section 4.2.4.

data) on R CrA.

As R CrA is variable from 5 - 20μm, and is also flagged as a variable (with 50% certainty) in the IRAS PSC, it is unsurprising that the IRAS 12 and 25μm fluxes did not match the 10 and 20μm SAAO data. The extent of the variability of R CrA observed by IRAS was determined from the original IRAS database from the range in the (non-colour corrected) fluxes at each band in the original IRAS database. The extent of the variation at bands I - IV over a 200 day period was ≃ 40, 60, 8 and 180 Jy respectively. The range of variation (not colour corrected) is indicated as vertical bars on the IRAS data points in Fig. 4.2.11.

Now, because of the intrinsic variability of R CrA and because R CrA is also significantly reddened by circumstellar dust (reddening which is also variable), the normalisation of the fitted model atmosphere to the dereddened optical photometry is unlikely to give a reliable estimate of the stellar radius. Therefore the expected radius of an A5II-III star, estimated to be ≃ 6 $R_\odot$ from Allen (1973) will be taken as an estimate of the stellar radius of R CrA.

If $R_* \simeq 6\ R_\odot$ and $T_{eff} = 8500K$ are adopted for R CrA, then the calculated luminosity is $L_{Bol} \simeq 170\ L_\odot$. Normalising the bolometric luminosity estimate of 130 $L_\odot$ (at an assumed d = 130pc) obtained by Wilking et al. (1986), to a distance of 150pc (the distance to R CrA adopted in this work) gives $L_{Bol} \simeq 173\ L_\odot$. Therefore stellar parameters of 8500 K, 6 $R_\odot$ and 170 $L_\odot$ for R CrA are considered to be consistent estimates, and will therefore be the values adopted here for further discussion.

From the peaks of the fitted blackbody components in the dereddened power (λF_λ) distribution from combined near- and far-IR

data (including the IRAS PSC data), the total IR luminosity (for d = 150pc) is estimated to be $L_{IR} \simeq 111\ L_{\odot}$. As $L_{Bol} \simeq 170\ L_{\odot}$, this gives $L_{IR}/L_{Bol} \simeq 0.65$.

Now, the balance of radiative equilibrium for a population of "real" (as opposed to grey) circumstellar grains, gives that,

$$r^2 = L_{Bol}(\langle Q_* \rangle / \langle Q_{IR} \rangle)/16\pi\sigma T_d^4 \qquad (4.1)$$

where r is the distance to grains heated to a temperature T_d around a star of bolometric luminosity L_{Bol}, and σ is Stefan's constant. $\langle Q_* \rangle$ is the Planck mean absorption of grains at stellar temperatures, and $\langle Q_{IR} \rangle$ is the Planck mean absorption of grains at grain temperatures. For $a \simeq 0.1\ \mu m$ silicate grains around a cool stellar source ($T_{eff} \leq$ 8500K), $\langle Q_* \rangle \simeq 0.042$ and $\langle Q_{IR} \rangle \simeq 0.0928\ T_{eff}^{-0.3}$ (Mayes 1983).

Assuming a distance of 150pc, the mean value of the normalised (R/D) values for the 1300K blackbody component indicates that the radius of emission from the inner dust shell has an upper limit of $\simeq 260\ R_{\odot}$ from R CrA. This is assuming that the dust shell is optically thick, which in view of the large IR excess and significant extinction ($A_V \simeq 3.5$ mag.) of R CrA is a not unreasonable assumption. From Eq. (4.1) for a star of $T_{eff} = 8500$K and $L_{Bol} = 170\ L_{\odot}$, the corresponding theoretical radius estimate for a thermally heated dust shell at 1300K is 340 $R_{\odot}$. Thus the possibility that the inner dust shell is thermally heated by absorption of stellar radiation would, from theoretical considerations, be not unreasonable.

To consider the likely disposition of the circumstellar dust around R CrA, it will be instructive to consider a quantitative estimate of the overall energy budget of R CrA and then to see if this

is consistent with the assumption that the circumstellar dust is distributed isotropically in a spherical halo around R CrA.

For a spherically symmetric, thermally heated dust shell, it can be shown that,

$$L_{IR}/L_{Bol} = [\ 1 - \exp(-\langle\tau\rangle)\ ] \qquad (4.2)$$

where $\langle\tau\rangle$ is the Planck mean optical depth. For a R = 5.3 anomalous reddening law, the optical depth at a wavelength λ can be estimated from $\langle\tau\rangle$ using the relation

$$\tau(\lambda) = 4667\ \langle\tau\rangle\ (\lambda T_{eff})^{-0.8} \qquad (4.3)$$

(A. Evans 1988, private communication). In Eq. (4.3), T_{eff} is in Kelvins and λ is in microns. The form of this expression is dependent on the adopted reddening law.

With the given ratio $L_{IR}/L_{Bol} \simeq 0.65$, the Planck mean optical depth from Eq. (4.2) is 1.1. With T_{eff} = 8500K and λ = 0.55μm, this gives an estimate for the visual optical depth of $\tau_V \simeq 6.0$. In comparison, the estimate of the actual circumstellar $A_V \simeq 3.2$ mag. implies a value of $\tau_V \simeq 3.0$. Obviously this result is dependent on the assumed reddening law. For a R = 4 reddening law for example, the inferred τ_V would have been 0.88, i.e. much less than the observed visual optical depth.

Thus the assumption that the circumstellar dust is isotropically distributed across 4π steradians is not a good one. As the observed extinction is less than would be expected from the observed IR excess (assuming a R = 5.3 reddening law), it would seem plausible that the

circumstellar dust is, to an extent, confined either to an inclined disc and/or discrete cloudlets. However, it is noted that in the case of a R = 4 reddening law, the result would indicate that the dust is essentially constrained to an edge-on disc. Thus it must be stressed that this result cannot be necessarily taken as being conclusive, as the R = 5.3 reddening law has not been explicitly derived for R CrA.

However, it is noted that the former suggestion would not be inconsistent with the inferred presence of a circumstellar disc from polarimetric mapping of R CrA by Ward-Thompson et al. (1985), and the latter suggestion would not be inconsistent with the occasional significant increases in circumstellar extinction (Section 4.2.3) and the polarimetric variability (Section 4.2.5). Therefore both suggestions are tenable, and a picture of R CrA surrounded by an inner disc with an outer halo of "orbiting" dust clumps would not be inconceivable.

In view of the observations of Ward-Thompson et al. (1985) and the significant IR excess and reddening of R CrA, attempts to resolve a circumstellar dust shell around R CrA when this becomes practicable (e.g. with the Hubble Space Telescope), would be of considerable interest in giving an insight into the spatial geometry of the circumstellar dust shell surrounding R CrA.

4.2.5. Polarimetric observations.

As reviewed in Section 4.2.1, analysis of the polarisation of R CrA would indicate that the polarisation arises in an optically thick region of dust (Vrba et al., 1979) close to R CrA (Serkowski 1969b), strongly indicating that the polarisation arises in a circumstellar dust shell. The fact that the polarisation has been observed

at 18% (Serkowski 1969b), a degree of polarisation higher than could be expected to be produced in an optically thick dust shell containing non-aligned grains ($p \simeq 11$-12%; Daniel 1980), and in view of the polarisation map of Ward-Thompson et al. (1985) (see Fig. 2.3.3), it would seem evident that some degree of grain alignment, presumably magnetic in nature, occurs in a disc-shaped circumstellar shell surrounding R CrA. In the light of this, a disc-like geometry will be assumed in the remaining discussion.

As the wavelength dependence of polarisation peaks at R (Vrba et al., 1979), a comparison with the computed curves in Section 7.2 indicates that the polarisation could be attributable to scattering by $\simeq 0.12\mu m$ graphite grains, but note that the polarisation map of Ward-Thompson et al. (1985) suggests that scattering by partially aligned ferro-magnetic (e.g. iron) grains is not unlikely.

Given that grains may be partially aligned along "frozen-in" magnetic field lines in a circumstellar disc, long-term variability ($\simeq$ months - years) in the polarisation could potentially arise from rotation of a disc. Also short-term ($\simeq$ days - weeks) changes in the structure of the magnetic field, e.g. due to reconnection or "warping" of field lines, could potentially lead to small scale "disorganisation" of grain alignment within the disc, thereby reducing the overall polarisation. However, realignment of grains (i.e. leading to an increase in the overall degree of polarisation) would be expected to occur only on a timescale of many years. Thus whilst it is conceivable that gradual, long-term changes in the degree of polarisation can occur due to large scale motion of frozen-in field lines, it is more difficult to see how changes in the actual magnetic field structure within the disc could give rise to anything other than

short-term *decreases* in the observed degree of polarisation.

The polarisation of R CrA was followed closely at SAAO (using a clear filter) over a period of ten days in September, 1987. Over this ten day period R CrA exhibited a steady rise in polarisation from p ≃ 1.5% to p ≃ 7% (Fig. 4.2.12). This rise in polarisation is similar in scale (a rise of 5% over 10 days) to the rise observed by Serkowski (1969b), with a rise of 10% over 38 days.

Two things are notable from these observations. One is the rapid (≃ days) rise in the polarisation and the second is the low level of polarisation observed over the first few days - in only the last two observations is the polarisation observed to be at a similar level to the more "typical" level of ≃ 7% (Section 4.2.1).

In view of the rapid rise seen in the polarisation, the bulk of the scattering dust must lie close in to R CrA, within about several light hours to a light day. i.e. less than ≃ 200 A.U. With changes in the magnetic field structure within the disc being considered unlikely as a plausible mechanism for a rapid increase in the polarisation (see above), two alternative mechanisms for the rapid variability are therefore considered: variation in the illumination of the dust shell (cf. Section 7.4) or structural changes in the dust shell.

From simultaneous photometry obtained over this period, the concurrent photometric variations are complex. The behaviour of V and B-V over the ten day period are shown in Figs. 4.2.13 and 4.2.14 respectively. As R CrA is observed to both redden whilst fading (between HJD 2447048 and HJD 2447050) and become bluer whilst fading (HJD 2447042 and HJD 2447044), the light and colour variations are probably due to simultaneous changes in the circumstellar dust shell opacity and in the intrinsic emission from R CrA (cf. Section 4.2.3).

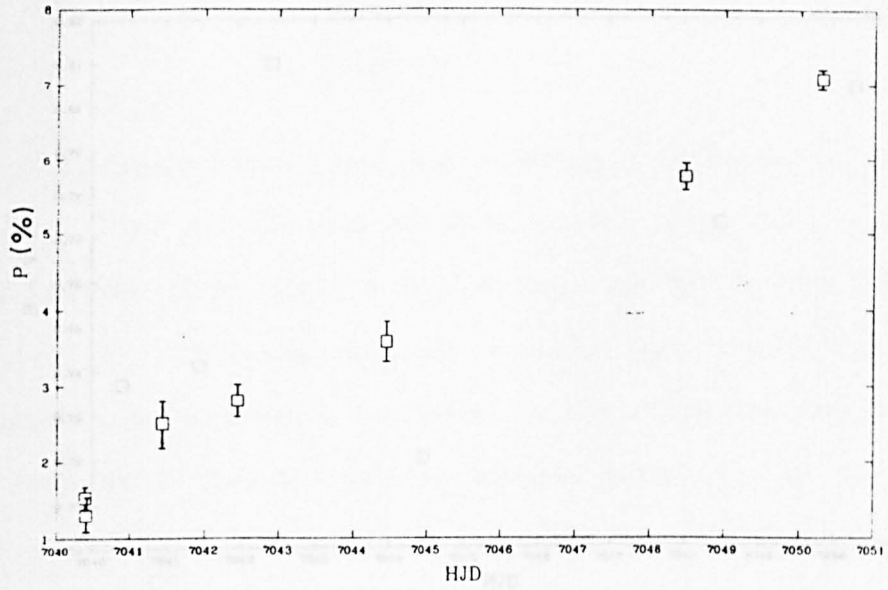

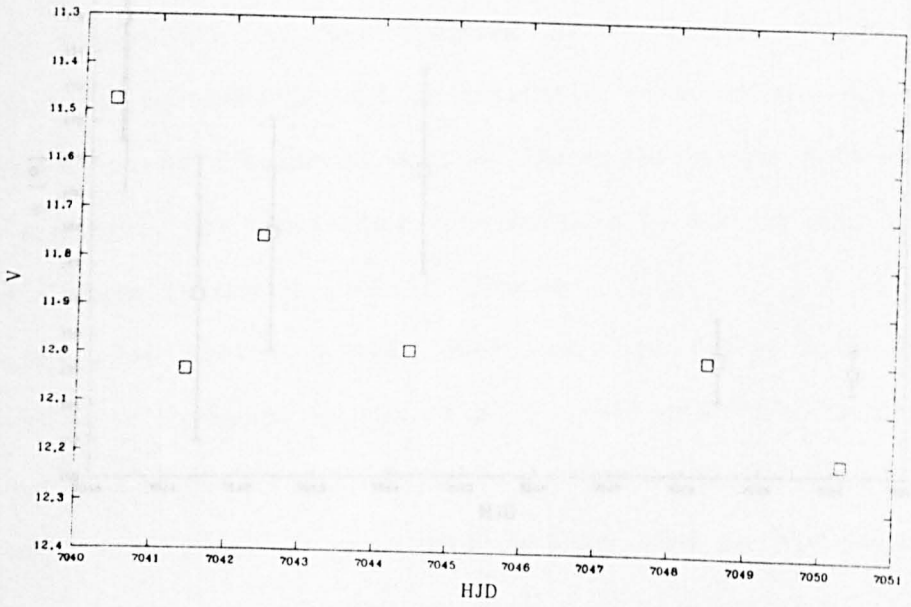

Fig. 4.2.12. The optical polarisation of R CrA observed from HJD 2447040 to HJD 2447050. The date is given in HJD 2440000+ and the polarisation in %. See also Section 4.2.5.

Fig. 4.2.13. The V photometry of R CrA observed from HJD 2447040 to HJD 2447050. The date is given in HJD 2440000+. See also Section 4.2.5.

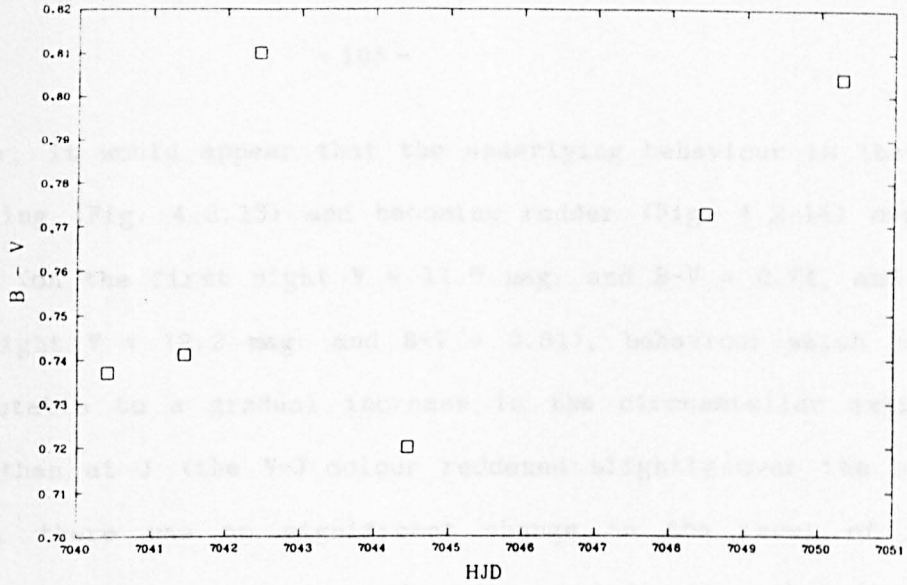

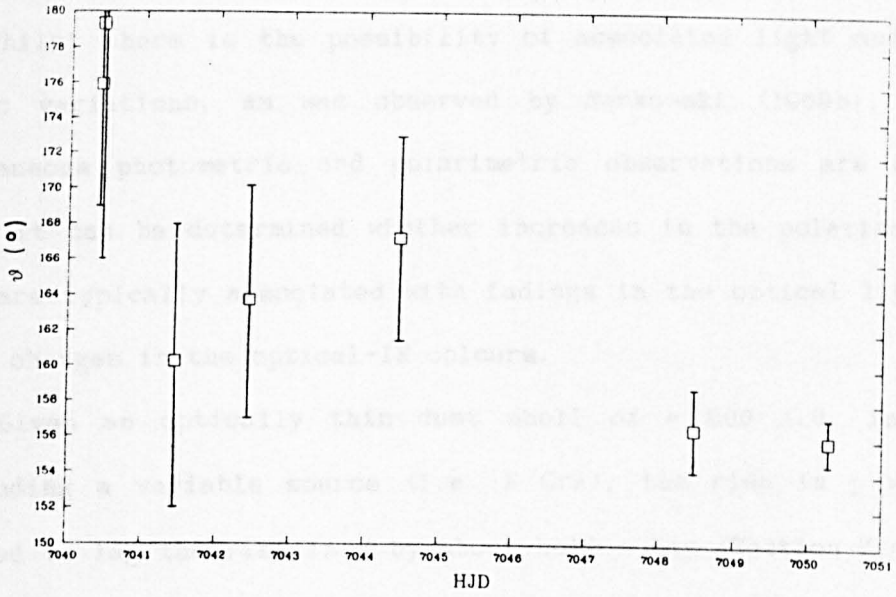

Fig. 4.2.14. The B-V colour of R CrA observed from HJD 2447040 to HJD 2447050. The date is given in HJD 2440000+. See also Section 4.2.5.

Fig. 4.2.15. The position angle of R CrA observed from HJD 2447040 to HJD 2447050. The date is given in HJD 2440000+ and the position angle in degrees. See also Section 4.2.5.

However, it would appear that the underlying behaviour is that R CrA is fading (Fig. 4.2.13) and becoming redder (Fig. 4.2.14) over this period (on the first night V ≃ 11.5 mag. and B-V ≃ 0.74, and on the last night V ≃ 12.2 mag. and B-V ≃ 0.81), behaviour which could be attributable to a gradual increase in the circumstellar extinction. Other than at J (the V-J colour reddened slightly over the observed epoch), there was no significant change in the level of near-IR emission at this epoch, i.e. there is no indication that there were any significant changes in the heating of the dust at this time.

Whilst there is the possibility of associated light and polarimetric variations, as was observed by Serkowski (1969b), further simultaneous photometric and polarimetric observations are required before it can be determined whether increases in the polarisation of R CrA are typically associated with fadings in the optical lightcurve and/or changes in the optical-IR colours.

Given an optically thin dust shell of ≃ 200 A.U. in extent surrounding a variable source (i.e. R CrA), the rise in p would be expected to lag the rise in V by about half a day (Section 7.4). Even with an optically thick dust shell giving rise to the polarisation, the phase lag between changes in V and p is considered unlikely to be much greater than a day. Therefore the lack of any correlated increase in V with the increase in p would seem to rule out variable illumination of the dust shell as the source of the polarimetric variability.

The variation of the position angle over the observed period is shown in Fig. 4.2.15. Given the observational errors, it would seem that the position angle has rotated by at least 10° over the ten night period. Along with the observed rise in the polarisation, Serkowski (1969b) also observed a rotation in the polarisation angle in both the

blue and visual (although in opposite senses) of a similar extent. Thus it would seem evident that significant changes in the polarisation are accompanied by a change in the position angle, i.e. there is no fixed axis of symmetry. The observed range in position angle is from ≃ 189° (Ward-Thompson et al., 1985) to ≃ 156° (observed in 1987).

The fact that significant changes in the polarisation and position angle occur on a timescale of days, it is suggested that changes in the disposition of dust within the circumstellar disc on this timescale can best account for the polarimetric variability of R CrA. For example, an ensemble of dense "orbiting" condensations associated with the disc could potentially modulate the underlying "intrinsic" degree of polarisation from the disc.

In summary, the polarisation of R CrA is observed to be strongly variable on a timescale of days. The fact that no correlated changes in the photometric brightness nor in the optical-IR colours of R CrA were observed, and also given that light from R CrA is probably polarised by partially aligned grains within a circumstellar dust shell/disc, the rise in the polarisation is attributed to changes in the degree of "diffusion" of polarised starlight within the dust shell/disc by the motion of dense condensations within the dust shell/disc.

4.2.6. Summary and Conclusions.

R CrA exhibits strong line emission, notably Hα, Hβ and a spectrum of FeII emission lines. That HeI lines are also observed indicates that a hotter "chromospheric" region underlies the emission envelope of R CrA. In light of the fact that the spectral type of R CrA is known to be intrinsically variable, changes in T_{eff} are considered to

contribute significantly to the light and colour variations of R CrA. In addition, it is argued that variable circumstellar extinction also plays a not insignificant role in the light and colour behaviour of R CrA, particularly on a timescale of weeks - months. From the colour slope of variation, it is suggested that large grains probably contribute to the (variable) circumstellar extinction. Further, it is also argued that the observed light and polarimetric variability of R CrA would both point towards a degree of "clumpiness" within the circumstellar dust distribution around R CrA, cf. the "shadowing" effect in the illumination of the nebula NGC 6279 discussed by Graham and Phillips (1987).

Adopting an anomalous reddening law of R = 5.3, the intrinsic flux distribution of R CrA is determined. The optical emission from R CrA is found to be consistent with emission from a reddened A5II photosphere and the strong IR excess is interpreted essentially in terms of thermal re-emission from both hot ($\simeq$ 1300K) and warm ($\simeq$ 300K) dust.

The significant degree of polarisation which is generally exhibited by R CrA would be consistent with scattering of starlight by both aligned and non-aligned grains within a dense, possibly flattened circumstellar dust shell.

Therefore the circumstellar environment is determined to be playing a very active role in the observed characteristics of R CrA: line emission and shell absorption (Herbig and Rao 1972) from a circumstellar envelope; significant polarisation and absorption of light by circumstellar dust; IR emission from the circumstellar dust. In view of the presence of substantial circumstellar dust (supposedly remnant material from the process of star formation); the important role of circumstellar dust in the observed characteristics; and in view of the

fact that R CrA is associated with an optical jet (Ward-Thompson et al. (1985), is strongly exciting nebulosity, and is intrinsically variable; it would seem not unreasonable to suggest that R CrA is in a relatively early, "active" stage of visible PMS stellar evolution.

4.3 The Herbig Ae/Be Star T CrA.

4.3.1 Introduction.

T CrA is also associated with the variable nebula NGC 6729 in the R CrA dark cloud. Although R CrA is the dominant illuminating source of the nebula, T CrA does appear to contribute to the illumination at the south-eastern part of the nebula. A faint jet-like structure originating at T CrA, and pointing away from R CrA, is indicated in an optical plate by Ward-Thompson et al. (1985) and, as for R CrA (see Section 4.2.1), they infer the existence of a collimating circumstellar disc around T CrA from their polarisation map (see Fig. 2.3.3). The observed range in the polarisation of T CrA is from 2% (Serkowski 1969b) to 8% (Ward-Thompson et al., 1985).

The range of optical light variation of T CrA is $11.7 < V < 14.5$ mag., and $\langle V \rangle \simeq 11.67$ mag. (Herbig and Rao 1972), suggesting that the star may well spend much of its time towards the bright end of its lightcurve, although T CrA is not assigned a lightcurve class in Herbig and Rao (1972). T CrA is mentioned briefly in Joy's (1945) work on R CrA, where he designates the spectrum of T CrA as F0 and remarks that at minimum light, the spectrum exhibits no unusual spectral features. However, the Hα line is very variable and typically observed in emission (e.g. Herbig and Rao 1972, Marraco and Rydgren 1981).

Herbig and Rao (1972) designate the spectral type as F0eα.

Brown (1987b) failed to detect radio emission at 6cm from T CrA at a 3σ rms limit, implying an upper limit on the ionised mass-loss rate of $\simeq 10^{-8}$ $M_{\odot}yr^{-1}$. Similarly Walter and Kuhi (1981) failed to detect X-ray emission with an upper detection limit of 1.4×10^{30} ergs s^{-1}.

4.3.2. The Optical Spectrum.

The optical spectrum of T CrA, shown in Fig. 4.3.1, was obtained on HJD 2446999 when T CrA was observed photometrically at V = 12.97 mag., i.e. about mid-way in its variability range. The spectrum of T CrA is found to be either F0 (when faint) or F0e (Herbig and Rao 1972), i.e. the spectral type does not vary.

From the strengths of the higher Balmer lines, the observed spectrum of T CrA is F0. However, the Hα line is strongly in emission, and the Hβ line is weaker than expected in a F0 spectrum, and is thus also affected by emission. The strength of the Balmer emission is variable and the Balmer lines are unaffected by emission when the star is faint (Joy 1945). Such emission would indicate that T CrA has a cool envelope or shell with $T_{*} \simeq 6000K$.

The NaI D and CaII K and H resonance lines are also affected by shell emission as they are not as strong as would be expected in a normal F0 spectrum. In addition a spectrum of neutral metallic lines, particularly of FeI, TiI and CrI is seen.

With an appropriate dereddening (with an IS $E(B-V)_{IS} = 0.17$; and a cloud plus circumstellar $E(B-V)_{CS} = 0.4$, assuming a R = 5.3 reddening law) of the spectrum, it can be well fitted to a $T_{eff} = 7000K$, log g = 3.5 Kurucz (1979) model atmosphere appropriate for a F0IV spectral

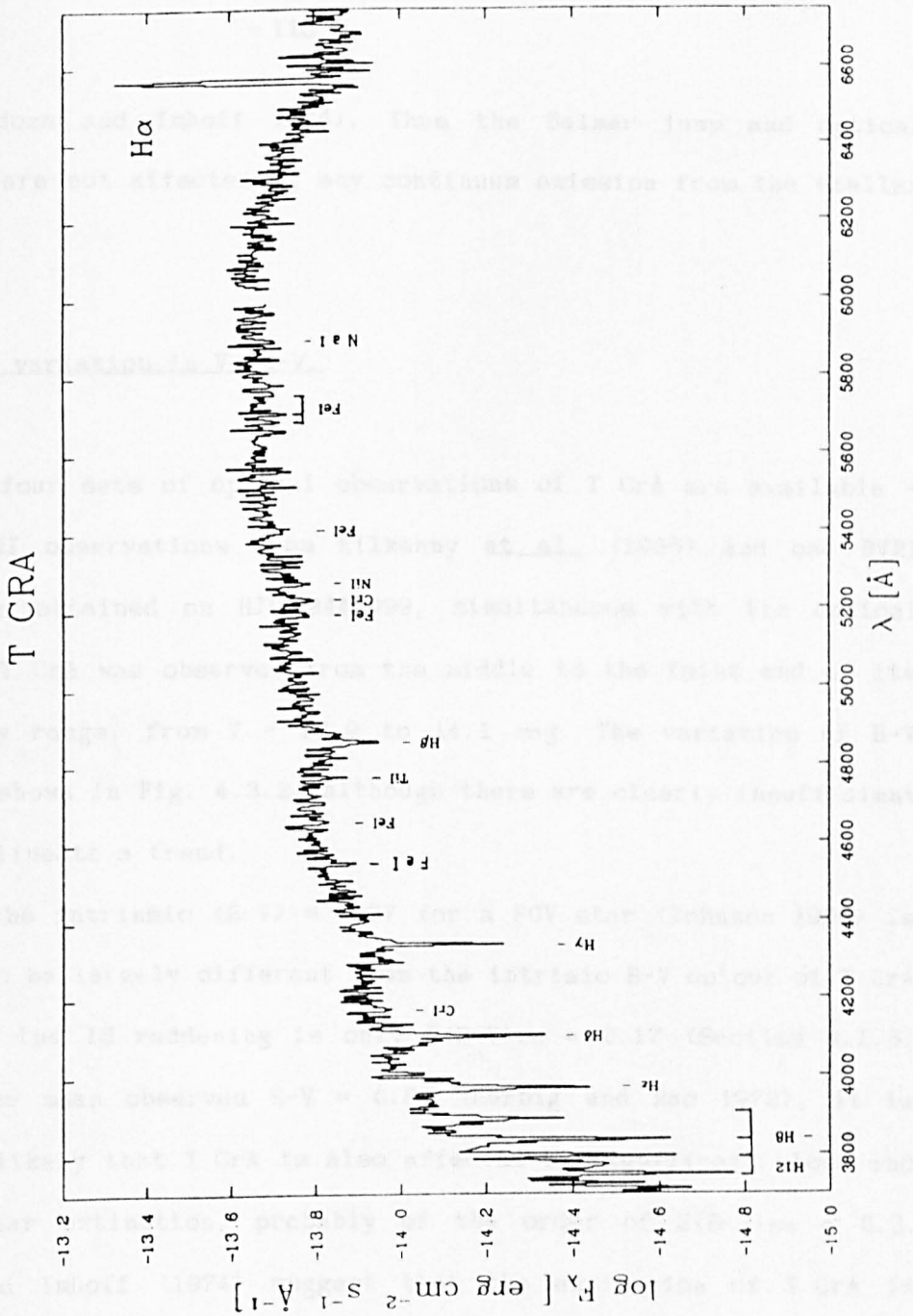

Fig. 4.3.1. Optical spectrum of T CrA.
See also Section 4.3.2.

type (Mendoza and Imhoff 1974). Thus the Balmer jump and optical continuum are not affected by any continuum emission from the stellar envelope.

4.3.3. The variation in V, B-V.

Only four sets of optical observations of T CrA are available - three UBVRI observations from Kilkenny et al. (1985) and one BVRI observation obtained on HJD 2446999, simultaneous with the optical spectrum. T CrA was observed from the middle to the faint end of its variability range, from V = 12.9 to 14.1 mag. The variation of B-V with V is shown in Fig. 4.3.2, although there are clearly insufficient data to delineate a trend.

Now, the intrinsic (B-V) = 0.37 for a F0V star (Johnson 1966) is unlikely to be largely different from the intrisic B-V colour of T CrA (F0IV). As the IS reddening is only $E(B-V)_{IS} \simeq 0.17$ (Section 4.1.3) and the the mean observed B-V = 0.84 (Herbig and Rao 1972), it is therefore likely that T CrA is also affected by significant cloud and circumstellar extinction, probably of the order of $E(B-V)_{CS} \simeq 0.3$. Mendoza and Imhoff (1974) suggest that the extinction of T CrA is probably largely circumstellar in origin. Therefore it would not be implausible that some of the light variations of T CrA could be caused by changes in the circumstellar extinction.

However, the circumstellar reddening law for T CrA is not known. If, like TY CrA and R CrA the circumstellar reddening law is anomalous, then changes in the circumstellar opacity would cause variations in the V, B-V plane which are steeper than $\Delta V/\Delta(B-V) = 3.1$. It is not unreasonable to suggest that the three observations when

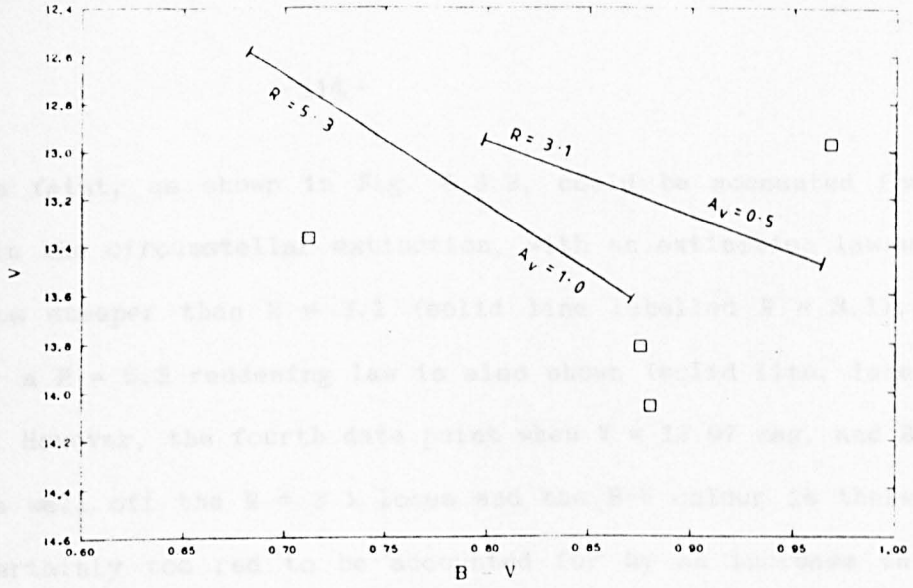

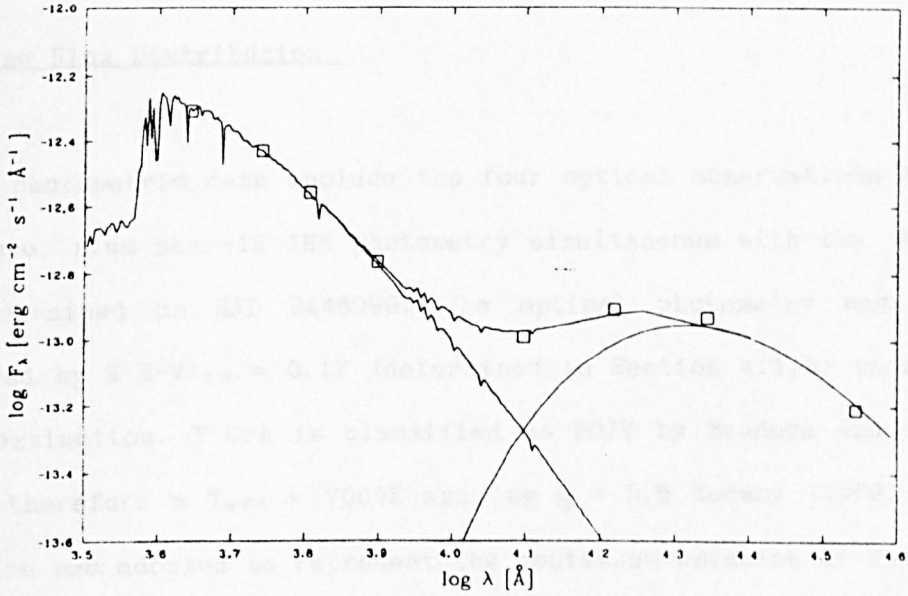

Fig. 4.3.2. V, B-V variation of T CrA. See also Section 4.3.3.

Fig. 4.3.3. Flux distribution of T CrA observed on HJD 2446999. See also Section 4.3.4.

T CrA was faint, as shown in Fig. 4.3.2, could be accounted for by changes in the circumstellar extinction, with an extinction law which is perhaps steeper than R = 3.1 (solid line labelled **R = 3.1**). The locus for a R = 5.3 reddening law is also shown (solid line, labelled **R = 5.3**). However, the fourth data point when V = 12.97 mag. and B-V = 0.97 lies well off the R = 3.1 locus and the B-V colour is therefore almost certainly too red to be accounted for by an increase in the circumstellar extinction.

4.3.4. The Flux Distribution.

The photometric data include the four optical observations discussed above, plus near-IR JHK photometry simultaneous with the observations obtained on HJD 2446999. The optical photometry was first dereddened by $E(B-V)_{IS}$ = 0.17 (determined in Section 4.1.3) to remove the IS extinction. T CrA is classified as F0IV by Mendoza and Imhoff (1974), therefore a T_{eff} = 7000K and log g = 3.5 Kurucz (1979) model atmosphere was adopted to represent the continuum emission of T CrA.

The circumstellar reddening law however is not known and thus fits to the adopted model atmosphere were carried out for both the normal IS reddening law (R = 3.1) and the anomalous cloud reddening law (taken to be R = 5.3). The anomalous extinction law adopted required a cloud plus circumstellar $E(B-V)_{CS} \simeq 0.4$ to fit the data to the model atmosphere, a value which is quite reasonable considering the estimate of the likely $E(B-V)_{CS} \simeq 0.3$ in Section 4.3.2. In contrast an $E(B-V)_{CS} \simeq 0.85$ is required to fit the data assuming a normal reddening law. Thus an anomalous reddening law for T CrA is considered to be more consistent with the observed colours of T CrA, and a R = 5.3 reddening

law is therefore adopted in dereddening the data. The fit of the dereddened BVRIJHK observations obtained on HJD 2446999, when V = 12.97 mag., to the model atmosphere is shown in Fig. 4.3.3. The fit to the near-IR excess was achieved with an additional 1400K blackbody component.

T CrA exhibits a notable increase in brightness from near-IR out to far-IR wavelengths from K ≃ 6.0 mag., through m(λ=12.6μm) ≃ 1.6 mag. (Vrba et al., 1976) and Q ≃ 1.0 mag. (Wilking et al., 1985). Therefore the IRAS PSC (Beichman et al., 1985) was searched for a far-IR source which could be identified with T CrA. However, no IRAS source was found to be co-incident (within the IRAS positional uncertainties) with the optical position of T CrA, the nearest adjacent IRAS source being the strong far-IR source R CrA. It would thus seem likely that at far-IR wavelengths, T CrA is dominated by its brighter neighbour R CrA (Q ≃ -3 mag., Wilking et al., 1985).

Assuming a radius of 1.5 $R_\odot$ (appropriate for a F0V star, Allen 1973), an effective temperature of 7000K and hydrostatic equilibrium, it is estimated that $L_{Bol} \simeq 4.8\ L_\odot$, a theoretically determined value which is consistent with the observational upper limit on L_{Bol} of 5 $L_\odot$ indicated by Wilking et al. (1985). Therefore values of 1.5 $R_\odot$, 7000K and 4.8 $L_\odot$ for the stellar radius, effective temperature and bolometric luminosity respectively are considered to represent the actual physical parameters of T CrA well.

If the far-IR data of Wilking et al. (1985) are included with the near-IR data obtained on HJD 2446999, the ratio L_{IR}/L_{vis} is estimated to be ≃ 3.1, a value which is independent of the assumed distance. This value compares well with the ratio of 2.5 determined by Knacke et al. (1973). Therefore about 60 - 75% (corresponding to $L_{IR}/L_{vis} = 2.5$

and 3.1 respectively) of the total luminosity of T CrA is emitted in the IR. In view of the form of the IR excess (fitted by a 1400K blackbody) and the not insignificant circumstellar reddening of T CrA, it is not unreasonable to interpret the near-IR excess of T CrA in terms of emission from thermally heated circumstellar dust.

4.3.4. Summary and Conclusions.

T CrA exhibits a F0IV spectrum with envelope emission affecting Hα, Hβ and the CaII and NaI resonance lines. In view of the fact that the spectral type is non-variable and that the observed continuum is unaffected by free-free envelope continuum emission, it is considered unlikely that the light variations of T CrA are due entirely to intrinsic changes in the continuum emission. As T CrA is reddened by circumstellar dust, it would therefore seem plausible to suggest that T CrA is affected by variable circumstellar extinction, although more photometric observations are required. Most of the luminosity of T CrA is emitted at IR wavelengths, and the near- and mid-IR excess can plausibly be interpreted in terms of emission by thermally heated (≈ 1400K) dust.

4.4. The YY Ori star S CrA.

4.4.1. Introduction.

S CrA is a YY Ori star located towards the south west edge of the R CrA dark cloud, and unlike the other bright association members

discussed here, is not associated with bright nebulosity. S CrA has a faint, V ≈ 13.5 mag. companion star (Joy 1945).

The lightcurve has no preference for any particular brightness level and although the light variations are generally irregular, the lightcurve can exhibit a quasi-period of 6.3 days (Herbig and Rao 1972). The observed range of variation is $10.49 < V < 13.2$ mag. (Kholopov et al., 1987). Therefore when S CrA is faint, the faint companion may contribute somewhat to the observed spectrum (see Appenzeller and Wolf 1977).

The optical spectrum of S CrA has been well studied. The extreme nature of the emission-line spectrum (strong Balmer and CaII K and H emission) prompted Joy (1945) to include S CrA in his original study defining the spectral characteristics of the InT stars. He noted that the strong lines were less variable than the other, weaker metallic lines. Amongst other studies of the spectrum include: Herbig and Rao (1972); Rydgren (1977); Marraco and Rydgren (1981). Also, in more recent years the optical spectrum has been extensively studied by European investigators: Appenzeller and Wolf (1977); Wolf et al. (1977); Bertout et al. (1982); Appenzeller et al. (1983); Mundt (1984); Appenzeller et al. (1986).

The characteristics of the optical spectrum of S CrA as elucidated from the above observations can be summarised as follows:

(i) The photospheric spectrum is affected by significant "blue veiling" (so called because the effects are most pronounced at blue wavelengths), ascribable to free-free, free-bound continuum emission, e.g. Appenzeller and Wolf (1977). Thus the underlying photospheric spectrum is typically only visible at red wavelengths. From the strength of the TiO bands observed when the star is faint, the

spectral type has been estimated as ≈ K5 (Appenzeller et al., 1986), although Herbig and Rao (1972) indicate a GV spectral type;

(ii) The majority of the strong lines (HI, FeII, TiII) exhibit variable inverse P Cygni (or YY Ori) line profiles, which thus includes S CrA in the YY Ori sub-class of InT variables (see Section 2.1) first discussed by Walker (1972). The nightly variation of the emission line profiles implies that the region from which these lines arise is extremely active;

(iii) The lowest lines of the Balmer series (with the exception of the strong Hα line) exhibit a very complex YY Ori structure. As well as the usual deep redward displaced absorption, there is also a central absorption reversal, which is slightly blueshifted. The notable variability in the lower Balmer lines, observed from night-to-night may be evidence for a clumpy, rather than a smooth inflow of matter towards S CrA (Appenzeller et al., 1986);

(iv) The observed resonance lines take several forms: LiI 6707Å is a strong photospheric line; the strong CaII K and H lines each have two emission peaks separated by a blueshifted absorption peak (Beals type III P Cygni profile); the NaI D lines have type I P Cygni profiles, with a strong blueshifted absorption feature, and a narrow, unshifted central absorption reversal which is almost certainly IS in origin;

(v) The HeI and HeII lines are considerably narrower than the other emission lines and are virtually unshifted, suggesting that they are formed in a hot, stationary region close to the star;

(vi) The forbidden lines of [OI] and [SII] have blueshifted, asymmetric emission profiles, indicating that they may arise in a bipolar wind. The unshifted [FeII] lines are weaker and their profiles resemble the Gaussian profiles of the permitted FeII lines.

Clearly, from the observed YY Ori profiles of the stronger lines, the envelope of S CrA is dominated by infall, whilst the profiles of the CaII K and H and NaI D resonance lines and the blueshifted forbidden lines indicate that S CrA also has a weak stellar wind.

The usual interpretation of the YY Ori sub-class of InT stars is that they are essentially intermediate between the visually obscured or embedded stage of low-mass PMS evolution and the visible low-mass PMS stars, i.e. YY Ori stars are the precursors of the more "typical" InT stars. In this view, the YY Ori stars have stellar winds which are in the process of dispersing the surrounding nebular matter within which the young star was formed, whilst the accretion of infalling matter onto the emerging protostar is still in its final stages. The youth of S CrA is evident from its position on the H-R diagram (see Appenzeller 1983).

However, this theory of YY Ori stars has not been without its critics and competing hypotheses. One alternative view has been proposed by Mundt (1984), who suggests that the observed inflow results from matter which has been accelerated in the wind, but then falls back towards the star under gravity. He points out that observations suggest that the infalling matter lies close to the star; this, Mundt claims, supports his hypothesis but not the idea that the infalling matter is remnant material from the pre-stellar nebula.

Another suggestion which challenges the usual interpretation of YY Ori stars, is the proposal that the observed emission line characteristics of YY Ori stars are due to infall of accreting matter from a binary companion (Grasdalen 1977). As S CrA has a faint companion, this would at least seem plausible in this case. But as there is no spectroscopic evidence for the motion of a binary companion in the

majority of YY Ori stars, this interpretation of YY Ori stars has gained very little support from other authors.

The UV spectrum of S CrA has been observed at low resolution on IUE by Appenzeller et al. (1980). In common with other YY Ori stars, S CrA exhibits an UV excess. Several emission lines of high ionisation are observed, including the resonance lines of SiIV 1394, 1403A and CIV 1548, 1550A, although these lines are quite weak. The blend of the MgII h and k resonance lines is the strongest emission feature. Also several FeII absorption blends are observable. The 2200A IS feature is pronounced, which is consistent with the value for the total observed reddening of E(B-V) ≈ 0.5 determined by Knacke et al. (1973).

The presence of optical (e.g. HeI) and UV (e.g. CIV) lines of high excitation/ionisation suggests the presence of a hot, accretion shock front formed close to the star by the infall of matter in the envelope of S CrA (Appenzeller and Wolf 1977). Free-free and free-bound emission from the inner, ionised region is expected to contribute to the observed UV and blue continuum (Appenzeller et al., 1980).

The optical polarisation of S CrA has been observed on two nights by Bastien (1985). The observed variation in the polarisation was only slight, and hence Bastien (1987) listed S CrA as a possible polarimetric variable.

4.4.2. The Optical Spectrum.

The optical spectrum of S CrA was obtained on HJD 2446999, whilst the star was at V = 11.77 mag., fainter than the <V> = 11.35 mag. (Herbig and Rao 1972). The observed spectrum of S CrA and the prominent lines which have been identified are shown in Fig. 4.4.1.

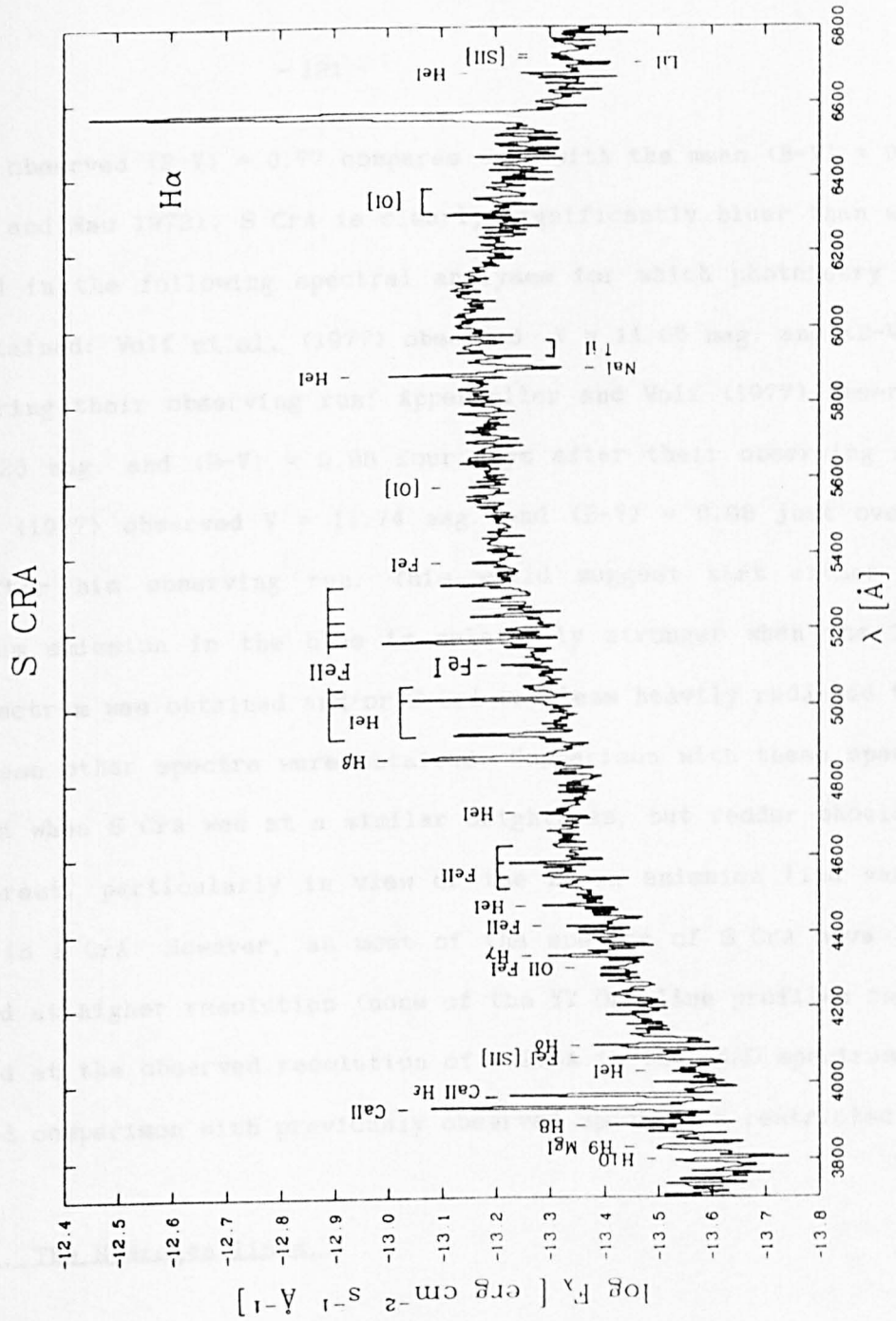

Fig. 4.4.1. Optical spectrum of S CrA observed on HJD 2446999.
See also Section 4.4.2.

The observed (B-V) = 0.77 compares well with the mean (B-V) = 0.78 (Herbig and Rao 1972). S CrA is clearly significantly bluer than when observed in the following spectral analyses for which photometry was also obtained: Wolf et al. (1977) observed V = 11.65 mag. and (B-V) = 0.88 during their observing run; Appenzeller and Wolf (1977) observed V = 11.28 mag. and (B-V) = 0.98 four days after their observing run; Rydgren (1977) observed V = 11.74 mag. and (B-V) = 0.98 just over a week after his observing run. This would suggest that either the continuum emission in the blue is relatively stronger when the 1987 SAAO spectrum was obtained and/or S CrA was less heavily reddened than when these other spectra were obtained. Comparison with these spectra obtained when S CrA was at a similar brightness, but redder should be of interest, particularly in view of the known emission line variability in S CrA. However, as most of the spectra of S CrA have been obtained at higher resolution (none of the YY Ori line profiles can be resolved at the observed resolution of $\simeq$ 2.8Å in the SAAO spectrum), a detailed comparison with previously observed spectra is restricted.

4.4.2.1. The Hydrogen lines.

Because of the limit of the resolution ($\Delta\lambda \simeq 2.8$Å), none of the self-absorption features in even the strongest lines, Hα and Hβ, can be resolved in the 1987 SAAO spectrum. Also, because of the blue veiling, the continuum is difficult to ascertain, particularly at low resolution. Thus a detailed comparison of the structure and fluxes of these lines cannot be made. The Balmer lines from H14 onwards are identifiable.

Rydgren (1977) notes that the peak intensity of the Hα line on 6th

August, 1976 (when S CrA was probably redder than when observed on HJD 2446999 at SAAO; see above) is more than 20 times the intensity of the continuum. In most of the other spectra of S CrA, the Hα line is clearly of a similar intensity, e.g. see Appenzeller et al. (1983). In contrast, in the 1987 SAAO spectrum the peak intensity of Hα was only 10 times as intense as the continuum. Similarly, the other Balmer lines are reduced in strength when compared to many of the other spectrograms of S CrA. Variability in the strength of the Balmer emission of S CrA is particularly well seen in the four spectrograms of Appenzeller and Wolf (1977).

Two near-IR (K and L) spectra of S CrA were obtained at CTIO in June, 1987. The Bγ line at 2.167μm is in emission in the K spectrum, but the possible Pfγ 3.74μm line is lost in the L spectrum due to the light leak around this wavelength. As no prominent lines are observed in the L spectrum, only the K spectrum is shown (Fig. 4.4.2).

4.4.2.2. The Helium lines.

Several HeI emission lines were observed in the optical spectrum. However, because of other strong lines in the spectrum (notably FeII lines) forming blends at the resolution obtained, the presence of some of the possible HeI lines cannot be reliably ascertained.

Lines which are unambiguously present (i.e. unblended lines) are the 4026Å $5d^3$ - $2p^3$, 4471Å $4d^3$ - $2p^3$, 4713Å $4s^3$ - $2p^3$, 5047Å $4s^1$ - $2p^1$, 5875Å $3d^3$ - $2p^3$, and 6678Å $3d^1$ - $2p^1$ lines. Likely blends of HeI lines with FeII lines are the 4921Å $4d^1$ - $2p^1$ (a line previously identified by Appenzeller et al., 1986) and 5015Å $3p^1$ - $2s^1$ (a line not previously identified) HeI lines. For an energy level diagram of

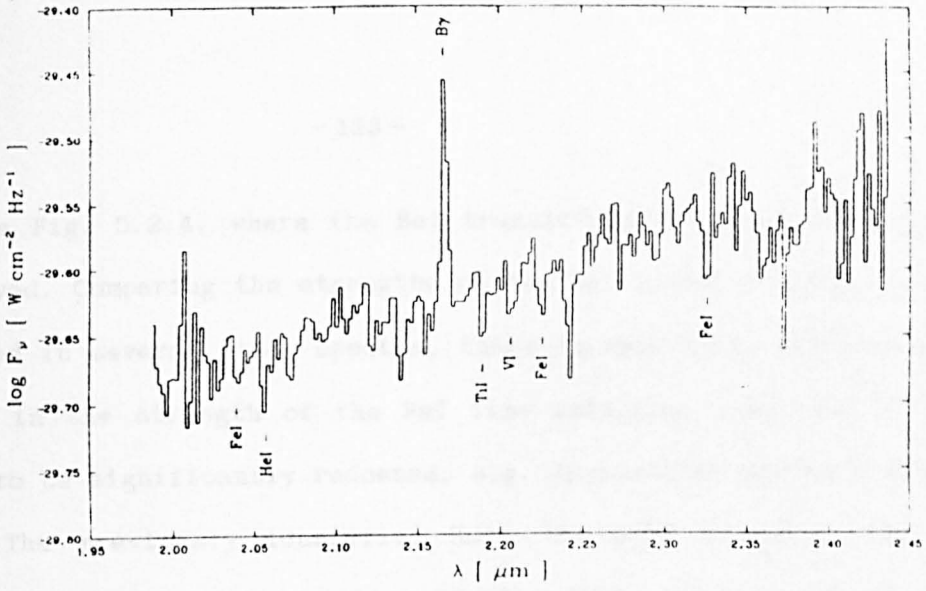

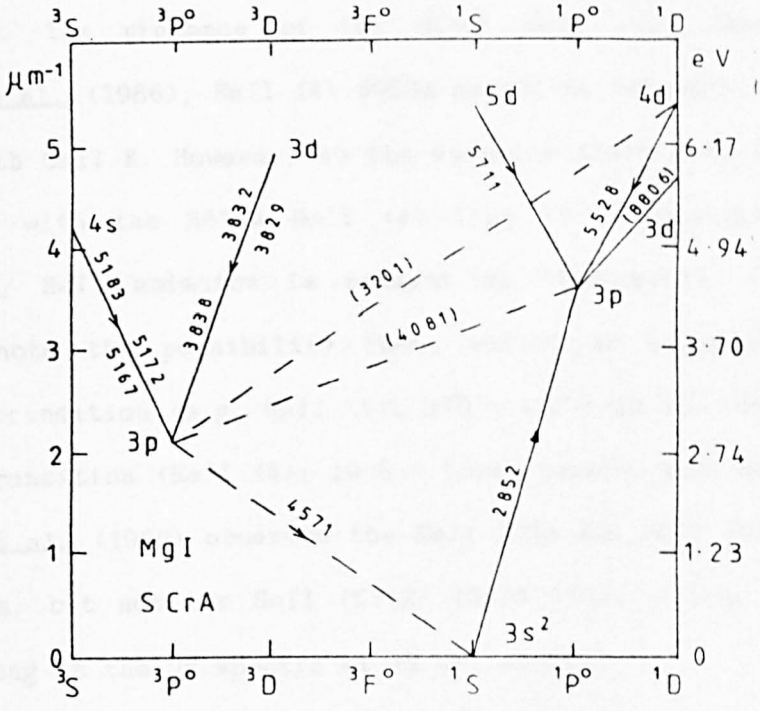

Fig. 4.4.2. K band IR spectrum of S CrA. See also Sections 4.4.2.1 and 4.4.2.2.

Fig. 4.4.3. MgI Grotrian diagram for observed optical transitions in S CrA. Also included is the $3s^2$ - 3p UV transition observed by Appenzeller et al. (1980). See also Section 4.4.2.5.

HeI see Fig. 5.2.4, where the HeI transitions observed in RU Lup are displayed. Comparing the strengths of the HeI lines with the strengths observed in several other spectra, there is seen to be little apparent change in the strength of the HeI line emission, even when S CrA is known to be significantly reddened, e.g. Appenzeller and Wolf (1977).

The previously identified HeII (5) 3781 and HeII (1) 4686Å emission lines (e.g. Appenzeller et al., 1986) are not present in the SAAO spectrum. The presence of the other HeII line observed by Appenzeller et al. (1986), HeII (4) 3923Å cannot be determined because of a blend with CaII K. However, as the emission feature at 3811Å can be identified with the 3814Å HeII (4) line it is plausible that, although weak, HeII emission is present at this epoch. It is of interest to note the possibility that, whilst an expected strong optical HeII transition (e.g. HeII (1): $3^2D - 4^2P^o$) is not observed, a weaker HeII transition (HeII (4): 19^2G - lower levels) may be present. Appenzeller et al. (1980) observed the HeII 2733 and HeII (UV1) 3202Å emission lines, but not the HeII (UV12) 1640Å line, a line which is typically strong in the UV spectra of YY Ori stars.

A comparison with previous spectra would thus suggest that whilst the degree of HeII emission is variable, the degree of HeI emission is not strongly variable. As the observed strength of the HeI lines blueward of $\simeq$ 5200Å will be affected by changes in the strength of the blue continuum emission it is suggested that the intrinsic strength of these blue HeI lines may well scale with the strength of the envelope continuum emission. This would not be inconsistent with both the HeI and the blue free-free continuum emission arising in the same region of the infalling envelope, i.e. the accretion shock (Appenzeller and Wolf 1977). A possible suggestion for the observed variability in the

HeII emission is that the degree of ionisation to HeII may well be dominated by episodic infall of material heating the accretion shock.

In the K spectrum of S CrA obtained at CTIO in June, 1987 (Fig. 4.4.2), the 2.085μm singlet 2p - 2s IR line of HeI was in absorption. As the optical transitions down to the 2p' level are always observed in emission, i.e. the 2p' level is well populated (cf. Fig. 5.2.4, the HeI Grotrian diagram for RU Lup), this is an unexpected result and it is not clear how conditions in the accretion shock could lead to absorption in this line. A possible interpretation may be that there was substantial infall of matter onto the accretion shock at this epoch, with the resultant strong 2.085μm HeI YY Ori line profile appearing as an absorption feature at the observed resolution. It has to be said however that YY Ori profiles have never been observed in the optical HeI lines. Clearly high resolution observations of this IR HeI line (preferably with simultaneous optical spectroscopy) would be of interest.

4.4.2.3. The CaII K and H lines and the FeI fluorescent lines.

From the relative strengths of the H8 and Hδ lines compared to the strong CaII K 3934Å line in the high resolution spectra of S CrA it would seem evident that the major contributor to the feature at 3867Å (a blend of Hϵ and CaII H) is the CaII H 3869Å line. That the CaII K line is of a similar strength when compared with other spectra, when S CrA was known to be redder, indicates that the strength of the CaII K emission is not particularly affected by the strength of the continuum.

However, in most of the previous spectra, the strengths of the

CaII K and H lines are very similar, whereas in the 1987 spectrum, the CaII H, Hε blend at 3967Å is not as strong as CaII K 3869Å. Variation in the relative strengths of the CaII K and the CaII H, Hε blend over one night have been noted by Appenzeller and Wolf (1977). If the CaII H, Hε blend were only marginally weaker than CaII K, then the lower flux could have been attributed to the likely weakness of the Hε line (the Balmer lines are weak at this epoch; Section 4.4.2.1). However, it is difficult to see how the notable shortfall in intensity of the CaII H, Hε blend (dominated by CaII H) could be attributed to a lower Hε flux than is usually observed. Also, it is doubtful whether the contribution of an iron line (either FeI 3930Å or FeII 3930Å; two lines generally not observed) to the flux of the strong CaII K line could account for the discrepency in the intensities of CaII K and H.

It is suggested that a possible explanation of this observation could be the fluorescence effect which results in the enhancement of the FeI (43) 4063.6 and 4132.1Å lines relative to the FeI (43) 3969 and 4071Å lines, i.e. the other FeI lines in the same multiplet. The fluorescence process is due to absorption of 3968.5 CaII H and 3970.1Å Hε photons via the FeI (43) 3969Å transition, which effectively "pump" the $^3F^o$ state by the 3969.3Å transition from the ^3F level, resulting in the enhanced emission observed in the 4064 and 4132Å lines (Joy 1945). The reader is referred to the FeI Grotrian diagram of RU Lup, Fig. 5.2.6 (see also Section 5.2.2.5), where the relevant transitions discussed here can be seen.

When the CaII K and H lines are of similar intensity, Hε is presumed to be the predominant "pumping" line. But as the CaII H, Hε blend is observed to be weaker than the CaII K line in the 1987 spectrum, it is conceivable that, at this epoch, the "missing" flux

from the CaII H line is also contributing to the FeI fluorescence process. Such a process is not implausible, as the CaII K and H and the FeI (43) fluorescent lines may well have a common region of formation, as is found in solar flares.

4.4.2.4. The NaI D resonance lines.

The NaI D resonance lines at 5890 and 5896Å cannot be resolved in the 1987 spectrum, although they do form a very strong absorption feature centred at 5894Å. In the higher resolution spectra, the NaI D lines exhibit an emission component and a strong blueward absorption component, indicative of outflow (e.g. Appenzeller et al., 1986). The NaI D emission features are sometimes observed to be stronger than the absorption components, e.g. Appenzeller et al. (1986) and *vice versa*, e.g. Bertout et al. (1982). Evidently, in the 1987 SAAO spectrum the NaI D emission features are weak, and the blueshifted NaI D absorption components dominate the blend. In none of the other spectra of S CrA inspected does the NaI D absorption appear as strong. As the NaI D absorption components are known to be blueshifted, i.e. indicating outflow, and are therefore presumably formed primarily in a stellar wind, it would seem probable that the stellar wind of S CrA was stronger at this epoch than is typically observed.

4.4.2.5. The MgI lines.

An interesting feature of the 1987 spectrum when compared to previous spectra is the strength of the usually weak MgI 3829, 3832 and 3838Å lines (e.g. Appenzeller et al., 1986) which form a wide,

unresolved feature with H9. A weak line which may be present in the blend is FeI 3828Å. It is very doubtful that the H9 line alone could account for the strength and width of this feature.

Strong MgI emission is also observed at 5167 and 5172Å (blended with FeII 5169Å) and at 5183Å. Also the presence of the 4571Å MgI line in emission, a usually inhibited transition, lends support to the identification of these MgI lines, as these MgI transitions (see Fig. 4.4.3) populate the 3p level, which de-populates to the $3s^2$ level via emission of a 4571Å photon. The other two optical MgI lines observed are at 5711 and 5528Å, which both populate another degenerate state of the 3p level. Most of these lines (excepting the 5528Å line) were also observed by Appenzeller et al. (1986), and the transitions are indicated by thin arrows in Fig. 4.4.3. Transitions not observed are indicated by the wavelength of the line being enclosed in brackets.

In view of the observed transitions, the 3p - $3s^2$ transition would be expected, i.e. the MgI (UV1) line would be expected in emission. However, in a 1978 IUE spectrum, the MgI 2852Å line was observed in absorption (a transition indicated in Fig. 4.4.3 by a filled arrow) by Appenzeller et al. (1980). Thus it would seem likely that the MgI lines are strongly variable.

4.4.2.6. The FeII lines.

The strongest lines observed in the optical spectrum of S CrA, after the Hα, Hβ and CaII K and H lines are the FeII lines. In fact many strong FeII lines are observable, many of which are stronger than is generally observed. Notable FeII lines are indicated in Fig. 4.4.4 and listed as follows.

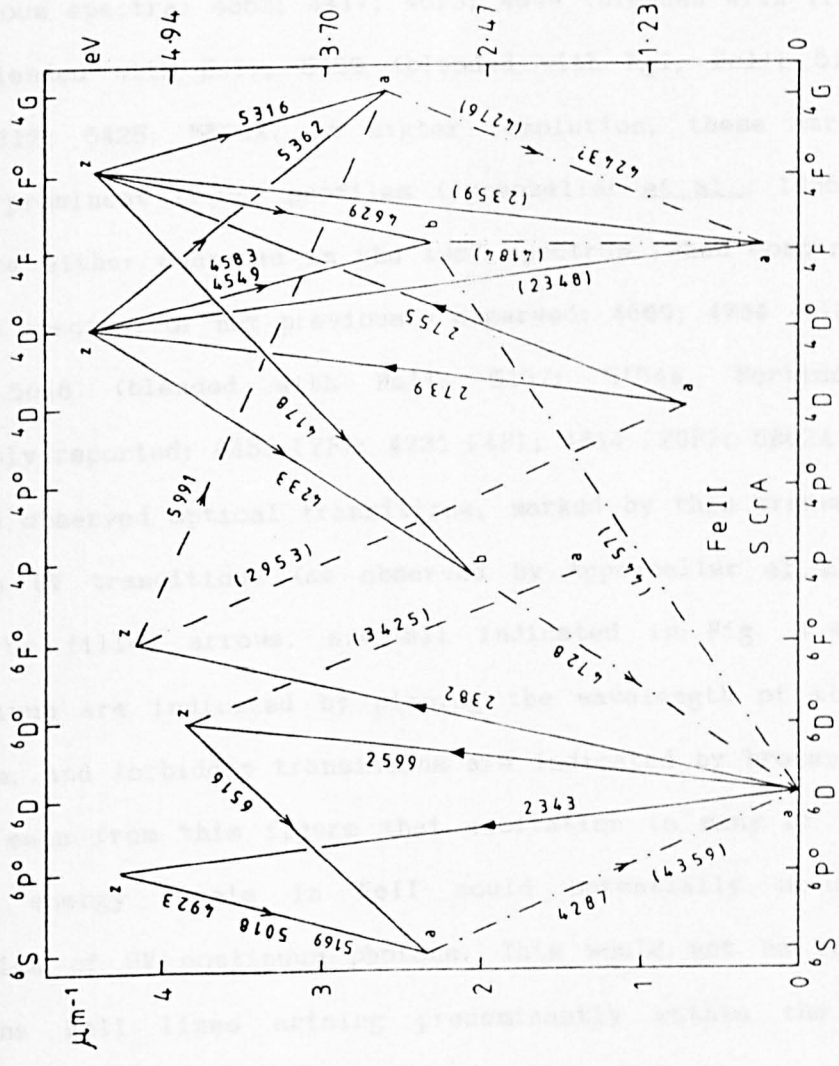

Fig. 4.4.4. FeII Grotrian diagram for observed optical transitions in S CrA. Included are the UV transitions observed by Appenzeller et al. (1980). See also Section 4.4.2.6.

Strong lines observed in the 1987 spectrum which have been observed in previous spectra: 4352; 4417; 4523; 4549 (blended with TiII); 4583; 4924 (blended with HeI); 5169 (blended with MgI, FeI); 5198; 5235; 5276; 5317; 5425; 5525Å. At higher resolution, these strong lines exhibit prominent YY Ori profiles (Appenzeller et al., 1986). Lines which are either enhanced in the 1987 spectrum, when compared to the previous spectra, or not previously observed: 4669; 4764 (blended with TiII); 5018 (blended with HeI); 5137; 5154Å. Forbidden lines previously reported: 4452 [7F]; 4731 [4F]; 4814 [20F]; 5262Å [18F].

The observed optical transitions, marked by thin arrows, and the possible UV transitions (as observed by Appenzeller et al., 1980), marked by filled arrows, are all indicated in Fig. 4.4.4. Other transitions are indicated by placing the wavelength of the line in brackets, and forbidden transitions are indicated by broken lines. It can be seen from this figure that excitation to many of the higher (≈ 5eV) energy levels in FeII could potentially occur by the absorption of UV continuum photons. This would not be inconsistent with the FeII lines arising predominantly within the infalling envelope (Appenzeller et al., 1986), thus lying outside of the accretion shock where the UV excess continuum emission arises (Appenzeller et al., 1980). As both the blue (and thus presumably also the UV) continuum and the FeII emission appear to be strong at this time, this mechanism of excitation of the strong optical FeII lines is not implausible. However, it must be stressed that simultaneous optical and UV spectra would clearly be required to verify this possibility.

As the FeII emission lines are prominent, and also that [FeII] lines are observed, it would seem that excitation of FeII (as with HI; see e.g. Appenzeller and Wolf 1977) may well occur essentially

throughout the stellar envelope.

4.4.2.7. The [SII] and [OI] Forbidden lines.

Weak [SII] 4069, 6715 and 6731Å forbidden lines, and the more prominent [OI] 5577, 6300, 6363Å lines are all observed in the 1987 spectrum. The [SII] lines are known to be particularly variable, and are often not observable. The fact that the [SII] lines are observed and that the [OI] lines are strong in the 1987 spectrum, would not be inconsistent with the suggested enhancement of the stellar wind from the strength of the NaI D absorption (Section 4.4.2.4).

4.4.2.8. The Photospheric lines.

The photospheric continuum is only generally observed redward of ≈ 5200Å, but because of the blue veiling, is only occasionally observed at blue wavelengths when the blue veiling is weak, e.g. (B-V) ≈ 0.98; Appenzeller and Wolf (1977). No strong photospheric lines are observable blueward of ≈ 5500Å in the 1987 spectrum, but given the low resolution of the spectrum, it cannot be determined unambiguously whether the photospheric spectrum at blue wavelengths is strongly veiled or not. Amongst the photospheric lines observed (e.g. TiI and ScI lines), is the characteristic InT LiI 6707Å resonance line.

4.4.2.9. Summary.

A strong optical emission line spectrum is observed, which is dominated by Hα, Hβ, CaII K and H and FeII lines. The Balmer lines are

found to be intrinsically weaker than is typically observed. The CaII H line (blended with Hε) is observed to be weaker than the CaII K line, which may indicate that flux from the CaII H line is contributing to the fluoresence of the FeI (43) 4064, 4132Å lines. It is suggested that the strength of the optical FeII emission should be directly correlated with the strength of the UV continuum emission.

Prominent HeI emission and weak HeII emission lines are observed. The strong HeI triplet lines dominate the HeI emission line spectrum and the 2.085μm IR singlet line is observed in absorption.

The NaI D lines are dominated by an absorption blend and strong [OI] and weak [SII] emission is observed. That these lines are likely formed in a stellar wind, it would seem that the wind at this time was stronger than is typically observed; as they are clearly variable, monitoring of these lines at high resolution would be worthwhile.

4.4.3. The Colour-colour variations.

Optical and IR photometry of S CrA has been obtained at SAAO over the period from 1981 - 1984 (Kilkenny *et al.*, 1985) and during 1987. Unfortunately insufficient observations were obtained to investigate the short-term (≃ days) variability of the lightcurve, and also too few U photometric observations were obtained to permit an analysis of the blue excess continuum emission from the variation in U-B. However, it is noted that the U-B colour did not necessarily redden when S CrA faded and that the observed (U-B) ≃ - 0.20 clearly indicates a considerable blue excess: $(U-B)_{intrinsic} \simeq 0.82$ for a K2V star (Johnson 1966). This blue excess is attributable to free-free emission from the emission envelope (Appenzeller *et al.*, 1980).

The observed variation of B-V with V, shown in Fig. 4.4.5, exhibits the general trend found in InT stars that the colours appear redder when the star is fainter. Although it is noted that over the four observations obtained from HJD 2447041 to HJD 2447048, whilst S CrA brightened and then faded again, B-V remained essentially constant at ≈ 0.80. As can be seen from the reddening line appropriate for a R = 5.3 reddening law (solid line), the V, B-V slope would not be inconsistent with variable circumstellar extinction by large grains. The occasional times when S CrA does not redden at B-V when it fades (such as indicated above) would be explicable in terms of changes occurring in the strength of the stellar continuum and/or the blue continuum emission (as mentioned in Section 4.4.2).

The B-V, V-I and the V-R, R-I colour-colour plots are shown in Figs. 4.4.6 and 4.4.7 respectively. Again, the observed optical colour slopes are relatively well-defined (the greater scatter in V-R, R-I is attributable to the strong, variable Hα line) and are not incompatible with S CrA being affected by variable circumstellar extinction with an extinction law of R = 5.3. It is interesting to note that the three well studied stars in the R CrA cloud, TY CrA, R CrA and S CrA, stars which are intrinsically quite different from one another, should have very similar colour slopes. A plausible interpretation of this would seem to be that they all suffer underlying variable extinction by a similar population of large grains. If so, such grains would presumably be essentially "cloud" grains in the intra-cloud and circumstellar environment associated with each star. Monitoring of other Orion Population stars in this association, e.g. T CrA, VV CrA, DG CrA would be welcomed in determining the colour slope of variation and/or reddening law for these stars.

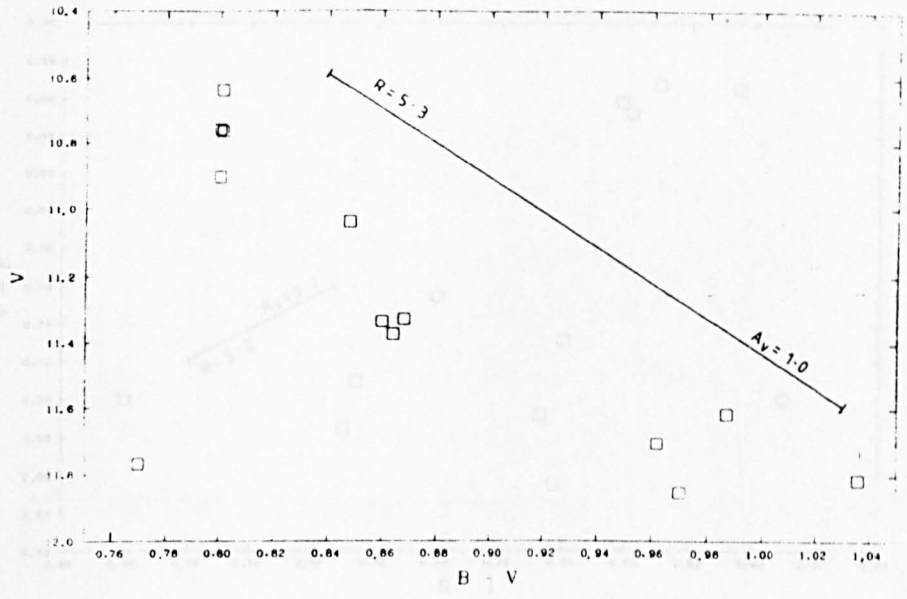

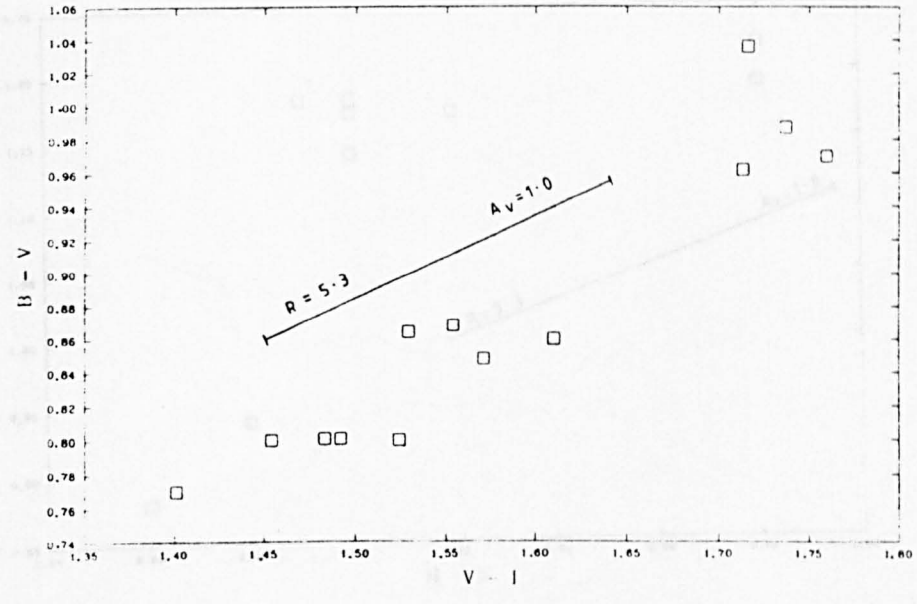

Fig. 4.4.5. V, B-V variation of S CrA.
See also Section 4.4.3.

Fig. 4.4.6. B-V, V-I variation of S CrA.
See also Section 4.4.3.

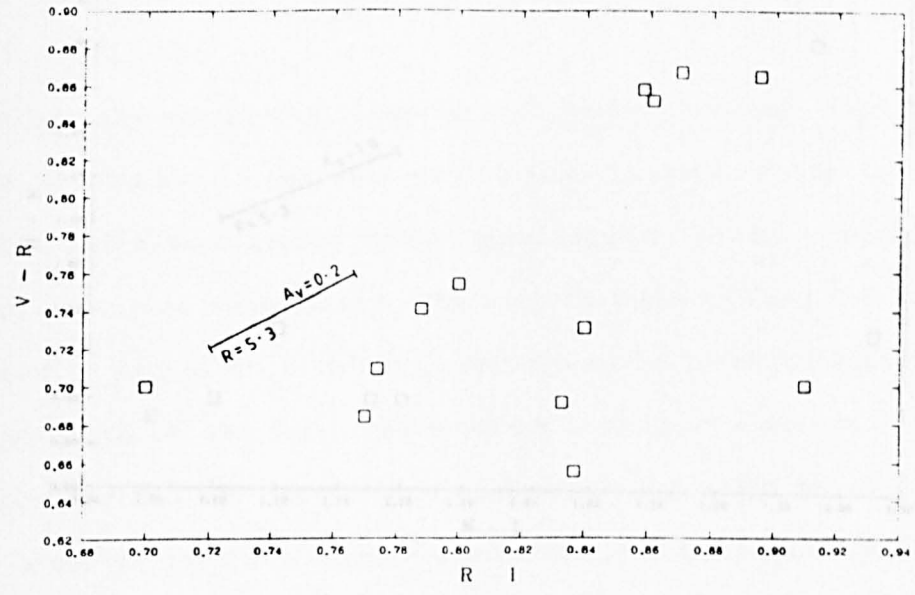

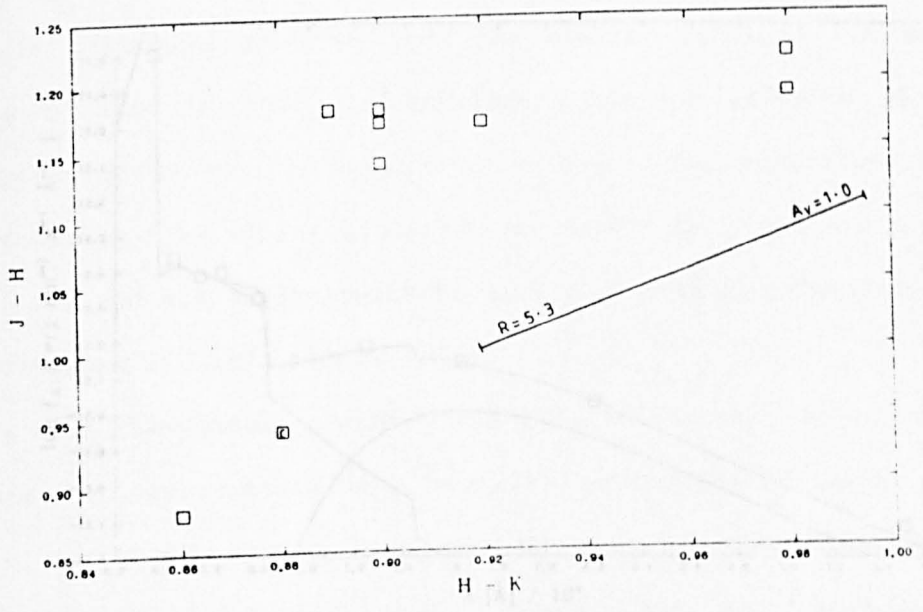

Fig. 4.4.7. V-R, R-I variation of S CrA. See also Section 4.4.3.

Fig. 4.4.8. J-H, H-K variation of S CrA. See also Section 4.4.3.

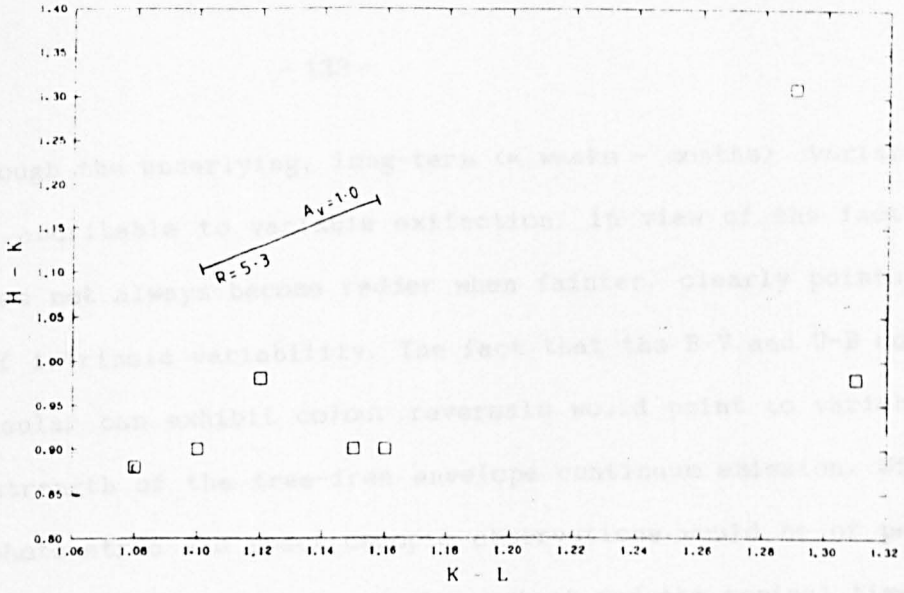

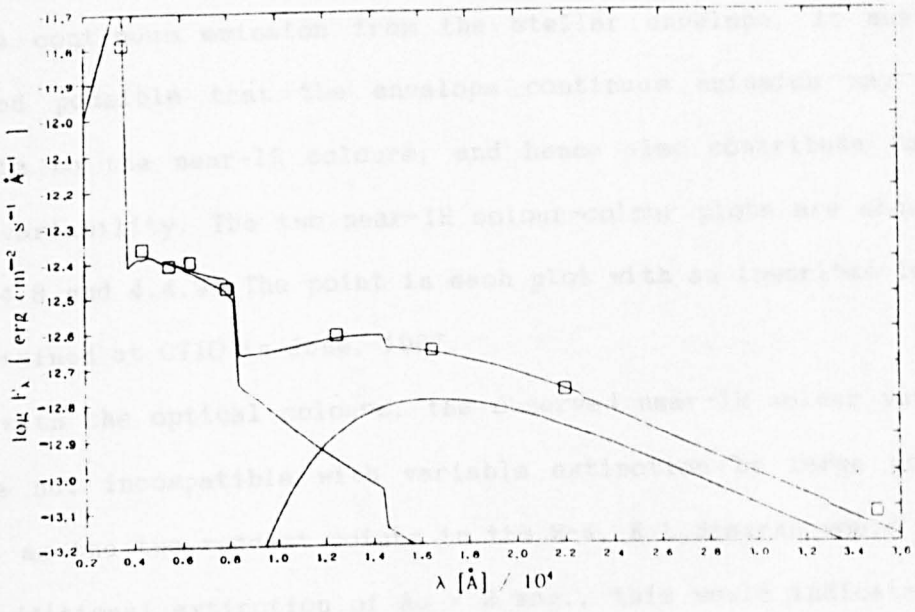

Fig. 4.4.9. H-K, K-L variation of S CrA. See also Section 4.4.3.

Fig. 4.4.10. Flux distribution of S CrA observed on HJD 2445101 (UBVRI) and HJD 2445102 (JHKL). See also Section 4.4.4.

Although the underlying, long-term (≃ weeks - months) variability could be ascribable to variable extinction, in view of the fact that S CrA does not always become redder when fainter, clearly points to a degree of intrinsic variability. The fact that the B-V and U-B colours in particular can exhibit colour reversals would point to variability in the strength of the free-free envelope continuum emission. Simultaneous photometric and spectroscopic observations would be of particular interest in identifying both the extent and the typical timescale of the variability in the continuum envelope emission.

Given that the UV and blue excess of S CrA is attributable to free-free continuum emission from the stellar envelope, it must be considered possible that the envelope continuum emission may also contribute to the near-IR colours, and hence also contribute to the near-IR variability. The two near-IR colour-colour plots are shown in Figs. 4.4.8 and 4.4.9. The point in each plot with an inscribed letter C was obtained at CTIO in June, 1987.

As with the optical colours, the observed near-IR colour variations are not incompatible with variable extinction by large grains. However, as the two reddest points in the H-K, K-L diagram would require an additional extinction of $A_V \simeq 2$ mag., this would indicate that the intrinsic near-IR continuum emission (i.e. free-free emission from the stellar envelope) must have been particularly weak at this time. Thus variability of the envelope continuum emission also likely contributes to the observed near-IR variability.

4.4.4. The Flux Distribution.

One near simultaneous UBVRI (on HJD 2445101) and JHKL (on HJD

2445102) observation of S CrA was obtained at SAAO by Kilkenny et al. (1985), and in addition, simultaneous BVRI, JHKL and occasional MNQ photometry was obtained during both July and September, 1987. This presents a database for determining the reddening and thereby the intrinsic flux distribution of S CrA out to 20μm.

The first requirement in analysing the data is to unambiguously determine the total reddening of the emergent flux from S CrA. The IS reddening towards the R CrA cloud has been determined to be $E(B-V)_{IS}$ = 0.17 (Section 4.1.4.1). Thus the photometry of S CrA is initially dereddened by an $E(B-V)_{IS}$ = 0.17 with an IS (R = 3.1) reddening law.

Knacke et al. (1973) derive a total reddening of E(B-V) ≈ 0.5 for S CrA, but their method of directly comparing the observed B-V colour with the expected B-V colour of a 5000K MS dwarf is unlikely to be reliable because of the strong blue veiling of S CrA. However, from the strength of the 2200Å feature observed in the 1978 IUE spectrum of S CrA, Appenzeller et al. (1980) comment that an estimate of the total E(B-V) ≈ 0.5 would not be inconsistent with the observed strength of this feature.

In view of the observed optical colour variations (Section 4.4.3), a reddening law of R = 5.3 is considered to be a reasonable estimate for the circumstellar reddening law, and will therefore be adopted in correcting the photometry for circumstellar extinction.

The spectral type of S CrA is estimated to lie in the range GV - K5 (Herbig and Rao 1972 and Bertout et al., 1982 respectively). According to the temperature calibration for young stars of Cohen and Kuhi (1979), this would indicate a range in effective temperature of ≈ 5800 - 4400K. In the following, the coolest available Kurucz (1979) model atmosphere of T_{eff} = 5500K (with a log g = 3.5 for a dwarf star) was

adopted to represent the photospheric emission from S CrA, i.e. it is assumed that S CrA was towards the upper limit of the range in T_{eff}. Ideally, simultaneous high resolution spectroscopy should be obtained to determine the effective temperature of S CrA at the observed epoch.

As discussed in Section 4.4.2, the optical photospheric continuum is observable longwards of ≃ 5200Å, and therefore the optical photometry is further dereddened for circumstellar reddening until a good fit of the V and I photometry (the R photometry is not considered reliable due to the strong Hα line) to the adopted Kurucz (1979) model atmosphere. Once the IS reddening had been removed, it was found that the best fits of the V and I colour slopes to the adopted model atmosphere were obtained with a cloud plus circumstellar $E(B-V)_{cs} \simeq 0.25 \pm 0.05$, given the adopted R = 5.3 reddening law. This gives the total visual extinction of S CrA to be $A_V \simeq 1.9$ mag., which is in reasonable agreement with the total $A_V \simeq 1.5$ mag. (Appenzeller et al., 1980) and the $A_V \simeq 2.0$ mag. indicated in the extinction map of Rossano (1978a).

In order to fit the blue U-B colour slope, a free-free emission component (Appenzeller et al., 1980) is required. However, given that the physical conditions of the accretion shock are not well known and that the level of the theoretical free-free continuum emission should be normalised against an observed HeII 1640Å flux (as the strength of this line would be expected to correlate with the strength of the continuum emission from the accretion shock), the fit of a theoretical free-free continuum to the dereddened U and B photometry (with the stellar contribution removed) is necessarily quite arbitrary. Use of a Hβ flux as a normalisation would probably not be as reliable as the Hβ line arises from several different regions of the envelope.

Various theoretical optically thin nebular continua were produced in an attempt to fit the blue excess emission, with an estimated range in $T_e \simeq 15000 - 40000K$ (from the relative strengths of the observed HeI and HeII lines) and a density of $N_e \simeq 10^{12} cm^{-3}$ (the likely density of the inner infalling envelope - Appenzeller et al., 1986). It is found that the dereddened UBVRI data of S CrA can, in general, be best fitted with a 5500K model atmosphere component and a free-free continuum component with $T_e \simeq 25000K$, normalised to a HeII 1640Å flux of $10^{-11.6}$ erg cm^{-2} s^{-1}. As the HeII lines are probably quite variable (Section 4.4.2.2), simultaneous observation of the HeII 1640Å line would be required to determine whether the strength of the fitted continuum was compatible with the observed strength of the HeII 1640Å line (although note that the HeII 1640Å line can be absent; Appenzeller et al., 1980). In addition, the near-IR excess emission can be successfully fitted at each epoch by a 1300K blackbody component. The three component fit for the UBVRI (HJD 2445101) and the JHKL (HJD 2445102) photometry of Kilkenny et al. (1985) is shown in Fig. 4.4.10.

Inclusion of the IRAS PSC (Beichman et al., 1985) data of S CrA (S CrA is flagged as a non-variable IRAS source) with the combined optical, near- and far-IR SAAO data obtained on HJD 2447044 (when S CrA was observed to be brightest) is shown in Fig. 4.4.11. The band IV 100μm IRAS flux of S CrA was a lower limit. The excess emission at 25μm and 60μm can be fitted with addition of a 70K blackbody. Note however the excess flux at 12 and 20μm. Whatever the blackbody used in an attempt to fit the 10 - 60μm data, the IR fluxes cannot be well fitted. It is suggested therefore that the 10 - 60μm emission of S CrA is probably variable (although no variability was seen by IRAS), although the possibility that a silicate feature affects the 20μm flux

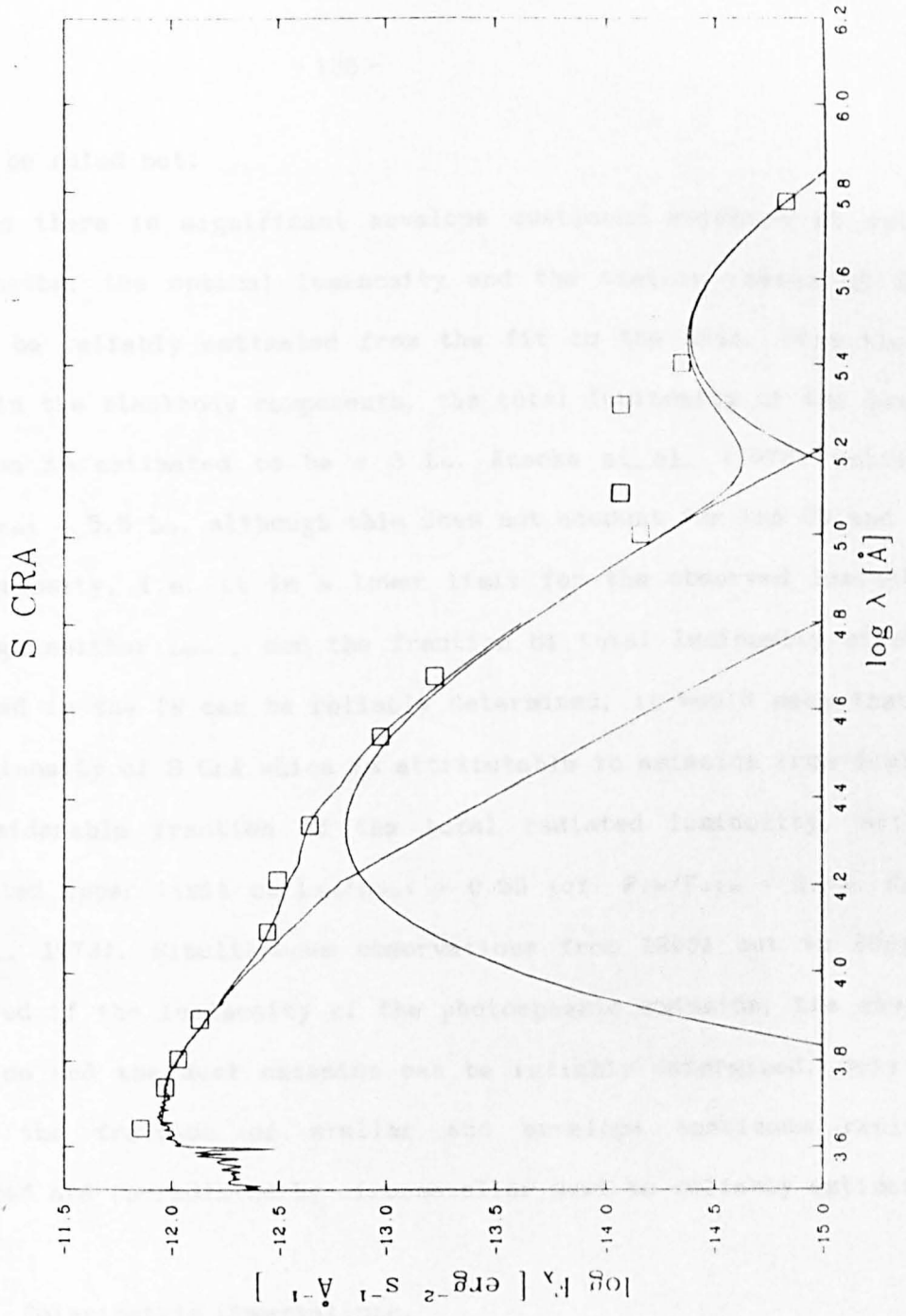

Fig. 4.4.11. Flux distribution of S CrA observed on HJD 2447044 with IRAS data included. See also Section 4.4.4.

cannot be ruled out.

As there is significant envelope continuum emission at optical wavelengths, the optical luminosity and the stellar radius of S CrA cannot be reliably estimated from the fit to the data. From the λF_λ peaks in the blackbody components, the total luminosity of the dust IR emission is estimated to be $\simeq$ 3 $L_\odot$. Knacke et al. (1973) estimated that $L_{Bol} \simeq 5.5\ L_\odot$, although this does not account for the UV and far-IR luminosity, i.e. it is a lower limit for the observed luminosity. Although neither L_{Bol}, nor the fraction of total luminosity of S CrA radiated in the IR can be reliably determined, it would seem that the IR luminosity of S CrA which is attributable to emission from dust, is a considerable fraction of the total radiated luminosity, with an estimated upper limit on $L_{IR}/L_{Bol} \simeq 0.55$ (cf. $F_{IR}/F_{vis} \simeq 2.84$; Knacke et al., 1973). Simultaneous observations from 1200Å out to 20μm are required if the luminosity of the photospheric emission, the envelope emission and the dust emission can be reliably determined. Only then could the fraction of stellar and envelope continuum radiation absorbed and re-radiated by circumstellar dust be reliably estimated.

4.4.5. Polarimetric Observations.

Polarimetric observations (obtained using a clear filter) of S CrA were obtained at SAAO in July and September, 1987. The polarimetric observations, along with the simultaneous V photometry, are tabulated in Table 4.4.1. The only previous polarimetric measurements of S CrA that have been found in the literature were obtained by Bastien (1985), where he observed $p(\lambda=5895Å) \simeq 1.1\%$, and the position angle at this wavelength was $\simeq 156°$. Based on these observations Bastien notes

Table 4.4.1.

Polarimetric and photometric observations of S CrA.

Date (HJD)	p (%)	σ(p) (%)	θ (°)	$\sigma(\theta)$ (°)	V (mag.)
2446991	0.82	0.03	156	3	11.34
2447041	1.07	0.14	145	11	10.91
2447042	0.97	0.14	149	11	10.64
2447044	0.85	0.09	141	9	10.76
2447048	0.78	0.06	138	6	10.76
2447050	0.82	0.04	135	4	11.04

The polarisation p, position angle θ and the visual magnitude, with the corresponding observational errors σ(p) and $\sigma(\theta)$ of S CrA observed in July and September 1987 at SAAO are tabulated.

that S CrA may be a polarimetric variable (Bastien 1987).

As S CrA is known to have an ionised envelope and also a circumstellar dust shell, the polarisation may originate from electron scattering in the envelope and/or from scattering within the dust shell. In view of the fact that the polarisation has not been observed to be greater than 1.1%, both mechanisms are plausible. However, as the wavelength dependence of the polarisation has not been observed, the origin of the polarisation cannot be determined.

Given the observational errors, the observations show that the polarisation is slightly variable on a timescale of days, although the extent of the variability is clearly not as extreme as is observed in several InT stars, e.g. RY Tau (Fig. 2.2.6), RY Lup (Fig. 5.1.16). The position angle clearly rotated by $\simeq 10^{o}$ between HJD 2446991 and 2447050, although the degree of variation over the last five observations (over a period of nine nights) is not significant within the errors, i.e. there is no evidence for variability in the position angle on a timescale of days. However, in view of the fact that the polarisation is variable on a timescale of days, the polarisation is therefore essentially intrinsic (as opposed to IS) in origin, and must originate fairly close to the star itself.

S CrA was fading during the last four observations, whilst the polarisation was also decreasing. Thus it is plausible that the optical photometric and polarimetric variations may be directly correlated. There was however no obvious correlation between the polarisation and the optical-IR colours (e.g. V-L; cf. Bastien 1985), indicating that the polarimetric variations are unlikely to be caused by changes in the dust shell opacity. Correlated variations in p and V would not be incompatible with variable illumination of the circum-

stellar dust shell (see Section 7.4) and more observations are needed to investigate this possibility further.

In summary, it can be reported that S CrA is a definite polarimetric variable, and thus the polarisation is clearly intrinsic. Also the timescale of the variability constrains the polarisation to originate close to S CrA. The optical polarisation and optical brightness may possibly be directly related in S CrA. In view of this and the level of polarisation observed (≃ 1%), scattering within a stellar envelope and within a circumstellar dust shell are both considered to be plausible mechanisms for interpreting the polarisation. Further observations, particularly of the wavelength dependence of polarisation, would therefore be of considerable interest.

4.4.6. Summary and Conclusions.

Although, given the spectral resolution, none of the YY Ori line profiles could be resolved, the optical spectrum of S CrA gives useful information about the strength of the line emission whilst S CrA was known to be bluer than has typically been observed spectroscopically. The UV excess and the blue spectral veiling of S CrA (S CrA exhibits a strong blue U-B excess) is attributable to free-free emission from the stellar envelope. The fact that the FeII emission is strong at this time (when S CrA is blue) would not be incompatible with FeII line emission being promoted by absorption of UV continuum radiation. In addition, there is a definite indication that the stellar wind is also strong at this epoch.

Other than the U-B blue excess, the optical colours exhibit a red excess, which is attributable to extinction by circumstellar dust.

There does not appear to be one single mechanism giving rise to the light variability in S CrA. The relatively well-defined colour variations indicate a degree of underlying variable extinction by large circumstellar grains, whilst changes in the strength of the envelope (and also the photospheric) continuum emission clearly also make S CrA appear blue at blue wavelengths, even when relatively faint.

The dereddened optical and IR emission of S CrA can be decomposed into essentially three components: envelope continuum emission; photospheric continuum emission; radiation from heated circumstellar dust. It would seem that there is significant emission in the IR (emission which is also variable), although further observations are required to reliably ascertain the luminosity of the IR emission due to dust.

The polarisation of S CrA has for the first time been observed to be definitely variable on a timescale of days, and may possibly be directly correlated with the visual flux. The polarisation may arise in the circumstellar envelope and/or in the circumstellar dust shell.

Chapter 5. The T Tauri Stars RY Lup and RU Lup.

5.1. The T Tauri star RY Lup.

5.1.1. Introduction.

RY Lup is one of the members of the dark nebula within the Lupus T association. Estimates of the spectral type of RY Lup have varied, ranging from Herbig and Rao's (1972) classification of G0V, to the classification of Appenzeller et al., (1983) of K4V. The most recent determination of the spectral type by Liseau et al. (1987) gave K0-1V, in reasonable agreement with the observations of Herbig (1977a) giving K1V, and of Gahm (1981, unpublished) giving G8IV. The spectrum often exhibits Hα in emission, but the other Balmer lines are typically only observed when RY Lup is faint (Evans et al., 1982).

The lightcurve of RY Lup is most frequently at the bright end of its range ($9.6 < V_{pg} < 13.5$ mag.; Herbig and Rao 1972), with occasional rapid activity of a few days duration being superposed upon more quiescent, long-term variations. Such rapid changes invariably involve sharp drops in the lightcurve by as much as $V \simeq 2$ mag. The lightcurve of RY Lup has been best studied by Hoffmeister (1965), where he was able to estimate a period of 3.76 days in the lightcurve. Bouvier et al. (1986b) determined a periodicity of 3.9 days and the rotation velocity to be $v \sin i = 25.0 \pm 4.6$ kms^{-1}.

Despite indications that the lightcurve can exhibit periodic variations, and the inference that the variations were likely due to brightness inhomogeneities on the stellar disc (Hoffmeister 1965), it

took many years before a starspot model was used in a quantitative attempt to interpret the light variations of RY Lup (Liseau et al., 1987; Hutchinson et al., 1987). However, both groups found the fitted parameters of a spot model to be physically unrealistic. The other proposal for a likely mechanism causing the light variations was forwarded by Evans et al. (1982), who suggested that the variations were due to variable circumstellar extinction.

Observations have shown that RY Lup has a near-IR excess which has been attributed to free-free envelope emission (Evans et al., 1982). RY Lup is also a notable polarimetric variable (Bastien 1985).

5.1.2. The Optical Spectrum.

The optical spectrum of RY Lup (of resolution $\Delta\lambda$ = 2.8Å) was obtained on HJD 2446998. Optical photometry, taken both the same night and the subsequent night, indicates that the star was fading rapidly at this time, from V = 11.87 mag. on HJD 2446998 to V = 12.34 mag. on HJD 2446999; the star was also observed to redden from (B-V) = 1.20 to 1.34 on the respective nights.

5.1.2.1. Spectral Classification.

The spectrum was carefully examined in order to identify spectral features which would classify the spectrum. The pertinent lines for late G - K dwarf stars (see Cohen and Kuhi 1979, and references therein) were all found to be present: the CaII K and H 3934 and 3969Å and NaI D 5890 and 5896Å resonance lines; the FeI 3820, 4046, 4383 and 5227Å lines; the CaI 4226 and 6162Å lines; and the 5210Å blend of CrI

lines. These lines are shown in Fig. 5.1.1. However, as can be seen, only a few of these features are particularly prominent (the NaI D and CaI 6126Å lines), and there are other, stronger lines also present, e.g. CrI 5784Å. This would indicate that the observed spectrum of RY Lup can be no earlier than mid-late K.

Although this is not readily seen in Fig. 5.1.1, a careful examination of the spectrum indicates that the continuum fades slightly around 5100 and 6200Å, suggesting the possible presence of weak bands of TiO. TiO band heads were thus looked for with a view to classifying the spectrum on the basis of the relative strengths of any TiO bands present. Use was made of the classification scheme for luminosity classes III-V adopted by Cohen and Kuhi (1979).

In order to better examine the continuum, the spectrum was processed with, in one instance, a 10Å and in a second instance, a 40Å Gaussian spectral filter. The re-plotted spectrum as processed by a 40Å filter is shown in Fig. 5.1.2. A TiO band commencing at ≈ 4955Å can be seen more clearly on this smoothed spectrum, but because of the weakness of the bands and the sharp fall in the continuum beyond 6000Å, the 6159 and 6200Å bands (expected in a mid-late K spectral type) are lost in the smoothed spectrum. The position of the band heads at 4955 and 6159Å are indicated in Fig. 5.1.2. From both the weakness of these two bands, and the absence of the other TiO bands, the spectrum is clearly earlier than ≈ M0. For stars earlier than M3, Cohen and Kuhi (1979) indicate that it is not possible to distinguish between luminosity classes III-V on the basis of the relative strengths of the TiO bands, and so the comparative strength of the 4955Å band does not make possible a luminosity classification.

Thus, from the presence of the metallic lines (although some are

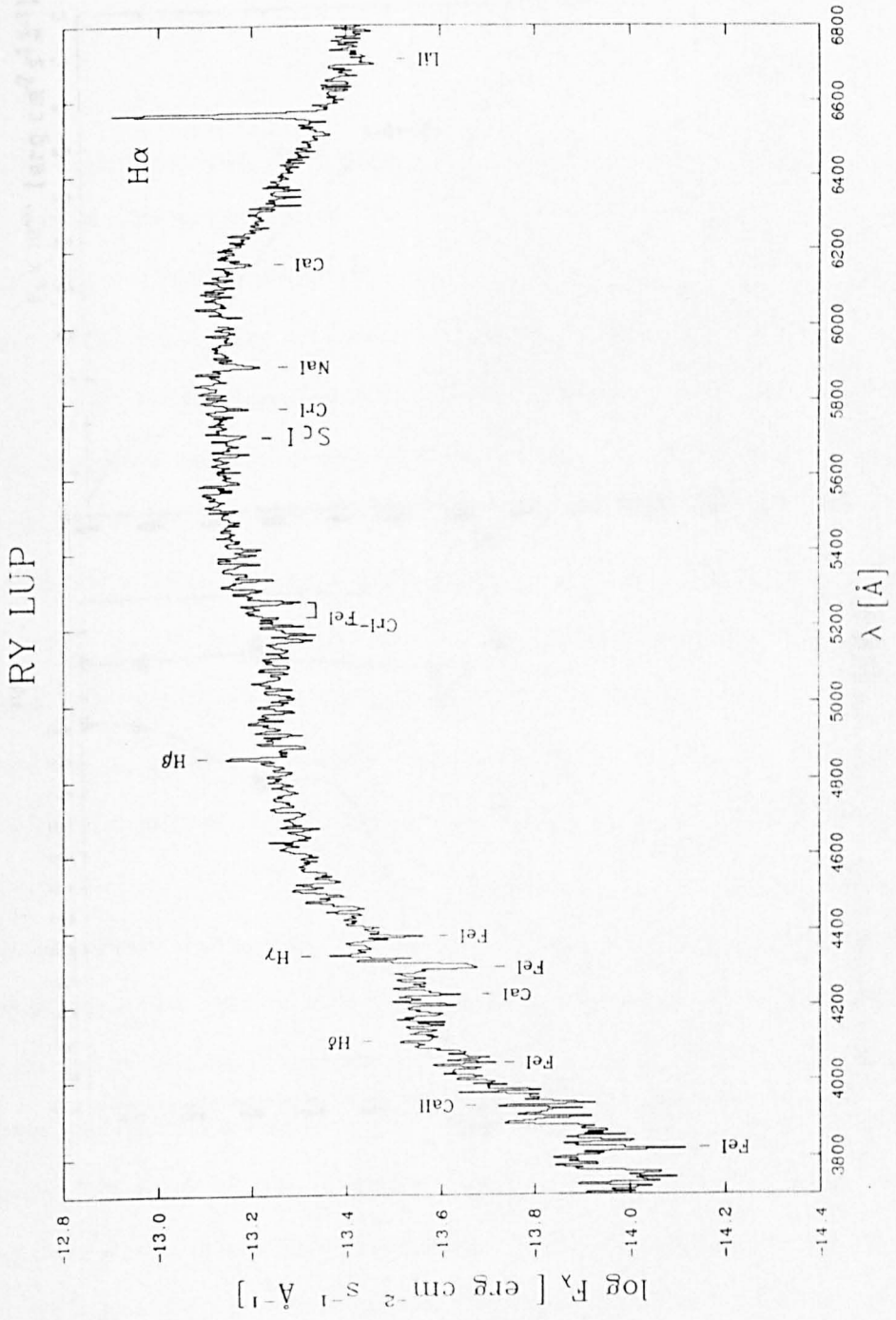

Fig. 5.1.1. Optical spectrum of RY Lup. See also Section 5.1.2.

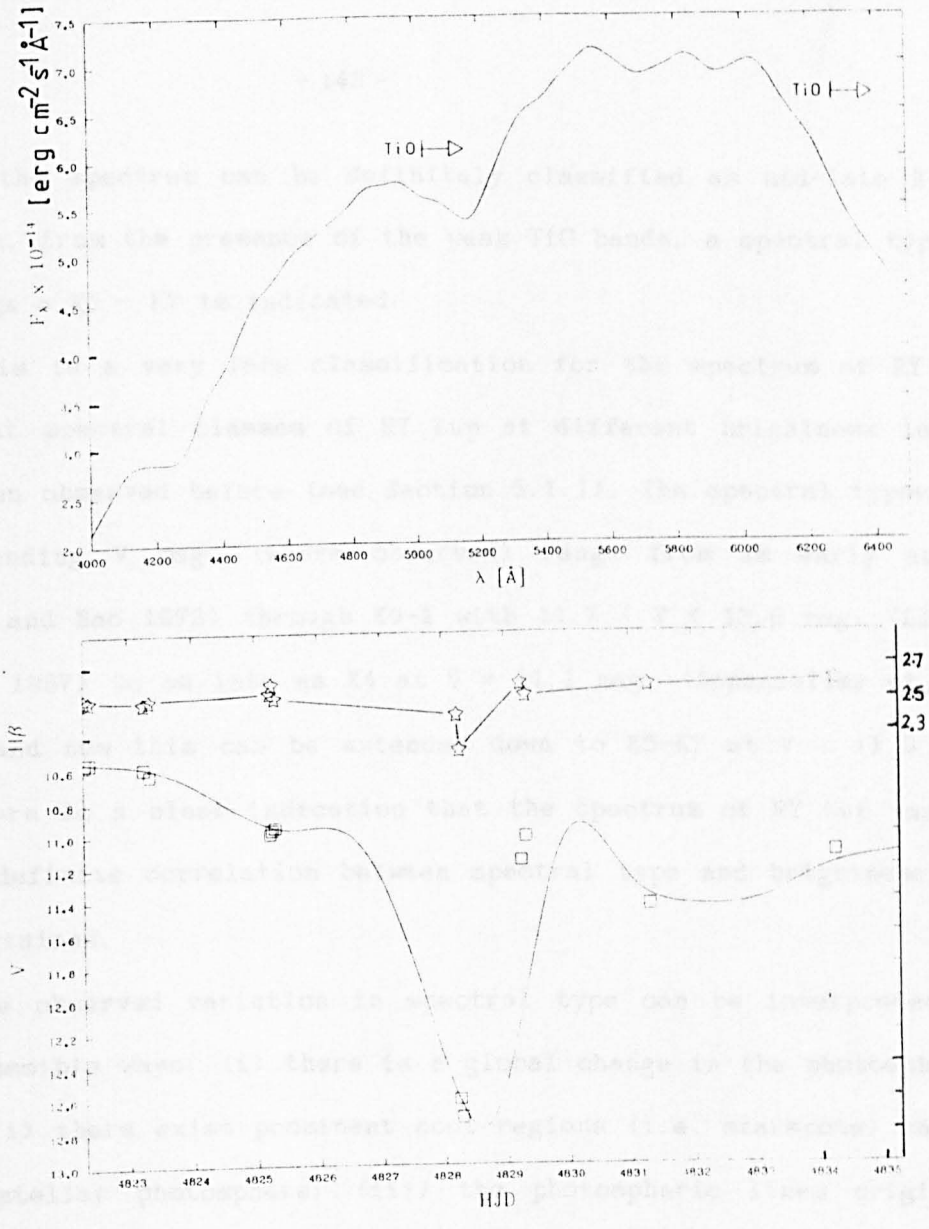

Fig.5.1.2. Smoothed spectrum of RY Lup showing positions of the 4955 and 6200Å bands. See also Section 5.1.2.1.

Fig. 5.1.3. Fitted spline curve to the V photometry of RY Lup with the Hβ photometry also shown. The date is given in HJD 2440000+. See also Section 5.1.3.2.

weak), the spectrum can be definitely classified as mid-late K. In addition, from the presence of the weak TiO bands, a spectral type in the range ≃ K5 - K7 is indicated.

This is a very late classification for the spectrum of RY Lup. Different spectral classes of RY Lup at different brightness levels have been observed before (see Section 5.1.1). The spectral types and corresponding V mag. (where observed) range from as early as G0 (Herbig and Rao 1972) through K0-1 with 11.7 < V < 13.0 mag. (Liseau et al., 1987) to as late as K4 at V = 11.1 mag. (Appenzeller et al., 1983), and now this can be extended down to K5-K7 at V ≃ 11.9 mag. Thus there is a clear indication that the spectrum of RY Lup varies, but no definite correlation between spectral type and brightness can be ascertained.

The observed variation in spectral type can be interpreted in three possible ways: (i) there is a global change in the photospheric T_{eff}; (ii) there exist prominent cool regions (i.e. starspots) on the normal stellar photosphere; (iii) the photospheric lines originate from a normally ≃ G8-K1 photosphere, whilst molecular TiO bands arise either within a circumstellar envelope (as with, e.g. Mira variables) or in a circumstellar dust shell. The fact that the spectrum of RY Lup has been observed no later than K7 places a definite constraint on the lowest value of either T_{eff} or T_{spot} respectively (of ≃ 4000K; Cohen and Kuhi 1979) permitted in (i) or (ii) above.

Each of these mechanisms could, in principle, account for the observed variations in the lightcurve of RY Lup, and the possibility of an intrinsic or circumstellar origin of the light variability in RY Lup will be examined in Section 5.1.3. The three mechanisms ought to be distinguishable in a simultaneous photometric and spectroscopic

monitoring programme which followed RY Lup during phases of minimum light: mechanisms (i) and (ii) would result in noticable changes in the photospheric line strengths; (ii) would also result in clearly defined sinusoidal photometric variations; (iii) would result in changes in the TiO band strengths but not significantly affect the photospheric lines.

5.1.2.2. The Hydrogen lines.

The Balmer lines are very variable in RY Lup (Gahm and Krautter 1982). Balmer line emission is observable only when the star is faint (Evans et al., 1982), but not even Hα is generally observable in emission when the star is brighter than V ≃ 11 mag. (Appenzeller et al., 1983).

In the 1987 SAAO spectrum, the Balmer lines, with the notable exception of Hα, are not strong, and of these, only Hβ - Hδ are evident, exhibiting a weak emission component. Thus, in view of the fact that the star was fading at the time when the SAAO spectrum was obtained, it is unsurprising that the Hα emission line is strong and that the Hβ - Hδ lines have an emission component. Balmer emission could arise either from a deep chromosphere or an extended envelope. However, a deep chromosphere would also be expected to give rise to metallic emission lines (e.g. Cram 1979) when RY Lup is faint, which are not observed. Thus it would seem that the Balmer emission more likely arises from an extended envelope.

The fact that Balmer emission (other than Hα, which is also seen at "normal" light) from an extended envelope is only observable when RY Lup is faint can be best explained in terms of a mechanism by which

only the photospheric continuum emission is "supressed" at minimum light. This suggests two possibilities, both of which may well be important with regards to RY Lup (as discussed in Section 5.1.2.1):

(a) a large area of the observable disc is covered by many starspot regions, supressing only the photospheric emission;

(b) a significant density enhancement in the circumstellar dust cloud of about the right size ($\simeq R_*$) passes across the stellar disc, dimming only the photospheric continuum (cf. a solar eclipse).

Mechanism (a) can apply to both a deep chromosphere or an extended envelope for RY Lup, but (b) is only applicable if RY Lup has an extended envelope.

A high resolution spectrum of the Hα - Hϵ lines obtained by Evans et al. (1982) led them to favour the Balmer emission arising in an extended envelope (as is favoured here), and the Balmer line profiles indicated that both infall and outflow is probably occurring in the envelope. Further high resolution spectroscopy of the variation of the Balmer line profiles when RY Lup is faint would be useful in determining the nature (i.e. excitation temperature, possible size) of the envelope and the constancy/variability of the line profiles (e.g. whether the lines indicate expansion, infall or both) arising from the envelope. An estimate of the size of the envelope would place useful constraints on plausible mechanisms causing the photometric minima.

5.1.2.3. Resonance lines.

The fact that the CaII K and H resonance lines are not as strong as would be expected in a normal K-type photosphere indicates that these lines are probably also affected by emission. Emission of CaII K

and H could arise either in a dense chromospheric region or in an extended envelope. The likelihood that the Balmer emission, observable when RY Lup is faint, probably arises within a stellar envelope (as is favoured here and also by Evans et al., 1982) would tend to suggest a similar (i.e. envelope) origin for the weak CaII K and H emission.

The fact that the NaI D resonance lines are in absorption, whilst the CaII resonance lines are not, would indicate that the NaI and CaII resonance lines arise essentially in different regions of the atmosphere of RY Lup (cf. Evans et al., 1982). The characteristic InT LiI 6707Å resonance line is also evident in the spectrum of RY Lup.

5.1.2.4. Summary.

Optical spectroscopy, together with simultaneous photometry provides further evidence for two interesting features of the spectrum of RY Lup. The first is that the spectral type of RY Lup shows a tendency to vary as the star varies in brightness, although there seems to be no direct correlation between the two. The second is that, when at minimum light, weak Balmer and CaII K and H line emission is evident, a fact which is attributable to the enhancement of emission from an extended envelope relative to the continuum emission from the photosphere. An understanding of the spectral behaviour of RY Lup through phases of minimum light would be integral in reliably determining the cause(s) of the photometric minima.

5.1.3. The Light and Colour variations.

This section comprises an estimation of the IS reddening, an

analysis of the optical lightcurve, and an analysis of the optical and IR colour-colour variations of RY Lup. The latter two sub-sections will consider which of the two possible interpretations of the variability, intrinsic light variations or changes in the extinction within a circumstellar dust shell, best describe the observed variability.

5.1.3.1. Estimate of the Interstellar Reddening.

The tightest locus of variation in the colours of RY Lup lies in the V-R, V-I colour-colour plane, and thus V-R and V-I were chosen as the colours least affected by reddening (cf. Imhoff and Mendoza 1974). Using the calibrations of Johnson (1966) for a K0 MS dwarf, and assuming a normal IS reddening law, the E(V-R) and E(V-I) colour excesses were estimated. From the colour excess ratios based on the the reddening law of Savage and Mathis (1979), this gives an estimate of $E(B-V)_{IS} \simeq 0.12$, assuming there is no circumstellar extinction at observed maximum light (V = 10.4 mag.). If the reddening curve (assuming the colours of a K0 dwarf) is plotted, a value of $E(B-V)_{IS} \simeq 0.18$ is indicated. However, as RY Lup is more luminous than a normal K0V star (see Section 5.1.4), the intrinsic colours of a K0 dwarf may not be totally accurate for RY Lup. A value of $E(B-V)_{IS} \simeq 0.18$ is adopted as an initial estimate in dereddening the photometry in Section 5.1.4.

5.1.3.2. The Optical Lightcurve.

In the period 1981-1984, over a hundred sets of simultaneous UBVRI photometric observations of RY Lup were obtained (see Kilkenny et al.,

1985), which gives very good coverage of the lightcurve, particularly over the following three epochs (given in HJD 2440000+): 4822 - 4834; 5416 - 5428; and 5808 - 5814. The remaining dataset covers an additional six epochs. A considerable fraction of the dataset is also complemented by simultaneous Hβ photometry (see Section 3.4.1) and near-simultaneous JHKL photometry.

Over the four year period, RY Lup varied from V = 10.44 to V = 12.72 mag., with the lightcurve experiencing rapid fadings into deep minimum (V > 12.0 mag.) in no less than six of the nine epochs covered. Where sufficient coverage is available, each period of deep minimum is seen to last no longer than a single night - similar behaviour has been reported in the lightcurves of a few other InT stars, e.g. RY Tau and SV Cep (Wenzel 1969); thus in agreement with previous studies of the lightcurve, RY Lup is observed most frequently at the bright end of its range, i.e. Parenago lightcurve type I (Herbig and Rao 1972). Although in order for the star to have been observed fainter than V ≃ 12.0 mag. on several occasions, it would seem that RY Lup can fade to minimum light with quite a high frequency of occurrence (≃ 1 - 2 times per month).

Significant (≃ 0.3 mag.) rapid (≃ hours) variations were looked for in the U lightcurve, which would be indicative of notable "flaring" activity (cf. Gahm 1986), but none were found. However it is noted that the largest scatter in the optical colour variations occurs in the U-B colour plane (see Fig. 5.1.9), which would point towards a small degree of chromospheric or "flaring" activity in RY Lup.

If the optical lightcurves were modulated by photospheric inhomogeneities (e.g. starspots), a periodicity in the lightcurve should be evident despite the obvious breaks in the dataset. Previous observ-

ations of the lightcurve of RY Lup have indeed revealed quasi-sinusoidal variations and corresponding estimates of the rotation period (P_{rot}) have been suggested in interpreting the data in terms of a rotational modulation by a spotted photosphere: Hoffmeister (1965) gave P_{rot} = 3.76 days; P. Bastien (private communication, 1986) gave P_{rot} = 3.62 days; Bouvier et al. (1986b) gave P_{rot} = 3.9 days. The similarity of these independently measured periods strongly suggests that such quasi-sinusoidal light variations are indeed rotationally modulated.

The visual lightcurve of RY Lup during the three well-observed epochs delineated above was carefully studied in order to look for quasi-sinusoidal and/or periodic variations. Efforts were concentrated on the visual lightcurve as the V photometry will neither be affected by any strong lines (e.g. Hα at R) nor from irregular fluctuations due to chromospherically active regions (e.g. any "flaring" activity at U; although as indicated above there are no sharp rises seen in the U lightcurve). In the first instance sine curves of varying amplitudes and periods (ranging from 3.5 to 4.0 days) were used in an attempt to fit the light variations, but this procedure met with little success. At best, in the epoch HJD 2445417 - 2445428, the light variations could only be poorly approximated by a sine curve.

A second approach consisted of fitting the lightcurve data by a least-squares spline curve in order to represent the observed variations by equally spaced data, data which could then be easily and accurately Fourier analysed, i.e. a good, regular sampling of data gives better signal-to-noise in the Fourier transform than when using the original data. The spline curve fitting algorithm used was developed by J. White and the Fourier analysis routine used is a

STARLINK software sub-routine developed from the procedure outlined in Scargle (1982).

The first two datasets each include a night where the star fades below 12.0 mag. As there is also simultaneous Hβ photometry for these two epochs, the visual lightcurve, the fitted spline curve and the Hβ photometry are shown for both epochs in Figs. 5.1.3 and 5.1.4. It can be seen that the Hβ index tends to indicate net emission ($\beta < 2.5$) when RY Lup is fainter than $V \simeq 11.4$ mag.

It was found however, that none of the Fourier power spectra of the fitted spline curves gave any statistically significant peaks. The only pertinent peaks in the power spectra were at $\simeq 2.7$ and 3.5 days. Thus, even allowing for changes in the phase and/or amplitude of variation, there is no real evidence for any underlying rotational modulation in any of the three well-observed epochs.

Therefore, it is only possible to conclude that, within the limits (imposed by the frequency of sampling of the lightcurve) of an analysis of the data, there is no compelling evidence for a strong periodicity due to rotation within the Kilkenny et al. (1985) optical dataset of RY Lup from 1981 - 1984. This conclusion would suggest that RY Lup goes through phases where starspots play only a very minor role in modulating the light variability, i.e. another variability mechanism(s) becomes dominant. For example, surface activity may be essentially quiescent whilst variable circumstellar extinction dominates the light variability.

The other optical lightcurves observed in the epoch HJD 2445416 - 2445428, the only epoch for which there is any indication of quasi-sinusoidal variation, were also approximated by sine curves. Whilst the fits were not good, this procedure does allow a determination of

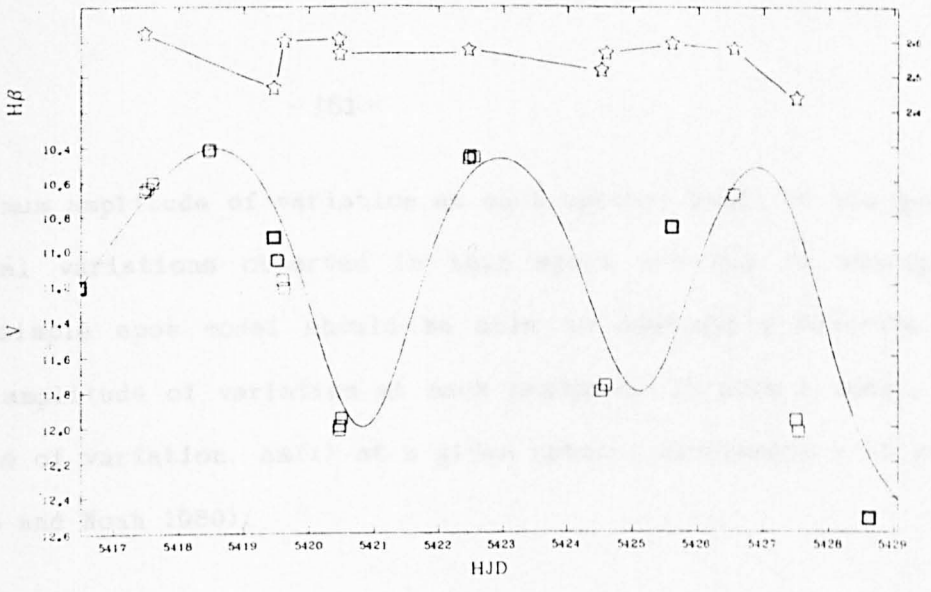

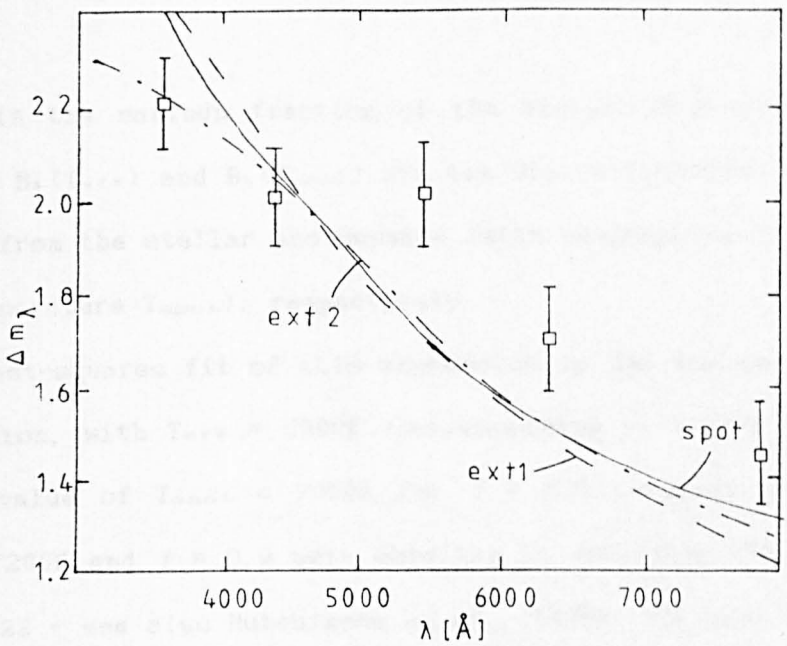

Fig. 5.1.4. Fitted spline curve to the V photometry of RY Lup with the Hß photometry also shown. The date is given in HJD 2440000+. See also Section 5.1.3.2.

Fig. 5.1.5. Maximum amplitude of variation at UBVRI observed over the epoch HJD 2445416-2445428 (see also Fig. 5.1.4). The curves spot, ext1 and ext2 are explained in Section 5.1.3.2.

the maximum amplitude of variation at each optical band. If the quasi-sinusoidal variations observed in this epoch are due to starspots, then a simple spot model should be able to adequately describe the maximum amplitude of variation at each bandpass. In such a model, the amplitude of variation, $\Delta m(\lambda)$ at a given optical wavelength λ is given by (Bopp and Noah 1980):

$$\Delta m(\lambda) = 2.5 \log_{10} [\ 1 - f\ (1 - B_\lambda(T_{eff})/B_\lambda(T_{spot}))\ ] \qquad (5.1)$$

where f is the maximum fraction of the stellar disc covered by the spot, and $B_\lambda(T_{eff})$ and $B_\lambda(T_{spot})$ are the Planck functions representing emission from the stellar photosphere (with temperature T_{eff}) and spot (with temperature T_{spot}), respectively.

A least-squares fit of this expression to the observed amplitudes of variation, with T_{eff} = 5000K (corresponding to a K0-1 photosphere) gives a value of T_{spot} = 7000K for f = 0.9 (similar parameters of T_{spot} = 7200K and f = 0.9 were obtained in modelling the data around HJD 2444822 - see also Hutchinson et al., 1989). The best fit starspot model to the data is shown in Fig. 5.1.5, and labelled **spot**. If the constraint on T_{eff} representing a K0-1 photosphere is eased, a similar fit can be obtained for a cooler photosphere with a hotter, similar-sized spot. Two other curves are shown, which represent the amplitude of variation corresponding to a normal (R = 3.1) extinction law (labelled **ext1**) and an anomalous (R = 5.3) extinction law (labelled **ext2**), both normalised to ΔV = 0.15 mag. Although none of the curves fit the amplitudes particularly well, it is interesting to note that whilst RY Lup was passing through two successive minima fainter than V $\simeq$ 11.4 mag., of the three curves, an anomalous reddening curve (R $\simeq$

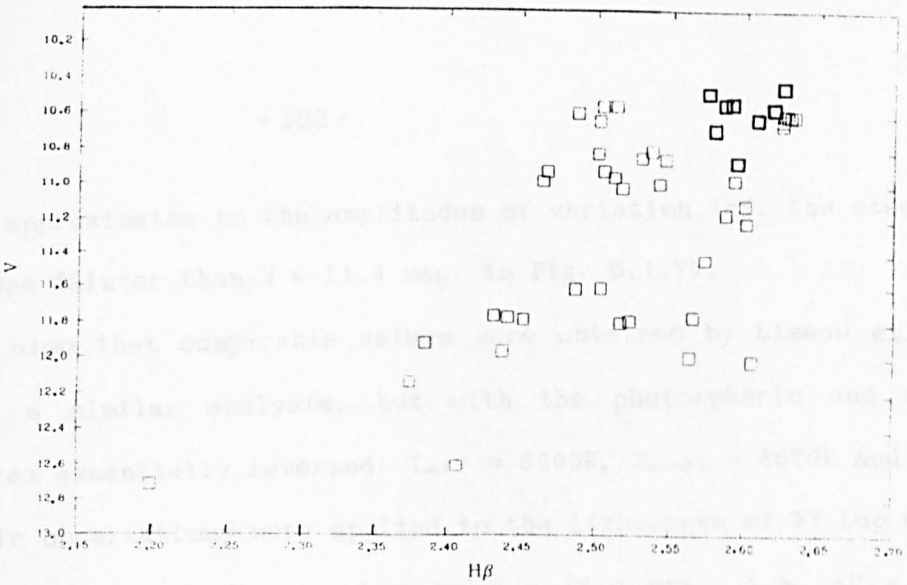

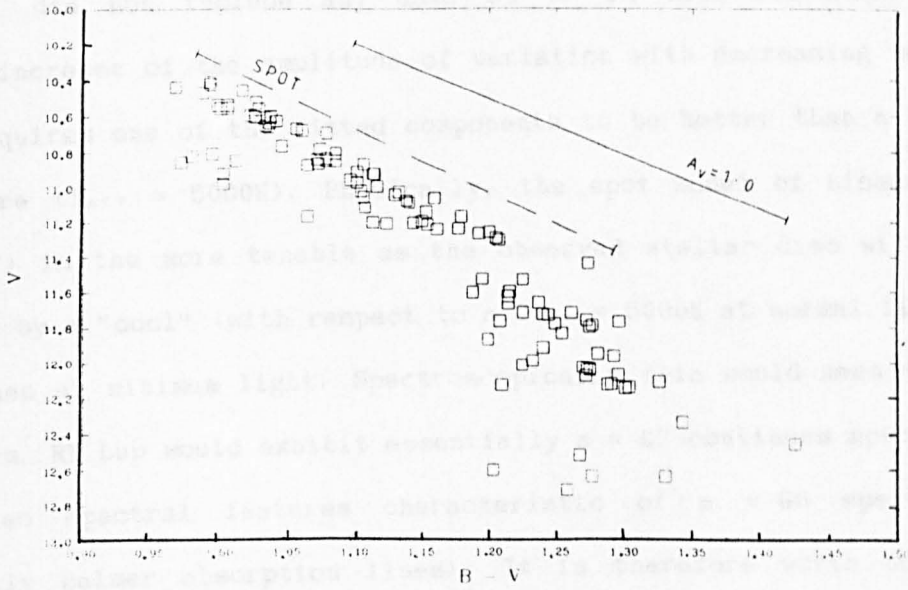

Fig. 5.1.6. V, Hβ variation of RY Lup.
See also Section 5.1.3.2.

Fig. 5.1.7. V, B-V variation of RY Lup.
The loci shown are discussed in Section 5.1.3.3.

5.3) best approximates to the amplitudes of variation (cf. the steeper V, B-V slope fainter than V ≃ 11.4 mag. in Fig. 5.1.7).

Note also that comparable values were obtained by Liseau et al. (1987) in a similar analysis, but with the photospheric and spot temperatures essentially reversed: T_{eff} = 6000K, T_{spot} = 4070K and f = 0.79. Their observations were applied to the lightcurve of RY Lup when it varied from V ≃ 11.7 mag. down to V ≃ 13.0 mag., i.e. ΔV ≃ 1.3 mag., but did not include any data at U. In both instances the observed increase of the amplitude of variation with decreasing wavelength requires one of the fitted components to be hotter than a K0-1 photosphere (T_{eff} ≃ 5000K). Physically, the spot model of Liseau et al. (1987) is the more tenable as the observed stellar disc will be dominated by a "cool" (with respect to a T_{eff} = 5000K at normal light) region when at minimum light. Spectroscopically this would mean that, at minimum, RY Lup would exhibit essentially a ≃ K7 continuum spectrum (with also spectral features characteristic of a ≃ G0 spectrum, essentially Balmer absorption lines). It is therefore worth noting that these parameters could conceivably reproduce the SAAO spectrum discussed in Section 5.1.2 if sufficient Balmer emission arose from an additional envelope component/deep chromosphere.

As has been already indicated, there is a tendency for the Hβ index to indicate net emission (β < 2.5) when the star is fainter than V ≃ 11.4 mag. This behaviour is evident in the minima shown in Figs. 5.1.3 and 5.1.4. However, as is shown in Fig. 5.1.6, there is no clear correlation between the general variation of the Hβ index with V. Although there is a tendency for the Hβ index to decrease as the star fades, the Hβ index can occasionally take values less than 2.5 when the star is bright. However, the Hβ index is *always* lower than 2.45

when the star is fainter than V ≈ 12 mag., i.e. there is always an emission component when the star is in deepest minimum. This behaviour at deep minimum was first described by Evans et al. (1982), cf. the SAAO optical spectrum which shows weak emission components of the Hδ - Hβ Balmer lines when the star is at V = 11.87 mag. (see Section 5.1.2.2). Thus it would seem clear that the "enhancement" of the Balmer line emission at minimum light is a fairly common occurrence and therefore this phenomenon must be included in a realistic interpretion of the minima.

One final note on the Hβ photometry of RY Lup should also be mentioned. Normally the Hβ index varies by no more than 0.05 per night. However, within a single hour on the night of HJD 2444828 the Hβ index decreased considerably from β = 2.407 to 2.199, whilst the star only faded from V = 12.61 to 12.72 mag. As it is evident from the optical photometry that the strength of the continuum did not change by a significant amount during this time, this would imply that the Hβ line profile (as monitored by the Hβ index) must have changed significantly at this time, i.e. of all the observed variations in Hβ, the only rapid change in the strength or profile of the Balmer line emission is seen when RY Lup is faint. This is consistent with the idea that the level of Balmer line emission in "enhanced" (relative to the photospheric continuum) when RY Lup is faint.

Therefore it is concluded that intrinsic variability of RY Lup (i.e. a simple starspot model or global changes in effective temperature) cannot realistically describe the observed amplitudes of the optical light variations (ΔV ≈ 2 mag.) in the well observed epochs in the period 1981-1984, and thus a mechanism of variable circumstellar extinction must be invoked, although contributions from both mechan-

isms acting simultaneously cannot be ruled out. A similar conclusion was reached by Liseau et al. (1987).

5.1.3.3. The Colour-colour variations.

Fig. 5.1.7 shows the variation in B-V with V. There is a noticable break in the data at V ≃ 11.4 mag., where a greater slope of variation in the V, B-V plane is indicated for V > 11.4 mag., although the scatter of points in this region is clearly greater. This change in slope can be seen clearly against the solid line of slope 3.1, included in Fig. 5.1.7, which is essentially parallel to the locus of variation for V < 11.4 mag. This line corresponds to an A_V = 1 mag. and reddening following a normal IS ($R = A_V/E(B-V) = 3.1$) reddening law, i.e. the variability at normal light can be described by variable circumstellar extinction by a population of IS-like grains.

The observed locus for V < 11.4 mag. can also be described by a simple spot model (see also Hutchinson et al., 1989). Assuming a distance d = 150 pc and $E(B-V)_{IS}$ = 0.2 (corresponding to the distance and reddening estimates of the associated InT star RU Lup, Gahm et al., 1981) the best-fit locus for a spot model is applied to the observed V, B-V locus. The fit is given with a stellar T_{eff} = 5000K (corresponding to a K0-1 spectral type at maximum light) and a spot temperature T_{spot} = 3000K. The plotted locus (dashed line, labelled **SPOT**) therefore corresponds to an "unspotted" disc at V ≃ 10.2 mag., and a completely "spotted" disc at V ≃ 11.4 mag., and thus also effectively represents the observed variation of a star cooling globally from T_{eff} = 5000K to T_{eff} = 3000K.

However, such a cool photospheric temperature (either in terms of

T_{spot} or T_{eff}) of 3000K (≃ M5-6 spectral type) covering the observed disc is not tenable, otherwise strong TiO bands would be clearly evident in an optical spectrum of RY Lup when the star was fainter than V ≃ 11.0 mag. - there exists no spectroscopic evidence for starspots cooler than ≃ 4000K (Section 5.1.2.1). In view of this locus, it would thus seem extremely unlikely that RY Lup could fade from V ≃ 10.2 mag. (corresponding to spectral type ≃ G8-K1) down to V = 11.87 mag., but still only exhibit a spectral type as early as K5-7 *unless* there was also a significant increase in the circumstellar reddening.

Therefore it is reasonable to interpret the weak TiO bands observed in the spectrum of RY Lup on HJD 2446998 (Section 5.1.2.1) as intrinsic, although the photospheric continuum must also be fairly heavily reddened by circumstellar dust at this epoch.

Therefore it is evident that only the locus of variation due to an IS-like reddening law (with a gradient of 3.1) can interpret the normal light variability (V < 11.4 mag.) in the V, B-V plane with least difficulty. Thus the observed normal light variability can be ascribed either to variable circumstellar extinction by a population of IS-sized grains (cf. Evans et al., 1982), or to superposed contributions from both cool "spotted" regions and variable circumstellar extinction. But the "normal" light variability *cannot* be ascribed to a simple starspot model (or global changes in T_{eff}) alone.

From a least-squares fit to the data for V ≥ 11.4 mag., the slope of variation when RY Lup is faint is $\Delta V/\Delta(B-V) \simeq 5.5$. This is an indication that when the star is close to minimum light, a population of larger grains (a ≃ 0.3μm) typically contribute to the observed extinction (Hutchinson et al., 1989).

The observed variation in the optical colour-colour plots, as shown in Figs. 5.1.8 (B-V, V-I), 5.1.9 (U-B, V-I) and 5.1.10 (V-R, R-I) are also consistent with the suggestion that the observed variability is due largely to variable circumstellar extinction by a normal population of IS-like grains (solid line, from the averaged IS reddening curve of Savage and Mathis 1979). That the colour variations do not follow the reddening locus exactly may well indicate that there is a level of concurrent colour variability due to starspots. The larger scatter observed in the U-B colour is explicable in terms of a normal extinction law, which affects the flux at shorter wavelengths to a greater degree and also due to limited "chromospheric" activity. The scatter in the V-R, R-I plane can be attributed to the variable Hα line. Again, when the colours are reddest, a slight change in slope can be seen, indicative of further reddening by an additional population of large grains.

The locus of variation in the near-IR J-H, H-K (Fig. 5.1.11) and H-K, K-L (Fig. 5.1.12) plots do not follow the slope expected from a normal extinction law (solid line) as well as is found in the optical colours. However, this is not unexpected in view of the near-IR excess of RY Lup, i.e. the near-IR variations will not be modulated by variable extinction of the photospheric continuum alone, but also by the strength of the excess emission (attributable to thermal re-emission by circumstellar dust: see Section 5.1.4). The dashed locus labelled T_{max} = 1300K represents thermal emission from circumstellar dust heated to 1300K around a central K0 star. The position of this locus indicates that the J-H, H-K colour plane is dominated by emission from dust heated to $\simeq$ 1400K, whilst a lower temperature is indicated in the H-K, K-L plane, i.e. the dust is heated to a maximum

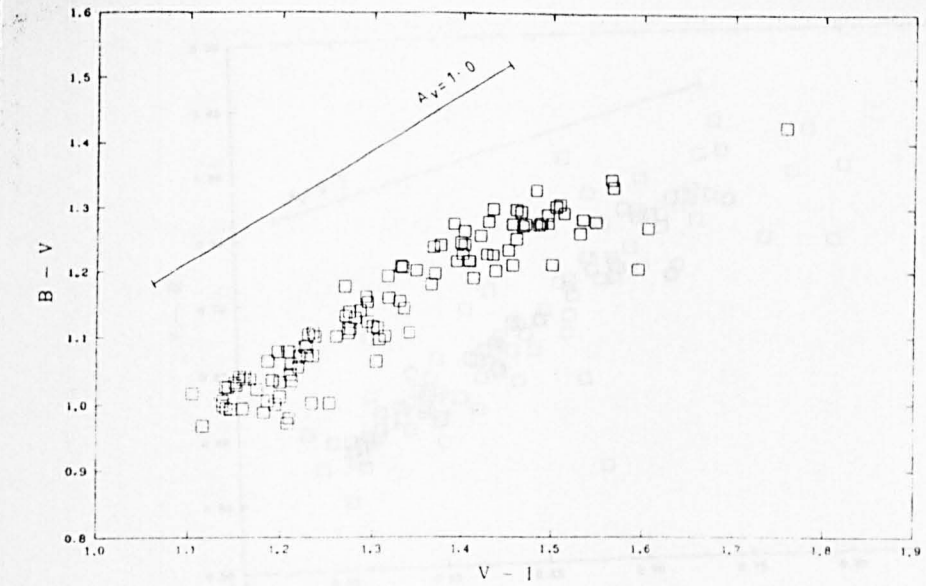

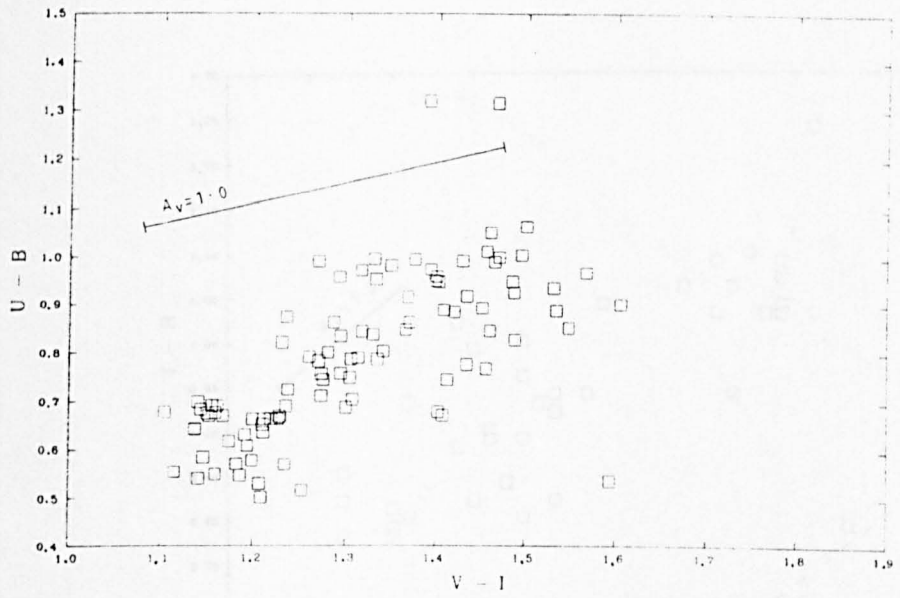

Fig. 5.1.8. B-V, V-I variation of RY Lup.
See also Section 5.1.3.3.

Fig. 5.1.9. U-B, V-I variation of RY Lup.
See also Section 5.1.3.3.

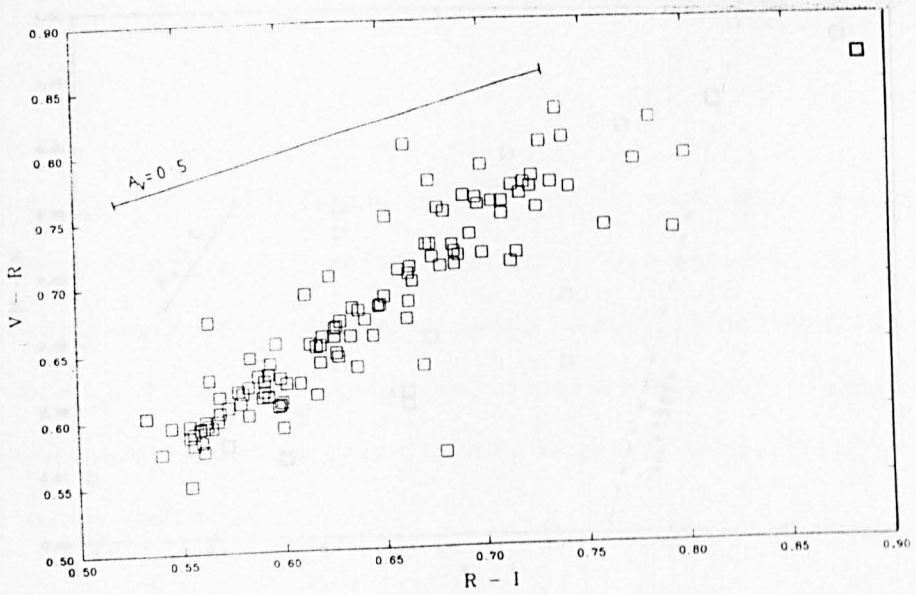

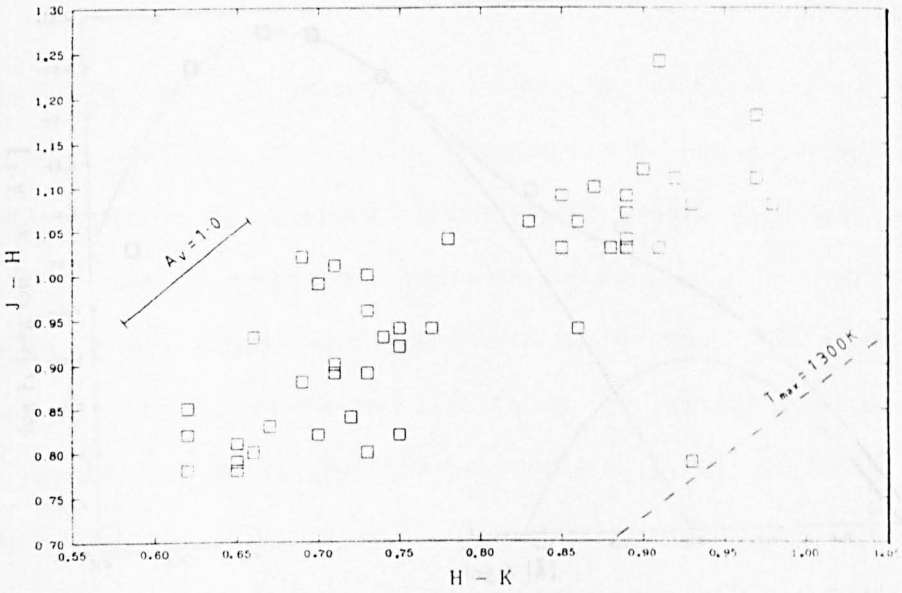

Fig. 5.1.10. V-R, R-I variation of RY Lup.
See also Section 5.1.3.3.

Fig. 5.1.11. J-H, H-K variation of RY Lup.
See also Section 5.1.3.3.

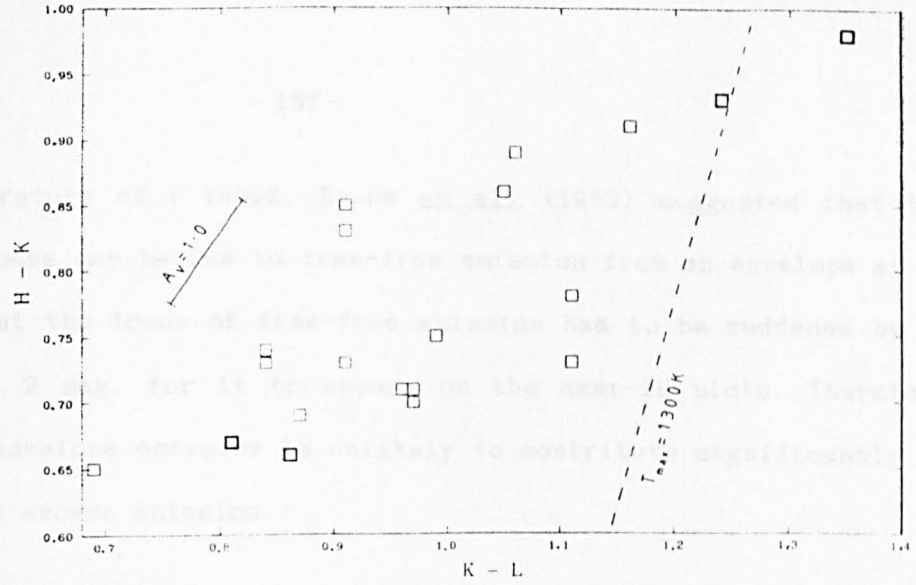

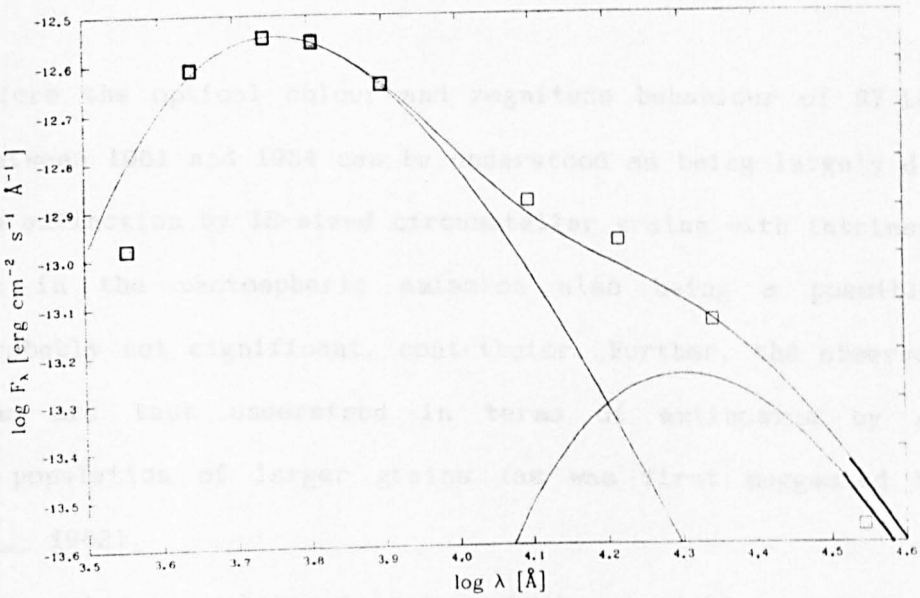

Fig. 5.1.12. H-K, K-L variation of RY Lup. See also Section 5.1.3.3.

Fig. 5.1.13. Flux distribution of RY Lup on HJD 2447042. See also Section 5.1.4.

dust temperature of ≃ 1400K. Evans et al. (1982) suggested that the near-IR excess may be due to free-free emission from an envelope at T_* ≃ 7500K, but the locus of free-free emission has to be reddened by at least A_V ≃ 2 mag. for it to appear on the near-IR plots. Therefore free-free envelope emission is unlikely to contribute significantly to the near-IR excess emission.

5.1.3.4. Summary and Discussion.

Therefore the optical colour and magnitude behaviour of RY Lup observed between 1981 and 1984 can be understood as being largely due to variable extinction by IS-sized circumstellar grains with intrinsic variability in the photospheric emission also being a possible, although probably not significant, contributor. Further, the observed deep minima are best understood in terms of extinction by an additional population of larger grains (as was first suggested by Evans et al., 1982).

This is not to say however that periodic sinusoidal variations (attributable to starspots) do not occur in RY Lup: in view of previous observations of the lightcurve, e.g. Hoffmeister (1965), sinusoidal variations in the optical lightcurves clearly do occur, and at such times starspots evidently dominate the short-term (≃ days) light variability of RY Lup. Also it would seem reasonable that starspot regions which may cover a considerable fraction of the stellar disc can account for the observed variation in the spectral type of RY Lup, such as was observed on HJD 2446998. Note however that when RY Lup is fainter than ≃ 11.5 - 12 mag., the light output from RY Lup is clearly significantly reddened by circumstellar dust.

Thus the observed sharp ($\simeq$ 1 - 2 days) falls in the optical light curve which are often correlated with changes in the Hβ line (and presumably also with enhanced Balmer line emission as discussed in Section 5.1.2.2) would indicate that emission from the stellar photosphere is typically inhibited relative to emission from the stellar envelope by a considerable increase in the line-of-sight circumstellar opacity, i.e. regions of enhanced density in the circumstellar shell.

The size of such condensed regions (or cloudlets) in the circumstellar dust shell must typically be $\simeq R_*$ in order to give changes in $\Delta V \simeq 2$ mag., but smaller than $R_{envelope}$ so that the envelope emission is not significantly affected. The size of the envelope is probably no greater than a few stellar radii. The short timescale of the deep minima also requires the cloudlets to be $\simeq R_*$, and the observed frequency of minima require a large number of such cloudlets to be present around RY Lup.

The observational requirements of the inferred eclipses therefore place tight constraints on the nature of such cloudlets, and the possibility of such cloudlets existing as isolated, gravitationally bound clumps can be examined.

As a clump passes across the disc in $\simeq$ 1 - 2 days, a clump must travel at a tangential velocity $\simeq$ 10 - 20 kms^{-1}, suggestive of planetary distances from RY Lup ($\simeq$ 1 - 2 A.U.). From the change in colour slope at deepest minimum, the size of the grains within the central condensation of a clump is probably a few times the size of a normal IS grain, i.e. $\simeq 0.3\mu m$. Unless the central condensation is much smaller than the size of the stellar disc (in which case the extinction from the core will be limited by the size of the covered

disc), then the observed visual extinction caused by the large grains is no greater than 1 mag., which implies that, for $\simeq 10\mu m$ grains (a size chosen in order to estimate an upper bound for the core mass) in a clump of diameter $\simeq R_{\odot}$, an upper limit on the mass of a typical core (a substantial fraction of the total clump mass) is only of the order of a few x 10^{19}g. This mass is roughly 1 - 10 times the mass of a typical comet. As pointed out by Evans (1981) for RU Lup, such low-mass clumps in planetary orbits would not be stable against gravitational shear. Therefore the light variations of RY Lup cannot be attributed to clumps travelling in planetary orbits and if they do form physically isolated clumps, such clumps must therefore be moving in essentially hyperbolic orbits (cf. Ulrich 1976, Chevalier 1983).

5.1.4. The Flux Distribution.

Extensive simultaneous UBVRI and JHKL photometry of RY Lup is available (Kilkenny et al., 1985) from 1981 to 1984, and simultaneous BVRI, JHKL and MNQ photometry of RY Lup was also obtained on several nights in 1987. This provides an ideal database with which to look for variations both in the effective temperature and reddening of the star (although it is not always easy to distinguish the two) and in the temperature of the inferred hot dust near-IR excess. Luminosity and size estimates of the circumstellar shells can also be made.

In view of the fact that the light variations over the period 1981 - 1984 are best interpreted in terms of variable circumstellar extinction, the reddening correction applied to the photometric data will be left as a free parameter, with a value of $E(B-V)_{IS} \simeq 0.18$ being assumed for the IS reddening (see Section 5.1.3.1). If the

possibility is considered that the effective temperature of the star varies, the required range of T_{eff} fits to the data dereddened by just the assumed IS $E(B-V)_{IS}$ of 0.18, was investigated. It was found that, in order to successfully fit the data, temperatures in the range 5100K - 3800K were required. As pointed out in Sections 5.1.2 and 5.1.3, the lower limit on a cool photosphere is ≃ 4000K, and the lower range of these fits is therefore unacceptable. This is again consistent with the conclusion of the previous section that the observed light variations, in particular the deep minima, cannot be ascribed to photospheric starspots; variable circumstellar extinction being the only mechanism which fits the data consistently.

The coolest available Kurucz (1979) model atmosphere is 5500K and thus a 5100K blackbody is chosen as the best approximation to the "typical" K0-1V photosphere of RY Lup, although using a blackbody does neglect the effects of line blanketing at blue wavelengths. The data at each epoch are thus dereddened until the V-I colour slope (i.e. avoiding Hα emission at R) of the 5100K blackbody is successfully fitted. With this procedure, it is found that there is a fairly large range in the values of the total E(B-V) required to deredden the data (which reflect the large changes, $\Delta V \simeq 2$ mag., in visual flux of RY Lup), as is indicated in Table 5.1.1, where the total reddening required and the resultant fits obtained are summarised. It was found that a blackbody in the range ≃ 1400 - 1450K could successfully fit the near-IR excess at each epoch.

Although near-IR data were obtained on HJD 2447043, in view of the large nightly variation in both the optical and IR fluxes of RY Lup, it was not appropriate to combine these data with the optical photometry of HJD 2447044. One of the fits is shown when the star

Table 5.1.1.

Parameters of the fits to RY Lup photometry.

Date (HJD 2440000+)	E(B-V)	$(R/D)_*$ ($R_\odot kpc^{-1}$)	T_{dust} (K)	$(R/D)_1$ ($R_\odot kpc^{-1}$)
4742	0.48	16.6	1450	190
4743	0.18	20.0	1450	205
4823	0.20	22.7	1450	175
4828	0.50	13.0	1450	180
5079	0.37	17.1	1450	185
5104	0.18	22.6	1450	185
5418	0.20	24.5	1450	180
5420	0.42	16.1	1450	180
6998	0.43	17.4	-	-
6999	0.53	16.2	1400	195
7041	0.30	20.9	1400	185
7042	0.72	20.1	1400	215
7044	0.42	20.1	-	-
7049	0.22	22.2	1400	210

The total reddening of the photometry at each date is given by E(B-V). The normalisation of the fits of a stellar (T_{eff} = 5100K) blackbody and a dust (T_{dust}) blackbody to the optical and near-IR photometry are given by $(R/D)_*$ and $(R/D)_1$ respectively, where R represents the radius of the fitted component and D represents the distance to RY Lup (in appropriate units).

appears most heavily reddened (HJD 2447042 - Fig. 5.1.13).

Also, in view of the observed variation in V, B-V when the star is faint (see discussion in Section 5.1.3.3), an attempt could have been made to separate the reddening into three components when RY Lup was faint, namely: an IS component; a circumstellar component with a normal extinction law; and a circumstellar component with an anomalous reddening law. However, with the uncertainty in $E(B-V)_{IS}$ this would be unlikely to lead to any meaningful results, and a normal reddening law was therefore assumed throughout.

In the far-IR, RY Lup is flagged as a variable source in the IRAS PSC (Beichman et al., 1985), and so the range of the variation within the raw (i.e. non-colour corrected) IRAS data was inspected. The range of variation seen in the raw data over a timescale of ≈ 215 days, in bands I - IV were 0.36, 0.42, 0.82 and 0.69 Jy respectively. Therefore the Band I and II IRAS fluxes of RY Lup cannot be expected to tie in with the 1987 far-IR photometry.

The IRAS fluxes (the vertical bars indicate the extent of the variability observed by IRAS) were plotted with the optical, near- and far-IR data obtained on HJD 2447049 in λF_λ in order that the luminosity out to 100μm could be estimated (see Fig. 5.1.14). The photometry from this night is chosen as the star was bright - thus the luminosity should not be over-estimated as may occur if the photometry is over-reddened. Three blackbody components were required to fit the photometry, with temperatures of 5100K, 1400K and 110K. It was also possible to fit the near-IR excess of RY Lup with thermal emission from an optically thin dust disc (see Hutchinson et al., 1989).

A temperature of ≈ 1400K is therefore the maximum dust temperature T_{max} surrounding RY Lup, which compares well with the value of T_{max}

indicated in the near-IR colour-colour diagrams (Section 5.1.3.3). From the peaks of the three blackbody components in λF_λ, the total bolometric luminosity is estimated to be 2.54 $L_\odot$ (assuming a distance of 150 pc; Gahm et al., 1979), with the ratio $L_{IR}/L_{Bol} = 0.45$ (independent of distance). This estimate of the observed luminosity agrees well with the estimate of 2.63 $L_\odot$ obtained by Bouvier et al. (1986b), and is considerably brighter than the luminosity of a normal K0V star of 0.4 $L_\odot$ (Allen 1973).

Although the ratio of L_{IR}/L_{Bol} is large, given that RY Lup is often affected by $\simeq$ 2 mag. of circumstellar extinction, re-radiation by a "clumpy" dust shell extending over essentially 4π steradians is not implausible. From Eq. (4.1), the expected distance of "real" silicate grains thermally heated to $\simeq$ 1400K around RY Lup (with L = 2.54 $L_\odot$) is 33 $R_\odot$. This value is in very good agreement with the estimated upper limit on the size of the fitted $\simeq$ 1400 - 1450K dust shell of 29 $R_\odot$, which was determined by averaging the $(R/D)_1$ values in Table 5.1.1 (with d = 150pc) obtained from fitting the IR excess with a $\simeq$ 1400 - 1450K blackbody. This finding is consistent with the representation of the near-IR excess of RY Lup by thermal re-emission by a circumstellar shell of silicate dust. Note also that the wavelength dependence of the polarisation also indicates the presence of silicate dust associated with RY Lup (Section 7.3.2.9).

The stellar radius is estimated, assuming hydrostatic equilibrium with T_{eff} = 5100K (for a K0-1 star) and L = 2.54 $L_\odot$, to be $R_* \simeq$ 2.1 $R_\odot$. At an assumed distance of 150pc, the mean value of $(R/D)_*$ in Table 5.1.1 gives $R_* \simeq$ 3.0 $R_\odot$, a value which would require RY Lup being either more luminous or slightly cooler than indicated, although the disagreement in the values of R_* is not particularly significant.

Taking the radius estimate of 2.1 $R_\odot$ together with the measured rotational velocity of v sin$i$ = 25.0 ± 4.6 kms^{-1} (Bouvier et al., 1986b), and assuming a rotational period of 3.7 ± 0.2 days, suggests an inclination angle of ≃ 60° (with a likely error of ± 15° due to the uncertainties in the assumed values). Within the errors, this would indicate that RY Lup is being viewed between about 15° - 45° away from its equatorial axis.

With this result, if RY Lup does have a disc (although there is no compelling evidence for one), provided such a disc had an opening angle of ≃ 30°, it would be reasonable to suggest that dust constrained to a disc-like geometry around RY Lup could conceivably affect the line-of-sight extinction.

In conclusion, the optical and IR photometry indicates that a considerable fraction of the total luminosity of RY Lup is radiated at IR wavelengths. The IR excess requires a sizable circumstellar dust shell, much of which probably subtends essentially 4π steradians and attenuates and re-radiates nearly half the stellar radiation. Inhomogeneities in such a dust distribution could, in principle, account for the observed frequency of minima due to obscuration by circumstellar dust (Section 5.1.3.4).

5.1.5. Polarimetric observations.

RY Lup is a polarimetric variable, and the observed position angle is markedly different from the IS position angle in the vicinity of RY Lup (Bastien 1985). Thus the polarisation of RY Lup is evidently intrinsic to the star. In Section 7.3.2.9 it is shown that the wavelength dependence of the polarisation close to polarimetric

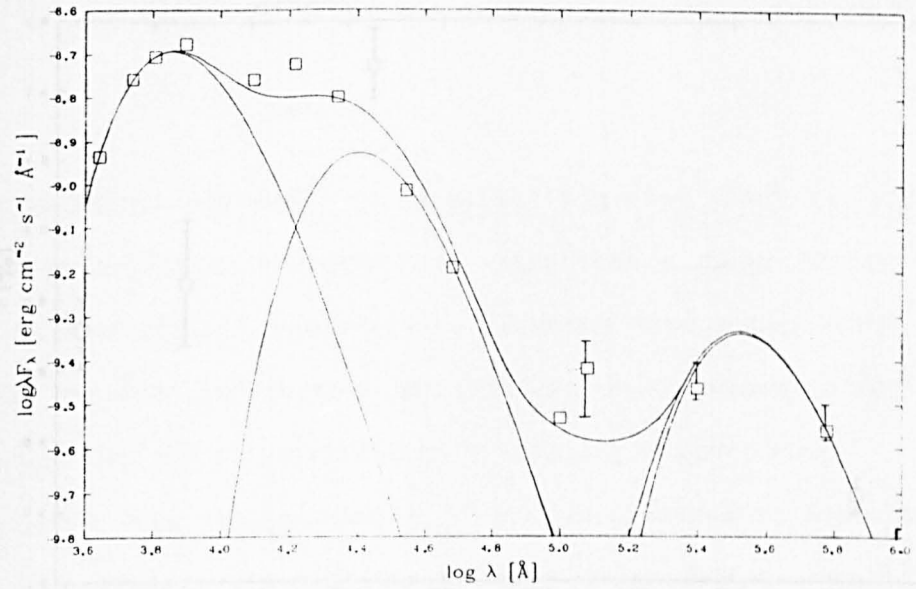

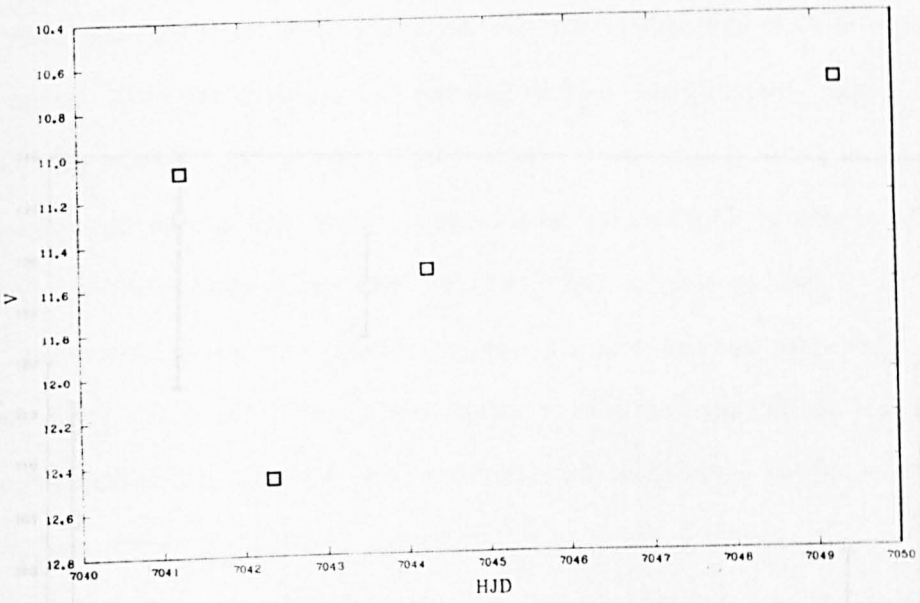

Fig. 5.1.14. Flux distribution of RY Lup on HJD 2447049 with IRAS data included. Vertical bars indicate the range of variability observed by IRAS. See also Section 5.1.4.

Fig. 5.1.15. V photometry of RY Lup from HJD 2447041 to HJD 2447049. The date is given in HJD 2440000+.
See also Section 5.1.5.

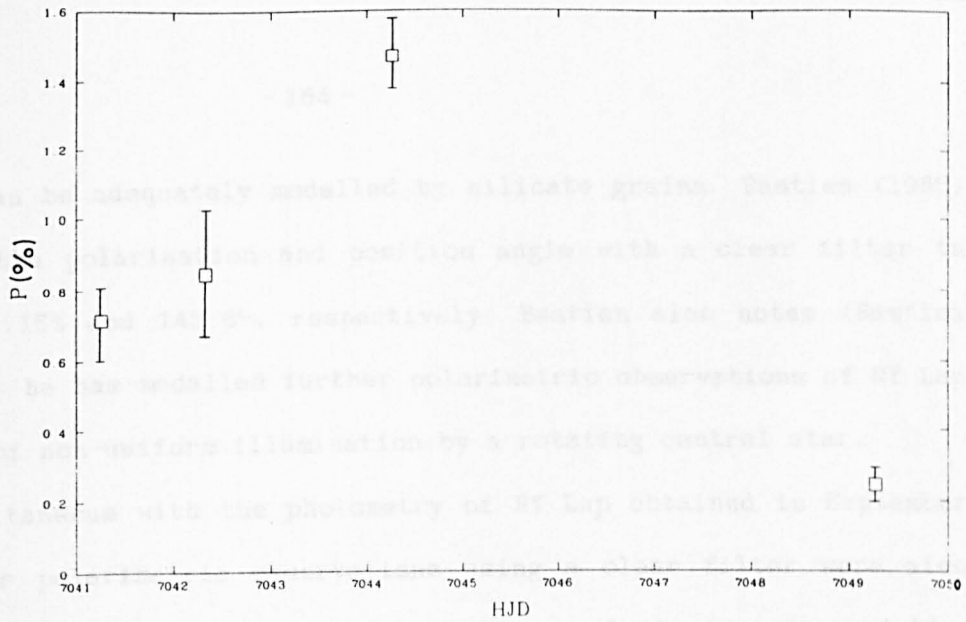

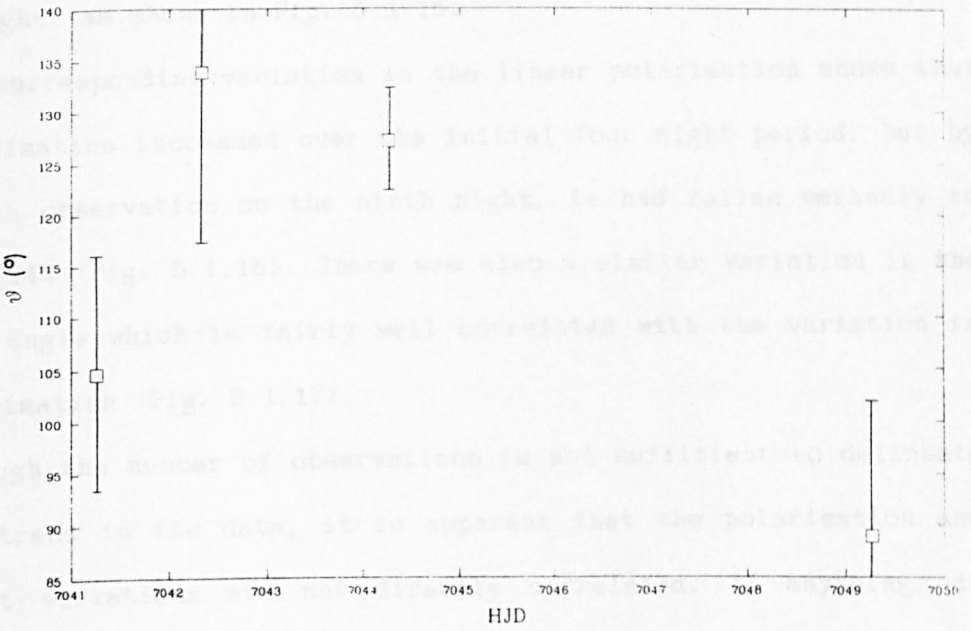

Fig. 5.1.16. Optical polarisation of RY Lup observed from HJD 2447041 to HJD 2447049. The date is given in HJD 2440000+ and the polarisation in %.
See also Section 5.1.5.

Fig. 5.1.17. Position angle of RY Lup observed from HJD 2447041 to HJD 2447049. The date is given in HJD 2440000+ and the position angle in degrees.
See also Section 5.1.5.

minimum can be adequately modelled by silicate grains. Bastien (1985) measured the polarisation and position angle with a clear filter in 1985 as 1.15% and 143.6°, respectively. Bastien also notes (Bastien 1987) that he has modelled further polarimetric observations of RY Lup in terms of non-uniform illumination by a rotating central star.

Simultaneous with the photometry of RY Lup obtained in September 1987, four polarimetric observations using a clear filter were also made. The polarisation and position angle were both strongly variable. Over the observed period, the star faded over the first two days, becoming redder when fainter, and subsequently brightened again to normal light, as shown in Fig. 5.1.15.

The corresponding variation in the linear polarisation shows that the polarisation increased over the initial four night period, but by the fourth observation on the ninth night, it had fallen markedly to only $\simeq$ 0.24% (Fig. 5.1.16). There was also a similar variation in the position angle which is fairly well correlated with the variation in the polarisation (Fig. 5.1.17).

Although the number of observations is not sufficient to delineate a clear trend in the data, it is apparent that the polarisation and the light variations are not directly correlated. If anything, it would seem that the optical light and polarimetric variations are anti-correlated. However, there is a limited correlation between the degree of polarisation, p, and the V-L colour (cf. Bastien 1985), which is seen in three of the four observations. The value of p in the four observations is 0.72, 0.84, 1.45 and 0.24%, and the value of V-L in the four observations is 5.14, 6.24, 5.63 and 4.68.

Variability in the optical polarisation which is unrelated to the visual light variations but may be related to the degree of IR excess

(i.e. dust) emission is most easily interpreted in terms of multiple scattering in a non-uniform asymmetrical dust shell. Multiple scattering is required to reproduce the degree of maximum polarisation, and a non-uniform asymmetric dust shell is required to account for the variability in both p and θ. An asymmetric dust shell confined to a narrow solid angle (i.e. a lop-sided, inclined disc) would probably be less likely to produce large variations in p than would a more spherical, asymmetric dust shell (see Section 2.2.5). The timescale of the variability constrains the bulk of the scattering dust to lie close to the star (within the region of $\simeq 10^2$ A.U.).

It is not unreasonable to consider such a non-uniform dust shell covering 4π steradians (such as could explain the IR excess) in terms of a randomly distributed ensemble of "clumps" or cloudlets of enhanced density such as are required to account for the deep minima in the lightcurve of RY Lup.

However, when starspot regions are present on the photosphere of RY Lup, the proposal mentioned in Bastien (1987) is certainly tenable and such a model would produce essentially correlated, periodic variations in V and p, as a phase lag of only a few hours at most is expected in view of the likely distance of the circumstellar dust, between $\simeq$ 0.5 and 25 A.U. (see also Section 7.4.2.1), determined from the dust temperatures, 1400K and 110K respectively, which were required to fit the IR excess (Section 5.1.4). Such a model clearly could not be reasonably expected to interpret the rise in polarisation discussed here as there was no correlated rise in V.

Therefore it is concluded that the observed variation in the polarisation and the limited correlated variation in V-L would not be

inconsistent with an ensemble of dust cloudlets, such as was discussed in Section 5.1.3.4 in order to interpret the frequency of optical light minima. If this view is correct, it is interesting to note that another InT star, RY Tau, which also exhibits occasional deep minima in its lightcurve (see Fig. 2.2.5) has also been observed to undergo similar polarimetric variations to RY Lup, variations which have been interpreted in terms of scattering by an ensemble of "orbiting" dust clouds (Efimov 1980).

5.1.6. Summary and Conclusions.

The spectrum of RY Lup has been observed whilst the star was fading and shows evidence of weak TiO bands. The spectrum was classified at K5-7, which is the latest spectral type that has been observed for RY Lup. It is suggested that the spectral variability of RY Lup is essentially due to the appearance of large, cool ($\simeq$ 4000K) starspot regions.

It has been shown however, that in the period between 1981 - 1984, the observed lightcurve of RY Lup did not show any periodic variations that could be attributed to an intrinsic, rotational modulation due to starspots. Also the V, B-V variability cannot be reasonably modelled by an intrisically variable photosphere. The observed light and colour variability can be more convincingly modelled by a mechanism of variable circumstellar extinction, although the occurrence of additional, low-amplitude intrinsic variability is not unlikely. This is in view of the fact that RY Lup can exhibit both variation in spectral type (as has been affirmed here) and also periodic ($\simeq$ 3.7 days) variability (e.g. Hoffmeister 1965) attributable to starspots.

In addition, RY Lup was observed to suffer several deep ($\Delta V \simeq 1.5$ - 2 mag.), short-term ($\simeq$ 1-2 days) minima which can be attributed to near-total occultations of the stellar disc by circumstellar dust cloudlets. The term "cloudlet" refers here to either a density enhancement, or a clump in a hyperbolic orbit, within the circumstellar dust shell. During several of these minima, RY Lup is more heavily reddened than would be expected from a normal extinction law, and therefore it is proposed that such dust cloudlets have cores which contain large grains. Also, as enhanced Balmer line emission (observed either directly, or inferred from Hβ photometry) has been observed to be associated with some of these minima, the size of the cloudlets must typically be of the order of a stellar radius. It is also suggested that the observed frequency of dust eclipses and the observed variation in the optical polarisation requires an ensemble of such dust cloudlets in motion around RY Lup.

The wavelength dependence of polarisation and the nature of the near-IR excess are both consistent with the presence of silicate grains around RY Lup. The variability in the position angle of polarisation, the frequency of occurrence of deep minima, the likely inclination of the rotation axis of RY Lup and the large fraction of total luminosity radiated in the IR each provide some level of constraint on possible dust shell geometries. A "clumpy" distribution of dust across essentially 4π steradians seems not unlikely, although it would not be a simple matter to convincingly ascertain a preferred dust shell geometry for RY Lup.

5.2. The "extreme" T Tauri star RU Lup.

5.2.1. Introduction.

Joy (1945) included RU Lup in his original work on the spectra of emission line variable stars associated with nebulosity. RU Lup is observed in the Lupus T association against a dark galactic dust lane in a region of high IS reddening (Gahm et al., 1975), although RU Lup is itself not heavily reddened (e.g. Gahm et al., 1981).

Whitmore et al. (1987) obtained CCD images (centred at the wavelengths of Hα and [OI] emission) of the nearby Herbig-Haro emission nebula HH55 (2' distant from RU Lup). They concluded that as RU Lup is an active star and the only adjacent IRAS source, it is probably the exciting source of HH55. RU Lup is also associated with a H_2O maser source (Whitmore et al., 1987).

The photometric variability of RU Lup at V was closely monitored for two periods of several months by Hoffmeister (1958, 1965), and from his observations obtained a periodicity for the light variations of 3.54 days. A later analysis of the first set of data by Plagemann (1969) gave a period of 3.7 ± 0.2 days. The lightcurve varies from 9.6 < V < 13.4 mag. and shows a tendency to reside at a mean brightness of V ≈ 11.0 mag. (Kholopov et al., 1987). The observed variations are slow and rarely dramatic.

Due to the extreme nature of the observed emission line optical spectrum (RU Lup is a prime example of an "extreme" InT star) causing heavy veiling of the photospheric spectrum, RU Lup is not an easy candidate to classify on the MK system. The veiling in RU Lup may be due to overlying free-free and free-bound continuum emission from an

extended envelope and/or the blending of many weak emission lines such as FeI (Rydgren et al., 1976) originating in a deep chromosphere. Because of the strong veiling of the photospheric absorption spectrum, Joy (1945), Herbig (1962) and Kuhi (1964) were unable to assign RU Lup a spectral class.

The first observation and analysis of the photospheric spectrum, thereby facilitating the first reliable estimate of the spectral class of RU Lup, was by Schwartz and Heuermann (1981) who obtained a high-dispersion spectrum of RU Lup whilst the star was at minimum light (V $\simeq$ 11.7 mag.). They suggested a spectral classification in the range K0 - K5. Subsequent detection of TiO bands in the spectrum by Appenzeller et al., 1983) suggested that RU Lup has a $\simeq$ K7 spectral type.

The blue veiling strongly affects the U-B colour of RU Lup (which has a mean value of $\simeq$ - 0.87, Gahm 1980), which is far bluer than the intrinsic U-B colour (U-B = 1.22, Johnson 1966) of a normal late KV star. However, unlike InT stars which have a strongly veiled optical spectrum and a considerable UV continuum excess attributable to an active chromosphere with a deep temperature minimum, RU Lup does not have a strong UV flux excess (Appenzeller et al., 1980). This would therefore suggest that a significant fraction of the veiling in RU Lup is due to continuum emission from an extended envelope.

RU Lup has been extensively studied in the UV using the IUE, with no less than 17 SWP spectra and 24 LWP spectra taken. It is one of the few InT stars with lines bright enough to be observed at high resolution. There have been many strong UV emission lines observed, particularly those of MgII (2795, 2803Å), CIV (1548, 1551Å) and SiIV (1394, 1403Å). The CIV and SiIV resonance lines are strongly broadened which indicates that they are formed in a very turbulent region (Brown

et al., 1984). Cram et al. (1980) have used the fluxes of the CII - CIV and SiII - SiIV lines in order to infer the temperature distribution and the emission measure of the line emitting region of RU Lup. Their results give a rough estimate of the temperature and electron density of the region of high excitation, $T_e \simeq 7 \times 10^4$ K and $N_e \simeq 1.6 \times 10^{10}$ cm^{-3}. This would indicate that the source depth of the UV emission between $T_e \simeq 6 \times 10^4 - 6 \times 10^5$K, is about 10% of the stellar radius.

A near-IR flux excess in RU Lup was first noted by Geisel (1970), and fitting of this excess was included in the work of Gahm et al. (1974). They fitted the optical photometry with a 4400K blackbody and free-free and free-bound emission from an extended envelope to fit the excess at U. The free-free and free-bound continuum could not however fully account for the near-IR excess, and an additional 700K blackbody component was required, which they attributed to thermal re-emission of stellar radiation by circumstellar dust.

Kuhi (1964) was the first to attempt an analysis of the line profiles of the Hγ, Hδ and CaII K emission lines. His spherically symmetric mass loss model gave an early estimate of the mass loss rate in RU Lup of 1.42×10^{-7} $M_\odot yr^{-1}$, which is about an order of magnitude higher than subsequent estimates. For example, Brown (1987a) observed a 3σ upper limit of the 6cm radio emission from RU Lup which constrains the rate of ionised mass loss to be $\leq 10^{-8}$ $M_\odot$ yr^{-1}.

In Lago and Penston (1982) and Lago (1982, 1984), a more detailed analysis and modelling of the observed line emission of RU Lup was carried out. Four emitting regions within the expanding envelope were defined, each characterised by a different velocity, density and temperature. From each of the regions arise emission from (i) the

metallic lines; (ii) the Balmer lines and optical resonance lines; (iii) the helium lines and the UV resonance lines; (iv) the forbidden lines. The blueshifted velocities of the [OI] and [SII] lines (Schwartz and Heuermann 1981) indicate outward motion of a well-defined (from the persistence of these lines) region of low density, and also that the receding shell of forbidden emission may possibly be obscured by a circumstellar disc (cf. Edwards et al., 1987).

Within the observational constraints of the physical parameters (the characteristic T_* and N_* of each ionised species) defining the emitting region, an Alfvénically driven wind model was developed by Lago (1984) for the emission envelope. A model with parameters of $B_\odot$ = 600 Gauss, $N_* = 10^{13}$ cm^{-3}, $T_* = 10^4$K, provides a good fit to some of the observed higher Balmer line profiles, and hence to the velocity law of expansion of the emitting region. A similar model has also been developed by Kuin (1986), a model which Brown (1987a) indicates is more compatible with the observed upper limit on the rate of ionised mass loss imposed from 6cm radio observations (see above).

Gahm et al. (1974) observed rapid ($\simeq$ 6 hrs) increases of $\approx$ 0.5 mag. in the U band, which they suggest may be taken as evidence for flaring activity in RU Lup, and their narrow-band photometry at various optical bandpasses showed correlated variations in brightness, with a trend towards decreasing amplitude of variation from blue to red wavelengths (a characteristic of the lightcurve noted by Herbig 1961). From their spectroscopic measurements, they noted that the relative intensities of the observed emission lines are very similar to those observed in the solar chromosphere.

Observations such as these help to underline Joy's (1945) original comment that the emission line spectrum of RU Lup is similar to that

of the sun when observed during a solar eclipse. This can be a useful analogy to make, although the emission envelope of RU Lup is clearly more complex than simply a scaled-up version of the solar chromosphere (see e.g. Giovannelli et al., 1986). Neither is there any evidence that RU Lup has a "solar-type" corona, following unsuccessful searches for X-ray emission (Feigelson and DeCampli 1981) and the 6375Å [Fe X] coronal line (Gahm et al., 1981) in RU Lup. As discussed in Section 2.2.1, X-rays in InT stars are probably formed in coronae or coronal flares and not in stellar winds. The transfer of heat energy out from the transition region by an Alfvénically driven wind (Lago 1984) would be likely to prevent the formation of a "coronal" X-ray emitting region (see Section 2.2.1). This explanation of the absence of X-ray emission is to be favoured in the case of RU Lup.

Further, from their blue spectral observations, Gahm et al. (1974) point out that as the stellar continuum varied, the line-to-continuum ratio for the emission lines remained essentially constant. Their interpretation of this observation is that most, if not all, of the observed luminosity variations of the star are due to changes in opacity of a surrounding circumstellar dust envelope. This led to a further discussion (Gahm et al., 1975) of the possibility that RU Lup is orbited by circumstellar dust clumps. Whilst commenting on the plausibility of this mechanism to interpret the observed spectroscopic variations, and quoting the required velocities and (planetary) distances for such orbiting clumps, their analysis failed to quantitatively investigate whether their proposition of such clumps orbiting the star at planetary distances was actually viable.

Evans (1981) showed that such a propositon was actually not physically plausible, as such condensations would be affected by

considerable gravitational shear and thus would be susceptible to tidal disruption. He did however, suggest two possible ways in which the condensations could remain stable against gravitational shear; either large grains ($\rangle$ 100μm) could gravitationally bind the clumps, or if the grains had an electric charge, then a strong stellar magnetic field ($\rangle$ 10^4 Gauss) could sustain bound condensations.

A 2.3σ detection of a magnetic field of $\simeq$ 550 Gauss associated with RU Lup was reported by Johnstone and Penston (1986). However their subsequent observations (Johnstone and Penston 1987) failed to confirm this detection and placed a 3σ upper limit of 495 Gauss for the magnetic field of RU Lup. Thus, unless RU Lup exhibits a strong far-IR excess and/or anomalous reddening at minimum light (both of which would suggest the presence of very large grains), it would therefore seem unlikely that circumstellar dust clumps can orbit RU Lup as was proposed by Gahm et al. (1975).

Indeed, high resolution spectroscopic observations of RU Lup by Boesgaard (1984) over five nights, unlike the observations of Gahm et al. (1974), showed definite changes in the line-to-continuum ratio of many of the metallic lines as RU Lup varied, thus indicating that the observed brightness variations of RU Lup are more likely due to intrinsic changes in the "chromospheric" activity rather than variable circumstellar extinction. Further, Boesgaard (1984) proposed that the variability in the widths of the strong lines is due to a rotational modulation of the emission envelope. The blueshifted absorption feature which is always observed in the profile of the strong Hα line at high resolution (Schwartz and Heuermann 1981, Boesgaard 1984) has been related to a previously ejected shell of matter (Boesgaard 1984). This further affirms that the extended envelope of RU Lup is in a

state of expansion.

5.2.2. The Optical and Infrared spectra.

5.2.2.1. Introduction.

A low resolution ($\Delta\lambda \simeq 2.8$Å) optical spectrum of RU Lup was obtained at SAAO on HJD 2446998 whilst the star was probably fading (from V = 10.74 mag. on HJD 2446995 to V = 11.06 mag. on HJD 2446998) and also becoming redder (from B-V = 0.57 to B-V = 0.69 on the same respective nights). The spectrum is shown, along with identification of the strong lines, in Fig. 5.2.1.

The optical emission line spectrum of RU Lup has been observed many times, and is always found to be variable. Therefore, the nature of the envelope can only be properly understood when account of the variability of the lines is made. Thus the observed spectrum will be compared with previous studies of the optical spectrum.

Because the spectrum contains many emission lines, several of the lines (particularly HeI and FeII) form blends at the observed resolution. Where this did lead to difficulty in the unambiguous identification of particular lines, the stronger lines within blends noted by previous authors (Schwartz and Heuermann 1981; Lago and Penston 1982) were taken as being the dominant contributing species.

Two IR spectra (at J, Fig. 5.2.2 and K, Fig. 5.2.3) were obtained a month earlier at CTIO in June, 1987. From simultaneous near-IR photometry obtained with the optical and IR spectra, RU Lup was slightly fainter (by 0.1 mag.) in the IR when the CTIO IR spectra were obtained. The J spectrum is fairly flat, whilst the K spectrum shows a

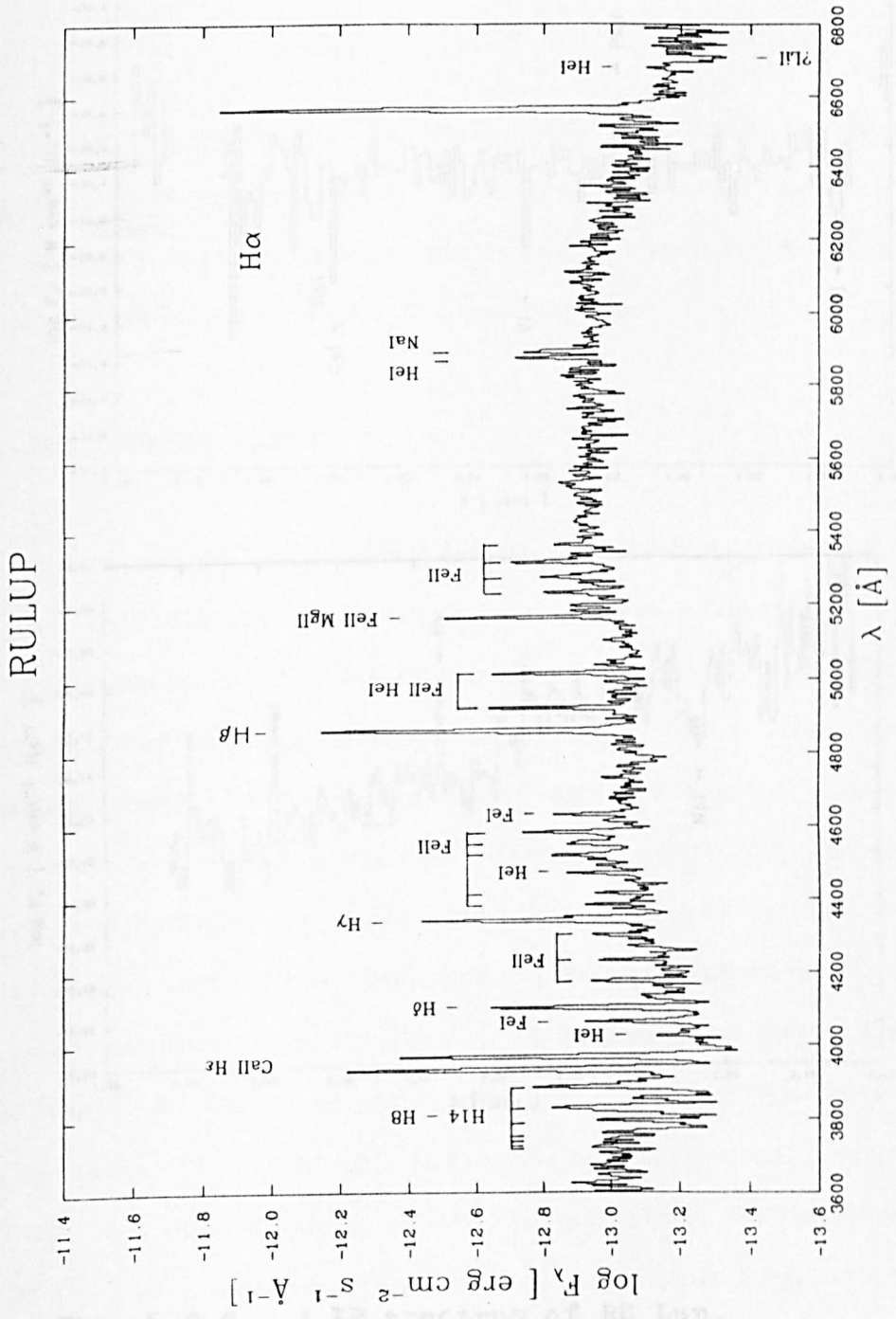

Fig. 5.2.1. Optical spectrum of RU Lup.
See also Section 5.2.2.

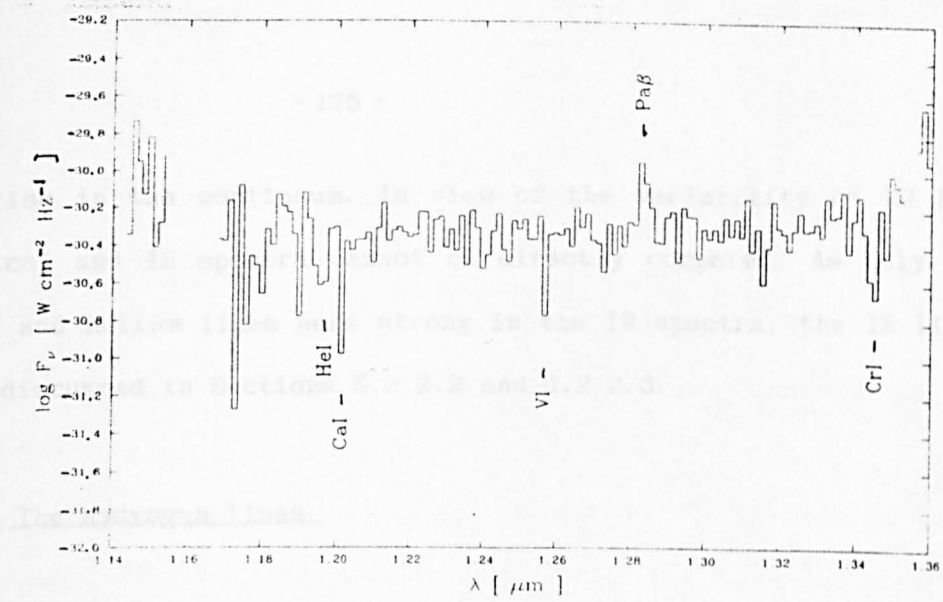

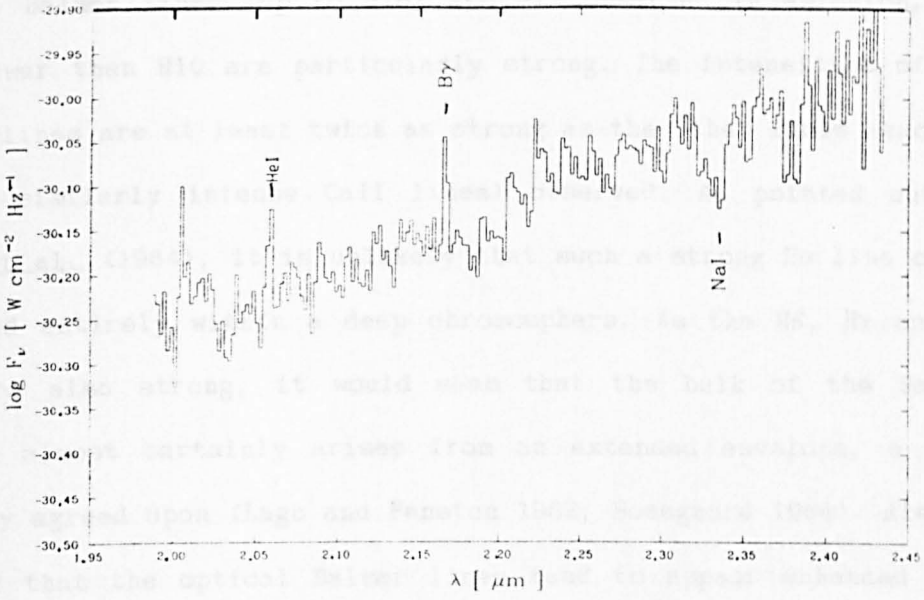

Fig. 5.2.2. J IR spectrum of RU Lup.
See also Sections 5.2.2.1, 5.2.2.2 and 5.2.2.3.

Fig. 5.2.3. K IR spectrum of RU Lup.
See also Sections 5.2.2.1, 5.2.2.2 and 5.2.2.3.

slight rise in the continuum. In view of the variability of RU Lup, the optical and IR spectra cannot be directly compared. As only the hydrogen and helium lines were strong in the IR spectra, the IR lines will be discussed in Sections 5.2.2.2 and 5.2.2.3.

5.2.2.2. The Hydrogen lines.

The Balmer lines (up to H19) are all observed in emission, the lines lower than H10 are particularly strong. The intensities of the Hδ - Hα lines are at least twice as strong as the other lines (excluding the similarly intense CaII lines) observed. As pointed out by Calvet et al. (1984), it is unlikely that such a strong Hα line could be formed entirely within a deep chromosphere. As the Hδ, Hγ and Hβ lines are also strong, it would seem that the bulk of the Balmer emission almost certainly arises from an extended envelope, a view generally agreed upon (Lago and Penston 1982, Boesgaard 1984). Also it is noted that the optical Balmer lines tend to appear enhanced when RU Lup is faint (Schwartz and Heuermann 1981; Giovannelli et al., 1986). The observed strength of the Balmer lines on HJD 2446998, whilst RU Lup was probably fading, is thus not inconsistent with this.

Two near-IR HI lines (Paα and Bβ) have also been observed by Giovannelli et al. (1986) using filter-wheel spectroscopy. These lines were observed in both emission and absorption. Giovannelli et al. (1986) indicate that the lines appeared in absorption only when RU Lup was both brightest (J = 8.35 mag.) and reddest (H-K = 1.23) in the IR. Two higher, and thus "weaker" near-IR transitions were detected in the CTIO spectra when RU Lup was both fainter (J = 8.83 mag.) and bluer (H-K = 0.75) in the IR than when observed by Giovannelli et al.

(1986): the Paβ (1.282μm - Fig. 5.2.2) and Brγ (2.166μm - Fig. 5.2.3) lines, both of which were observed in emission. Thus the behaviour in the near-IR HI lines observed by Giovannelli et al. (1986), that the near-IR lines are in emission when the near-IR continuum of RU Lup is both faint and blue, is confirmed.

Intrinsic stellar (photospheric and chromospheric) and envelope emission from RU Lup probably dominate both the near-IR line and continuum emission, whilst thermal continuum emission from dust (as proposed by Gahm et al., 1974) is probably only important beyond ≈ 2μm (suggested by the rise in the continuum at K; see also Fig. 5.2.8). That the optical and near-IR HI emission from the envelope is inversely correlated with the strength of the free-free, free-bound continuum emission from the envelope could potentially be explained in one of two ways:

RU Lup is dimmed either by cool surface regions or by circumstellar dust. Thus when RU Lup is faint, the envelope HI line emission is enhanced by a "supression" of the photospheric emission (similar to that discussed for RY Lup) produced by either starspots or cloudlets of circumstellar dust;

The HI line emission and the free-free, free-bound emission essentially arise in two separate regions of the envelope, with the HI line emission region lying within the free-free, free-bound region. Thus when the envelope continuum is strong, the near-IR HI transitions are strongly affected by self-absorption.

The first proposal effectively supposes that the optical and near-IR variability is dominated by changes in the observed photospheric continuum emission. Such a supposition is difficult to support however in view of the strong veiling of the photospheric continuum. Thus the

second proposal is probably the more likely. Also in view of the well-stratified emission line regions in the envelope (Lago and Penston 1982), it would not be inconsistent to suggest that much of the Balmer line emission forms in a region of the envelope separate from the highly excited region where free-free continuum emission and the lines of high excitation arise.

5.2.2.3. The Helium lines.

As with the Balmer series, many members of the HeI series were observed in emission, although at the observed spectral resolution, several of the HeI lines form blends with other strong lines of HI and FeII. The observed optical and (non-simultaneous) IR singlet and triplet transitions are indicated in Fig. 5.2.4. In this, and the subsequent Grotrian diagrams, an observed transition is indicated by an arrow. The wavelengths which are included in brackets denotes transitions which were either not reliably covered in the spectra or not observed, and transitions which were possibly present, but are not certain, are denoted by a question mark. Also any forbidden or semi-forbidden transitions are marked with a dashed line.

Although strong, the HeI optical spectrum is not as strong as is usually observed (cf. Giovannelli et al., 1986). With the poor signal-to-noise redward of ≈ 6800Å it is impossible to determine whether the expected HeI lines at 7065 and 7281Å are present. The HeI triplet 4471 and 5875Å lines are not blended with other strong lines, and are therefore clearly strong. From the strength and position of the singlet HeI 4921Å and FeII (42) 4923Å blend at 4925Å, and in view of the fact that the other FeII (42) multiplet lines are strong, it is

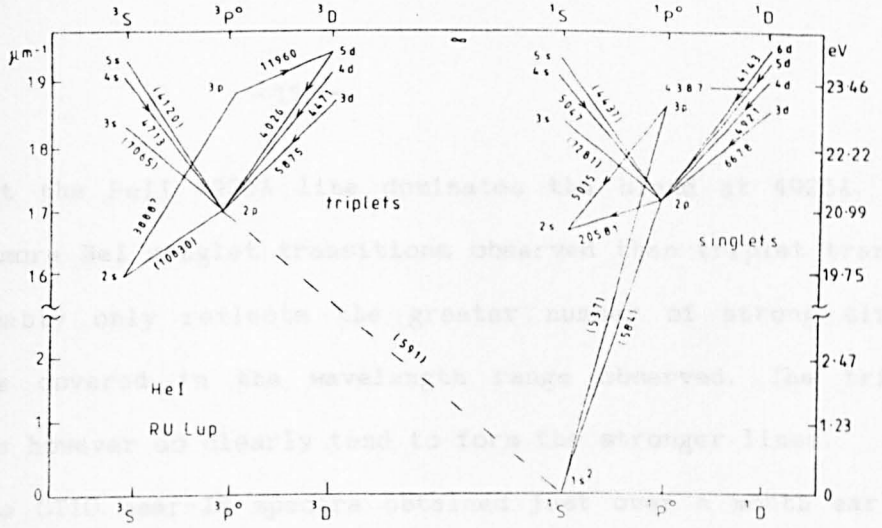

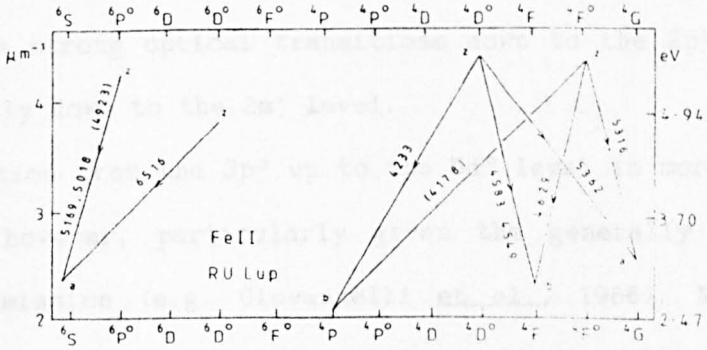

Fig. 5.2.4. HeI Grotrian diagram for optical transitions observed in RU Lup.
See also Section 5.2.2.3.

Fig. 5.2.5. FeII Grotrian diagram for optical transitions observed in RU Lup.
See also Section 5.2.2.5.

likely that the FeII 4923Å line dominates the blend at 4925Å. That there are more HeI singlet transitions observed than triplet transitions, probably only reflects the greater number of strong singlet transitions covered in the wavelength range observed. The triplet transitions however do clearly tend to form the stronger lines.

In the CTIO near-IR spectra obtained just over a month earlier, the singlet HeI 2p - 2s 2.058μm line is clearly in emission and the absorption feature at 1.195μm is attributed to the triplet HeI 3p - 5d 1.196μm transition. The strong HeI 2.058μm emission line is certainly expected as the strong optical transitions down to the $2p^1$ level can decay radiatively down to the $2s^1$ level.

The transition from the $3p^3$ up to the $5d^3$ level is more difficult to understand however, particularly given the generally strong HeI optical line emission (e.g. Giovannelli et al., 1986). Now, at the resolution of the SAAO spectrum, it is impossible to determine whether the 3888Å $3p^3$ - $2s^3$ HeI line is present because of the strong 3889Å H8 line. Given the strength of the other optical HeI transitions from the similarly energetic $4s^3$ and $4d^3$ levels (see Fig. 5.2.4), it would be expected that the 3888Å HeI line should be observable in emission. However, even in low resolution spectra the 3888Å line is not observed (e.g. Schwartz and Heuermann 1981, Lago and Penston 1982), and it is therefore suggested that the HeI 3888Å line is weak because it is affected by significant self-absorption. Self-absorption of the $3p^3$ - $2s^3$ transition is important because radiative transition from $2s^3$ down to $1s^1$ is strongly forbidden (Osterbrock 1974).

If this view is correct, then it would be expected that the $3p^3$ - $3s^3$ 4.3μm line should be observable in emission, and this line should be looked for. But whether population of the $3p^3$ level could also give

rise to the 1.196μm $3p^3$ - $5d^3$ transition, by collisional excitation say, is not certain, and the 1.196μm line should also be monitored.

Weak HeII emission lines are also seen in the optical spectrum. The lines observed are the 3814, 4686 (blended with FeI) and possibly the 6560Å line (a possible blend with the intense Hα line) may also be present, but this is impossible to ascertain. It is also noted that the HeII 1640Å line is usually (but not always: Gahm et al., 1979) observed in the UV spectrum of RU Lup (e.g. Giovannelli et al., 1986).

If the emission envelope is formed by a magnetically accelerated wind as is suggested by Lago (1984) and Kuin (1986), such a wind will tend to transfer heat away from the transition region, and when the wind decelerates (within ≃ a few R_*), will commence depositing its energy in the form of heat (Lago 1984). Such a deceleration region could potentially produce the high temperatures required to form the HeII, SiIV and CIV lines (formed at $T_e \simeq 10^5 - 10^6$ K) typically observed in RU Lup. In addition, Brown et al. (1984) indicate that the UV resonance lines are probably formed in a very turbulent region. The formation of lines of high excitation in a deceleration region is therefore not improbable. Note that in this picture, continuum emission from the deceleration region would originate exterior to the bulk of the HI emission, cf. the proposal suggested in Section 5.2.2.2. to explain the near-IR HI line variability.

5.2.2.4. The Forbidden lines and the Iron lines.

The forbidden 5577, 6300 and 6363Å lines of [OI] and the 4069, 6715 and 6731Å lines of [SII] are all seen in the spectrum, lines which are generally observable.

Many strong FeII lines are observed in the spectrum of RU Lup. The dominant transitions are indicated in Fig. 5.2.5. In agreement with Boesgaard (1984), most of the strong optical lines observed arise in upper levels having excitation potential ≈ 5eV.

The spectrum was carefully searched for [FeII] lines; these forbidden lines are extremely variable and not always observed in the optical spectrum of RU Lup (Giovannelli et al., 1986). The 5750Å (2F) line (observed by Lago and Penston 1982) is the only [FeII] line which may be present, but the blend is almost certainly dominated by the 5753Å (1107) FeI line. The lack of [FeII] emission at certain epochs (as here) indicates that the FeII emission region does not usually extend out to low densities (where the forbidden lines are formed).

Although the FeI emission lines are not as strong as the singly ionised metallic lines (e.g. FeII, CaII, TiII), there are many more FeI lines observed than for any other species. The FeI transitions which could be identified are shown in Fig. 5.2.6. The two FeI multiplets which have lines enhanced by a fluoresence effect in RU Lup are shown and are denoted by the letter F. The "pumping" transitions for these fluorescent lines are also shown and are denoted by the letter P. The fluorescent lines are the 4063, 4132Å (43) (noted in both RU Lup and S CrA by Joy 1945) and the 4202, 4308Å (42) (noted by Lago 1982) lines. Both sets of lines are observed in the SAAO spectrum, although the two fluoresecent (42) multiplet lines are not as enhanced as the two (43) multiplet lines.

An extensive spectrum of weak FeI lines can be readily produced within a deep chromosphere without recourse to emission from an envelope, e.g. Cram (1979). Although the strong lines are clearly dominated by emission from the envelope, the formation of the weaker

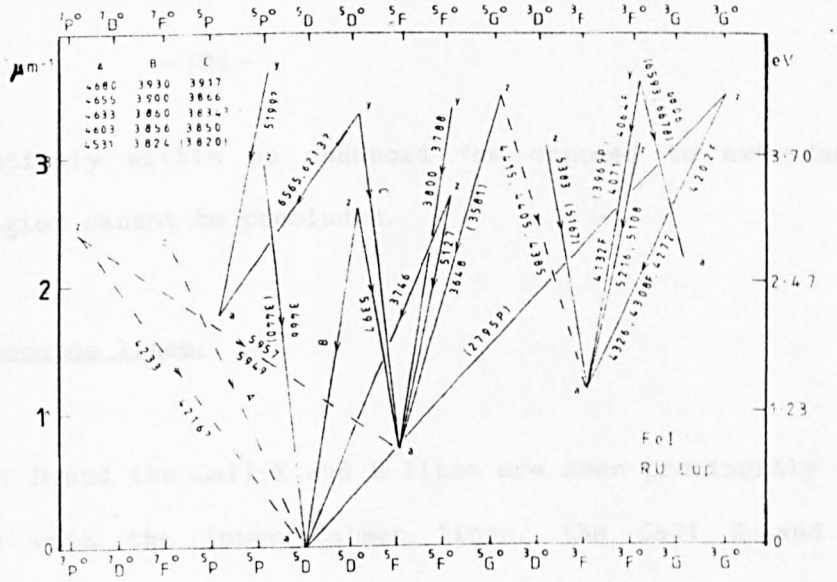

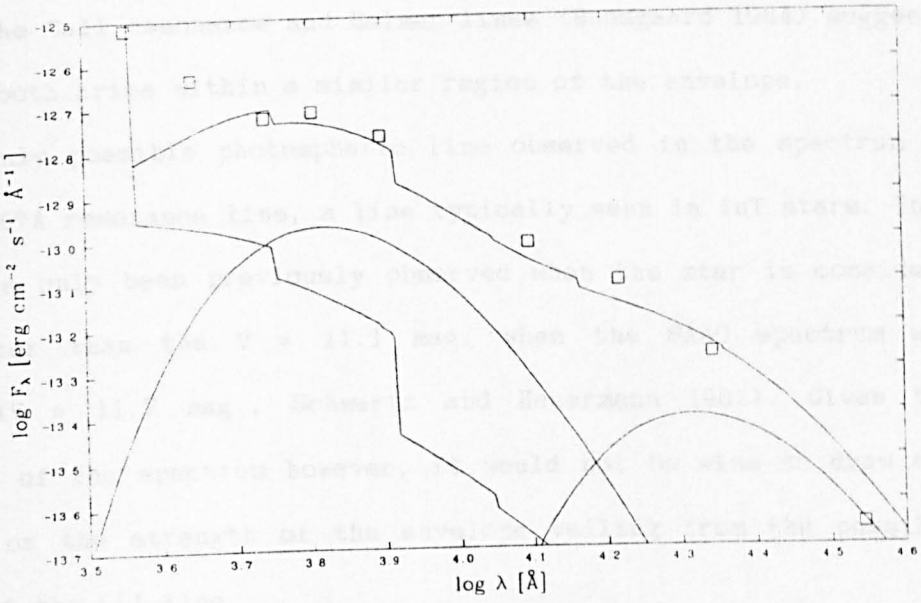

Fig. 5.2.6. FeI Grotrian diagram for optical transitions observed in RU Lup. See also Section 5.2.2.5.

Fig. 5.2.7. Flux distribution of RU Lup on HJD 2444825. See also Section 5.2.3.

FeI lines essentially within an enhanced (as opposed to extended) chromospheric region cannot be precluded.

5.2.2.5. The Resonance lines.

Both the NaI D and the CaII·K and H lines are seen prominently in emission. Along with the lower Balmer lines, the CaII K and H resonance lines are the strongest lines in the spectrum, of a similar strength to the Hβ and Hγ lines. The strengths and correlated variations of the CaII resonance and Balmer lines (Boesgaard 1984) suggests that they both arise within a similar region of the envelope.

The only possible photospheric line observed in the spectrum is the LiI 6707Å resonance line, a line typically seen in InT stars. This feature has only been previously observed when the star is considerably fainter than the V ≃ 11.1 mag. when the SAAO spectrum was obtained (V ≃ 11.7 mag., Schwartz and Heuermann 1981). Given the resolution of the spectrum however, it would not be wise to draw any inference on the strength of the envelope veiling from the possible presence of the LiI line.

5.2.2.6. Summary.

The optical emission line spectrum of RU Lup consists of strong lines of both low (e.g. FeII, CaII K and H) and high (e.g. HeI) excitation. The bulk of the line emission (with the possible exception of the FeI lines) probably arises within the stellar envelope, although any distinction between the outer extent of the chromosphere and the inner extent of the envelope is probably not a clear one.

In view of the many different lines which form under different physical conditions, e.g. FeII, HeI and [OI], the emission from the envelope is probably very well-stratified, as has been indicated by Lago and Penston (1982). The veiling of the photospheric continuum is ascribable to free-free, free-bound continuum emission, much of which could well originate in the region of the envelope from which the highly excited line emission arises. The HI emission is expected to predominantly arise from a different region of the envelope, possibly inner to the region from which much of the free-free continuum emission arises. In view of the forbidden emission, the blueshifted Hα absorption feature and the nearby HH55 nebulosity, the envelope almost certainly forms an extensive wind, a wind which is probably Alfvénically driven (Lago 1984, Kuin 1986).

5.2.3. The Flux Distribution.

Simultaneous UBVRI and JHKL photometry was obtained at SAAO by Kilkenny et al. (1985) from 1981 - 1984, and a few additional observations at SAAO in 1987 were also obtained.

As pointed out in Section 5.2.1, the significant blue excess of RU Lup evidently requires an additional, non-stellar component to fit the observed optical continuum flux. It is the extended envelope, from which the strong optical line emission arises, which is expected to give rise to this additional, non-stellar component, namely continuum free-free, free-bound emission. There are probably two components of this emission: emission from a cool region (which also gives rise to the Balmer emission) and emission from a hot region (which also gives rise to the HeI, HeII emission). The initial parameters determining

the free-free and free-bound continuum emission were therefore adopted from the physical parameters determined for the HI and HeI line emitting regions (Lago and Penston 1982).

In view of the mid-K spectral type of RU Lup (see Section 5.2.1), a 4400K (from the temperature calibration of Cohen and Kuhi 1979) blackbody will be adopted to represent the stellar continuum. A 4400K blackbody has typically been used to represent the photospheric continuum of RU Lup, e.g. Gahm et al., (1974). However, a 4400K blackbody clearly fails to account for the significant line-blanketing expected in a normal mid-K spectrum.

The reddening of RU Lup has been essentially determined from the strength of the IS 2200Å feature observed using IUE. Gahm et al. (1979) estimate $0.3 < A_V < 1.0$ mag. (the lower value is determined from the optical colour slope of a 4400K star), and Giovannelli et al. (1986) suggest that $E(B-V) = 0.1 \pm 0.02$. Thus values in the range $0.1 < E(B-V) < 0.2$ were initially adopted in fitting the photometry.

RU Lup was observed when both bright ($V \simeq 10.5$ mag.) and faint ($V \simeq 11.6$ mag.). The optical spectrum is dominated by lines such as HI, CaII and FeII, lines which typically form at temperatures $T_e \simeq 6000$K. However, the relative fluxes at B, V and R when the star is both bright and faint and given the above range in the reddening, are found to be incompatible at each epoch with the continuum derived for a cool ($T_e \simeq 6000 - 10000$K) theoretical free-free, free-bound optically thin nebular continuum. It would therefore seem that the continuum emission from the inner envelope (which gives rise to the strong optical lines) is not a major contributor to the blue optical continuum emission.

A grid of hot ($T_e \simeq 15000 - 50000$K) nebular continua were produced (with an estimated $N_e \simeq 3.0 \times 10^{11}$ cm^{-3} from Lago and Penston 1982;

the continua of such models are relatively insensitive to the input density) in order to attempt a fit to the data at U, B and V. The flux from a superposed 4400K stellar (blackbody) continuum does not significantly contribute to the total flux at U or B.

In principle, the nebular continua should be normalised by an observed Hβ and/or HeII 1640Å flux. However, as no simultaneous spectroscopy (except for optical spectroscopy at one epoch) was obtained, this was not possible, and thus all the continua were fitted to the optical photometry directly. The required normalisation for each fit, as represented by the required "input" Hβ flux lies in the range $f(H\beta) = 10^{-10.1} - 10^{-10.45}$ erg cm^{-2} s^{-1}.

Only one simultaneous optical spectrum (on HJD 2446998) was obtained with which the "input" Hβ flux can be compared with the dereddened, observed Hβ flux. It is found that the "input" Hβ flux is a factor of ≈ 8 greater than the lower limit of the dereddened, observed Hβ flux. However, it is noted that free-free emission almost certainly arises from both a cool region (which would be best normalised to a simultaneous Hβ flux) and a hot region (which would be best normalised to a simultaneous HeII 1640Å flux) of the envelope, and so this discrepancy is probably not significant.

It was found that the better fits resulted with 1.6 - 2.0 x 10^4 K nebular continua fitted to the data dereddened by a total E(B-V) = 0.2 (R = 3.1), although these models do give a high UV flux and underestimate the flux at B. Note however, that the effects of line-blanketing in the photospheric emission from RU Lup are not accounted for here. This will particularly affect the reliability of the fit to the U and B fluxes.

Now, IUE spectra were obtained by Brown et al. (1984) (SWP 19739

and LWR 15745 on HJD 2445411), five nights prior to optical photometry obtained at SAAO on HJD 2445416 and by Giovannelli et al. (1986) (SWP 22683 and LWP 3098 on HJD 2445796), twelve nights prior to optical photometry obtained on HJD 2445808.

When the dereddened UV continua are plotted against the various nebular continua fitted to the nearest optical photometry dataset, it would seem that the hotter continua ($T_* \geq 25000$K) probably over-estimate the UV flux observed in RU Lup. However, as the optical and UV data are not simultaneous, with simultaneity being required in view of the variability of RU Lup, and also bearing in mind that the photospheric continuum emission is only represented by a blackbody, a comparison between these optical and UV data cannot be regarded as wholly reliable.

Simultaneous photometry and UV/optical spectroscopy (from which the UV and optical continua, and the envelope parameters can be determined) are clearly desirable in reliably fitting a free-free continuum and an appropriate blanketed model atmosphere to the UV, blue and near-IR excesses of RU Lup. With a blanketed model atmosphere a better fit of the photospheric continuum, and thus also of the free-free continuum component(s), to the UV and blue excess of RU Lup will almost certainly result.

Even so, it is possible to fit the optical (although the B point is clearly under-estimated) and near-IR photometry, dereddened by $E(B-V) = 0.2$, with the following three components: an optically thin 20000K nebular continuum, a 4400K blackbody (to represent the photospheric continuum) and a hot dust shell blackbody component, with a temperature $\simeq$ 1300 - 1400K.

It is noted that the blackbody dust temperature of $\simeq$ 1300 - 1400K

is hotter than the blackbody temperature of 700K fitted to the near-IR excess by Gahm et al. (1974). However, in view of the fact that the form of the remaining near-IR excess (attributable to dust emission), once the stellar and the nebular continuum components have been removed, is dependent on the form of the fitted nebular continuum, it would be unwise to draw any conclusions from the different dust temperatures, as Gahm et al. (1974) fitted a very different, cool (T_e = 6000K) nebular continuum to their photometry. Only when the UV and optical continuum emission has been reliably fitted (see above), could the form of the near-IR excess due to emission from dust, be unambiguously ascertained.

Two of the fits obtained are shown, one when RU Lup is faint, on HJD 2444825 (Fig. 5.2.7), and the other when the star is bright, on HJD 2445416 (Fig. 5.2.8). Note again that the fitted models underestimate the flux at B. When the star is brightest (HJD 2445416), the luminosity (estimated from 1.36 $(\lambda F_\lambda)_{max}$) of the stellar component is 0.9 $L_\odot$ and the hot ($\simeq$ 1300 - 1400K) dust component is 0.6 $L_\odot$, both assuming a distance of 150pc. If the IRAS PSC data (Beichman et al., 1985) of RU Lup are also included, a 200K blackbody can be fitted to the dereddened far-IR fluxes, and from this fit, the total luminosity of the far-IR emission is estimated to be $\simeq$ 0.6 $L_\odot$. As RU Lup is flagged as a non-variable in the IRAS PSC, the estimate of the far-IR flux from the combined dataset is considered to be reliable.

Therefore the total UV, optical and IR luminosity (the UV luminosity estimate of 0.3 $L_\odot$ from Gahm et al., 1979 has been included) of RU Lup is $\simeq$ 2.4 $L_\odot$. However, no account has been made here of the significant contribution of the envelope emission in the optical and near-IR. However, it is seen that the total luminosity derived here

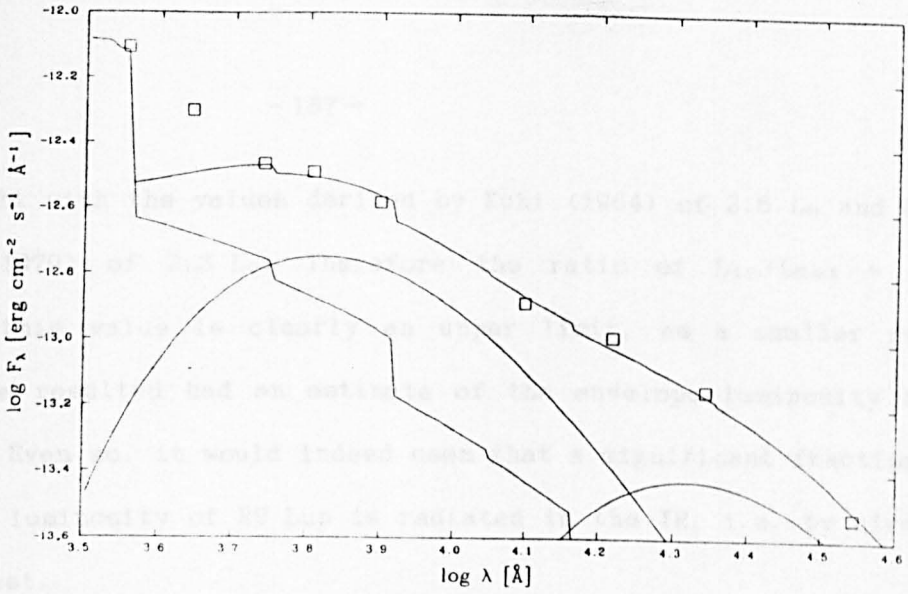

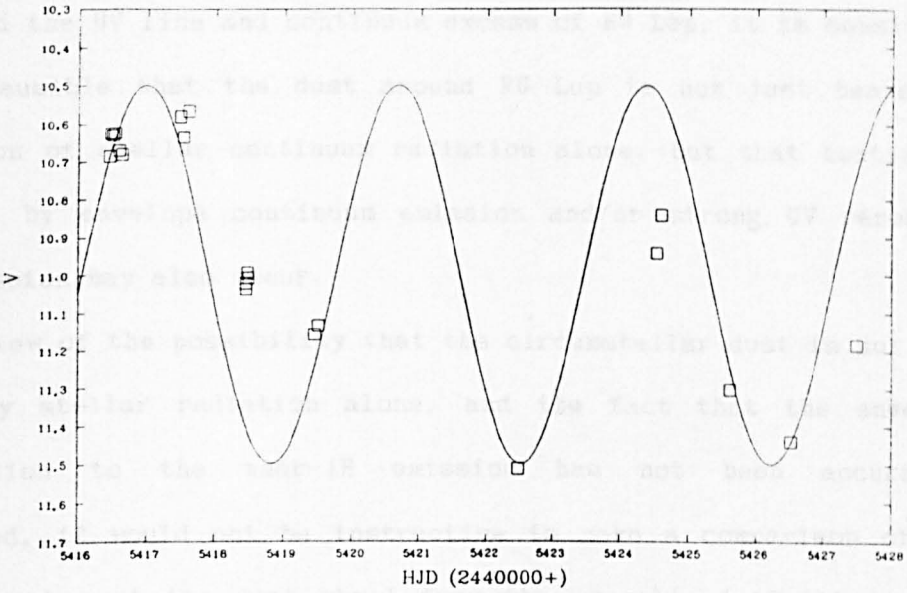

Fig. 5.2.8. Flux distribution of RU Lup on HJD 2445416. See also Section 5.2.3.

Fig. 5.2.9. V lightcurve of RU Lup from HJD 2445416 to HJD 2445427 fitted with a sine curve of period 3.7 days. See also Section 5.2.4.1.

agrees well with the values derived by Kuhi (1964) of 2.5 $L_\odot$ and Gahm et al. (1979) of 2.3 $L_\odot$. Therefore the ratio of $L_{IR}/L_{Bol} \simeq 0.5$, although this value is clearly an upper limit, as a smaller ratio would have resulted had an estimate of the envelope luminosity been included. Even so, it would indeed seem that a significant fraction of the total luminosity of RU Lup is radiated in the IR, i.e. by circumstellar dust.

In view of the significant IR excess attributable to emission from dust, and the UV line and continuum excess of RU Lup, it is considered not implausible that the dust around RU Lup is not just heated by absorption of stellar continuum radiation alone, but that heating of the dust by envelope continuum emission and/or strong UV resonance line emission may also occur.

In view of the possibility that the circumstellar dust is not just heated by stellar radiation alone, and the fact that the envelope contribution to the near-IR emission has not been accurately determined, it would not be instructive to make a comparison of the estimated size of the dust shell from the normalised blackbody fits and Eq. (4.1). Also, in view of the fact that the 4400K blackbody (taken to represent the photospheric emission) was not directly fitted to the optical photometry, it would also be unwise to estimate the radius of RU Lup from the normalisation of the stellar blackbody component obtained in the fits.

In conclusion, it is found that the optical and near-IR continuum emission of RU Lup cannot easily be modelled because of the likely two-component free-free and free-bound emission from the stellar envelope and also because of the dominance of this continuum emission from UV to near-IR wavelengths. Simultaneous with optical and near-IR

photometry, UV and optical spectra would also be required if L_{Bol} is to be reliably estimated and if the continuum from the UV out to the near-IR is to be reliably fitted. It would however seem that a significant fraction of the total luminosity of RU Lup is emitted in the IR from both free-free envelope and dust continuum emission.

5.2.4. The Light and Colour variations.

Simultaneous UBVRIHβ and JHKL photometry of RU Lup was obtained by Kilkenny *et al.* (1985) between 1981 and 1984, and BVRI and JHKL photometry was obtained at SAAO in 1987. The optical lightcurves were examined for any regularities in the lightcurve, attributable to rotational modulation and for any sharp rises in flux, attributable to "flares". The colour-colour plots are then used to examine the nature of the light variations observed.

5.2.4.1. The Optical Lightcurves.

With several independent studies of the light variations exhibited by RU Lup indicating a periodicity of ≈ 3.7 days, a rotational modulation of the light output from RU Lup would seem highly likely; further, this is not inconsistent with the star being observed generally at mean brightness (Herbig and Rao 1972).

With this in mind, an attempt was made to fit the photometry obtained in the epoch HJD 2445416 - 2445427, the only sample of data in Kilkenny *et al.* (1985) which follows the lightcurve adequately over a few rotation periods, with a sine curve of period 3.7 days (Section 5.2.1). A reasonable fit was made to the optical lightcurves, and the

fit to the V lightcurve is shown in Fig. 5.2.9. Allowing for superposed rapid (≃ hours) variations and slight changes in both the phase and amplitude of variation, changes which are considered likely as the optical continuum emission of RU Lup is affected by emission from an active stellar envelope, then the plausibility of an underlying rotational modulation during this epoch seems quite reasonable. Also, as both the stellar and envelope continuum emission contribute to the optical flux, a rotational modulation of the lightcurve probably reflects not only rotation of the star itself, but also of the envelope (cf. spectroscopic evidence for rotational modulation of the envelope line emission, Boesgaard 1984).

Also the U lightcurve was studied in an attempt to identify any significant rapid (≃ hours) rises in flux, greater than 0.3 mag., which may be attributed to "flare"-like events (cf. Gahm 1986). A similar criterion was employed by Gahm et al. (1974), who observed several "flare"-like events in their data. Similarly, Plagemann (1969) looked for rapid rises in the V lightcurve observed by Hoffmeister (1958, 1965). Using this dataset Plagemann (1969) reported four "flare"-like events.

In the Kilkenny et al. (1985) dataset, RU Lup was observed more than once in the same night at U on a total of 14 nights. On each of these nights, no evidence for any rise in the flux at U greater than 0.2 mag. was found. As RU Lup was observed to vary between $10.52 < V < 11.59$ mag. in this dataset, i.e. around "normal" light ($\langle V \rangle \simeq 11.0$ mag.; Kholopov et al., 1987), the possibility of the observation of "flares" due a selection effect, i.e. "flares" being more apparent when RU Lup is faint, is ruled out. As the degree of "activity" at U in 1981 - 1984 is evidently much reduced when compared to previous

epochs, it is concluded that the observed "flaring" or "chromospheric" activity of RU Lup may well be intermittent from year to year.

The tendency of the amplitude of light variation in RU Lup to decrease with increasing wavelength (e.g. Gahm et al., 1974) is confirmed here. In the Kilkenny et al. (1985) dataset, the range in variation observed at each optical bandpass was: $10.20 < U < 11.55$ mag.; $11.00 < B < 12.26$ mag.; $10.52 < V < 11.59$ mag.; $9.99 < R < 10.84$ mag.; $9.47 < I < 10.18$ mag. As noted by Gahm et al. (1974) the form of $\Delta m(\lambda)$ would not be incompatible with that expected from variable circumstellar extinction.

The variation of the Hβ index with V magnitude is shown in Fig. 5.2.10. Although there is no obvious trend between the Hβ index and V, the observed variation in Hβ would seem to reflect, to a degree, the expected enhancement of Balmer line emission (smaller values of Hβ index) when RU Lup is faint (e.g. Giovannelli et al., 1986).

5.2.4.2. The Colour-colour variations.

The optical colours of RU Lup tend to become redder as RU Lup fades, as can be seen for example, in the variation of V with B-V (Fig. 5.2.11). This is a typical trend amongst InT stars. Also, as noted above, the range in variation decreases towards longer wavelengths. Neither fact would be incompatible with variable circumstellar extinction affecting the long-term light behaviour of RU Lup.

Now, as was seen in Section 5.2.3, both photospheric and envelope continuum emission contribute to the optical broadband emission. The envelope contribution is dominant in the blue, whereas the photospheric emission peaks towards the red, e.g. see Fig. 5.2.8. Therefore

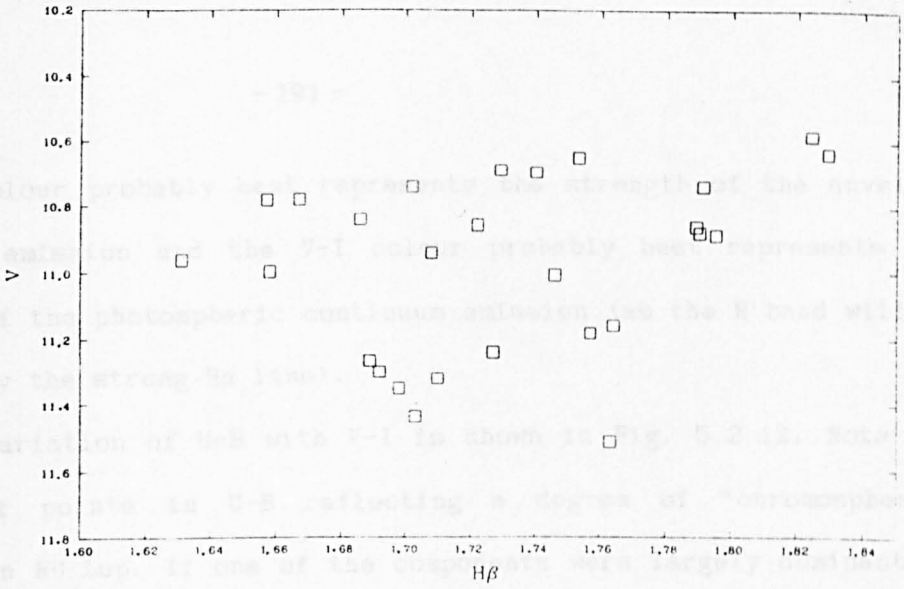

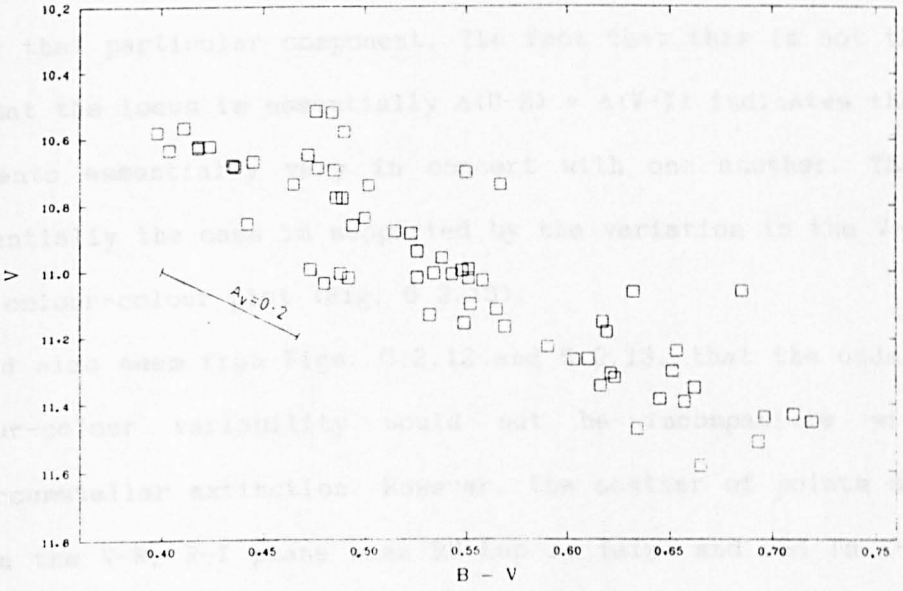

Fig. 5.2.10. V, Hβ variation of RU Lup.
See also Section 5.2.4.1.

Fig. 5.2.11. V, B-V variation of RU Lup.
See also Section 5.2.4.2.

the U-B colour probably best represents the strength of the envelope continuum emission and the V-I colour probably best represents the strength of the photospheric continuum emission (as the R band will be affected by the strong Hα line).

The variation of U-B with V-I is shown in Fig. 5.2.12. Note the scatter of points in U-B reflecting a degree of "chromospheric" activity in RU Lup. If one of the components were largely dominant in causing the optical light variability, then the locus of variation would tend to be parallel to the axis of the colour index best representing that particular component. The fact that this is not the case, and that the locus is essentially $\Delta(U-B) \simeq \Delta(V-I)$ indicates that both components essentially vary in concert with one another. That this is essentially the case is supported by the variation in the V-R, R-I optical colour-colour plot (Fig. 5.2.13).

It would also seem from Figs. 5.2.12 and 5.2.13, that the underlying colour-colour variability would not be incompatible with variable circumstellar extinction. However, the scatter of points off the locus in the V-R, R-I plane when RU Lup is faint and red in R-I, but blue in V-R, can be attributed to contamination of strong (variable) Hα emission affecting R. Such colour behaviour would argue against variable circumstellar extinction by IS-sized grains (solid line) causing the light variations when RU Lup is blue in V-R.

It is noted that, although RU Lup and RY Lup are two very different InT stars and exhibit very different lightcurves in the period 1981-1984 (RU Lup exhibits a Parenago type II lightcurve, whereas RY Lup exhibits Parenago type I), the variation in the optical colour-colour planes of both stars are strikingly similar (except for V-R, R-I), i.e. they both run closely parallel to the IS reddening

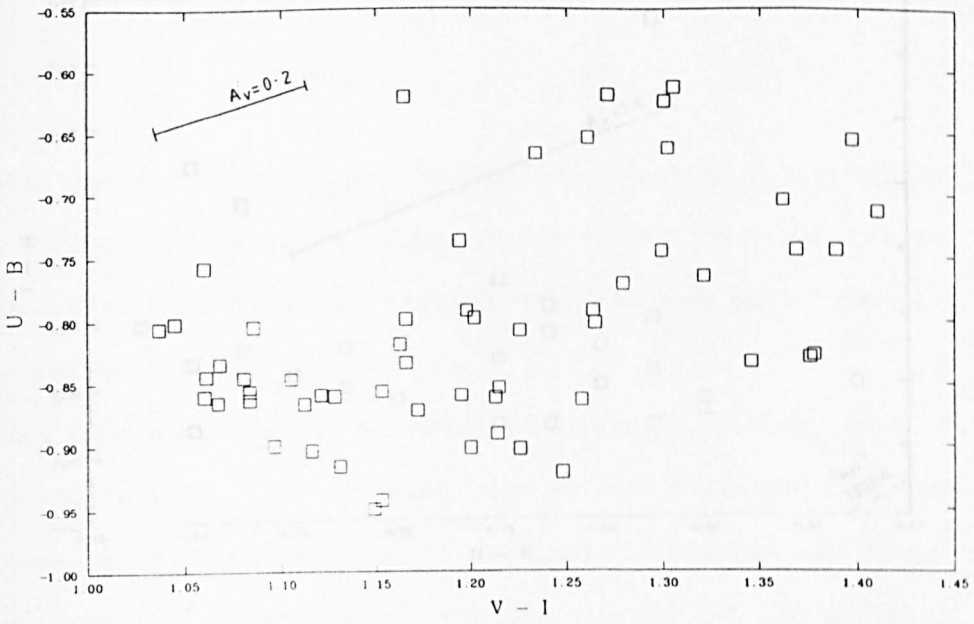

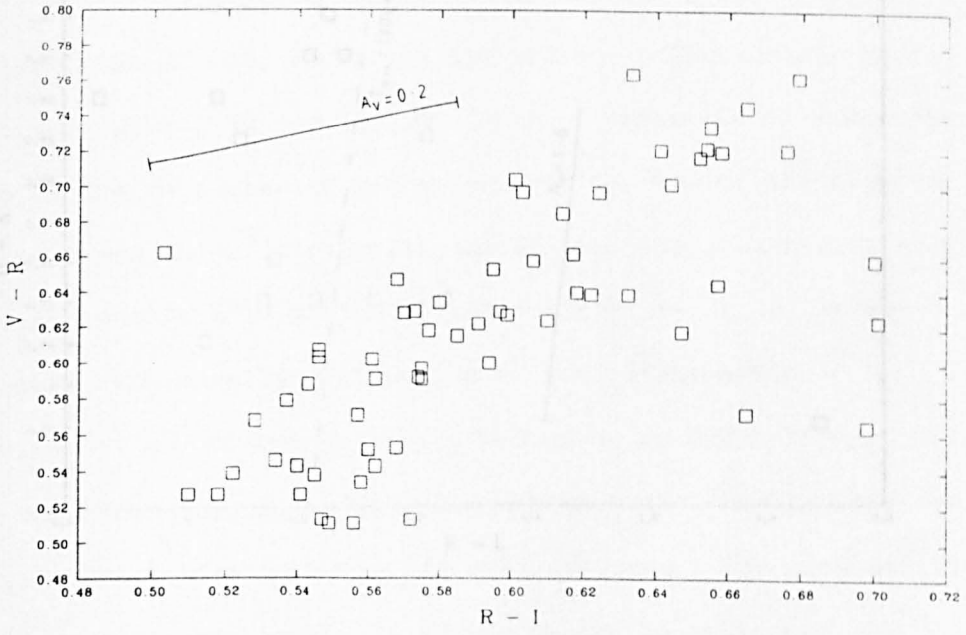

Fig. 5.2.12. U-B, V-I variation of RU Lup.
See also Section 5.2.4.2.

Fig. 5.2.13. V-R, R-I variation of RU Lup.
See also Section 5.2.4.2.

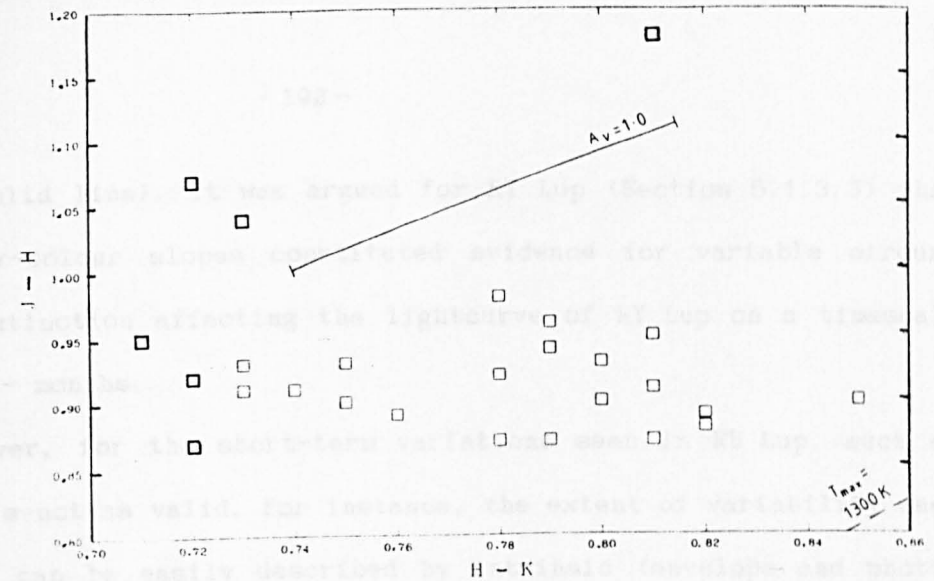

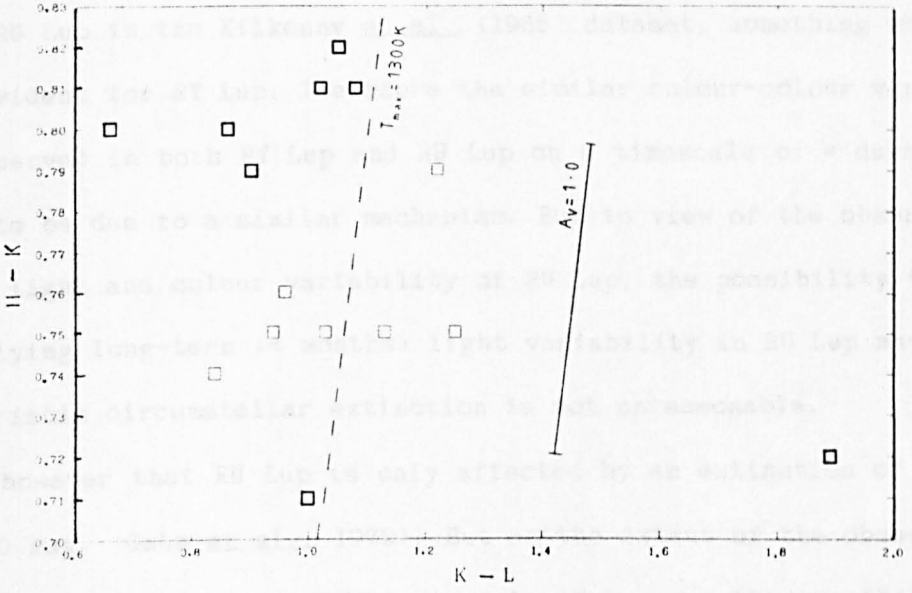

Fig. 5.2.14. J-H, H-K variation of RU Lup. See also Section 5.2.4.2.

Fig. 5.2.15. H-K, K-L variation of RU Lup. See also Section 5.2.4.2.

vector (solid line). It was argued for RY Lup (Section 5.1.3.3) that the colour-colour slopes constituted evidence for variable circumstellar extinction affecting the lightcurve of RY Lup on a timescale of ≃ days - months.

However, for the short-term variations seen in RU Lup, such an argument is not as valid. For instance, the extent of variability seen in RU Lup can be easily described by intrinsic (envelope and photospheric) variability, which was not the case for RY Lup. In addition, there is evidence for a rotational modulation of the optical light curve of RU Lup in the Kilkenny et al. (1985) dataset, something which was not evident for RY Lup. Therefore the similar colour-colour variability observed in both RY Lup and RU Lup on a timescale of ≃ days is unlikely to be due to a similar mechanism. But in view of the observed long-term light and colour variability of RU Lup, the possibility that the underlying long-term (≃ months) light variability in RU Lup may be due to variable circumstellar extinction is not unreasonable.

Note however that RU Lup is only affected by an extinction of 0.3 < A_V < 1.0 mag. (Gahm et al., 1979). But as the extent of the observed optical light variability in RU Lup is only $\Delta V \simeq 1$ mag., the possibility of long-term variable extinction in RU Lup cannot be ruled out.

The variation in the near-IR colours, J-H, H-K (Fig. 5.2.14) and H-K, K-L (Fig. 5.2.15), do not follow the IS reddening vector. Also the near-IR colour variation cannot be represented by free-free and free-bound continuum emission from neither a hot (T_e ≃ 20000K: (K-L) ≃ 0.5), nor a cool (T_e ≃ 6000K: (K-L) ≃ 0.2) plasma, for stellar and envelope parameters representative of RU Lup, unless the intrinsic colours from such emission are reddened by several visual magnitudes (cf. Fig. 12, Cohen and Kuhi 1979), which is unlikely. It should be

noted that larger variation in the L magnitude in comparison with the other near-IR colours is probably due to the faintness of RU Lup at L (L $\simeq$ 5.6 - 6.4 mag.), a fact which means that the errors at L are $\simeq$ 0.15 mag. (Kilkenny et al., 1985).

The near-IR colours can however be more readily interpreted in terms of re-emission of optical and UV radiation by circumstellar grains. The dashed locus labelled T_{max} = **1300K** represents dust emission surrounding a mid-K dwarf star where the dust is heated to T_{max} = 1300K, cf. Rydgren et al. (1982). The H-K, K-L colour locus follows the T_{max} = 1300K locus well, but that the J-H, H-K colour locus lies above the T_{max} = 1300K locus is attributed to the stronger free-free, free-bound envelope contribution towards shorter IR wavelengths. A dust temperature of $\simeq$ 1300K is roughly consistent with the fits obtained in Section 5.2.3 to the dereddened near-IR photometry.

5.2.4.3. Summary.

The colour behaviour of RU Lup can be interpreted in terms of variable circumstellar extinction and/or intrinsic variability. However, with the observed periodicity, the colour reversal seen in V-R and the absence of any sharp drops in the lightcurves (cf. RY Lup), intrinsic variability clearly dominates the variability on a timescale of days. No evidence for any rapid "flare"-like activity at U was found during the period 1981 - 1984.

5.2.5. Polarimetric observations.

The polarisation of RU Lup has been measured by Bastien (1985) and

he observed the polarisation to vary by $\simeq$ 0.4% over a four day period, which led him to classify RU Lup as a suspected polarimetric variable. He observed the polarisation and position angle in the blue (4300Å) to be p = 0.51 ± 0.10% and θ = 139 ± 6°, and in the red (7543Å) to be p = 0.21 ± 0.07% and θ = 18 ± 10° on HJD 2444729.

These observations of Bastien (1985) can be compared with the observations of RU Lup at B (4400Å) with p = 0.67 ± 0.19% and θ = 155 ± 23°, and at I (7900Å) with p = 0.51 ± 0.13% and θ = 114 ± 20°, taken on HJD 2446994. Thus between two observations six years apart, the level of the polarisation is not significantly different, the only notable change being in the position angle at red wavelengths (7900Å).

In addition, the polarisation of RU Lup through a clear filter was measured on two nights, eight weeks apart. The polarisation was observed at 0.68 ± 0.00% on HJD 2446994, when the star was bright (V = 10.70 mag.) and at 1.00 ± 0.10% on HJD 2447049, when the star was fainter (V = 11.06 mag.). Also, the position angle was observed at 114° on both nights (the error was 20° in the first observation, and 8° in the second).

It would therefore seem from the four sets of observations discussed here, that the polarisation of RU Lup can vary slightly over a period of several weeks, although on a timescale of years no real change in the level of polarisation is evident. The position angle does not seem particularly variable except on a timescale of years, a change which was only in evidence at red wavelengths. Whether significant changes occur on a shorter timescale than observed here requires further monitoring.

In view of the limited variability, the observed polarisation of RU Lup is essentially intrinsic, and must therefore either arise in

the stellar emission envelope (from electron scattering) and/or within the circumstellar dust shell. The wavelength dependence of polarisation (observed on HJD 2446994) does not favour a contribution from electron scattering, although observations at several bandpasses are required to rule out entirely a contribution from the stellar envelope. The observations (at B and I) can be fitted by a dust scattering model with 0.18μm ice grains (see Section 7.4.2.7). However, since RU Lup exhibits an IR excess due to emission from dust, scattering by ice grains (which sublime at ≃ 100K) is not plausible, and scattering by silicate grains must be regarded as being more realistic.

Thus RU Lup is observed to exhibit limited variation in polarisation on a timescale of ≃ weeks. Scattering by dust grains is considered to be the more likely origin of the polarisation. If variability of the polarisation on a timescale of days is confirmed, then scattering by silicate grains (which have similar scattering properties to ice grains) would certainly be favoured, as the scattering dust would be constrained to lie fairly close to the star.

5.2.6. Summary and Conclusions.

The extreme emission line spectrum and blue veiling of RU Lup can both be interpreted in terms of emission from an extended stellar envelope. Lines of both low (e.g. CaII, FeII) and high (e.g. HeI, HeII) excitation were observed, as well as forbidden line emission. Thus the envelope of RU Lup clearly has different characteristic emitting regions. It is suggested that the nature of the observed near-IR hydrogen line variability of RU Lup is plausibly due to the hydrogen line emission arising predominantly within a region of the

envelope interior to the envelope continuum emission.

Alfvénically driven wind models (Lago 1984, Kuin 1986) applied to RU Lup give a good interpretation of the characteristics of the line and continuum emission from RU Lup. Such a model also potentially explains the lack of X-ray emission from RU Lup.

In view of the adjacent H_2O maser and the likely association of RU Lup with the Herbig-Haro object HH55 (Whitmore et al., 1987), the interaction of an extended wind from RU Lup with its surrounding medium would seem highly likely, i.e. the stellar wind is extensive.

The observed optical and near-IR fluxes can be fitted by emission from three components: free-free, free-bound emission from the stellar envelope; emission from a mid-K photosphere; and emission from circumstellar dust. It would seem plausible that the (variable) polarisation is due to scattering within the circumstellar dust shell and/or within the circumstellar envelope.

The degree of "chromospheric" activity of RU Lup was clearly not pronounced in the observations obtained in 1981 - 1984. Both intrinsic (variation in the photospheric and envelope emission and/or rotation of the star and stellar envelope) and extrinsic (variable circumstellar extinction) mechanisms have been invoked to account for the optical line and continuum variability in RU Lup. In view of the fact that the optical line (Boesgaard 1984) and continuum variations (e.g. Hoffmeister 1965; this work) of RU Lup has been observed to vary with a period of $\simeq$ 3.7 days, an intrinsic origin of the short-term variability is preferred. It is however seen that the long-term ($\simeq$ months) colour variability of RU Lup would not be incompatible with limited ($1 \lesssim \Delta V \lesssim 0.5$ mag.), underlying changes in the line-of-sight dust shell opacity.

Chapter 6. Additional Stars of the Orion Population.

6.1. The Herbig Ae/Be star V856 Sco.

6.1.1. Introduction.

V856 Sco (HR 5999, HD 144668), an Ina variable (Kholopov et al., 1987), and HD 144667 (HR 6000) form a wide (45"), true visual binary system (both stars have a common proper motion; Bessel and Eggen 1972) in a cluster of low-mass Orion Population, Hα emission stars known as Δ199 (Thé 1962) associated with the Lupus dark cloud (Imhoff and Appenzeller 1987). Although the star of interest is V856 Sco, the companion star, HD 144667 (HR 6000) is an ideal comparison star, and therefore this star was also observed, and thus will also be briefly introduced.

HD 144667 is a bright (V = 6.4 mag.) star with a peculiar spectrum, which exhibits weak helium emission and strong PII lines. The spectral type of HD 144667 has been observed to be Bp (Bessel and Eggen 1972) and A0-3IIIp (Kholopov et al., 1987). The star is reddened by only E(B-V) ≈ 0.06 (Bessel and Eggen 1972); Thé and Tjin A Djie (1978) give a similar estimate of E(B-V) = 0.08. The distance to this star (and therefore the cluster) has been estimated as 270pc assuming a B6 spectral type for HD 144667 (Thé and Tjin A Djie 1978). Although physically associated with V856 Sco, HD 144667 is not itself a PMS star (Bessel and Eggen 1972). HD 144667 is known to be neither a polarimetric nor a photometric variable.

V856 Sco has a shell spectrum with variable Balmer lines and Hα in

emission (with a central absorption reversal), these lines being the only strongly variable spectral features (Bessel and Eggen 1972). The blueshifted Balmer absorption features indicate expansion of the shell, and the upper limit on the ionised mass loss rate (assuming spherical symmetry) was estimated by Brown (1987a) to be $\propto 1.5 \times 10^{-8}$ $M_{\odot}$ yr^{-1} from his 3σ upper limit measurement of 0.15 mJy at 6 cm. V856 Sco has been determined to be a PMS variable (Thé 1962; Thé and Tjin A Djie 1978), particularly in view of its association in a young cluster, although Bessel and Eggen (1972) did in fact suggest it is a star that has evolved *from* the MS.

The other strong optical lines are FeII, TiII, the CaII K and H and NaI D resonance lines. The spectral type of V856 Sco is usually taken to be A7III-IVe (Petersen and Jørgensen 1972; Bessel and Eggen 1972). From spectroscopic and photometric observations of V856 Sco, the range in the estimates of temperature and gravity are from T_{eff} = 7500K and log g = 3.2 - 3.4 (Bessel and Eggen 1972; Petersen and Jørgensen 1972) to T_{eff} = 8400K and log g = 4.1 (Thé and Tjin A Djie 1978). It should be noted that no variation in the size of the Balmer jump nor in the strengths of the metallic lines has been reported in any of the spectroscopic observations, which would indicate that the photometric variations are not intrinsic to the star. Also observations indicate a particularly high rotation velocity (v sin*i* $\propto$ 180 kms^{-1}) for V856 Sco (Imhoff and Appenzeller 1987).

The UV spectrum of V856 Sco is described by Tjin A Djie et al. (1982). The strong emission line spectrum (including lines of MgII, CIV and SiIV) is interestingly more similar to the UV spectra generally exhibited by InT stars rather than that of Ina stars.

The optical lightcurve of V856 Sco varies irregularly when at the

bright end of its variability range of $6.8 < V < 8.0$ mag. (Kholopov et al., 1987), but has been observed to suffer quasi-periodic minima, which occur approximately once a month (Bessel and Eggen 1972). The behaviour of the lightcurve has been likened to the lightcurve behaviour of the evolved R CrB stars (Hecht et al., 1984) and semi-detatched binary systems. But it is unlikely that V856 Sco is an evolved star, and the timescale of the quasi-periodicity refutes the latter suggestion. The colour variations (Bessel and Eggen 1972; Thé and Tjin A Djie 1978) and associated polarimetric variations (Bessel and Eggen 1972) all indicate that the variations are due to variable circumstellar extinction.

6.1.2. The Optical and Infrared Spectra.

The optical spectrum ($\Delta\lambda \simeq 2.8$Å) of V856 Sco was obtained at SAAO on HJD 2446999. From photometry obtained the same night and the following night, V856 Sco was at the extreme bright end of its photometric range, $V = 6.79$ mag. and marginally varied photometrically around this time: V varied by only 0.04 mag. and B-V by only 0.08. Also IR spectra from 0.9 to 5.0μm were obtained at CTIO in June, 1987, although no simultaneous photometry was obtained. Thus the spectra are plotted normalised to the SAAO near-IR photometry obtained a month later. The optical and IR spectra and identification of the strong lines are shown in Figs. 6.1.1 and 6.1.2 respectively. Typically only the strong HI and HeI lines are identifiable in the IR spectra (see Section 3.3.3). Although the spectra are non-simultaneous, as only the hydrogen lines are known to be strongly variable, a comparison of the helium transitions observed ought to be fairly reliable.

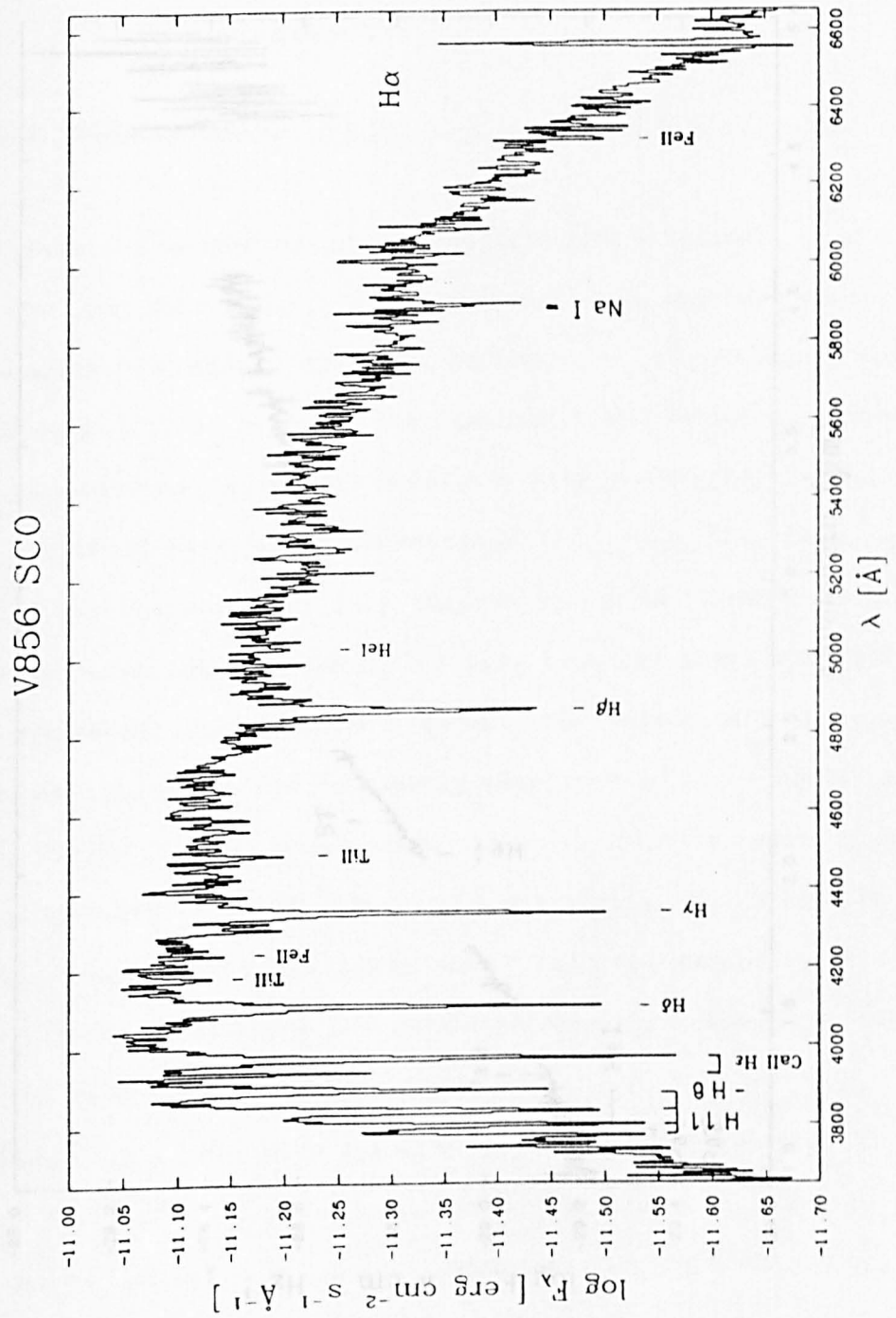

Fig. 6.1.1. Optical spectrum of V856 Sco. See also Section 6.1.2.

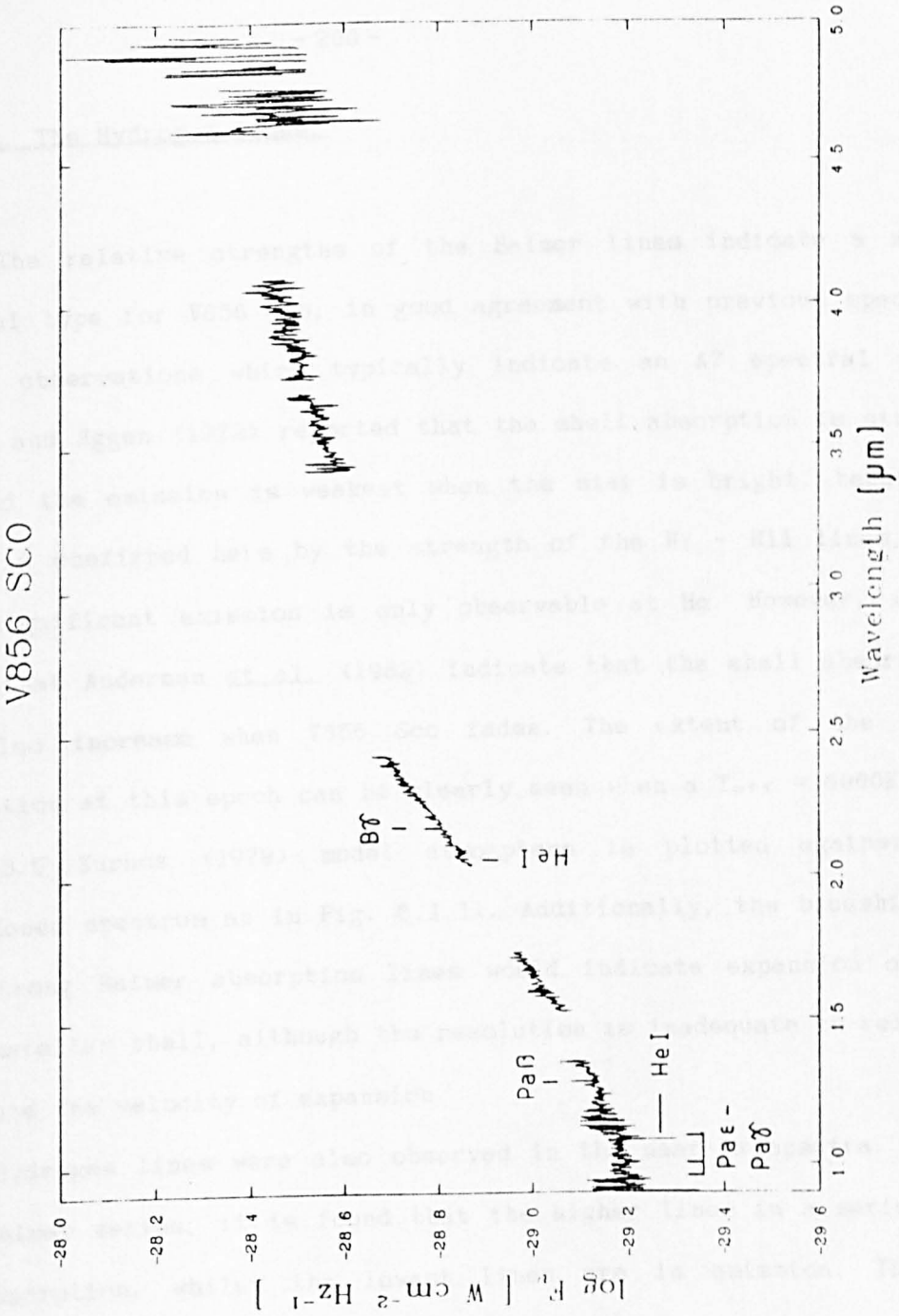

Fig. 6.1.2. Infrared spectra of V856 Sco.
See also Section 6.1.2.

6.1.2.1. The Hydrogen lines.

The relative strengths of the Balmer lines indicate a mid-A spectral type for V856 Sco, in good agreement with previous spectroscopic observations which typically indicate an A7 spectral type. Bessel and Eggen (1972) reported that the shell absorption is strongest and the emission is weakest when the star is bright, behaviour which is confirmed here by the strength of the Hγ - H11 lines, and that significant emission is only observable at Hα. However, it is noted that Andersen et al. (1982) indicate that the shell absorption can also increase when V856 Sco fades. The extent of the shell absorption at this epoch can be clearly seen when a T_{eff} = 8000K, log g = 3.5 Kurucz (1979) model atmosphere is plotted against the dereddened spectrum as in Fig. 6.1.11. Additionally, the blueshift of the strong Balmer absorption lines would indicate expansion of the circumstellar shell, although the resolution is inadequate to reliably estimate the velocity of expansion.

Hydrogen lines were also observed in the near-IR spectra. As in the Balmer series, it is found that the higher lines in a series are in absorption, whilst the lowest lines are in emission. The Paε (0.955μm) and Paδ (1.005μm) lines were observed in absorption, whilst the Paβ (1.282μm) and Bγ (2.166μm) lines were observed in emission (see Fig. 6.1.2). The (B10 - B22) Brackett lines were not strong enough to be evident in the H band spectrum, and the possible Pfγ (3.740μm) line was lost due to the light leak in the L spectrum.

6.1.2.2. The Metallic lines.

The resonance K and H lines of CaII (3934, 3969Å) and the NaI D resonance lines (5890, 5896Å) form very strong shell absorption features, although at this resolution, an IS contribution to the NaI D lines cannot be ruled out.

The strongest metallic lines (other than NaI D and CaII K and H) are the FeII and TiII lines. The strongest of the FeII lines observed are (with known multiplets shown in brackets) 4233 (27), 4314 (32), 4489 (37) and 6317Å; the strongest TiII lines are 3761 (13), 4177, 4300 (41) and 4468Å (31).

The strong FeII transitions represent excitation to the $^4D^o$, $^4F^o$ and $^4H^o$ levels; the strong TiII transitions represent excitation to the $^2F^o$, $^3F^o$, $^2D^o$ and ^4D levels. Bessel and Eggen (1972) found that the most well-defined lines of FeII (4923, 5018Å) and TiII (3759, 3761Å) came from the metastable levels; but only the latter TiII line is found to be strong in the 1987 spectrum. This would indicate that both the FeII and TiII lines are variable, i.e. the excitation of the envelope varies with time. Variability in the strength of the metallic lines (≈ weeks) was observed by Andersen et al. (1982).

6.1.2.3. The Helium lines.

A few HeI lines in absorption are evident in both the optical and IR spectra: 3888 ($2s^3 - 3p^3$; a possible blend with H8), 5015Å ($2s^1 - 3p^1$), 1.083μm ($2s^3 - 2p^3$) and possibly also 2.0581μm ($2s^1 - 2p^1$), i.e. the HeI lines of lowest excitation. These lines are *not* expected from a mid-A spectral class star, and thus they indicate a region of

reasonably high excitation ($T_e \simeq 1 - 2 \times 10^4$ K) within the stellar envelope. Again, the presence of HeI lines (not observed by Bessel and Eggen 1972) indicates variability of the excitation of the shell.

6.1.2.4. Summary.

It is seen that hydrogen, singly ionised metals and helium are excited in a shell surrounding V856 Sco and that the extent of the excitation is probably variable with time. The degree of shell absorption observed would appear to be directly correlated with the photometric brightness at certain epochs, and anti-correlated with the photometric brightness at other epochs. More spectroscopic observations of V856 Sco are required in order to establish the timescale of this phenomenon and spectroscopic observations as V856 Sco passes through photometric minimum would be of particular interest in successfully interpreting the variable degree of shell absorption.

6.1.3. The Colour-colour variations.

HD 144667 was observed by Kilkenny et al. (1985) between 1981 and 1984, and did not vary by more than 0.1 mag. from a mean brightness of V = 6.65 mag. However, the V-I colour was observed to vary from - 0.01 to - 0.46. The observed mean value of (B-V) = - 0.075, suggests an intrinsic (B-V) $\simeq$ - 0.14 (from the reddening estimate of Thé and Tjin A Djie 1978), which is appropriate for a B5 giant. A similar result was obtained by Thé and Tjin A Djie (1978).

In estimating the distance modulus of HD 144667, Thé and Tjin A Djie (1978) use a M_v = - 0.7 mag., appropriate for a B6III star, which

gives a distance estimate of 270 - 300pc. However, spectra of the star typically exhibit an A0-3IIIp spectral type (Kholopov et al., 1987). Although the spectrum is peculiar, a distance estimate assuming the intrinsic colours of an A0III spectral type, rather than a B6III spectral type, is likely to be the more reliable.

Thus using a M_v = 0.7 mag. (Allen 1973) appropriate for an A0III star, the distance is determined to be 160pc (≃ 170pc allowing for an A_v = 0.2 mag.). Thus the distance to the binary system of HD 144667 and V856 Sco will be assumed to be ≃ 170pc.

The light variations of V856 Sco were well studied by Bessel and Eggen (1972) who found that the star faded gradually from normal light (V ≃ 6.9 mag.) to minimum (V ≃ 7.8 mag.) with a quasi-period of about one month. Although Thé and Tjin A Djie (1978) made fewer observations, their photometry also showed a similar behaviour. However, in their study, Andersen et al. (1982) indicate that the minima are not periodic, but occur infrequently.

The light and colour variations seen in V856 Sco have been found to be consistent with the variability being caused by variable circumstellar extinction. However, Bessel and Eggen (1972) and Tjin A Djie and Thé (1978), who included the dataset of Bessel and Eggen in their analysis, report different colour slopes.

In their 42 observations (covering 5 minima in total), Bessel and Eggen (1972) found colour slopes indicative of a normal IS-type reddening law; whilst in the combined dataset of V856 Sco from 1971 - 1977, Tjin A Djie and Thé (1978) (including the 5 minima observed by Bessel and Eggen 1972, and the minimum observed by Thé and Tjin A Djie 1978) report colour slopes (when V856 Sco is varying between minimum and maximum) indicative of an anomalous (R = 5.0 ± 0.9) reddening law.

In view of the fact that the observations of Bessel and Eggen (1972) alone cover successive minima, their data must be taken to be more representative of the colour behaviour of V856 Sco around minimum light, i.e. colour slopes corresponding to variable extinction by IS-sized circumstellar grains.

In the observations of V856 Sco including the data of Kilkenny et al. (1985) and the data obtained in June and September, 1987, V856 Sco was observed close to normal light (V ≈ 6.8 - 7.2 mag.), *except* for only two nights, when the star faded to V = 7.69 mag. on HJD 2444779 and to V = 7.47 mag. on HJD 2447044. From an examination of the observed lightcurve from 1981 - 1984, the Kilkenny et al. (1985) dataset has sufficiently long gaps for successive minima (apart from one) to have potentially been "missed" during each gap in the coverage. However, the fact that V856 Sco was observed to be fainter than 7.2 mag. in only 2 out of 27 observations obtained over a three year period does suggest that quasi-periodic minima of the form observed by Bessel and Eggen (1972) were not prevalent during this period, cf. Andersen et al. (1982). Therefore the total dataset (31 observations) only provides good coverage of the photometric behaviour of the star when at normal light.

There was very little variation of the Hβ index with V, as is shown in Fig. 6.1.3, which indicates that there is no significant change in the Hβ line profile (a line affected by shell absorption) whilst the star varies around normal light. This result would not be inconsistent with the finding of Bessel and Eggen (1972) that notable changes in the shell absorption occur only when the star fades.

The optical colour behaviour of V856 Sco from 1981 - 1984 when at normal light (see Figs. 6.1.4 - 6.1.7) are found to match the behav-

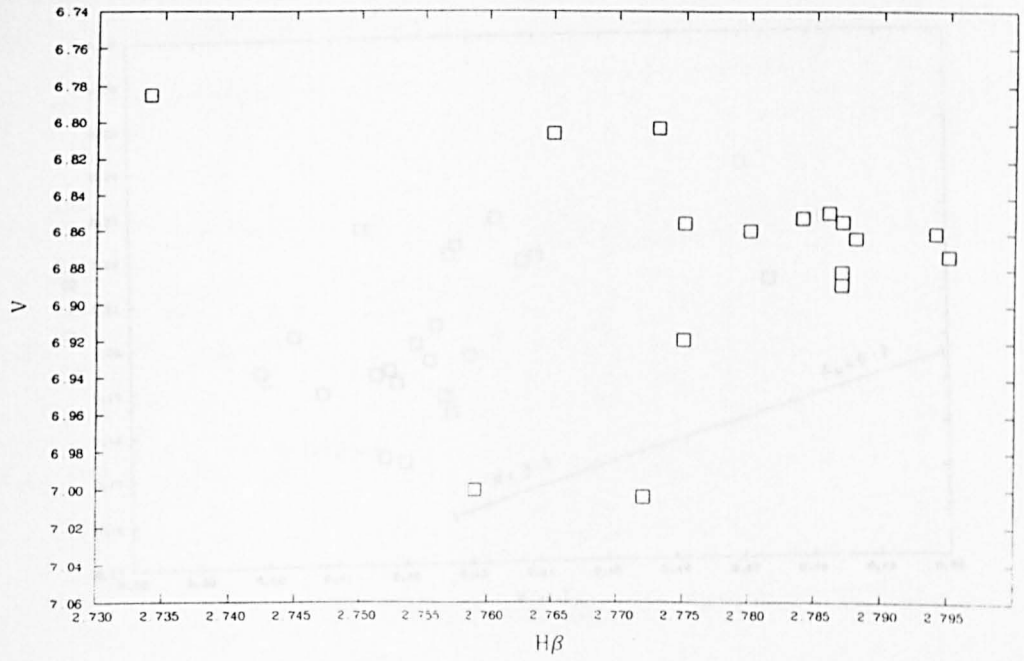

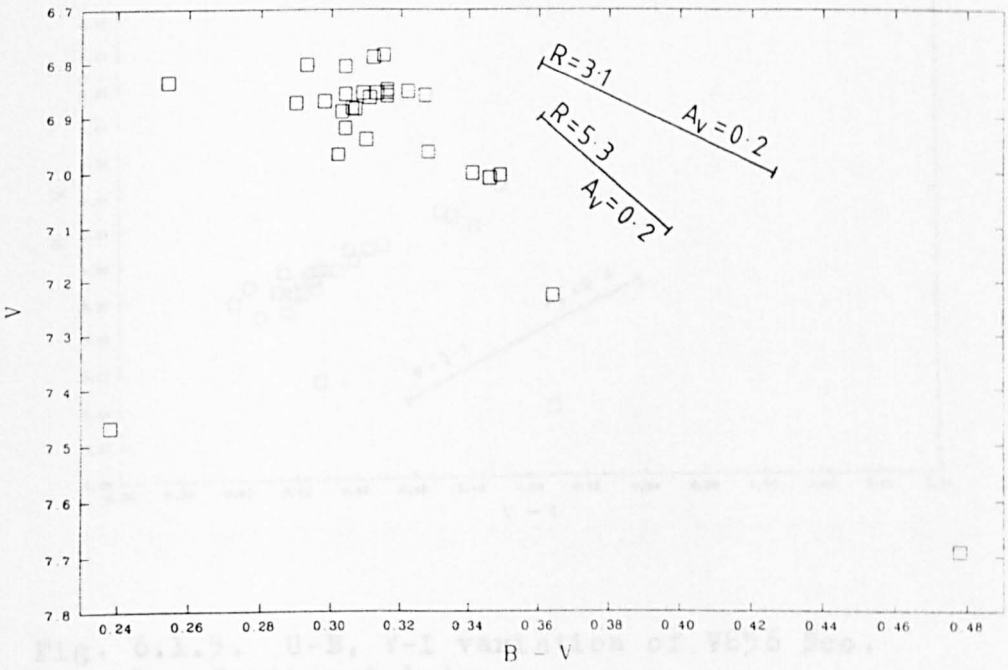

Fig. 6.1.3. V, Hβ variation of V856 Sco.
See also Section 6.1.3.

Fig. 6.1.4. V, B−V variation of V856 Sco.
See also Section 6.1.3.

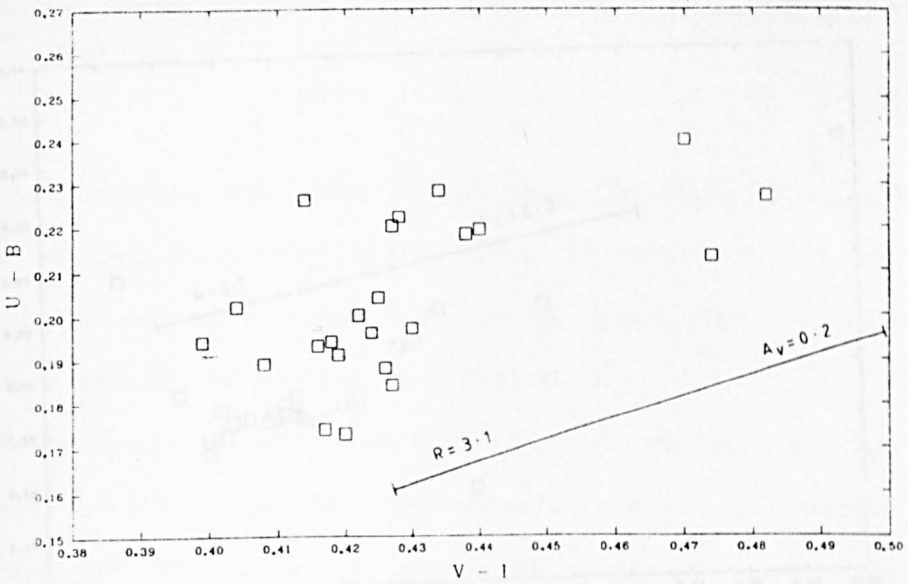

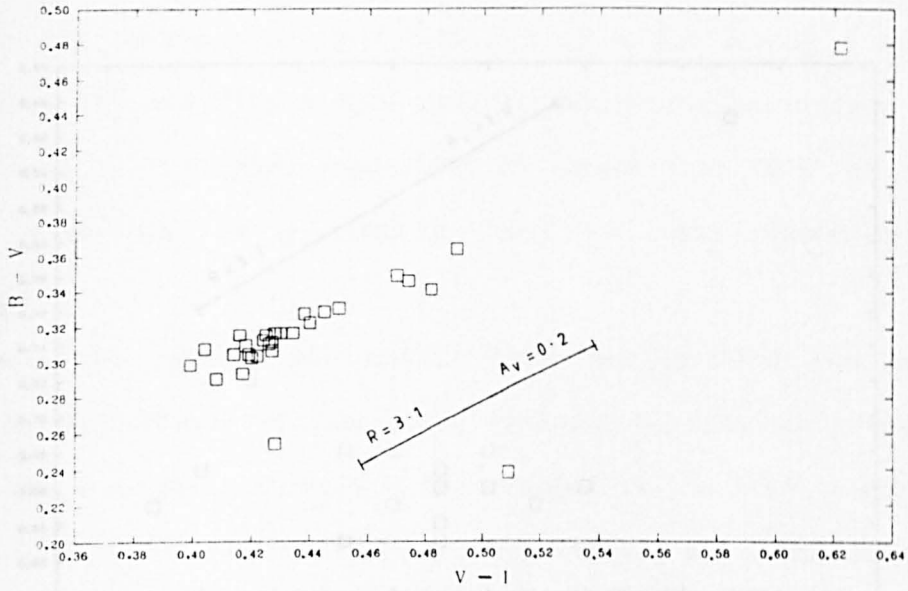

Fig. 6.1.5. U-B, V-I variation of V856 Sco. See also Section 6.1.3.

Fig. 6.1.6. B-V, V-I variation of V856 Sco. See also Section 6.1.3.

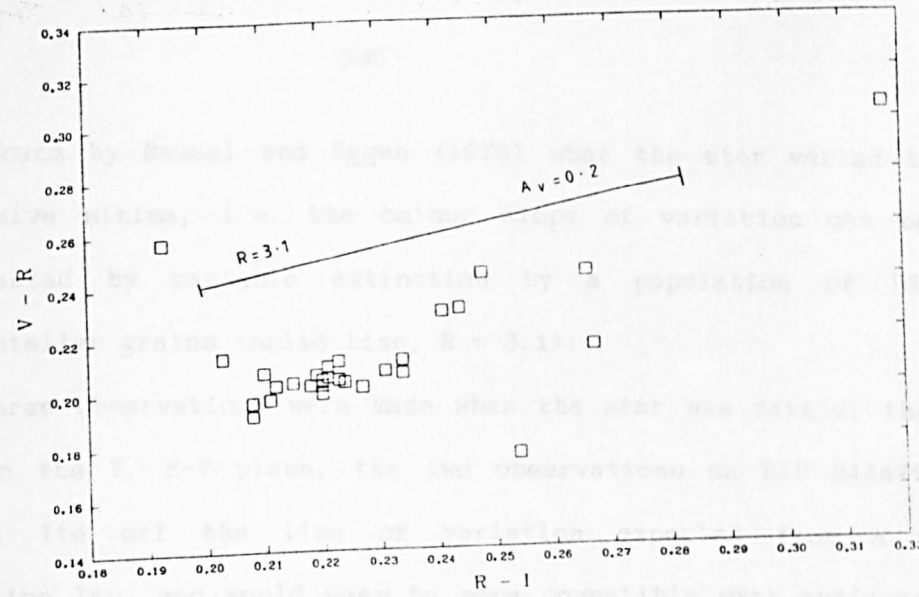

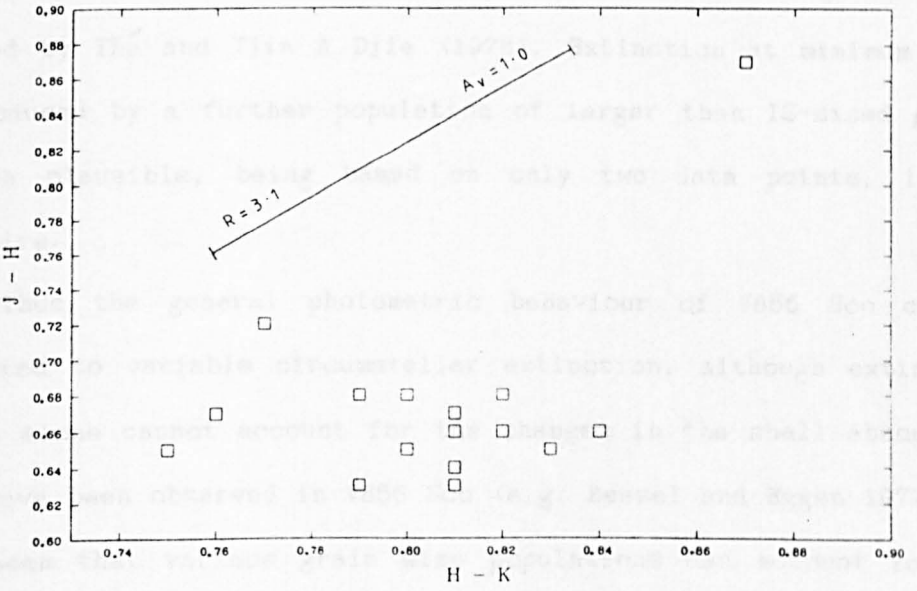

Fig. 6.1.7. V-R, R-I variation of V856 Sco. See also Section 6.1.3.

Fig. 6.1.8. J-H, H-K variation of V856 Sco. See also Section 6.1.3.

iour found by Bessel and Eggen (1972) when the star varied through successive minima; i.e. the colour slope of variation can be well represented by variable extinction by a population of IS-sized circumstellar grains (solid line, R = 3.1).

Three observations were made when the star was fainter than 7.2 mag. In the V, B-V plane, the two observations on HJD 2444779 and 2444781 lie off the line of variation expected from a normal extinction law, and would seem be more compatible with extinction by larger than IS-sized grains, corresponding to an anomalous extinction law, R = 5.3 (solid line, R = 5.3), cf. R ≃ 5.5 during a minimum observed by Thé and Tjin A Djie (1978). Extinction at minimum light being caused by a further population of larger than IS-sized grains although plausible, being based on only two data points, is not persuasive.

Thus the general photometric behaviour of V856 Sco can be attributed to variable circumstellar extinction, although extinction by dust alone cannot account for the changes in the shell absorption which have been observed in V856 Sco (e.g. Bessel and Eggen 1972). It would seem that various grain size populations can account for the different colour slopes observed at different epochs and at different brightness levels. More photometric and spectroscopic observations following V856 Sco through a few consecutive periods of minimum light (i.e. observations every few nights over a period of a few months) would clarify the observational constraints on the variability of this star, and allow a consistent interpretation of the minima.

Thus the optical photometry presented here, whilst confirming the general colour behaviour observed by Bessel and Eggen (1972), attributable to variable circumstellar extinction by IS-sized grains, do

not appear to substantiate the gradual, quasi-periodic light variations observed by Bessel and Eggen (1972). From theoretical considerations (cf. Evans 1981), it would seem unlikely that bound clumps, stable against gravitational shear, could persist in regulated "orbits" of periods of ≃ a month, i.e. it is not unsurprising that quasi-periodic minima on this timescale do not persistently occur in the lightcurve of V856 Sco.

The locus of variation in the near-IR colours, Figs. 6.1.8 - 6.1.9, do not follow the reddening slope as well as is found for the optical colours. This indicates that there is some intrinsic variation in the near-IR emission (attributable to dust: see Section 6.1.4) as well as variation in the dust shell opacity.

6.1.4. The Flux Distribution.

The simultaneous optical and near-IR photometry of V856 Sco (and HD 144667) obtained by Kilkenny et al. (1985) and the optical, near- and far-IR data obtained in 1987 formed the database for investigating the intrinsic flux distribution.

The intrinsic spectral type (A0-3III; Bessel and Eggen 1972) and reddening ($E(B-V)_{IS}$ = 0.06 - 0.08; Bessel and Eggen 1972, Thé and Tjin A Djie 1978) have been fairly well determined for HD 144667. It is found that both the optical and near-IR data of HD 144667 can be well represented by a 10000K, log g = 3.5 Kurucz (1979) model atmosphere (consistent with the given spectral type) which is dereddened by E(B-V) = 0.06, as is shown in Fig. 6.1.10, i.e. there is no IR excess out to 3.5μm. Thus an $E(B-V)_{IS}$ = 0.06 will be adopted at the IS reddening to both HD 144667 and V856 Sco.

From the normalisation required to fit the dereddened data, the stellar radius of HD 144667 is estimated to be $\simeq$ 4.6 $R_\odot$ at a distance of 170pc (as determined in Section 6.1.3). With R = 4.6 $R_\odot$ and T_{eff} = 10000K, and assuming hydrostatic equilibrium, the luminosity is estimated to be 190 $L_\odot$, cf. $L_{Bol} \simeq 79\ L_\odot$ for a normal A0IV star (Allen 1973).

Assuming the same IS reddening for V856 Sco and a R = 3.1 circumstellar reddening law for V856 Sco at normal light (Section 6.1.3), the optical photometry of V856 Sco was further dereddened until a good fit to an 8000K, log g = 3.5 Kurucz (1979) model atmosphere (adopted as a compromise between the parameters derived by various authors - see Section 6.1.1) was obtained. The additional reddening required to fit the photometry to the model atmosphere is typically $E(B-V)_{cs} \simeq$ 0.16, which is therefore taken to be the circumstellar reddening affecting V856 Sco at normal light. At minimum light an $E(B-V)_{cs} \simeq$ 0.22 is required to fit the photometry.

In addition, an $E(B-V)_{cs} \simeq 0.16$ is required to fit the model atmosphere to the SAAO optical spectrum and is shown in Fig. 6.1.11. This confirms the spectral type and helps to show the extent of the Balmer shell absorption.

From the normalisation of the model atmosphere required to fit the photometry at normal light (e.g. on HJD 2445101 - Fig. 6.1.12), the radius estimate of V856 Sco is $\simeq$ 4.4 $R_\odot$ at d = 170pc. A normal A5III-IV star has a radius of $\simeq$ 3 - 4 $R_\odot$ (Allen 1973). Assuming hydrostatic equilibrium, the luminosity of a T_{eff} = 8000K and R_* = 4.4 $R_\odot$ star is $L_{Bol} \simeq 71\ L_\odot$. The bolometric luminosity of a normal A5 sub-giant is only 20 $L_\odot$ (Allen 1973), and thus an A7III spectral classification of V856 Sco is perhaps the more appropriate.

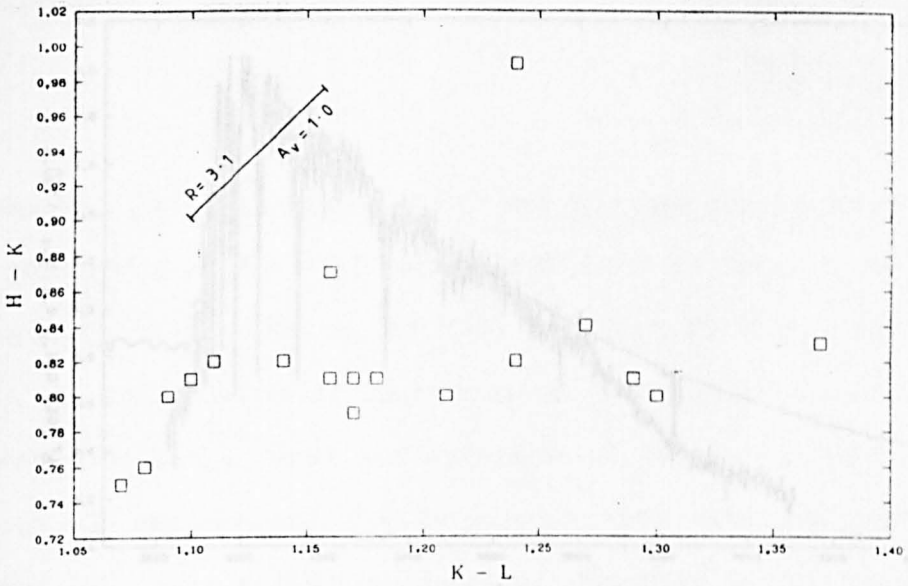

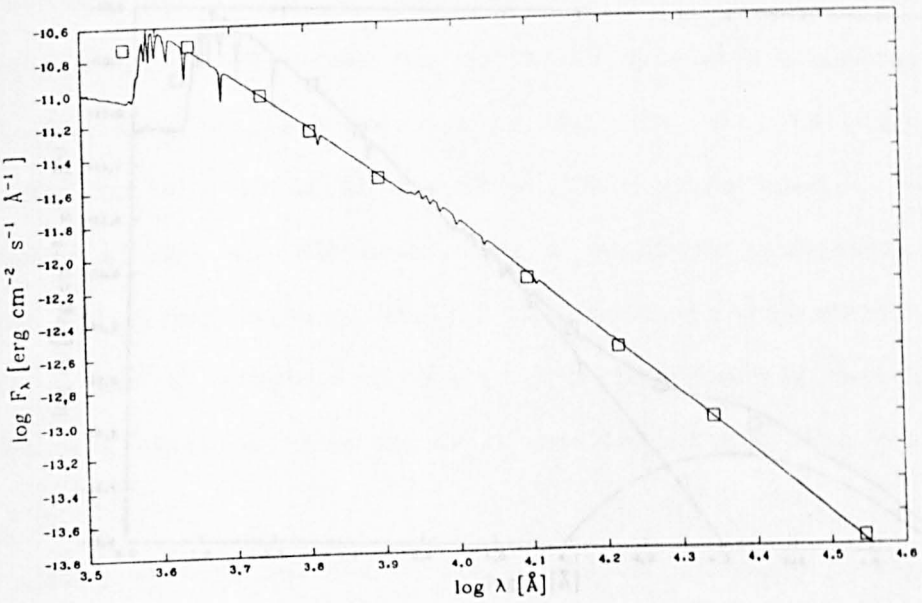

Fig. 6.1.9. H-K, K-L variation of V856 Sco. See also Section 6.1.3.

Fig. 6.1.10. Flux distribution of HD144667. See also Section 6.1.4.

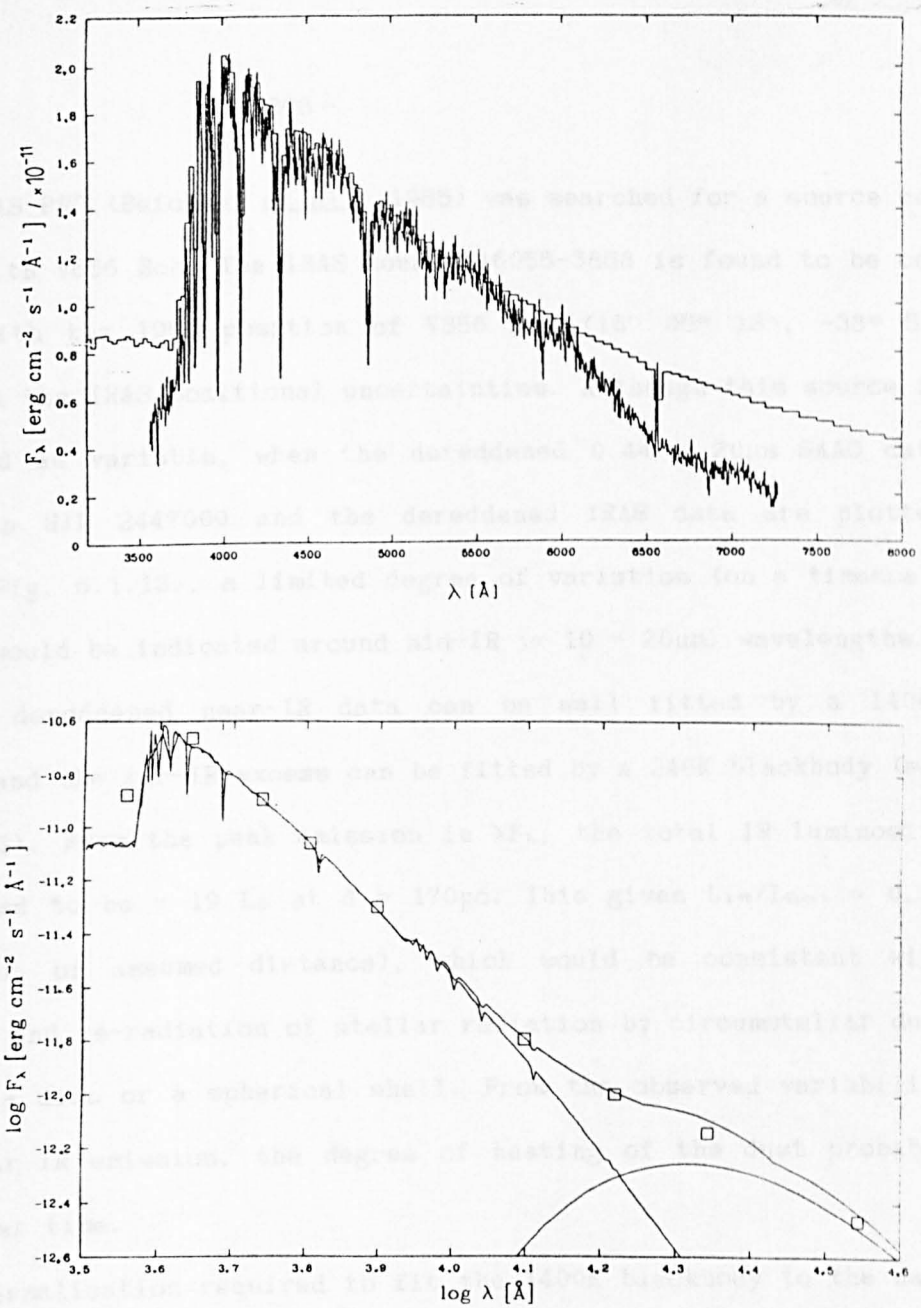

Fig. 6.1.11. Model atmosphere fit of optical spectrum of V856 Sco.
See also Section 6.1.4.

Fig. 6.1.12. Flux distribution of V856 Sco on HJD 2445101.

The IRAS PSC (Beichman et al., 1985) was searched for a source coincident with V856 Sco. The IRAS source 16055-3858 is found to be coincident with the 1950 position of V856 Sco (16^h 05^m 13", -38° 57' 36") within the IRAS positional uncertainties. Although this source is not flagged as variable, when the dereddened 0.44 - 20μm SAAO data obtained on HJD 2447000 and the dereddened IRAS data are plotted together (Fig. 6.1.13), a limited degree of variation (on a timescale of years) would be indicated around mid-IR (≃ 10 - 20μm) wavelengths.

The dereddened near-IR data can be well fitted by a 1400K blackbody and the far-IR excess can be fitted by a 240K blackbody (see Fig. 6.1.13). From the peak emission in λF_λ, the total IR luminosity is estimated to be ≃ 19 $L_\odot$ at d = 170pc. This gives $L_{IR}/L_{Bol} \simeq 0.26$ (independent of assumed distance), which would be consistent with absorption and re-radiation of stellar radiation by circumstellar dust either in a disc or a spherical shell. From the observed variability in the near-IR emission, the degree of heating of the dust probably changes over time.

The normalisation required to fit the 1400K blackbody to the data at each epoch is fairly constant, and indicates an upper limit for the inner dust shell radius of ≃ 122 $R_\odot$. For the stellar parameters of V856 Sco, using Eq. (4.1) for thermally heated, "real" silicate grains, the expected distance is ≃ 183 $R_\odot$.

6.1.5. Polarimetric observations

The polarisation of HD 144667 through a clear filter was measured on HJD 2447044 to be 0.92 ± 0.04% with a position angle of 3 ± 4°. The polarisation observed through a clear filter is significantly differ-

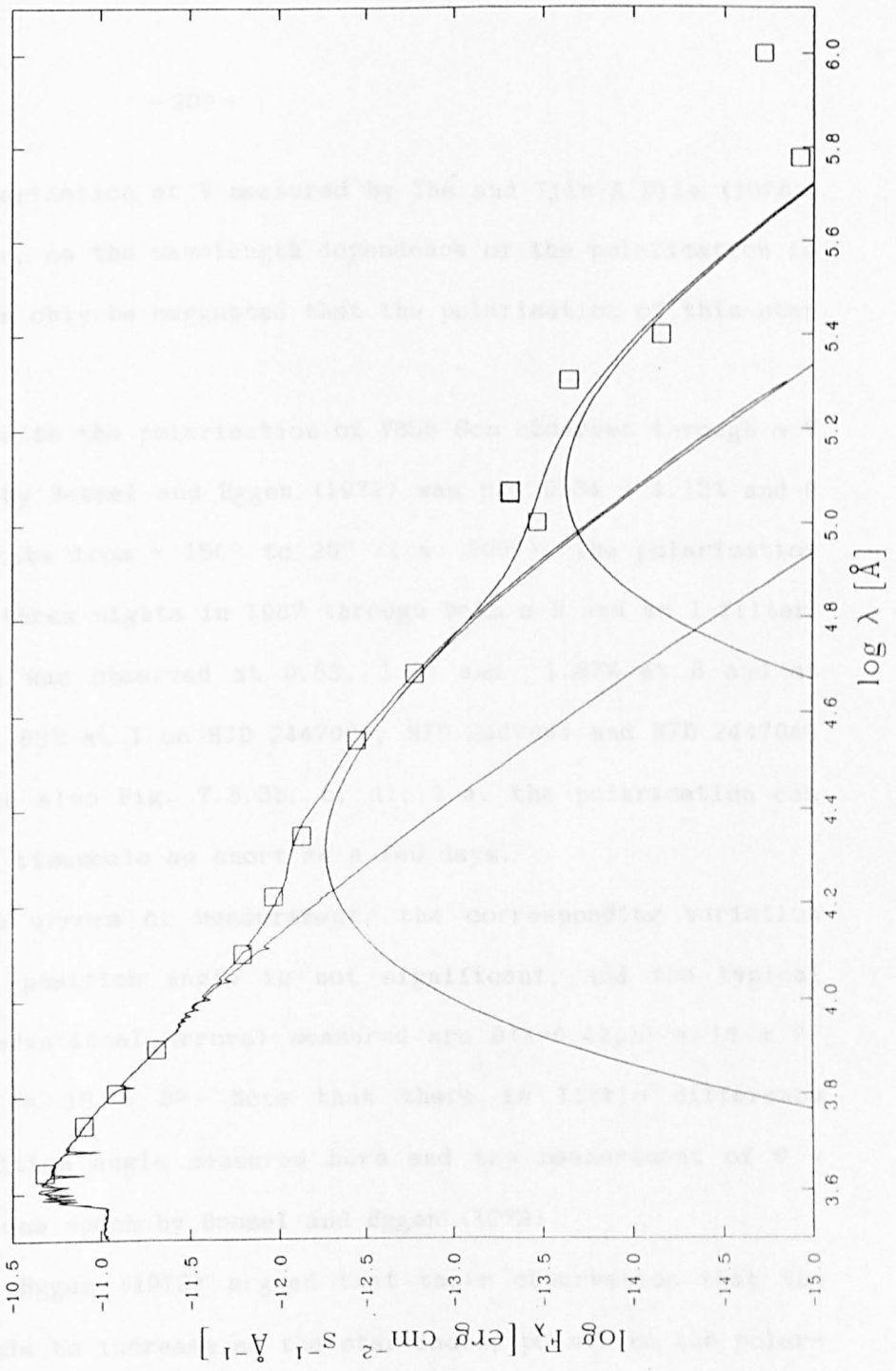

Fig. 6.1.13. Flux distribution of V856 Sco on HJD 2447000 with IRAS data included. See also Section 6.1.4.

ent from the polarisation at V measured by Thé and Tjin A Djie (1978), of 0.46%. However, as the wavelength dependence of the polarisation is not known, it can only be suggested that the polarisation of this star may be variable.

The variation in the polarisation of V856 Sco observed through a V filter measured by Bessel and Eggen (1972) was p = 0.34 - 1.13% and θ was found to rotate from ≃ 150° to 20° (i.e. 200°). The polarisation was observed on three nights in 1987 through both a B and an I filter. The polarisation was observed at 0.83, 1.04 and 1.87% at B and at 0.92, 1.04 and 1.83% at I on HJD 2447000, HJD 2447044 and HJD 2447049 respectively (see also Fig. 7.3.3b, c, d), i.e. the polarisation can be variable on a timescale as short as a few days.

Within the errors of measurement, the corresponding variation observed in the position angle is not significant, and the typical values (and observational errors) measured are $\theta(\lambda=0.44\mu m) \simeq 18 \pm 7^{\circ}$ and $\theta(\lambda=0.79\mu m) = 18 \pm 3^{\circ}$. Note that there is little difference between the position angle measured here and the measurement of $\theta \simeq 20^{\circ}$ obtained at one epoch by Bessel and Eggen (1972).

Bessel and Eggen (1972) argued that their observation that the polarisation tends to increase as the star fades, points to the polarisation arising within the circumstellar dust shell. Although only three observations on different dates were obtained here (i.e. not enough to conclusively identify a trend), the fact that the polarisation was observed to increase from $p(\lambda=0.44\mu m) = 0.83 - 1.87\%$ (from HJD 2447000 - 2447044), an increase which was associated with a fading in the lightcurve from V = 6.84 - 7.47 mag. (observed on HJD 2447000 and 2447040 respectively), would not be inconsistent with the conclusion reached by Bessel and Eggen (1972).

The extent of the variation between two observations obtained only five days apart does argue that the polarisation must arise from a region which extends no more than about a light day from the star. This places a definite constraint on the grain temperature and composition. The observed polarisation can be modelled by scattering by graphite grains (see Section 7.3.2.8), which is not inconsistent with the constraints imposed by the polarimetric variability and the near-IR excess (see Section 6.1.4).

6.1.6. Summary and Conclusions.

V856 Sco is an Ina star which lies within Δ199, a cluster of InT stars, although its binary companion, HD 144667 exhibits a peculiar spectrum and is probably not a PMS star. No notable photometric variability of HD 144667 is observed from 1981 - 1987, although it may possibly have varied polarimetrically. From the observed magnitude of HD 144667 and assuming an A0III spectral type, the distance to the cluster has been estimated to be ≈ 170pc.

The spectrum of V856 Sco was observed to have pronounced shell absorption lines when the star was bright (as was observed by Bessel and Eggen 1972), and also singly ionised metallic and some HeI absorption lines. The degree of the excitation within the stellar envelope has clearly changed since 1972 (Bessel and Eggen 1972). Only the lowest hydrogen lines observed (Hα, Paß and Bγ) are seen in emission, but in non-simultaneous optical and IR spectra.

V856 Sco is found to radiate about a quarter of its total luminosity in the IR, which can be attributed to re-radiation of optical radiation by heated dust in either a disc or a spherical halo.

V856 Sco has been observed to exhibit a slowly varying lightcurve attributable to changes in the opacity of circumstellar dust, e.g. Bessel and Eggen (1972). The data presented here support the mechanism of light variability forwarded for V856 Sco, variable circumstellar extinction. However, quasi-periodic minima (such as were observed by Bessel and Eggen 1972) are not evident in the lightcurve, although given the breaks in the dataset, quasi-periodic minima occurring between 1981 and 1984, although unlikely, cannot be totally ruled out.

The fact that minima have been observed to be accompanied by rises in optical polarisation (as has also been indicated by data presented here) as well as changes in the strength of the shell absorption lines, would indicate that the spectroscopic, polarimetric and photometric variations may well be related, and potential models must account for this.

The suggested periodicity of light minima, ≃ one month (Bessel and Eggen 1972) is too short for "orbiting" dust clumps, and thus "unbound" density enhancements ("cloudlets") in the circumstellar dust shell are thought to be more plausible. Changes in the line-of-sight opacity due to isolated "cloudlets" would not however be expected to significantly affect the polarisation, but more global changes (e.g. motion of an ensemble of dust "cloudlets") would be needed, and further work is required to interpret the polarimetric changes.

6.2. The T Tauri star CoD -33° 10685.

6.2.1. Introduction.

CoD -33° 10685 (Sz 68) is an InT star included in Herbig and Rao's

(1972) list of Orion variables and is associated with the bright B228 nebula near the Lupus T association. In their catalogue, Hα is noted as the only emission line, and the spectral type is given as Geα. Elsewhere (Herbig 1977a; Appenzeller et al. 1983; Bouvier et al., 1986b) it is designated as a K2eα star. Bouvier et al. (1986b) give an estimate of the bolometric luminosity, $L_{bol} \simeq 4.9\ L_{\odot}$, and the rotation velocity v sin i = 48.0 ± 6.6 kms^{-1}.

The star is neither a notable photometric nor polarimetric variable. The observed range in V is 10.5 (Appenzeller et al., 1983) to 10.8 mag. (Bouvier et al., 1986b). Bastien (1985) notes that the polarisation in the red varies by no more than 0.2% and the position angle varies by no more than 2°. However Bastien's measurements do indicate that the polarisation has both an IS and an intrinsic component, and he interprets the wavelength dependence of the polarisation in terms of scattering by graphite or iron grains.

6.2.2. Optical and Infrared photometry.

Simultaneous optical and IR photometry of CoD -33° 10685 was obtained on four nights in July and September, 1987. In both the July observations V ≃ 10.25 mag., and the only notable change in V occurred in the last two observations when the star was observed to fade from V = 10.26 mag. on HJD 2447041 to V = 10.48 mag. on HJD 2447042, i.e. on all but the last night, the star is consistently ≃ 0.25 mag. brighter than has been typically observed.

On the last two nights, both the V-R and V-I colours became redder by only 0.04 mag. and there was no change in B-V. This would indicate that the circumstellar reddening did not change significantly between

these two nights, and thus the prolonged phase at which CoD -33° 10685 was brighter than usual is more likely to have been due to the star being intrinsically brighter, rather than being less heavily reddened, over this time than is usual. But the fact that the mean colours in July and September, respectively, were B-V = 1.27, 1.32; V-R = 0.75, 0.77; V-I = 1.52, 1.54 indicates that neither was there any significant change in the effective temperature of the star over this period.

The optical photometry was dereddened to fit a 5000K blackbody (from the temperature calibration of Cohen and Kuhi 1979 for a K2 star). A Kurucz (1979) model was not used as the coolest available Kurucz model is for T_{eff} = 5500K, and also the gravity of CoD -33° 10685 is not known. A total E(B-V) = 0.45 with R = 3.1, gave the best fit to the data (allowance was made for Hα emission at R). It is noted that on the night of HJD 2447042 (when CoD -33° 10685 was at more "normal" light of V = 10.48 mag.), a slightly greater E(B-V) = 0.50 gave a better fit to the data, although this possible difference in reddening cannot be regarded as significant (see above).

No variation in the IR colours was observed. The most complete wavelength coverage from 0.4 - 10μm was obtained on HJD 2447041, and a 1400K blackbody was found to give the best fit to the dereddened IR data, shown in Fig. 6.2.1. The colour slope of the MNQ data obtained concurrently with the optical photometry on HJD 2446991 (no JHKL photometry was obtained on this date however) indicates that emission from cooler dust (≃ 200K) is required to explain the far-IR emission.

From the fits to the dereddened optical and IR data, the luminosity from 0.44μm out to 20μm is estimated to be 7.6 $L_\odot$ (with an assumed distance of 150pc to the Lupus T association). The ratio $L_{IR}/L_{bol} \simeq 0.18$ (independent of assumed distance), i.e. the IR

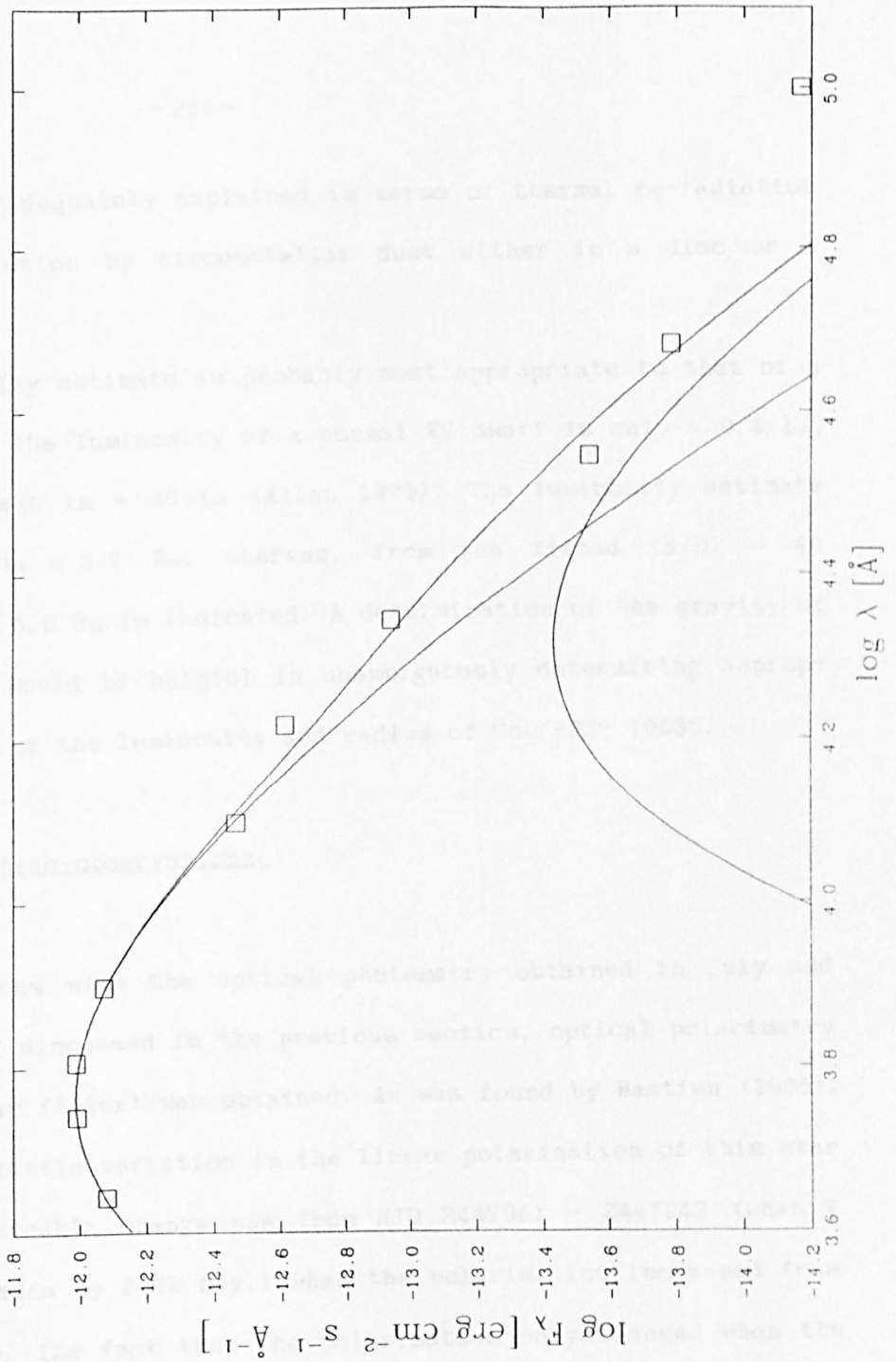

Fig. 6.2.1. Flux distribution of CoD- 33°10685 on HJD 2447042.

emission can be adequately explained in terms of thermal re-radiation of stellar radiation by circumstellar dust either in a disc or a spherical shell.

The luminosity estimate is probably most appropriate to that of a K2 sub-giant as the luminosity of a normal K2 dwarf is only $\simeq 0.4\ L_\odot$, and of a K2 giant is $\simeq 80\ L_\odot$ (Allen 1973). The luminosity estimate suggests that $R_* \simeq 3.7\ R_\odot$, whereas, from the fitted (R/D) = 40 $R_\odot kpc^{-1}$, a $R_* \simeq 6.0\ R_\odot$ is indicated. A determination of the gravity of CoD -33° 10685 would be helpful in unambiguously determining appropriate estimates of the luminosity and radius of CoD -33° 10685.

6.2.3. Polarimetric observations.

Simultaneous with the optical photometry obtained in July and September, 1987 discussed in the previous section, optical polarimetry (through a clear filter) was obtained. As was found by Bastien (1985), there is very little variation in the linear polarisation of this star - the only noticable change was from HJD 2447041 - 2447042 (when V concurrently faded by 0.22 mag.) when the polarisation increased from 1.36% to 1.50%. The fact that the polarisation only changed when the brightness of the star varied suggests that the two may possibly be anti-correlated (although this is based on only four observations) and subsequent related changes should be looked for. Also, from two simultaneous near-IR JHK observations, the optical-IR colours (e.g. V-K) were found to be correlated with the observed increase in p.

On one night, HJD 2446991, the position angle was observed to vary from 185° to 173° (the error in both measurements was $\simeq 3°$), values which are both significantly different from the $\theta(\lambda=0.53\mu m) = 196 \pm 2°$

observed by Bastien (1985).

Although these changes in polarisation and position angle are smaller than exhibited by many other InT stars, they represent the first significant polarimetric variations of CoD -33°10685 observed, and, as they occurred within 24 hours (although a different 24 hour period in each case), they place a constraint on the size of the scattering volume of dust. Possible related variation in the optical-IR colours with the polarisation may indicate that changes in the distribution of circumstellar dust may be responsible for the polarimetric variability. Further simultaneous polarimetry and optical and near-IR photometry are required. The wavelength dependence of the linear polarisation can only be poorly fitted by a model using graphite grains (see Section 7.3.2.10) and thus the polarisation may be caused by scattering by iron grains (cf. Bastien 1985).

6.2.4. Summary and Conclusions.

In three out of four observations, CoD -33°10685 was observed to be about 0.25 mag. brighter than is usually observed. An IR excess is observed out to 20μm which is consistent with thermal re-radiation by heated (up to ≃ 1400K) circumstellar grains. For the first time, notable changes in the polarisation and position angle of CoD -33° 10685 can be reported. With a timescale of variation of only hours being indicated, further monitoring of the polarisation of this star (preferably with simultaneous optical and near-IR photometry) should be pursued.

6.3. The T Tauri star AK Sco.

6.3.1. Introduction.

The InT star AK Sco (HD 152404), has a spectral type F5V (Herbig and Rao 1972) and can exhibit Hα in emission and the characteristic InT photospheric LiI 6707Å line is also seen (Herbig and Rao 1972). The star lies in the Sco-Oph dark cloud region. The visual lightcurve varies between 8.7 and 11.7 mag., and is most frequently at mean brightness, $\langle V \rangle \simeq 9.0$ mag. The polarisation (Serkowski 1969a) and wavelength dependence of the polarisation (Bastien 1987) of AK Sco are both variable.

6.3.2. The IR continuum.

IR spectra, from 0.94 - 2.4 μm, of AK Sco were obtained at CTIO in June, 1987. No hydrogen or other strong lines were observed. This indicates that hydrogen line emission (which can be observed affecting Hα) does not extend to the IR transitions. The JH and K spectra are displayed together (Fig. 6.3.1), normalised to the fluxes from the IR photometry obtained within 24 hours of the spectra being observed (as the I photometry could not be reduced, the I spectrum could not be appropriately normalised and is not shown; but there are no features observed in the spectrum). It is noted that the shape of the observed near-IR continuum would not be appropriate for a F5 photosphere (given the reddening of AK Sco determined in Section 6.3.4), and thus there may possibly be a near-IR excess. However, the lack of any significant Balmer emission (except for emission at Hα) indicating the lack of a

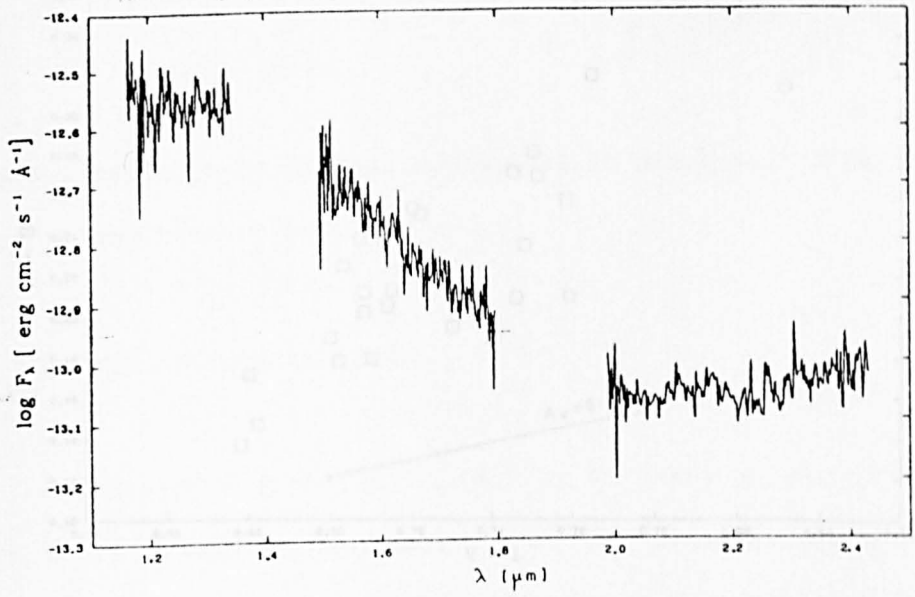

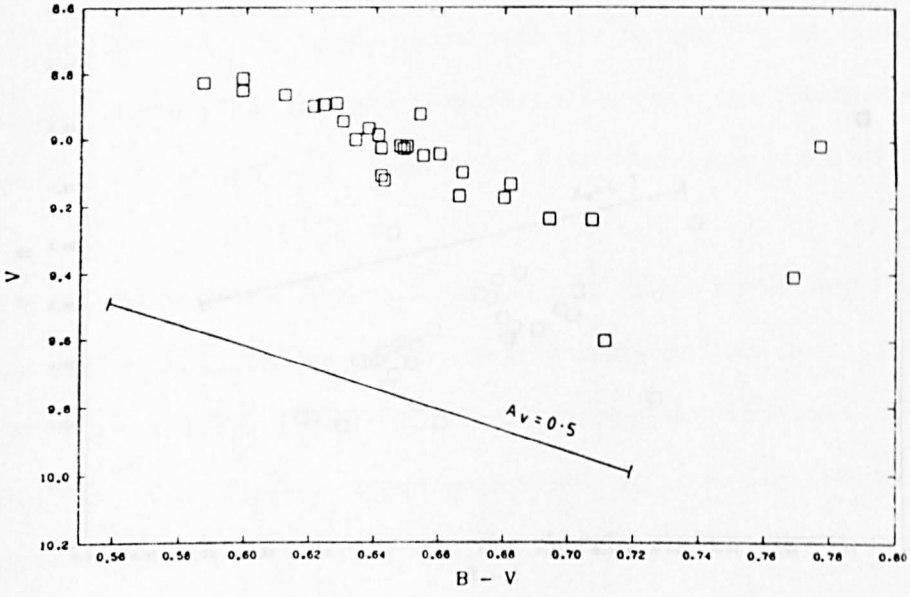

Fig. 6.3.1. Infrared spectra of AK Sco.
See also Section 6.3.2.

Fig. 6.3.2. V, B-V variation of AK Sco.
See also Section 6.3.3.

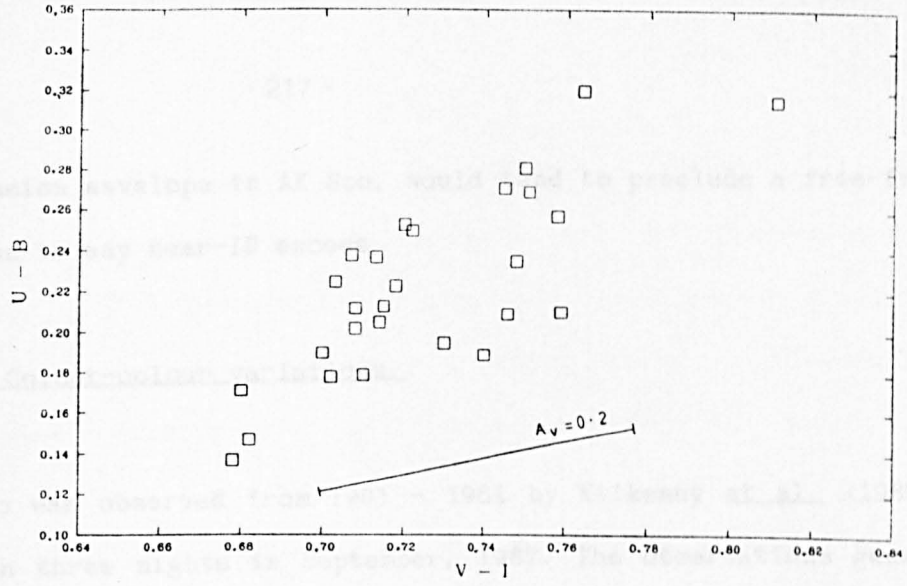

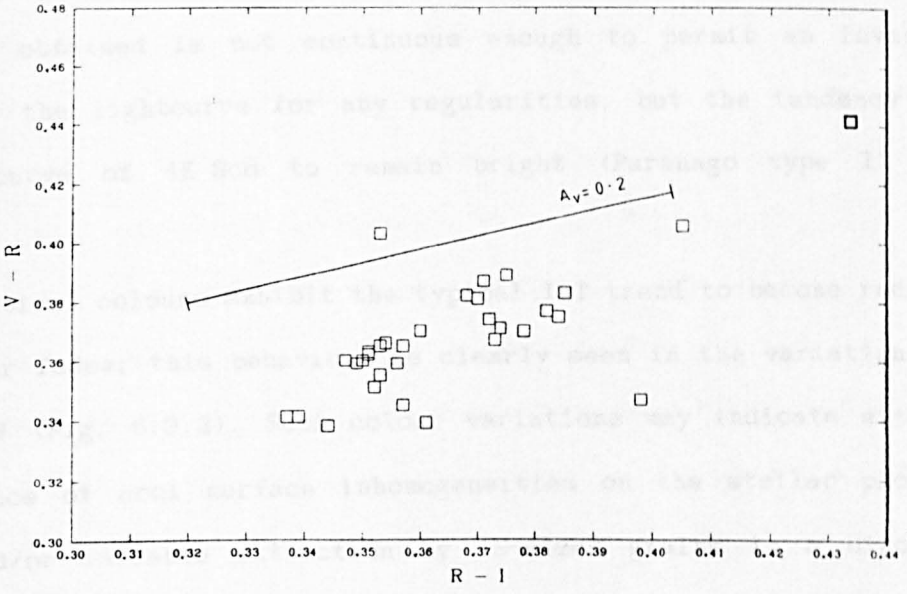

Fig. 6.3.3. U-B, V-I variation of AK Sco.
See also Section 6.3.3.

Fig. 6.3.4. V-R, R-I variation of AK Sco.
See also Section 6.3.3.

strong emission envelope in AK Sco, would tend to preclude a free-free contribution to any near-IR excess.

6.3.3. The Colour-colour variations.

AK Sco was observed from 1981 - 1984 by Kilkenny et al. (1985), and also on three nights in September, 1987. The observations generally show a variation around normal light between V = 8.83 and 9.20 mag., except on two nights, when the star faded below V = 9.4 mag. The photometry obtained is not continuous enough to permit an investigation of the lightcurve for any regularities, but the tendency of the lightcurve of AK Sco to remain bright (Parenago type I) is confirmed.

The optical colours exhibit the typical InT trend to become redder as the star fades; this behaviour is clearly seen in the variation of B-V with V (Fig. 6.3.2). Such colour variations may indicate either the presence of cool surface inhomogeneities on the stellar photosphere and/or variable extinction by IS-sized grains in a circumstellar dust shell (i.e. a R = 3.1 reddening law, solid line). On one night (HJD 2447044) when the star was fainter than V = 9.4 mag., the B-V colour became significantly redder (from B-V = 0.65 to 0.77), but on the other night when AK Sco was fainter than V = 9.4 mag. (HJD 2444739), it did not. This suggests that although increases in the circumstellar extinction can cause AK Sco to fade towards minimum light, intrinsic variations must also be responsible for some minima (cf. Section 6.3.4).

The U-B, V-I and V-R, R-I colour-colour slopes, shown in Figs. 6.3.3 and 6.3.4, respectively, follow a definite locus, and indicate

that the general variation when the star is at normal light can indeed be ascribed to variable circumstellar extinction by IS-sized grains (solid line). The larger scatter in the U-B plane can be plausibly attributed to occasional, relative brightening of the U band emission caused by weak "chromospheric" or "flaring" activity (cf. Worden and Schneeberger 1981).

Thus, in view of the fact that AK Sco almost always appears redder when fainter and that the observed colour variations would not be inconsistent with variable circumstellar extinction caused by IS-sized grains, this mechanism for the light variability typically seen in AK Sco is favoured. However some intrinsic changes in the photospheric emission, particularly when AK Sco is faint, would also seem to occur.

The Hβ index exhibits very little variation (Fig. 6.3.5), i.e. the Hβ profile is always in absorption (β > 2.5), although what variation there is, is seen to be essentially independent of visual brightness.

The loci of variation of the near-IR colours (Figs. 6.3.6 and 6.3.7) are less distinct, and there is a significant scatter in points (especially in K-L). But as AK Sco is only ≃ 5.5 mag. at L, the scatter in K-L is due in part to the errors in measurement at L (≃ 0.15 mag.) on the 0.75m telescope at SAAO. In view of this, the observed near-IR variations would not be inconsistent with changes in the circumstellar extinction (solid line). However, the possibility of additional near-IR emission (Section 6.3.2) contributing to the near-IR variability cannot be excluded.

6.3.4. The Flux Distribution.

Simultaneous optical, near- and far-IR photometry of AK Sco was

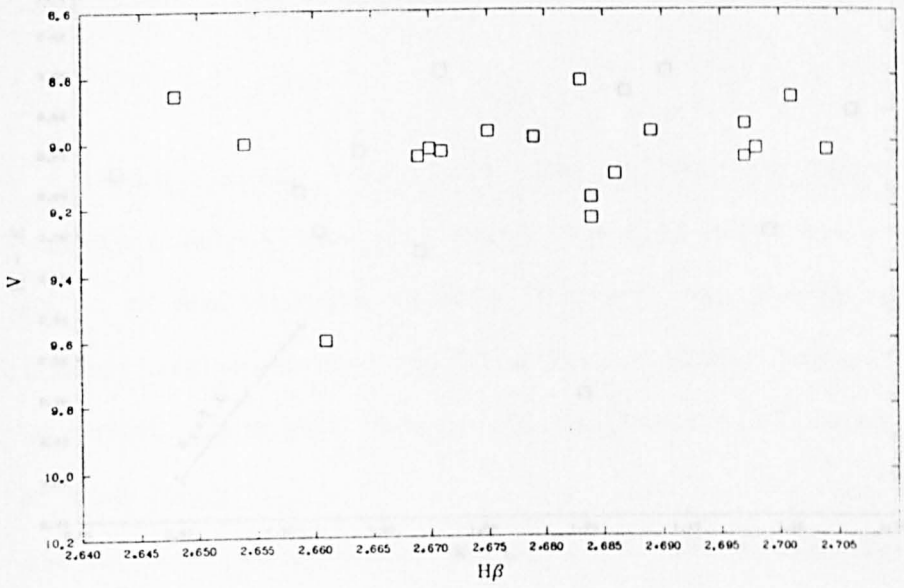

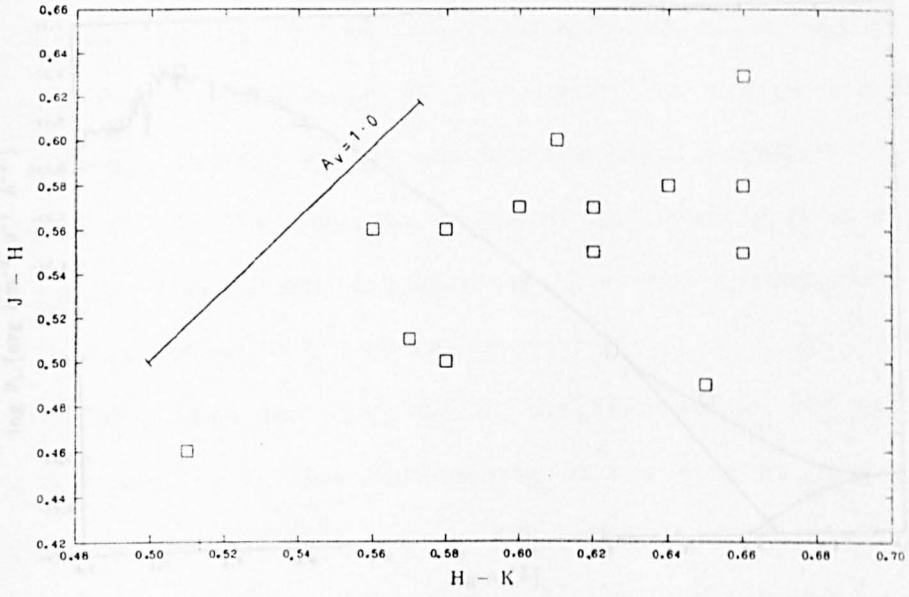

Fig. 6.3.5. V, Hβ variation of AK Sco.
See also Section 6.3.3.

Fig. 6.3.6. J-H, H-K variation of AK Sco.
See also Section 6.3.3.

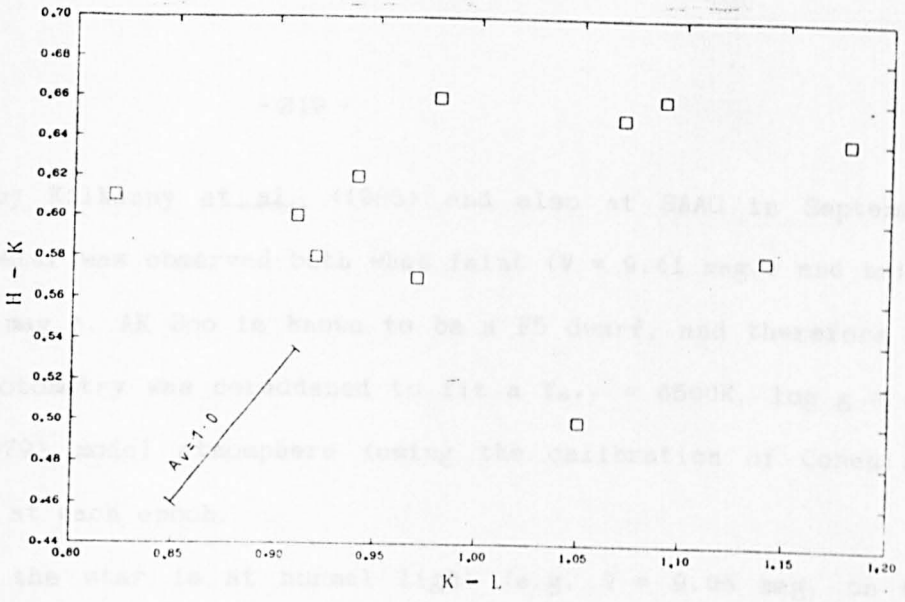

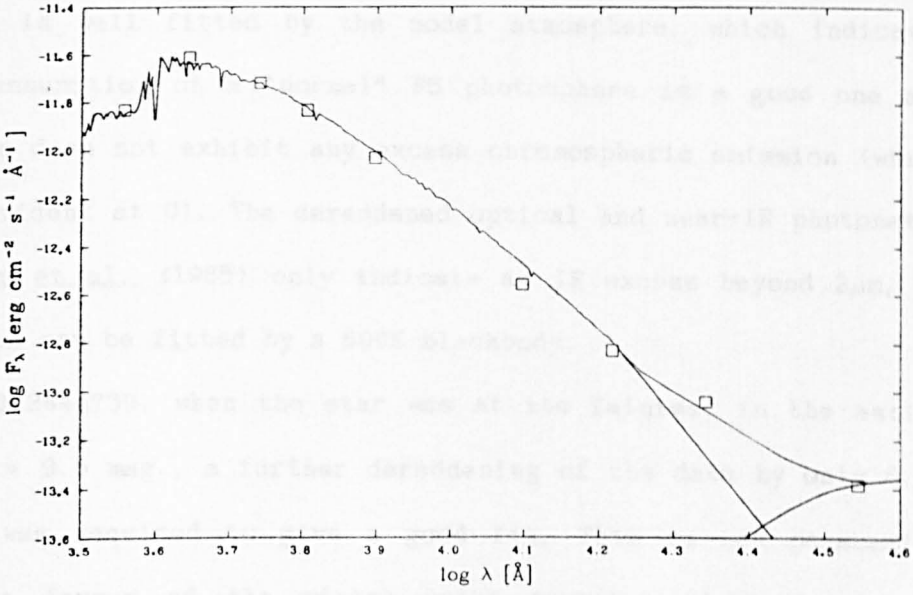

Fig. 6.3.7. H-K, K-L variation of AK Sco.
See also Section 6.3.3.

Fig. 6.3.8. Flux distribution of AK Sco on HJD 2445104.
See also Section 6.3.4.

obtained by Kilkenny et al. (1985) and also at SAAO in September, 1987. The star was observed both when faint (V = 9.41 mag.) and bright (V = 8.93 mag.). AK Sco is known to be a F5 dwarf, and therefore the optical photometry was dereddened to fit a T_{eff} = 6500K, log g = 4.0 Kurucz (1979) model atmosphere (using the calibration of Cohen and Kuhi 1979) at each epoch.

When the star is at normal light (e.g. V = 9.05 mag. on HJD 2445104; see Fig. 6.3.8), the optical data require dereddening by E(B-V) = 0.27 in order to fit the model atmosphere. The optical photometry is well fitted by the model atmosphere, which indicates that the assumption of a "normal" F5 photosphere is a good one and that AK Sco does not exhibit any excess chromospheric emission (which would be evident at U). The dereddened optical and near-IR photometry of Kilkenny et al. (1985) only indicate an IR excess beyond 2μm, an excess which can be fitted by a 800K blackbody.

On HJD 2444739, when the star was at its faintest in the entire dataset, V ≃ 9.6 mag., a further dereddening of the data by only 0.05 in E(B-V) was required to give a good fit. This is not persuasive evidence in favour of the minima being caused exclusively by an increase in the circumstellar extinction (cf. Section 6.3.3).

The distance of AK Sco is not well known, but if the star is assumed to lie about 150pc away (that estimated for the nearby Lupus dark cloud), then the required normalisation of the Kurucz (1979) model atmosphere to fit the data gives $R_* \simeq 2.3\ R_\odot$, which is significantly larger than the 1.2 $R_\odot$ of a normal F5 dwarf (Allen 1973): but as PMS stars can be known to have larger radii than MS stars of the same spectral class (Vrba et al., 1985), this result is not too unexpected.

The corresponding estimate of the bolometric luminosity, assuming $R_* = 2.3\ R_\odot$, $T_{eff} = 6500K$ and hydrostatic equilibrium, is 2.1 $L_\odot$, which is not unreasonable given that a normal F5V star has a luminosity of 2.5 $L_\odot$ (Allen 1973). Thus it would seem that 150pc is a not unreasonable distance estimate for AK Sco.

The non-variable IRAS source 16514 -3648 in the IRAS PSC (Beichman et al., 1985) co-incides well with the 1950 optical co-ordinates of AK Sco ($16^h\ 51^m\ 23^s$, $-36^\circ\ 48'\ 26''$). Therefore the PSC fluxes of this source were included with the optical and IR fluxes of AK Sco obtained on HJD 2447044 when AK Sco was fairly bright (V = 9.0 mag.). The IR excess out to 100μm (the band IV flux is an upper limit, and thus does not necessarily indicate further emission from cooler dust) can be fitted by emission from two blackbody components at 750K and 200K. The fit to these data is shown in Fig. 6.3.9. However, it can be seen that the fit to the near-IR data at this epoch is not as good as was obtained with the 1981 - 1984 SAAO data of Kilkenny et al. (1985), cf. Fig. 6.3.8.

This result would indicate that either the adopted reddening correction at this epoch (September, 1987) is incorrect (i.e. the circumstellar reddening and/or the effective temperature of AK Sco may have changed since 1984), or that there is additional near-IR emission at this epoch which cannot be fitted simply in terms of blackbody emission. Note that the B-V colour (= 0.77) of AK Sco was significantly redder than is usual on this night, and thus the first suggestion, that the reddening correction is incorrect, is not improbable (particularly in view of the fact that the general colour behaviour is attributable to variable circumstellar extinction, Section 6.3.3).

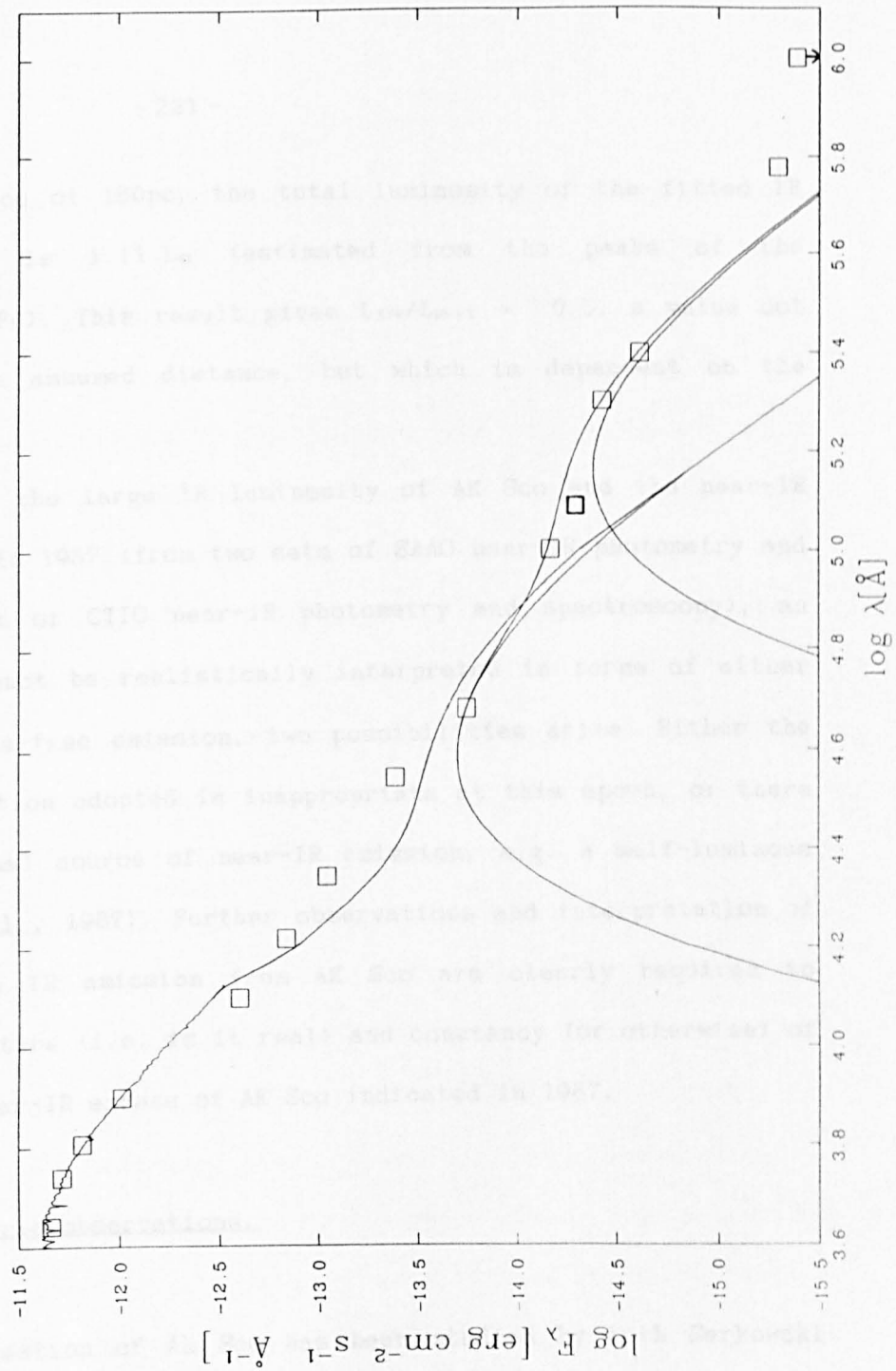

Fig. 6.3.9. Flux distribution of AK Sco on HJD 2447044 with IRAS data included. See also Section 6.3.4.

At a distance of 150pc, the total luminosity of the fitted IR excess emission is 1.11 $L_{\odot}$ (estimated from the peaks of the blackbodies in λF_{λ}). This result gives $L_{IR}/L_{Bol} \simeq 0.5$, a value not dependent on the assumed distance, but which is dependent on the assumed reddening.

In view of the large IR luminosity of AK Sco and the near-IR excess observed in 1987 (from two sets of SAAO near-IR photometry and one combined set of CTIO near-IR photometry and spectroscopy), an excess which cannot be realistically interpreted in terms of either blackbody or free-free emission, two possibilities arise. Either the reddening correction adopted is inappropriate at this epoch, or there is some additional source of near-IR emission, e.g. a self-luminous disc (Adams at al., 1987). Further observations and interpretation of the optical and IR emission from AK Sco are clearly required to ascertain the nature (i.e. is it real) and constancy (or otherwise) of the anomalous near-IR excess of AK Sco indicated in 1987.

6.3.5. Polarimetric observations.

The polarisation of AK Sco has been studied by both Serkowski (1969a) and Bastien (1985). They both found erratic variations in both the polarisation and position angle, and although there is likely to be a strong IS polarisation component (as AK Sco is located close to the galactic plane), variability in the polarisation and the wavelength dependence of the polarisation point towards a significant degree of intrinsic polarisation.

AK Sco was observed on three nights in September, 1987 through a B and an I filter, and the linear polarisation is shown in Fig. 7.3.4c.

Given the errors, there was no significant change observed over a four day period, with (at I), $p \simeq 1.31 \pm 0.05\%$ and $\theta = 125 \pm 5^{\circ}$ (the uncertainty given is the typical observational error).

As with previous studies of the polarisation, the observations indicate limited variability in the polarisation over a timescale of days. This timescale of variation implies that the polarisation must arise close to the star itself. This would be consistent with the fitting of the data in Section 7.3.2.11 with 0.14μm graphite grains, grains which would be expected to radiate strongly in the IR, i.e. not inconsistent with the substantial warm (≃ 750K) dust IR excess of AK Sco (Section 6.3.4).

6.3.6. Summary and Conclusions.

The known tendency of the lightcurve of AK Sco to remain close to maximum light is confirmed. The optical and near-IR colour variability around maximum light indicates that the variations are predominantly ascribable to variable circumstellar extinction, although an extent of intrinsic variability is also indicated, notably when AK Sco is faint.

No strong lines were observed in the IR spectra, although the possibility of a near-IR excess at this epoch as indicated by the near-IR spectral slope, is substantiated by the slight excess in the near-IR photometry observed a few months later at SAAO in September, 1987. Either this excess is real, in which case it is unlikely to be attributable to free-free or thermal dust emission, or it is caused by anomalous circumstellar extinction of the star at this time.

Warm, ≃ 800 - 750K thermal dust emission is observed at each epoch. Also, the high inferred luminosity of the IR emission (beyond

≃ 2μm) and the wavelength dependence of polarisation would both be consistent with the presence of graphite grains in the circumstellar dust shell of AK Sco.

6.4. The "isolated" T Tauri star V4046 Sgr.

6.4.1. Introduction.

V4046 Sgr (HDE 319139, AS 292, HEN 1636, CPD-32°5229, BID 319139) is an untypical InT star in several respects. It is classified as a dKV5e variable (although Heneize (1976) suggests that the star may not be a dwarf), and was proposed by de la Reza et al. (1986) to be an "isolated" InT star (i.e. an InT star not associated with a region of star formation; see Section 2.1.1), the other well-known member of this class being TW Hya (Rucinsky and Krautter 1983).

V4046 Sgr is also unusual amongst InT-type variables in that it is a known binary system and exhibits dramatic flare-like activity (Busko and Torres 1978), more reminiscent of the behaviour of UV Cet (eruptive, flare-like variables) and BY Dra type variables (rotationally modulated variable stars with surface inhomogeneities, e.g. spots, flares).

This behaviour is evident when the levels of variability at V and U are contrasted. The variation at V is only $10.32 < V < 10.39$ mag. (Kholopov et al., 1987), whereas the flux at U can brighten rapidly (≃ minutes), and the range in variation at U is significantly greater, $11.1 < U < 12.4$ mag. (Kholopov et al., 1987).

The variable U-B colour excess (de la Reza et al. 1986); the rotational modulation of the U lightcurve (Busko and Torres 1978) with

a period of 1.7 days (Kholopov et al., 1987); and the rotational modulation of the spectral lines (with a period of 2.45 days; de la Reza et al., 1986); would all indicate that the line and continuum variations are either rotationally modulated, i.e. the Hα emission is inhomogeneously distributed around one of the binary companions, and/or orbitally modulated, i.e. either one or both of the components has an extended Hα envelope, the emission from which is modulated by the orbital motion.

The spectrum of the primary component includes lines characteristic of InT spectra: emission lines of hydrogen, Hα and Hβ; emission lines of high excitation, such as CIV (1548, 1551Å), HeII (1640Å), MgII (2795, 2803Å) and HeI (5876Å); the characteristic strong absorption line of LiI (6707Å).

The orbital elements of the binary system were evaluated by de la Reza et al. (1986), and they estimate the parameters of the primary component to be $M_* \simeq 0.69\ M_\odot$ and $R_* \simeq 1.0\ R_\odot$. The secondary component is estimated to be a K7 dwarf of a similar mass, and these authors suggest that the secondary is probably also a PMS object.

The optical position of V4046 Sgr was carefully measured by de la Reza et al. (1986) and they identified the IRAS source (18108 -3248) (IRAS PSC, Beichman et al., 1985) with the optical position of V4046 Sgr. In view of the IR excess observed by IRAS, they conclude that the inferred circumstellar dust is remnant material from star formation.

6.4.2. The Flux Distribution.

In view of the lack of near-IR observations of V4046 Sgr, optical

(HJD 2446674-5) and near-IR JHK (HJD 2446667) photometry was obtained at SAAO, and narrowband 8 - 12μm photometry and L' and 20μm bolometer data was also obtained at a later date on a service run at UKIRT (on HJD 2446894). Only the L' and 20μm data was reduced however to complement the SAAO IR data, but the UKIRT data (and errors) are tabulated in Table 6.4.1.

Table 6.4.1.

Band (μm)	L'	[8.75]	[9.7]	[10.5]	[11.5]	Q
mag.	6.98	6.04	5.51	5.25	4.78	2.9
error	0.08	0.18	0.11	0.16	0.19	0.24

Although the observations were not simultaneous, as the star is not known to be strongly variable (except at the U band) the fluxes from the optical and near-IR wavelength ranges can be reliably combined. These latest observations confirm the non-variability of the optical emission, other than at U: the star was observed at V = 10.44 mag. (cf. V = 10.40 mag., de la Reza et al., 1986) and B-V = 1.19 (cf. B-V = 1.17, de la Reza et al., 1986) on both HJD 2446674 and 2446675; but the U-B colour was observed to vary from 0.74 to 0.81 (cf. U-B = 0.72, Byrne 1985).

The reddening of V4046 Sgr is not known, but the spectral type is K5. Thus the optical photometry was dereddened until a good fit of a 4400K blackbody (from the temperature calibration of Cohen and Kuhi 1979) to the BV and I points was obtained (the U-B colour is known to be anomalous, and the flux at R will be slightly contaminated by emission from the Hα line). The resultant estimate of the reddening is

$E(B-V) = 0.20$.

When the IR photometry and the IRAS PSC (Beichman et al., 1985) fluxes from the IRAS source 18108 - 3248 are included, there is clearly no IR excess out to $\simeq$ 3.5μm. The fit to the dereddened data (where the UKIRT data has been plotted as circles) is given in Fig. 6.4.1. The IR excess provides clear evidence for the presence of cold dust associated with V4046 Sgr. The dust temperature is estimated to be $\simeq$ 120 K from the fit obtained to the 20μm and the IRAS data. From the fitted components, the ratio L_{IR}/L_{bol} is estimated to be 0.44, i.e. much of the luminosity of V4046 Sgr is emitted in the IR.

Comparing the observed 20μm flux with the IRAS fluxes, a degree of variability in the mid-IR emission would seem likely, and thus future monitoring of the 10 and 20μm fluxes in V4046 Sgr would be welcomed.

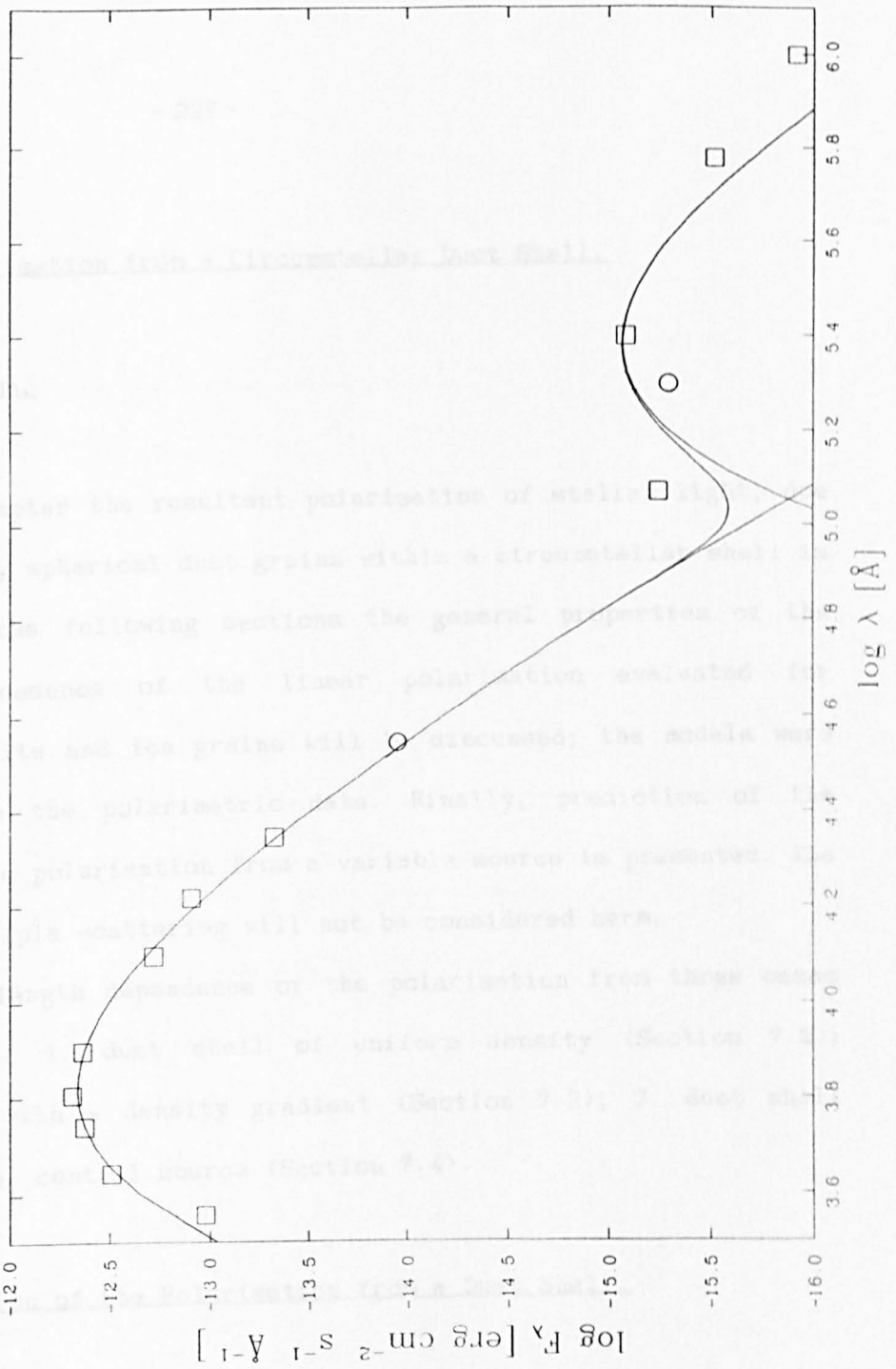

Fig. 6.4.1. Flux distribution of V4046 Sgr from combined SAAO photometry (squares), UKIRT photometry (circles) and IRAS data (squares). See also Section 6.4.2.

Chapter 7. Polarisation from a Circumstellar Dust Shell.

7.1. Introduction.

In this chapter the resultant polarisation of stellar light, due to scattering by spherical dust grains within a circumstellar shell is evaluated. In the following sections the general properties of the wavelength dependence of the linear polarisation evaluated for silicate, graphite and ice grains will be discussed; the models were then fitted to the polarimetric data. Finally, prediction of the behaviour of the polarisation from a variable source is presented. The effects of multiple scattering will not be considered here.

The wavelength dependence of the polarisation from three cases are considered: 1. dust shell of uniform density (Section 7.2); 2. dust shell with a density gradient (Section 7.2); 3. dust shell with a variable, central source (Section 7.4).

7.1.1. Derivation of the Polarisation from a Dust Shell.

The basic method used to determine the polarisation from a uniform, ellipsoidal dust shell is taken from Zellner (1971), and is extended in Sections 7.1.2 and 7.1.3. An outline of the mathematical derivation is now given, and the relevant algorithm is described in Appendix 1.

The co-ordinate system of the dust shell is centred on the star, and the observer is located along the x-axis and the yz plane represents the plane of the sky (see Fig. 7.1.1, shown in the xz

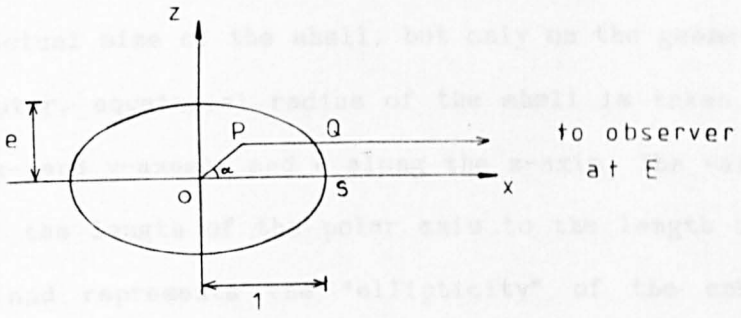

Fig. 7.1.1

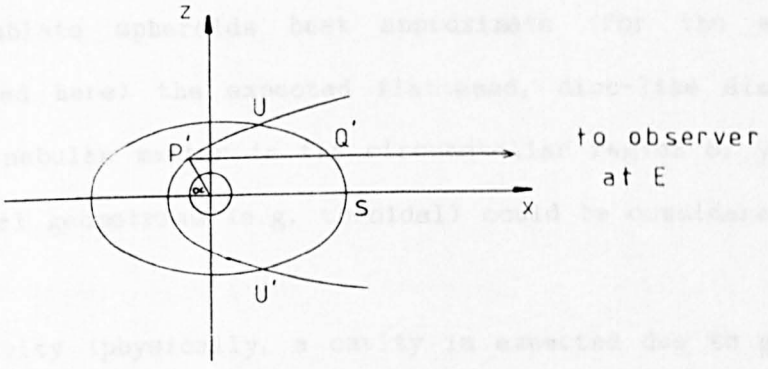

Fig. 7.1.2

Fig. 7.1.1. Co-ordinate system of a homogeneous dust shell centred on a star at O. See text for details.

Fig. 7.1.2. Co-ordinate system of a dust shell with a central cavity, centred on a variable source at the origin. See text for details.

plane). As the polarisation is a ratio of intensities, it is not dependent on the actual size of the shell, but only on the geometrical shape. Thus the outer, equatorial radius of the shell is taken to be unity (along the x- and y-axes), and e along the z-axis. The value of e is the ratio of the length of the polar axis to the length of the equatorial axis, and represents the "ellipticity" of the spheroid (ellipsoid of revolution): $e > 1$ representing a prolate spheroid; $e = 1$ a sphere; $e < 1$ an oblate spheroid (smaller values of e represent increasingly more oblate spheroids). Cases for $e < 1$ only will be considered, as oblate spheroids best approximate (for the shell geometry considered here) the expected flattened, disc-like distribution of dusty, nebular matter in the circumstellar region of young stars. Less general geometries (e.g. toroidal) could be considered in future models.

A central cavity (physically, a cavity is expected due to grain evaporation) can be introduced, but as the absolute dimensions of a circumstellar shell around PMS stars cannot be observationally determined at present, the relative position of the cavity radius is essentially quite arbitrary. For a cavity radius ≤ 0.01 of the normalised, outer radius, the computed polarisation is not significantly affected by the introduction or non-introduction of a cavity for a homogeneous shell (case 1 above; see Sections 7.2.1.3, 7.2.2.3 and 7.2.3.3). Thus the presence of a cavity will not yet be considered: it is only for a shell with a density gradient (case 2 above) that the introduction of a cavity is a mathematical requirement (see Section 7.1.2), and for a variable source (case 3 above) that absolute dimensions enter the calculations (see Section 7.1.3).

The equation of the shell is, in the adopted dimensionless units,

$$x^2 + y^2 + z^2/e^2 = 1 \qquad (7.1).$$

Light of wavelength λ, passing directly to the observer, passes through unit radius OS, and thus through an optical depth $\tau_o = N\pi a^2 Q_{ext}$. N is the density of grains, with all grains within the shell being considered to be identical spherical grains of radius a and refractive index $m = n - i\,k$. For fixed grain parameters, Q_{ext} is thus dependent purely on wavelength.

If B_λ represents the emission from the star, then the observed flux (seen through the dust shell) is

$$F_* = B_\lambda\ \Omega_*\ \exp(-\tau_o) \qquad (7.2)$$

where Ω_* is the observed solid angle of the star, a distance D from the observer.

A light ray passes through an optical depth τ_1, until it is scattered in the x direction by a grain at a point P (x_p, y_p, z_p). Hence the path length OP before scattering is simply, $r = (x_p^2 + y_p^2 + z_p^2)^{1/2}$ and τ_1 is given by $\tau_o r$. The incident flux at P is therefore

$$F_p = B_\lambda\ \Omega'_*\ \exp(-\tau_1) \qquad (7.3)$$

where Ω'_* is the solid angle of the star as seen from P.

The light is scattered through an angle $\alpha = \arccos(x/r)$ towards the observer, into intensity components I_1 and I_2 parallel and perpendicular respectively, to the original direction of propagation. The point at which the scattered ray leaves the cloud is Q (x_q, y_p, z_p). Thus, from the equation of the spheroid, x_q is given by

$$x_q = (1 - y_p^2 - z_p^2/e^2)^{1/2} \qquad (7.4)$$

Hence the scattered intensity components (traversing path length PQ) are viewed through an optical depth of $\tau_2 = \tau_0 (x_q - x_p)$, and therefore the observed intensity components are,

$$I_1^{obs} = I_p (\lambda^2/8\pi^2) i_1 D^{-2} \exp(-\tau_2) \qquad (7.5)$$

and

$$I_2^{obs} = I_p (\lambda^2/8\pi^2) i_2 D^{-2} \exp(-\tau_2) \qquad (7.6)$$

(from van de Hulst 1957), where i_1 and i_2 are the squares of the complex amplitude functions $S_1(\theta)$ and $S_2(\theta)$ respectively, computed from Mie theory (Wickramasinghe 1973), and are dependent on m, a, λ and the scattering angle α.

From (7.2) and (7.3), and realising that $I_p/I_* = F_p/F_* = \Omega'_*/\Omega_* \exp(\tau_0-\tau_1) = D^2/r^2 \exp(\tau_0-\tau_1)$, substituting into (7.5) and (7.6), gives the observed intensity components as,

$$I_1^{obs} = F_* (\lambda^2/8\pi^2) i_1 r^{-2} \exp(\tau_0-\tau_1-\tau_2)$$

$$I_2^{obs} = F_* (\lambda^2/8\pi^2) i_2 r^{-2} \exp(\tau_0-\tau_1-\tau_2) \qquad (7.7).$$

The observed components parallel to the y- and z-axes are respectively, in terms of I_1^{obs} and I_2^{obs},

$$I_y^{obs} = I_1^{obs} \sin^2 \beta + I_2^{obs} \cos^2 \beta,$$

$$I_z^{obs} = I_1^{obs} \cos^2 \beta + I_2^{obs} \sin^2 \beta, \qquad (7.8)$$

where β is the angle of scattering, and is given by $\beta = \arctan(z/y)$. If the intensity components of the scattered ray are now resolved perpendicular and parallel to the equatorial plane of the spheroid, they are respectively (dropping the superscript **obs**),

$$I_r = N \int I_2 \, dV + F_*/2 \qquad \text{(perpendicular)}$$

$$I_1 = N \int I_y \, dV + F_*/2 \qquad \text{(parallel)}$$

The observed polarisation is $p = (I_r - I_1)/(I_r + I_1)$, which, in terms of I_1 and I_2 becomes

$$p = \frac{N \int_V \{ (I_1 \cos^2\beta + I_2 \sin^2\beta) - (I_1 \sin^2\beta + I_2 \cos^2\beta) \} \, dV}{N \int_V \{(I_1 \cos^2\beta + I_2 \sin^2\beta) + (I_1 \sin^2\beta + I_2 \cos^2\beta) \} \, dV + F_*}$$

where the integration is carried out over the volume of the ellipsoid, V.

This equation simplifies to

$$p = \frac{N \int_V (\cos^2\beta - \sin^2\beta)(I_1 - I_2) \, dV}{N \int_V (I_1 + I_2) \, dV + F_*}$$

and from the values of I_1 and I_2 in (7.7), gives,

$$p = \frac{N\exp(\tau_o)F_*(\lambda^2/8\pi^2)\int_V (\cos^2\beta-\sin^2\beta)\ (i_1-i_2)\exp(-\tau_1-\tau_2)\ dV/r^2}{N\exp(\tau_o)F_*(\lambda^2/8\pi^2)\int_V (i_1+i_2)\ \exp(-\tau_1-\tau_2)\ dV/r^2 \ + \ F_*} \qquad (7.9).$$

Now multiplying both upper and lower terms by the term $\pi a^2 Q_{ext}(8\pi^2/\lambda^2)/F_*$, and recognising that $N\pi a^2 Q_{ext}$ is simply the equatorial optical depth, τ_o, the resultant expression for the polarisation, p is

$$p = \frac{\tau_o \exp(\tau_o)\int_V (\cos^2\beta - \sin^2\beta)\ (i_1-i_2)\ \exp(-\tau_1-\tau_2)\ dV/r^2}{\tau_o \exp(\tau_o)\int_V (i_1+i_2)\ \exp(-\tau_1-\tau_2)\ dV/r^2 \ + \ 2\pi\chi^2 Q_{ext}} \qquad (7.10)$$

where $\chi = 2\pi a/\lambda$.

This equation is used as the basis for the computation of the polarisation in this, the general case, and also in the cases considered below (with relevant modifications). The algorithm and a listing of the program which evaluates Eq. (7.10) are given in Appendix 1.

7.1.2. Dust shell with a density gradient.

The number density of grains in the dust shell is now considered to follow a law of the form

$$N(r) = N_o\ (\ r_o\ /\ r\ )^{\gamma} \qquad (7.11)$$

where N_o is the grain number density at the now introduced inner radius of the shell, r_o (not shown in Fig. 7.1.1). For values of $\gamma > 1$, a cutoff radius is mathematically essential (as well as being

expected physically), otherwise the integral in the evaluation of p will not converge.

The equation for the polarisation (7.10), is slightly modified to read

$$p = \frac{\tau_o \exp(\tau_o) \int_V (\cos^2\beta - \sin^2\beta)\ (i_1 - i_2)\ \exp(-\tau_1 - \tau_2)\ r^{-(\gamma+2)}\ dV}{\tau_o \exp(\tau_o) \int_V (i_1 + i_2)\ \exp(-\tau_1 - \tau_2)\ r^{-(\gamma+2)}\ dV + 2\pi\chi^2 Q_{ext}\ W(r)} \qquad (7.12)$$

for $\gamma \neq 1$,

where $W(r) = (1 - r_o^{1-\gamma})/(1-\gamma)$. The expression for $\gamma = 1$ can be obtained by carrying out appropriate integrations.

The corresponding expressions for the optical depths are now

$$\tau_o = N_o\ r_o^{\gamma}\ \pi a^2\ Q_{ext}\ (1 - r_o^{1-\gamma})/(1-\gamma) \qquad (7.13)$$

$$\tau_1 = \tau_o\ (\ r^{1-\gamma} - r_o^{1-\gamma}\ )/(1 - r_o^{1-\gamma}) \qquad (7.14)$$

$$\tau_2 = \frac{\tau_o\ (1 - \gamma)}{(1 - r_o^{1-\gamma})} \int_{\psi_2}^{\psi_1} \frac{y\ \mathrm{cosec}^2\ \psi\ d\psi}{(y^2\ \mathrm{cosec}^2\ \psi + z^2)^{\gamma/2}} \qquad (7.15)$$

where $\psi_1 = \arctan\ (y/x_1)$ and $\psi_2 = \arctan\ (y/x_2)$. These expressions simplify to the values obtained in Section 7.1.1 for $\gamma = 0$ and $r_o = 0$. Again, the expressions when $\gamma = 1$ can be obtained by carrying out appropriate integrations.

7.1.3. Illumination by a variable central source.

The central source will now be taken to be variable (i.e. the emitted flux at a given wavelength is time dependent, $F_*(t)$) and the resultant effect on the polarised light from the shell (taken to have an inner cavity) will be evaluated.

Light which is emitted isotropically from the central source at a given time t (i.e. the emitted flux is $F_*(t)$), then scattered by a grain at P' into the direction of the observer (located at a very distant point E) has a longer path length (OP'E) than light which reaches the observer directly from the star (OE). For a variable source, this increased path length now becomes important as it introduces a phase lag between the scattered and unscattered light rays.

Because of the time delay (taken to be δt) between a scattered and an unscattered light ray, the observer will simultaneously receive unscattered light emitted when the stellar flux was $F_*(t+\delta t)$ and scattered light originally emitted when the stellar flux was $F_*(t)$. Each ray of scattered light with the same time lag δt with respect to the unscattered light, has therefore the same light travel time, or path length (OP'E), and will thus arise from an expanding parabaloid of revolution (UP'U'), where P' is a general point on the parabaloid between U and U'. The 3-D parabaloid is represented by a 2-D parabola in Fig. 7.1.2.

The net effect of this will be that the observer receives scattered light of various intensities, from confocal paraboloids of revolution surrounding the star. Thus the net observed polarisation at a given time will be given by the scattered and unscattered light rays

integrated over the whole volume of the shell.

The variation of light, emitted at a given wavelength, from the central source at time t will be assumed to be of the form

$$F_*(t) = F_m + F_b \sin \omega t \qquad (F_b < F_m) \tag{7.16}$$

where ω is the angular frequency of the variation (thus the period of variation is $2\pi/\omega$). Extension to other forms of lightcurve is straightforward.

Thus the 3-D parabaloid of uniform "illumination" (see Fig. 7.1.2) as seen by the observer is given by (in spherical polar co-ordinates),

$$r = \frac{ct}{1 - \cos \phi \sin \theta} \tag{7.17}$$

where c is the velocity of light, $\theta = \arctan \{ (x^2 + y^2)^{1/2}/z \}$ and $\phi = \arctan (y/x)$.

Thus a grain at P', a distance r from the source, will be "illuminated" by light emitted from the star a time δt earlier, where δt is from (7.17), given by

$$\delta t = r (1 - \cos \phi \sin \theta) / c \tag{7.18}.$$

Thus the "illumination" of a grain as a function of distance from the central source and of time is, from (7.16) and (7.18),

$$F_*(r,t) = F_m + F_b \sin \omega [t - r (1 - \cos\phi \sin\theta)/c] \tag{7.19}.$$

For this case, because a light signal traversing across the dust shell has to be considered, the size of the dust shell will now be a parameter in determining the polarisation. Dimensionless units of distance and time are used in order to simplify the computation. The dimensionless units of distance, $\rho = r/R_o$ and of time, $\Gamma = ct/R_o$ are defined, in terms of c and R_o, the velocity of light and the equatorial radius of the dust shell, respectively.

Hence (7.19) becomes,

$$F_*(\rho,\Gamma) = F_* + F_b \sin \{ \omega R_o/c \, [\Gamma - \rho \, (1 - \cos\phi \sin\theta)] \} \qquad (7.20).$$

Following the algebra as in the general case, the analagous expression of (7.10) for $p(\Gamma)$ is obtained,

$$p(\Gamma) = \frac{\tau_o \exp(\tau_o) \int_V (1+\epsilon \sin\Sigma) \, (\cos^2\beta - \sin^2\beta) \, (i_1 - i_2) \exp(-\tau_1 - \tau_2) \, dV/\rho^2}{\tau_o \exp(\tau_o) \int_V (1 + \epsilon \sin \Sigma) \, (i_1 + i_2) \exp(-\tau_1 - \tau_2) \, dV/\rho^2 + M(\Gamma)} \qquad (7.21)$$

where $M(\Gamma) = 2 \pi \chi^2 Q_{sca} \{1 + \epsilon \sin (\omega \Gamma R_o/c)\}$, $\epsilon = F_b/F_*$, $\Sigma \equiv \Sigma(\Gamma) = (\omega R_o/c) \{\Gamma - \rho \, (1 - \cos\theta \sin\phi)\}$ and the optical depths used depend on the density distribution considered. Eq. (7.21) reduces to (7.10) for the case $\epsilon = 0$.

7.2. Properties of the Wavelength dependence of the Polarisation.

The evaluation of the polarisation given by Eqs. (7.10) and (7.12) allows several free parameters (m, a, N, e, γ), thereby enabling the

variation in the polarisation curve (the wavelength dependence of the polarisation) with (i) shell ellipticity - e, (ii) grain size - a, (iii) radial density-law - γ, to be investigated for different grain types. Three grain types which may exist in the circumstellar environments of young stars are considered here: amorphous silicate grains, graphite grains and ice grains. Unless otherwise indicated, the wavelengths at which the polarisation is evaluated are at the Johnson (1966) optical wavelengths: U = 0.36μm; B = 0.44μm; V = 0.55μm; R = 0.64μm; I = 0.79μm.

The following checks on the performance of the program (which is more fully described in Appendix 1) were initially made:

(a) Computation of Q_{ext} with the subroutine EXCOEFF (see Appendix 1) for various values of the refractive index and $\chi = 2\pi a/\lambda$ were checked against the tabulations of Wickramasinghe (1973), and excellent agreement was found (to within a factor of $\simeq 10^{-3}$). In view of the slightly different values of τ_0 (dependent on Q_{ext}) obtained by Zellner (1971) for identical input parameters, it would seem his calculations of Q_{ext} were slightly erroneous;

(b) The integrals evaluated by the subroutines TOPANS and BOTANS (see Appendix 1), corresponding to the upper and lower integrals in Eq. (7.10), were evaluated using three different NAG library routines, and a variation in the results of $\simeq$ 20% was found between routines used. For some values of χ, the convergence of the integrals is poor and the agreement between routines is reduced for such cases. The most efficient routine to run was the NAG routine D01JAF, which also computed an error estimate, and thus this routine was used in all the subsequent computations. The computational errors in evaluating the integrals using D01JAF for the cases (i) and (ii) above were typically

1 - 2%, and the number of volume elements used in evaluating the integrals were typically 534 - 2200 (cf. ≃ 500, Zellner 1971). However, when considering case (iii), a power-law density distribution, it was found that the integrals could only be computed to an accuracy of ≃ 5 - 10%. Therefore, it is only for case (iii) that the error bars in the figures are greater than the plotted symbol;

(c) Equivalent computations (i.e. with the same input parameters) to those performed by Zellner (1971) were carried out, and broad agreement was found - the form of the wavelength dependence of the polarisation is similar in both sets of calculations. In view of the reliable evaluation of Q_{ext} and the high accuracy of the NAG routine used, the results presented here are considered to be very reliable;

(d) the program was run for e = 1, corresponding to a spherical dust distribution, and the polarisation was determined to be effectively zero.

Finally, for the above case (iii), the values of γ chosen represent those thought most likely to occur in the circumstellar shells of young stars: γ = 1/2 and γ = 3/2, corresponding to free-fall at different distances within the circumstellar region (Chevalier 1983). A value of γ = 2, representative of the equatorial density law in a steady-state accretion disc, was also attempted. However, because of the high inner densities inherent with such a distribution, the integrals were either found not to converge, or where convergence occurred, the computed error was poor (> 50%).

7.2.1. Silicate grains.

The program was run with a refractive index of m = 1.65 - 0.01 i

to approximate the properties of amorphous silicate grains (Mayes 1983; Wickramasinghe 1973). In Sections 7.2.1.1 and 7.2.1.2, the polarisation is evaluated for a number density of grains of 2 cm^{-3}.

7.2.1.1. Variation with shell ellipticity.

Fig. 7.2.1 shows the polarisation from silicate grains (of radius 0.14μm) for dust shells of different values of oblateness, from a nearly spherical shell with e = 0.8, to a flattened spheroid with e = 0.1. In each of the figures, a connecting line is drawn between the computed points. This is intended as an aid to the eye, and does not necessarily imply continuity in the variation between the points.

The wavelength dependence of the polarisation for silicate grains does not change markedly with shell ellipticity. The polarisation generally rises towards shorter wavelengths, with a "plateau" around B, V and R. The form of this "plateau" changes only slightly with ellipticity.

The wavelength dependence of the polarisation (Fig. 7.2.1) can be contrasted with the wavelength dependence of Q_{ext} for 0.14μm silicate grains which is plotted in Fig. 7.2.2a. A comparison is meaningful in the case of silicate grains as $Q_{ext} \simeq Q_{sca}$ for dielectrics ($k \simeq 0$), and both the polarisation and Q_{sca} are dependent upon the scattering properties of the grains. Efficient scattering of light will also give a higher degree of polarisation. For all values of e, both p and Q_{ext} show a rise with decreasing wavelength, but with the form of $Q_{ext}(\lambda)$ steeper than for the polarisation, $p(\lambda)$.

The polarisation at U is found to increase as the shell becomes more flattened (decreasing values of e) to e = 0.1; whereas at the

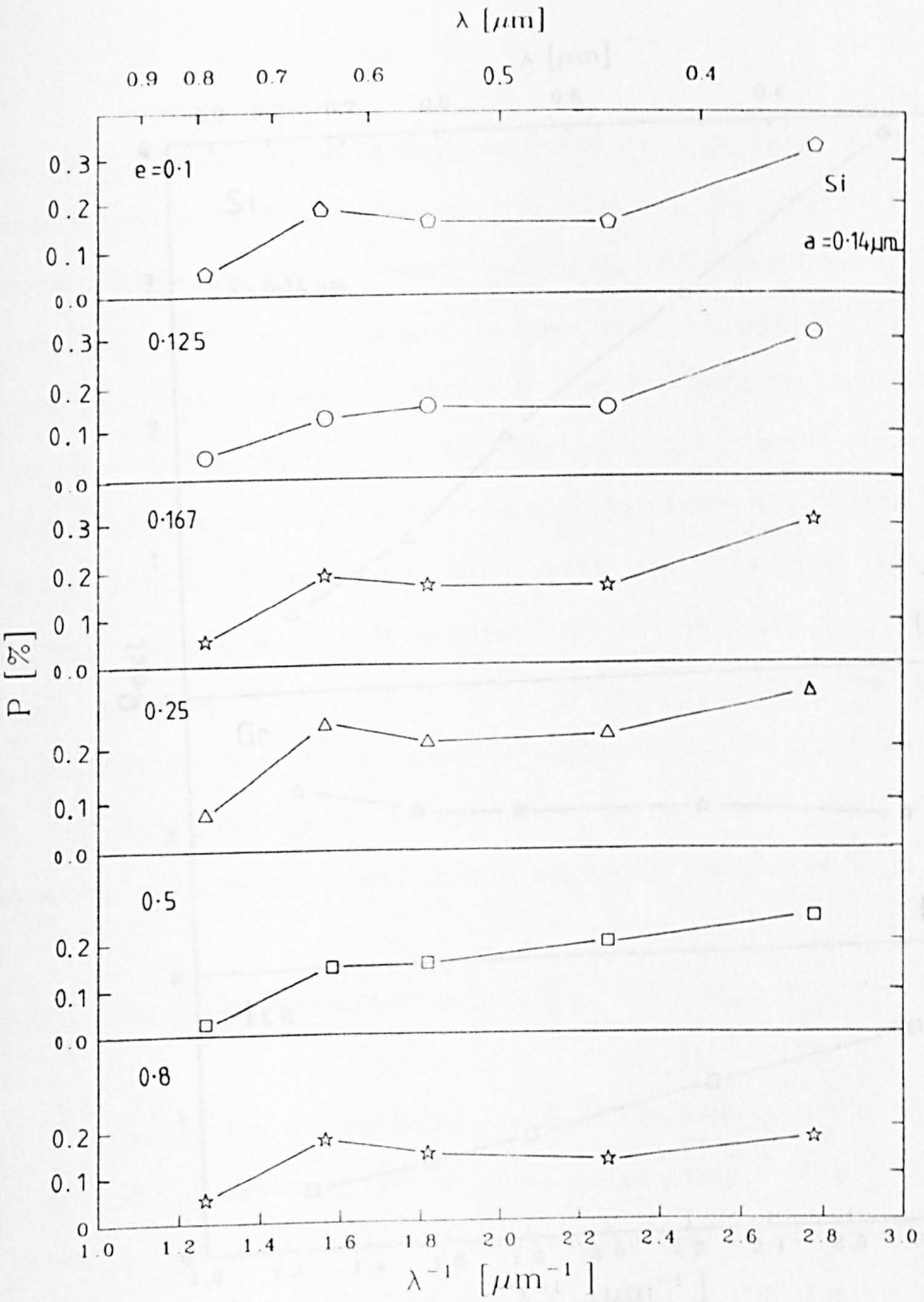

Fig. 7.2.1. The polarisation from silicate grains of radius 0.14μm evaluated at various values of e = 0.1, 0.125, 0.167, 0.25, 0.5 and 0.8. See also Section 7.2.1.1.

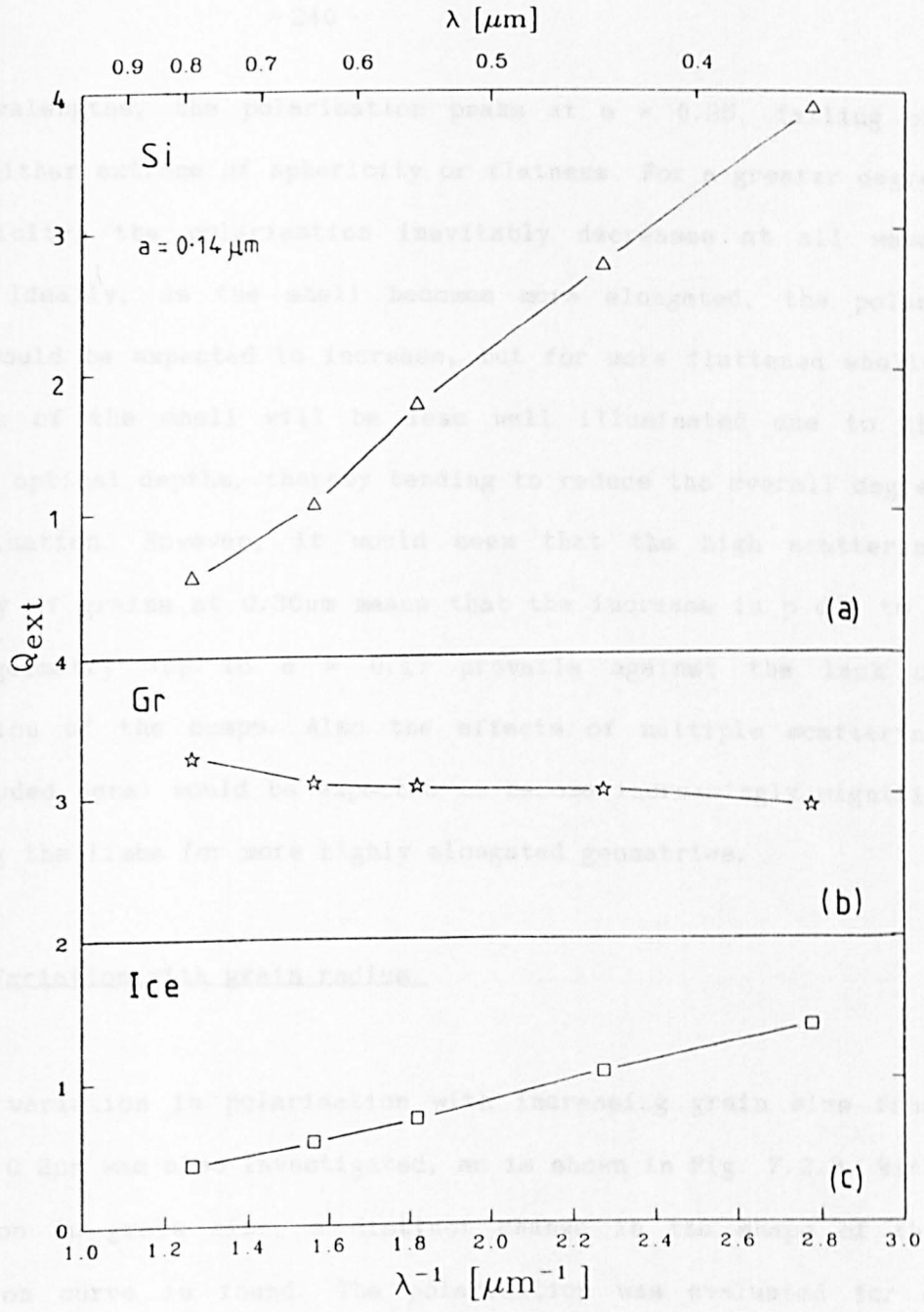

Fig. 7.2.2. $Q_{ext}(\lambda)$ for (a) silicate grains, (b) graphite grains and (c) ice grains.

other wavelengths, the polarisation peaks at e = 0.25, falling off towards either extreme of sphericity or flatness. For a greater degree of sphericity, the polarisation inevitably decreases at all wavelengths. Ideally, as the shell becomes more elongated, the polarisation would be expected to increase, but for more flattened shells, the cusps of the shell will be less well illuminated due to the increased optical depths, thereby tending to reduce the overall degree of polarisation. However, it would seem that the high scattering efficiency of grains at 0.36μm means that the increase in p due to a flatter geometry (up to e = 0.1) prevails against the lack of illumination of the cusps. Also the effects of multiple scattering (not included here) would be expected to become increasingly significant along the limbs for more highly elongated geometries.

7.2.1.2. Variation with grain radius.

The variation in polarisation with increasing grain size from 0.08μm to 0.2μm was also investigated, as is shown in Fig. 7.2.3. With a variation in grain size, a distinct change in the shape of the polarisation curve is found. The polarisation was evaluated for a shell with an ellipticity of e = 0.25.

For small, 0.08μm grains the polarisation is small (p_V = 0.01%), and the wavelength dependence is fairly flat, with a slight increase towards shorter wavelengths. For 0.12 and 0.14μm grains, the polarisation curve still increases towards shorter wavelengths, with the peak occurring at V and R respectively. However, between 0.14 and 0.16μm grains, there is a definite change in the wavelength dependence: the polarisation at V, R and I is still increasing, whilst the

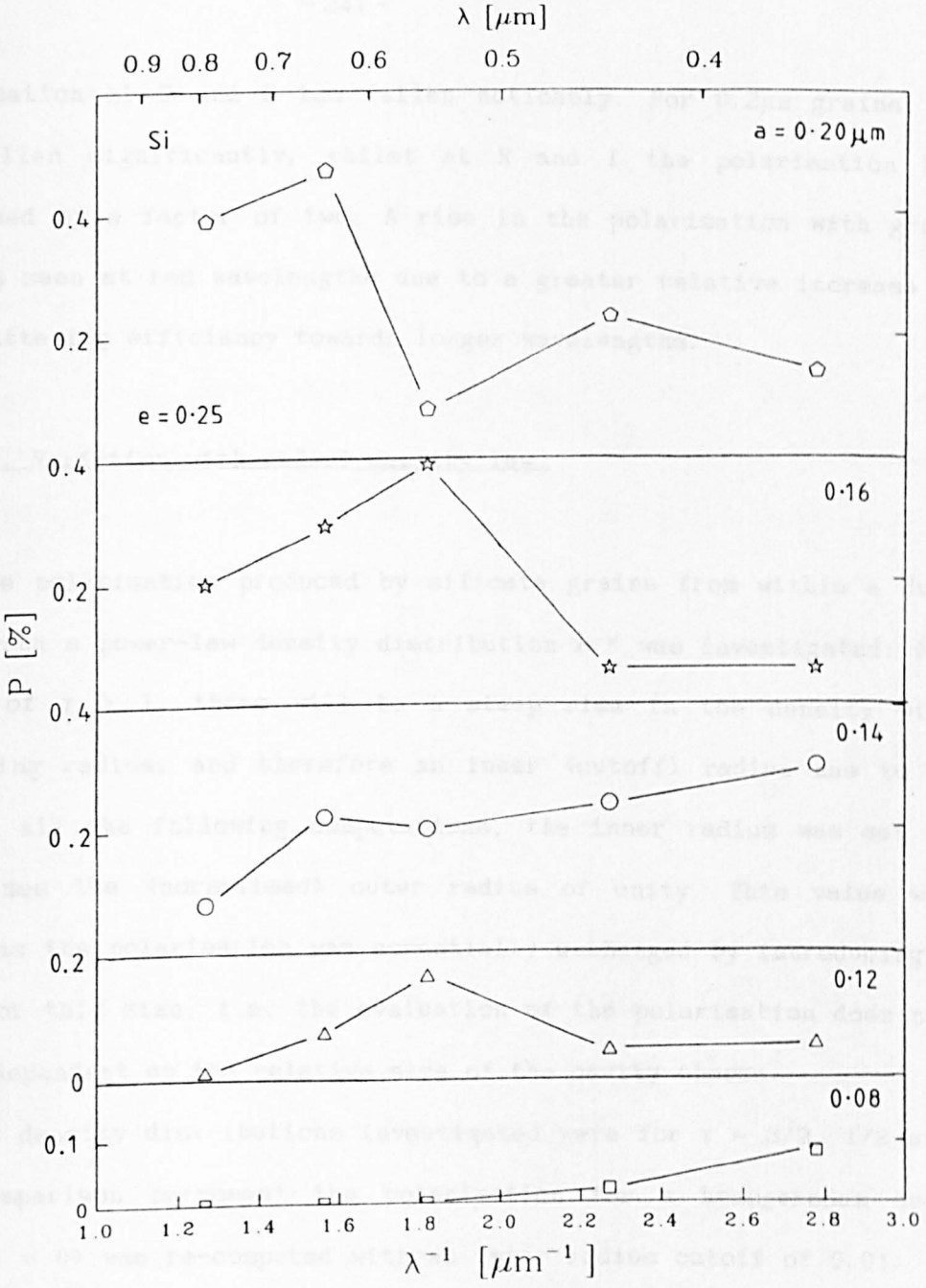

Fig. 7.2.3. The polarisation from silicate grains of radii a = 0.20, 0.16, 0.14, 0.12 and 0.08μm evaluated for e = 0.25. See also Section 7.2.1.2.

polarisation at U and B has fallen noticably. For 0.2μm grains, p_V has fallen significantly, whilst at R and I the polarisation has increased by a factor of two. A rise in the polarisation with grain size is seen at red wavelengths due to a greater relative increase in the scattering efficiency towards longer wavelengths.

7.2.1.3. Variation with radial density law.

The polarisation produced by silicate grains from within a dust shell with a power-law density distribution $r^{-\gamma}$ was investigated. For values of $\gamma > 1$, there will be a steep rise in the density with decreasing radius, and therefore an inner (cutoff) radius has to be set. In all the following computations, the inner radius was set as 0.01 times the (normalised) outer radius of unity. This value was chosen as the polarisation was essentially unchanged by introducing a cavity of this size, i.e. the evaluation of the polarisation does not become dependent on the relative size of the cavity chosen.

The density distributions investigated were for γ = 3/2, 1/2 and (for comparison purposes) the polarisation for a homogeneous dust shell (γ = 0) was re-computed with an inner radius cutoff of 0.01. In this section computations were made for 0.14μm grains and a shell with e = 0.25.

For the γ = 0 density law, the inner density was once again set to 2 cm^{-3}, which at V gives an equatorial optical depth τ_0 = 0.21 (Q_{ext} = 1.76), and a polarisation p_V = 0.15%. The other density distributions were normalised to the same equatorial optical depth at V in order that there will be the same number of (scattering) grains within the volume of the shell. Independent of grain type, the inner densities

required were 11 cm^{-3} (for γ = 1/2) and 110 cm^{-3} (for γ = 3/2).

The computation for γ = 0 and an inner radius of 0.01 matched the computations for no inner radius cutoff within the computed errors (see Fig. 7.2.4). It was found however, for increasing values of γ, the computed errors became significantly greater as the integrals converged less quickly. The errors are shown in Fig. 7.2.4, and were typically $\simeq$ 5% for γ = 1/2 and $\simeq$ 10% for γ = 3/2. At each wavelength, the magnitude of the result TOPANS evaluated (see Appendix 1) is found to increase for increasing values of γ.

For γ = 1/2, the polarisation curve is not significantly different from the γ = 0 case - the polarisation has only increased by 0.05% (except at I, where the increase is less), i.e. within the computed errors. In both cases the optical polarisation increases towards U.

There is a notable change however, for the γ = 3/2 case, where the polarisation increases at long wavelengths, but decreases at short wavelengths. With an increasingly steeper density law, a greater fraction of the scattering particles lie closer to the central source, and thus there is an increasing likelihood that a grain near the inner radius will scatter a light ray. But this effect is countered by the tendency towards a spherically symmetric distribution of grains as the effect of the radial density law dominates. There is no significant change for a γ = 1/2 density law, but the observed rise in the polarisation at long wavelengths and the decrease in the polarisation at short wavelengths when γ is increased to 3/2, is due to the rise in Q_{ext} towards shorter wavelengths, i.e. light at longer wavelengths penetrates deeper into the shell than light at shorter wavelengths, effectively illuminating or "reaching" a greater number of scattering particles. The overall effect of more "efficient" illumination towards

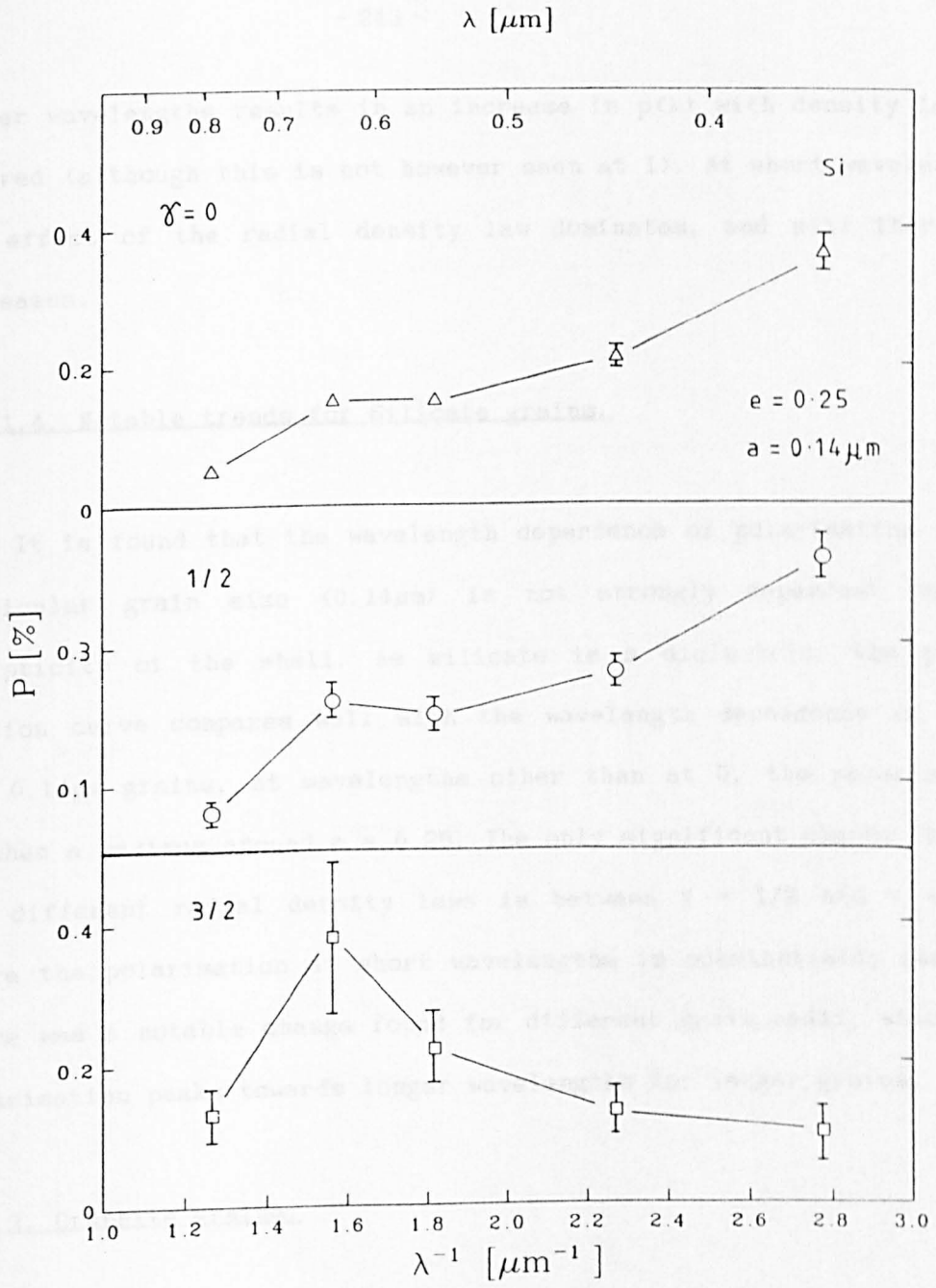

Fig. 7.2.4. The polarisation from silicate grains of radius 0.14μm evaluated for e = 0.25 and for γ = 0, 1/2 and 3/2.
See also Section 7.2.1.3.

longer wavelengths results in an increase in p(λ) with density law in the red (although this is not however seen at I). At short wavelengths the effect of the radial density law dominates, and p(λ) therefore decreases.

7.2.1.4. Notable trends for Silicate grains.

It is found that the wavelength dependence of polarisation for a particular grain size (0.14μm) is not strongly dependent on the ellipticity of the shell. As silicate is a dielectric, the polarisation curve compares well with the wavelength dependence of Q_{ext}. For 0.14μm grains, at wavelengths other than at U, the polarisation reaches a maximum around e = 0.25. The only significant change in p(λ) for different radial density laws is between γ = 1/2 and γ = 3/2, where the polarisation at short wavelengths is substantially reduced. There was a notable change found for different grain radii, where the polarisation peaks towards longer wavelengths for larger grains.

7.2.2. Graphite grains.

The variation of the wavelength dependence of polarisation was investigated for grains with a refractive index of m = 2.54 - 1.405 i to approximate the properties of graphite grains (Mayes 1983).

7.2.2.1. Variation with shell ellipticity.

The variation of the polarisation curve with shell ellipticity was evaluated for 0.14μm grains, and is shown in Fig. 7.2.5. The

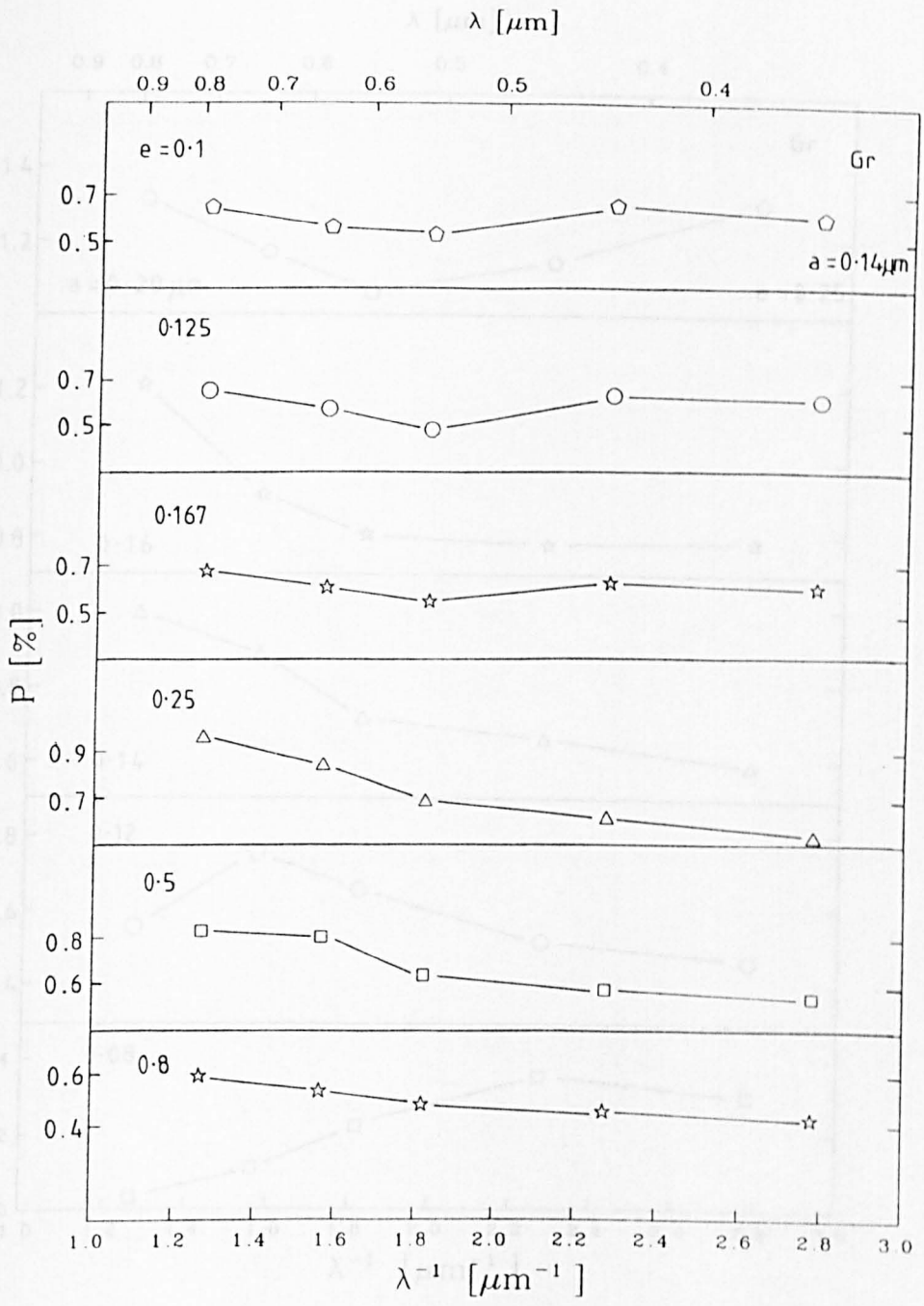

Fig. 7.2.5. The polarisation from graphite grains of radius 0.14μm evaluated at various values of e = 0.1, 0.125, 0.167, 0.25, 0.5 and 0.8. See also Section 7.2.2.1.

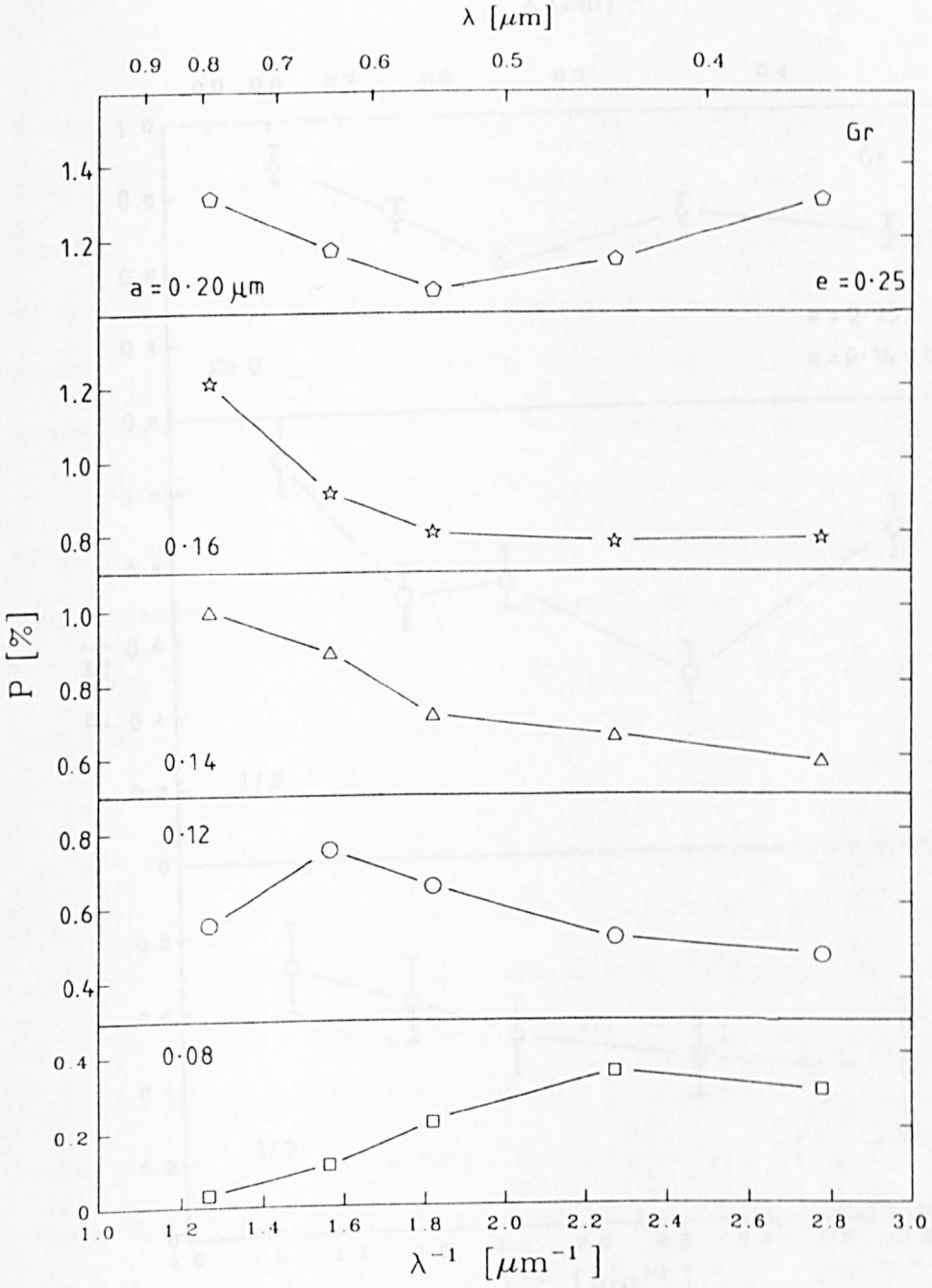

Fig. 7.2.6. The polarisation from graphite grains of radii a = 0.20, 0.16, 0.14, 0.12 and 0.08μm evaluated for e = 0.25.
See also Section 7.2.2.2.

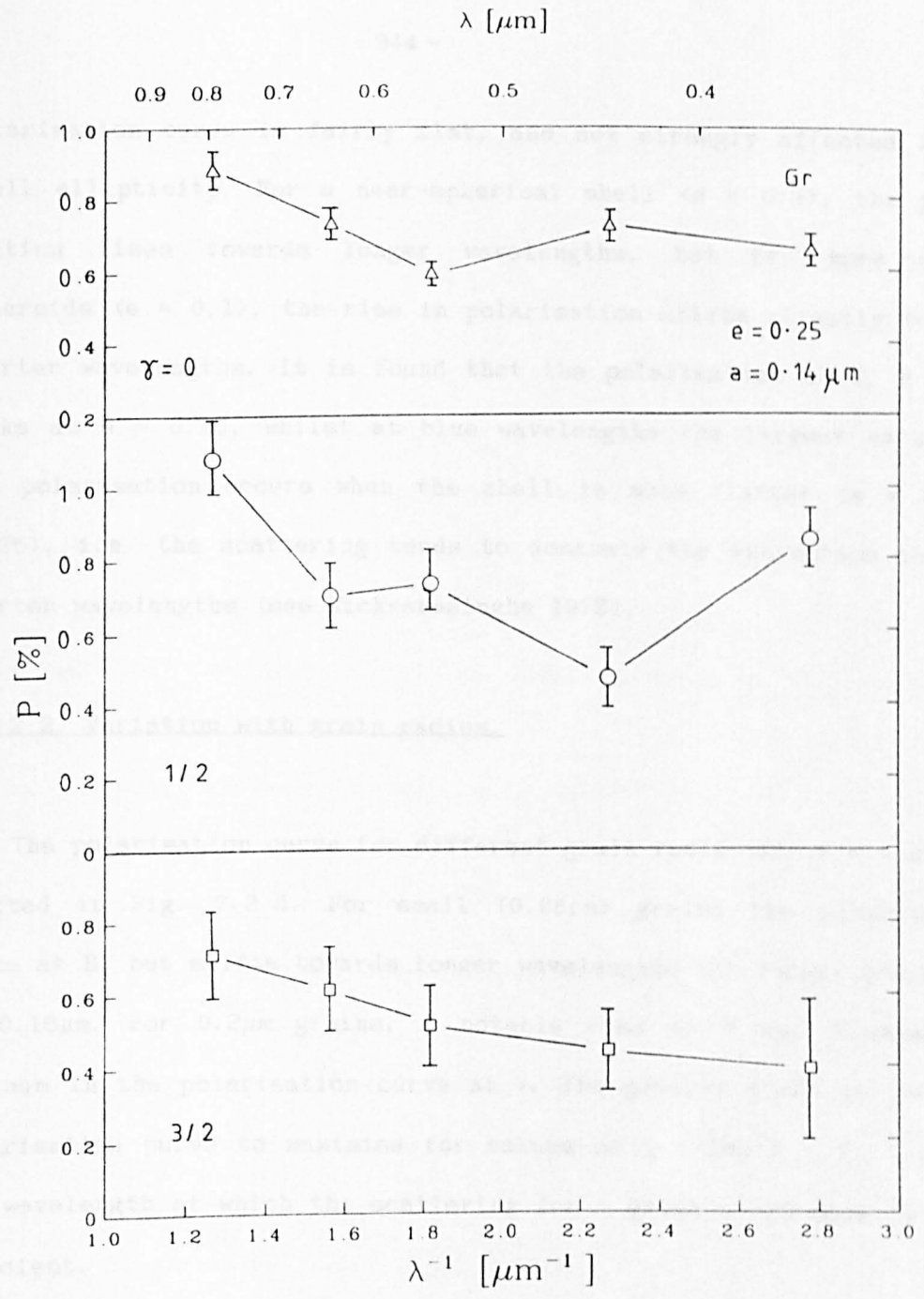

Fig. 7.2.7. The polarisation from graphite grains of radius 0.14μm evaluated for e = 0.25 and for γ = 0, 1/2 and 3/2.
See also Section 7.2.2.3.

polarisation curve is fairly flat, and not strongly affected by the shell ellipticity. For a near-spherical shell (e = 0.8), the polarisation rises towards longer wavelengths, but for more oblate spheroids (e ≈ 0.1), the rise in polarisation shifts slightly towards shorter wavelengths. It is found that the polarisation at V, R and I peaks at e = 0.25, whilst at blue wavelengths the largest value for the polarisation occurs when the shell is much flatter (e = 0.1 - 0.125), i.e. the scattering tends to dominate the extinction towards shorter wavelengths (see Wickramasinghe 1973).

7.2.2.2. Variation with grain radius.

The polarisation curve for different grain radii (for e = 0.25) is plotted in Fig. 7.2.6. For small (0.08μm) grains the polarisation peaks at B, but shifts towards longer wavelengths for larger grains up to 0.16μm. For 0.2μm grains, a notable rise at U and B causes a minimum in the polarisation curve at V. The general trend is for the polarisation curve to maximise for values of $\chi = 2\pi a/\lambda \approx 1$, i.e. at the wavelength at which the scattering for a given grain size is most efficient.

7.2.2.3. Variation with radial density law.

The polarisation was re-computed for a homogeneous shell with e = 0.25 and an inner radius of 0.01. The grain radius was set to a = 0.14μm. The plot of the polarisation produced from shells with power-law density distributions with exponents γ = 1/2 and 3/2 is shown in Fig. 7.2.7. The inner density was normalised to an equatorial optical

depth at V of $\tau_0 = 0.37$. For $\gamma = 0$, this gives $p_V = 0.60\%$ for 0.14μm grains.

Except at V, no significant change within the errors is found for a homogeneous density law when considering the effect of an inner radius cutoff. However, the form of the polarisation curve for $\gamma = 1/2$ is quite different from $\gamma = 0$, the major change being a significant rise (when compared to the errors) in the polarisation at U. The same counter-balancing effects discussed in Section 7.2.1.3 are at work here, but as Q_{ext} now increases with wavelength, the polarisation only increases from $\gamma = 0$ to $\gamma = 1/2$ at short wavelengths. For a steeper density law than $\gamma = 1/2$, the effect of the radial density law dominates, and thus the polarisation is reduced at all wavelengths for $\gamma = 3/2$.

7.2.2.4. Notable trends for Graphite grains.

The parameter which was found to most significantly affect the polarisation curve was grain radius. The peak in the polarisation shifts from blue (0.44μm) wavelengths for small, 0.08μm grains, to longer wavelengths for increasingly larger grains. Unlike silicate grains, the peak in the polarisation curve was also found to be somewhat affected by shell ellipticity, which shifted towards shorter wavelengths as the shell became more oblate.

7.2.3. Ice grains.

The variation of the polarisation curve was investigated for grains with a refractive index of $m = 1.3 - 0.1\,i$, to represent the

properties of ice grains (Wickramasinghe 1973).

7.2.3.1. Variation with shell ellipticity.

The variation with shell ellipticity is plotted in Fig. 7.2.8 for 0.14μm grains with a density of 2 cm^{-3}. When the shell is near-spherical, the polarisation peaks towards blue wavelengths, tending to rise more steeply at blue wavelengths for more oblate shells. It is when the dust shell is most oblate in Fig. 7.2.8, that the wavelength dependence of the polarisation best matches the wavelength dependence of Q_{scm} (as ice is a dielectric $Q_{scm} \simeq Q_{ext}$; see Fig. 7.2.2c) for 0.14μm grains. At each wavelength the polarisation is found to peak for e = 0.25.

7.2.3.2. Variation with grain radius.

The variation of p(λ) with grain radius for a shell with e = 0.25 is plotted in Fig. 7.2.9. For 0.08μm grains the polarisation at red wavelengths is nearly zero, rising gently towards blue wavelengths. For increasingly larger grains, the polarisation curve tends to become flatter, peaking around red wavelengths for 0.2μm grains, although the form of the curve is still fairly flat.

7.2.3.3. Variation with radial density law.

The polarisation for different density distributions within a shell with e = 0.25 was computed for 0.14μm ice grains, and are plotted in Fig. 7.2.10. For γ = 0, with a density of 2 cm^{-3}, the

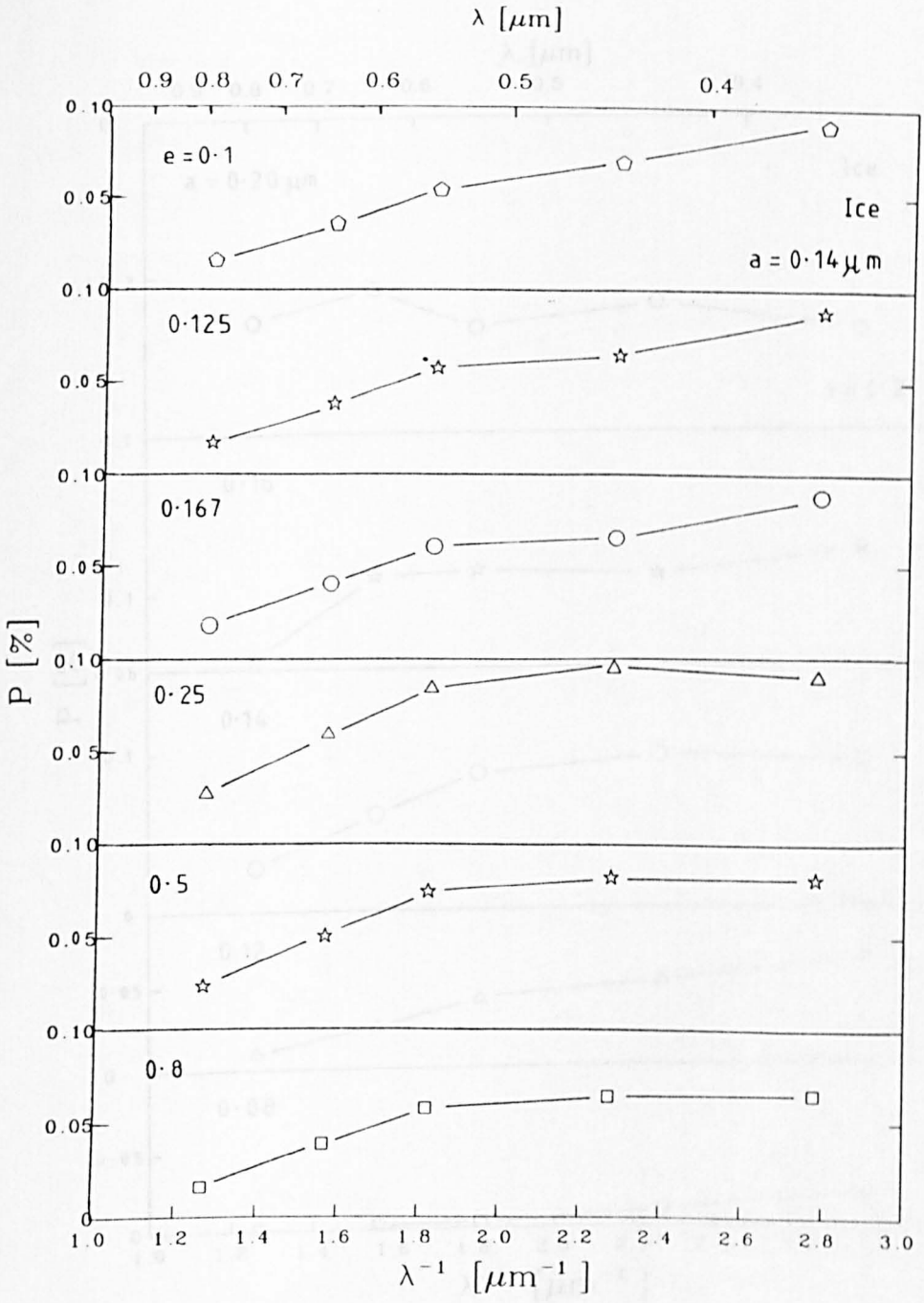

Fig. 7.2.8. The polarisation from ice grains of radius 0.14μm evaluated at various values of e = 0.1, 0.125, 0.167, 0.25, 0.5 and 0.8. See also Section 7.2.3.1.

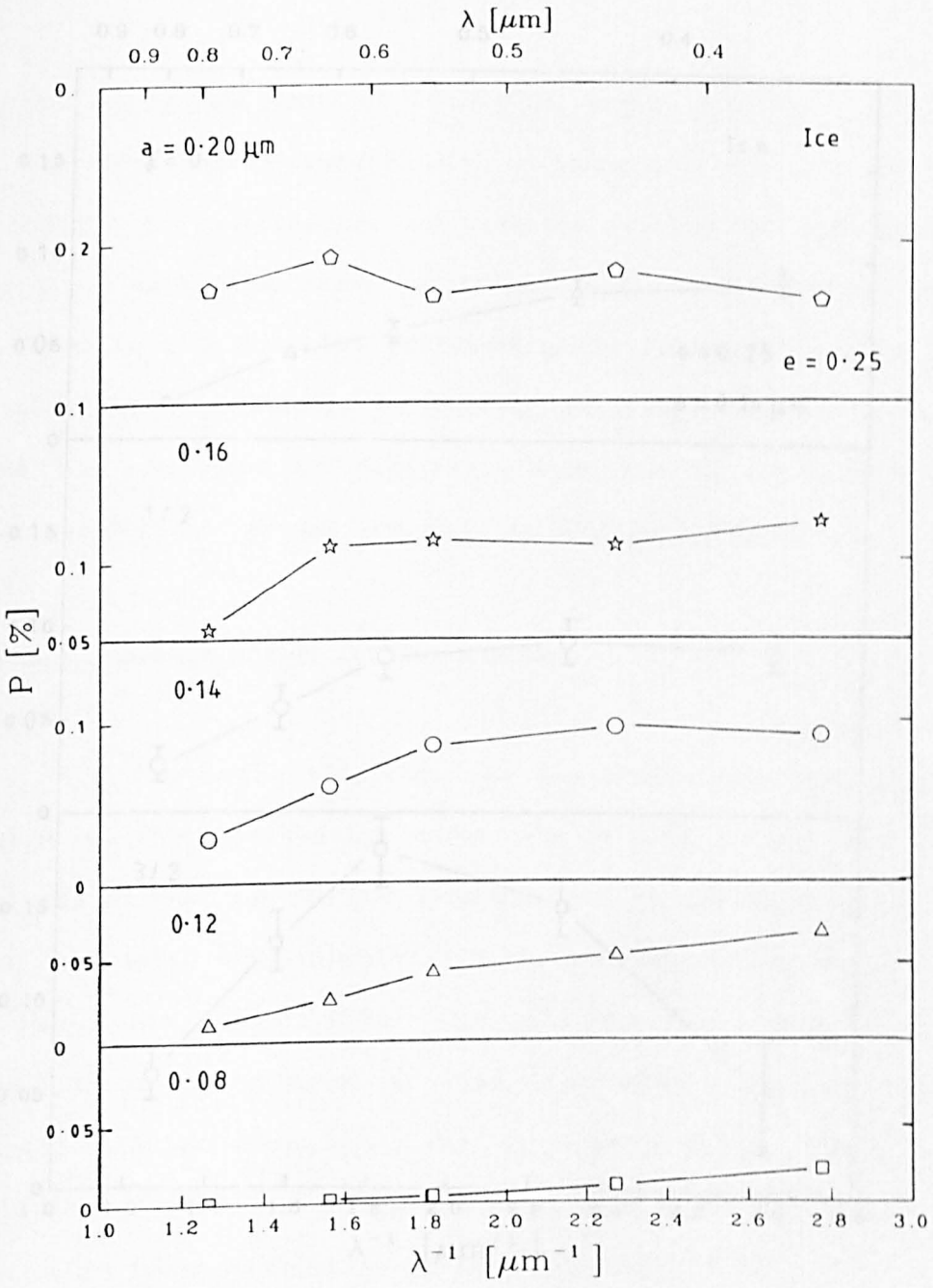

Fig. 7.2.9. The polarisation from ice grains of radii a= 0.20, 0.16, 0.14, 0.12 and 0.08μm evaluated for e= 0.25.
See also Section 7.2.3.2.

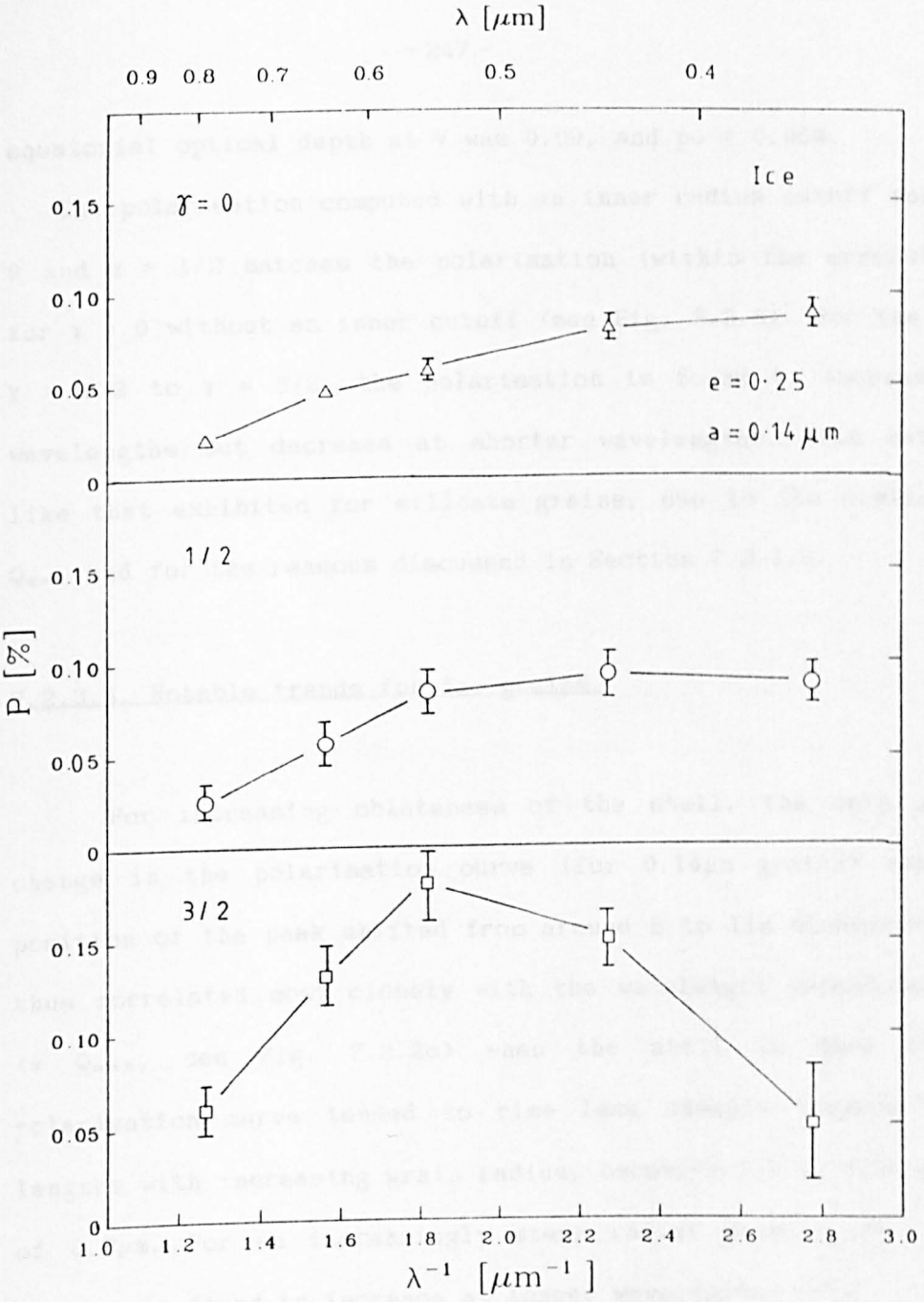

Fig. 7.2.10. The polarisation from ice grains of radius 0.14μm evaluated for e = 0.25 and for γ=0, 1/2 and 3/2.
See also Section 7.2.3.3.

equatorial optical depth at V was 0.09, and p_V = 0.06%.

The polarisation computed with an inner radius cutoff for both γ = 0 and γ = 1/2 matches the polarisation (within the errors) computed for γ = 0 without an inner cutoff (see Fig. 7.2.8). For the change in γ = 1/2 to γ = 3/2, the polarisation is found to increase at long wavelengths but decrease at shorter wavelengths. This behaviour is like that exhibited for silicate grains, due to the similar form of Q_{ext} and for the reasons discussed in Section 7.2.1.3.

7.2.3.4. Notable trends for Ice grains.

For increasing oblateness of the shell, the only significant change in the polarisation curve (for 0.14μm grains) was that the position of the peak shifted from around B to lie bluewards of U, and thus correlated most closely with the wavelength dependence for Q_{sca} ($\simeq Q_{ext}$, see Fig. 7.2.2c) when the shell is more oblate. The polarisation curve tended to rise less steeply towards blue wavelengths with increasing grain radius, becoming fairly flat at a radius of 0.2μm. For an increasingly steep radial density law, the polarisation is found to increase at longer wavelengths only.

7.2.4. Conclusions.

From the above investigation of the variation in polarisation for three different grain types, the following conclusions can be made:

(i) The general trend found in the variation of the polarisation for a shell of increasing oblateness (from e = 0.8 to e = 0.1) is that the polarisation at a particular wavelength increases up to an ellipticity

of 0.25, and then subsequently decreases again as the ellipsoid becomes flatter. This general behaviour of p(e) is explained in Section 7.2.1.1. This variation with shell ellipticity is found to be essentially independent of grain type and also (from additional computations) grain radius. The main exception from this trend, was for the polarisation at U for 0.14μm silicate grains, for which the polarisation was found to increase for decreasing values of e. The general trend that the polarisation tends to peak around e = 0.25 was also found by Zellner (1971). However, the form of the polarisation curve is largely unaffected by changes in the shell geometry;

(ii) As the grain radius is increased, the peak in the polarisation curve tends to shift towards longer wavelengths. This trend is also essentially independent of grain type;

(iii) For 0.14μm dielectric grains, the trend in $p(\lambda)$ and $Q_{ext}(\lambda)$ were found to be similar. This is not unsurprising, as for dielectrics, $Q_{scat} \simeq Q_{ext}$;

(iv) When considering radial power-law density distributions expected within an infalling envelope, the important trend observed is that the polarisation essentially decreases for increasingly steeper density laws, although the polarisation can increase if $Q_{ext}(\lambda)$ is low. The basic trend that $p(\lambda)$ decreases with an increasingly steep density law is essentially because the shell geometry becomes less and less important as the radial density law dominates the effective "size" and geometry of the scattering volume - the scattering particles become more concentrated within a smaller spherical volume, thereby reducing the polarisation. The value of γ at which $p(\lambda)$ begins to decrease is seen to be dependent on the grain properties;

(v) In view of (i), (ii) and (iv) above it is seen that the form of

the polarisation curve $p(\lambda)$ for a given grain type is essentially independent of shell geometry, not strongly affected by radial density law, but is strongly dependent on grain radius.

7.3. Fitting of the Polarimetric data.

7.3.1. Introduction.

Following the analysis of the wavelength dependence for three grain types for different grain sizes and shell geometries, fits to the polarimetric observations at more than one wavelength, carried out at both SAAO and at La Palma (Section 3.5), will now be discussed. To supplement the available data for three stars of particular interest, fits to the polarimetric data of Bastien (1985) were also used: CoD $-33^{\circ}10685$, RY Lup and AK Sco.

The aim of this section is to determine plausible grain types and grain radii for the stars discussed here, parameters which will be of use in subsequent modelling of the polarisation of these stars.

Before the fits are discussed, the reasonableness of the somewhat simple model used here must be considered in view of previous analyses of the polarisation associated with young stars. A similar model to that considered here has been used by several previous authors, e.g. Zellner (1971), Shawl (1975), McCall and Hough (1980). These and other authors indicate that the wavelength dependence of the polarisation is largely independent of the assumed dust geometry (e.g. Hough et al., 1981), the grain properties being the important factor determining the form of $p(\lambda)$. This conclusion is similar to that drawn here (Section 7.2.4).

An important constraint in considering whether the fitted model is plausible is the equatorial optical depth, and thus whether it is reasonable to neglect higher order scatterings. The higher the observed polarisation, then the higher the shell opacity required. Zellner (1971) suggests that multiple scattering effects are negligible up to optical depths of $\simeq 0.5$, whereas Bastien (1987) suggests the limit is $\simeq 0.3$. Thus single scattering models can only realistically reproduce a polarisation of $\simeq 1\%$ at most.

However, Monte Carlo computations which do include the effects of multiple scattering (e.g. Daniel 1980) indicate that the first scatter is essentially that which determines the observed wavelength dependence, subsequent scattering affecting only the magnitude of the polarisation. Thus, where single scattering models have been employed to fit a value of $p(\lambda)$ in excess of $\simeq 0.5 - 1\%$, it has been usual to normalise the polarisation curve to the data, and in light of the conclusion of Daniel (1980), this would seem a not unreasonable approach. Thus the form of the polarisation curve calculated by the single scattering model can be taken to be reliable, and is therefore useful in determining likely grain parameters.

It should be borne in mind therefore, that as the scope of this work is limited to single scattering only, the results presented here are best viewed as pointing the way to more realistic fits. Both from the point of view of neglecting multiple scattering and with the observational limit on the line-of-sight optical depth imposed by the observed extinction, the optical depths required to fit many of the observations are found to be unrealistically large. In individual cases where this is clearly the case, this point will be discussed.

Although attempting fits for radial density laws other than $\gamma = 0$

would have eased the observational constraint on τ_0 somewhat in several cases, it was decided against introducing another degree of freedom because already there are four variable parameters in the model: m, a, N and e; and also there is a reduction in accuracy in computing the polarisation for $\gamma > 0$.

Finally, for stars in which the observed polarisation is greater than $\simeq$ 4% (e.g. BF Ori), fits with the model employed here were not attempted as the circumstellar optical depth must obviously be high in such instances. It is noted however that as $p(\lambda)$ for BF Ori tends to increase with decreasing wavelength, scattering by small ($\lesssim$ 0.1μm) grains would seem to be required. Also, as is seen in RY Tau, the wavelength dependence of the polarisation (and the degree of polarisation) is clearly too variable to justify a fit using a single model. For example, Bastien and Landstreet (1979) find that silicate grains of $a \simeq 0.06\mu m$ give a good fit to one dataset, but that $a \gtrsim 0.3\mu m$ silicate grains are required to fit another dataset of RY Tau. Clearly, in the case of RY Tau, different grain populations give rise to the polarisation at different epochs.

7.3.2. Model fits to the Observations.

The stars for which fits have been made will now be discussed. Unless otherwise stated, the stars discussed are InT stars. All the stars considered have IR excesses and are significantly reddened, so the presence of a circumstellar dust shell for each star is not implausible.

Also, as was discussed in Section 2.2.5 and 2.3.5, recent studies of the polarisation curve $p(\lambda)$ observed in the majority of both InT

and Ina stars (and this includes all the stars discussed here), such as Bastien and Landstreet (1979), Bastien (1981), and Hough et al. (1981), conclude that the observed wavelength dependence is best explained by scattering by dust particles. As many of the stars observed exhibit some kind of silicate feature, fits using silicate grains were always looked for, but in many instances ice or graphite grains (the presence of which cannot always be precluded) fit the data better, and in each case, the best fit to the data will be shown. Discussion will be made in each individual case, but it is clear that in the instances where graphite gives the best fit, that scattering by dielectric (i.e. silicate or ice) grains almost certainly cannot account for the observed wavelength dependence.

In the figures, lines are drawn as a guide to the eye between each observational point (circle), and the error for each observational point is indicated by a vertical bar; the fitted points are represented by a filled symbol, and where the computed error is greater than the size of the symbol, it is represented by two vertical arrows.

7.3.2.1. FM Tau.

The polarisation of FM Tau was observed on two dates, HJD 2447160 (Fig. 7.3.1b) and HJD 2447162 (Fig. 7.3.1a), and was found to be variable. The observed steep rise in the polarisation towards the UV (particularly seen in Fig. 7.3.1b) clearly indicates that the scattering is by dielectric grains. The initial fit was based on the second observation (Fig. 7.3.1a), as the polarisation at all five Johnson bands was observed, and also the observational uncertainty was lower. On HJD 2447162 the polarisation peaks at U and B; thus fits

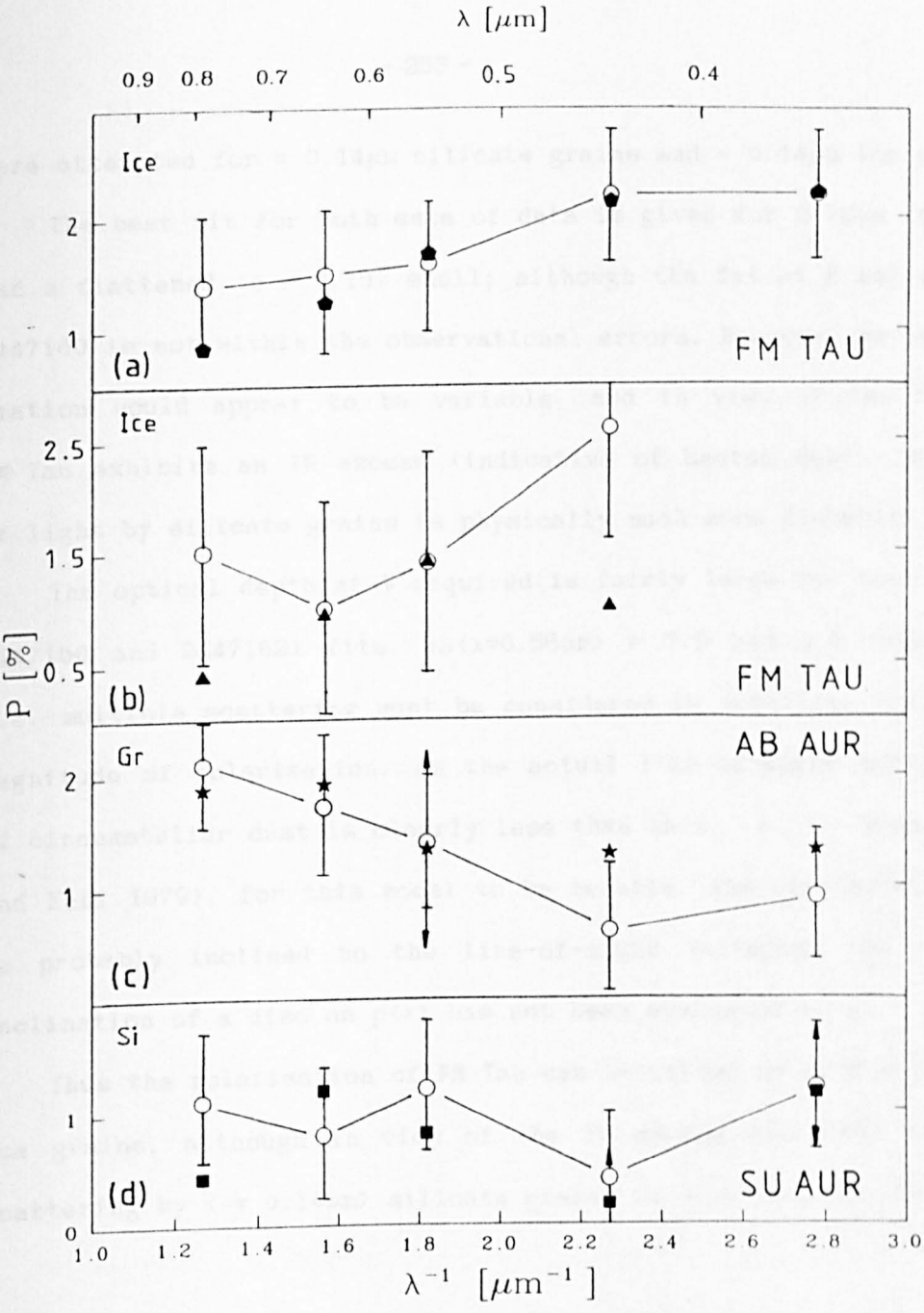

Fig. 7.3.1. Model fits to the observations of (a) FM Tau on HJD 2447162, (b) FM Tau on HJD 2447160, (c) AB Aur on HJD 2447163 and (d) SU Aur on HJD 2447161.
See also Sections 7.3.2.1, 7.3.2.2 and 7.3.2.3.

were attempted for ≃ 0.14μm silicate grains and ≃ 0.14μm ice grains.

The best fit for both sets of data is given for 0.13μm ice grains and a flattened (e = 0.15) shell; although the fit at B and I for HJD 2447160 is not within the observational errors. However, as the polarisation would appear to be variable, and in view of the fact that FM Tau exhibits an IR excess (indicative of heated dust), scattering of light by silicate grains is physically much more plausible.

The optical depth at V required is fairly large for both the (HJD 2447160 and 2447162) fits, $\tau_{\odot}(\lambda=0.55\mu m)$ = 3.5 and 2.8 respectively, i.e. multiple scattering must be considered in modelling the observed magnitude of polarisation. As the actual line-of-sight optical depth of circumstellar dust is clearly less than this, ($A_V \simeq 0.9$ mag.; Cohen and Kuhi 1979), for this model to be tenable, the circumstellar shell is probably inclined to the line-of-sight (although the effect of inclination of a disc on p(λ) has not been evaluated here).

Thus the polarisation of FM Tau can be fitted by both silicate and ice grains, although in view of the IR excess exhibited by FM Tau, scattering by (≃ 0.14μm) silicate grains is much more likely.

7.3.2.2. AB Aur.

Although Cohen and Kuhi (1979) indicate that the near-IR excess (out to 8μm) of this star can be fitted by a free-free continuum alone, recent near- and far-IR photometry (Rydgren and Zak 1987) indicate the presence of emission from cold dust. Indeed, AB Aur exhibits a 10μm silicate emission feature, indicating the presence of silicate grains at ≃ 500K (Cohen and Whitteborn 1985).

The polarisation of AB Aur (an Ina star) was observed on HJD

2447163. The polarisation of AB Aur increases towards longer wavelengths, thus the polarisation is unlikely to be due to dielectric grains, and a fit using graphite grains was looked for. A good fit to the data was found for 0.16μm graphite grains with shell parameters of e = 0.25 and $\tau_0(\lambda=0.55\mu m)$ = 0.94 (see Fig. 7.3.1c). The fit is best at longer wavelengths (although note the high uncertainty in the computation of p_v indicated by the vertical arrows).

Although the scattering of light within both a gaseous stellar envelope (Catala et al., 1984) and by silicate grains in a dust shell (Cohen and Whitteborn 1985) cannot be ruled out, the wavelength dependence of polarisation can be best interpreted in terms of scattering by graphite grains within an optically thin dust shell.

7.3.2.3. SU Aur.

The 10μm silicate feature has been observed in emission in SU Aur, suggesting the presence of silicate grains at ≈ 415K (Cohen and Whitteborn 1985). Hough et al. (1981) observed that the polarisation in the near-IR, $p(\lambda=2.2\mu m) \approx 0.94\%$, is substantially greater than that observed in the optical, $p(\lambda=0.55\mu m) \approx 0.25\%$. Therefore, Hough et al. (1981) suggest that the polarisation arises from a circumstellar dust shell by scattering from both medium-sized (≈ 0.1μm) and small (≪ 0.1μm) silicate grains, with a lower number density of small-sized grains to account for the low optical polarisation.

Hough et al. (1981) also observed a 90° reversal in position angle between the optical and the IR polarisation. Note that such a 90° reversal is characteristic of scattering by dielectric grains (Daniel 1980). Therefore the interpretation forwarded by Bastien (1987), that

the optical and IR polarisation arises in a mutually orthogonal dust distribution (i.e. a disc and bipolar lobes) does not seem necessary. Indeed, in view of the fact that the optical position angle of SU Aur is variable (by ≃ 25°, Bastien 1985), the dust distribution cannot be symmetrical. Although the dust distribution is unlikely to be symmetric, the limited variation usually exhibited in the degree of polarisation and the more significant variation in position angle, does suggest that the dust is confined to a narrow solid angle, e.g. a disc (see also Section 2.2.5).

The polarisation was observed on HJD 2447161, and is greater than the level of optical polarisation usually observed of ≃ 0.2% (Hough et al., 1981; Bastien 1982; Schulte-Ladbeck 1983). This would indicate that the dust giving rise to the polarisation is not necessarily confined to a circumstellar disc (see above). In fitting the data, several dielectric grain sizes were tried, and the best fit (see Fig. 7.3.1d) was given with 0.14μm silicate grains with shell parameters e = 0.125 (i.e. a flattened, disc-like ellipsoid) and $\tau_0(\lambda=0.55\mu m)$ = 4.39 - but in view of previous observations, the optical depth of dust which scatters the optical light is typically substantially lower than this. The fit to the polarisation curve would thus indicate that a significant number of medium-sized grains were contributing to the optical polarisation at this time to a greater extent than is perhaps usual.

Therefore for SU Aur, the case for scattering by silicate grains is very strong. Single scattering models should be able to adequately model the usual level of optical polarisation that is observed. The usual low level of polarisation and the flattened shell geometry favoured in the fit obtained here suggests that much of the dust lies

in a disc, although the polarisation "flare" observed indicates the presence of a substantial fraction of medium-sized grains which may not be confined to a disc.

7.3.2.4. RW Aur.

The observed 10μm silicate emission feature indicates the presence of silicate dust at ≈ 415K around RW Aur (Cohen and Whitteborn 1985). The polarisation and the wavelength dependence are both time-variable (Schulte-Ladbeck 1983; Bastien 1985). However, two analyses of the observed polarisation lead to contradictory conclusions on the likely dust shell geometry: Bastien (1985) notes that rotation of the position angle > 25° occurs, thus indicating that there is no fixed axis of symmetry; whereas the limited variation in the position angle observed by Schulte-Ladbeck (1983) led her to conclude that a fixed-axis of symmetry is indicated. The former conclusion (based on more observations), would seem the more tenable.

The polarisation was observed on HJD 2447161 and 2447163. Again, several models were attempted, with the best fit to both observations being given by 0.16μm ice grains for a shell with e = 0.25. For the fit to the HJD 2447161 observations (Fig. 7.3.2a), $\tau_o(\lambda=0.55\mu m)$ = 1.75; and for HJD 2447163 (Fig. 7.3.2b), $\tau_o(\lambda=0.55\mu m)$ = 3.64. A reasonable fit with 0.16μm silicate grains can also be made, although the polarisation at U is under-estimated by a factor of 3.

However, in view of the IR excess (precluding scattering by ice grains), the 10μm silicate feature and the time variation in the wavelength dependence of the polarisation, it is suggested that a fit with a bimodal silicate grain distribution, with ≈ 0.16μm and small

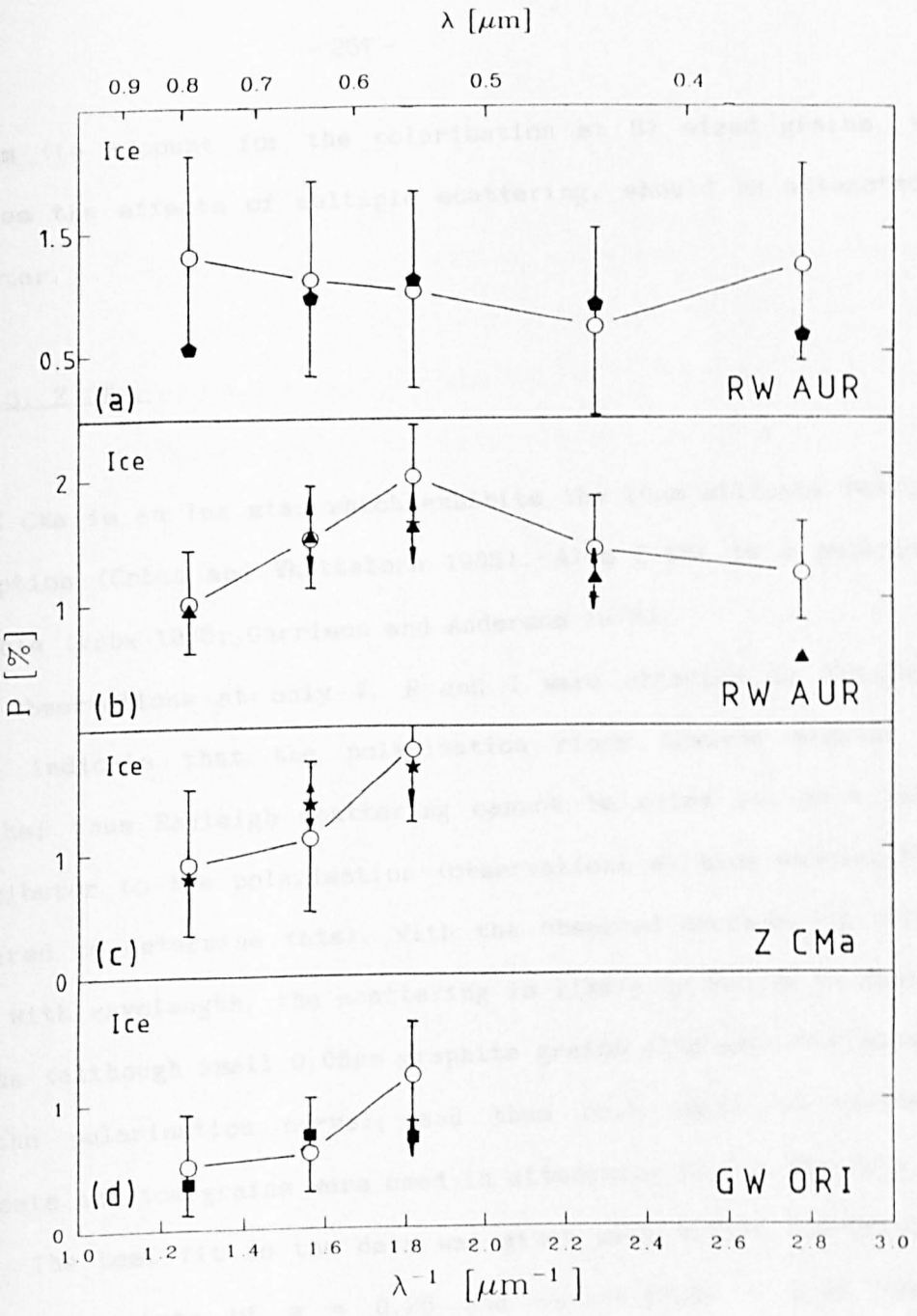

Fig. 7.3.2. Model fits to the observations of (a) RW Aur on HJD 2447161, (b) RW Aur on HJD 2447163, (c) Z CMa on HJD 2447166 and (d) GW Ori on HJD 2447164.
See also Sections 7.3.2.4, 7.3.2.5 and 7.3.2.6.

$\leq$ 0.1μm (to account for the polarisation at U) sized grains, which includes the effects of multiple scattering, should be attempted for this star.

7.3.2.5. Z CMa.

Z CMa is an Ina star which exhibits the 10μm silicate feature in absorption (Cohen and Whitteborn 1985). Also Z CMa is a polarimetric variable (Vrba 1975; Garrison and Anderson 1978).

Observations at only V, R and I were obtained on HJD 2447166, which indicate that the polarisation rises towards shorter wavelengths; thus Rayleigh scattering cannot be ruled out as a possible contributor to the polarisation (observations at blue wavelengths are required to determine this). With the observed decrease in polarisation with wavelength, the scattering is likely to be due to dielectric grains (although small 0.08μm graphite grains also give a similar form of the polarisation curve), and thus both small to medium-sized silicate and ice grains were used in attempting to fit the data.

The best fit to the data was given with 0.15μm ice grains with shell parameters of e = 0.25 and $\tau_o(\lambda=0.55\mu m)$ = 3.46 (see Fig. 7.3.2c). However, in view of the presence of the 10μm silicate absorption feature and the IR excess, the fit obtained with 0.12μm silicate grains would seem physically much more plausible. The 10μm absorption feature and the large extinction of Z CMa ($A_V \propto$ 2.82 mag.; Cohen and Kuhi 1979) point towards a significant line-of-sight opacity. Thus the effects of multiple scattering are very important if the observed polarisation is to be reliably fitted.

7.3.2.6. GW Ori.

GW Ori exhibits the 10μm silicate feature in emission, which indicates the presence of silicate dust at ≈ 375K (Cohen and Whitteborn 1985). GW Ori is a suspected polarimetric variable (Bastien 1985), and the IR excess of this star is attributable to both free-free emission and dust (Cohen and Kuhi 1979).

As for Z CMa, only three observations at V, R and I were made, on HJD 2447164, and a similar rise towards shorter wavelengths was observed. Again, this leaves open the possibility of a contribution from Rayleigh scattering in a stellar envelope.

The best fit was obtained with 0.14μm ice grains with shell parameters of e = 0.25 and $\tau_0(\lambda=0.55\mu m)$ = 1.53 (see Fig. 7.3.2d), although the fit at V lies just within the errors. A less accurate, but physically more plausible fit (in view of the IR excess) was obtained for 0.16μm silicate grains, although as GW Ori is not known to be rapidly variable, a small contribution to the polarisation by ice grains cannot be totally ruled out. In both cases the optical depth required means that the effects of multiple scattering should be included in accurately fitting the data.

7.3.2.7. RU Lup.

RU Lup exhibits only small changes in polarisation (Bastien 1985). However, the IR excess consists of emission likely arising from both a stellar envelope and a circumstellar dust shell (e.g. Gahm et al., 1975; Section 5.2.3). As far as the author is aware, no IR spectral features due to circumstellar grains have been looked for in RU Lup.

The observation on HJD 2446994 at only B and I indicates that the polarisation decreases with increasing wavelength (as was observed at three wavelengths by Bastien 1985). Observations at more wavelengths are clearly required.

The rise towards shorter wavelengths is not steep enough to be explained by Rayleigh scattering (which can be expected to occur within the hot stellar envelope). The observed wavelength dependence suggests that ice or silicate grains may be responsible for a significant component of the polarisation observed for this star.

With the available polarimetric data (obtained here and by Bastien 1985), no tight constraints on a plausible dust model for RU Lup can yet be placed. A model with 0.18μm ice grains (e = 0.25 and $\tau_o(\lambda=0.55\mu m) = 1.75$), shown in Fig. 7.3.3a, gives the best fit to the data. In view of the limited variability of the polarisation, the possibility of ice grains contributing to the observed polarisation would seem reasonable, although RU Lup does exhibit an IR excess attributable to warm dust (Section 5.2.3), thus ruling against scattering by ice grains. Dependent on the actual relative contributions from scattering within a stellar envelope (Section 5.2.2) and within a dust shell, multiple scattering effects in the dust shell may not be important.

7.3.2.8. V856 Sco.

V856 Sco is an Ina star which has an IR excess attributable to thermal emission from dust (Section 6.1.4). The polarisation from this star is highly variable (see Section 6.1.5) and is therefore largely intrinsic to the stellar environment.

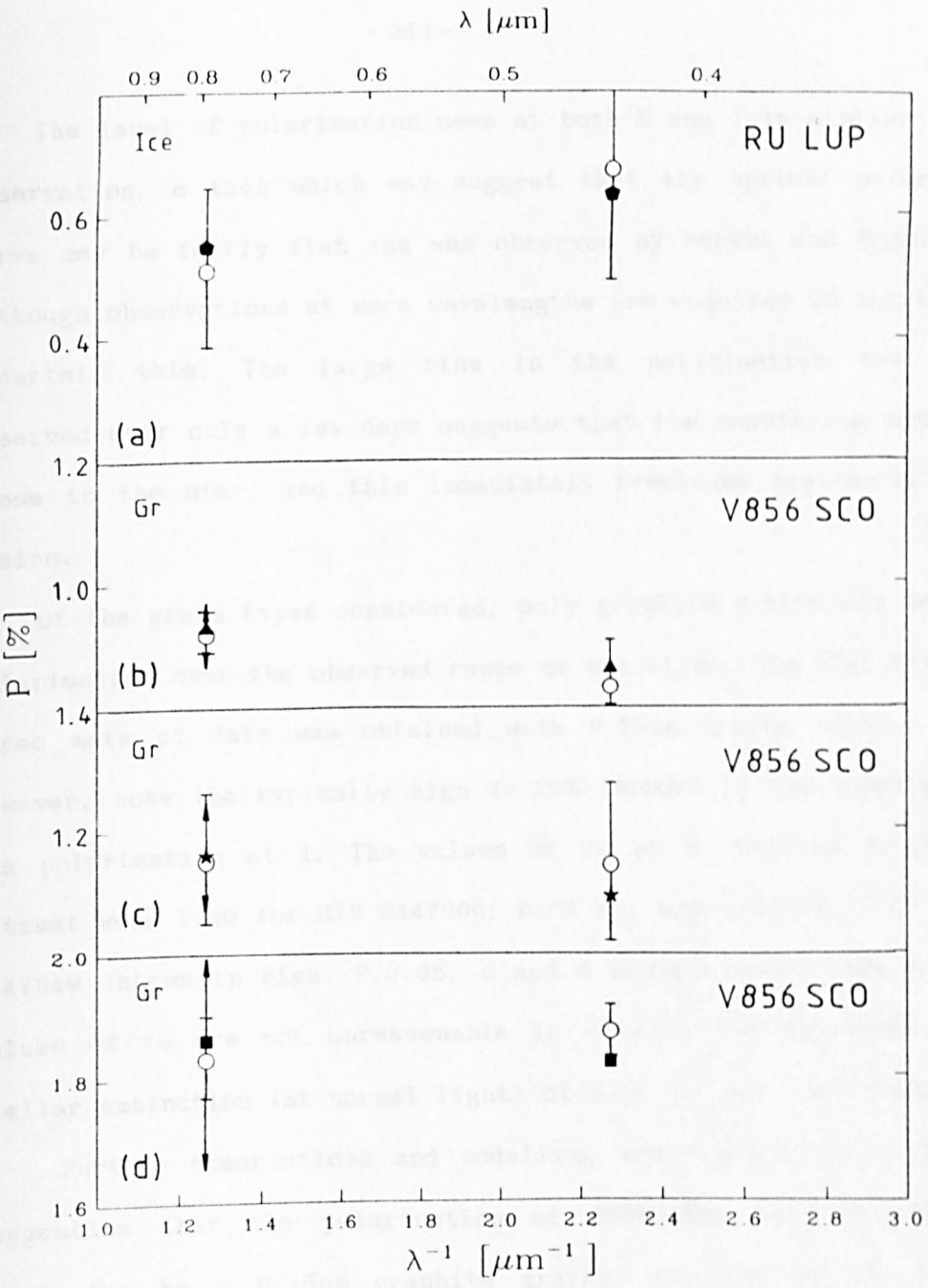

Fig. 7.3.3. Model fits to the observations of (a) RU Lup on HJD 2446994, (b) V856 Sco on HJD 2447000, (c) V856 Sco on HJD 2447044 and (d) V856 Sco on HJD 2447049.
See also Sections 7.3.2.7 and 7.3.2.8.

The level of polarisation seen at both B and I is similar in each observation, a fact which may suggest that the optical polarisation curve may be fairly flat (as was observed by Bessel and Eggen 1972), although observations at more wavelengths are required to convincingly ascertain this. The large rise in the polarisation (by $\propto$ 0.8%) observed over only a few days suggests that the scattering must occur close to the star, and this immediately precludes scattering by ice grains.

Of the grain types considered, only graphite grains can match the polarisation over the observed range of variation. The best fit to the three sets of data was obtained with 0.15μm grains with e = 0.15. However, note the typically high ($\simeq$ 10%) errors in the computation of the polarisation at I. The values of τ_0 at B required to fit each dataset were 0.50 for HJD 2447000; 0.59 for HJD 2447044; 1.25 for HJD 2447049 (shown in Figs. 7.3.3b, c and d respectively). The first two values of τ_0 are not unreasonable in view of the estimated circumstellar extinction (at normal light) of A_V = 0.7 mag. (Section 6.1.4).

Further observations and modelling are required to confirm the suggestion that the polarisation of V856 Sco is attributable to scattering by $\propto$ 0.15μm graphite grains. In view of the range of variability observed, the effects of multiple scattering where graphite grains are used need only be considered when the polarisation is greater that $\propto$ 1%.

For the remaining three stars, observations by Bastien (1985) have been used to supplement the polarimetric data of RY Lup, CoD -33°10685 and AK Sco obtained at SAAO. For the data of Bastien (1985), the observations were obtained at the following wavelengths: 0.36, 0.44,

0.59, 0.75 and 0.84μm. Thus the model computations were carried out at these different wavelengths.

7.3.2.9. RY Lup.

This star has a near-IR excess which is attributable to thermal emission by warm dust grains (see Section 5.1.4). The fact that dust does lie close to the star, means that the observed rapid time variability (≃ days) is compatible with polarisation by dust grains. Bastien (1987) indicates that he can apply a single-scattering dust model to account for both the magnitude of the polarisation and the (correlated) polarimetric and photometric variability he observed.

The dataset of Bastien (1985) for RY Lup was obtained on HJD 2444731 (when the polarisation of the star was low), and the polarisation is seen to increase with decreasing wavelength; thus fits were attempted for both ice and silicate grains. The best fit was obtained for 0.16μm ice grains with shell parameters e = 0.25 and $\tau_o(\lambda=0.59\mu m)$ = 0.85, although the model does not match the rise in polarisation at U, and over-estimates the polarisation at V (see Fig. 7.3.4a). A less good, but adequate fit can also be given with 0.14μm silicate grains for a similar optical depth, although the polarisation from this model at 0.75 and 0.84μm (0.22 and 0.09% respectively) give a poor fit to the observations (0.44 and 0.22% respectively). However, in view of the rapid variability of the polarisation (Bastien 1985; Section 5.1.5) and the near-IR excess, the silicate model must be favoured. Also in view of the fact that the polarisation of RY Lup can be much higher than when observed by Bastien (1985), cf. Section 5.1.5, multiple scattering cannot be neglected when the star is more

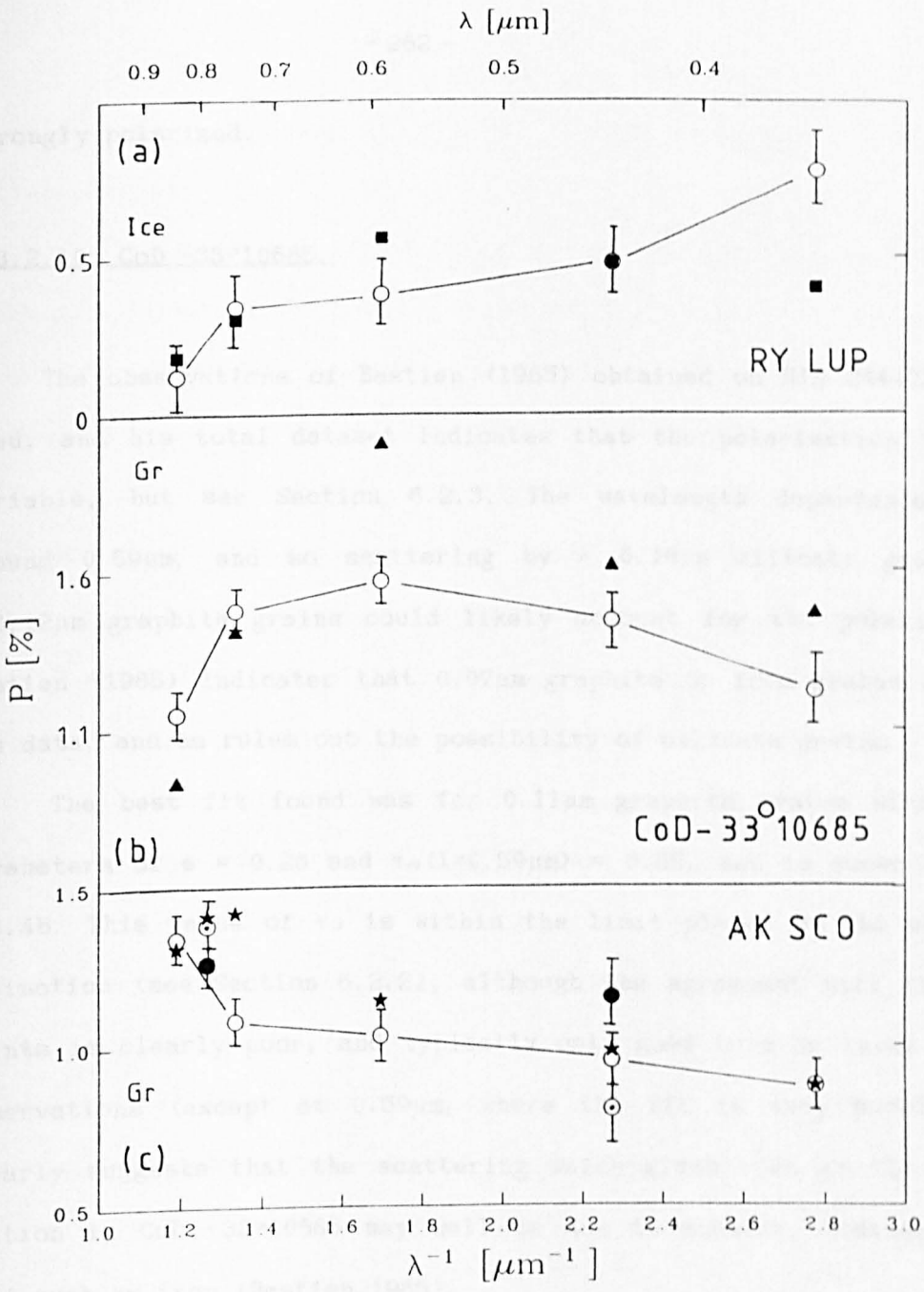

Fig. 7.3.4. Model fits to the observations of RY Lup on HJD 2444731, (b) CoD -33°10685 on HJD 2444731 and (c) AK Sco on HJD 2444730 (empty circles), HJD 2447041 (filled circles) and HJD 2447042 (dotted circles).
See also Sections 7.3.2.9, 7.3.2.10 and 7.3.2.11.

strongly polarised.

7.3.2.10. CoD -33°10685.

The observations of Bastien (1985) obtained on HJD 2444731 were used, and his total dataset indicates that the polarisation is non-variable, but see Section 6.2.3. The wavelength dependence peaks around 0.59μm, and so scattering by ≃ 0.16μm silicate grains or ≃ 0.12μm graphite grains could likely account for the polarisation. Bastien (1985) indicates that 0.07μm graphite or iron grains can fit his data, and he rules out the possibility of silicate grains.

The best fit found was for 0.11μm graphite grains with shell parameters of e = 0.25 and $\tau_0(\lambda=0.59\mu m)$ = 0.85, and is shown in Fig. 7.3.4b. This value of τ_0 is within the limit placed by the observed extinction (see Section 6.2.2), although the agreement with the data points is clearly poor, and typically only good to a 3σ level in the observations (except at 0.59μm, where the fit is very poor). This clearly suggests that the scattering which gives rise to the polarisation in CoD -33°10685 may well be due to another, similar grain type such as iron (Bastien 1985).

7.3.2.11. AK Sco.

The IR excess of AK Sco is attributable to emission from warm dust (Section 6.3.4), and the polarisation of AK Sco is quite variable on a timescale of days (Serkowski 1969a, Bastien 1985). Three datasets, obtained when AK Sco was in a similar polarimetric state, are plotted in Fig. 7.3.4c and are indicated thus: Bastien (1985), obtained on HJD

2444730 - empty circles; HJD 2447041 - filled circles; HJD 2447042 - dotted circles.

The observations all display a rise in the polarisation with increasing wavelength. The fit plotted (Fig. 7.3.4c) was that which adequately fits all three datasets (except for Bastien's data at 0.75μm) and was given by 0.14μm graphite grains, with e = 0.25 and $\tau_o(\lambda=0.59\mu m)$ = 0.60. Fitting the datasets individually shows that the observed range in variability only requires a range in τ_o of ≈ 0.1, i.e. a single model can adequately interpret more that one set of data. The value of $A_v \simeq 0.84$ mag. (Section 6.3.4) is not inconsistent with the fitted line-of-sight τ_o. Therefore, scattering by graphite grains within an optically thin disc-like shell which is not significantly inclined, can potentially interpret the data successfully.

7.3.3. Summary and limitations of the model.

The initial model does provide useful constraints, particularly on possible grain types and sizes, as well as possible general shell geometries (if a simple, symmetric shell geometry is plausible for a given star) in interpreting the polarisation around young stars. Despite the model being simple (i.e. neglecting higher order scatterings and assuming symmetry in the xy-plane), it is expected that in most of the cases considered, it isolates the best grain type of the three grain types considered, and reasonably predicts the typical grain size which produces the polarisation associated with the stars discussed above.

However, as also pointed out by Bastien (1981), as different grain models can reproduce the same form of $p(\lambda)$ if enough grain types are

actually considered, the fact that only three grain types were investigated here does leave room for other fits. Thus the fits obtained here are best viewed as being indicative of the grain properties (e.g. dielectric) and grain size responsible for the observed polarisation in each case. Although where other observations (e.g. IR spectroscopy) substantiate the presence of a grain material which can successfully fit $p(\lambda)$, the model is clearly to be favoured.

A further constraint on plausible dust models would also be provided by computing the thermal IR emission from the dust shell required to fit the polarisation. This constrains ice grain models, as ice grains will not give rise to thermal near-IR ($\simeq$ 1 - 5μm) emission. The computed IR emission can then be compared to the observed IR excess of a star.

In conclusion, it is possible to fit most of the polarimetric observations reasonably well (with the notable exception of CoD $-33^{\circ}10685$) assuming single scattering and only three grain types, although the assumption that multiple scattering can be neglected is clearly not a good one in some cases. However, single scattering models do reproduce a fairly accurate determination of the form of $p(\lambda)$, and normalised, single scattering models have been previously used to provide a reliable indication of the typical grain properties and sizes required to fit the data. Thus the parameters obtained here are of value in applying future multiple scattering models. A more precise determination of grain and dust shell parameters would require a more extensive long-term observational and theoretical investigation.

7.4. Polarisation with a variable central source.

7.4.1. Introduction.

The majority of young stars which exhibit significant polarisation ($p \gtrsim .1\%$) also exhibit variability of their polarisation (e.g. Bastien 1985). Thus the prospect for the successful interpretation of the variability with the dust shell model must therefore be considered.

An interpretation of the polarimetric variability can be sought by considering that the light and polarimetric variations are related. This could arise naturally in one of two ways:

(i) For a non-isotropic dust distribution, the polarimetric variability can be considered as arising from changes in the disposition of dust around the star (e.g. orbiting dust clumps), which will also result in changes in the line-of-sight extinction of the star. But in order to account for the short-term timescale of the variability observed for many young stars ($\simeq$ days; e.g. Serkowski 1969a, b; Bastien 1982, 1985), such an approach would require the bulk of the dust which scatters the light to be placed close to the star. This would necessarily require the dust grains to have a reasonably high sublimation temperature ($\simeq$ 1300K; cf. the dust temperature maximum "observed" in many young stars, e.g. Rydgren et al., 1982), and therefore precludes ice grains in interpreting any short-term variability due to structural variations occurring in the circumstellar dust distribution;

(ii) The central source can be regarded as intrinsically variable, and variation in the polarisation will arise due to differences in the illumination of the shell. It is this case which lends itself to an

initial analysis here.

7.4.2. Analysis of the Polarisation with a variable source.

The expression which is used to evaluate the polarisation as a function of time for a variable source is given by Eq. (7.21). Only sinusoidal light variations will be considered here. This is an over-simplification, as young stars are usually irregularly variable (in both V and p), but is the most straightforward case to consider here. However, a sinusoidal lightcurve is a very good approximation for light variations caused by an inhomogeneous (spotted) photosphere, for which there is increasing evidence as the cause of the variability in some InT stars (e.g. Vrba et al., 1986; see also Section 2.2.4).

A general case only will be considered here, but it is chosen in order to be representative of the typical timescale and magnitude of light variation exhibited by most young stars. From this one case, the behaviour of the polarisation can be predicted for a variety of dust shells.

In each case the variation will be contrasted against the visual light variability of the central source. The computed lightcurve was evaluated for a 5000K star with $\langle V \rangle = 10.45$ mag., an amplitude of variation of 0.5 mag. (which corresponds to a fractional variation in light of 0.2 in the visual) and a period of variation of a day. The computed polarisation is for silicate grains with a grain radius of 0.14μm. The general results are not affected by the grain type or size chosen.

7.4.2.1. Variation with size of dust shell.

The polarimetric variability from a shell of outer radius R_o around a source varying with a period t, will be expected to be most pronounced for grains concentrated around $R \simeq ct$ in appropriate units ($R \simeq R_o$ for a homogeneous shell). For t = 1 day, this corresponds to a shell of several hundred A.U.'s radius. From the form of the IR excesses, dust around young stars is likely to be distributed from a few tenths of an A.U. ($T_{dust} \simeq 1300K$) out to a few tens of thousand A.U. ($T_{dust} \simeq 50K$). For a dust shell lying only within a few A.U.'s around a star varying with a period of 1 day, the (observable) variation in the polarisation is negligible, as the shell is less than one light-hour across, and will thus best respond to a variation in the illumination on the timescale of $\simeq$ 1 hour. For a range of larger shells (from R_o = 10 - 10000 A.U.), the variation of $p(\lambda=0.55\mu m)$ is displayed in Fig. 7.4.1. The period of variation in V is a day, as shown in the upper curve, but there is a significant shift in phase of the polarimetric variations relative to the photometric variation as increasingly larger shell radii are considered. In the computations, the value of e for the shell was set to 0.25, in order to maximise the magnitude of the polarisation.

For a shell of 10 A.U. radius (second curve down), the polarimetric variations are essentially in phase with the visual lightcurve (uppermost curve), and the variation from the mean polarisation of 0.19% is 0.08%, a significant fraction of the total polarisation. Thus the largest fractional variation in p that can be expected with a typical source which varies by $\simeq$ 0.5 mag., is estimated to be $\simeq$ 0.4. For a shell of 100 A.U. radius (third curve) the polarisation lags the

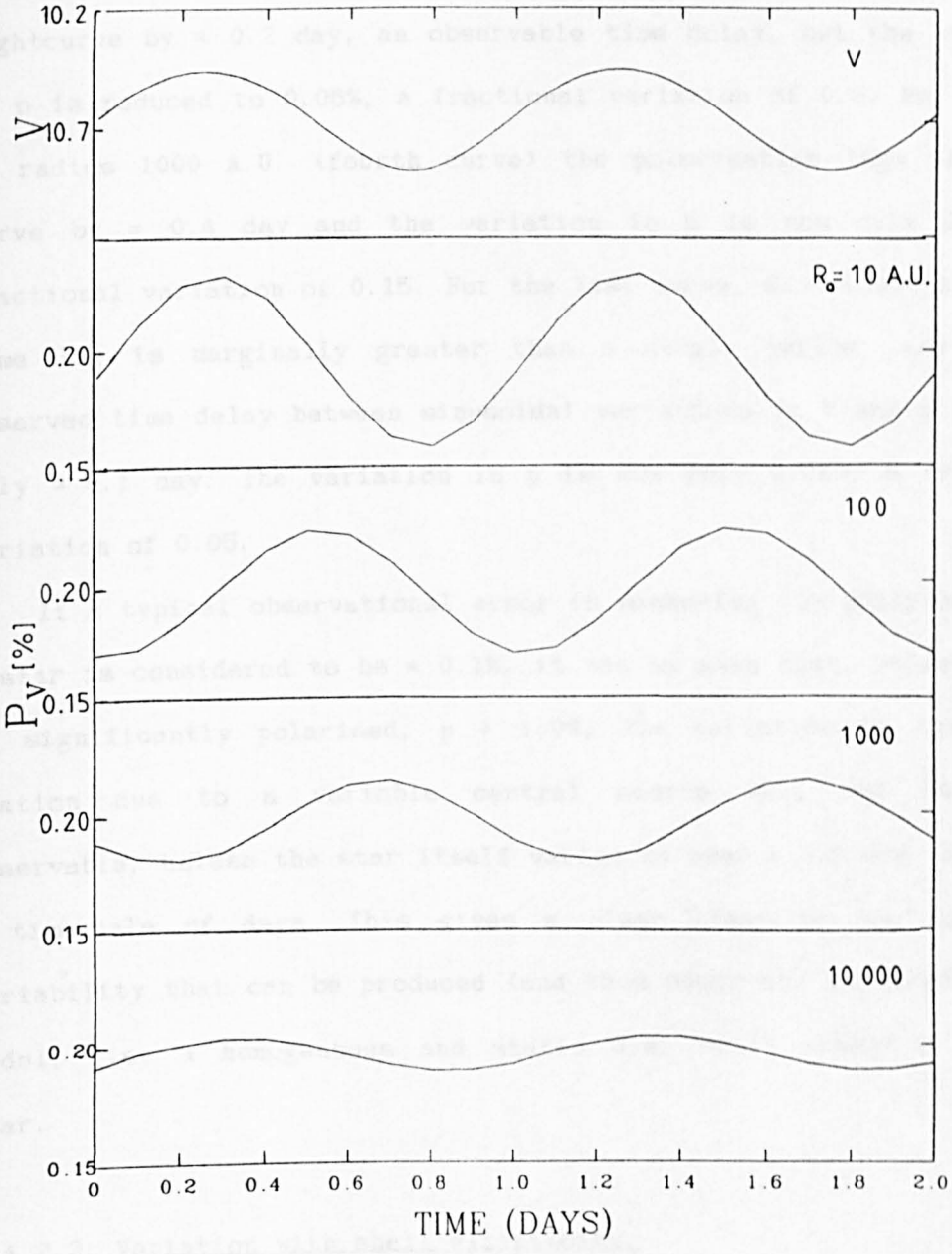

Fig. 7.4.1. The polarisation from a variable source (upper curve) for dust shells with equatorial radii of 10, 100, 1000 and 10000 A.U. See also Section 7.4.2.1.

lightcurve by ≃ 0.2 day, an observable time delay, but the variation in p is reduced to 0.06%, a fractional variation of 0.3. For a shell of radius 1000 A.U. (fourth curve) the polarisation lags the light curve by ≃ 0.4 day and the variation in p is now only 0.03%, a fractional variation of 0.15. For the last curve, R_o = 10000 A.U., the time lag is marginally greater than a single period, and so the observed time delay between sinusoidal variations in V and p would be only ≃ 0.1 day. The variation in p is now only 0.01%, a fractional variation of 0.05.

If a typical observational error in measuring the polarisation of a star is considered to be ≃ 0.1%, it can be seen that, unless a star is significantly polarised, p ≳ 1.0%, the variation in the polarisation due to a variable central source will **not** be easily observable, unless the star itself varies by over ≃ 0.5 mag. at V over a timescale of days. This gives a clear limit on the extent of variability that can be produced (and thus observed) in terms of this model, i.e. a homogeneous and static dust shell around a variable star.

7.4.2.2. Variation with shell ellipticity.

The variation of p for a shell of 100 A.U. radius for values of e = 0.1, 0.25 and 0.5 was investigated, and the results are plotted in Fig. 7.4.2. The choice of e will affect the mean value of p as well as the range in variation of p. It is found that as the dust shell becomes more spherical, both the magnitude of p and the magnitude of variation of p decrease. The magnitude of variation of p decreases and the time delay in p relative to V increases for more spherical shells,

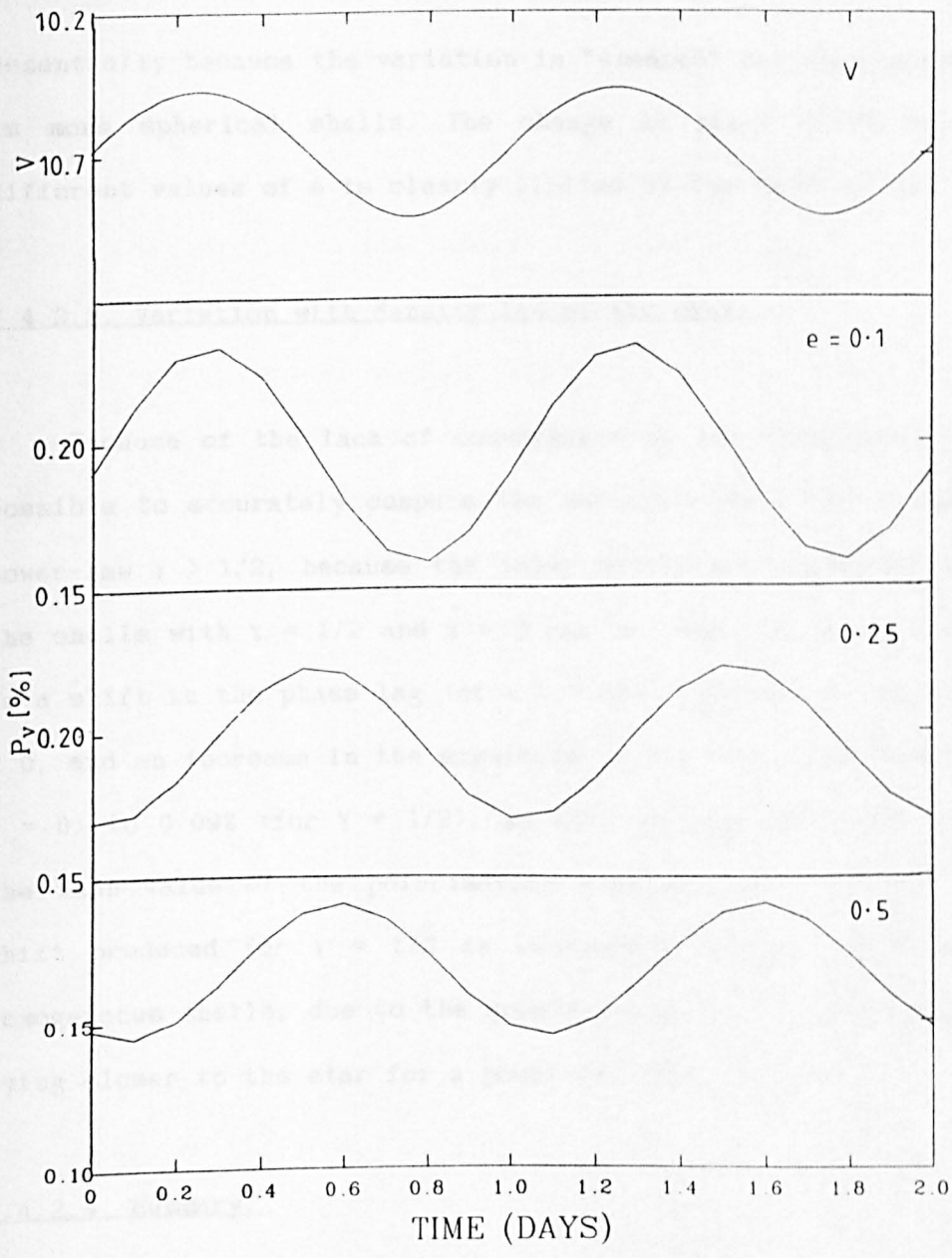

Fig. 7.4.2. The polarisation from a variable source (upper curve) for dust shells with e= 0.1, 0.25 and 0.5.
See also Section 7.4.2.2.

essentially because the variation is "smeared" out to a greater extent in more spherical shells. The change in phase shift possible for different values of e is clearly limited by the value of R_0.

7.4.2.3. Variation with density law of the shell.

Because of the lack of convergence of the integrals, it was not possible to accurately compute the variation in p for a shell with a power-law $\gamma > 1/2$, because the inner densities become too great, but the shells with $\gamma = 1/2$ and $\gamma = 0$ can be compared. For $\gamma = 1/2$, there is a shift in the phase lag (of $\simeq 0.3$ day) relative to that seen for $\gamma = 0$, and an increase in the magnitude of the variation from 0.07% (for $\gamma = 0$) to 0.09% (for $\gamma = 1/2$), as well as the associated increase in the mean value of the polarisation (see Section 7.2.1.3). The phase shift produced for $\gamma = 1/2$ is equivalent to that given by smaller homogeneous shells, due to the greater proportion of scattering grains lying closer to the star for a power-law distribution.

7.4.2.4. Summary.

It has been shown that where the polarisation is considered to arise within an isotropic, optically thin dust shell surrounding a variable source, a fractional variation of $\simeq 0.4$ in p can be produced by a corresponding fractional variation in visual stellar flux of 0.2. Thus for many of the stars which exhibit a significant level of polarisation ($p \gtrsim 1\%$), variation in the illumination of the circumstellar dust can plausibly account for the observed variation in p (provided that the variation in p and V are essentially directly correlated),

without having to invoke changes in the distribution of the circumstellar dust.

A phase delay is noted for shells which are comparable to, or greater in size than, ct, where t is the typical timescale of the light variations. It is found that both for increasing shell sizes and increasingly spherical shells, that the magnitude of variation in the polarisation decreases and the phase delay increases. The variation with radial shell density law could not be fully examined, but for a shell of radius R_o with a $r^{-1/2}$ density law, the variation in the polarisation is similar to the variation seen in smaller homogeneous dust shells.

Thus for stars which exhibit essentially correlated variations in V and p, the observed phase lag and magnitude of variability of the polarisation do not uniquely define the shell radius; but if one of R_o or e can be estimated from other observational constraints, then it may be possible to specify the other (unknown) parameter from polarimetric observations.

7.5. Conclusions.

A simple model to evaluate the wavelength dependent polarisation for single scattering in a series of ellipsoidal dust shell geometries surrounding a central star, is formulated and applied to the observed polarisation of several PMS stars. As the form of $p(\lambda)$ is not strongly dependent on the shell geometry and higher order scatterings, the model is useful in indicating the type of grain and typical grain size which may give rise to the polarisation observed in each star.

An analysis of the level of variability produced by this simple

model with a variable central source also shows that it should, in principle, be able to produce the level of short-term polarimetric variability observed in stars which are significantly polarised, provided that the variation in the polarisation and the visual lightcurve are reasonably well correlated.

More refined dust shell models are clearly required before polarimetric observations can be comfortably fitted within all the observational constraints. It is suggested that further models should include some of the following effects: e.g. multiple scattering within an inclined disc; scattering by an ensemble of "orbiting" circumstellar dust clumps; scattering in a disc-like geometry by partially aligned non-spherical grains in a magnetic field; scattering by grains with a simple grain size distribution; scattering by grains which increase in size over time.

Chapter 8. Summary and Conclusions.

8.1. Summary.

Several stars of the Orion Population have been observed and analysed using optical and IR data, and in one case (TY CrA) also using UV data. Further, the polarisation of several of these stars, and an additional number of Orion Population stars has also been studied. Although insufficient stars have been observed to draw any statistically significant conclusions as regards the Orion Population as a whole, most of the stars observed here are probably not "untypical" representatives of the some of the various sub-classes of the Orion Population. The general findings will now be summarised, and then the conclusions and implications of this work can be drawn.

To aid discussion, and also to indicate possible correlations in the limited sample of stars observed here, both the results of the fits to the intrinsic flux distribution and the overall polarimetric characteristics of each star studied in Chapters 4, 5 and 6 are summarised in Table 8.1.1.

It has been seen that the circumstellar environment can play an important role in the observational characteristics of both InT and Ina stars. In the first instance, optical spectroscopy shows that stellar envelopes are probably not uncommon in Ina stars, and both shell absorption (TY CrA, V856 Sco) and envelope emission (R CrA) are seen. Also it is evident that envelope emission occurs in both "extreme" InT stars, such as RU Lup, and YY Ori stars, such as S CrA. Additionally, it has been seen that an enhancement of envelope

Table 8.1.1.

Summary of results.

Star	A_V (mag.)	L_{IR}/L_{Bol}	T_{max} (K)	$\langle p \rangle$ (%)	Δp (%)	Refs.
TY CrA	2.90	0.38	320	1.21	0.25	
R CrA	3.76	0.65	1300	7	17	1,2,3
T CrA	2.65	0.60	1400	4	6	1,2,3
S CrA	1.85	$\leq$ 0.55	1300	0.98	0.53	4
RY Lup	1.14	0.45	1400	1.52	3.16	4
RU Lup	0.62	$\leq$ 0.50	1300	0.59	0.93	4,5
V856 Sco	0.68	0.26	1400	1.04	1.53	6
CoD-33°10685	1.40	0.18	1400	1.42	0.27	4
AK Sco	0.84	0.50	800	0.79	0.84	4,5
V4046 Sgr	0.62	0.44	120	-	-	

The results of the investigation of the flux distribution and optical polarisation for each star studied in Chapters 4, 5 and 6 are summarised. Each respective column tabulates the star, the total extinction, the ratio of IR to bolometric luminosity (the inequality $\leq$ indicates that the value given is an upper limit), the maximum dust temperature fitted to the IR excess, the mean polarisation and the total range in polarisation that has been observed here and by various authors (labelled under **Refs.**). The numbered references refer to the following polarimetric observations:

1. Serkowski (1969b)
2. Vrba *et al.* (1979)
3. Ward-Thompson *et al.* (1985)
4. Bastien (1985)
5. Serkowski (1969a)
6. Bessel and Eggen (1972)

emission is evident in one InT star, RY Lup, when the star is faint. The idea of an extended envelope and/or stellar "wind" in Orion Population stars is not inconsistent with the association of optical jets/nebulosity and molecular emission in both InT (e.g. see Sections 2.2.3 and 5.2.1) and Ina stars (e.g. see Chapter 4).

Also the presence of circumstellar dust, presumably essentially remnant material from the earliest stages in the process of star formation, is found to be essentially ubiquitous in both the InT and Ina stars observed. This fact is determined from the interpretation of the IR excesses and the reddened optical colours (see Table 8.1.1; cf. Rydgren et al., 1982).

It is found that blackbodies can be fitted to the IR excesses of the stars studied here, i.e. the excess IR radiation can be interpreted in terms of thermal emission from circumstellar dust shells. As is seen in Table 8.1.1, for most of the stars studied, the maximum dust temperature is determined to be $T_{max} \simeq 1300 - 1400K$ from the fitting of a blackbody to the near-IR excess, a process which is dependent on the intrinsic stellar colours adopted and the reddening correction used. It is therefore interesting to note that this temperature maximum is very similar to the maximum dust temperature determined by Rydgren et al. (1982) for a large number of InT stars in the Taurus and NGC 2264 regions.

Also, the fact that the thermal dust emission typically extends out into the far-IR would indicate that the dust shells are generally quite extensive. Further, the large ratio of L_{IR}/L_{Bol} ($\simeq 0.4 - 0.6$) found in most of the stars studied, as is seen in Table 8.1.1, indicates that the total mass of the circumstellar dust shell is often considerable. The fact that L_{IR}/L_{Bol} is found not to exceed unity in

any of the stars is consistent with thermal re-emission from circumstellar dust.

Not only does circumstellar dust manifest itself by emission at IR wavelengths, but also it is seen that most of the stars studied are affected by significant circumstellar extinction. The fact that there is a limited correlation between the IR excess and the visual extinction seen in Table 8.1.1, i.e. the stars which have the larger values of L_{IR}/L_{bol} tend also to be most heavily reddened, is consistent with the reddening being essentially circumstellar in origin (cf. Rydgren et al., 1982).

In addition, it is shown to be plausible that variable circumstellar extinction modulates the light output in a number of the stars observed. The database of Kilkenny et al. (1985) used here allows, in some cases for the first time, investigation of the long-term (≈ weeks - months) colour behaviour in several of the stars studied. For example, it is found that the long-term colour behaviour observed in TY CrA, R CrA and S CrA would indicate an underlying degree of variable extinction by larger than IS-sized grains. In the case of TY CrA this is clearly consistent with the anomalous R = 5.3 reddening law of the star as explicitly derived here and by Whittet et al. (1983).

Also the underlying, long-term light behaviour of RY Lup, AK Sco, V856 Sco, and possibly also RU Lup, is found to be modulated by variable extinction by IS-sized circumstellar grains. It is also seen that the short-term (≈ days) deep minima of RY Lup, and possibly also the minima of V856 Sco, are due to extinction by an additional population of larger grains.

It is however stressed that, for most of the stars for which long-term variation in the dust shell opacity has been ascertained, the

short-term (≃ hours - days) light variability is almost certainly dominated by intrinsic variations. This is clearly the case for those stars which can exhibit quasi-periodic variations (e.g. RU Lup), variation in spectral type (e.g. R CrA) and/or strong envelope continuum emission (e.g. S CrA). In only RY Lup is there any clear evidence for modulation of the lightcurve by variable extinction on a timescale as short as days.

It can be seen in Table 8.1.1 that, in the sample of stars studied, there is a limited correlation between the total extinction and the degree of polarisation. R CrA and T CrA, which exhibit the strongest degree of polarisation, are both heavily reddened (also they both have the largest IR excesses found here); in comparison, the two stars which exhibit a mean polarisation of less than 0.8%, RU Lup and AK Sco, are only slightly reddened. Such a correlation would be compatible with the polarisation arising essentially within the circumstellar dust shells.

The polarisation exhibited by a number of the stars is either shown to be (e.g. as in RY Lup, AK Sco) or is known to be (e.g. as for R CrA) due to the scattering of light by circumstellar grains. For these stars therefore, the variation in the degree of polarisation and the position angle typically exhibited could indicate changes in the illumination of circumstellar dust and/or changes in the disposition of circumstellar dust. As the photometric and polarimetric behaviour in several of these stars has been observed simultaneously, it has been possible to determine the likely origin of the variability in these stars.

The polarisation from an optically thin dust shell around a variable source is computed here and the typical time lag between the

light and the polarimetric variations are determined. Although none of the observations discussed here can be clearly interpreted in terms of such a model, it is to be expected that sources which are found to exhibit closely correlated light and polarimetric changes would find a ready interpretation in terms of this model. The only possible candidate found here for related light and polarimetric variations was S CrA.

Therefore it is argued that the polarimetric variations observed in R CrA, RY Lup and V856 Sco must be essentially due to changes in the distribution of the circumstellar dust. Thus in these three stars in particular, it would seem that there is both photometric and polarimetric evidence for the existence of an ensemble of "clumpy" regions in motion within the circumstellar dust shells of these stars.

Finally, the wavelength dependence of polarisation observed in an additional number of Orion Population stars is found to be successfully interpreted in terms of a simple model of scattering of light by circumstellar dust grains in ellipsoidal dust shells. Thus likely grain parameters have been suggested in each of the stars fitted.

8.2. Conclusions.

The implication of a characteristic maximum dust temperature, $T_{max} \simeq 1300K$, observed in many Orion Population stars would point towards a common process in the development of the circumstellar dust shells around both InT and Ina stars. The value of T_{max} is almost certainly determined by the sublimation temperature of the circumstellar grains (Nakano 1987), i.e. the common temperature maximum is probably due to similar grain types occurring in a similar circumstellar environment

associated with different stars.

In view of this, plausible explanations of the common temperature maximum would include: the formation and/or destruction of a particular grain type in the circumstellar environment, e.g. grain formation in a stellar wind, destruction by strong UV radiation; the occurrence of circumstellar discs around many PMS stars, where the temperature maximum is set by the grain type and the inner disc radius. However, as only a limited number of InT stars have been conclusively shown to possess stellar winds, and as Ina stars do not generally exhibit strong UV excesses, the latter suggestion is thought to be the more plausible interpretation for a similar value of T_{max} in the Orion Population as a whole. Further observations and modelling of the near-IR excesses, particularly in Ina stars, is required to establish how predominant a characteristic temperature maximum is in the Orion Population of young stars.

From the possible presence of large circumstellar grains in the dust shells of some stars (e.g. TY CrA, RY Lup, V856 Sco), it is not implausible that grain growth and/or coagulation may be occurring in the circumstellar dust shells of such stars.

It is seen to be feasible that polarimetric variability and long-term variable circumstellar extinction have a common origin in some of the stars studied, i.e. bulk motion of an ensemble of dust condensations. If this is true of most Orion Population stars, the fact that, in the Orion Population as a whole, short-term variable circumstellar extinction is less common than is short-term polarimetric variability, would tend to suggest that the likely disposition of the inner dust shell distribution tends to be constrained to a disc-like geometry. This is because as circumstellar discs would be

viewed at different orientations, it would be expected that an observational selection effect due to orientation would affect the preferential observation of variable extinction to a greater extent than the observation of variable polarisation.

Another qualitative argument which may well favour a disc-like geometry in a large number of Orion Population stars is that whilst most stars exhibit IR dust excesses and circumstellar reddening, only a minority of Orion Population stars are very heavily reddened ($A_V > 3$ mag.), i.e. a similar observational selection effect explicable in terms of orientation of circumstellar discs.

In principle therefore, the placing of a cluster of young stars in the E(V-I), (H-K) plane (cf. Rydgren et al., 1982) should also indicate the likely geometry of a circumstellar dust shell, e.g. a heavily reddened star with a low IR excess would be expected to have a circumstellar disc which is being observed essentially edge-on. However, as Orion Population stars are often very variable, and as the distribution of dust may well be far from homogeneous (i.e. "clumpy") in a number of stars, e.g. as is plausible for both R CrA and RY Lup, determination of a possible dust shell geometry simply by placing the star on a colour-colour diagram may not always be instructive.

The limited correlation found between the degree of polarisation and the circumstellar reddening, and also the fact that the stars which are most strongly polarised, R CrA and T CrA, also have strong IR excesses (cf. the correlation found between p and $\langle V \rangle - \langle L \rangle$ in a larger number of stars; Bastien 1985), would tend to indicate that the more massive the circumstellar dust shell, then the greater is the degree of polarisation observed.

Finally, the inferred presence of large circumstellar grains,

sizable circumstellar dust shells (or discs) and the likely motion of condensations associated with such dust shells, as is suggested by both the polarimetric and photometric variability exhibited by three stars in this work (R CrA, RY Lup and V856 Sco), has obvious implications in view of the existing models involving the coagulation of circumstellar dust grains to form planetary (e.g. Nakano 1987) and cometary (e.g. Gahm and Greenberg 1984, Bailey 1987) bodies around PMS stars.

8.3. Suggestions for Further Work.

The value of long-term photometric monitoring of Orion Population stars at optical and IR wavelengths has been shown here. Further monitoring should be pursued, with simultaneous optical polarimetry and high-resolution spectroscopy being obtained where possible. Such additional observations (and any correlations found) would help delineate both the degree of variability due to the star and due to the disposition of the circumstellar dust. As has been observed in R CrA, it may be expected that stars which are heavily reddened and which have considerable near-IR excesses (i.e. stars with substantial amounts of dust close in to the star) would exhibit both a greater degree of polarisation and a stronger degree of variability on short timescales ($\simeq$ hours - days).

Detailed modelling of the wavelength dependence of the polarisation observed in heavily reddened young stars (such as R CrA) which exhibit both large and variable polarisation on short timescales is clearly required. It is suggested that such modelling should attempt to include multiple scattering by non-spherical, aligned grains and

also the effects of dilution of polarised light by inhomogeneous, time-varying dust distributions.

Information on the characteristic grain sizes around Orion Population stars can be determined from both polarimetric and photometric observations. For stars which exhibit both variable circumstellar extinction and significant polarisation (e.g. R CrA, RY Lup), observations of the wavelength dependence of polarisation, which would indicate the characteristic grain size a_{gr} giving rise to the polarisation, and observations of the extinction law and/or the optical colour slopes (where relevant), which would help determine the ratio of total-to-selective extinction, R, would be welcome. From such observations, investigation of any possible relation between the value of R and the value of a_{gr} and/or λ_{max} (the peak in the polarisation curve) would be of considerable interest.

Further, in view of the possibilty that grain growth/coagulation may be occurring in the dust shells of some of the stars studied here (e.g. RY Lup, V856 Sco), long-term monitoring of the values of R and $p(\lambda)$ in such stars may well help establish whether the grain size distribution in the circumstellar dust shells changes with time.

As it would seem likely that copious amounts of circumstellar dust, probably in excess of the mass of a planetary system such as our own, are still present around Orion Population stars, further work would be useful in estimating the timescale of removal of such quantities of dust by both steady-state (e.g. as in RU Lup) and episodic winds (as in FU Ori stars). As the circumstellar dust shell is dispersed and/or the dust condenses into planetesimals, it would be expected that the level of near-IR emission from dust should decrease as the star evolves towards the MS, i.e. the strength of the near-IR

excess emission would be expected to decrease with age. Observational and theoretical (i.e. estimating the age of a young star by placing it on the H-R diagram) investigations of a statistically large number of Orion Population stars (including "naked" InT stars) are required to see whether such a relation can be observationally discerned.

Although the Ina and InT stars are obviously different in many respects because of differences in stellar mass, it is unclear why particular differences should relate to the likely distribution of the circumstellar dust. An attempt to resolve some of the following questions may well help to better understand the dust environment around Orion Population stars.

Why is it that Ina stars generally exhibit a much larger degree of optical polarisation than InT stars (Section 2.3.5; cf. Section 2.3.4)? Is it because the more massive Ina stars have the more massive dust shells, or because there is a greater degree of grain alignment in the dust shells associated with Ina stars?

Why is it that a significant fraction of Ina stars, but not InT stars, exhibit Parenago type I lightcurves (presumably due, in many cases, to variable circumstellar extinction; Section 2.3.4)? Might this fact reflect the more likely formation of discs (Section 8.2) and/or "clumpy" dust distributions around the more massive Ina stars?

If FU Ori outbursts (seen in InT stars) are triggered by instabilities occurring in circumstellar discs, as has been suggested by Hartmann and Kenyon (1985), should it not be expected that Ina stars will also exhibit FU Ori-type outbursts? Is the reason why no FU Ori-type outbursts have (yet) been observed in Ina stars an observational selection effect or because discs around Ina stars are gravitationally more stable than discs around InT stars?

Appendix 1. Description of the Polarisation Program.

The basic program, which calculates the polarisation of an ellipsoidal shell of uniform density around a non-variable star, will be described here; but as discussed in Chapter 7, the program was also modified to compute other cases.

The equation (7.10) which is used to compute the polarisation is evaluated in three separate parts: the top and bottom integrals are evaluated by the routines TOPANS and BOTANS. The remaining denominator term $2\pi\chi^2 Q_{ext}$ is simply evaluated using the computed value of Q_{ext}. The routines TOPANS and BOTANS, used to evaluate the top and bottom integrals are very similar, and thus only the routine evaluating the top integral is described.

The basic flow chart, describing the structure of the program is given in Fig. A.1.1, and the program itself is printed in Fig. A.1.2. The basic mathematical content of the program is described in Chapter 7, and the Mie formulae used in the program can be found in Wickramasinghe (1973).

The program will now be briefly described. Each numbered section corresponds to the labelled section in Fig. A.1.2.

(i) The constants to be used are input and assigned to COMMON blocks for transfer to sub-routines. In the interactive program, the constants are input from the terminal, but example parameters are shown within the program displayed in Fig. A.1.2. The output data are written to a file.

(ii) The sub-routine EXCOEFF (described in part (xi)) is called to evaluate Q_{ext} using the formulae given in Wickramasinghe (1973) for

the given values of λ and a. The equatorial optical depth, TAU0 (τ_0) is then evaluated.

(iii) The NAG library routine D01JAF is now called to evaluate the volume integral (in this case, the top integral in Eq. (7.10)). The input parameters determine the efficiency of the library routine. If the accuracy requested cannot be accomplished then the program will fail and the exit value of IFAIL will be non-zero.

The output parameters are: RESULT which outputs the evaluated integral; ESTERR which gives an estimate of the absolute error obtained (normally a relative error $\approx 10^{-2}$ is achieved); NEVALS is the number of evaluations used (typically 534 - 2200).

(iv) Evaluates the output term TOPANS.

(v) The user-defined function F(x,y,z) describes the integrand (see Eq. (7.10)). The Mie constants used to evaluate OTA1 (i_1) and OTA2 (i_2), see Eq. (7.10), are set up (see Wickramasinghe (1973) for details).

(vi) The library routine integrates over a sphere of unit radius. Thus the function is set to zero if the current (x,y,z) position lies outside of the ellipsoidal dust distribution of unit equatorial radius.

(vii) The angles of the light-rays are evaluated (incident angle BETA, β = arctan (z/y); scattered angle ALPHA, α = arccos (x/r)), and the sums used in evaluation of the Mie terms are initialised.

(viii) The initial Mie terms (dependent on position) are determined.

(ix) The recurrent Mie terms are now evaluated. The Mie scattering terms, SUM1 ($S_1(\theta)$) and SUM2 ($S_2(\theta)$), are determined by summation. Until convergence is reached (current term $< 10^{-6}$ x sum), the program loops back to label 20.

(x) The integrand is now evaluated in terms of the functions (of position): β; τ_1; τ_2; i_1; i_2. In evaluating F within BOTANS the factor ONE is omitted and (OTA1-OTA2) becomes (OTA1+OTA2) (see Eq. (7.10)).

(xi) The sub-routine EXCOEFF evaluates Q_{ext} by summing over the Mie terms (as in F(x,y,z)).

Fig. A.1.1.

PROGRAM POLAR

Step 1. Evaluate top integral.

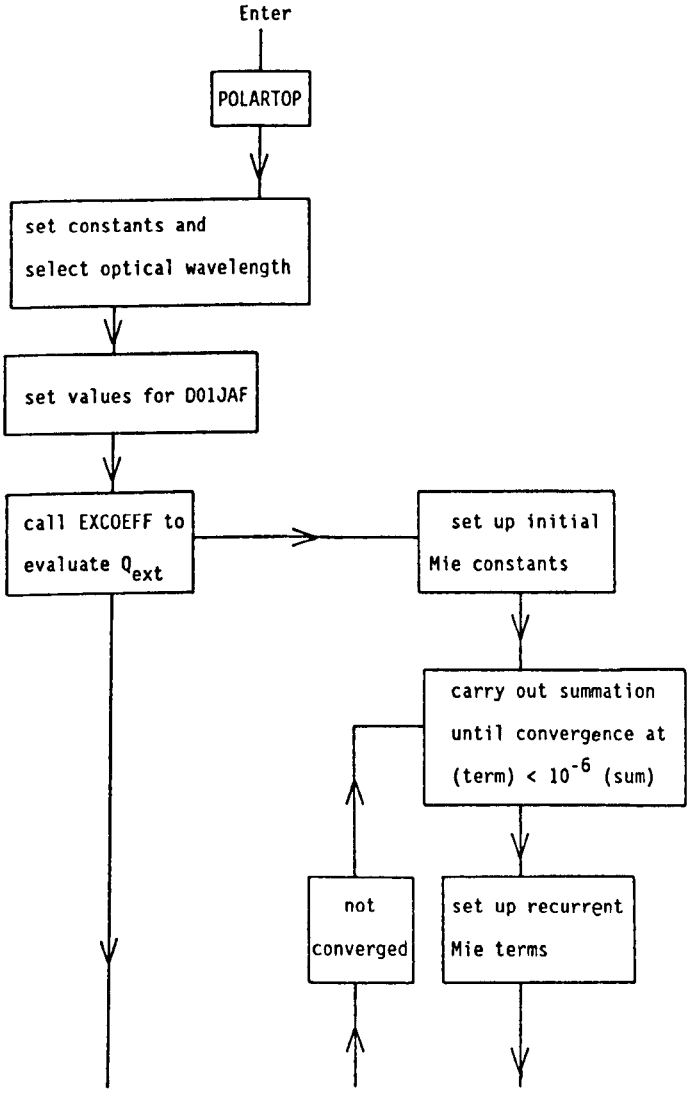

Fig. A.1.1. Flow chart for polarisation program POLAR.

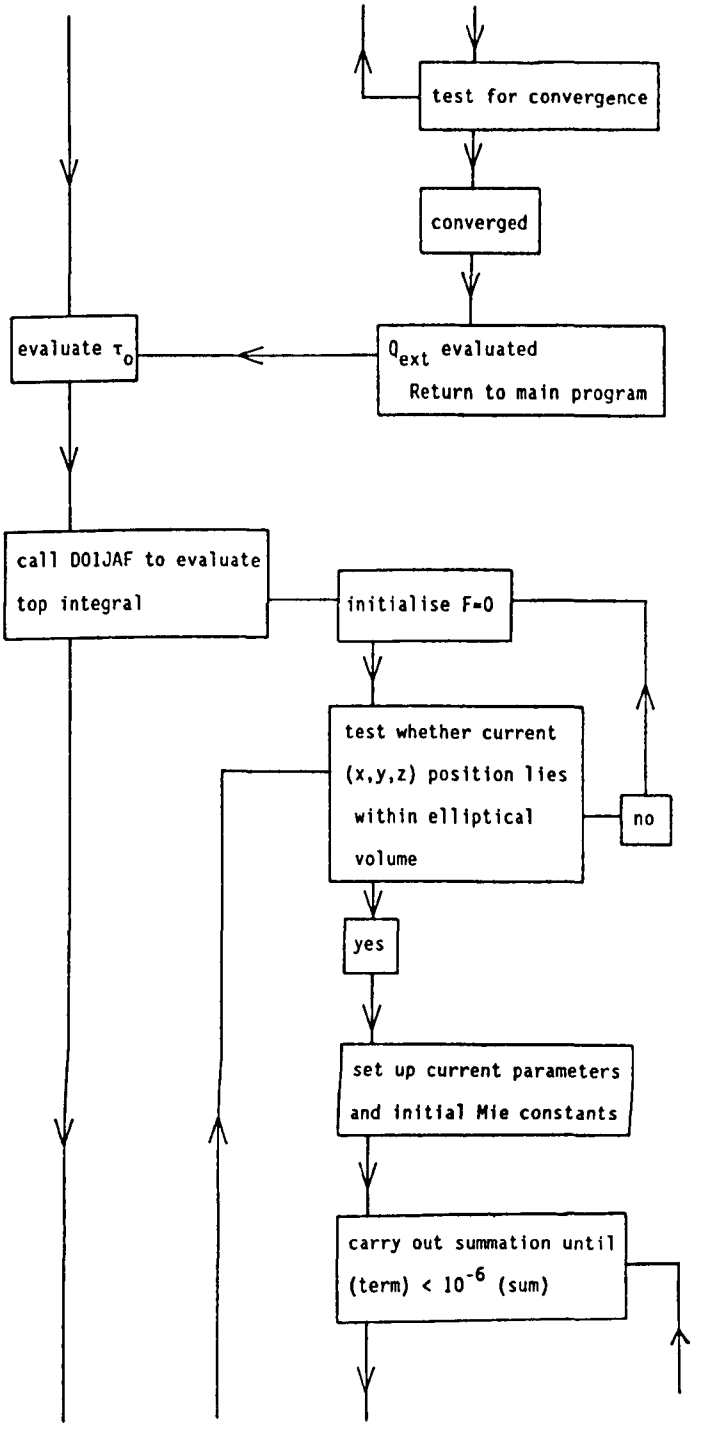
test for convergence
converged
Q_{ext} evaluated
Return to main program
evaluate τ_o
call D01JAF to evaluate top integral
initialise F=0
test whether current (x,y,z) position lies within elliptical volume
no
yes
set up current parameters and initial Mie constants
carry out summation until (term) < 10^{-6} (sum)

Fig. A.1.1. (Cont.)

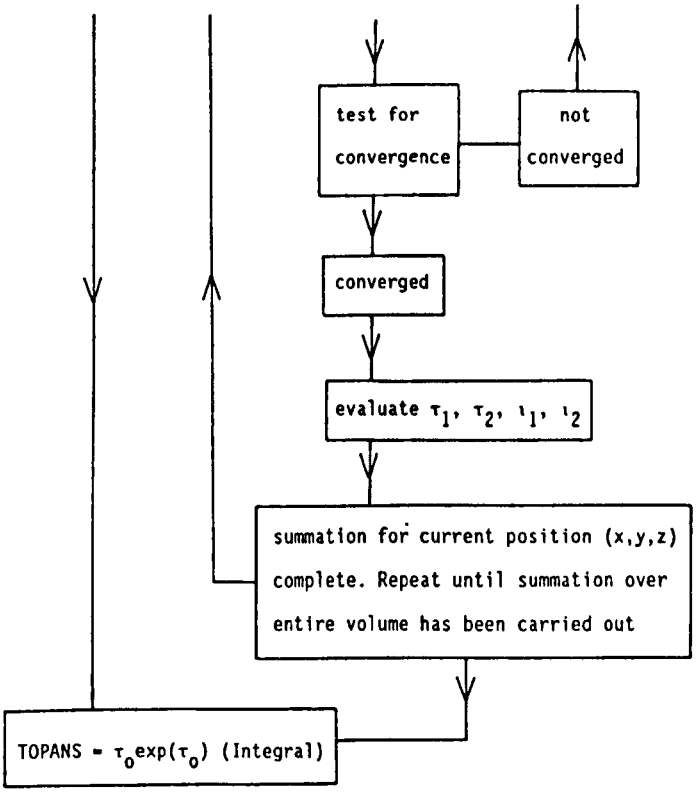

Step 2. Repeat above procedure for bottom integral, which will evaluate BOTANS

Step 3. Evaluate other bottom term

$$TERM = 2\pi x^2 Q_{ext}$$

Step 4. Evaluate polarisation, $P = \dfrac{TOPANS}{BOTANS + TERM}$

Fig. A.1.1. (Cont.)

Fig A.1.2.

```
C-----------------------------------------------------------------
C                                                                  ↑
      PROGRAM POLARTOP                                             ↑
      IMPLICIT DOUBLE PRECISION(A-H,O-Z)                           ↑
      COMMON/CONST/AG,CN,CK,PI                                     ↑
      COMMON/LIMITS/WV,ECC                                         ↑
      COMMON/Q/QEXT,TAU0                                           ↑
C                                                                  ↑
C     CONSTANTS ARE AG=GRAIN RADIUS(um),  WV=WAVELENGTH(um)        ↑
C     CM=REFRACTIVE INDEX = CN - iCK, CY = 2*PI*AG*CM/WV           ↑
C     ECC=ELLIPTICITY OF THE SPHEROID                              ↑
C                                                                  ↑
      EXTERNAL F,EXCOEFF,D01JAF                                    ↑
      OPEN(2,FILE='TOPJAF.DAT',STATUS='NEW')
C                                                                 (i)
C     EXTERNAL FUNCTIONS F,EXCOEFF AND D01JAF HAVE BEEN DECLARED
C     TOPJAF IS FILE WHICH WILL OUTPUT THE DATA.  INPUT CONSTANTS  ↓
C                                                                  ↓
      CN=1.65D0                                                    ↓
      CK=1.0D-1                                                    ↓
      WV=5.5D-1                                                    ↓
      ECC=2.50D-1                                                  ↓
      DENSITY=2.44D0                                               ↓
      PI=4.0D0*DATAN(1.0D0)                                        ↓
      AG=1.4D-1                                                    ↓
C                                                                  ↓
C-----------------------------------------------------------------
C                                                                  ↑
C     EVALUATE QEXT AND TAU0                                       ↑
C
      CALL EXCOEFF(QEXT)                                          (ii)
      TAU0=DENSITY*PI*AG*AG*QEXT
      WRITE(2,1000)QEXT,TAU0                                       ↓
 1000 FORMAT(1X,'QEXT IS',E14.6,'TAU0 IS',E14.6)                   ↓
C                                                                  ↓
C-----------------------------------------------------------------
C                                                                  ↑
C     SET UP CONSTANTS FOR NAG LIBRARY ROUTINE D01JAF              ↑
C                                                                  ↑
      NDIM=3                                                       ↑
      RADIUS=1.0D0                                                 ↑
      EPSA=1.0D-2                                                  ↑
      EPSR=1.0D-2                                                  ↑
      METHOD=6                                                     ↑
      ICOORD=0
      IFAIL=0                                                     (iii)
C
C     NDIM = NO. OF DIMENSIONS; RADIUS = RADIUS OF SHELL (IN       ↓
C     NORMALISED UNITS); EPSA AND EPSR ARE ABSOLUTE AND RELATIVE   ↓
C     ERROR REQUIRED; METHOD = 6 (HIGH ACCURACY); ICOORD = 0       ↓
```

Fig. A.1.2. (Cont'd)

```
C   (USE CARTESIAN COORDS); IFAIL=0 (IFAIL.GT.0 GIVES ERROR CODE (iii)
C   IF PROGRAM FAILS). CALL SUB-ROUTINE TO EVALUATE INTEGRAL  (cont'd)
C                                                                      ↓
      CALL D01JAF(F,NDIM,RADIUS,EPSA,EPSR,METHOD,ICOORD,               ↓
     1  RESULT,ESTERR,NEVALS,IFAIL)                                    ↓
C                                                                      ↓
C     RESULT OUTPUTS INTEGRAL; ESTERR GIVES AN ESTIMATE                ↓
C     OF THE ABSOLUTE ERROR; NEVALS = NO. OF EVALUATIONS               ↓
C                                                                      ↓
C-----------------------------------------------------------------------
C                                                                      ↑
C     TOP TERM OF POLARISATION IS EVALUATED                            ↑
C                                                                      ↑
      TOPANS=TAU0*DEXP(TAU0)*RESULT                                    ↑
      WRITE(2,1001)WV,RESULT,ESTERR,TOPANS,NEVALS,IFAIL
 1001 FORMAT(1X,'WAVELENGTH=',E10.6,'RESULT=',E14.6,'ESTERR=',     (iv)
     1 E14.6,/1X,'TOPANS=',E14.6,'NEVALS=',I6,'IFAIL=',I2)
      END                                                              ↓
C                                                                      ↓
C     END OF MAIN PROGRAM                                              ↓
C                                                                      ↓
C-----------------------------------------------------------------------
C                                                                      ↑
C     DEFINE FUNCTION F(X,Y,Z) TO EVALUATE VOLUME INTEGRAL             ↑
C                                                                      ↑
      DOUBLE PRECISION FUNCTION F(NDIM,X)                              ↑
      IMPLICIT DOUBLE PRECISION(A-H,O-Z)                               ↑
      DOUBLE COMPLEX CM,CY,S1,S2,EP(-1:20),AP(0:20),                   ↑
     1 AM(20),BM(20),SINCY,COSCY,DENOM1,DENOM2                         ↑
C                                                                      ↑
C     S1,S2 SUM TERMS; EP, AP, AM, BM ARE MIE CONSTANTS                ↑
C     TO BE EVALUATED; SINCY AND COSCY ARE SIN AND COS TERMS;          ↑
C     DENOM1 AND DENOM2 HOLD DENOMINATOR ARGUMENTS                     ↑
C                                                                      ↑
      INTEGER NDIM
      DOUBLE PRECISION X(NDIM),PIE(0:20),T(0:20)                  (v)
C
C     PIE AND T HOLD RECURRENT MIE TERMS                               ↓
C                                                                      ↓
      COMMON/CONST/AG,CN,CK,PI                                         ↓
      COMMON/LIMITS/WV,ECC                                             ↓
      COMMON/Q/QEXT,TAU0                                               ↓
C                                                                      ↓
C     SET INTEGRAND INITIALLY TO ZERO                                  ↓
C                                                                      ↓
      F=1.0D-33                                                        ↓
      CM=DCMPLX(CN,-CK)                                                ↓
      CX=2.0D0*PI*AG/WV                                                ↓
      CY=CM*CX                                                         ↓
C                                                                      ↓
C     EVALUATE INITIAL MIE CONSTANTS                                   ↓
```

Fig. A.1.2. (Cont'd)

```
C                                                                    (v)
      SINCY=SIN(CY)                                                (cont'd)
      COSCY=COS(CY)                                                  ↓
      AP(0)=COSCY/SINCY                                              ↓
      EP(-1)=DCMPLX(DCOS(CX),-DSIN(CX))                              ↓
      EP(0)=DCMPLX(DSIN(CX),DCOS(CX))                                ↓
      PIE(0)=1.0D-6                                                  ↓
      T(0)=1.0D-6                                                    ↓
C                                                                    ↓
C--------------------------------------------------------------------
C                                                                    ↑
C     ZTEST DETERMINES WHETHER CURRENT Z POSITION IS WITHIN          ↑
C     THE REGION TO BE SUMMED OVER. IF NOT F = 0.                    ↑
C                                                                    ↑
      ZTEST=DABS(ECC*DSQRT(1.0D0-X(2)*X(2)-X(1)*X(1)))               ↑
      IF (DABS(X(3)).GT.ZTEST) THEN                                  ↑
      F=1.0D-33
      GOTO 90                                                      (vi)
      ENDIF
C                                                                    ↓
C     R = RADIUS VECTOR TO GRAIN                                     ↓
C                                                                    ↓
      R = DSQRT(X(1)*X(1)+X(2)*X(2)+X(3)*X(3))                       ↓
C                                                                    ↓
C--------------------------------------------------------------------
C                                                                    ↑
C     BETA = ANGLE OF INCIDENCE AND ALPHA = ANGLE OF SCATTER         ↑
C                                                                    ↑
      BETA=DATAN2(X(3),X(2))                                         ↑
      ALPHA=DACOS(X(1)/R)
      SUM1=1.0D-33                                                 (vii)
      SUM2=1.0D-33
C                                                                    ↓
C     HAVE (RE)SET SUMMATION CONSTS (TO EVALUATE THE SUM OF          ↓
C     THE MIE SCATTERING TERMS, S1 AND S2) TO ZERO                   ↓
C                                                                    ↓
C--------------------------------------------------------------------
C                                                                    ↑
C     N IS A COUNTER TO EVALUATE TERMS LESS THAN N = 2               ↑
C                                                                    ↑
      N = 0                                                          ↑
      PIE(1)=1.0D0                                                   ↑
      T(1)=DCOS(ALPHA)
      PIE(2)=3.0D0*DCOS(ALPHA)                                     (viii)
      T(2)=3.0D0*DCOS(2.0D0*ALPHA)
   20 IPOINT=1                                                       ↓
      N=N+1                                                          ↓
      IF (N.LT.3) GOTO 33                                            ↓
C                                                                    ↓
C     20 IS LABEL FOR SUMMATION LOOP. IF N.LT.3 GOTO 33              ↓
C                                                                    ↓
C--------------------------------------------------------------------
```

Fig. A.1.2. (Cont'd)

```
C     EVALUATE RECURRENT MIE TERMS AND START SUMMATION                  ↑
C                                                                       ↑
      PIE(N)=DCOS(ALPHA)*DBLE(2*N-1)*PIE(N-1)/DBLE(N-1)                 ↑
     1 - DBLE(N)*PIE(N-2)/DBLE(N-1)                                     ↑
      T(N)=DCOS(ALPHA)*(PIE(N)-PIE(N-2)) - DBLE(2*N-1)*                 ↑
     1 (DSIN(ALPHA))**2*PIE(N-1) + T(N-2)                               ↑
C                                                                       ↑
  33  IPOINT=1                                                          ↑
C                                                                       ↑
      EP(N)=(DBLE(2*N-1)/CX)*EP(N-1)-EP(N-2)                            ↑
      AP(N)=-DBLE(N)/CY + (1.0D0/(DBLE(N)/CY - AP(N-1)))                ↑
      DENOM1=( (AP(N)/CM + DBLE(N)/CX)*EP(N) - EP(N-1) )                ↑
      AM(N)=( (AP(N)/CM + DBLE(N)/CX)*DREAL(EP(N)) -
     1 DREAL(EP(N-1)) )/(DENOM1)                                        (ix)
      DENOM2=( (CM*AP(N) + DBLE(N)/CX)*EP(N) - EP(N-1) )
      BM(N)=( (CM*AP(N) + DBLE(N)/CX)*DREAL(EP(N)) -                    ↓
     1 DREAL(EP(N-1)) )/(DENOM2)                                        ↓
C                                                                       ↓
C     SET UP S1 AND S2 TERMS AND THEN EVALUATE SUMS                     ↓
C                                                                       ↓
      S1=DBLE(2*N+1)*(AM(N)*PIE(N)+BM(N)*T(N))/DBLE(N*(N+1))            ↓
      S2=DBLE(2*N+1)*(BM(N)*PIE(N)+AM(N)*T(N))/DBLE(N*(N+1))            ↓
      SUM1=SUM1+DBLE(S1)                                                ↓
      SUM2=SUM2+DBLE(S2)                                                ↓
      TEST1=DBLE(S1)/SUM1                                               ↓
      TEST2=DBLE(S2)/SUM2                                               ↓
C                                                                       ↓
C     CHECK FOR CONVERGENCE. GOTO 20 IF NOT CONVERGED                   ↓
C                                                                       ↓
      IF(DABS(TEST1).GT.1.0D-6 .AND. DABS(TEST2).GT.1.0D-6)GOTO 20      ↓
C                                                                       ↓
C-----------------------------------------------------------------------
C                                                                       ↑
C     EVALUATE INCIDENT AND EXIT OPTICAL DEPTHS TAU1 AND TAU2           ↑
C                                                                       ↑
      TAU1=TAU0*R                                                       ↑
      TAU2SQRD=(1.0D0 - X(2)*X(2) - X(3)*X(3)/ECC**2)                   ↑
      TAU2=TAU0*(DSQRT(TAU2SQRD) - X(1) )
C                                                                       (x)
C     EVALUATE IOTA TERMS AND ONE WHICH HOLDS (COS2BETA-SIN2BETA)
C                                                                       ↓
      OTA1=DABS(SUM1)**2                                                ↓
      OTA2=DABS(SUM2)**2                                                ↓
      ONE=(DCOS(BETA))**2 - (DSIN(BETA))**2                             ↓
      F = ONE*(OTA1 - OTA2)*DEXP(-TAU1-TAU2)/R**2                       ↓
  90  ICOORD=1                                                          ↓
C     HAVING EVALUATED F(X,Y,Z) NOW RETURN TO MAIN PROGRAM              ↓
      RETURN                                                            ↓
      END                                                               ↓
C-----------------------------------------------------------------------
```

Fig A.1.2. (Cont'd)

```
C     SUBROUTINE TO EVALUATE QEXT                                          ↑
C                                                                          ↑
      SUBROUTINE EXCOEFF(QEXT)                                             ↑
      IMPLICIT DOUBLE PRECISION(A-H,O-Z)                                   ↑
      DOUBLE COMPLEX CM,CY,S1,S2,EP(-1:40),AP(0:40),                       ↑
     1 DENOM1,DENOM2,SINCY,COSCY,AM(40),BM(40)                             ↑
      COMMON/CONST/AG,CN,CK,PI                                             ↑
      COMMON/LIMITS/WV,ECC                                                 ↑
      CM=DCMPLX(CN,-CK)                                                    ↑
      CX=2.0D0*PI*AG/WV                                                    ↑
      CY=CM*CX                                                             ↑
C                                                                          ↑
C     INITIALISE SUM (QSUM) AND EVALUATE MIE CONSTANTS                     ↑
      N=0                                                                  ↑
      QSUM=1.0D-33                                                         ↑
      SINCY=SIN(CY)                                                        ↑
      COSCY=COS(CY)                                                        ↑
      AP(0)=COSCY/SINCY                                                    ↑
      EP(-1)=DCMPLX(DCOS(CX),-DSIN(CX))                                    ↑
      EP(0)=DCMPLX(DSIN(CX),DCOS(CX))                                      ↑
   40 IPOINT=1                                                             ↑
      N=N+1
C                                                                         (xi)
C     LOOP ROUND TO LABEL 40 UNTIL SUM CONVERGES
C                                                                          ↓
      EP(N)=(DBLE(2*N-1)/CX)*EP(N-1)-EP(N-2)                               ↓
      AP(N)=-DBLE(N)/CY + (1.0D0/(DBLE(N)/CY - AP(N-1)))                   ↓
      DENOM1=( (AP(N)/CM + DBLE(N)/CX)*EP(N) - EP(N-1) )                   ↓
      AM(N)=( (AP(N)/CM + DBLE(N)/CX)*DREAL(EP(N)) -                       ↓
     1 DREAL(EP(N-1)) )/(DENOM1)                                           ↓
      DENOM2=( (CM*AP(N) + DBLE(N)/CX)*EP(N) - EP(N-1) )                   ↓
      BM(N)=( (CM*AP(N) + DBLE(N)/CX)*DREAL(EP(N)) -                       ↓
     1 DREAL(EP(N-1)) )/(DENOM2)                                           ↓
C                                                                          ↓
      Q = DBLE(2*N+1)*DREAL(AM(N)+BM(N))                                   ↓
      QSUM=QSUM+Q                                                          ↓
C                                                                          ↓
C     TEST FOR CONVERGENCE                                                 ↓
C                                                                          ↓
      QTEST=Q/QSUM                                                         ↓
      IF (DABS(QTEST).GT.1.0D-6) GOTO 40                                   ↓
C                                                                          ↓
C     EVALUATE QEXT AND THEN RETURN TO MAIN PROGRAM                        ↓
C                                                                          ↓
      QEXT=2.0D0*QSUM/CX**2                                                ↓
      RETURN                                                               ↓
      END                                                                  ↓
C                                                                          ↓
C-------------------------------------------------------------------------
```

Appendix 2. Observations of the unusual star XX Oph.

A.2.1. Introduction.

XX Oph is a bright, variable (8.59 < V < 10.2 mag., Kholopov et al., 1987) B0IIIe (Lockwood et al., 1975) shell star which lies near the obscured ρ Oph region. The near-IR spectrum of XX Oph contains strong CO, VO and TiO bands which point to the presence of a cool M6 giant or supergiant companion star which is reddened by an $A_v \simeq 4$ mag. (Lockwood et al., 1975). Some of the other unusual features of this star will now be outlined.

The B-type optical spectrum is rich in narrow emission lines, which are predominantly lines of singly ionised metals, e.g. TiII and FeII (hence the nickname of XX Oph: the "iron star"). The intensities of many of these lines are enhanced (relative to other multiplets) with respect to the expected laboratory *gf* values.

The wide hydrogen line profiles are strongly variable and often exhibit blue-displaced absorption features (although redshifted lines are also observed), suggestive of a strong, variable stellar wind. The extent of the blueshifted features (up to 5Å in some cases) indicates very high velocities ($\simeq$ 400 kms^{-1}) in the wind. Merril (1961) indicates that the required rapid accelerating force must be proportional to the velocity, and proposes that radiation pressure from strong Lyα emission may well be the likely acceleration mechanism.

The optical lightcurve of XX Oph is symbiotic in nature; the variations are irregular, with occasional deep ($\Delta V \simeq 1$ mag.), persistent minima occurring. Although recurrent novae and symbiotics

can exhibit TiO bands at such minima, XX Oph shows neither the large optical light variations nor the high-excitation nebular lines that are characteristic features of such stars.

The combination of a hot and cool binary stellar system with a symbiotic-type lightcurve and rich emission spectrum, may suggest that XX Oph is a VV Cephei or Mira variable. But in both these types of star, the M star dominates the optical light output from the system, which is not the case for XX Oph.

A.2.2. The Optical and Infrared Spectra.

Non-simultaneous optical (from SAAO) and IR (from CTIO) spectra of XX Oph were obtained in 1987. The optical spectrum, with identified strong lines, is shown in Fig. A.2.1. The IR spectra are displayed in Fig. A.2.2: unfortunately, due to problems with the stepping motor (see Section 3.3.3), only the J spectrum is of good quality. The Paβ 1.282μm line was not evident in absorption (the 1.28μm emission feature in the figure is an artefact of the reduction process, see Section 3.3.3) - thus the cool companion evidently dominates the IR continuum, although the spectra did not cover any strong molecular bands expected (particularly around ≃ 0.8μm) from the companion.

Many lines, both in absorption and emission, were observed in the optical spectrum; because of the low resolution ($\Delta\lambda \simeq 2.8$Å), many of the lines form blends, but most of the lines observed by Merril (1961) were clearly present.

The predominant lines observed are lines of singly ionised metals, which form many emission and absorption features, including some wide p Cygni features, although the resolution is not adequate to resolve

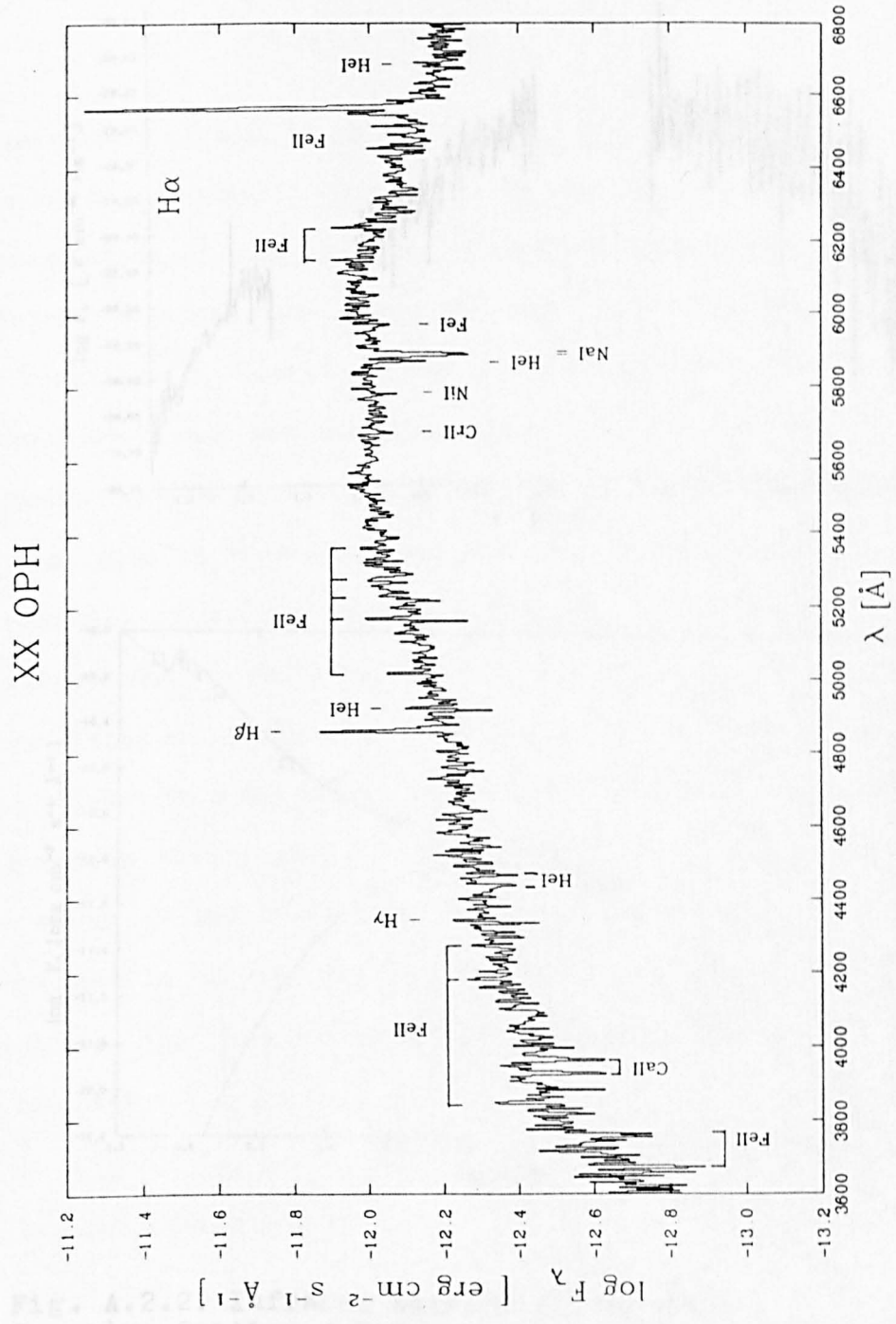

Fig. A.2.1. Optical spectrum of XX Oph.
See also Section A.2.2.

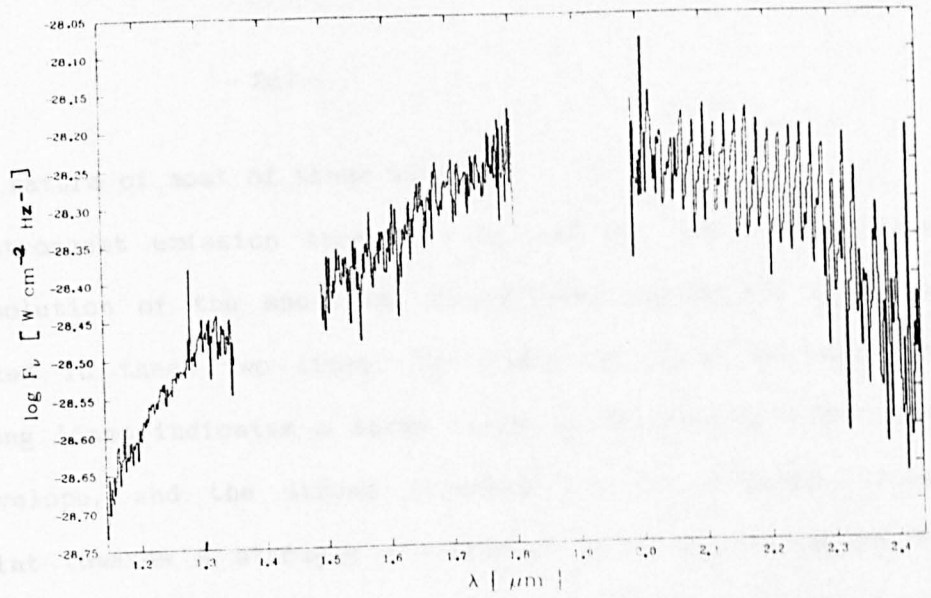

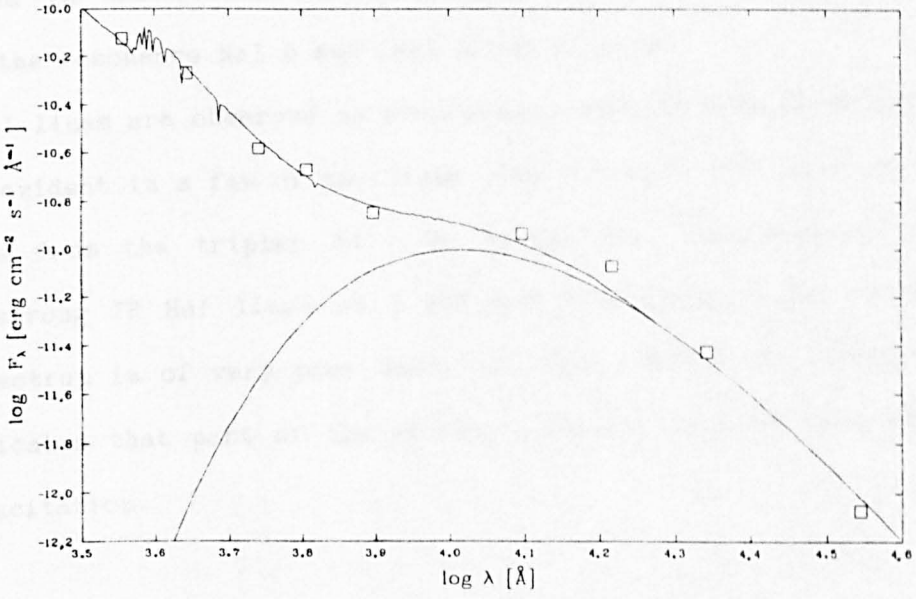

Fig. A.2.2. Infrared spectra of XX Oph. See also Section A.2.2.

Fig. A.2.3. The flux distribution of XX Oph. See also Section A.2.3.

the P Cygni nature of most of these lines.

The strongest emission lines are Hα and Hβ, and even at the limited resolution of the spectrum, blueshifted absorption features are indicated in these two lines. The width of these (as well as other) strong lines indicates a large range in velocities within the stellar envelope, and the strong blueshift in the stronger lines clearly point towards a strongly accelerated outflow. The weaker Hγ and Hδ lines also have emission and absorption components, with the other lines in the series in absorption. The strongest absorption lines are the resonance NaI D and CaII K and H lines.

Many HeI lines are observed in absorption, with perhaps an emission component evident in a few of the lines. The strongest HeI line is the 5875Å line from the triplet 3d - 2p transition. Unfortunately the expected strong IR HeI lines at 1.083 and 2.058μm were not covered (the K spectrum is of very poor quality). The presence of strong HeI lines indicates that part of the stellar envelope must be in a state of high excitation.

A.2.3. The Flux Distribution.

Lockwood et al. (1975) indicate that the reddening correction required to correctly interpret the inferred spectral types of the (optical) primary (B0III) and the (IR) secondary (M6III) components is A_V = 4.0 mag. This correction was applied, adopting a normal IS extinction law, and a good fit to the photometric data obtained at SAAO (1981 - 1984: Kilkenny et al., 1985; and in 1987) at each epoch was obtained with a T_{eff} = 20000K, log g = 4.0 Kurucz (1979) model atmosphere representing the primary component, and a 2800K blackbody

representing the secondary component. No subsequent IR excess out to 3.5μm is found (see Fig. A.2.3; photometry obtained on HJD 2445422).

The normalisation obtained in fitting the data gives $R_*/D \simeq 16$ $R_\odot kpc^{-1}$ for XX Oph. The expected radius of a normal B0III star is 16 $R_\odot$ (Allen 1973), which suggests that a distance estimate of ≃ 1 kpc for XX Oph would be appropriate. The corresponding radius estimate of the M6 companion, at a distance of 1 kpc would be 530 $R_\odot$, which is more appropriate for a M5I-II star (Allen 1973).

If a radius of 16 $R_\odot$ is assumed, then the inferred luminosity of XX Oph, assuming hydrostatic equilibrium and T_{eff} = 20000K, is 3.7 x 10^4 $L_\odot$. The luminosity of the M6 companion is estimated from the peak in λF_λ to be 5.1 x 10^{-3} $L_\odot$ at a distance of 1 kpc.

Although there are regions of significant extinction in Sco-Oph (Rossano 1978b), given that the distance to XX Oph is probably only ≃ 1 kpc, and yet XX Oph suffers 4 mag. of visual extinction, it would seem likely that XX Oph may also suffer from significant circumstellar extinction. That no significant near-IR excess nor far-IR excess (no co-incident IRAS source was found for XX Oph in the IRAS PSC; Beichman et al., 1985) is evident for XX Oph, would indicate that any circumstellar dust must be located far from the star.

A.2.4. The Light and Colour variation.

In the period 1981 - 1984 covered by the observations of Kilkenny et al. (1985), XX Oph only varied from V = 8.87 - 9.09 mag., and (B-V) = 0.97 - 1.14. No periodic variations in their dataset could be discerned. The observed variation in V, B-V is shown in Fig. A.2.4, and it is seen that XX Oph can appear blue (B-V ≳ 1.04) both when

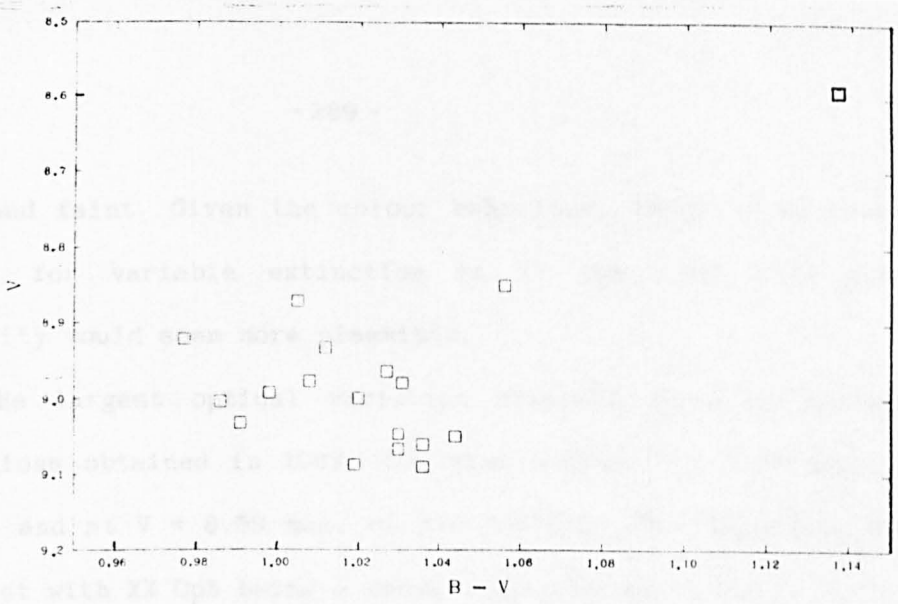

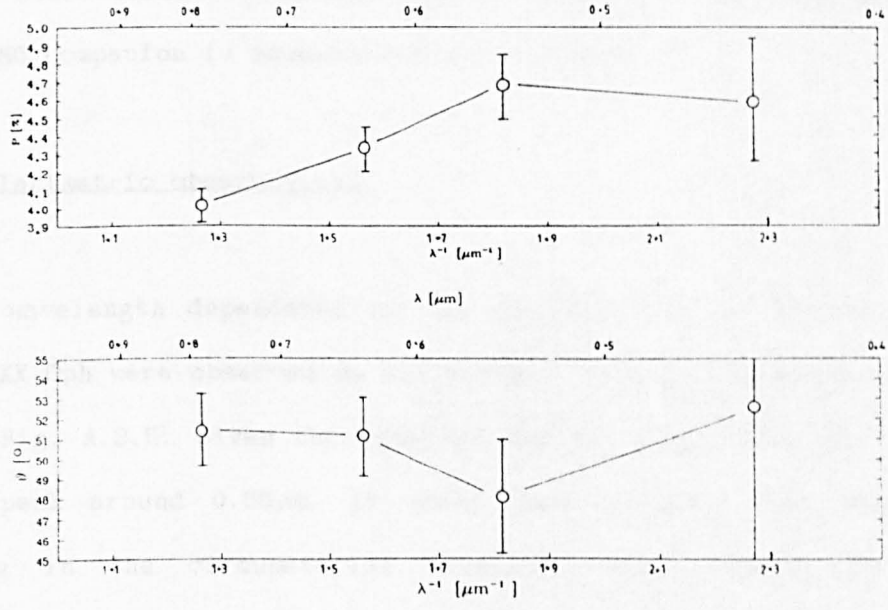

Fig. A.2.4. V, B-V variations of XX Oph. See also Section A.2.4.

Fig. A.2.5. The polarisation and position angle of polarisation with wavelength for XX Oph. See also Section A.2.5.

bright and faint. Given the colour behaviour, there is no convincing evidence for variable extinction in XX Oph, and thus intrinsic variability would seem more plausible.

The largest optical variation observed occurred between two observations obtained in 1987. The star was at V = 8.85 mag. on HJD 2446998, and at V = 8.59 mag. on HJD 2447044. This behaviour at V is consistent with XX Oph being a known long-term variable.

The near-IR emission at J, H and K (predominantly from the M6 companion star) varied by no more than 0.07 mag. in the observations, i.e. the M6 companion is essentially non-variable.

A.2.5. Polarimetric observations.

The wavelength dependence of the polarisation and the position angle of XX Oph were observed on HJD 2447044, and the observations are shown in Fig. A.2.5. Given the observed degree of polarisation ($\simeq$ 4%) and the peak around 0.55μm, it would seem unlikely that Rayleigh scattering in the circumstellar envelope could account for the polarisation. Instead, scattering by dust grains in an optically thick dust shell is favoured. The observed wavelength dependence indicates scattering by possibly $\simeq$ 0.10μm graphite grains or $\simeq$ 0.14μm dielectric (ice or silicate) grains. It is not known whether the polarisation of XX Oph is variable, and thus the possibility of scattering by ice grains cannot be ruled out.

A.2.6. Summary and Conclusions.

Photometric observations confirm XX Oph as a distant (≃ 1 kpc) binary system which is heavily reddened ($A_V \simeq 4$ mag.). The observed optical fluxes would be consistent with emission from a reddened B0III star, and near-IR emission from a reddened M6II-III star. The optical photometric variability would be more consistent with intrinsic variability of XX Oph, although there is no indication of variability in the M6 companion. The optical spectrum observed indicates the highly excited nature of the stellar envelope, and in view of the profiles of the stronger lines, significant mass loss from XX Oph is also likely. In view of the lack of any evidence for IR emission from dust, the high extinction and the observed wavelength dependence of polarisation of XX Oph, it is suggested that the 3μm ice absorption feature should be looked for.

List of Publications.

Hutchinson, M.G., Evans, A., Davies, J.K., Bode., M.F., Whittet, D.C.B. & Kilkenny, D., 1987, In: *Circumstellar Matter*, IAU Symp. 122, 102. Eds. I. Appenzeller & C. Jordan, D. Reidel, Dordrecht.

Catchpole, R.M., Whitelock, P.A., Feast, M.W., Menzies, J.W., Glass, I.S., Marang, F., Laing, J.D., Spencer Jones, J.H., Roberts, G., Balona, L.A., Carter, B.S., Laney, C.D., Lloyd Evans, T., Sekiguchi, K., Hutchinson, M.G., Maddison, R., Albinson, J.S., Evans, A., Allen, D.A., Winkler, H., Fairall, A., Corbally, C., Davies, J.K. & Parker, A., 1987, *Mon. Not. R. astr. Soc.*, **231**, 75P.

Hutchinson M.G., Evans, A., Davies, J.K. & Bode, M.F., 1989, *Mon. Not. R. astr. Soc.*, **237**, 683.

List of References.

Abuladze, O.A., et al., 1975, *Perem. Zvezdy*, **20**, 47.

Adams, F.C., Lada, C.J. & Shu, F.H., 1987, *Astrophys. J.*, **312**, 788.

Adams, F.C. & Shu, F.H., 1985, *Astrophys. J.*, **296**, 655.

Adams, F.C. & Shu, F.H., 1986, *Astrophys. J.*, **308**, 836.

Allen, C.W., 1973, *Astrophys. Quantities*, Athalone Press.

Ambartsumian, V.A., 1947, *Stellar Evolution & Astrophys.*, Acad. Sci. Armenian SSR.

Andersen, J., Gahm, G.F. & Krelowski, J., 1982, *Astron. Astrophys.*, **113**, 176.

Appenzeller, I., 1983, *Rev. Mexicana Astron. Astrophys.*, **7**, 151.

Appenzeller, I., Chavarria, C. & Krautter, J., 1980, *Astron. Astrophys.*, **90**, 184.

Appenzeller, I. & Dearborn, D.S.P., 1984, *Astrophys. J.*, **278**, 689.

Appenzeller, I., Jankovics, I. & Jetter, R., 1986, *Astron. Astrophys. Supp. Ser.*, **64**, 65.

Appenzeller, I., Jankovics, I. & Krautter, J., 1983, *Astron. Astrophys. Supp. Ser.*, **53**, 291.

Appenzeller, I. & Wolf, B., 1977, *Astron. Astrophys.*, **54**, 163.

Astronomical Almanac, 1987, Eds. C.K. Roberts & A. Boksenberg, HMSO.

Bailey, M.E., 1987, *Icarus*, **69**, 70.

Barrett, P., 1987, Private communication.

Bastien, P., 1981, *Astron. Astrophys.*, **94**, 294.

Bastien, P., 1982, *Astron. Astrophys. Supp. Ser.*, **48**, 153.

Bastien, P., 1985, *Astrophys. J. Supp. Ser.*, **59**, 277.

Bastien, P., 1986, Private communication.

Bastien, P., 1987, Review paper presented at the Vatican Conference

Polarised Radiation of Circumstellar Origin.

Bastien, P. & Landstreet, J.D., 1979, *Astrophys. J. Lett.*, **299**, L137.

Beckwith, S., Zuckerman, B., Skruskie, M.F. & Dyck, H.M., 1984, *Astrophys. J.*, **287**, 793.

Beichman, C.A., Neugebauer, G., Habing, H.J., Clegg., P.E. & Chester, T.J., 1985, *IRAS Point Source Catalogue*, JPL-D-1855.

Bertout, C., Carrasco, L., Mundt, R. & Wolf, B., 1982, *Astron. Astrophys. Supp. Ser.*, **47**, 419.

Bessel, M.S. & Eggen, O.J., 1972, *Astrophys. J.*, **177**, 209.

Bieging, J.H., Cohen, M. & Schwartz, P.R., 1984, *Astrophys. J.*, **282**, 699.

Bisnovatyi-Kogan, G.S. & Lamzin, S.A., 1977, *Sov. Astron.*, **21**, 720.

Boesgaard, A.M., 1984, *Astron. J.*, **89**, 1635.

Bopp, B.W. & Noah, P.V., 1980, *Publ. Astron. Soc. Pac.*, **92**, 717.

Bouvier, J. & Bertout, C., 1986, In: *Cool Stars, Stellar Systems, and the Sun*, Lecture notes in Physics, **254**, 132.
Eds. M. Zelik & D. M. Gibson, Springer-Verlag, Heidelberg.

Bouvier, J., Bertout, C., Benz, W. & Mayor, M., 1986b, *Astron. Astrophys.*, **166**, 110.

Bouvier, J., Bertout, C. & Bouchet, P., 1986a, *Astron. Astrophys.*, **158**, 149.

Breger, M., 1974, *Astrophys. J.*, **188**, 53.

Brown, A., 1987a, In: *Circumstellar Matter*, IAU Symp. 122, 63.
Eds. I. Appenzeller & C. Jordan, D. Reidel, Dordrecht.

Brown, A., 1987b, *Astrophys. J. Lett.*, **322**, L31.

Brown, A., Penston, M.V., Johnstone, R.M., Jordan, C., Kuin, N.P.M., Lago, M.T.V.T., Gross, B. & Linsky, J.L., 1984, In: *Future of UV Astron.*, 388. NASA CP-2349.

Burke, J.R. & Silk, J., 1976, *Astrophys. J.*, **210**, 341.

Busko, I.C. & Torres, C.A.O., 1978, *Astron. Astrophys.*, **64**, 153.

Byrne, P.B., 1985, *Irish Astron. J.*, **17**, 3.

Calvet, N., Basri, G. & Kuhi, L.V., 1984, *Astrophys. J.*, **277**, 725.

Canto, J., 1983, *Rev. Mexicana Astron. Astrophys.*, **7**, 109.

Cassinelli, J.P. & Lamers, H.J.G.L.M., 1987, In: *Exploring the Universe with IUE*, 139. Ed. Y. Kondo, D. Reidel, Dordrecht.

Catala, C., 1988, *Astron. Astrophys.*, **193**, 222.

Catala, C., Kunasz, P.B. & Praderie, F., 1984, *Astron. Astrophys.*, **134**, 402.

Catala, C., Praderie, F. & Felenbok, P., 1986, In: *New Insights into Astrophysics: 8 Years of IUE.*, 125. ESA SP-263.

Catchpole, R.M. et al., 1987, *Mon. Not. R. astr. Soc.*, **231**, 75P.

CTIO List of Spectroscopic and Photometric Standards.

CTIO IR Spectrometer Users Manual 1986, Ed. B. Gregory.

Chevalier, R.A., 1983, *Astrophys. J.*, **268**, 753.

Cohen, M., 1982, *Publ. Astron. Soc. Pac.*, **94**, 266.

Cohen, M., 1983, *Astrophys. J. Lett.*, **270**, L69.

Cohen, M. & Kuhi, L.V., 1979, *Astrophys. J. Supp. Ser.*, **41**, 743.

Cohen, M. & Witteborn, F.C., 1985, *Astrophys. J.*, **249**, 245.

Cram, L.E., 1979, *Astrophys. J.*, **234**, 949.

Cram, L.E., Giampapa, M.S. & Imhoff, C.L., 1980, *Astrophys. J.*, **238**, 905.

Cudworth, K.M. & Herbig, G.H., 1979, *Astron. J.*, **84**, 548.

Daniel, J.Y., 1980, *Astron. Astrophys.*, **87**, 204.

DeCampli, W.M., 1981, *Astrophys. J.*, **244**, 124.

Dijab, E.A. & Esipov, V.F., 1968, In: *Non-Periodic Phenom. in*

Var. Stars, 107. Ed. L. Detre, Acad. Budapest.

Eaton, J.A. & Hall, D.S., 1979, *Astrophys. J.*, **227**, 907.

Edwards, S. & Snell, R.L., 1982, *Astrophys. J.*, **261**, 151.

Edwards, S., Cabrit, S., Strom, S.E., Heyer, I., Strom, K.M. & Anderson, E., 1987, *Astrophys. J.*, **321**, 473.

Efimov, Yu. S., 1980, *Perem. Zvezdy.*, **21**, 273.

Elias, J., 1978, *Astrophys. J.*, **224**, 483.

Evans, A., 1981, *Astrophysics and Space Science*, **74**, 235.

Evans, A., 1988, Private communication.

Evans, A., Bode, M.F., Whittet, D.C.B., Davies, J.K., Kilkenny, D. & Baines, D.W.T., 1982, *Mon. Not. R. astr. Soc.*, **199**, 37P.

Evans, A., Davies, J.K., Kilkenny, D. & Bode, M.F., 1989, *Mon. Not. R. astr. Soc.*, **237**, 695.

Feigelson, E.D., 1983, In: *Cool Stars, Stellar Systems and the Sun*, Third Cambridge Workshop, 27. Eds. S.L. Baliunas & L. Hartmann, Springer-Verlag, Heidelberg.

Feigelson, E.D. & DeCampli, W.M., 1981, *Astrophys. J.*, **243**, 289.

Felli, M. & Panagia, N., 1981, *Astron. Astrophys.*, **102**, 424.

Finkenzeller, U., 1985, *Astron. Astrophys.*, **151**, 340.

Finkenzeller, U. & Mundt, R., 1984, *Astron. Astrophys. Supp. Ser.*, **55**, 109.

Gahm, G.F., 1980, *Astrophys. J. Lett.*, **242**, L163.

Gahm, G.F., 1981, unpublished.

Gahm, G.F., 1986, In: *Flares, Solar and Stellar*, 124. Ed. P.M. Gondhalekar, R.A.L. Publ.

Gahm, G.F., Fredga, K., Liseau, R. & Dravins, D., 1979, *Astron. Astrophys. Lett.*, **73**, L4.

Gahm, G.F. & Greenberg, J.M., 1984, In: *Asteroids, Comets, and Meteors*, 375. Eds. C-I. Lagerqvist & H. Rickman, Uppsala Univ. Publ.

Gahm, G.F. & Krautter, J., 1982, *Astron. Astrophys.*, **106**, 25.

Gahm, G.F., Lago, M.T.V.T. & Penston, M.V., 1981, *Mon. Not. R. astr. Soc.*, **195**, 59P.

Gahm, G.F., Nordh, H.L. & Olofsson, S.G., 1975, *Icarus*, **24**, 372.

Gahm, G.F., Nordh, H.L., Olofsson, S.G. & Carlborg, N.C.J., 1974, *Astron. Astrophys.*, **33**, 399.

Gaposchkin, S. & Greenstein, J.L., 1936, *Harvard Obs. Bull.*, **904**, 8.

Garrison, L.M. & Anderson, C.M., 1978, *Astrophys. J.*, **221**, 601.

Geisel, S.L., 1970, *Astrophys. J. Lett.*, **161**, L105.

Gezari, D.Y., Schmitz, M. & Mead, J.M., 1984, NASA Tech. Mem. 83819.

Giampapa, M.S., 1983, In: *Cool Stars, Stellar Systems and the Sun*, Third Cambridge Workshop, 14. Eds. S.L. Baliunas & L. Hartmann, Springer-Verlag, Heidelberg.

Giovannelli, F, Vittone, A.A., Rossi, C., Nastari, I., Bisnovatyi-Kogan, G.S, Golynskaya, I.M., Kurt, V.G., Mizyakina, T.A., Shafer, E., Shamolin, V.M., Sheffer, E.K., Smirnoff, A.S., Lamzin, S.A., Larinov, M.G. & Sidorenko, V.N., 1986, 95. In: *New Insights in Astrophysics*, ESA SP-263.

Golay, M., 1974, *Astronomical Photometry*, D. Reidel, Dordrecht.

Goodrich, R.W., 1987, *Publ. Astron. Soc. Pac.*, **99**, 116.

Graham, J.A. & Phillips, A.C., 1987, *Publ. Astron. Soc. Pac.*, **99**, 91.

Grasdalen, G.L., 1977, In: *Proc. IAU Coll. 42*, 25.

Grasdalen, G.L., Strom, S.E., Strom, K.E., Capps, R.W., Thompson, D. & Castelaz, M., 1984, *Astrophys. J.*, **261**, 151.

Hartigan, P. & Graham, J.A., 1987, *Astron. J.*, **93**, 913.

Hartigan, P. & Lada, C.J., 1985, *Astrophys. J.*, **59**, 383.

Hartmann, L. & Kenyon, S.J., 1985, *Astrophys. J.*, **299**, 462.

Hartmann, L., Hewett, R., Stahler, S. & Mathieu, R., 1986, *Astrophys. J.*, **309**, 275.

Hecht, J.H., Holm, A.V., Ake III,T.B., Imhoff, C.L., Oliversen, N.A. & Sonneborn, G., 1984, 318. In: *Future of UV Astronomy*, NASA CP-2349.

Heck, A., 1987, In: *Exploring the Universe with IUE*, 121. Ed. Y. Kondo, D. Reidel, Dordrecht.

Heck, A., Egret, D., Jaschek, M. & Jaschek, C., 1984, *IUE low dispersion Spectral Reference Atlas:Part I Normal Stars*, ESA Publ.

Heneize, K.G., 1976, *Astrophys. J. Supp.*, **30**, 491.

Herbig, G.H., 1958, *Mem. Soc. Roy. Sci. Liege*, 4th Ser., **18**, 251

Herbig, G.H., 1960, *Astrophys. J. Supp. Ser.*, **4**, 337.

Herbig, G.H., 1961, *Astrophys. J.*, **133**, 337.

Herbig. G.H., 1962, *Ann. Rev. Astron. Astrophys.*, **1**, 47.

Herbig, G.H., 1970, *Mem. Soc. R. Sci. Liege*, **19**, 13.

Herbig, G.H., 1977a, *Astrophys. J.*, **214**, 747.

Herbig, G.H., 1977b, *Astrophys. J.*, **217**, 693.

Herbig, G.H. & Rao, N.K., 1972, *Astrophys. J.*, **174**, 401.

Herbig, G.H. & Soderblom, D.R., 1980, *Astrophys. J.*, **242**, 628.

Herbig, G.H., Vrba, F.J. & Rydgren, A.E., 1986, *Astron. J.*, **91**, 575.

Herbst, W., 1986, *Publ. Astron. Soc. Pac.*, **98**, 1088.

Herbst, W., Holtzmann, J.A. & Klasky, R.S., 1983, *Astron. J.*, **88**,1648.

Herbst, W., Holtzmann, J.A. & Phelps, B.E., 1982, *Astron. J.*, **87**,1710.

Herbst, W. & Stine, P.C., 1984, *Astron. J.*, **89**, 1716.

Hoffmeister, C., 1958, *Veroff. Stern. Sonn.*, **3**, 333.

Hoffmeister, C., 1965, *Veroff. Stern. Sonn.*, **6**, 97.

Hough, J.H., Bailey, J., Cunningham, E.C. & McCall, A., 1981, *Mon. Not. R. astr. Soc.*, **195**, 429.

Hsu, J-C. & Breger, M., 1982, *Astrophys. J.*, **262**, 732.

Hulst, H.C. van de, 1957, *Light Scattering by Small Particles*, Wiley, New York.

Hunger, K. & Kron, G. E., 1957, *Publ. Astron. Soc. Pac.*, **96**, 347.

Hutchinson, M.G., Evans, A., Davies, J.K., Bode., M.F., Whittet, D.C.B. & Kilkenny, D., 1987, In: *Circumstellar Matter*, IAU Symp. 122, 109. Eds. I. Appenzeller & C. Jordan, D. Reidel, Dordrecht.

Hutchinson M.G., Evans, A., Davies, J.K. & Bode, M.F., 1989, *Mon. Not. R. astr. Soc.*, **237**, 683.

Imhoff, C. & Appenzeller, I., 1987, In: *Scientific Accomplishments of the IUE.*, 295. Ed. Y. Kondo, D. Reidel, Dordrecht.

Imhoff, C.L. & Mendoza V, E.E., 1974, *Rev. Mexicana Astron. Astrophys.*, **1**, 25.

IUE Notes for Applicants, 1988, ESA Publ.

Johnson, H.L., 1966, *Ann. Rev. Astr. Astrophys.*, **4**, 193.

Johnstone, R.M. & Penston, M.V., 1986, *Mon. Not. R. astr. Soc.*, **219**, 927.

Johnstone, R.M. & Penston, M.V., 1987, *Mon. Not. R. astr. Soc.*, **227**, 797.

Joy, A.H., 1945, *Astrophys. J.*, **102**, 193.

Kaifu, N., 1987, In: *Star Forming Regions*, IAU Symp. 115, 275.

Kenyon S.J. & Hartmann, L., 1988, *Astrophys. J.*, in press.

Kilkenny, D., Whittet, D.C.B., Davies, J.K., Evans, A., Robinson, E.I. & Banfield, R.M., 1985, *South African Astr. Obs. Circ.*, No. 9, 55.

Kholopov, P.N., et al., 1987, *General Catalogue of Variable Stars*, Fourth Edition. General Editor P.N. Kholopv.

Knacke, R.F., Strom, S.E., Strom, K.M., Young, Y. & Kunkel, W., 1973, *Astrophys. J.*, **179**, 847.

Kuhi, L.V., 1964, *Astrophys. J.*, **140**, 1409.

Kukarkin, B.V., et al., 1969, *General Catalogue of Variable Stars*, Third Edition. General Editor B.V. Kukarkin.

Kuin, N.P.M., 1986, In: *Cool Stars, Stellar Systems & the Sun*, Lecture notes in Physics, **254**, 466.
Eds. D. Zelik & D.M. Gibson, Springer-Verlag, Heidelberg.

Kurucz, R.L., 1979, *Astrophys. J. Supp.*, **40**, 1.

Kurucz, R.L. & Peytremann, E., 1975, *SAO Special Report* No. 362.

Lada, C.J., 1985, *Ann. Rev. Astron. Astrophys.*, **23**, 267.

Lago, M.T.V.T., 1982, *Mon. Not. R. astr. Soc.*, **198**, 445.

Lago, M.T.V.T., 1984, *Mon. Not. R. astr. Soc.*, **210**, 232.

Lago, M.T.V.T. & Penston, M.V., 1982, *Mon. Not. R. astr. Soc.*, **198**, 429.

Larson, R.B., 1980, *Mon. Not. R. astr. Soc.*, **190**, 321.

Levreault, R.M., 1984, unpublished.

Liseau, R., Lindroos, K.P. & Fischerstrom, C., 1987, *Astron. Astrophys.*, **183**, 274.

Lockwood, G.W., Dyck, H.M. & Ridgway, S.T., 1975, *Astrophys. J.*, **195**, 385.

Loren, R.B., 1975, Ph.D. Thesis.

Loren, R.B., 1979, *Astrophys. J.*, **227**, 832.

Marraco, H.G. & Rydgren, A.E., 1981, *Astron. J.*, **86**, 62.

Massachusetts Institute of Technology Wavelength Tables, 1969, Ed. G.R. Harrison.

Mayes, A. 1983, Ph. D. Thesis, University of Keele.

McCall, A. & Hough, J.H., 1980, *Astron. Astrophys. Supp.*, **42**, 141.

Mendoza V, E.E., 1968, *Astrophys. J.*, **151**, 977.

Mendoza V, E.E., Jaschek, M. & Jaschek, C., 1969, *Bol. Obs. Tonantzintla Tacubaya*, **5**, 107.

Merril, P.W., 1961, *Astrophys. J.*, **133**, 503.

Mestel, L. & Spitzer, L. 1956, *Mon. Not. R. astr. Soc.*, **187**, 337.

Montmerle, T., Koch-Miramond, L., Falgarone, E. & Grindlay, J., 1983, *Astrophys. J.*, **269**, 182.

Moore, C.E., 1972, *A Multiplet Table of Astrophysical Interest*, NBRDS - NBS (US) No. 40.

Moore, C.E. & Merril, P.W., 1968, NSRDS - NBS (US) No. 23.

Mould, J.R., Hall, D.N.B., Ridgway, S.T., Hintzen, P. & Aaronson, M., 1978, *Astrophys. J. Lett.*, 222, L123.

Mullan, D.J., 1975, *Astrophys. J.*, **200**, 641.

Mundt, R., 1984, *Astrophys. J.*, **280**, 749.

Mundt, R. & Fried, J.W., 1983, *Astrophys. J. Lett.*, **274**, L83.

Nadeau, R. & Bastien, P., 1986, *Astrophys. J. Lett.*, **307**, L5.

Nakano, T., 1987, *Mon. Not. R. astr. Soc.*, **224**, 107.

Osterbrock, D.E., 1974, *Astrophysics of Gaseous Nebulae*, Freeman and Co., New York.

Panagia, N. & Felli, M., 1975, *Astron. Astrophys.*, **39**, 1.

Parenago, P., 1954, *Publ. Sternberg Astr. Inst.*, No. 25.

Petersen, J.O. & Jørgensen, H.E., 1972, *Astron. Astrophys.*, 17, 367.

Petrov, P. & Shcherbackov, A., 1976, In: *Stars and Galaxies*, 163. Ed. E.K. Kharadze, Tbilisi: Abastumani Astrophys. Obs.

Plagemann, S., 1969, *Mem. Soc. R. Sci. Liege*, **19**, 331.

Poeckert, R. & Marlborough, J.M., 1978, *Astrophys. J.*, **220**, 940.

Pogodin, M.A., 1985, *Astron. Zh.*, **62**, 918.

Reza, R. de la, Quast, G., Torres, C.A.O., Mayor, M., Meylan, G. & Llorente de Andres, F., 1986, In: *New Insights in Astrophysics*, 107. ESA SP263.

Ridgway, S., 1984, In: *Galactic and Extragalactic Infrared Spectroscopy*, 309. Eds. M.K. Kessler & J.B. Phillips, D. Reidel, Dordrecht.

Rossano, G.S., 1978a, *Astron. J.*, **83**, 234.

Rossano, G.S., 1978b, *Astron. J.*, **83**, 241.

Rucinski, S.M., 1985, *Astron. J.*, **90**, 2321.

Rucinski, S.M. & Krautter, J., 1983, *Astron. Astrophys.*, **121**, 219.

Rydgren, A.E., 1977, *Publ. Astron. Soc. Pac.*, **89**, 557.

Rydgren, A.E., Schmelz, J.T. & Vrba, F.J., 1982, *Astrophys. J.*, **256**, 168.

Rydgren, A.E., Strom, S.E. & Strom, K.M., 1976, *Astrophys. J. Supp. Ser.*, **30**, 307.

Rydgren, A.E. & Zak, D.S., 1987, *Publ. Astron. Soc. Pac.*, **99**, 141.

Sargent, A.I. & Beckwith, S., 1987, *Astrophys. J.*, **323**, 294.

Savage, B.D. & Mathis, J.S., 1979, *Ann. Rev. Astron. Astrophys.*, **17**, 73.

Scargle, J.D., 1982, *Astrophys. J.*, **263**, 835.

Schaefer, B.E., 1983, *Astrophys. J. Lett.*, **266**, L45.

Schmelz, J.T., 1984, *Astron. J.*, **89**, 108.

Schulte-Ladbeck, R., 1983, *Astron. Astrophys.*, **120**, 203.

Schwartz, R.D. & Heuermann, R.W., 1981, *Astron. J.*, **86**, 1526.

Serkowski, K., 1969a, *Astrophys. J. Lett.*, **156**, L55.

Serkowski, K., 1969b, *Astrophys. J. Lett.*, **158**, L107.

Serkowski, K., 1970, *Astrophys. J.*, **160**, 1083.

Serkowski, K., Mathewson, D.S. & Ford, V., 1975, *Astrophys. J.*,

196, 261.

Shawl, S.J., 1975, *Astron. J.*, **80**, 595.

Shu, F.C. & Adams, F.C., 1987, In: *Circumstellar Matter*, IAU Symp. 122, 7. Eds. I. Appenzeller & C. Jordan, D. Reidel, Dordrecht.

Skumanich, A., 1972, *Astrophys. J.*, **171**, 565.

Smith, B.A. & Terrile, R.J., 1984, *Science*, **226**, 1421.

Snow, T.P. & Stalio, R., 1987, In: *Exploring the Universe with IUE*, 183. Ed. Y. Kondo, D. Reidel, Dordrecht.

SAAO IR Photometers Tech. Ed., 1980, Ed. I.S. Glass.

Stickland, D.J., 1980, *ESA IUE Newsletter* No. 5, 30.

Strom, S.E., 1983, *Rev. Mex. Astron. Astrophys.*, **7**, 201.

Taylor, K.N.R. & Storey, J.W.V., 1984, *Mon. Not. R. astr. Soc.*, **209**, 5P.

Thé, P.S., 1962, *Contrib. Bosscha Obs.*, No. 15.

Thé, P.S. & Dawanas, D.N, 1987, In: *Circumstellar Matter*, IAU Symp. 122, 99. Eds. I. Appenzeller & C. Jordan, D. Reidel, Dordrecht.

Thé, P.S. & Tjin A Djie, H.R.E., 1978, *Astron. Astrophys.*, **62**, 439.

Tjin A Djie, H.R.E. & Thé, P.S., 1978, *Astron. Astrophys.*, **70**, 311.

Tjin A Djie, H.R.E., Thé, P.S., Hack, M. & Selvelli, P.L., 1982, *Astron. Astrophys.*, **106**, 98.

Ulrich, R.K., 1976, *Astrophys. J.*, **210**, 377.

UK Optical Telescopes Observers Guide, La Palma Obs., 1983, R.G.O.

Vardanian, R.A., 1964, *Soobsch. Biurak Obs.*, **35**, 3.

Vogel, S.T. & Kuhi, L.V., 1981, *Astrophys. J.*, **245**, 960.

Vrba, F.J., 1975, *Astrophys. J.*, **195**, 101.

Vrba, F.J., Coyne, G.V. & Tapia, S., 1981, *Astrophys. J.*, **243**, 489.

Vrba, F.J. & Rydgren, A.E., 1984, *Astron. J.*, **90**, 1490.

Vrba, F.J., Rydgren, A.E., Chugainov, P.F., Shakovskaya, N.I. &

Zak, D.S., 1986, *Astrophys. J.*, **306**, 199.

Vrba, F.J., Rydgren, A.E., Zak, D.S. & Schmelz, J.T., 1985, *Astrophys. J.*, **90**, 326.

Vrba, F.J., Schmidt, G.D. & Hintzen, P.M., 1979, *Astrophys. J.*, **227**, 185.

Walker, H.J. & Marsden, P.L., 1986, In: *Light on Dark Matter*, 91. Ed. F.P. Israel, D. Reidel, Dordrecht.

Walker, M.F., 1972, *Astrophys. J.*, **175**, 89.

Walter, F.M., 1987, *Publ. Astron. Soc. Pac.*, **99**, 31.

Walter, F.M. & Kuhi, L.V., 1981, *Astrophys. J.*, **250**, 254.

Ward-Thompson, D., Warren-Smith, R.F., Scarrott, S.M. & Wolstencroft, R.D., 1985, *Mon. Not. R. astr. Soc.*, **215**, 537.

Wenzel, W., 1969, In: *Non-Periodic Phenom. in Var. Stars*, 61. Ed. L. Detre, Acad. Budapest.

Whitmore, B., Cameron, D.H.M. & Warren-Smith, R.F., 1987, In: *Circumstellar Matter*, IAU Symp. 122, 189. Eds. I. Appenzeller & C. Jordan, D. Reidel, Dordrecht.

Whittet, D.C.B., Williams, P.M., Bode, M.F., Davies, J.K. & Zealey, W.J., 1983, *Astron. Astrophys.*, **123**, 301.

Wickramasinghe, C., 1973, *Light Scattering Functions for Small Particles*, Wiley, New York.

Wilking, B.A., Taylor, K.N.R. & Storey, J.W.V., 1986, *Astron. J.*, **92**, 103.

Wolf, B., Appenzeller, I. & Bertout, C., 1977, *Astron. Astrophys.*, **58**, 163.

Worden, S.P. & Schneeberger, T.J., 1981, *Astrophys. J.*, **244**, 520.

Zajtseva, G.V., 1982, *Astrofizika*, **18**, 67.

Zellner, B., 1971, *Astron. J.*, **76**, 651.